THE UNIVERSITY
of EDINBURGH

Cellular Delivery using Peptoid Carriers

By

Géraldine Escher

Thesis for the Degree of Doctor of Philosophy

THE UNIVESITY OF EDINBURGH

COLLEGE OF SCIENCE AND ENGINEERING
SCHOOL OF CHEMISTRY

April 2013

To my parents and my husband,

UNIVESITY OF EDINBURGH

COLLEGE OF SCIENCE AND ENGINEERING
SCHOOL OF CHEMISTRY

Abstract for Doctor of Philosophy

Cellular Delivery using Peptoid Carriers

By Géraldine Escher

Efficient delivery into cells is essential for many applications. However, cellular access of "cell-impermeable" molecules, such as drugs, sensors, proteins and oligonucleotides, can often be severely limited due to the plasma membrane which protects cells from unregulated influx of hydrophilic materials. In order to solve this issue, several physical techniques and bio-chemical products are today available. One of them is called peptoids (N-alkylglycines). These compounds are peptidomimetics which are resistant to enzymatic degradation, non-immunogenic and are readily prepared by an Fmoc chemical approach. Peptoids based on the "TAT"-peptide (RKKRRQRRR) offer rapid cellular uptake/delivery and low cytotoxicity.

In this thesis, based on previous works using fluorescein-cationic peptoids, various fluorescent N-substitued glycines (lysine-like) were prepared by the monomer method followed by solid-phase synthesis. Their cellular uptakes *in vitro* into several cell lines (such as HeLa, B16F10, HEK293T and primary immune cells) were examined via flow cytometry and microscopy. The cellular delivery of small molecules mediated by the 9mer polymer achieved an efficient and rapid penetration. These results open up a vast number of applications for delivery of macromolecules using nonalysine-like peptoid. In order to demonstrate this ability, the nonalysine-like carrier was used to deliver various biopolymer molecules such as peptides, GFP protein and DNA (in collaboration with Dr. Stefano Caserta). In addition, thanks to the non-cytotoxicity of this cellular transpoter (MTT assays); experiments were carried out *in vivo* in mice using peptoids labelled near-infrared dyes. The first results have shown that the peptoid is not toxic for the mouse and does not block cell movements. These results allowed the use of 9mer-peptoid as a cellular tracking agent. Based on the development on antimicrobial peptides, the polylysine-like peptoid was also tested as an antibiotic. Recent experiments carried out in collaboration with Dr. Kevin Dhaliwal have revealed a new antimicrobial property of the peptoids. *In vitro* and *in vivo* studies have been carried out using both gram positive and negative bacteria. These results present a promising alternative to conventional antibiotics and antimicrobial peptides (AMPs).

TABLE OF CONTENTS

DECLARATION OF AUTHORSHIP

I, Géraldine Escher, declare that the thesis entitled *"Cellular Delivery using Peptoid Carriers"* and the work presented in it are my own work.

I confirm that:

• The research described in this thesis was carried out under the supervision of Prof. Mark Bradley at the University of Edinburgh;

• Where I have consulted the published work of others, this is always clearly attributed;

• Where I have quoted from the work of others, the source is always given. With the exception of such quotations, this thesis is entirely my own work;

• I have acknowledged all main sources of help;

• Where the thesis is based on work done by myself jointly with others, I have made clear exactly what was done by others and what I have contributed myself;

• No part of this thesis has been previously submitted at this or any other university for any other degree or a professional qualification

• Parts of the work presented herein have been published or are in the process of being published as:

- Dhaliwal, K., Alexander, L., Escher, G., Unciti-Broceta, A., Jansen, M., Mcdonald, N., Cardenas-Maestre, J. M., Sanchez-Martin, R., Simpson, J., Haslett, C., Bradley, M., Multi-modal molecular imaging approaches to detect primary cells in preclinical models. *Faraday Discussions*, **2011**, 149, 107-114, discussion 137-157.

- Dhaliwal, K., Escher, G., Unciti-Broceta, A., Mcdonald, N., Simpson, J., Haslett, C., Bradley, M., Far red and NIR dye-peptoid conjugates for efficient immune cell labelling and tracking in preclinical models. *MedChemComm*, **2011**, 2, (11), 1050-1053.

Signed:…….

Date:…….

ACKNOWLEDGMENTS

Firstly, I would like to thank my supervisor, Professor Mark Bradley, for not only the chance to do a PhD in his world-class research group, but also for his continued support, his patience, his help and advices over the past years.

A massive thank you goes out to Dr. Rosario Sánchez-Martín for teaching me everything that I know about cellular delivery and cell culture. I also thank her for always understanding what I meant and her inconditional friendship and kindness. I am also very thankful to Dr. Asier Unciti-Broceta for our collaboration, his help, his invaluable advice, his patience and our long discussions.

I would like to thank to my major collaborator, Dr. Kevin Dhaliwal (Medical Research Council, Centre for Inflammation Research, Queen's Medical Research Centre, University of Edinburgh) for making this PhD so exciting, for staying optimistic and for the great work that we did together. Thanks to his team (Manuelle, Niel and Jagath), in particular to Manuelle for our conference in Kyoto and her explanations. I also thank Dr. Stefano Caserta for our collaboration on DNA delivery into immune cells and for his advices.

I also thank Dr. Dominic Campopiano and his group for giving me access to their protein synthesis facilities. A massive thanks goes to Marine, my dear friend, and Jonathan for their help, their advice and their kindness. I thank Dr. Nick Gilbert, from Edinburgh Cancer Research UK Centre, for his help and his advice with the GFP expression and purification. I must acknowledge the important contribution of the staff in the King's Building particularly, Dr. Juraj Bella (School of Chemistry) for the countless times he has helped me with my NMR queries, Dr. Andrew Cronshaw (School of Biological Sciences) for all of the expert help he has provided during my use of the MALDI-TOF MS facility and Martin Waterfall (Ashworth Laboratories) for all his advice, his time and his teaching during my use of flow cytometry facility.

Thank you to all members of the Bradley group (past and present) for providing a fun place to work and for all the great times over the years. Massive thank you to the Spanish team, Juan Jo, Mentxu, Salvo (by adoption), Ana and to my dear Juan Ma (we made it, we made it…) for being such motivating, smiling and kind friends. Thanks to you, Mariona, my sweet Catalan friend for sharing our good and bad days. Thanks to the French team (Guilhem, Delphine, Christophe, Anjali and Aurélie) for our French chat. Thanks to the British team, Lois, Adam and Frank B, for educating me into the British culture and for their friendship. Thanks to the peptoid-peptide team, Antonio F., Nikos, Thingsoon and Martha for our scientific discussion and support. Thanks to my partners of the Biolab team (Emma, Nanna and Anne) for our work, our collaboration and our gossips, in particular Emma and Nanna for our house diner. A special thank you for Ivan, my friend, for your English lessons and Maria for teaching, during her last year of PhD, the synthesis of Cyanine dyes.

I would also like to acknowledge Marie Curie fellowship for the funding of my first year of PhD.

I also thank all my friends from France (Petite Elo, Grande Elo, Isaline, Virginie, Emilie, Thomas and Mathieu) who are fantastic friends for 10 years now. Thanks to the Edinburgh French connection (Aline, Nicolas, Marine, Didier, Marie, Anne Fred) for our lovely cheesy evenings.

Finally, I thank my family; my parents, Christine and François, for their love and support during all my studies and Julien for being such a good brother. And it would all be pointless without my husband, my best friend, Yan, whose love has kept me shining during my darkest hour.

ABBREVIATIONS

Abbreviation	Full name
A_{570}	Absorbance at $\lambda = 570$nm
AA	Amino acid
abs	Absorbance
Abu	Aminobutyric acid (three letter code for amino acids)
Ahx	Aminohexanoic
ADP	Adenosine-5'-diphosphate
AIBN	α,α'-Azoisobutyronitrile
AMP	Antimicrobial peptide
AntpHD	Antennapedia's homeodomain
AQ	Acquisition time (NMR)
Arg	Arginine (three letter code for amino acids)
ATP	Adenosine-5'-triphosphate
B16F10	Murine melanoma cells
BMDMs	Bone marrow-derived macrophages
BMRPA1	Rat pancreaticacinar cells
Boc	*Tert*-butyloxycarbonyl
br	Broad (NMR)
Bu^t	*Tert*-butyl
C	Cystine (one letter code for amino acids)
^{13}C-NMR	Carbon-13 nuclear magnetic resonance
Cbz	Carboxybenzyl
$CDCl_3$	Deuterated chloroform
CO_2	Carbon dioxide
CPP	Cell penetrating peptide
Cy	Cyanine
Cy5.5	Cyanine dye 5.5
Cy7	Cyanine dye 7
Cys	Cysteine (three letter code for amino acids)
d	Doublet (NMR)
D1	Relaxation delay (NMR)
DAPI	4',6-diamidino-2-phenylindole
D_2O	Deuterated water
DCM	Dichloromethane
dd	Double doublet (NMR)
Dde	*N*-(1-(4,4-Dimethyl-2,6-dioxocyclohex-1-ylidene)ethyl)

Dha	Didehydroalanine (three letter code for amino acids)
DHAA	Dehydroabietylamine
Dhb	Didehydroaminobutyric acid (three letter code for amino acids)
DIC	*N*,*N*-Diisopropylcarbodiimide
DilC18	1,1'-Dioctadecyl-3,3,3',3'-tetramethylindocarbocyanine perchlorate
DIPEA	Diisopropylethylamine
DMEM	Dulbecco's modified eagle medium
DMF	*N*,*N*-Dimethylformamide
2,5-DMFu	2,5-Dimethylfuran
DMSO	Dimethyl sulfoxide
DNA	Deoxyribonucleic acid
dt	Doublet of triplet (NMR)
E49	Rat brain capillary endothelial cells (cancer cells)
EDTA	Ethylenediaminetetraacetic acid
EGTA	Ethylene glycol tetraacetic acid
ELSD	Evaporative light-scattering detector
em	Emission
equiv.	Equivalent
ES^+	Electrospray mode positive
Et_4NCl	Tetrabutylammonium chloride
Et_2O	Diethyl ether
EtOAc	Ethyl acetate
FA	Formic acid
FACS	Fluorescence activated cell sorting
FBS	Foetal bovine serum
Fmoc	9*H*-Fluoren-9-ylmethoxycarbonyl
Fmoc-OSu	*N*-(9-Fluorenylmethoxycarbonyl) succinimide
FRET	Fluorescence resonance energy transfert
FS	Forward scatter
FT-ICR MS	Fourier transform ion cyclotron resonance mass spectrometry
G	Glycine (one letter code for amino acids)
GAA	Glacial acetic acid
GFP	Green fluorescent protein
Gly	Glycine (three letter code for amino acids)
H_2	Hydrogen gaz
^{1}H-NMR	Proton nuclear magnetic resonance
16HBE14o-	Human bronchial epithelial cells
HBS	HEPES (4-(2-hydroxyethyl)-1-piperazineethanesulfonic acid)-buffered saline
HEK293T	Human embryonic kidney 293T cells

HeLa	Helacyton Gartleri , human cervical tumour cells
HIV	Human immunodeficiency virus
HMDS	Hexamethyldisiloxane
HOBt	1-Hydroxybenzotriazole
HOECHST 33342	2'-(4-Ethoxyphenyl)-5-(4-methyl-1-piperazinyl)-2,5'-bi-1*H*-benzimidazole trihydrochloride
HPLC	High performance liquid chromatography
HRMS	High resolution mass spectrometry
Hz	Hertz
IPTG	Isopropyl β-D-1-thiogalactopyranoside
2-IT	2-Iminothiolane
IR	Infrared
J	Coupling constant (NMR)
K	Lysine (one letter code for amino acids)
K562	Human erythomyeloblastoid leukemia cells
kb	Kilo bases (DNA)
KCl	Potassium chloride
KCN	Potassium cyanide
KH_2PO_4	Potassium dihydrogen phosphate
L929	Murine aneuploidy fibrosarcoma cells
Lan	Lanthionine (three letter code for amino acids)
LPS	Lipopolysaccharides
Lys	Lysine (three letter code for amino acids)
NLys	*N*-(4-Aminobutyl)glycine
m	Multiplet (NMR) or medium (IR)
m/z	Mass-to-charge ratio
MALDI	Matrix assisted laser desorption ionisation
MBC	Minimal bactericidal concentration
MeCN	Acetonitrile
MeLan	Methyllanthionine
MeOH	Methanol
$MgCl_2$	Magnesium chloride
$MgSO_4$	Magnesium sulfate anhydrous
MHz	Mega hertz
MI	Molecular imaging
MIC	Minimum inhibitory concentration
MIR	Magnetic resonance imaging
Mp	Melting point
MS	Mass spectrometry
α-MSH	α-Melanocyte stimulating hormone
MTT	3,-(4,5-Dimethylthiazol-2-yl)-2,5-diphenyletrazolium bromide

MTS	Membrane translocating sequence
Mw	Molecular weight
N_2	Nitrogen gas
N/S	Ratio noise/signal (NMR)
NaCl	Sodium chloride
NADH	Nicotinamide adenine dinucleotide
Na_2HPO_4	Disodium hydrogen phosphate
NaN_3	Sodium azide
NH_4Cl	Ammonium chloride
NH_2OH	Hydroxylamine
NIR	Near infrared
NMP	*N*-Methyl-2-pyrrolidone
NMR	Nuclear magnetic resonance
NLLP	Nonalysine-like peptoid
NLS	Nuclear localization signal
NS	Number of scans (NMR)
NSG	N-Substituted glycine
O_2	Oxygen gaz
OD_{600}	Optical density at 600 nm
OMI	Optical molecular imaging
ON	Over night
Orn	Ornithine
Oxyma	Ethyl 2-cyano-2-(hydroxyimino) acetate
PBS	Phosphate buffered saline
PEBBLE	Probes encapsulated by biologically localized embedding
PET	Positron emission tomography
pEGFP-C1	Plasmid enhanced green fluorescence protein
pI	Isoelectric point
PI	Propidium iodide
Pmc	2,2,5,7,8-Pentamethyl-chroman-6-sulphonyl
ppm	Parts per million
PTD	Protein transduction domain
PyBOP	(Benzotriazol-1-yloxy)tripyrrolidinophosphonium hexafluorophosphate
PyBrOP	Bromo-tris-pyrrolidino phosphoniumhexafluorophosphate
Pyr	Pyridine
q	Quadruplet (NMR)
qNMR	Proton quantitative nuclear magnetic resonance
quin	Quintet (NMR)
Rf	Retention Factor
Rho	Rhodamine

RNA	Ribonucleic acid
rpm	Revolutions per minute
RPMI	Roswell park memorial institute medium
rt	Room temperature
s	Singlet (NMR) or strong (IR)
S	Serine (one letter code for amino acids)
S. aureus	Staphylococcus aureus
SDS-PAGE	Sodium dodecyl sulphate - polyacrylamide gel electrophoresis
Ser	Serine (three letter code for amino acids)
sg	Signal (NMR)
SiRNA	Small interfering RNA
SPE	Solid-phase extractor
SPPS	Solid-phase peptide synthesis
SS	Side scatter
TAT	Trans-activator of transcription
td	Triplet of doublet (NMR)
TEM	Transmission electron microscopy
TEA	Triethyl amine
TFA	Trifluoroacetic acid
THF	Tetrahydrofuran
TIS	Triisopropylsilane
TLC	Thin-layer chromatography
TOF	Time of flight
t_R	Retention time (HPLC)
Tris	Tris(hydroxymethyl)aminomethane
Trt	Trityl
UV	Ultraviolet
Vol^m	Volume
w	Weak (IR)
µw	Microwave
δ	Chemical shift
ε_{570}	Molar extinction coefficient at $\lambda = 570$ nm
λ	Wavelength

CHAPTER 1 : INTRODUCTION

1.1. Cellular entry

For many years, the focus of research in chemistry has been on the synthesis of fascinating compounds including small molecules, polymers and biologically intriguing macromolecules. Although chemists have great skills in producing a myriad of interesting biologically active compounds, the uptake and the delivery of these new materials into cells or tissues can be difficult. To enable efficient cellular uptake of foreign materials (such as drugs and sensors), the characteristics of bilipidic membranes as well as natural pathways through it have to be understood and cytoplasmic delivery of compounds of interest should be carried out while maintaining cell integrity.

1.1.1. Cell membrane-characteristics

Cells are the building blocks of life and are the place where DNA, RNA and proteins are synthesized. This natural laboratory is protected thanks to a membrane (**Figure 1.1**) which creates a remarkable barrier delimitating the intracellular space and providing excellent control of the movement between intra and extracellular fluids.

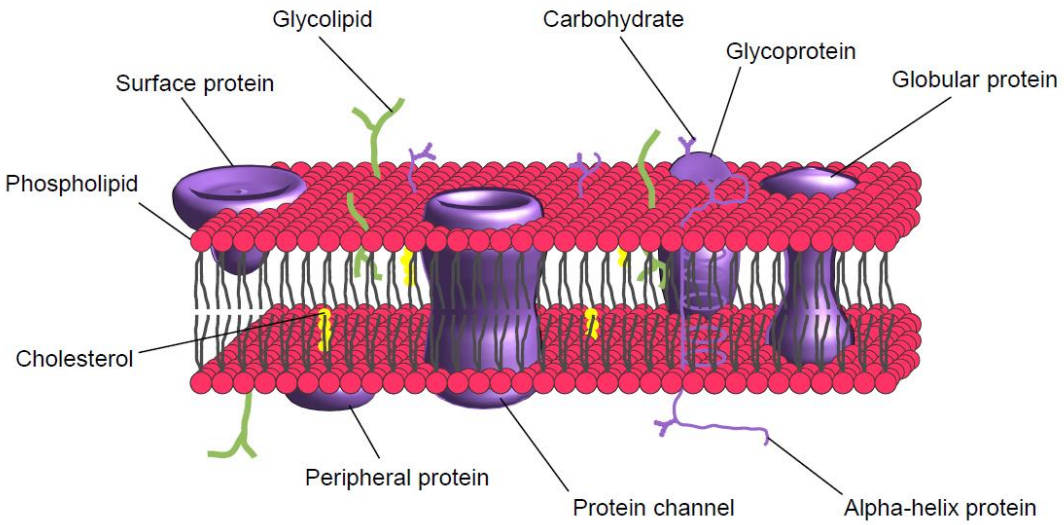

Figure 1.1: Pictorial representation of the cell membrane.
[Permission, **Appendix 1**][1]

'Traffic control' is mainly based on transport proteins, ionic charges (through ionic interactions) and hydrophobicity as the cell membrane is a lipid bilayer made of phospholipids. These lipids have hydrophilic heads and hydrophobic tails that organise themselves with their polar heads facing the aqueous extra and intracellular domains while their long hydrophobic carbon chains are held together by hydrophobic interactions (**Figure 1.2**).

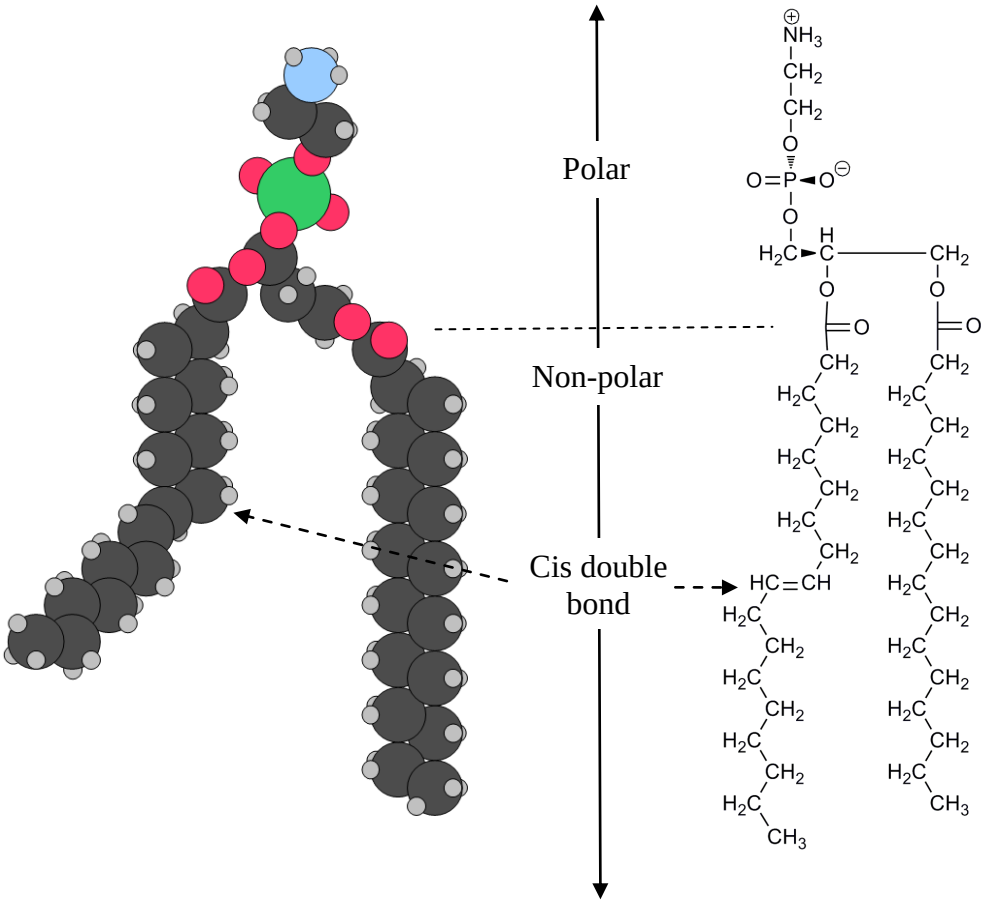

Figure 1.2: A phospholipid.
On the left: Spatial atomic representation; on the right: Chemical structure.
[Permission, **Appendix 1**][1]

Although cell membranes are mainly composed of phospholipids, they are much more complex and contain several other molecules. Inside and crossing the lipid bilayer are proteins and other lipids (e.g. cholesterol, sphingolipids and glycolipids) while carbohydrates are found on the outer cell surface (**Figure 1.1**). These other

buildings blocks allow numerous cellular functions to occur, including cell signalling, adhesion and transport of molecules (e.g. amino acids).[2]

1.1.2. Natural pathways for cellular uptake

Transport of compounds through the cell membrane depends on the nature of the molecules. Cellular phospholipid membranes are impermeable to most molecules, preventing loss of polar compounds such as proteins, nucleic acids or ions (e.g. H^+, K^+, Na^+, Cl^-, Mg^{2+}), but allowing the passive diffusion of certain small materials (non-polar and non-charged). Nevertheless, polar molecules can access the cytoplasm through active transport that requires adenosine-5'-triphosphate (ATP).

1.1.2.1. Passive diffusion

For molecules to diffuse freely through the cellular membrane they typically have to be small, hydrophobic, non-polar or non-charged.

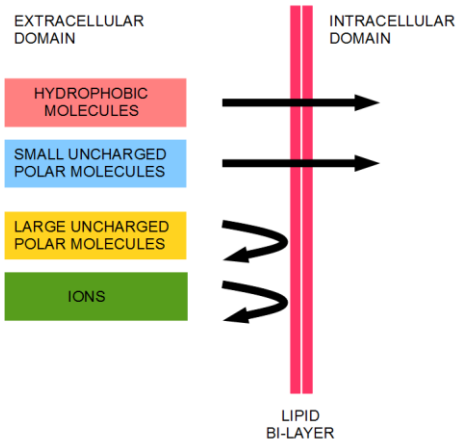

Figure 1.3: Selective permeability of cellular membrane and diffusion of small uncharged molecules.
[Permission, **Appendix 1**][1]

Small, non-polar molecules, including gases (e.g. O_2 and N_2), are able to dissolve into the lipidic bilayer and therefore rapidly diffuse across. Due to random vibration occurring in the membrane, small uncharged polar molecules that do not interact with the negatively charged head of the phospholipids, such as CO_2, water, alcohol and urea, are able to translocate slowly through the hydrophobic fatty region. The

diffusion of such molecules across the cellular membrane is not energy-dependent. Compounds cross the membrane according to a concentration gradient and thanks to their kinetic energy and to random motions due to the other molecules present in the lipid bilayer. However, the lipid bilayer is totally impermeable by diffusion to charged molecules, no matter how small they are, and to large polar compounds such as proteins, amino acids and other foreign materials (**Figure 1.3**).

1.1.2.2. ATP independent membrane transport

There are two major classes of energy free (ATP free) membrane transport proteins. In both of them, the protein creates a gate that allows the solutes to cross the cellular barrier without being in contact with the phospholipids.

The first class is **carrier proteins**, also known as facilitated diffusion. This mechanism requires the solute bounded to a specific binding site. This interaction causes various conformation changes of the protein that transfers the bounded solute from one side of the membrane to the other. Facilitated diffusion always goes down the concentration gradient and continues until equilibrium is reached. However, it is important to note that other carrier proteins act as a pump and use ATP (see ***Paragraph 1.1.2.3***).

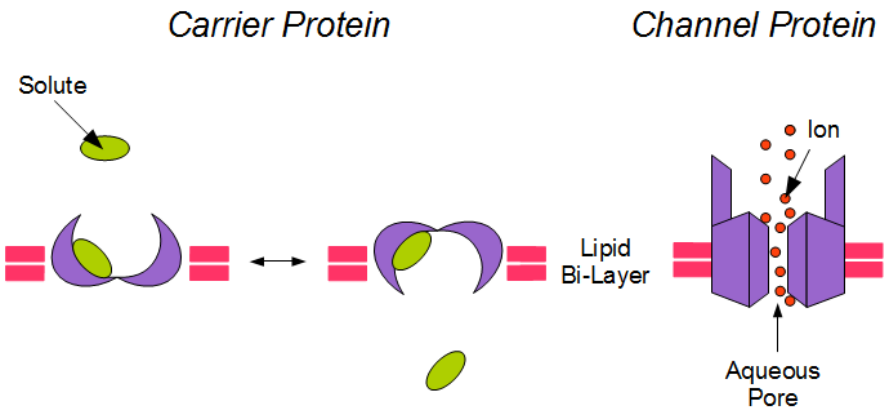

Figure 1.4: Principles of ATP free membrane transport proteins.
Left: Representation of carrier protein for carrier-mediated diffusion; Right: Representation of channel protein. [Permission, **Appendix 1**][1]

The second class is **ion channels**, pores made across the membrane by transmembrane proteins. This transport mode works as a voltage 'gate' that allows small ions (e.g. Cl^- and Ca^{2+}) to travel across the lipid bilayer according to a electrochemical gradient and does not require any binding between the solute and the protein channel (**Figure 1.4**).

Although these classes of protein transport offer efficient cellular penetration of ions, they are limited for the transport of macromolecules as each transporter protein is specific to one, and only one, molecule. Transport of polar molecules (such as amino acids and carbohydrates) cannot occur by diffusion or facilitated diffusion and requires an energy dependent pathway.

1.1.2.3. Energy dependent mechanisms

In synergy with passive diffusion, energy dependent mechanisms or active transport allows the transport of molecules or ions against their concentration gradient and requires the consumption of energy. The main source of energy comes from the hydrolysis of the adenosine-5'-triphosphate (ATP) that generates one molecule of adenosine-5'-diphosphate (ADP) and one of monophosphate (Pi). ADP can be further hydrolysed into adenosine-5'-monophosphate and another molecule of Pi to release more energy. Two main types of mechanism using chemical energy can be distinguished: **endocytosis** that creates a vesicle around the macromolecules and **pumps** that drive the compound across the membrane.

Endocytosis

Endocytosis is a process by which cells uptake materials (such as macromolecules, particles). A small portion of cellular membrane invaginates a foreign substance to form a vesicle that plays the role of carrier. Once internalised, the vesicle pinches off internally to form an endosome or endocytic vesicle that contains the material which is then released into the cytoplasm. Largely, the term 'endocytosis' describes this mode of encapsulation by the lipid bilayer. This general mechanism can be divided

in three sub-pathways: **phagocytosis**, **pinocytosis** and **receptor mediated endocytosis** (**Figure 1.5**).

Phagocytosis (cell eating) is a cellular process in which specific solid particles (typically 1 µm or more), such as apoptotic cells or microbes, are ingested.[3] This operation occurs only in specialist cells known as phagocytes, which include neutrophils, macrophages and monocytes. The specific particle binds onto the cell surface and is encapsulated into a vesicle called a phagosome. Once internalized, these phagosomes are transformed into lysosomes and the contents are degraded or transformed as nutriments.

Pinocytosis (cell drinking) is similar to phagocytosis. This non-specific process creates very small vesicles that typically contain extracellular fluids. Once the small pinocytic vesicle is created, it penetrates inside the cytosol where its contents are released.

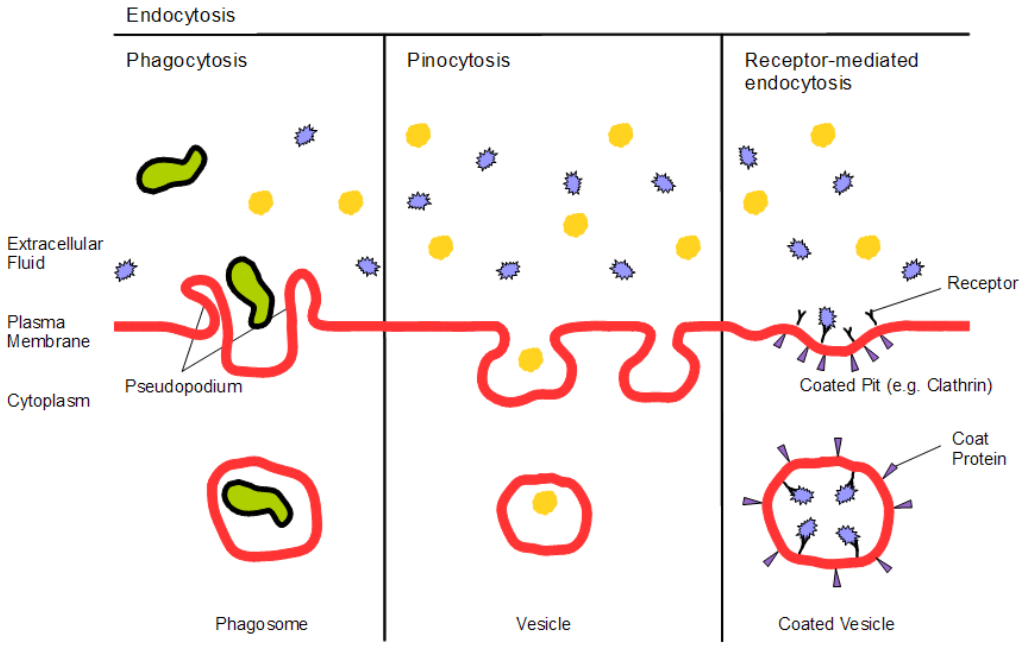

Figure 1.5: Pictorial representation of the three main endocytosis.
On the left: Phagocytosis uptake; in the middle: Transport by pinocytosis; on the right: Formation of coated vesicle through receptor-mediated endocytosis.

Receptor mediated endocytosis (RME) refers to specific endocytic mechanisms, which take place via an interaction between a particular cellular

membrane receptor and the macromolecule ligand. Once bound to each other, the complex transforms itself onto a specialist coated vesicle. These include clathrin-mediated endocytosis (such as for cholesterol using the Low-Density-Lipoprotein receptor)[4] or caveolae-mediated endocytosis.[5] Clathrin-mediated endocytosis depends on formation of clathrin-coated endocytic vesicles. Clathrins bind to the receptor through another protein called adaptin. After removal of their clathrin coats, these vesicles fuse together to form early endosomes, where the constructs receptor-ligand are acidified to separate them. Receptors are then sorted to be recycled back to the membrane or degraded in the late endosome. In the meantime, ligands are, often but not always, degraded inside the lysosomes. More than 25 receptors are known to use this uptake mechanism. For instance transferrin (blood plasma protein) accesses cells through this pathway. In comparison to clathrin-mediated endocytosis, caveolae mediated endocytosis are small distinct invaginations (50 to 100 nm) present on the plasma membrane. These small flask shaped vesicles are rich in caveolin, an integral membrane protein. Caveolae can be in most cells but are especially abundant in smooth tissues such as smooth muscle cells and pneumocytes (cells lining the alveoli in lung). Caveolae dependant cellular mechanism is used by the full length TAT (trans-activator of transcription) protein of human immunodeficiency virus type 1 (HIV-1) and heterologous proteins fused to the TAT.[6]

Sodium-potassium pump

The sodium-potassium pump (Na^+, K^+-ATPase) is an enzyme bound onto the cell membrane. This membrane-bound ion pump belongs to the family of P-type ATPases.[7] During each cycle of ATP hydrolysis, three sodium and two potassium ions are involved (**Figure 1.6**).

At the beginning of each cycle the enzyme is facing the cytoplasm and three sodium ions bind to the protein channel. Due to ATP, the channel changes its shape that in turn drives the Na^+ through the channel. Sodium ions are then released on the other side of the membrane. The channel now has a high affinity for two potassium ions. This potassium-protein interaction generates a new shape change and rotation of the channel toward the cytoplasm. The potassium ions are then released and a new cycle can start.[8]

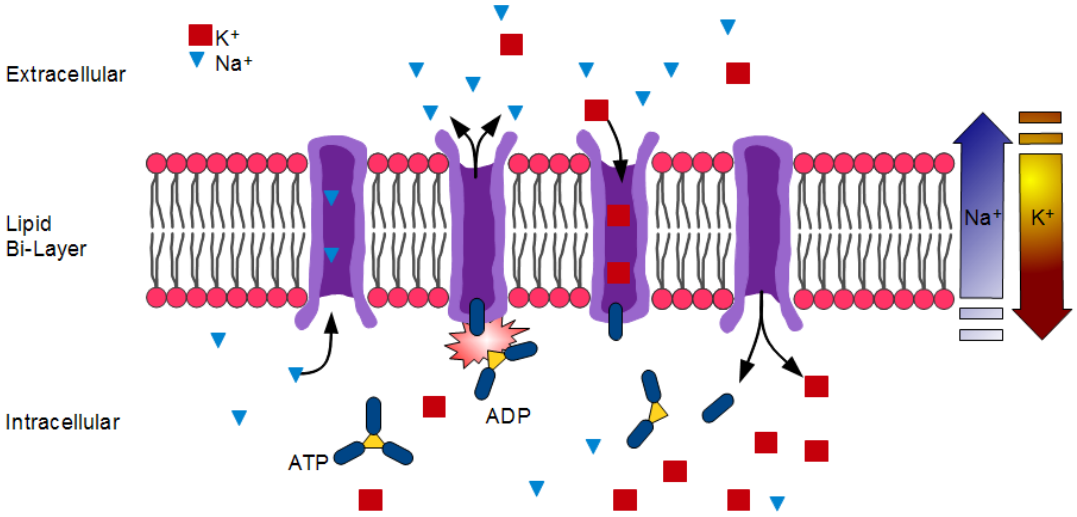

Figure 1.6: Schematic representation of a sodium-potassium pump.
After ATP hydrolysis, the enzyme begins to exchange sodium and potassium through the cell membrane.

In this pump system, sodium and potassium are both moving against their concentration gradient (from areas of low concentration to areas of high concentration). This transmembrane ATPase plays a vital role of osmoregulation in animal cells by regulating their volume (stopping water from entering into cells), intracellular pH and potential.

1.2. Available cellular delivery methods

As described above, cytoplasmic access to molecules is difficult and strongly regulated by various natural tools present on the cell membrane. In order to enable cellular penetration of exogenous materials (such as DNA, siRNA, organic drugs and proteins), a large number of techniques have been developed. These techniques can be grouped into three classes: physical, chemical and carrier based methods.

1.2.1. Physical methods

Physical methods (also defined as mechanical methods) allow cellular delivery of foreign materials to the cytoplasm by disturbing the lipidic bilayer. This disturbance generates a transitory hole in the cell membrane, which gives access to the cytoplasm

for any molecules present in the extracellular fluid. After a few moments, the cell membrane starts to repair itself and reorganises its phospholipids to become impermeable again. These mechanical techniques include microinjection[9] (**Figure 1.7**), scrape loading[10] and electroporation.[11] They have been used to deliver molecules from small organic drugs to DNA.[12,13]

Photoporation, or laser assisted cell poration, is a physical technique which allows the permeabilisation of single cells. In order to destabilise the cell membrane or to create a transient pore, a highly localised laser beam is applied onto the outer membrane of the target cell.[14] This permeability modification allows foreign DNA, siRNA, proteins or quantum dots present in the surrounding media to access the cytoplasm.[15]

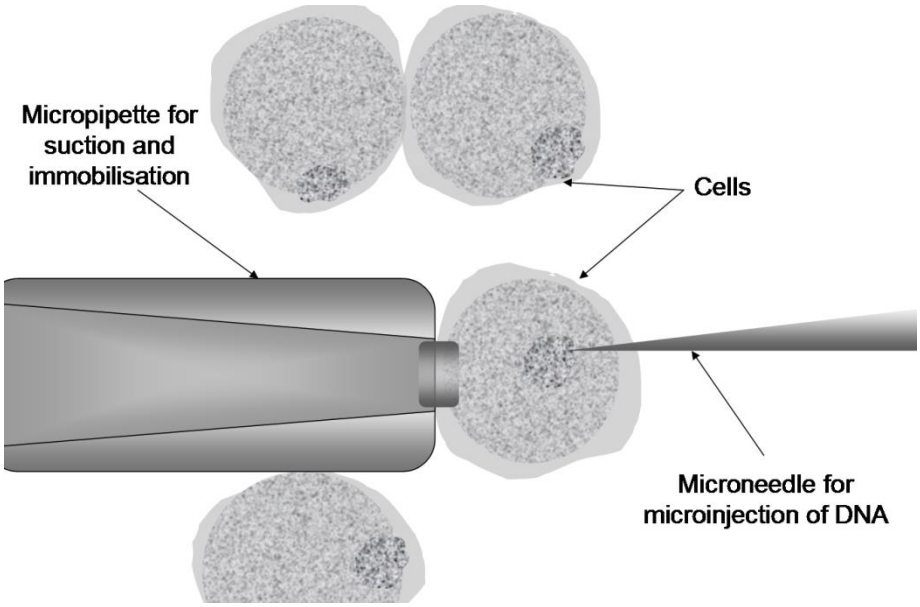

Figure 1.7: Pictorial representation of microinjection technique.

However, even if these methods are widely used by biologists, they can be laborious with low efficiency[16] and can often cause severe damage to cells or tissues.[17]

1.2.2. Chemical approaches

Some chemical techniques are based on the same principles as the physical methods. They disrupt for a short period of time the cell membrane allowing compounds to penetrate into the cytoplasm. This disruption can be carried out to deliver for

example DNA by the use of simple chemical agents such as DMSO[18] or proteins by complexation with the detergent SDS (sodium dodecyl sulphate).[19] However, like physical cellular delivery, the cytotoxicity caused by these methods is a major limitation.[20]

1.2.3. Carrier based cellular delivery

In order to overcome this cytotoxicity issue, scientists have developed less aggressive techniques. The molecules of interest are delivered through a carrier that is able to cross the cell membrane with a minimum effect on its natural organisation. Numerous cellular transporters offer various modes of uptake and two different linking techniques with their cargos: ionic and covalent.

Cationic lipids[21] were introduced in 1987 by Felgner.[22] These amphiphilic organic molecules are composed with a hydrophilic cationic head, which interacts with negatively charged oligonucleotides through ionic interactions, and one or two fatty acid 'tails'. In an aqueous environment, cationic lipids organise themselves around DNA[23] or RNA[24] to form stable complexes or micelles that promote cellular penetration thanks to their similarity with the cell membrane.

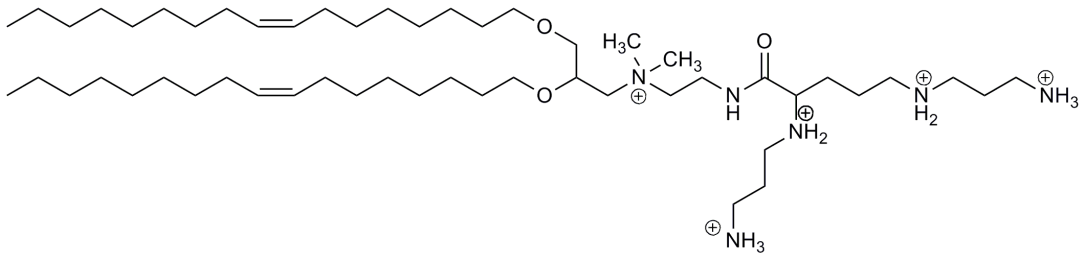

DOSPA : 2,3-DioleylOxy-N-[2(Spermine-carboxamido)ethyl]-N,N-dimethyl-1-PropanaminiumtrifluoroAcetate

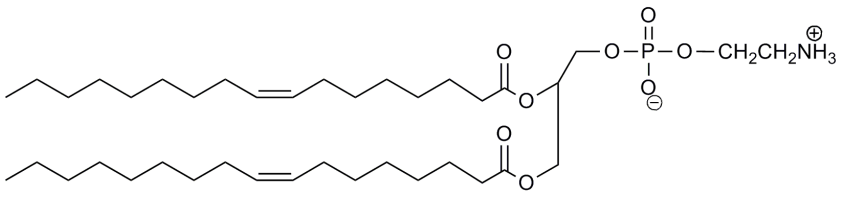

DOPE : DiOleoylPhosphatidylEthanolamine

Figure 1.8: Chemical structures of Lipofectamine (DOSPA/DOPE 3:1 (w: w)).[25]

Several of these non-viral vectors are commercially available, like Lipofectamine®[25] (**Figure 1.8**) and DOSPER®[26,27] (**Figure 1.9**). These lipids or mixture of lipids are used to efficiently transfect an important range of cell lines including stem cells.[28] However, cationic lipids are often associated with complex protocols and cytotoxicity.[29]

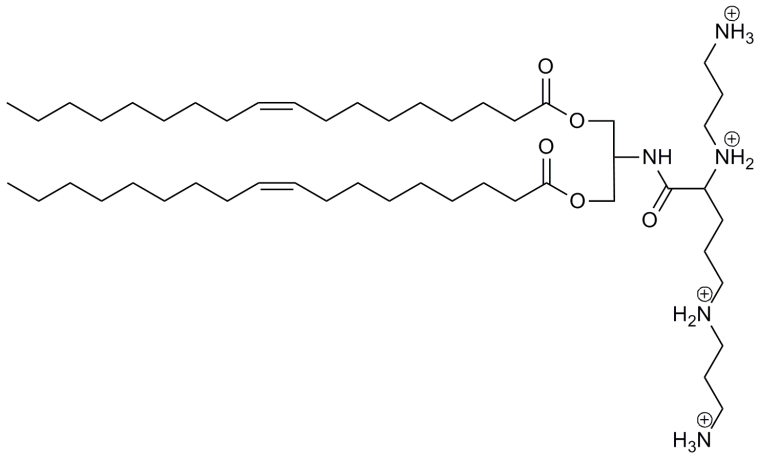

Figure 1.9: Chemical structure of DOSPER.[27]

Carbon nanotubes were first described in 1952, but only became popular almost 40 years later.[30] They exist in two types: single wall (SWNT) and multi wall (MWNT) and have been used to deliver various foreign materials into several cell types (e.g. small molecules,[31] nucleic acids[32] and proteins[33]). Although efficient and diverse, carbon nanotubes suffer from high cytotoxicity[34] and biocompatibility issues.[35]

Microspheres are small spherical particles made of various materials such as glass, ceramics or polymers (e.g. polystyrene or polyethylene), and have been used in research for decades. During the last few decades, the interest in microspheres as cellular delivery devices has kept increasing. These particles can be biodegradable when composed with biodegradable polymer such as poly(D, L-lactide) (PLA) and/or poly(D,L-lactide-co-glycotide) (PLGA)[36] or non-biodegradable (e.g. polystyrene).[37] Microspheres are now used to deliver any size of molecule (e.g. protein,[38,39] DNA,[40] sensors[41] and drugs[42,43]) either by encapsulation[44] or by covalent bonding.[37]

Even if the previous methods are very promising and efficient, cytotoxicity remains their main problem. In order to solve this problem, scientists get inspiration from Nature.

Dendrimers are polymeric hyperbranched structures (**Figure 1.10**). Their architecture, size and composition can be controlled to create a specific and efficient delivery system.[45]

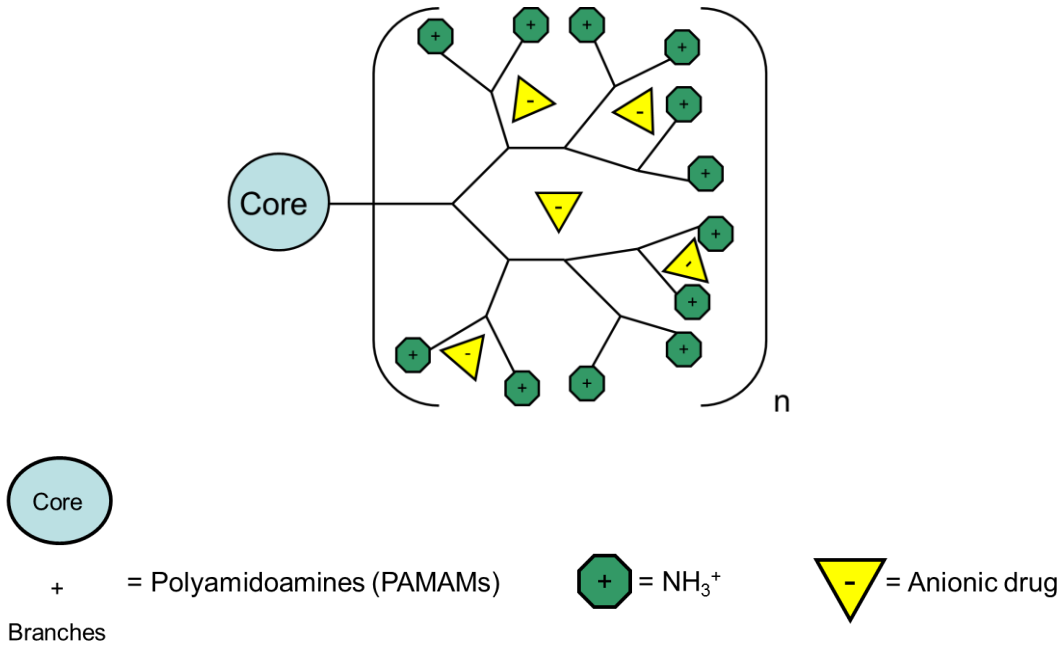

Figure 1.10: Schematic representation of dendrimer and drug incorporation.

Many foreign materials can be internalized using this technique. For instance, DNA is delivered into eukaryotic cells using dendrimers based on polyamidoamines (PAMAM)[46] while antisense oligodeoxynucleotides (OGNs) can be transfected using covalent bonding to an anionic dendrimer (pentaerythritol-based anionic dendrimer)[47] and drugs complexed with dendrimer to facilitate oral delivery.[48]

Another type of cellular delivery system involves the use of natural peptides.

1.3. From peptide domains of viral proteins to cell penetrating peptides

In Nature some proteins, cytokines, transcription factors, antibacterial peptides and transmembrane proteins, are able to interact and translocate across the cell membrane. These properties are often due to a short sequence of amino acids, known

as a protein transduction domain (PTD), which mediates the delivery of protein inside the cell in an energy independent mechanism (also termed as a membrane translocating sequence (MTS)). They are the basis of many cell penetrating peptides (CPPs).[49] The most famous of these "Trojan peptides" has a viral origin and is the HIV-1 transactivator of transcription (TAT).[50] This 86 amino acid protein was first described in 1988[51] and is known to transactivate genes that are expressed from HIV-LTR (long terminal repeat). Various studies of TAT resulted in the identification of two specific sequences allowing cellular penetration: a highly basic sequence (GRKKRRQRRR) between the amino acids 48 and 60[52] allowing ionic interactions with the cell membrane and a nuclear localization signal (NLS) at position 48-52 (GRKKR).[53] Although the TAT peptide is the most well-known of the CPPs, it is not the only one to be used.

1.3.1. Various cell penetrating peptides

The number of CPPs keeps on growing. They have been used to deliver various molecules from nucleic acids[54] to proteins[55] and small molecules into cells.[56] They can be organised into four main categories. Three of them are based on their physicochemical properties, while the forth one is based on natural peptides:

- Basic: based on amino acids like lysine, histidine and arginine.
- Basic-amphipatic: having both basic amino acids and hydrophobic regions.
- Hydrophobic: based on amino acids like valine, leucine and tryptophan.
- Chimera: also known as fusion peptides which are created through the joining of at least two natural peptides.

Category	Name	Sequence	Origin
Basic	HIV-1 TAT[57]	H-GRKKRRQRRRPPQ-OH	Viral transcriptional regulator
	Poly-Arginine R_8[58,59]	H-RRRRRRRR-OH	Synthetic
	FHV Coat (35-49)[59]	H-RRRRNRT RRNRRRVR-OH	Flock house virus coat protein
Basic-amphipathic	Penetratin (43-58)[60]	H-RQIKIWFQ NRRMKWKK-OH	*Antennapedia* homeodomain (pAnt-(43-58))
	Model Amphipatic Peptide (MAP)[61]	H-KLALKLALK ALKAALKLA-NH_2	Synthetic
Hydrophobic	Membrane Translocating Sequence peptide (MTS)[62]	H-KGEGAAVL LPVLLAAPG-OH	Hydrophobic-region from Kaposi-fibroblast growth factor (K-FGF)
	Pep-1[63]	H-KETWWETWWTEW SQPKKKRKV-OH	Synthetic and NLS (SV-40) large T antigen
Chimera	Transportan[64]	H-GWTLNSAGYLLG KINLKALAALAKKIL-NH_2	N-terminal sequence from neuropeptide Galanin (1-12) and C-terminal sequence from Wasp venon toxin Mastoparan[65]
	MPG[66]	H-GALFLGFLGAAGSTM GAWSQPKKKRKV-NH_2	HIV-1 gp41 associated with NLS of SV-40

Table 1.1: Selection of cell penetrating peptides.

Thanks to the efficiency and low cytotoxicity of cell penetrating peptides, biotechnology and pharmaceutical companies have shown an interest in this type of carrier. For instance, Transporter^{TM} peptides are a range of modified cell penetrating peptides commercialised by Cambridge Research Biochemicals. These peptides were described to deliver several cargos (proteins, DNA and organic dyes) that are coupled to the CPP through a disulphide bond.[67] DeliveryX is a siRNA transfection kit commercialised by Panomics and based on MPG[68] (**Table 1.1**). The nucleic acids interact with the cationic sequence of the peptide to generate a nanoparticle able to cross the cell membrane. The siRNA encapsulated within the peptide cluster can access the cytoplasm without using endocytic pathway and, thus, avoiding its degradation (lysosomal degradation).[69] SynB vectors are small linear synthetic peptides (e.g. SynB1 H-RGGRLSYSRRRFSTSTGR-OH) inspired by natural peptide protegrin-1.[70] They are covalently bound to the drug of interest (such as doxorubicin, an anticancer agent) and allow cellular penetration without disturbing the biological membrane.[71]

1.3.2. CPPs and cellular uptake mechanisms

Despite the fact that CPPs are widely used to deliver an important range of bioactive molecules into various cell lines and animals,[49,87] their cellular uptake is still subject to many discussions and several studies carried out with the same carrier have led to contradictory results. Early studies reported that CPP internalization was receptor,[72] energy[73] and temperature independent.[74] Nevertheless, in 2003, these results (CPP uptake through energy free mechanisms) were re-evaluated by Lebleu[75] and Temsamani.[76] Their experiments have shown that several cell-penetrating peptides containing a cationic sequence (e.g. TAT, R_9,[75] SynB5 and penetratin[76]) were found inside endocytic vesicles. These data suggest that this type of CPPs crossed the bilipidic membrane via an endocytosic pathway.

1.3.2.1. Energy free mechanism

Energy free mechanisms (**Figure 1.11**) were initially thought to describe the efficient cellular uptake of CPPs. The theory being that positively charged amino acids of the

peptides interact with the anionic head of the phospholipids. Where this ionic interaction takes place, the overall charge of the cell membrane is modified (neutral). This change leads to instability of the cell surface that could facilitate cavity, pore formation and/or membrane disruption. The cationic charges on the peptides are essential to link the CPP to the membrane. The following steps depend on the other amino acids present in the peptide sequence.

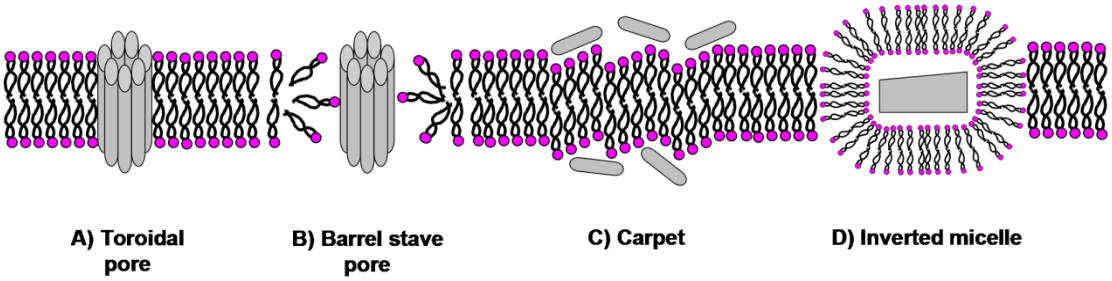

Figure 1.11: Mechanisms of direct translocation across the cellular membrane.
Grey structures represent CPPs. [Permission, **Appendix 1**][83]

In early studies on direct translocation, Derossi[72] described the formation of a hydrophilic cavity, known as an '**inverted micelle**' (**Figure 1.11-D**). The positive charges of penetratin peptides (homeodomain of Antennapedia, a *Drosophila* transcription factor) are attracted by the anionic phospholipids. This ionic bonding is a crucial step for the integration of the CPP. Thanks to this ionic interaction and the structure of the peptides, the tryptophan residues (known to be inducers of inverted micelles) are orientated to penetrate the cell membrane. This lipid disturbance leads to the formation a hexagonal phase, known as inverted micelle. This small pocket contains the peptide-cargo conjugate until its release inside the cytosol.

Pore formation was suggested by analogy with mechanisms of penetration across cell membrane by antimicrobial peptides (AMPs), such as Magainin-2 (GIGKFLHSAK KFGKAFVGEIMNS) and Buforin-2 (TRSSRAGLQFPVGRVHRLLRK).[77] These peptides penetrate into the cytoplasm thanks to an ionic disturbance and a channel through the phospholipid bilayer. As far as pore formation is concerned, three types of pore formation can be described.[78] The first of these mechanisms, the '**barrel-stave**' model (**Figure 1.11-B**), was described in the 1970s. Amphipatic peptides, after interacting with the cell surface, position themselves perpendicularly to the membrane. Thanks to their amphipathic alpha helix structures, antimicrobial peptides

or cell penetrating peptides generate an "aqueous hole", where the hydrophobic amino acids face the aliphatic chains of the phospholipids, while the polar regions face each other.[79] The second mechanism, called the '**toroidal-pore**' model (**Figure 1.11-A**), is very similar to the first one.[80] In both models, the final result is the formation of a perpendicular channel into the cell membrane. However in this pore formation mechanism, the peptides interact firstly with the polar groups of phospholipids to create a complex that forces the lipids to reorganize themselves inside the membrane to fashion a toroidal hole (similar to O-ring shape) composed by both peptides and phospholipids.[81] The last mechanism, known as the '**carpet model**' (**Figure 1.11-C**), begins by the parallel association of the cationic amino acids of the peptides, as single units or oligomers, onto the negative charges of the cell surface. At this stage, the membrane surface is covered by peptides. Then they reoriented themselves: non-polar amino acids towards the long carbon chains of phospholipids and the hydrophilic ones facing the phosphate head of the phospholipids. Once the peptide concentration is above a threshold concentration, they penetrate thanks to the low stability of the cell membrane. During the whole integration process, the peptides conserve the same organisation towards the phospholipids.[82] All these models seem to be efficient and applicable to various exogenous materials. However, due to the size of the inverted micelle, cellular access of macromolecules through this mechanism is not possible.[83]

Several studies have also demonstrated the uptake of CPPs via energy dependent mechanisms.

1.3.2.2. Endocytosis pathways

As discussed in ***Paragraph 1.1.2.3***, endocytosis is an energy dependent mechanism and can be easily detected, as endocytosis is inhibited at low temperature ($4^{o}C$).[84] Mechanism studies on CPPs have shown that several of these peptides are able to penetrate the cellular membrane by endocytosis, such as penetratin and TAT peptides.[75]

The exact endocytosis pathway is still up for discussion for most of these CPPs. Indeed, the same peptide has shown various energy dependent cell penetration mechanisms. For instance, it was shown that a TAT-fusion accessed the cytoplasm

thanks to interaction with lipid rafts (cholesterol and sphingolipids) and through caveolar mediated endocytosis.[85] Nevertheless, two years later, Chernomordik[86] using heparinase III (specific inhibitors of heparan sulfate receptor) reported that unconjugated TAT internalisation was based mainly on a clathrin-dependent endocytic pathway.

Collectively, these data have shown that cellular uptake is a function of the peptide (charge, size and secondary structure), its cargo and the cell type.[87] Furthermore, studies have demonstrated the importance of the interactions between the CPP and the cell surface that could lead to direct translocation and/or an endosome formation.

1.4. Analogues of CPPs

Analogues of peptides or peptidomimetics are mutants which can mimic natural peptides while modifying their biostability, action and/or bioavailability. Analogues of peptides have been developed to counteract various problems that limit the clinical applications of peptides as delivery systems (CPPs[88]) or as drugs.[89] One of the main concerns about peptides is their rapid degradation by proteases.[90] Although TAT peptide is the most used of all the CPPs, its *in vivo* applications are highly limited because of its cytotoxicity and proteolytic sensibility. For instance, trypsin can cleave the TAT sequence up to seven times.[91]

Many peptide modifications are available to give access to a range of peptidomimetics.

Peptidomimetics can be obtained from natural peptides by an inversion of the α-chiral centre (D-peptides[92]) or by a chemical modification of the amide structure (e.g. thioamides). Peptidomimetics can be organised into three categories: spatial, backbone and amide bond modification (**Figure 1.12**). These changes play important roles in their conformation and/or their proteolytic stability.

D-peptides are made of D-amino acids instead of the natural L-amino acids. Various D-enantiomeric peptides have shown similar cellular penetrating properties (cellular uptake and activities) to their L-isomers, while increasing dramatically their stability toward proteases.[92,93]

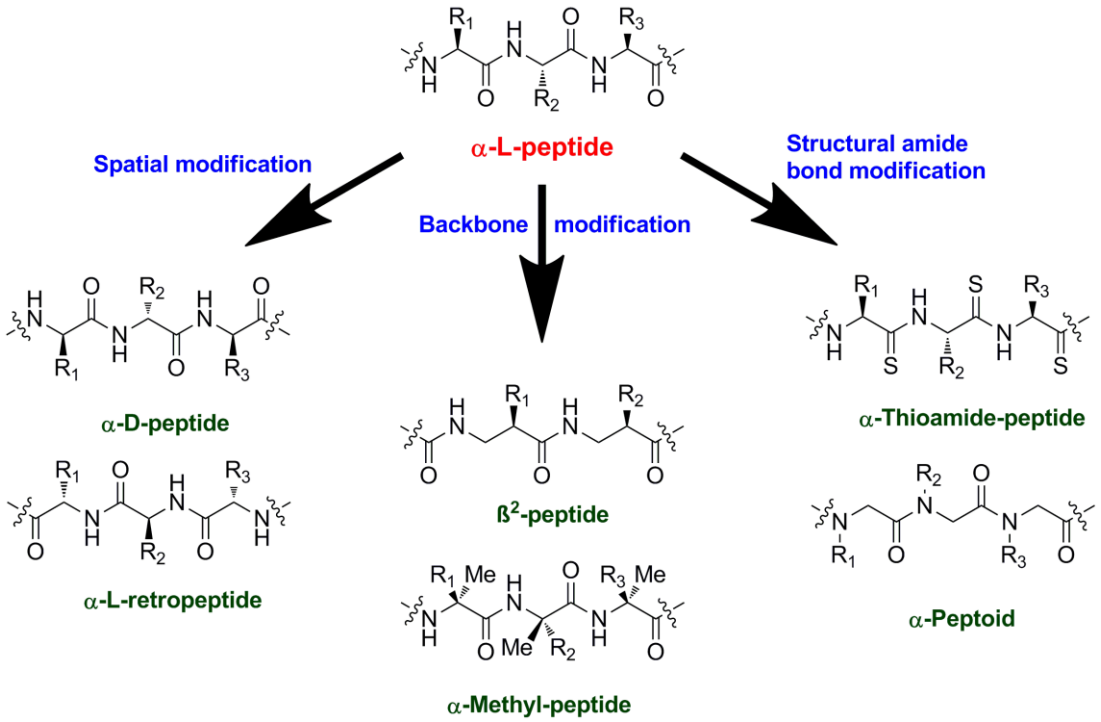

Figure 1.12: Examples of peptidomimetics and their structures.

Beta-peptides[94] (β-peptides) are made of β-amino acids that generate normal amide bonds while increasing the spacing between two consecutive side chains. Their secondary structures (α-helix and/or β-sheets) are stabilised thanks to the formation of intramolecular hydrogen bonds between their C=O and their NH. In β-amino acids, carboxyl group and nitrogen are separated by two carbons. This methylene group allows two types of β-peptides to be generated as a function of where the side chain is located. β^2 and β^3-peptides refer to the side chain positioned onto, respectively, the carbon C_2 (carbon next to carbonyl), and C_3 (carbon next to nitrogen). Thanks to this structural change, this type of peptidomimetics is usually as biologically active (e.g. delivery) as normal peptides, highly resistant toward protease degradation and offers extremely stable helical structure (sequence dependent).[94, 95] β-amino acids can be synthesised using a number of reactions, such as Arndt-Eistert homologation of an α-amino acid.[96]

Thioamide peptides are peptides in which the oxygen of one or more amide bonds has been replaced by sulphur. This atom substitution leads to retention of the planar amide bond but to a disruption or distortion of the secondary structure (β-sheet and α-helix), due to the larger size of the Van der Waals radius of sulphur (180 pm for S,

against 152 pm for O). This change has been reported to increase the enzymatic stability of these molecules against proteases.[97] Thioxopeptides can be prepared by a thioxylation of protected peptide with thiation agents typically via Lawesson's reagent (**Figure 1.13**).[98]

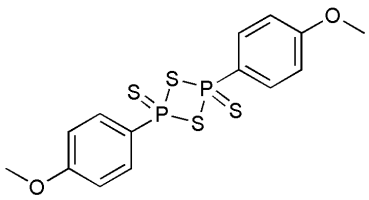

Figure 1.13: Chemical structure of the Lawesson's reagent.

1.5. Peptoids: a promising analogue

The term 'peptoid' was used for the first time in 1982 by Ariens[99] to describe small and flexible chemical structures with the ability to mimic peptidic biological activity without direct structural resemblance. 10 years later, Simon[100] published the first paper on peptoids as we know them today, an oligomer of N-substituted glycines. Like α-peptides, peptoids are composed by a succession of building blocks linked together by an amide bond. As opposed to α-amino acids, the side chains of peptoid building blocks (as suggested by the name N-substituted glycines) are attached to the nitrogen group on the backbone (**Figure 1.14**). This shift retains the distance between two consecutive side chains as in natural peptides and carbonyl.

Nevertheless, this small structural modification plays a crucial role in the properties of this compound. Indeed, in comparison with peptides and other peptidomimetics (**Figure 1.12**), peptoids are much more flexible polymers than peptides as they do not possess any chirality and any hydrogen bond donors on their backbone. Moreover, in comparison with structures containing secondary amide bond, the presence of the tertiary amide decreases the polarity of the oligomer, the formation of secondary structures (based on H-bonding) and the proteolytic sensibility.[101]

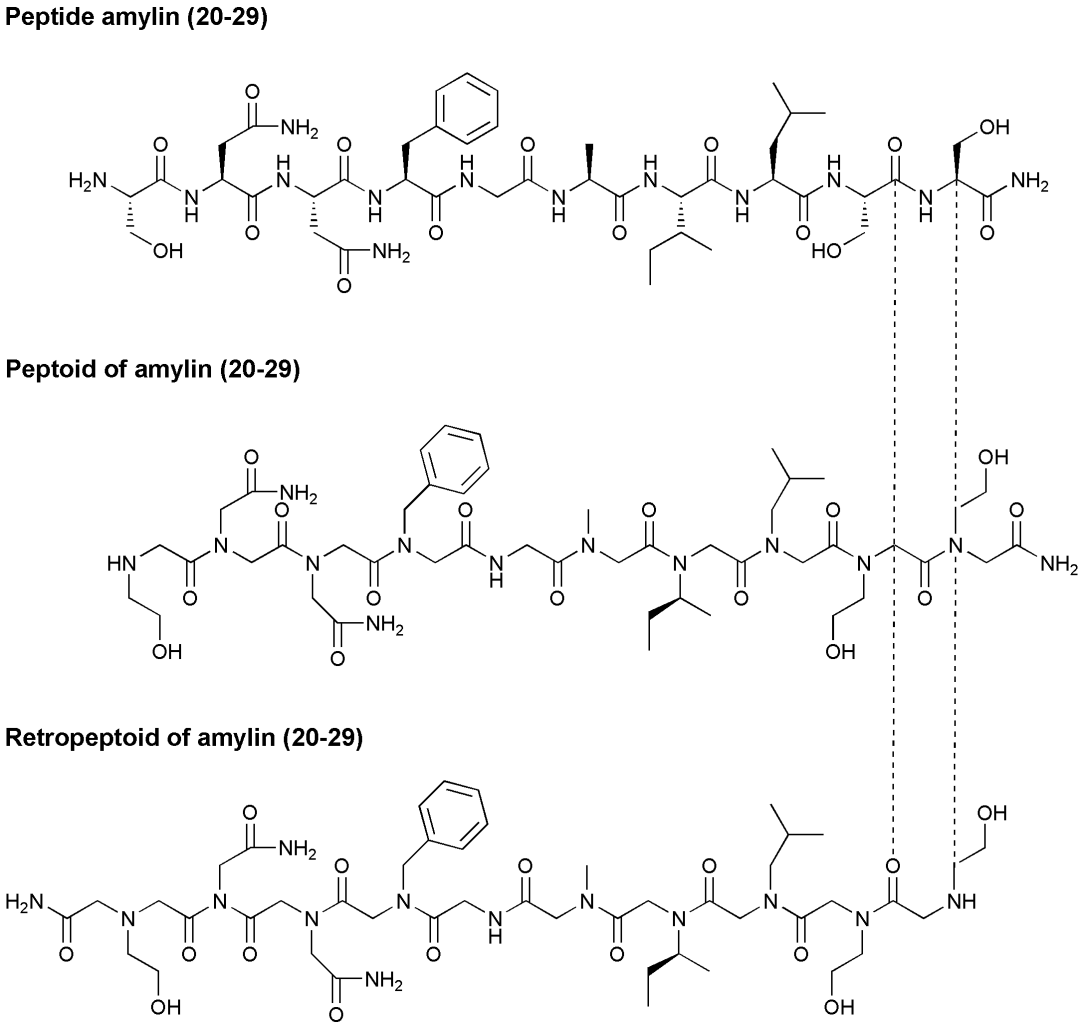

Figure 1.14: Schematic comparison between peptides and peptoids.[102]

Nowadays, peptoids are used in medical and biological chemistry[103] as an efficient cellular delivery system of small molecules[104,105] and macromolecules like DNA (dendrimer peptoids).[106] For instance, peptoids have been used to mimic antimicrobial peptides and have demonstrated promising antibacterial activities (***CHAPTER 5***).[107] Researches have shown that arginine rich N-substituted glycines were able, like proteins, to bind RNA with high affinity.[108] Peptoids have as well been used to coordinate metals. Zinc was bound with high affinity to a two-helix peptoid containing thiol and imidazole moieties. This work was carried out with the aim of mimicking protein nanostructures. When the ion was coordinated to the thiol and imidazole, the peptoid was folded up into two-helix bunbles (U shape).[109] In the same spirit, copper II and cobalt II were coordinated to small peptoids (pentamer or

hexamer) made with one or two units of hydroxyquinoline N-substituted glycine. The metal-peptoid coordination generates a well-defined secondary structure of the oligomer, introducing conformation contraints (helix type) and chiral environment to the metal center.[110]

1.6. Aim of this work and carrier design

The aim of the work in this thesis was the synthesis and study of peptoid-based cellular penetrating systems. Due to the data discussed in this chapter, the cellular penetrating system chosen was based on polycationic peptides like HIV-1 TAT (49-57). Although arginine is the most common amino acid in the TAT sequence, this thesis work focused on lysine-based transporters. This choice was determined by several studies, notably research that demonstrated polylysine oligomers are less cytotoxic than their corresponding polyarginine analogues.[111] In addition, even though polyarginines oligomers possess a more efficient cellular uptake, polylysine compounds (peptides or peptoids) have demonstrated great properties to deliver various cargos into cells.[104,112]

In addition to the choice of lysine N-side chain, the length of the carbon chain was increased from butyl to hexyl as this side chain extension was demonstrated by Wender to improve the cell penetration as it increases flexibility and the hydrophobic character of the side chain.[113]

Previously, several polylysine-like peptoids were synthesised (3, 5, 7 and 9mer) and tested with various cell lines.[104, 114] The studies showed that the number of monomer units played a major role on the cellular efficiency of the carrier. Indeed the 3mer was the least penetrating, while the 9mer was the most rapidly taken up by cells. In addition, the comparison of peptoids (N-alkylglycines) and their peptide homologues (polylysines or polyarginines) clearly demonstrated the greater efficiency (faster to penetrate cells) of the peptoids compared to the peptides. Even though, this type of cellular carrier had been synthesised previously and tested, numerous questions remain unanswered.

Following peptoid synthesis, the following questions about its properties and characteristics were targeted:

- Can small molecules be delivered into cells without cytotoxicity?
- Is the cellular uptake of the peptoid cargo dependent?
- Is peptoid delivery applicable for *in vivo* research?
- Could macromolecules be internalized into cells?
- Do they have any other interesting applications?

CHAPTER 2 : RHODAMINE-PEPTOID: SYNTHESIS AND *IN VITRO* CELLULAR DELIVERY STUDIES

Previously a fluorescein-9mer peptoid was synthesised and analysed with K562, L929 and HeLa cells.[104] In this chapter, the aim was to synthesise a rhodamine labelled 9mer peptoid and carry out a detailed analysis in several cell lines to demonstrate that labelling was dye independent.

2.1. Synthesis of N-Fmoc-N-(6-N'-Boc-aminohexyl)-glycine

2.1.1. Background

In order to synthesise a peptoid, two main routes are used. The first technique, the so-called "monomer" synthesis, was first described by Zuckermann[100] in 1992. This approach was optimised by Liskamp[115] in 1995, Peretto in 2003 and by Fara[116] in 2006. The second technique, the so-called "submonomer" synthesis route, was published at the end of 1992 by Zuckermann.[117]

2.1.1.1. Monomer synthesis

"Monomer" peptoid synthesis involves the synthesis of protected building blocks (monomers), which can then be coupled together using the techniques developed for solid-phase peptide synthesis (SPPS). As for peptides, peptoids are synthesised from the C-terminus to the N-terminus, by reaction between an activated carboxylic acid (AA+1) with an amino group of AA. In order to avoid side reactions, the side chains of amino acids and the amine group have to be orthogonally protected. In the first paper describing the "monomer" synthesis of peptoids,[100] side chain protecting groups were acid labile (Boc, Bu^t, Trt and Pmc) and the amino groups were protected using an Fmoc moiety (base labile).

The original methods used for peptoid "monomer" synthesis were carried out by reductive amination of an amine with a glyoxylic acid (**2.1)** (**Scheme 2.1-A**) or reaction of a glycine methyl ester (**2.2**) with an aldehyde (**Scheme 2.1-B**).

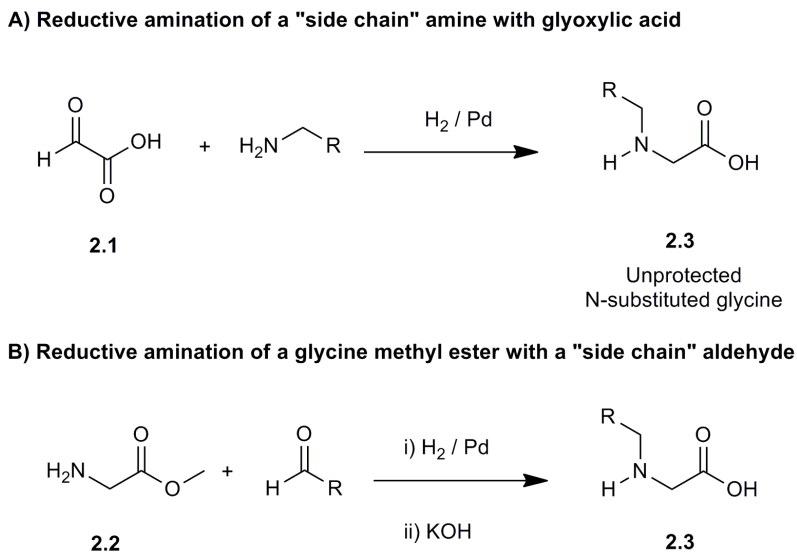

Scheme 2.1: Original synthetic routes towards N-substituted glycines (2.3).[100]
R = representing side chains, protected as necessary.

These original methods were very convenient bringing together two approximately equal fragments, but were not suitable for all side chains and protecting groups. Alternative routes were developed to overcome this issue including:

- Alkylation of an amine with chloroacetic acid (**2.4**) (**Scheme 2.2-A**).
- 1,4-addition of glycine (**2.5**) to acrylamide (**2.6**) (**Scheme 2.2-B**).

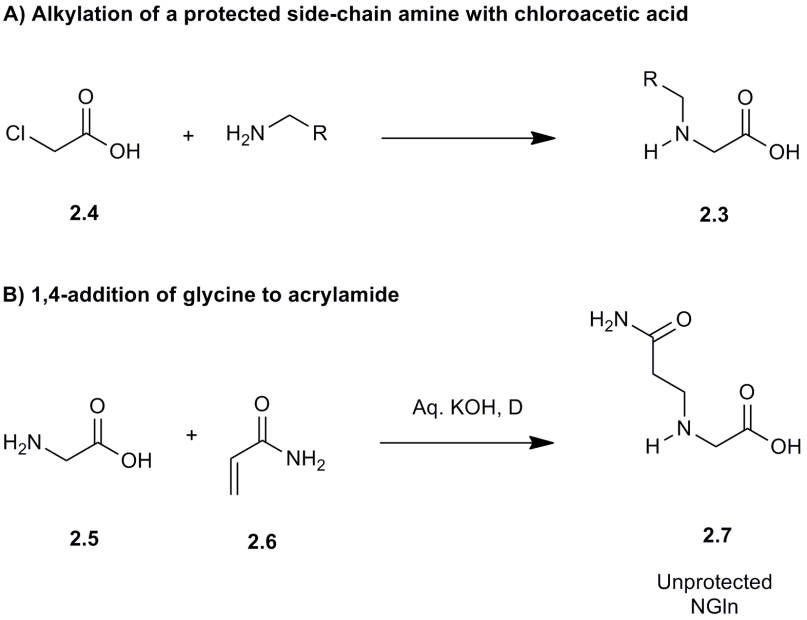

Scheme 2.2: Alternative synthetic routes toward N-substituted glycines.[100]
R = representing side chains, protected as necessary. NGln = N-substituted glutamine.

The amine group of the N-substituted glycines (NSGs) could then be protected using *N*-(9-fluorenylmethoxycarbonyl)succinimide (Fmoc-OSu).

In 1995, Liskamp described his three step monomer synthesis based on Zuckermann's work (**Scheme 2.3**). Ethyl bromoacetate (**2.8**), as a starting material, was alkylated with the desired primary amine. This N-alkylation was followed by a classical saponification of the ethyl ester using sodium hydroxide to obtain the salt that was then Fmoc protected. This method allowed an impressive variety of NSGs to be made as any amines (alkylamine, amino acid or diamine) could be used to alkylate the bromo ester.

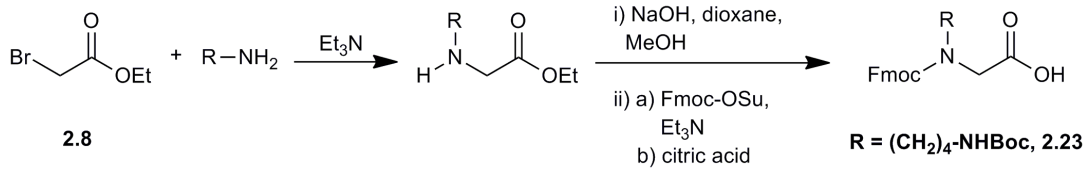

2.8

R = $(CH_2)_4$-NHBoc, 2.23

Scheme 2.3: Synthesis of peptoid monomer by Liskamp.[115]

Three years later, the same group proposed a modification of their synthetic route to access Fmoc-NArg(Boc)$_2$-OH (**2.16**) in high yield.[118] In this N-substituted glycine synthesis, *N*-Boc-1, 3-propanediamine (**2.9**) was alkylated using benzyl bromoacetate (**2.10**) instead of ethyl bromoacetate (**Scheme 2.4**). Once the protected N-substituted glycine of the non-standard amino acid ornithine (**2.11**) had been prepared, the amino group was protected by treatment with benzyl chloroformate to obtain Cbz-NArg(Boc)$_2$-OH (**2.12**). The side-chain amine was then deprotected selectively under acidic conditions and the free amine was guanylated with *N,N'*-bis(Boc)-1-guanylpyrazole (**2.13**) to give Cbz-NArg(Boc)$_2$-OBn (**2.14**). The benzyl ester and Cbz group were removed simultaneously by hydrogenolysis, followed by Fmoc protection of the free secondary amine to give Fmoc-NArg(Boc)$_2$-OH (**2.16**).

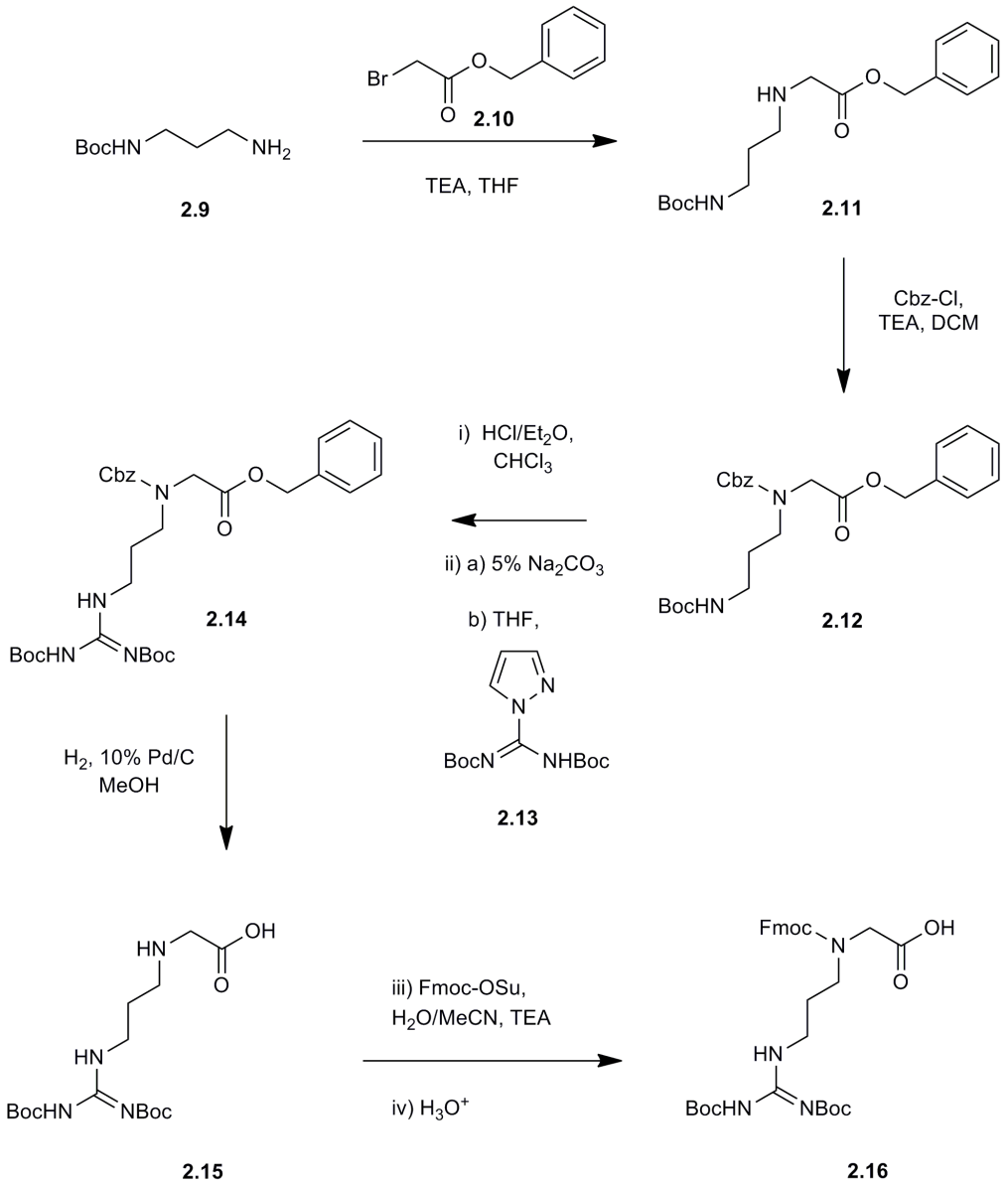

Scheme 2.4: Synthetic route proposed by Lyskamp to access Fmoc-NArg(Boc)$_2$-OH (2.16).[118]

Based on Liskamp's synthesis, other groups such as Bradley[104, 114] and Bräse,[119] have developed their own method to obtain specific peptoid monomers. Once the monomers were synthesised, they can be coupled using solid-phase synthesis. Solid-phase synthesis of the peptoid will be described later in this chapter.

2.1.1.2. Submonomer synthesis

The "submonomer" process was introduced by Zuckermann[117] in order to avoid the necessity of producing multiple peptoid building blocks as starting materials. In this

new approach (**Scheme 2.5**), each monomer is created directly on the solid-phase using two rapidly available "submonomers", a haloacetic acid and a primary amine. In this synthesis, each extension cycle is composed of two steps: an acylation followed by a nucleophilic displacement (**Scheme 2.5**).

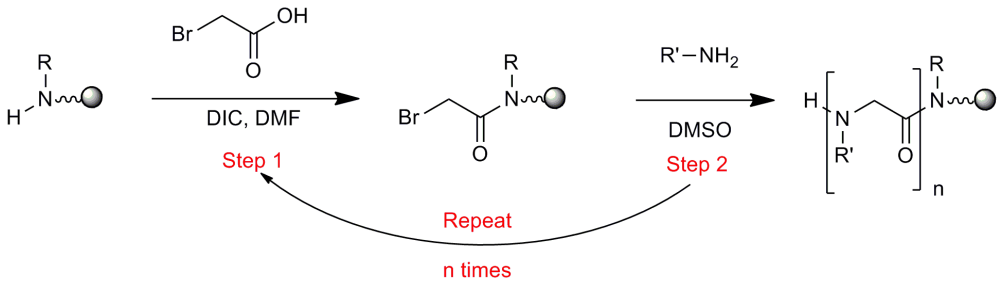

Scheme 2.5: "Submonomer" synthesis of peptoids
In this synthesis, Step 1 is an acylation and Step 2 is a nucleophilic displacement.
(R and R' = protected side chains)

The **acylation (Scheme 2.5**, Step 1) of the secondary amine on the solid support by the pre-activated α-haloacetyl submonomer (bromo, chloro or iodoacetic acid) was carried out using a carbodiimide as an activating agent. The combination of the high concentration of the haloacetic acid (0.6 M in DMF) and DIC (0.66 M in DMF) generates a highly potent acylating agent that facilitates secondary amine acylation.
The **nucleophilic displacement (Scheme 2.5**, Step 2) of the halogen was carried out in order to introduce the side chain (protected if needed). This reaction was carried out in presence of an excess of primary amine (40 equivalents, 2.5 M in DMSO). In his paper, Zuckerman studied the efficiency of nucleophilic displacement function of the halogen. His work revealed that the yield of this second step appeared to be greatly superior when carried out on an iodo and bromo solid support compared to chloro derivate. Zuckerman published the synthesis of nine peptoids (mainly pentamers) using a robotic synthesizer.[120] Each cycle taking approximately 3 hours with the peptoids obtained after TFA cleavage of the Rink amide linker.

Nowadays, numerous groups have modified the original submonomer synthesis in order to reduce the original reaction time from 3 hours to less than 30 minutes (use of microwave heating Kadaked,[121] Burgess,[122] and Blackwell[123]) or to be able to apply peptoid synthesis on arrays (e.g. photolithographic synthesis[124]).

2.1.1.3. Solid-phase synthesis of peptoids

As previously described in ***Paragraph 2.1.1.1***, monomers synthesised in solution phase have to be coupled to each other in order to prepare the desired peptoid. The easiest way to do so is to use a solid support.

Fmoc peptoid solid-phase synthesis is based on the same techniques as Fmoc-SPPS and can be divided in two parts:

- 1: Elongation of the peptide or peptoid chain (coupling and Fmoc deprotection).
- 2: Cleavage and deprotection.

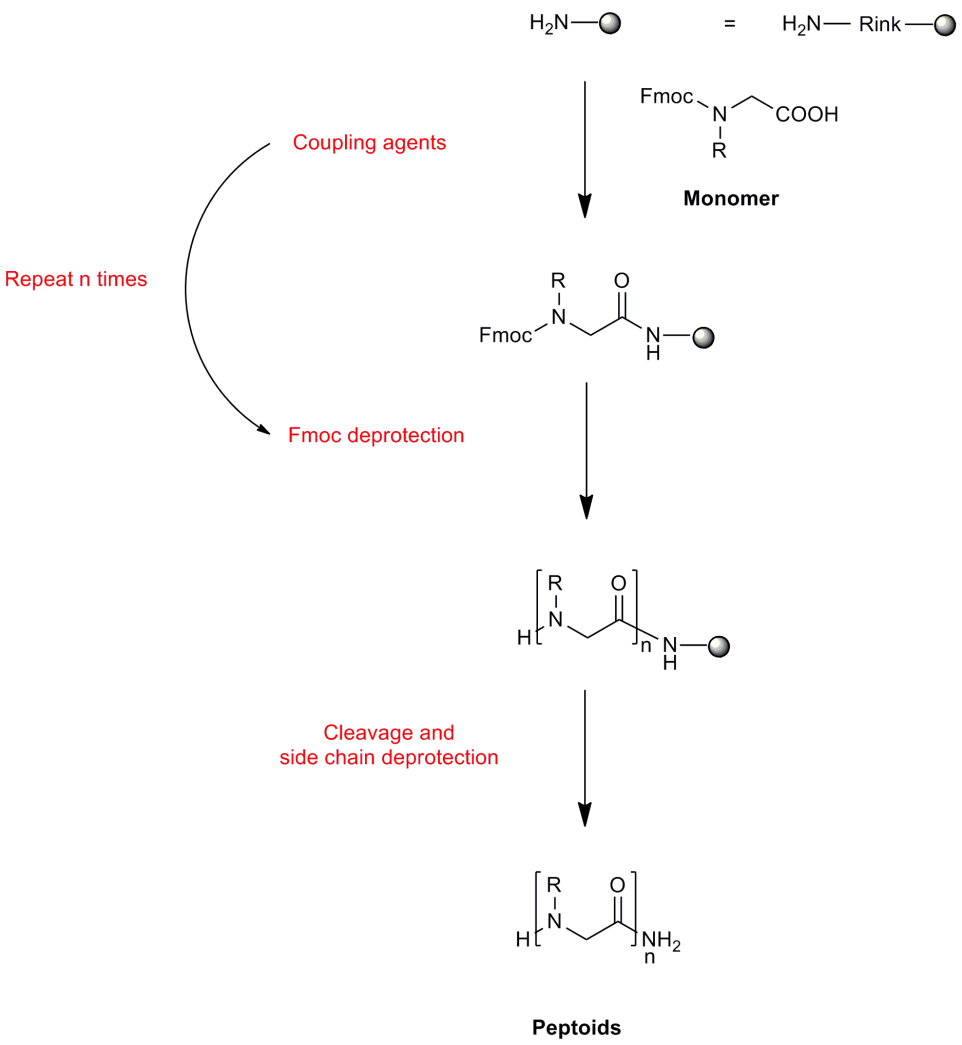

Scheme 2.6: Fmoc solid-phase synthesis of peptoids.
R=side chains, protected as necessary.

The nature of the amino group will affect the ease of the coupling reaction. Indeed, N-alkylamino acids (such as proline), due to their steric hindrance, are known to couple poorly under standard conditions[125], a problem that can affect the yield and purity of peptoid oligomers. In order to solve this issue, standard carbodiimide coupling reagents have often been substituted with PyBOP and PyBrOP, developed for the coupling of hindered or disubstituted amino acids.[126] In 2006, Fara[116] was able to reduce the coupling reaction time using a mixture of DIC/HOBt for 20 minutes at 60°C using microwave irradiation.

2.1.1.4. Monomer or submonomer synthesis - that is the question?

Nowadays, both techniques are used; Zuckermann and Barron work using the submonomer synthesis while Bradley and Bräse prefer the "monomer" approach.[103] Before starting any work on a peptoid, it is important to know which synthetic route will be the most efficient (time and material) for the project. In order to do so, the advantages and the disadvantages of both methods must be evaluated. Some of these criteria are summarised in the following table.

	Advantages	**Disadvantages**
Monomer synthesis route	- Usual Fmoc SPPS techniques - Monitoring of each coupling reaction and Fmoc deprotection using a colorimetric test - Automation possible - Microwave assisted DIC/HOBt protocol: 40 minutes per residue (including Fmoc deproctection) - High purity - High yield - Precise control of peptoids library using "split and mix"	- Synthesis of each protected monomer in large quantities

Submonomer synthesis route	- Full solid-phase process - Large range of commercially available primary amines - Efficient acylation mediated by the DIC/haloacetic acid mix - Automation - Ease of solid-phase synthesis - Microwave heating can be applied -Excess of amine can be recovered and reused	- High quantities of reagents - Need to purify final product - Low yield for hindered amines - 2.5 to 3 hours per residue at room temperature - Protection of side chains

Table 2.1: Comparison of both peptoid synthetic routes.[116, 121, 127]

The **submonomer** synthesis allows the creation of large libraries of peptoids thanks to the number of commercially available primary amines.[128] However this incredible flexibility has some important limitations. The main drawback is the use of large excesses of starting materials, up to forty equivalents at high concentrations (primary amine or haloacetic acid solutions up to 2.5 M). The second concern about this method resides in the efficiency of the SN_2 step. Indeed, incorporation of hindered, poor nucleophilic and low solubility amines cannot be carried out with high yield. Therefore, this step will decrease the synthesis efficiency of the peptoid (purity and yield).

The **"monomer" approach**, thanks to its analogy with peptide synthesis, uses well known and optimized conditions and requires a relatively small amount of material (3 equivalents) per residue. The oligomerisation progress can be easily monitored using the colorimetric methods (primary amine using ninhydrin test[129] and secondary amine using chloranil test[130]). Another advantage, based on the fact that peptoid solid-phase synthesis uses the same reagent as SPPS, is automation using commercially available peptide synthesisers. However, the main limitation of this method is the preparation of the protected monomer in large quantity.

To conclude, if the project requires the screening of numerous small peptoids the submonomer route is the method of choice. However, if the aim of the study is to analyse the capacity of a specific peptoid with a known sequence, the monomer approach is the best choice, as the purity using this second method is much higher.

This thesis project deals with a peptoid (**2.17, Figure 2.1**) as a cell penetrating peptidomimetic that is based on polylysine. As the peptoid structure is a repetition of the same building blocks the "monomer" synthesis was demonstrated to be the most efficient approach. Indeed, once the monomer unit synthesised, the peptoid polymer can be carried out on solid-phase allowing clean synthesis and awoiding purification.

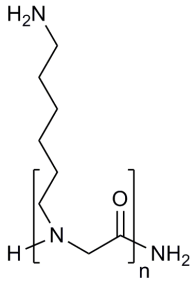

2.17

Figure 2.1: Structure of polylysine-like peptoids (2.17).

2.1.2. Synthesis of the Boc protected building block : *N*-Fmoc-*N*-(6-*N*'-Boc-aminohexyl)-glycine

The method used in this project for the synthesis of *N*-Fmoc-*N*-(6-*N*'-Boc-aminohexyl)-glycine (**2.22**) was previously published by Bradley[104, 114] and in the thesis of Fara.[131]

2.1.2.1. Previous synthetic routes

The first synthetic route of *N*-Fmoc-*N*-(6-*N'*-Boc-aminohexyl)-glycine (**2.22**) was described by Peretto[114] and began with the 1,6-diaminohexane (**2.18**) (**Scheme 2.7**). This synthesis was inspired by the synthetic work of Liskamp.[115] The choice of the monomer was guided by the several advantages of polylysine (described in ***CHAPTER 1***) and Wender's cellular uptake work.[113]

After Boc mono-protection of 1,6-diaminohexane (**2.18**),[132] the monoprotected reagent (**2.19**) was alkylated using one equivalent of ethyl bromoacetate (**2.20**) to give the lysine-like N-substituted glycine ethyl ester (**2.21**) (55% yield). The *tert*-butyloxycarbonyl group (Boc) chosen is extremely resistant under basic conditions and catalytic hydrogenolysis. These characteristics make it an ideal orthogonal partner to the Fmoc group. The ethyl ester was saponified under basic conditions, followed by *N*-Fmoc protection to give the desired monomer in a yield of 40%.

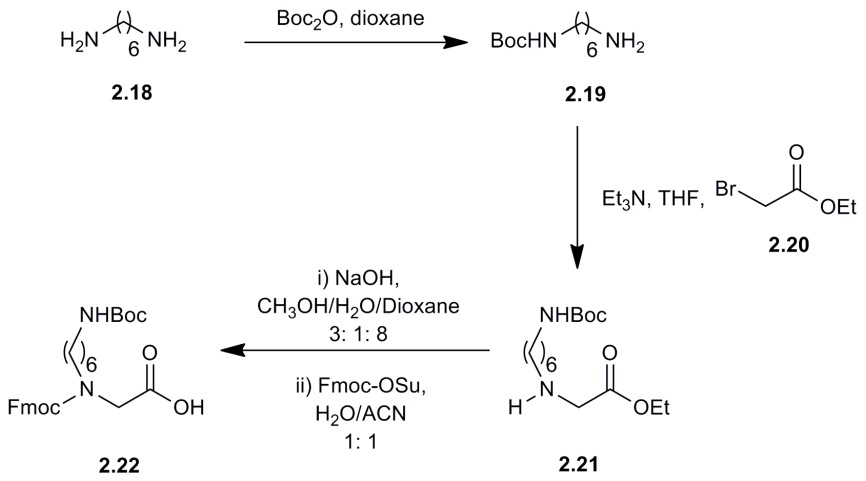

Scheme 2.7: Peretto monomer synthesis of *N*-Fmoc-*N*-(6-*N'*-Boc-aminohexyl)-glycine (2.22)

Despite the fact that the reaction worked, the global yield was fairly low (22%) compared to Liskamp's synthesis (72% for Fmoc-NLys(Boc)-OH, **2.23**, **Scheme 2.3**). This difference of yield was due to the lower efficiency of the mono-alkylation reaction (55% in Peretto's protocol and 75% in Liskamp's synthesis). Also the saponification/Fmoc protection step was lower in Peretto's synthesis (40% for the synthesis of **2.22** from **2.21** against 95% for Liskamp's product).[114, 118]

2.1.2.2. Fara's synthetic route

In order to increase the yield of this monomer (**2.22**) synthesis, ethyl bromoacetate was replaced with benzyl bromoacetate, as described for the synthesis of Fmoc-NArg(Boc)$_2$-OH (**2.16**).[118] Using the benzyl bromoacetate, saponification would not be required and Fmoc protection could be carried out with the acid group still protected (**Scheme 2.8**).[104]

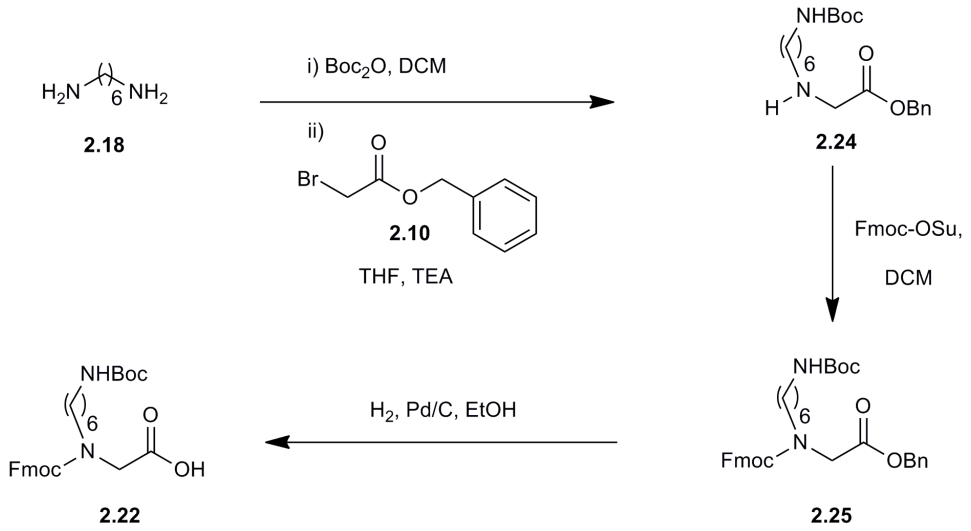

Scheme 2.8: Fara's synthesis of the *N*-Fmoc-*N*-(6-*N'*-Boc-aminohexyl)-glycine (2.22).[104]

The first step of Fara's synthesis[104] was the creation of the N-substituted glycine (**2.24**) from 1,6-diaminohexane (**2.18**). The Boc monoprotection was carried out using di-*tert*-butyl dicarbonate in DCM at room temperature for three hours. Without further purification, the free primary amine was monoalkylated with benzyl-2-bromoacetate (**2.10**) to obtain the desired N-substituted glycine protected by a benzyl ester and a Boc group (**2.24**). Compound **2.24** was isolated by column chromatography in a final yield of 68% over the first two steps. The non-protected secondary amine group was then protected by a Fmoc group using Fmoc-OSu. After purification by chromatography, **2.25** was obtained in a 94% yield. Benzyl group deprotection was carried out using Pd/C catalyst under H_2. After purification, the monomer **2.22** was obtained in 80% yield. In this thesis, the desired compound (**2.22**) was synthesised using Fara's method and a classical palladium-based hydrogenation with a global yield of 51% from the unprotected diamine.

2.2. Solid-phase synthesis of nonalysine-like peptoid

2.2.1. Previous work : solid-phase synthesis of nonalysine-like peptoid

Bradley described the preparation of 3 (**2.30**), 5 (**2.31**) and 7 (**2.32**) lysine-like peptoids using *N*-Fmoc-*N*-(6-*N*'-Boc-aminohexyl)-glycine (**2.22**) and Fmoc solid-

phase peptide chemistry using polystyrene aminomethyl resin (**2.27**) functionalised with a Fmoc Rink amide linker (**2.26**) (**Scheme 2.9**).[114]

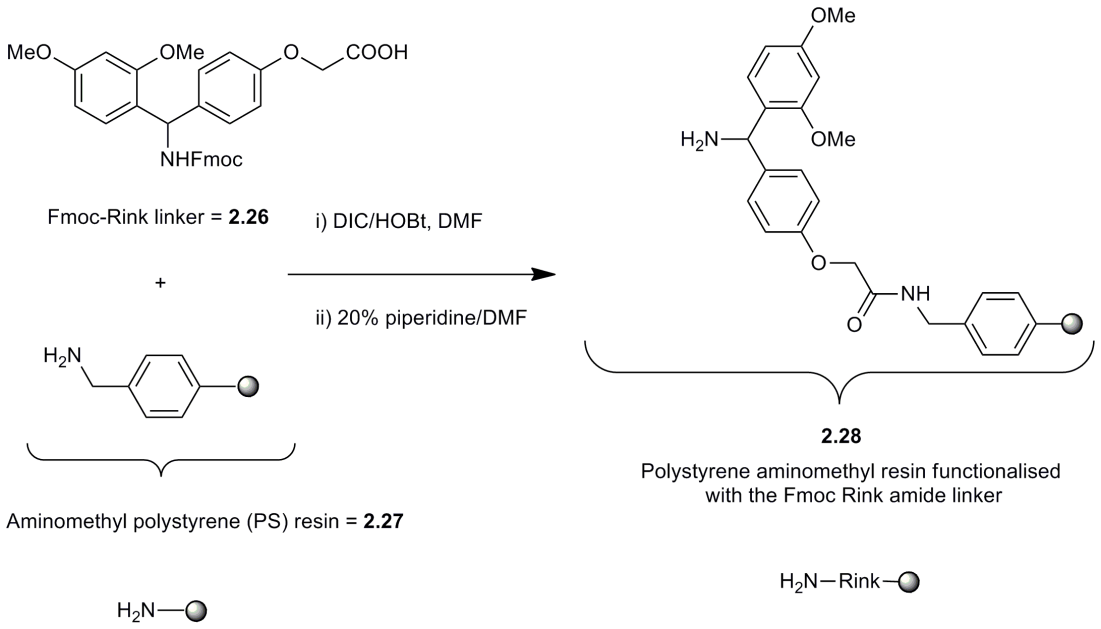

Scheme 2.9: Synthesis of the functionalised polystyrene aminomethyl resin with Rink amide linker (2.28).

This TFA-labile trialkoxybenzhydryl-type linker (**2.28**) was inspired by the 1987 design by Rink[133] for the preparation of peptide amides using an Fmoc-SPPS strategy.[134] In this original paper, peptide amides were prepared by direct "amide" attachment with the 4-(2',4'-dimethoxyphenyl-hydroxymethyl)-phenoxymethyl-polystyrene (the alcohol version of the Fmoc Rink linker).

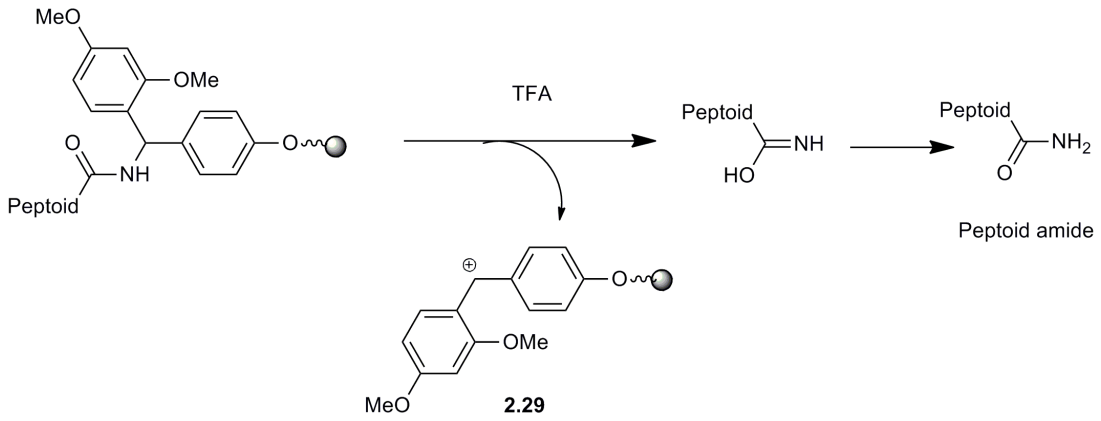

Scheme 2.10: TFA cleavage of the peptoid from the functionalised Rink amide polystyrene resin.

For the solid-phase synthesis of the polylysine-like peptoid (3mer (**2.30**), 5mer (**2.31**) and 7mer (**2.32**)), oligomerisation was carried out over 4 hours using 2 equivalents of **2.22**, 2 equivalents of bromo-tris(pyrrolidino)phosphonium hexafluorophosphate (PyBrOP)[126] and 4 equivalents of *N*,*N*-diisopropylethylamine (DIPEA) in DCM (concentration of monomer **2.22** = 0.08 M) (**Scheme 2.11**). Each building block coupling was alternated with a Fmoc group deprotection (20% piperidine in DMF). This succession of coupling and deprotection was repeated as desired to produce the required peptoid, after which the peptoid was released from the resin by TFA treatment (TFA/TIS, 95: 5)[114] (**Scheme 2.10**).

These coupling steps were difficult and long (4 hours) due to the nature of the building blocks. Indeed, since the reaction is carried out between a free acid and a secondary amine group it often had to be repeated in order to obtain an efficient coupling. Although PyBroP partially solves this problem,[126] this compound has some important drawbacks. First of all, this coupling reagent is very expensive. Secondly, truncated sequences were observed when using this phosphonium reagent under standard coupling conditions.[116]

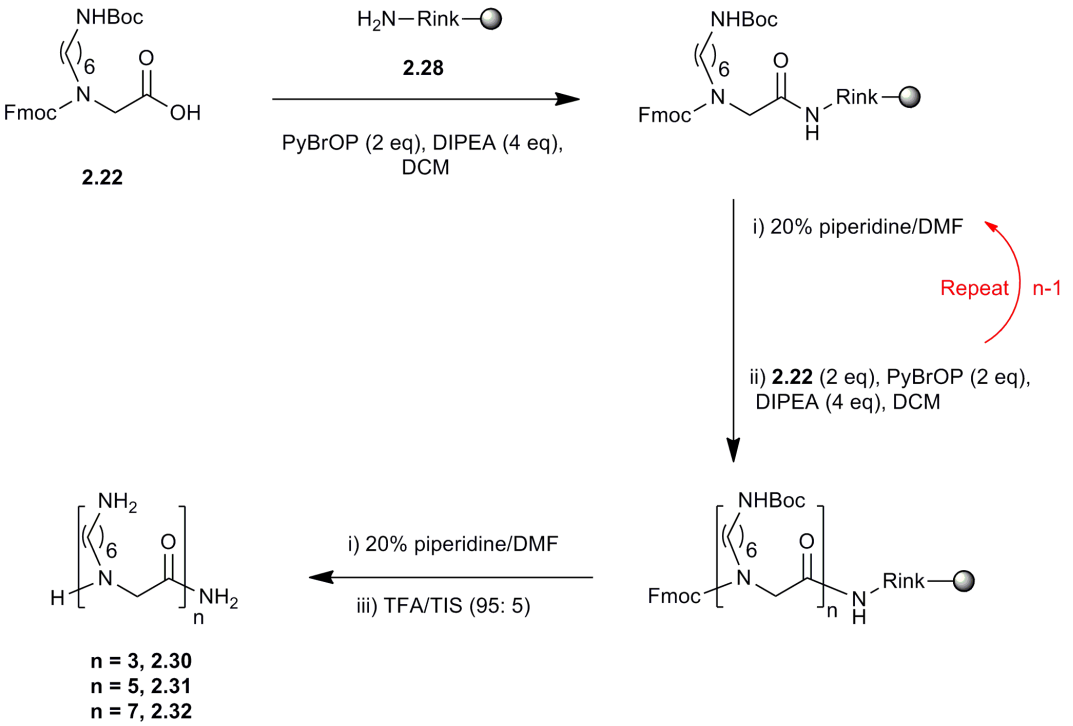

Scheme 2.11: Peretto's solid-phase synthesis of polylysine-like peptoid.
Coupling using PyBOP and DIPEA; n = 3, 3mer (**2.30**); n = 5, 5mer (**2.31**); n = 7, 7mer (**2.32**)

In order to obtain an efficient coupling (time and yield), the use of microwave heating was studied and described by Fara.[116] Microwave synthesis was first reported in 1986,[135] while microwave peptide coupling was described by Wang[136] to allow difficult peptide couplings. Microwave energy (2.45 GHz or 12.2 cm^{-1}) can be transferred to the substances present in a microwave vessel (polar solvent or conducting ions). Microwave heating is based on the ability of chemicals to absorb energy and convert it into heat. Microwaves are made of an electric and a magnetic field component. In chemistry, it is the electric part that plays the most important role. Two main mechanisms are causing the heat production: dipolar polarization and ionic conduction. Molecules with a dipole moment try to align themselves in the applied electric field. However, this field oscillates, so the molecule attempts to realign itself with the field. During this process, energy is lost as heat due to "molecular friction" and dielectric loss. For the ionic conduction, heat is produced due to the oscillation (back and forth) of the charged particles in solution. Under the influence of the microwave field, they move and enter in collision with their neighbours (molecules or atoms) producing heat.

In association with the microwave system, Fara used a standard and robust *N,N'*-diisopropylcarbodiimide and *N*-hydroxy-benzotriazole coupling protocol.[116] Peptoid couplings were carried out in a single-mode microwave reactor (Biotage Initiator instrument) in sealed vials using 3 equivalents of the Boc monomer (**2.22**), 3 equivalents of HOBt and 3 equivalents of DIC in DMF (C = 0.1 to 0.2 M). The reaction time dropped from 4 hours at room temperature to 20 minutes at 60°C under microwave radiation.

2.2.2. Synthesis of Rho-9mer peptoid

In a recent paper, Unciti-Broceta has shown that the cellular penetration of the lysine-like peptoid composed of nine units (Fluo-9mer) is more efficient than the peptoid with only 7 units.[104] In order to increase the knowledge about the capacity of this peptoid as cellular transporter, a Rhodamine-9mer lysine-like peptoid (Rho-9mer, **2.37**) was prepared using HOBt/DIC assisted microwave solid-phase synthesis (**Scheme 2.12**).

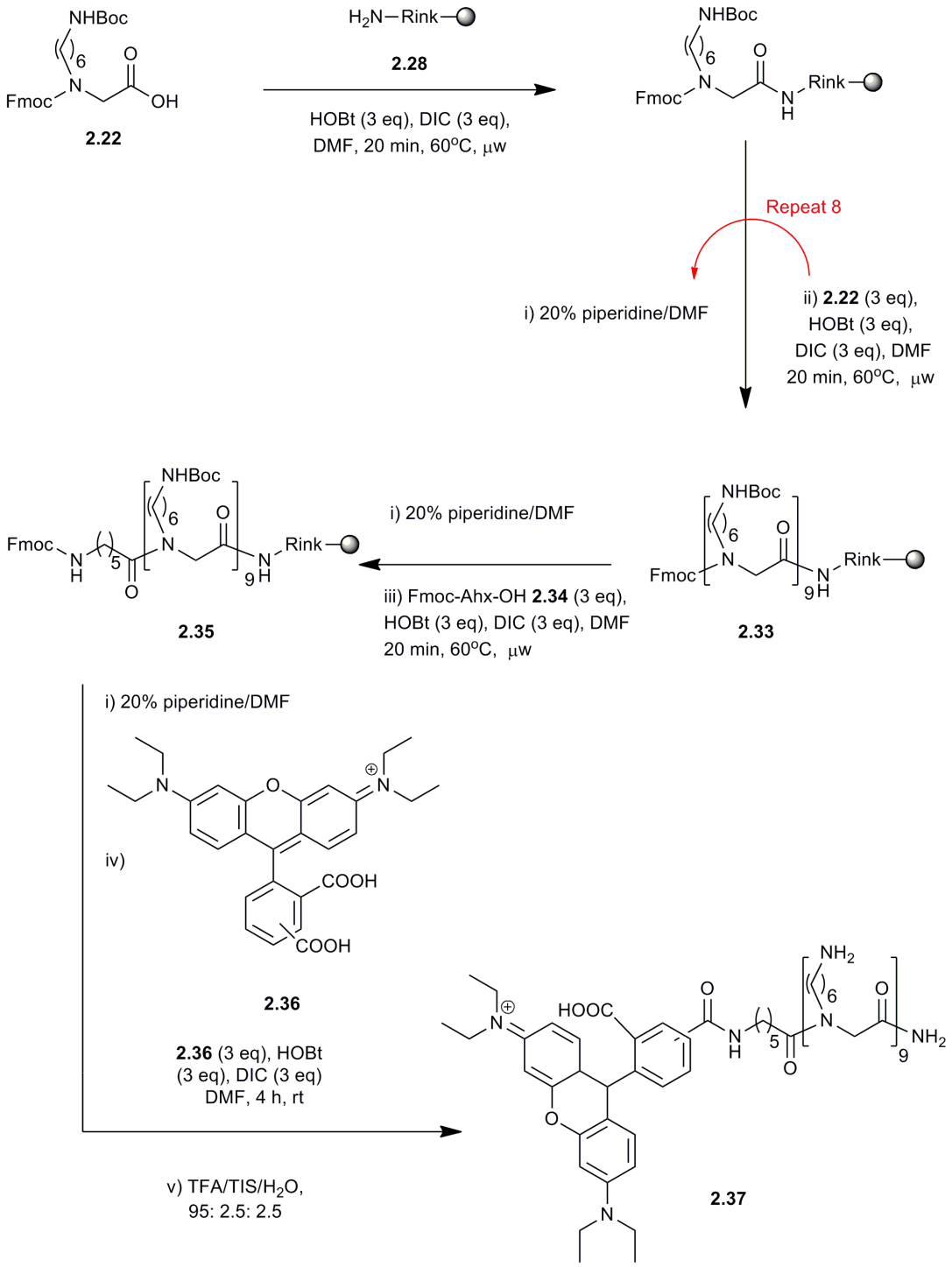

Scheme 2.12: HOBt/DIC microwave assisted solid-phase synthesis of Rho-9mer peptoid (2.37).

The 9mer lysine-like peptoid (**2.33**) was covalently linked to 5(6)-carboxyrhodamine (**2.36**) via an aminohexanoic spacer unit (**2.34**) (**Scheme 2.12**). The hexanoic spacer unit decreases the steric congestion between the peptoid and the dye. Furthermore,

spacer units have been described to enhance the biocompatibility and the interaction between cellular transporters and the cell surface.[137] Bräse have also shown that polyarginine-like peptoid functionnalised with the Ahx spacer had a more efficient cellular penetration.[105]

After TFA cleavage and precipitation in cold Et_2O, **2.37** was obtained in 94% yield (based on the loading of **2.28**) and analysed by MS (MALDI-TOF), HPLC (purity > 98% for both isomers), fluorescence spectroscopy (**Figure 2.2-A**) and NMR. The HPLC spectrum of Rho-9mer peptoid (**2.37**) (**Figure 2.2-B**) showed two peaks, though only one compound appeared on the MS analysis. The carboxyrhodamine (**2.36**) used for this peptoid synthesis has two isomers (5 and 6), therefore, these two peaks were expected to be both Rho-9mer (**2.37**). In order to confirm this, the peaks were separated by preparative HPLC and analysed.

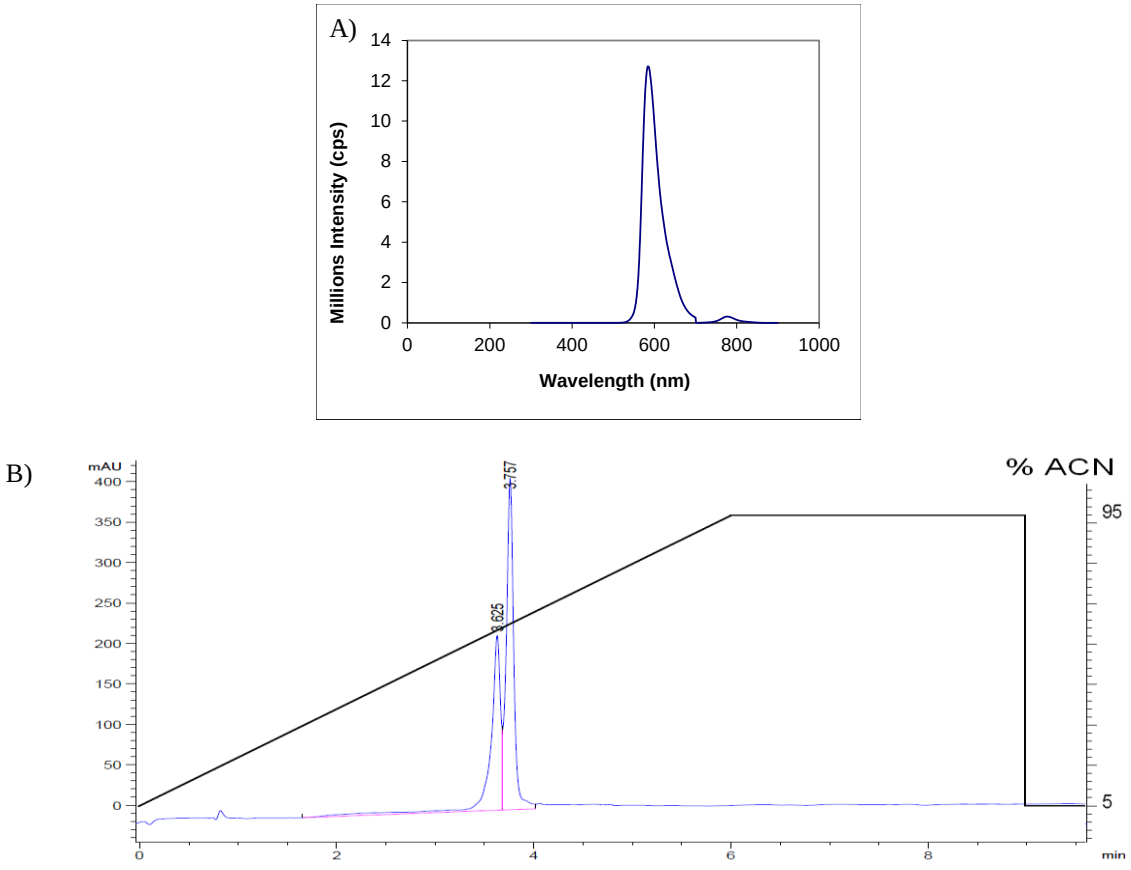

Figure 2.2: Analysis of Rho-9mer peptoid (2.37).
A) Emission spectrum of Rho-9mer peptoid **2.37** in MeOH (abs max = 525 nm; em max = 584 nm);
B) HPLC trace (λ = 540 nm) of Rho-9mer peptoid **2.37**, purity > 98%.

From the proton NMR analysis of 5(6)-carboxyrhodamine **2.36**, one third of the carboxyrhodamine corresponds to the isomer 6 which was also confirmed by the HPLC peak areas (**Appendix 2-1**). Isomer 6 of the Rho-9mer peptoid came first at 3.625 minutes, while the isomer 5 had a retention time of 3.757 minutes.

The successfully labelled peptoid could be now used to study its properties as a cellular delivery device.

2.3. In vitro studies of Rho-9mer

In order to study more deeply the efficiency of the 9mer lysine-like peptoid, the cellular uptake of the Rho-9mer peptoid (**2.37**) was tested in several cell lines and primary immune cells. The various cells were analysed using techniques such as flow cytometry and/or microscopy. The cytotoxicity of the labelled 9mer was also evaluated while mechanistical studies of the uptake were also carried out.

2.3.1. Cellular uptake

2.3.1.1. Flow cytometry analysis

Flow cytometry (**Figure 2.3**) is an analytical technique based on light scattering, excitation and emission of fluorophores. This method can generate various data for cells or particles in the size range of 0.5 to 40 μm diameter. In cellular analysis, it can be applied to an important range of studies such as cell counting and fluorophore analysis. The flow analyser performs these studies by passing thousands of cells per second through a laser beam and capturing the emerging light.

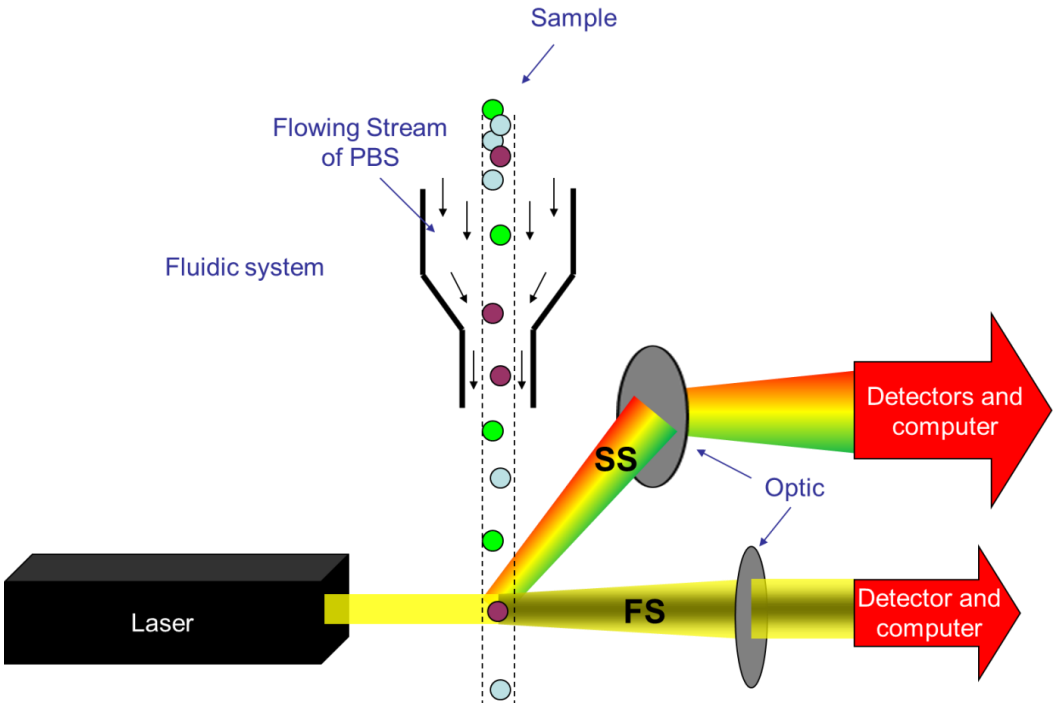

Figure 2.3: Pictorial representation of the flow cytometer.
SS: Side Scatter; FS: Forward Scatter

When a molecule passes through the laser, light is reflected in many directions. Forward scatter (FS) corresponds to the amount of light "going forward". This type of emerging light is proportional to the size of the cell passing through at a precise moment (**Figure 2.4-A**, X axis: small size toward the left). Side scatter (SS) refers to the light going to all angles, except forward. Usually the detector of SS is located at 90 degrees from the original laser path. This light derivation can be caused by granularity on the surface or by the complexity inside the cell (**Figure 2.4-A**, Y axis: low complexity toward the bottom). FS and SS data can be plotted as a histogram in order to give us information about cell size and complexity.[138]

Fluorescence is another parameter that can be analysed by flow cytometry. When the fluorophore on the particle of interest is struck by the laser (at the proper wavelength), a fluorescent signal is emitted. This signal travels on the same path as SS (usually analysed at 90^{o} to the particle) toward its specific detector.

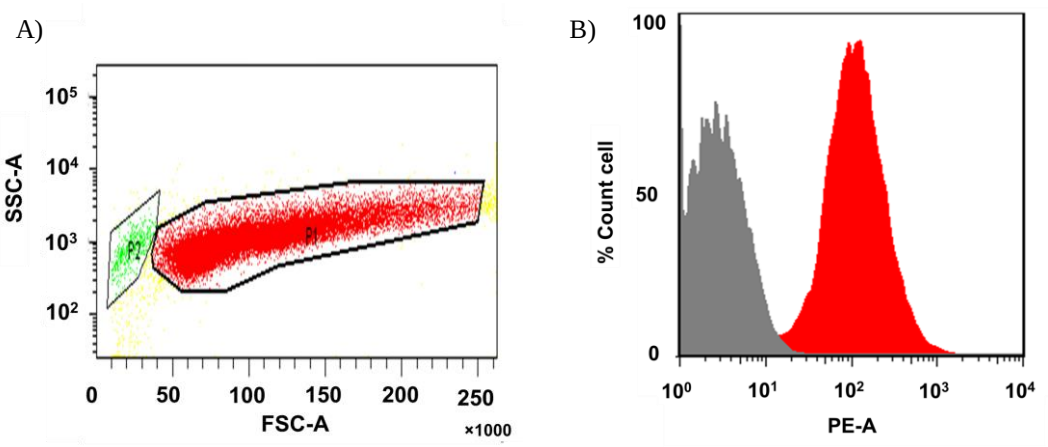

Figure 2.4: Flow cytometry histograms of HeLa cells.
A) Histogram of the FS against the SS of the untreated cells with P1 corresponding to the healthy population of HeLa cells, P2 corresponding to dying cells and the yellow color to other particles including cell debris and cell agglomerates; B) Analysis of number of cells against fluorescence; Grey peak: cell population before peptoid incubation; Red peak: cell population after peptoid incubation (10 µM of Rho-9Mer (**2.37**) for 24 hours). SSC axis: Complexicity level; FSC axis: Analyte size; PE axis: Rhodamine fluorescence intensity.

Fluorescent data can be plotted, like FS and SS data, as a histogram (**Figure 2.4-A**). Typically, the fluorescence is plotted on the X axis while the Y axis refers to the number of events (cells) passing through the laser (**Figure 2.4-B**).

The cellular uptake of Rho-9mer (**2.37**) was evaluated in three different cell lines:

-HeLa: Helacyton Gartleri, human cervical tumour cells,

- B16F10: Murine melanoma cells,

- HEK293T: Human embryonic kidney 293T cells.

The cells were labelled at 37°C using 10 µM of peptoid for incubation times of 5 minutes, 30 minutes, 2 hours, 4 hours and 24 hours. Afterwards, the cells were washed and detached. Prior to analysis by flow cytometry, extracellular fluorescence needs to be quenched. Indeed, it is essential to distinguish intracellular peptoids from those contained on the membrane. To do so, the cells were mixed with a solution of trypan blue (**2.38**, **Figure 2.5**) (0.2% trypan blue in foetal bovine serum (FBS)/phosphate buffered saline (PBS)). Trypan blue is an intercalating dye (excitation ~ 520 nm and emission ~ 650 nm) that is unable to penetrate in healthy cells. Instead, it coats the exterior surface of cell membrane. Any fluorophore emitting at less than 610 nm and localised on the cellular membrane will be quenched in a fluorescence resonance energy transfer (FRET)-like system.[139, 140, 141]

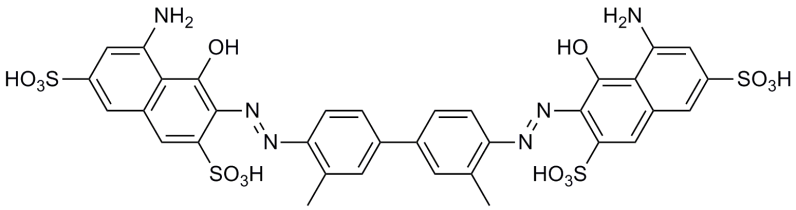

2.38

Figure 2.5: Structure of trypan blue (2.38).

Cellular uptake by various cell lines was measured by flow cytometry and was represented in the following graphs. Labelling time of the whole population of cells was first measured for Rho-9mer peptoid (**2.37**) (**Graph 2.1-A**). Then, the cellular uptake of Rho-9mer (**2.37**) was compared with the one of naked rhodamine dye (**2.36**) (as a negative control) (**Graph 2.1-B**) thanks to the fluorescence intensity of cells.

Uptake was found to be high across all the cell lines analysed with at least 95% of cells labelled after 24 hours of incubation with the Rho-9mer (**2.37**) (**Graph 2.1-A**). Cellular penetration was dependent on the incubation time and the cell lines. HEK293T cells showed an impressive and quick cellular uptake (> 90% in 2 hours), while for B16F10 cancer cells, which can be more difficult to deliver external cargo to, this high level of penetration was obtained after 4 hours. 90% of the HeLa cells, another type of cancer cells, were penetrated by the nonalysine-like peptoid after only 30 minutes of incubation with the compound. These data clearly illustrated that Rho-9mer (**2.37**) was able to label the whole population of cells in less than 24 hours. The relative fluorescence intensity of cells treated with Rho-9mer (**2.37**) was compared to carboxyrhodamine (**2.36**). Unsurprisingly, Rho-9mer (**2.37**) showed a much greater cellular uptake than naked Rhodamine (**2.36**). After 24 hours of incubation, cells treated with the Rho-9mer showed fluorescence intensity at least six times superior to the ones treated by the naked dye (**Graph 2.1-B**). Furthermore, the amount of uncoupled rhodamine inside the cells started to decrease after 4 hours of incubation suggesting diffused out, while the rhodamine labelled peptoid showed increasing cellular penetration.

A) Uptake of Rho-9mer

B) Comparison of cellular uptake between Rho-9mer (Red) and Rhodamine (Orange)

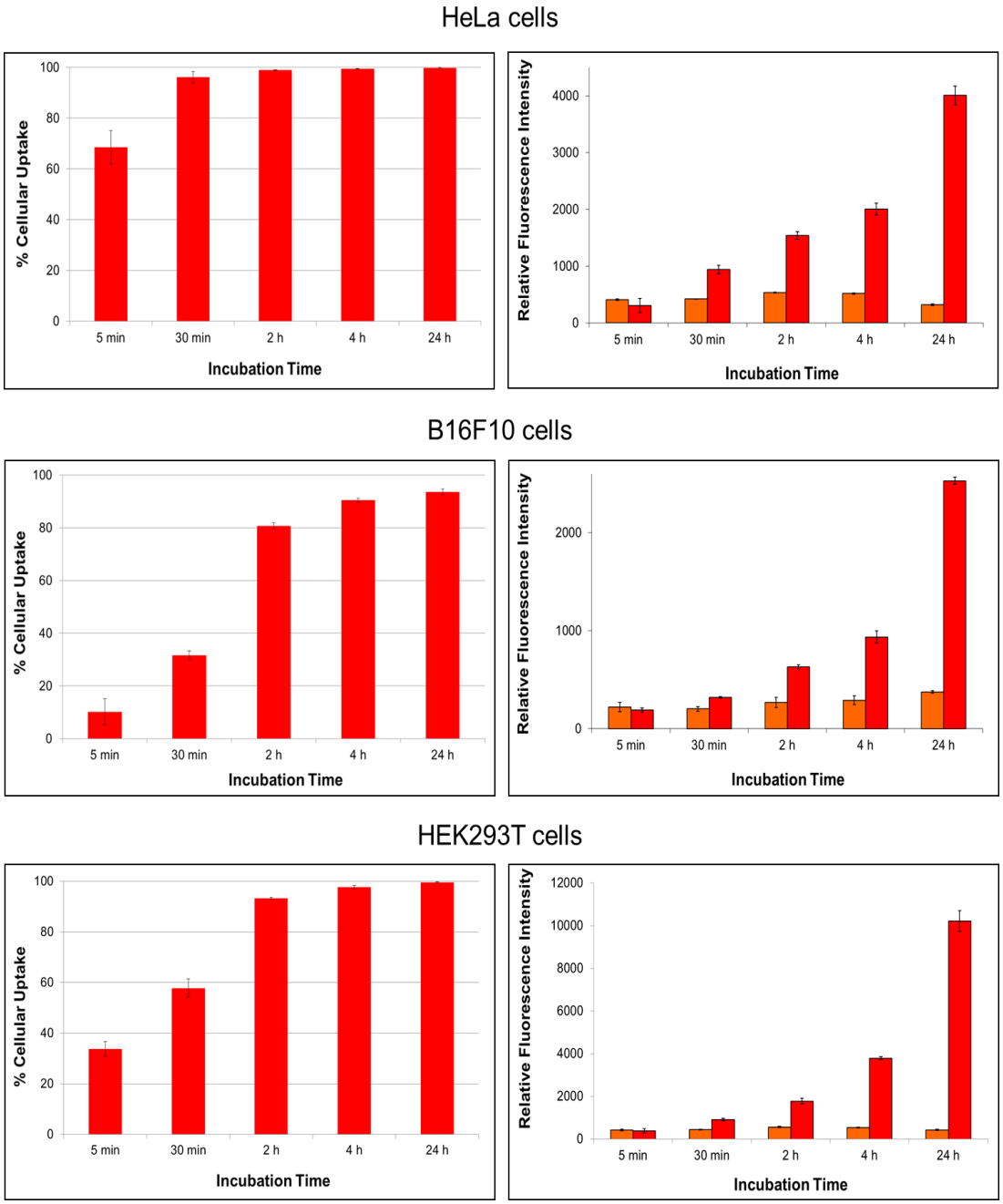

Graph 2.1: Uptake of Rho-9mer (2.37) and free 5(6)-carboxyrhodamine (2.36) (10 µM). A) % uptake measured for Rho-9mer (**2.37**) as the % of cells with a fluorescent emission exceeding untreated control as 0% uptake; B) Relative fluorescence intensity inside the cell for free 5(6)-carboxyrhodamine (**2.36**) and Rho-9mer (**2.37**). The errors bar represents the standard error of the average (n = 3).

By comparing the percentage of cellular uptake and the relative fluorescence intensity, it was shown that even though the whole population of cells were labelled

by the peptoid, the Rho-9mer was still able to penetrate the cells. For instance, all the HeLa cells were labelled by the peptoid after 4 hours (2006 units of fluorescence) but after 24 hours the units of fluorescence were doubled.

The cellular uptake of Rho-9mer peptoid (**2.37**) was also tested in immune cells during a collaboration with Dr. Stefano Caserta (from Professor Rose Zamoyska group). Three different cells were incubated for 1 hour with 1 and 10 μM of **2.37**:

- S2 - Drosophila cells: *Drosophila melanogaster* embryos Schneider 2 (S2) cells.
- Primary LN-derived cells: Primary Lymph Node-Derived cells.
- F5 hybridoma cells: mouse T cell hybridoma, F5.

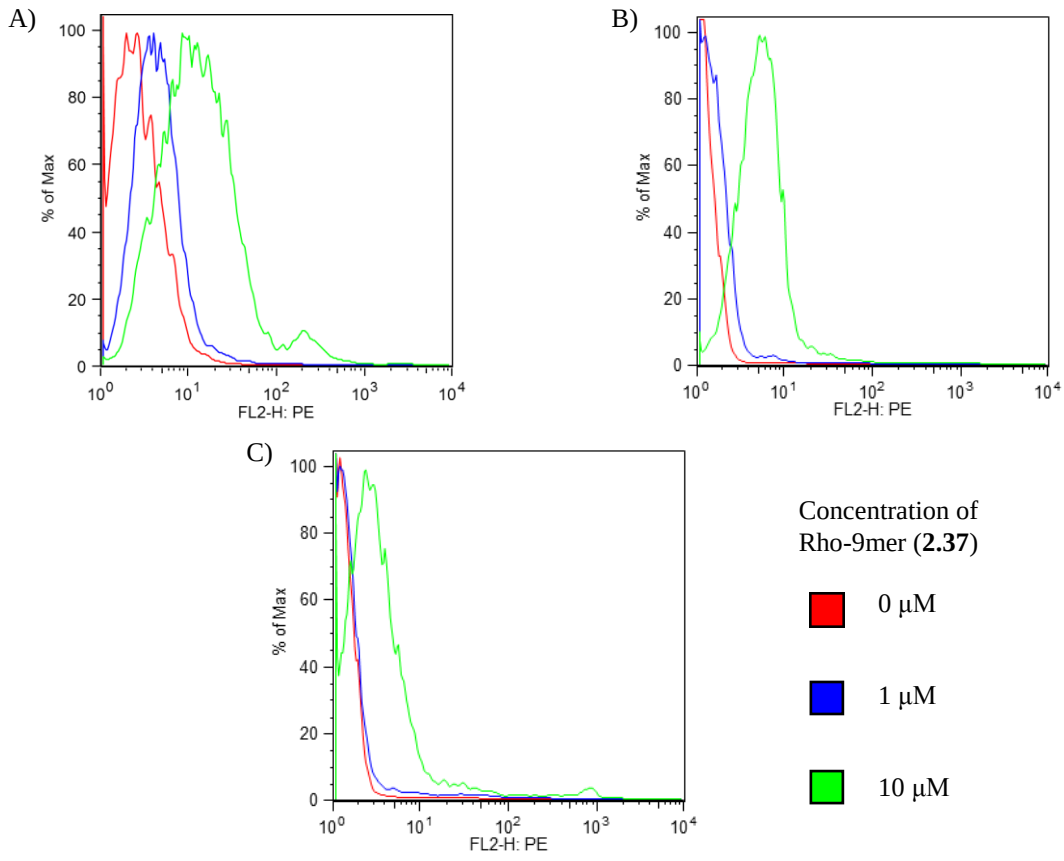

Figure 2.6: Uptake of Rho-9mer (2.37) in immune cells.
A) S2 - Drosophila cells; B) F5 hybridoma cells; C) Primary LN-derived cells. Cells were labelled for 1 hour at 37°C using 1 (blue line) and 10 μM (green line) of Rho-9mer (**2.37**). The percentage of cellular uptake measured as the percentage of cells with a fluorescent emission exceeding untreated cells. Control cell population was taken as 0% of uptake. PE axis: Rhodamine fluorescence intensity. Data courtesy of Dr. Stefano Caserta from the Institute of Immunology & Infection Research (Prof. Rose Zamoyska) at the University of Edinburgh.

The histograms (**Figure 2.6**) clearly showed that the rhodamine peptoid (**2.37**) was able to penetrate within the three primary immune cell types after 1 hour of incubation using 10 µM peptoid with the following cellular uptake:

- 58% for S2 Drosophila,
- 89% for mouse F5 hybridoma,
- 76% for primary LN-derived cells.

2.3.1.2. Microscopy analysis

Flow cytometry results were confirmed using microscopic techniques. Live cells images were taken using a Leica fluorescence microscope after a simple PBS wash to remove of the excess fluorescent probe.

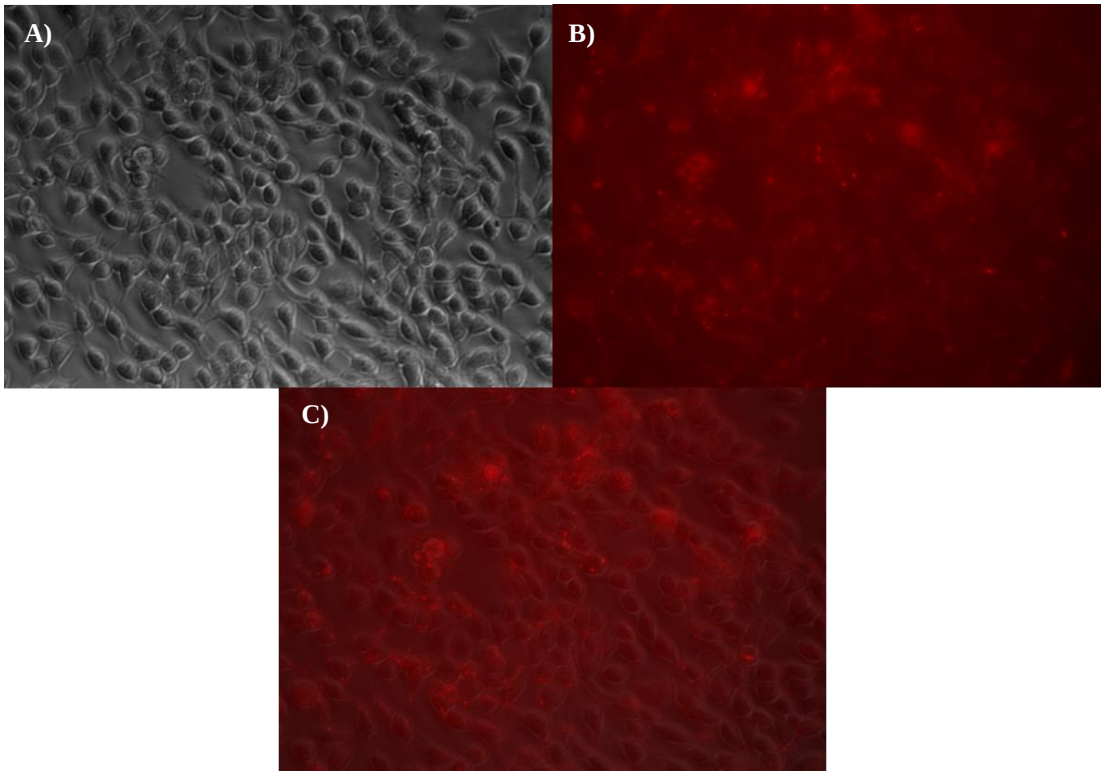

Figure 2.7: Live HeLa cells imaging with a Leica fluorescent microscope.
These images were taken after incubation of the HeLa cells for 4 hours at 37°C with 10 µM of Rho-9mer (**2.37**)**.** A) Brightfield image; B) Rhodamine fluorescent image (excitation 515-560 nm) (peptoid as red spots); C) Fluorescence image merge with brightfield.

Using this technique, the presence of Rho-9mer (**2.37**) inside HeLa cells could be confirmed. The peptoid appears in endosomes all around these cells (**Figure 2.7-B**

and **C**). However, this method is not precise enough to say if the cell penetrating peptoid is inside the cells or in the membrane. A more defined technique, called confocal microscopy, allows more precise pictures of the peptoid location inside cells. In order to do so, cells can be alive or fixed onto glass cover slips.

Confocal microscopy is an optical technique based on the use of pinhole and point-by-point illumination. Using this method, cells are imaged as a succession of slices ('Z-slices') taken along the vertical axis. At any one time, only one "slice" of cell is in focus. After acquisition, the slices can be stacked together and reconstructed to generate a 3-D model. In comparison with the standard fluorescence microscopy, this technique offers much sharper images by excluding most of the light from the specimen that is not within the microscope's focal plane.

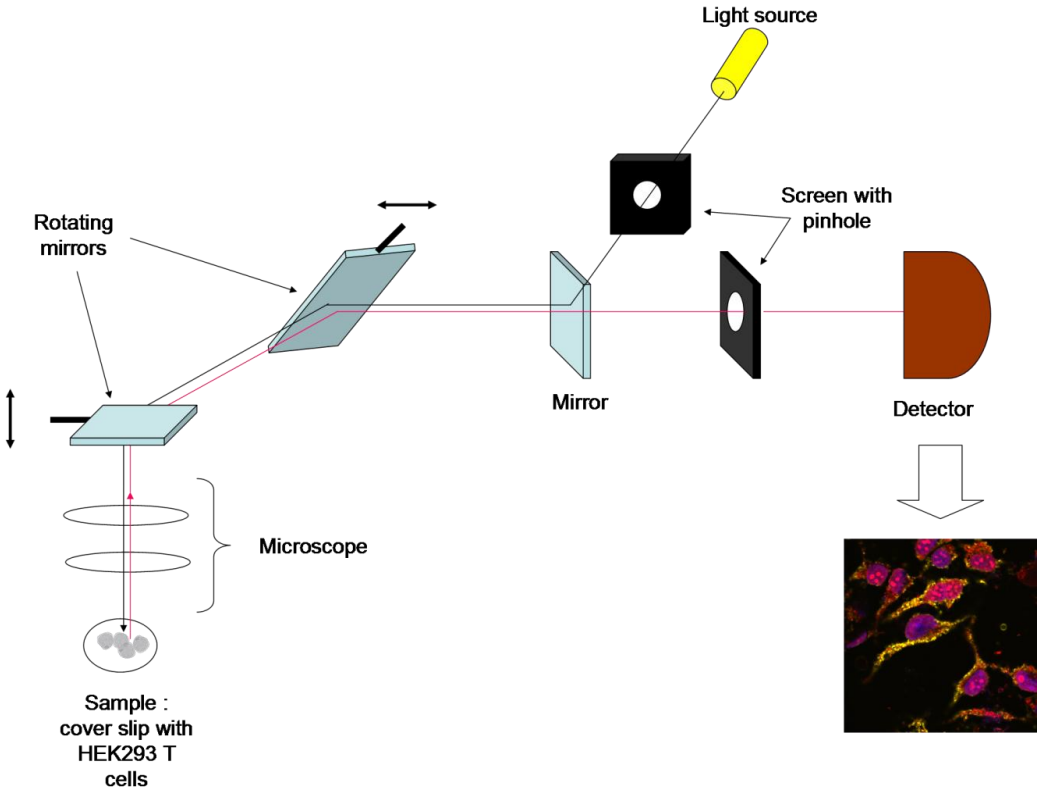

Figure 2.8: Pictorial representation of confocal microscopy

For confocal microscopy study, the cells were cultured on sterilised cover slips. After incubation (24 hours) with the Rho-9mer (**2.37**, concentration of 10 μM), the cells were washed with PBS and fixed using 4% paraformaldehyde. Nuclei were stained with HOECHST-33342 and membranes were labelled with 1,1'-dioctadecyl-

3,3,3',3'-tetramethylindocarbocyanine perchlorate (DilC18). The confocal images (**Figure 2.9**) clearly showed the intracellular presence of Rho-9mer (red dots).

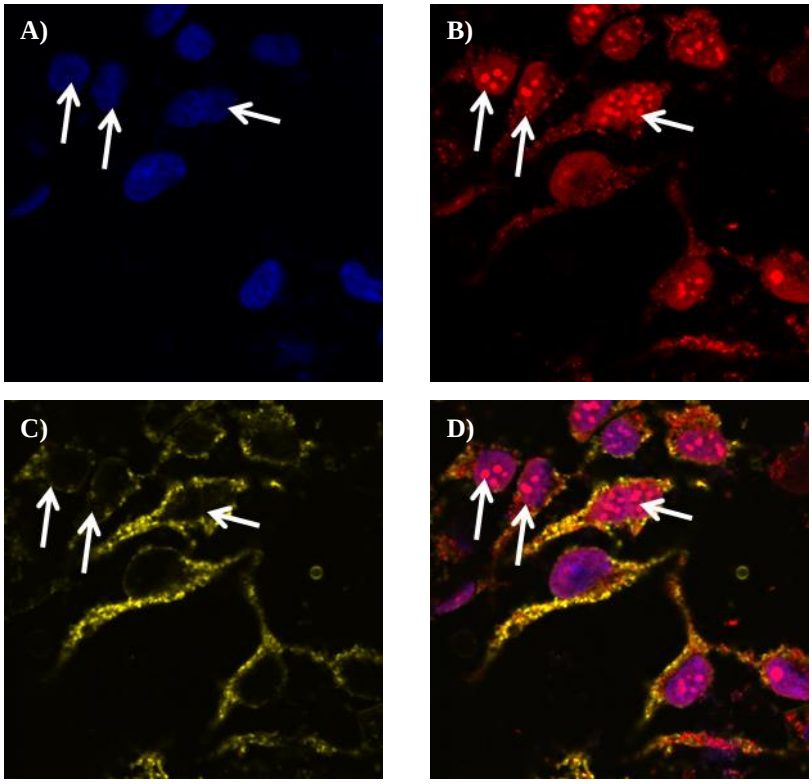

Figure 2.9: Confocal images of HEK 293T labelled with Rho-9Mer (2.37) (10 µM) for 24 hours
A) Nuclei staining using HOECHST-33342 (excitation at 405 nm and emission filter 413-482 nm); B) Cellular labelling with Rho-9mer (excitation laser 561 nm and emission filter 567-630 nm); C) Membrane staining with DilC 18 (excitation at 595 nm and emission filter 670-690 nm); D) Composite image. The arrows show the localisation of the Rho-9mer inside the cells.

2.3.1.3. Mechanistical studies

In order to confirm the possible uptake mechanism, a simple study of the effects of the temperature onto the cellular uptake of the rhodamine penetrating peptoid (**2.37**) was carried out. Low temperatures can have a substantial effect on cellular uptake. Energy dependant mechanisms, such as endocytosis, are generally 'blocked' as the transformation of ATP onto ADT dramatically slows down.[142] As far as the energy free mechanisms are concerned, the decrease of temperature will result in a hardening of the bilipidic membrane and consequently, slow down passive diffusion.[143]

HEK293T and HeLa cells were incubated for 3 hours with Rho-9mer (**2.37**) at several temperatures (4, 20 and 37°C), detached, and analysed.

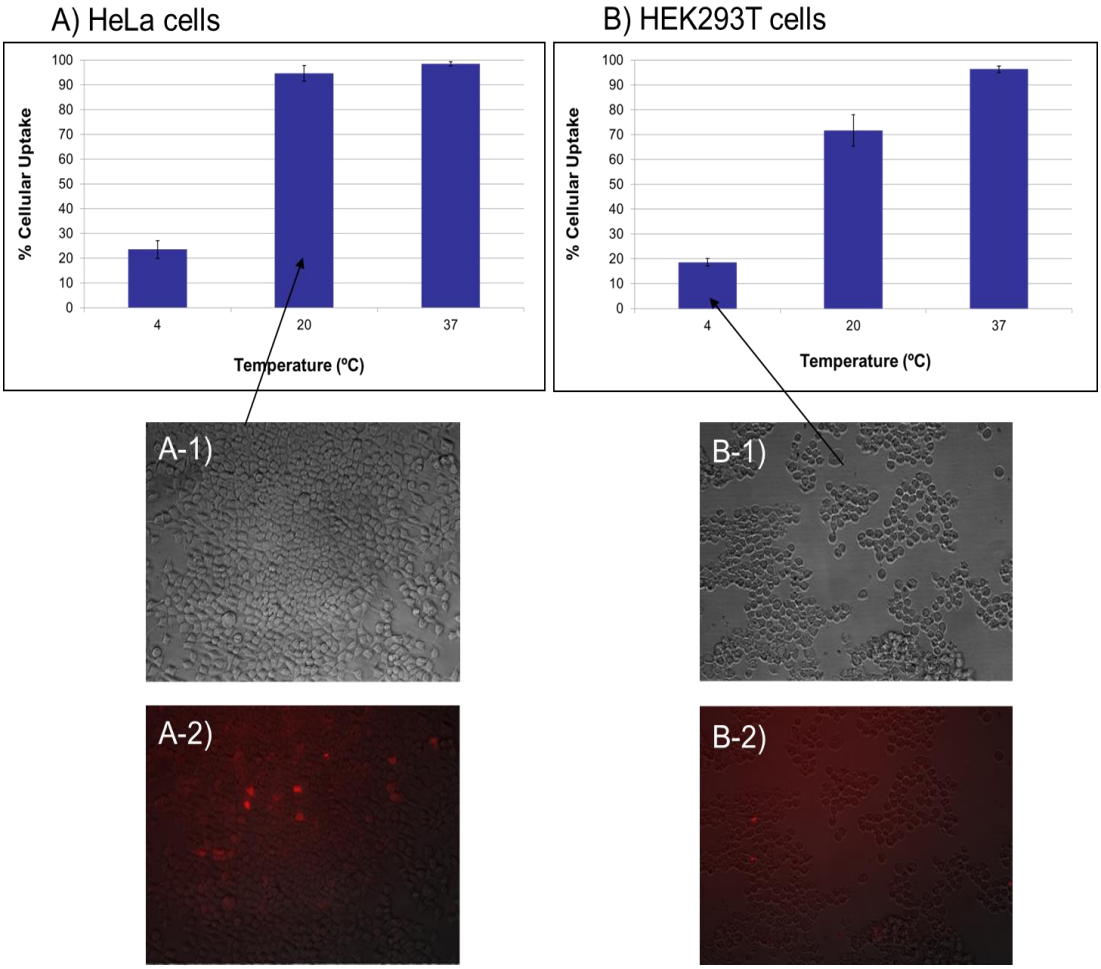

Figure 2.10: Effect of temperature on the cellular uptake of the Rho-9mer peptoid (2.37) (10 µM, 3 hours).
Top graphs: Flow cytometry analysis: A) HeLa uptake; B) HEK293T uptake;
Lower images: A-1) Brightfield image of HeLa cells incubated at 20°C; A-2) Fluorescence image merge with brightfield of HeLa cells incubated at 20°C; B-1) Brightfield image of HEK293T cells incubated at 4°C; B-2) Fluorescence image merge with brightfield of HEK293T cells incubated at 4°C. The errors bar represents the standard error of the average (n = 6).

Flow cytometry results (**Figure 2.10-A** and **B**) showed that peptoid uptake was affected by the decrease of temperature (especially at 4°C). At 20°C, uptake by both cell lines slightly decreased. As expected, at 4°C cellular access of Rho-9mer (**2.37**) to both cell lines was dramatically lowered with a maximum uptake of 24% for HeLa cells. These results were confirmed by fluorescence microscopy (**Figure 2.10**), but

diverged slightly with the results described by Peretto's paper.[114] Indeed, in this work from 2003, no internalisation was observed at 4ºC with none of the three fluorescein labelled peptoids (3mer, 5mer and 7mer), while only a few cells were showing green fluorescence at 20ºC. This difference of results could be explained by the length variation of the peptoid. In a previous paper,[104] a comparison between the Fluo-7mer and the Fluo-9mer peptoids showed that using 9mer doubled the amount of peptoid inside the cells. Furthermore, the uptake kinetic increased when cells were treated with the longer peptoid.

In order to confirm the result that some 9mer peptoid was able to penetrate cells without involving an energy dependant mechanism the cells were treated with sodium azide (NaN_3). Sodium azide is known to be a general inhibitor of adenosine triphosphate (ATP) production as it interferes with cytochrome oxidase in the mitochondria.[144] In previous work,[114] treatment of cells by NaN_3 has shown a total inhibition of polylysine-like peptoid (n = 3, 5 and 7) uptake. Therefore in this experiment HeLa and HEK293T cells were analysed using the same conditions. Both cell lines were treated with 0.5% of sodium azide for 30 minutes before being exposed to Rho-9mer peptoid (**2.37**) (10 µM).[114] After 3 hours of incubation with the Rho-9mer, the cells were analysed by flow cytometry and the results are summarised in **Graph 2.2**.

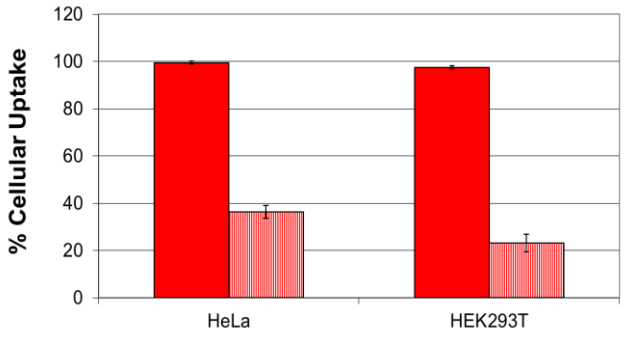

Graph 2.2: Effect of sodium azide on cellular uptake of Rho-9mer (2.37).
Red represents the uptake of Rho-9mer (10 µM) without ATP inhibition. The hatched red represents the uptake of Rho-9mer (10 µM) under ATP inhibition by 0.5% of sodium azide. The errors bar represents the standard error of the average (n = 6).

In opposition to the previous study,[114] 0.5% sodium azide did not completely inhibit the Rho-9mer internalisation. The peptoid uptake decreased to 36% in HeLa cells and to 23% in HEK293T cells. These results showed that there are multiple uptake

routes. The main mechanism for cellular uptake of the 9mer polylysine-like peptoid involves an energy dependent mechanism involving the formation of vesicles. Indeed during both microscopic studies, peptoids appeared like red dots inside cells (**Figure 2.9** and **Figure 2.10**). This confirms the previous observations obtained using Fluo-9mer.[104] Even though the main cellular uptake mechanism seems to be endocytosis, results (low temperature and sodium azide) have demonstrated the ability of the peptoids to penetrate the cells using other pathways that do not require ATP. This energy free penetration could be carried out thanks to the high number of positive charges on the 9mer peptoid. This finding is not surprising: various cationic cell penetrating peptides are known to use both type of mechanisms.[145,75.]

2.3.2. Cytotoxicity analysis

Cellular uptake of the Rho-9mer peptoid has been shown to be high in various cell lines. However, it is essential for the future of this compound as a cellular transporter that it does not exhibit cytotoxicity in cells.

In order to evaluate the toxic potential of the 9mer peptoid (**2.37**), MTT assays were carried out on HEK293T, HeLa and B16F10 cells. This test measured the cellular enzymatic activity. Cells were incubated using several concentrations of Rho-9mer (0, 1, 5, 10 and 20 μM). At the end of the incubation time, a solution of MTT (**2.39**) was added to the washed cells. MTT (3-(4,5-dimethylthiazol-2-yl)-2,5-diphenyltetrazolium bromide) is a tetrazole dye which is able to freely diffuse in healthy cells. Once inside, the soluble dye is reduced by mitochondria enzymes to form purple insoluble formazan crystals.[146] After 3 hours, the insoluble dye was dissolved and the absorbance measured at 570 nm.

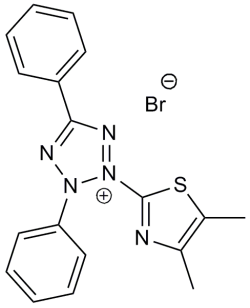

2.39

Figure 2.11: Structure of MTT (2.39).

Graph 2.3 summarises the effect of various concentrations of Rho-9mer peptoid **2.37** (1, 5, 10 and 20 µM) on the health of HEK293T, HeLa and B16F10 cells. After 24 hours of incubation, no cytotoxicity was revealed using any of the tested concentrations.

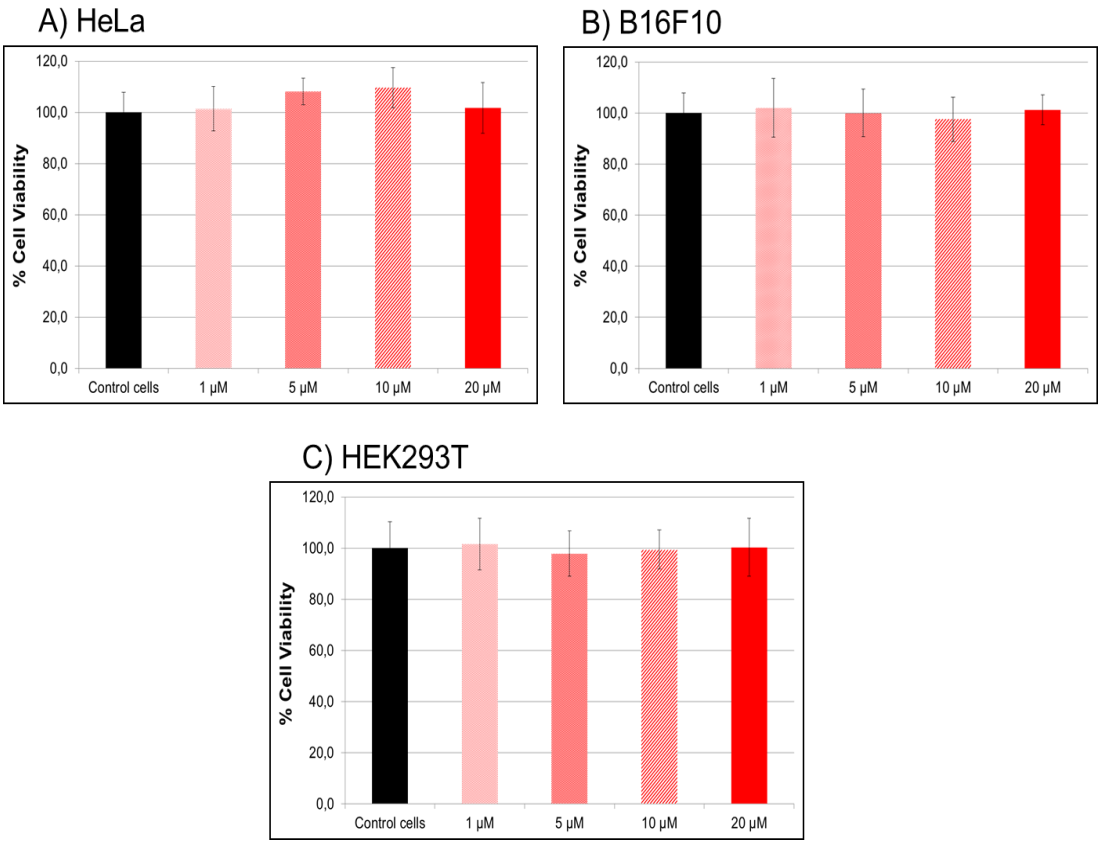

Graph 2.3: MTT assays to evaluate the cytotoxicity of Rho-9mer, 2.37.
A) HEK293T; B) HeLa and C) B16F10 cells treated with 1, 5, 10 and 20 µM of Rho-9mer for 24 hours prior to MTT analysis. The errors bar represents the standard error of the average (n = 10).

Cytooxicity of the Rho-9mer (**2.37**) was also tested on immune cells (S2 Drosophila, mouse F5 hybridoma and primary LN-derived cells). After the exposure to the delivery system, cell viability was evaluated by staining with TO-PRO-3 (**2.40, Figure 2.12**).[147]

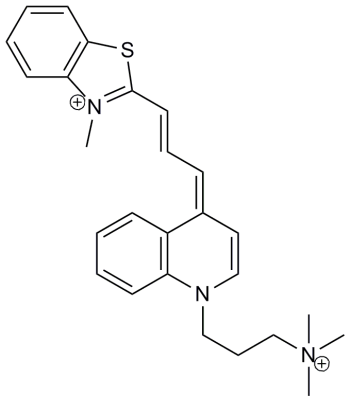

2.40

Figure 2.12: Structure of TO-PRO-3 (2.40).[147]

This cyanic dye (absorbance at 642 nm and emission at 661 nm) is a high affinity DNA binder but is unable to cross the membrane of healthy cells. In opposition to MTT assays, TO-PRO-3 analysis measures the amount of dead cells. Once a cell begins to die, its membranes are compromised (cytoplasmic and nuclear) allowing TO-PRO-3 to enter to bind to the nuclear DNA.[148]

The cells were first treated with the Rho-9mer (**2.37**) (1 and 10 μM) for 1 hour. Prior to flow cytometry analysis, TO-PRO-3 was added to each flow tube (final concentration 0.25 μM). Both rhodamine and TO-PRO-3 fluorescences were measured (**Figure 2.13**).

In **Figure 2.13-A**, the histogram showed two populations of labelled primary LN-derived cells. In order to know if one of the populations corresponded to dead cells, a second type of histogram was plotted. In this new graph, the X axis corresponded to the TO-PRO-3 fluorescence while the Y axis represented the rhodamine fluorescence.

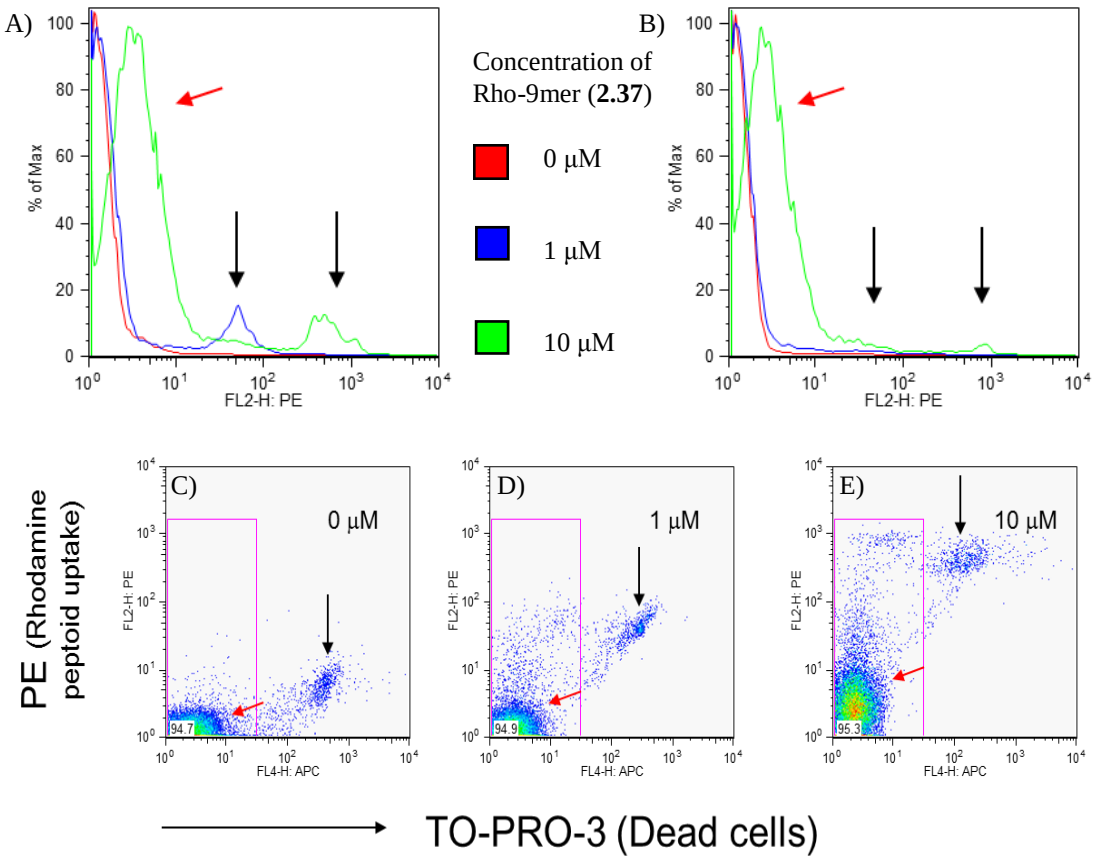

Figure 2.13: TO-PRO-3 analysis of primary LN-derived cell viability.
Cells were treated with 0, 1 and 10 µM of Rho-9mer (**2.37**) for 1 hour prior TO-PRO-3 analysis. A) Histogram plotting the rhodamine fluorescence (X axis) against the number of event (Y axis) before gating; B) Histogram plotting the rhodamine fluorescence (X axis) against the number of event after gating; C) Gating of the histogram plotting the TO-PRO-3 fluorescence (X axis) against rhodamine fluorescence (Y axis) for untreated cell; D) Gating of the histogram plotting the TO-PRO-3 fluorescence (X axis) against rhodamine fluorescence (Y axis) for cells treated with 1 µM of Rho-9mer (**2.37**) ; E) Gating of the histogram plotting the TO-PRO-3 fluorescence (X axis) against rhodamine fluorescence (Y axis) for cells treated with 10 µM of Rho-9mer (**2.37**). The red arrows show the healthy cells, while the black ones point the dead cells. PE axis: Rhodamine fluorescence intensity; APC axis: TO-PRO-3 fluorescence intensity. Data courtesy of Dr. Stefano Caserta from the Institute of Immunology & Infection Research (Prof. Rose Zamoyska) at the University of Edinburgh.

The healthy cells (low TO-PRO-3 fluorescence) were gated in the histograms (**Figure 2.13-C, D** and **E**). By doing this selection, the high rhodamine fluorescence population (pointed by the black arrows in **Figure 2.13-B**) was supressed, as only healthy cells appeared. Gating allowed a comparison of the percentage of dead cells between untreated and treated samples. Rho-9mer (**2.37**) did not affect the cell viability (94.7% of healthy for the negative control and 95.3% for the 10 µM positive control). Similar analyses were carried out for the S2 Drosophila and mouse F5

hybridoma cells (**Appendix 2-2**). The results of these studies were summarised in the following table (**Table 2.2**).

	Untreated Cells	Treated with 1 μM of Rho-9mer (**2.37**)	Treated with 10 μM of Rho-9mer (**2.37**)
S2 Drosophila cells	97.4	97.6	98.7
Mouse F5 hybridoma cells	81.7	87.3	84.2

Table 2.2: Percentage of healthy cells calculated by TO-PRO-3 cytotoxicity assay.

As shown in the above table, a one hour treatment of S2 Drosophila and mouse F5 hybridoma cells by 10 μM of Rho-9mer (**2.37**) did not induce any cytotoxicity.

2.4. Conclusions

Rhodamine-9mer peptoid was prepared via the monomer synthesis route and SPPS and characterised. As expected, the Rho-9mer peptoid (**2.37**) showed very good cellular uptake in various adherent cell lines, both human and murine. In HeLa and HEK293T cells, the whole populations of cells were labelled in less than 2 hours at 37^{o}C. This is two times faster than the 7mer polylysine-like peptoid that labelled 99% of HEK293T cells after 4 hours. Using MTT assays, the non-cytotoxic nature of this cellular carrier was confirmed over 24 hours and at a concentration up to 20 μM. Rho-9mer was also delivered, without any cytotoxicity (TO-PRO-3 analysis), to primary immune cells (S2 Drosophila, mouse F5 hybridoma and primary LN-derived cells). Over an hour, the peptoid (10 μM) enabled cellular labelling of at least 50%. During the mechanistic studies, the peptoid **2.37** showed some uptake at low temperature and when using an inhibitor of ATP synthesis. Even if these results do not allow any definitive conclusion about the cellular uptake mechanism of this

cellular penetrating peptoid, they do suggest the possibility that this peptoid enters cells via several mechanisms.

In the future, cellular delivery of the Rho-9mer peptoid could be compared to known CPPs such as TAT, polylysine and polyarginine. In addition, the penetrating pathway could be more deeply studied using, for instance, endosomal tracker (e.g. LysoTracker Red) to prove the presence of the peptoid within this type of vesicle.[149] The endocytosis pathway could also be evaluated more deeply using specific inhibitors allowing specific endocytosis inhibition. For instance, the cholesterol synthesis could be inhibited using mβ-cyclodextrin[150] as well as the caveolae-mediated endocytosis using filipin III and genistein.[151]

CHAPTER 3 : *IN VIVO* APPLICATIONS OF PEPTOIDS LABELLED WITH NEAR-INFRARED DYES

3.1. Imaging and near-infrared dyes

3.1.1. Imaging techniques

Over the past decades, numerous imaging techniques have been developed including in the molecular imaging area. Molecular imaging (MI) is a new biomedical discipline used in drug development and in diagnosis. This field combines several imaging techniques allowing the characterisation, quantification and determination of molecular events and pathways, ideally carried out in real-time (without interfering with the natural processes).[152]

Imaging techniques can be divided in two categories:

1. Morphological and anatomical imaging technologies: computerised tomography (CT), magnetic resonance imaging (MRI) [153] and ultrasound (US).
2. Molecular imaging technologies (including cellular changes): optical molecular imaging (OMI), positron emission tomography (PET)[154] and single photon emission computerised tomography (SPECT).

These techniques can be used on their own or by combining two or more of these imaging processes (e.g. PET-CT[154] or PET-MRI) to allow high structural resolution images to be obtained. Optical molecular imaging is widely used in cell biology as it offers an important number of advantages compared to other imaging methods such as MRI and PET. Indeed, OMI offers a moderate cost, sensitive, non-invasive and safe technique.[155]

Even though all the OMI techniques do not require the use of fluorescence probes, fluorescent labelling of biomolecules facilitates the visualisation of their location, interaction and migration and therefore the understanding of their activities.[156] Prior to performing *in vivo* fluorescent imaging studies, the choice of an appropriate labelling agent is essential. This molecule must not interfere with the innate biological functions of the studied cells, tissues or organs and offer suitable sensitivity for *in vivo* detection. Fluorescent optical imaging compounds are usually

composed of two units: a dye that allows visualisation and a targeting device that enables the covalent or non-covalent interaction with the biological entity of interest.

3.1.2. Cyanine dyes

Fluorescent molecules are an indispensable part of any fluorescent imaging agent, enabling real time analysis as tracking agents or as measures of enzyme activity (e.g. via a FRET system, **Figure 3.1**).

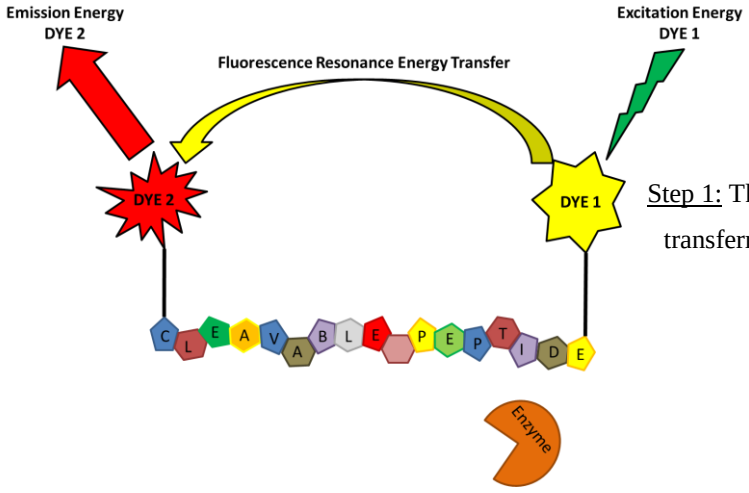

Step 1: The emission energy from dye 1 is transferred to dye 2 as excitation energy, therefore the dye 2 emits.

Step 2 : The enzyme recognises and cleaves the peptide on its cleavable site.

Step 3: Dye 1 is excited and emits. Now the dyes are too far apart so the emission energy of dye 1 is not transferred to dye 2.

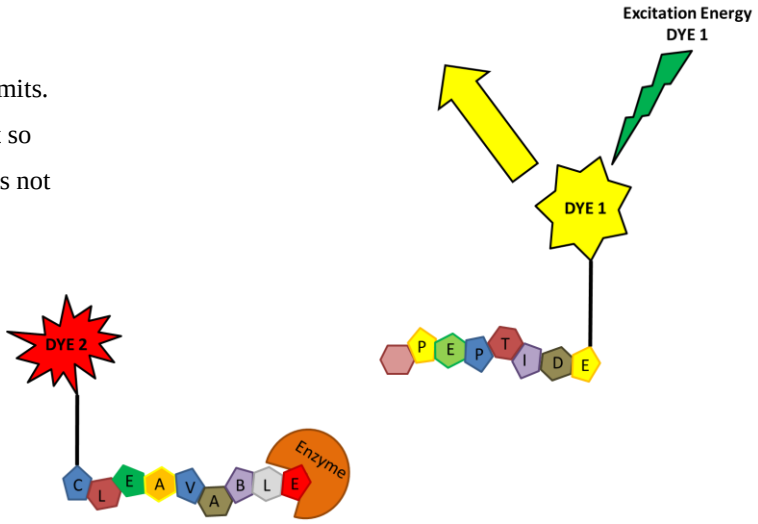

Figure 3.1: Principle of fluorescence resonance energy transfer (FRET).

Many dyes are available either commercially (**Figure 3.2**) or through laboratory synthesis. The main concern is the choice of the suitable one for any specific project.[157] Before selecting a fluorophore is essential to check the auto-fluorescence of the organ or cells related to the project. This fluorescence is due to endogenous components capable of emitting light at different wavelengths (**Table 3.1**).[158]

Organs and components	Emission wavelength
Lung	630-520 nm ratio
Cervix	450 nm
Esophagus	480 and 640 nm
Tryptophan	348 nm
Collagen	405 nm
NADH (Nicotinamide adenine dinucleotide) **3.1**	440-462 nm
Carotene (skin)	482 nm
Blood	Plasma 330-340 nm Oxy-hemoglobin 541 and 577 nm Porphyrin 590 and 630 nm

Table 3.1: Wavelenghts of some organs and cellular components.[158, 159]

In the case of an *in vivo* study, studies have shown that the autofluorescence of organs and tissues is at its maximum emission using blue filter (excitation blue filter 460-500, emission green filter 505-560 nm), with minimum emission detected using NIR filter set (725-775 nm/790-830 nm). Therefore dyes having a maximum wavelength inferior to 650 nm should not be used for tissue imaging.[160]

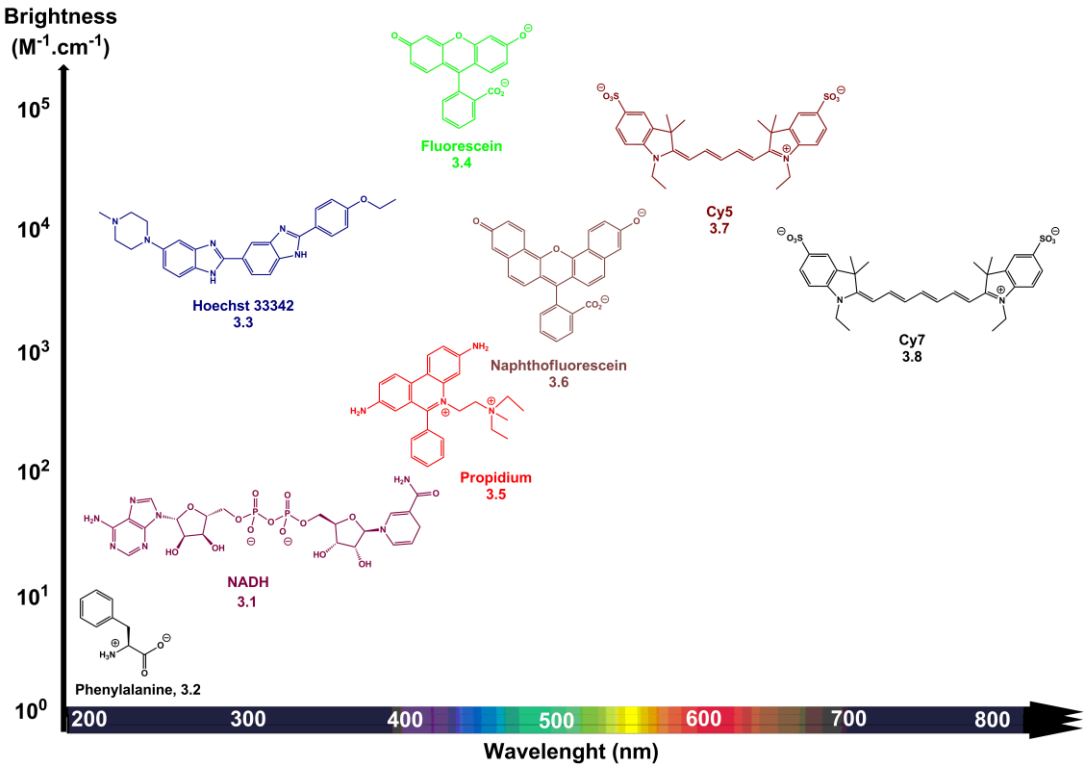

Figure 3.2: List of commercially available fluorophores with their λmax and brightness.[157] Brightness = ε × ϕ, where ε is the coefficient of extinction of a molecule at a given wavelength and ϕ is the quantum yield of the fluorophore. [Permission, **Appendix 1**]

The repertoire of fluorophores operating in the NIR window (between 650 nm and 1000nm) is increasing with new dyes such as naphthofluorescein **3.6** (λ_{abs} = 595 nm, λ_{em} = 660 nm, under basic conditions)[157] and seminaphthofluorones (λ_{em} maxima from 713 to 757 nm in aqueous solution)[161] having been synthesised. Polymethine cyanine (Cy) dyes, like Cy5 (**3.7**) and Cy7 (**3.8**), remain the most common NIR fluorophores due to their tunable wavelengths (λ_{em} from 506 for Cy2 up to 788 nm for Cy7 (**3.8**)), high coefficient of extinction and good quantum yields (e.g. 0.18 for Cy5, **3.7**). The generic structure of these dyes corresponds to two nitrogens (one positively charged) linked together by a conjugated chain of an odd number of carbon. In biology and chemistry, the Cy abbreviation (e.g. 2, 5.5 and 7) refers to the core of the dye only. The number following the Cy refers to the number of insaturated carbon between the two heteroaromatic cycles (indol). The notation ".5" can be added after the carbon referencing number. In that case, the indol group is replaced by benzoindol heteroaromatic cycle. The functionnalised group allowing its

coupling to a delivery system (carboxylic group) or increasing its solubility (sulfonated group) is usually omitted.

One of the most attractive subgroups is the indocyanine type (**Figure 3.3**) that, in contrast with other cyanine dyes, avoids self-aggregation when sulfonated.[160] In addition, since the discovery of cyanine dyes in 1856, the synthesis of this subclass NIR dyes has been widely studied and improved.[162] Today, indocyanine dyes can be synthesized in bulk and are easily modified to allow conjugation to molecules of interest.[163]

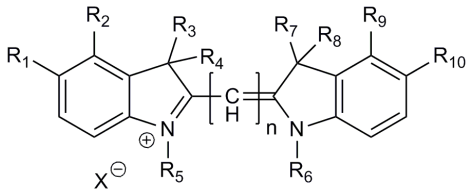

Figure 3.3: General structure of indocarbocyanine dye.[162]
n = 1, 3, 5, 7; R_1, R_2, R_9, R_{10} = H, -$(CH=CH)_2$-, SO_3^-; R_3, R_4, R_7, R_8 = H, CH_3, -$(CH_2)_n$-COOH; R_5 and R_6 = H, CH_3, -$(CH_2)_n$-COOH, -$(CH_2)_n$- SO_3^-, -$(CH_2)_n$-CH_3.

3.1.3. Cell mediated delivery of cyanine dyes

Once the fluorophore is chosen, labelling of the cells or organs of interest can be carried out. Physical cellular penetration can be carried out using the methods described in ***CHAPTER 1***. These techniques (e.g. electroporation) generate disturbance in the cell membrane allowing the penetration of the dye present in the surrounding environment. Chemical modification of the dye (often by sulfonation) aims to make the fluorophore more hydrophilic and less susceptible to aggregation in water.[164] Cellular uptake and cellular retention is mainly due to the relative hydrophobicity/hydrophilicity properties of these sulfonated species.[165] Sulfonated cyanines have been used to label tumour cells, tissues and to image cancer.[166]

The most famous of these dyes is the indocyanine green (**3.9**, **Figure 3.4**, λ_{abs} = 805 nm and λ_{em} = 835 nm in water). Since 1959, the FDA (U.S. food and drug administration) approved its intravenous application for diagnostic purposes. This dye is mainly used in determination of cardiac output, liver function diagnostics (liver clearance test) and retinal angiography. [167]

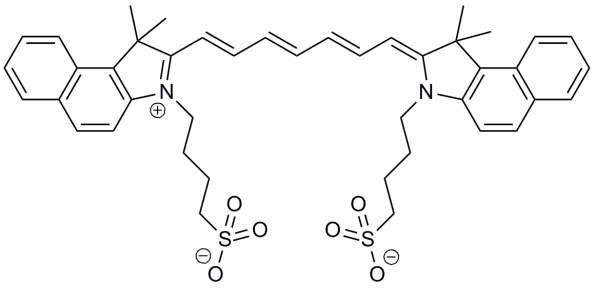

3.9

Figure 3.4: Structure of the indocyanine green (3.9)

Finally, delivery systems including microspheres,[168] cell-penetrating peptides[169] and copolymers[170] can be coupled to cyanine dyes and used as imaging agents. As far as peptoids are concerned, no studies have described peptoids coupled to an NIR dye and then applied in molecular imaging. The imaging applications reported with peptoids (as labelling agents) were the MRI and PET analysis of the tumours.

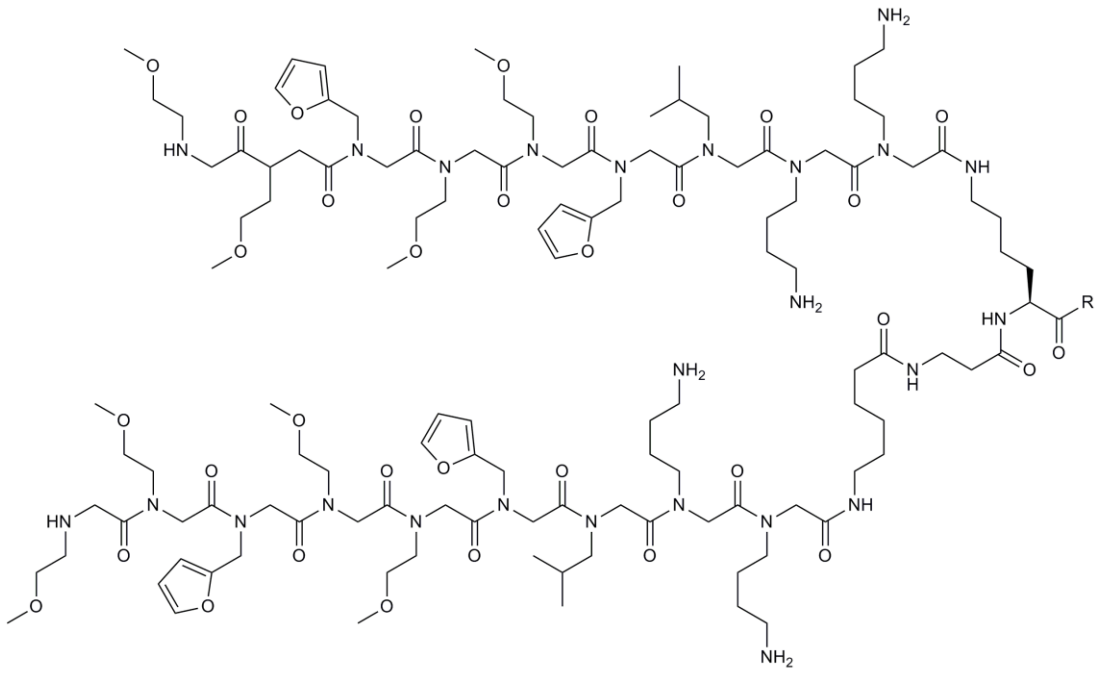

R = OH, **3.10**

R = Cys-LINKER-PAMAM-G4-DOTAGd^{3+}, **3.11**

R = Cys-LINKER-DOTA ^{64}Cu, **3.12**

Figure 3.5: Structure of the dimer peptoid coupled to imaging probe (peptoid dimer (3.10), peptoid-Gd^{3+} for MRI (3.11) [171] and peptoid-^{64}Cu for PET imaging (3.12) [172]).

In 2010, a peptoid dimer known (**3.10**, **Figure 3.5**) to have a high affinity for the vascular endothelial growth factor receptor 2 (VEGFR2) was conjugated to eight molecules of gadolinium (Gd^{3+}). The peptoid **3.11** was used to target and analysed via MRI tumours in mice.[171] The same peptoid dimer (**3.10**, **Figure 3.5**) was also applied to analyse the vascular activity of a tumour in a prostate cancer mouse model using PET imaging. For this study, the peptoid **3.10** was conjugated with ^{64}Cu (**3.12**, **Figure 3.5**) allowing the monitoring of tumour activity.[172]

In this project, carried out in collaboration with Dr. Kevin Dhaliwal, the first aim was to synthesise a peptoid coupled to a NIR cyanine dye. 9mer lysine-like peptoids were covalently linked to carboxy-Cy5.5 and carboxy-Cy7 dyes. The second aim was to test the cellular uptake of these peptoids into various cell lines and evaluate their cytotoxicity. The final aim was to apply this cellular labelling to *in vivo* models of inflammation leading to a greater understanding of the migration and trafficking of primary cells. Macrophages, neutrophils and monocytes were labelled *ex vivo* before being injected into mouse models of inflammation. Cell migration was tracked using OMI, tomographic imaging or MI coupled to X-ray.[173, 174]

3.2. Synthesis of peptoids labelled with NIR dyes

3.2.1. Catch-and-release synthesis of carboxy-Cy7 and carboxy-Cy5.5

The modified Cy7 (**3.20**) and Cy5.5 dyes (**3.26**) were synthesised using a microwave assisted catch-and-release strategy (**Scheme 3.3**) developed in 2008 by Lopalco.[163] This strategy allowed the synthesis of any cyanine dye with low time consuming purifications and high final yield. The first step to access carboxy-Cy7 (**3.20**) and carboxy-Cy5.5 (**3.26**) was the preparation of 4-aminophenol resin (**3.16**) (**Scheme 3.1**). *N*-^{t}butyloxycarbonyl-4-hydroxyaniline PS resin (**3.15**) was synthesised by nucleophilic substitution of chloromethyl resin (**3.13**) (Merrifield resin, 1% DVB cross-linking) by *N*-^{t}butyloxycarbonyl-4-hydroxyaniline (**3.14**), monitored using the chloromethyl group colorimetric test.[175] The formation of the desired resin was confirmed by IR analysis (peak at 1687 cm^{-1}, C=O stretch of the Boc group). The Boc protecting group was removed by treatment of the resin **3.15** with a solution of

20% TFA in DCM. The formation of **3.16** was monitored by ninhydrin colorimetric test[129] and loss of the peak at 1687 cm^{-1}.

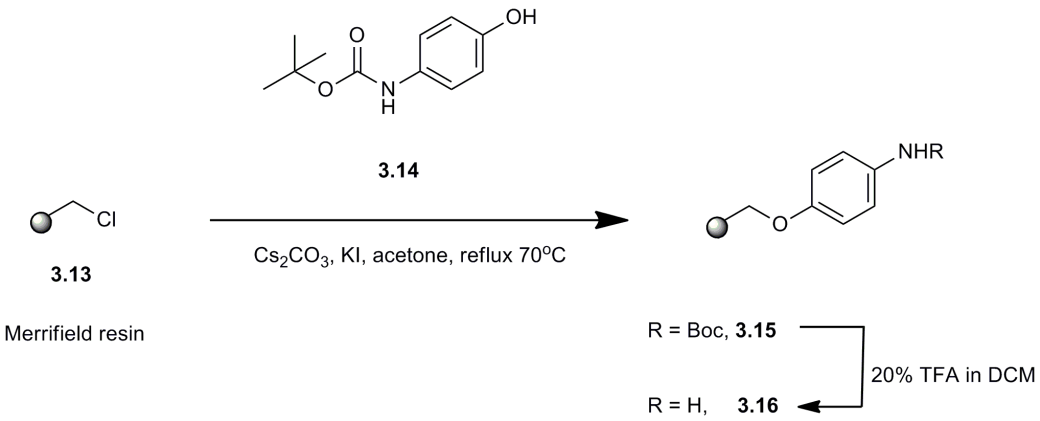

Scheme 3.1: Preparation of the 4-aminophenyl resin (3.16).

The synthesis of carboxy-Cy7 (**3.20, Scheme 3.3**) was carried out in two steps from the unprotected 4-aminophenol resin (**3.16**). The first step was the formation of the polymer-bound polyene-precursor **3.18** by loading of the hemicyanine intermediate **3.17** onto the solid support **3.16**. Compound **3.17** was synthesised in solution by nucleophilic attack of the quaternary indoleninium salt (**3.28**) onto the glutaconaldehyde dianilido hydrochloride (**3.27**) and acetylated using acetic anhydride (**Scheme 3.2**).[164] The formation of the desired hemicyanine intermediate **3.17** was monitored by UV/vis spectrometry to reduce the formation of the undesired symmetrical dye. Hemicyanine (**3.17**) had a maximum absorption around 489 nm while the starting material (**3.28**) absorbed at 290 nm and the symmetrical cyanine fluorophore at 750 nm. The compound **3.17** was isolated by precipitation in cold ether as a red solid (75%).

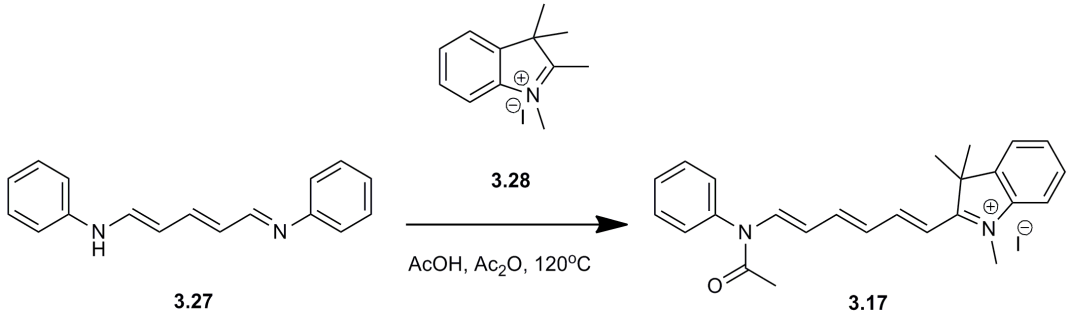

Scheme 3.2: Synthesis of the hemicyanine intermediate (3.17).

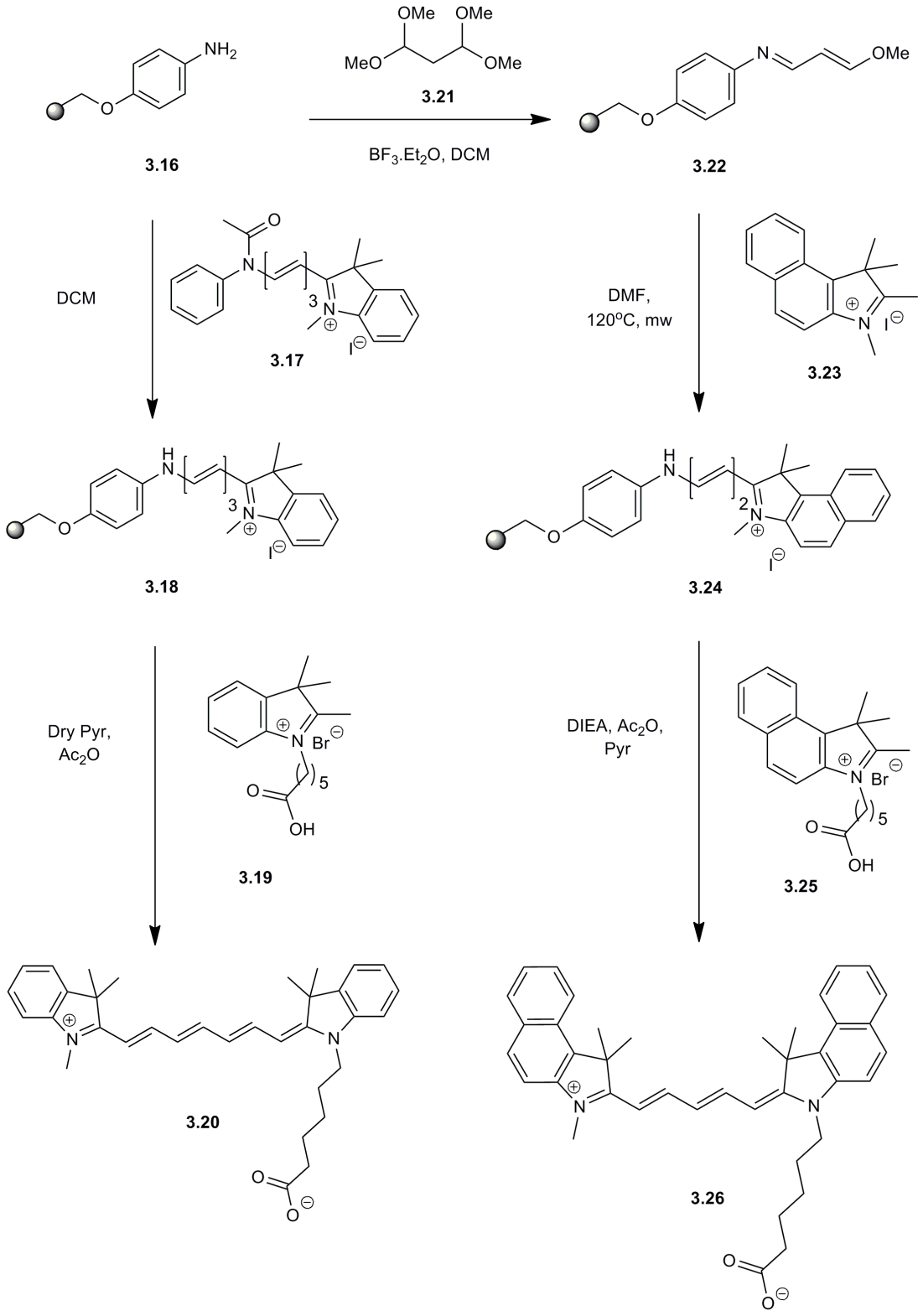

Scheme 3.3: Catch and release synthesis of the modified heptamethine dye, carboxy-Cy7 (3.20) and the modified pentamethine dye, carboxy-Cy5.5 (3.26).

Without further purification, the hemicyanine **3.17** was added to the polymer-bound aniline **3.16** giving the polymer-bound polyene-precursor **3.18** via the nucleophilic attack of the hemicyanine by the amine on the resin (**3.16**), generating the displacement of a molecule of acetanalide. The PS derivate **3.18** was isolated by filtration as a dark blue resin. The unsymmetrical heptamethine dye **3.20** (carboxy-Cy7) was cleaved from the resin **3.18** by nucleophilic attack of the modified quaternary indoleninium salt **3.19** onto the polymer-bound hemicyanine in the presence of pyridine and acetic anhydride. Carboxy-Cy7 (**3.20)** was obtained as a green-blue solid in high yield (92% based on the amount of heterocycle (**3.19**) used) and high purity (97%) as determined by HPLC (**Figure 3.6**) and ^{1}H NMR analysis.

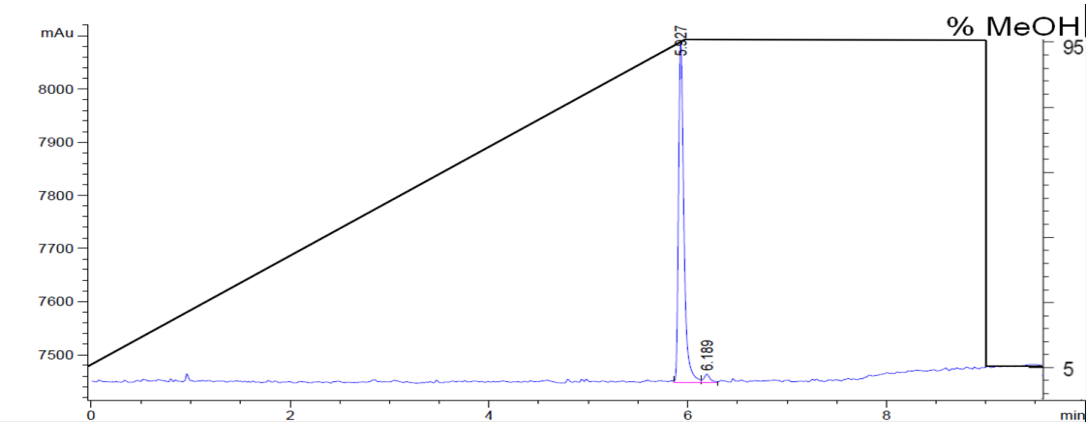

Figure 3.6: HLPC trace (ESLD) of the crude heptamethine dye carboxy-Cy7 (3.20), purity 97%.

As for the synthesis of the carboxy-Cy7 dye (**3.20**), preparation of the pentamethine dye carboxy-Cy5.5 (**3.26**) was carried out over three steps using the "catch and release" method. The fluorophore synthesis started with the polymer-bound precursor **3.24** (**Scheme 3.3**). The polyene-chain precursor **3.22** was prepared from the 4-aminophenol PS (**3.16**) using 1,1,3,3-tetramethoxypropane (**3.21**) in the presence of $BF_3.Et_2O$ (confirmed by a ninhydrin test and changes of colour). **3.16** had an orange colour while the resin **3.22** was dark blue. Furthermore, the formation of the imidate can be confirmed by IR detection of a sharp peak at 1624 cm^{-1} corresponding to the –C=N– stretch. Once the precursor **3.22** was synthesised, the next step was the preparation of the immobilised hemicyanine **3.24** by condensation of the quaternised indolenine derivative **3.23** onto the solid support. The

condensation reaction was carried out in DMF under microwave irradiation (120°C for 15 minutes). After filtration and washes, the formation of the desired immobilised hemicyanines was confirmed by IR analysis (loss of the sharp peak at 1624 cm^{-1}). The desired unsymmetrical pentamethine carboxy-Cy5.5 (**3.26**) was obtained by treatment of the modified quaternary indoleninium salt **3.25** onto the polymer-bound hemicyanine in the presence of pyridine and acetic anhydride.

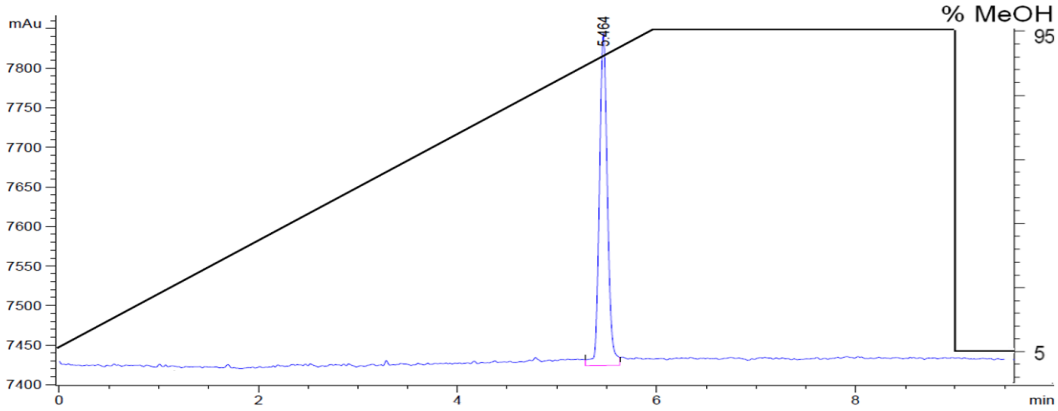

Figure 3.7: HLPC trace (ELSD) of the crude pentamethine dye carboxy-Cy5.5 (3.26), purity 100%.

After precipitation in ether and filtration, the carboxy-Cy5.5 **3.26** was obtained as a green-blue solid with high yield (90% based on **3.25**) and high purity (100%) determined by HPLC (**Figure 3.7**) and ^{1}H NMR analysis.

3.2.2. Preparation of peptoids labelled with NIR dyes

In order to deliver cyanine dyes into cells, carboxy-Cy7 (**3.20**) and carboxy-Cy5.5 (**3.26**) were coupled to the lysine-like peptoids functionalised with an aminohexanoic spacer (**2.35** for 9mer (***CHAPTER 2***) and **3.33** for 1mer). After Fmoc deprotection, the solid supports were coupled to the dyes (**3.20** and **3.26, Scheme 3.4**) with two activation techniques evaluated: a succimido (OSu) active ester or a 1-hydroxybenzotriazole (OBt) active ester.

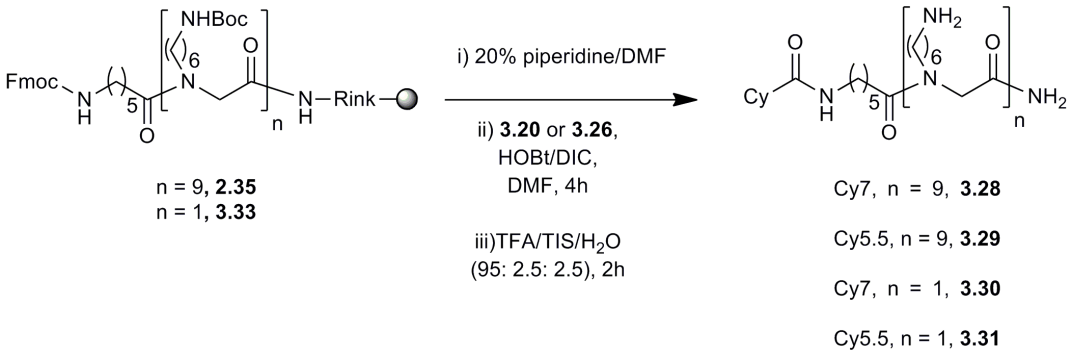

Scheme 3.4: Synthesis the cyanine dye labelled peptoids.
Cy7-9mer (**3.28**), Cy5.5-9mer (**3.29**), Cy7-1mer (**3.30**) and Cy5.5-1mer (**3.31**).

The first method (OSu active ester) was previously applied by Maria Lopalco to couple cyanine dyes for the synthesis of enzymatically cleavable fluorescent nucleotides.[176] This method was applied to these dyes as it allowed recovery of unreacted cyanine dyes. The carboxylic group of the carboxy-Cy7 (**3.20**) was activated using *N,N*'-disuccinimidyl carbonate (DSC) (reaction was monitored by HPLC and MS until completion). After precipitation, the activated cyanine dye was added to the previously Fmoc deprotected resin **2.35** and coupling completion monitored by a ninhydrin test. Unfortunately, this coupling method was not very efficient and had to be repeated in order to label all the free amino groups. The NHS-Cy7 was very sensitive to hydrolysis and free cyanine dye (**3.20**) was recovered after coupling. Resin-bound labelled Cy7-peptoid was deprotected and cleaved from the solid support by treatment with a mixture of TFA/TIS/H_2O (95: 2.5: 2.5) for 2 hours. The resulting product was impure mainly due to incomplete coupling. Once purified, the Cy7-9mer (**3.28**) (**Figure 3.8**) was isolated as a green-blue solid in a final yield of 60% (calculated from the theoretical loading of **2.35**) and a purity of 98% (ELSD). Although the desired compound was successfully synthesised, HOBt activation was tested to increase the yield and avoid purification.

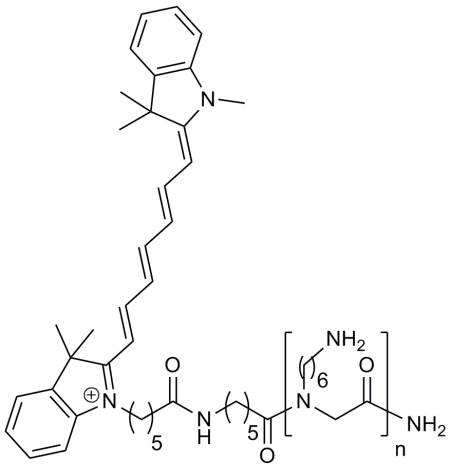

n = 9, **3.28**

n = 1, **3.30**

Figure 3.8: Structure of Cy7-9mer (3.28) and Cy7-1mer (3.30).

HOBt activation of cyanine dyes was previously described by Lois Alexander to couple carboxy-Cy5 and carboxy-Cy7 onto microspheres. The drawback of this synthesis was the number of equivalents used (10 equivalents of the dye, HOBt, PyBOP and DIPEA).[177] The HOBt/DIC coupling method was previously used to prepare nonalysine-like peptoids and was efficient for the coupling of rhodamine onto the 9mer peptoid (***CHAPTER 2***) with only three equivalents of each reagent. Therefore, HOBt/DIC was applied to couple the carboxy-Cy7 (**3.20**) to the Fmoc deprotected resin (**2.35**). After activation of the dye (mixture of **3.20**, HOBt and DIC in DMF), it was added to the resin and mixed for four hours. The coupling was monitored by ninhydrin test. Before running the colorimetric test, the resin supporting the Cy7-9mer was washed extensively to avoid Cy7 trace. The reaction was complete after only one coupling. Cleavage and deprotection of Cy7-9mer (**3.28**) (TFA/TIS/H_2O, 95:2.5:2.5) gave a green-blue solid (isolated after precipitation in Et_2O). MS (MALDI-TOF) and NMR analysis confirmed the synthesis of the compound while HPLC (**Figure 3.9-B**) showed the purity of **3.28** as 98% (ELSD) with a yield of 94% (calculated from the theoretical loading of **2.35**).

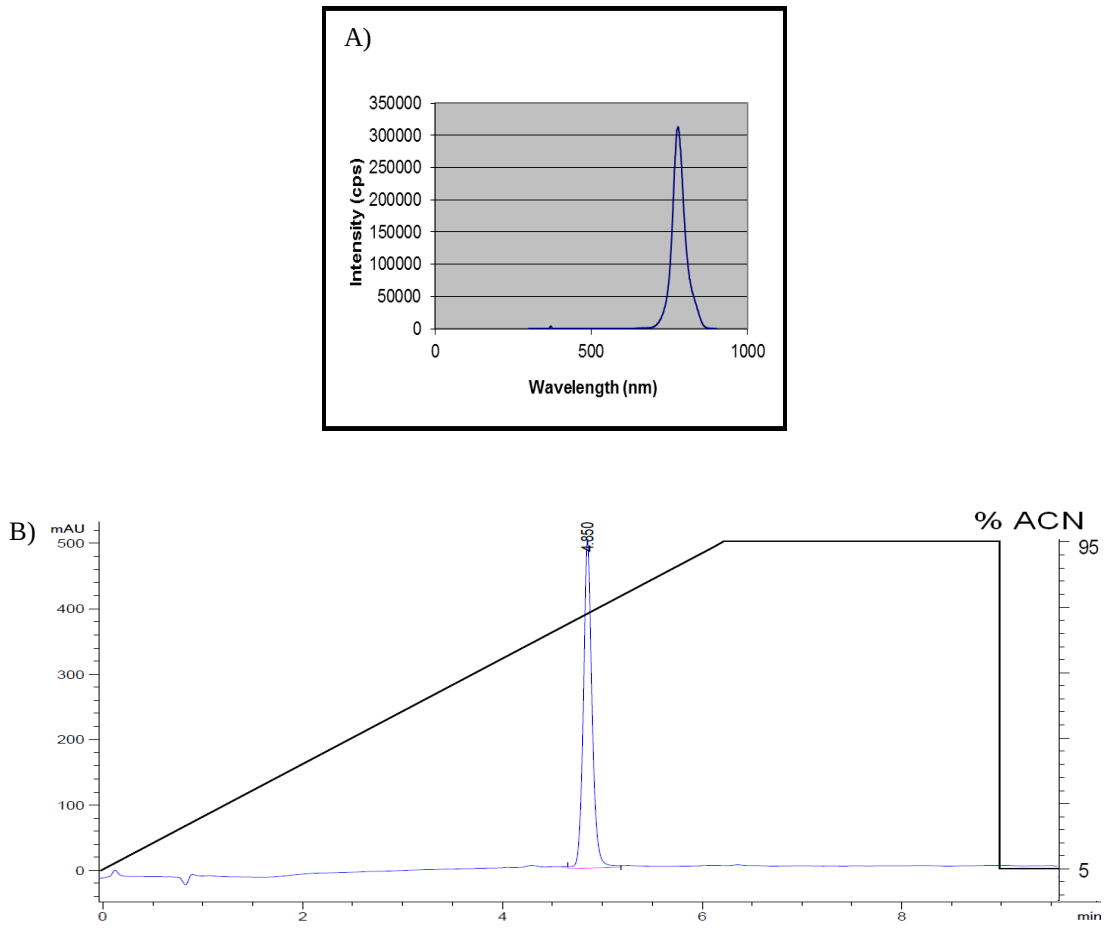

Figure 3.9: Analysis of the crude Cy7-9mer (3.28) obtained with HOBt/DIC activation.
A) Emission spectrum of Cy7-9Mer peptoid **3.28** in MeOH (λ_{abs} = 744 nm, λ_{em} = 777 nm); B) HPLC trace (λ = 750 nm) of Cy7-9mer peptoid **3.28**, purity > 98%

Cy5.5-9mer (**3.29, Figure 3.10**) was synthesised using the same protocol (HOBt/DIC activation) as Cy7-9mer (**3.28, Scheme 3.4**). The Cy5.5-9mer peptoid (**3.29**) was cleaved and deprotected (TFA/TIS/H_2O, 95: 2.5: 2.5) to give after precipitation (cold Et_2O) a blue solid in a yield of 87% (based on the theoretical loading of **2.35**) and a purity of 97% (HPLC (**Figure 3.11-B**) and confirmed by ^{1}H-NMR and MS analysis).

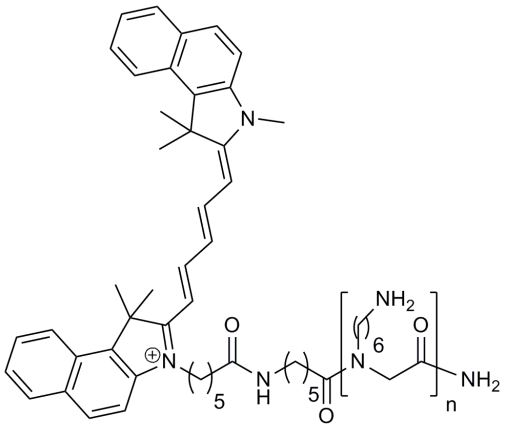

n = 9, **3.29**

n = 1, **3.31**

Figure 3.10: Structure of Cy5.5-9mer (3.29) and Cy5.5-1mer (3.31).

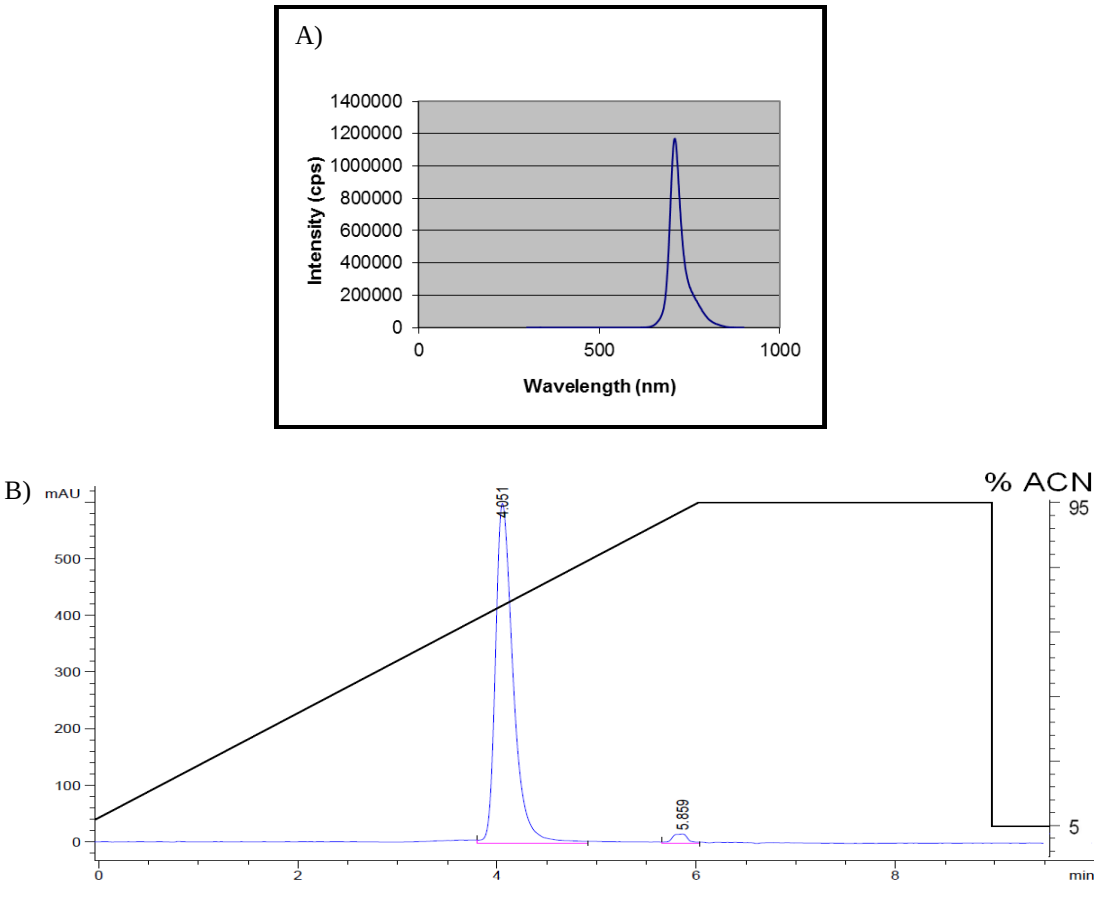

Figure 3.11: Analysis of the Cy5.5-9mer (3.29).
A) Emission spectrum of Cy5.5-9Mer peptoid **3.29** in MeOH (λ_{abs} = 678 nm, λ_{em} = 710 nm);
B) HPLC trace (λ = 675 nm) of Cy5.5-9mer peptoid **3.29**, purity > 97%.

As a negative control was required for cell analysis and as both carboxy-cyanine dyes (**3.20** and **3.26**) were not soluble in water (unless addition of DMSO), Cy7-1mer (**3.30, Figure 3.8**) and Cy5.5-1mer (**3.31, Figure 3.10**) were synthesised using the same protocol as their 9mer analogues (**Scheme 3.4**).

3.3. In vitro assays

3.3.1. Cell labelling

The cellular uptake of Cy7-9mer **3.28** and Cy5.5-9mer **3.29** by HeLa, B16F10 and HEK293T cells was carried out with a 10 μM peptoid concentration. The cells were incubated with the peptoids at 37°C for 5 minutes, 30 minutes, 2 hours, 4 hours and 24 hours. Afterwards, the cells were washed, trypsinated and analysed by flow cytometry. Results of representative cellular uptakes are shown in the **Graph 3.1**.
Uptake was found to be high across all the cell lines analysed with at least 95% of cells labelled after 24 hours of incubation with the Cy-9mer (**3.28** and **3.29**). Cellular penetration was dependent on the incubation time and the cell lines but the type of cyanine dye did not affect the uptake. HEK293T cells showed an impressive and quick cellular uptake (> 90% in only 30 minutes). Surprisingly, B16F10 cancer cells, which are known to be more difficult to deliver external cargo to, showed a high level of penetration (> 90%) after 2 hours. More than 80% of the HeLa cells (82% with Cy7-9mer and 99% with Cy5.5-9mer), another type of cancer cells, were penetrated by the nonalysine like peptoid after only 30 minutes of incubation.

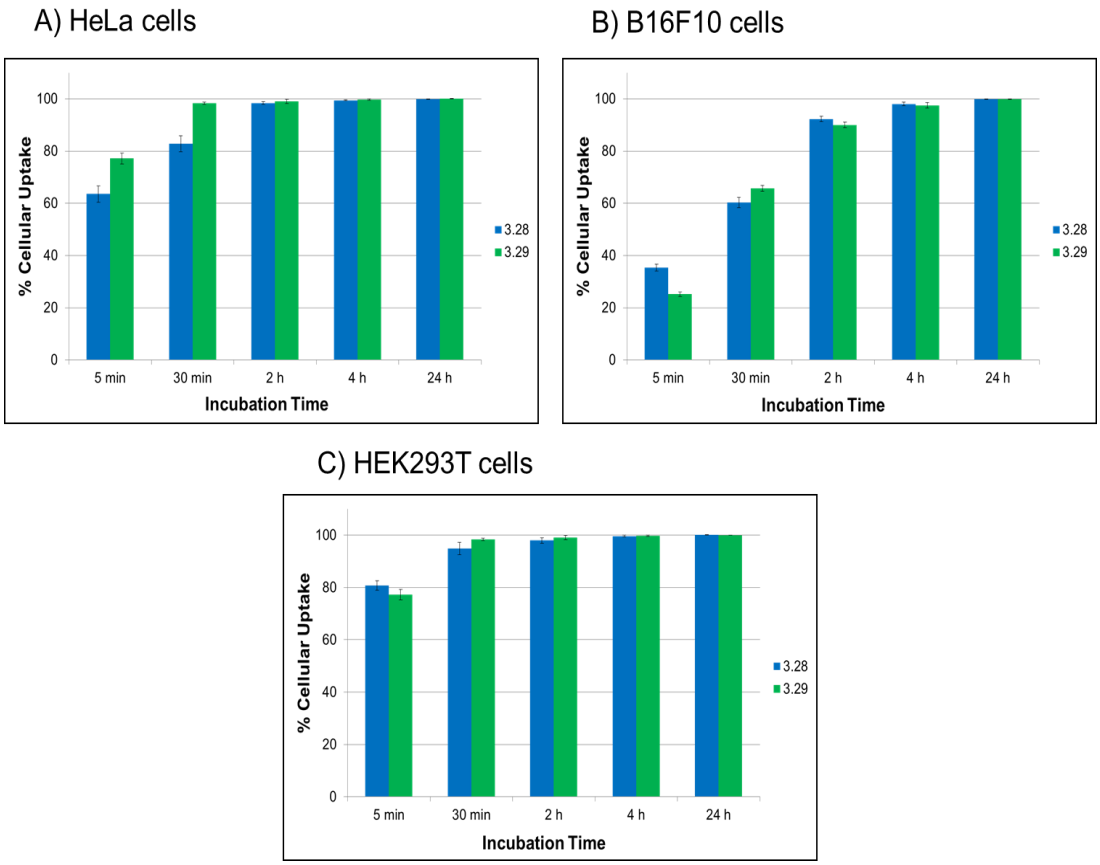

Graph 3.1: Cellular uptake of Cy7-9mer (3.28, blue) and Cy5.5-9mer (3.29, green).
A) HeLa cells; B) B16F10 cells; C) HEK293T cells. % uptake was measured as the % of cells with a fluorescent emission exceeding untreated control cells, which were defined as 0% uptake. Compound concentration 10 μM. The errors bar represents the standard error of the average (n = 6).

3.3.2. Cytotoxicity assays

Cellular uptake of both peptoids, Cy7-9mer (**3.28**) and Cy5.5-9mer (**3.29**), was shown to be high in various cell lines. Cell viability of HEK293T, HeLa and B16F10 cells was tested against Cy7-9mer and Cy5.5-9mer at various concentrations (1, 5, 10 and 20 μM) after 24 hours of incubation.

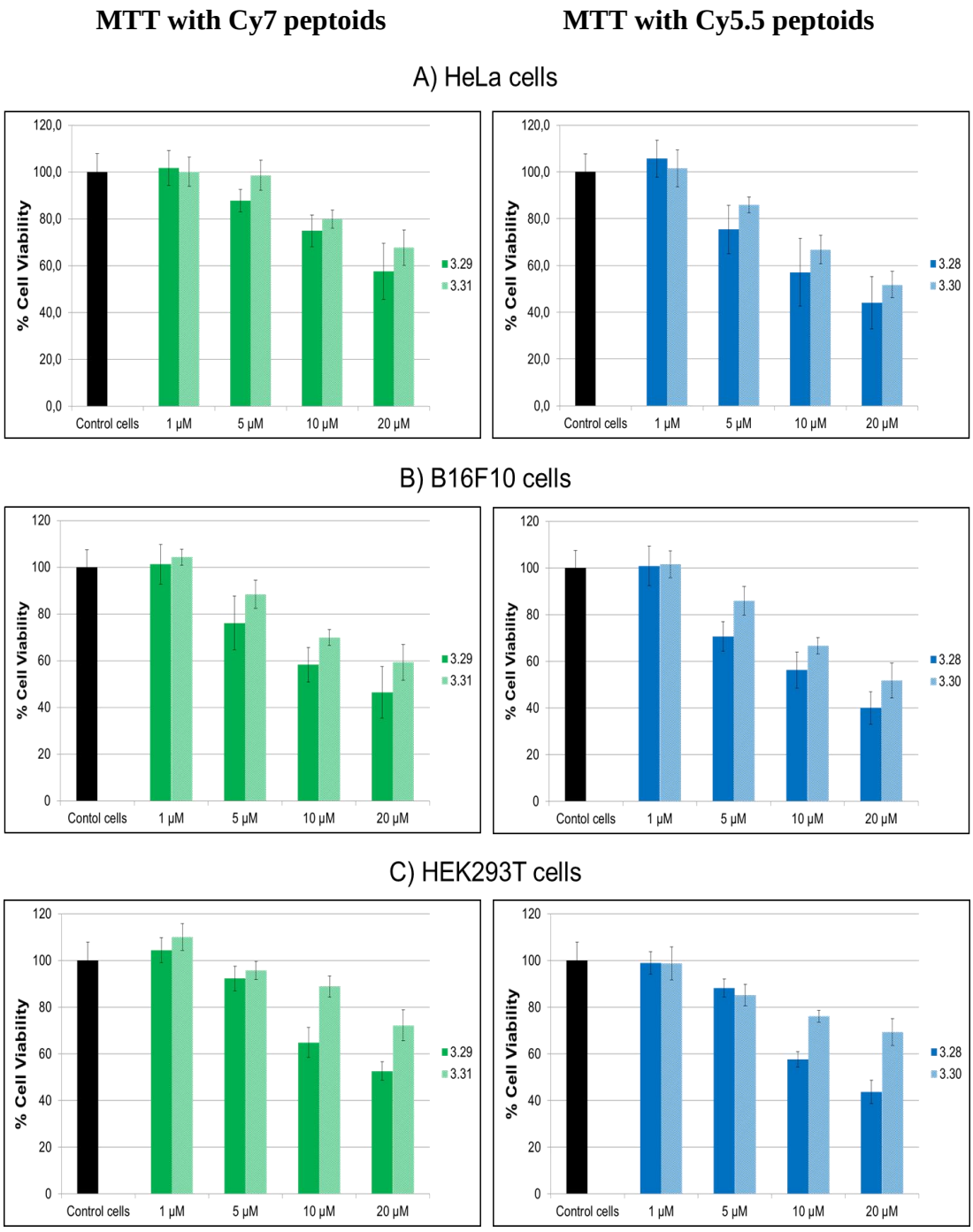

Graph 3.2: MTT results to evaluate cellular viability of cyanine peptoids.
HEK293T, HeLa and B16F10 cells in presence of 1, 5, 10 and 20 µM of peptoids (Cy7-9mer (**3.28**), Cy5.5-9mer (**3.29**), Cy7-1mer (**3.30**) and Cy5.5-1mer (**3.31**)) for 24 hours before being treated with MTT. The errors bar represents the standard error of the average (n = 5).

Surprisingly, both cyanine peptoids demonstrated some cytotoxicity in all the tested cell lines (**Graph 3.2**). Indeed, with 10 µM of Cy7-9mer (**3.28**) and Cy5.5-9mer (**3.29**), less than 60% of the cells were viable. These results were very surprising

after the non-cytotoxicity of the Rho-9mer peptoid shown in ***CHAPTER 2*** (**Graph 2.3**) and in previous papers.[104, 114] However, several studies have reported the cytotoxicity of cyanine dyes when delivered into cells even at low concentration (1 µM for 4 hours).[178,179] For instance, Cy5.5 labelled nanoparticles showed cellular toxicity in HeLa cells when incubated at a concentration of 20 µg/mL.[180] As far as the Cy7 was concerned, nothing about its cytotoxicity has been published so far in the literature.[181] Therefore, the cytotoxicity of the Cy-9mer could be due to the dye.

Although the cytotoxicity of the cyanine-1mer peptoids was less than for the cyanine-9mer peptoids, MTT assays showed similar results (**Graph 3.2**). As the Cy7-1mer (**3.30**) and Cy5.5-1mer (**3.31**) had a lower uptake than their 9mer analogues (**Appendix 3**), they were less toxic to cells. Cyanine-1mer peptoids demonstrated a maximum cytotoxicity with 50% of viable cells (HeLa) after 24 hours of incubation at 20 µM, while cyanine-9mers showed, under the same conditions, a maximum of 42% healthy cells.

MTT assays were carried out on unlabelled peptoid (**3.32**) (**Figure 3.12-A**) to prove the non cytotoxicity of the cellular transporter. In order to compare the cytotoxicity of each peptoid, MTT assays were done using the same conditions for all of them (concentrations of peptoids = 1, 5, 10 and 20 µM, 24 hour incubation time, 37^{o}C) on the HEK293T, HeLa and B16F10 cells.

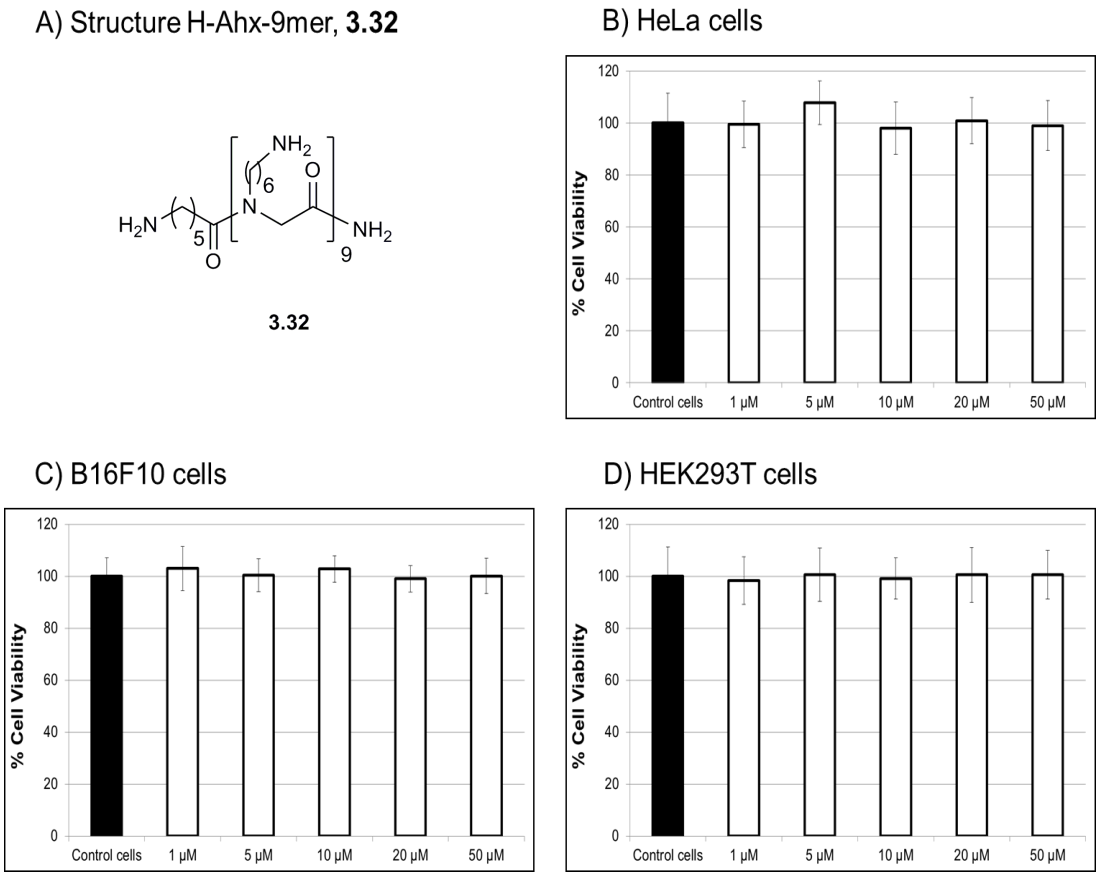

Figure 3.12: Structure of H-Ahx-9mer (3.32) and its cellular viability.
A) Structure of the H-Ahx-9mer (**3.32**); B) MTT assay in HEK293 T cells; C) MTT assay in HeLa cells; D) MTT assay in B16F10 cells. The errors bar represents the standard error of the average (n = 5).

As far as the H-Ahx-9mer (**3.32**) was concerned, MTT assays did not show any cytotoxicity. This result was obtained for all cell lines tested and for all the peptoid concentrations (**Figure 3.12**).

In view of these data, *in vivo* applications did not seem possible. Therefore, it was important to find an incubation time and a concentration that would allow good cellular penetration without cytotoxicity. Cells (HeLa and HEK293T cells) were treated with 5 µM of Cy7-9mer (**3.28**) and Cy5.5-9mer (**3.29**) for 15 and 30 minutes prior to cytotoxicity analysis (MTT assays, **Graph 3.3**).

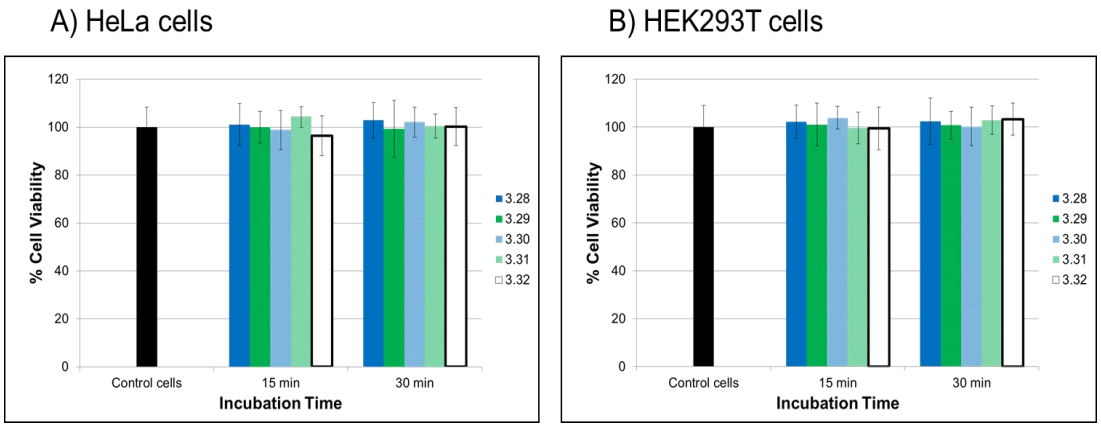

Graph 3.3: MTT results to evaluate cellular viability of cyanine peptoids.
HeLa (A) and HEK293T (B) cells in presence of 5 µM of peptoids (Cy7-9mer (**3.28**), Cy5.5-9mer (**3.29**), Cy7-1mer (**3.30**) and Cy5.5-1mer (**3.31**)) for 15 and 30 minutes before being treated with MTT. The errors bar represents the standard error of the average (n = 5).

As demonstrated in **Graph 3.3**, none of the 4 cyanine peptoids (Cy7-9mer (**3.28**), Cy5.5-9mer (**3.29**), Cy7-1mer (**3.30**) and Cy5.5-1mer (**3.31**)) showed cytotoxicity at 5 µM with an incubation time for 15 and 30 minutes. Therefore, the cellular labelling of Cy7-9mer and Cy5.5-9mer was assessed using the same conditions (5 µM for 15 and 30 minutes).

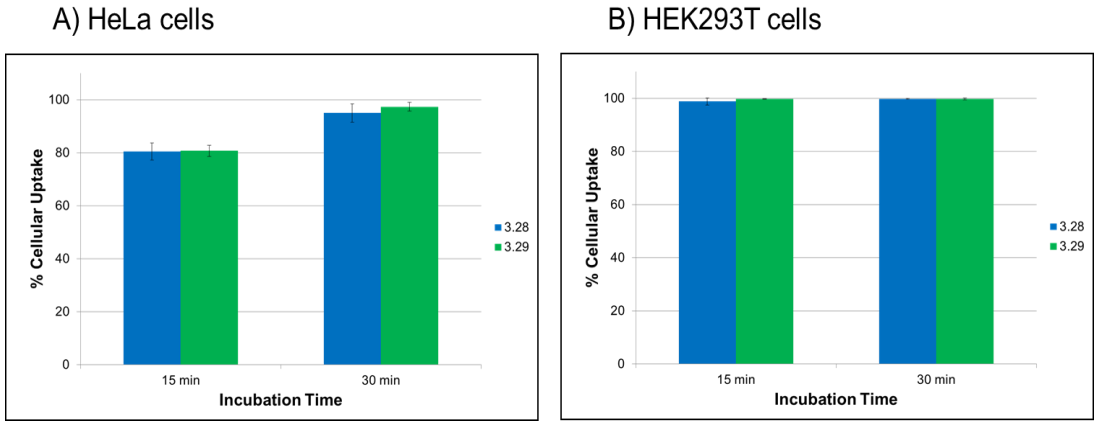

Graph 3.4: Cellular uptake of Cy7-9mer (3.28) and Cy5.5-9mer (3.29).
HEK293T (A) and HeLa (B) cells incubated with 5 µM of peptoids (Cy7-9mer (**3.28**) and Cy5.5-9mer (**3.29**)) for 15 and 30 minutes at 37°C. The errors bar represents the standard error of the average (n = 6).

5 µM of the cyanine peptoids (Cy7-9mer and Cy5.5-9mer) allowed efficient cellular labelling of HeLa and HEK293T cells with at least 80% of the cells labelled after 15

minutes of incubation and more than 90% labelled (HeLa) after 30 minutes (**Graph 3.4**). These results were confirmed by confocal microscopy. HeLa cells were more difficult to label in comparison to HEK293T, therefore they were incubated with 5 µM of Cy5.5-9mer (**3.29**) for 30 minutes at 37°C. At the end of the incubation time, cells were washed with PBS and their membrane and nucleus were stained (**Figure 3.13**).

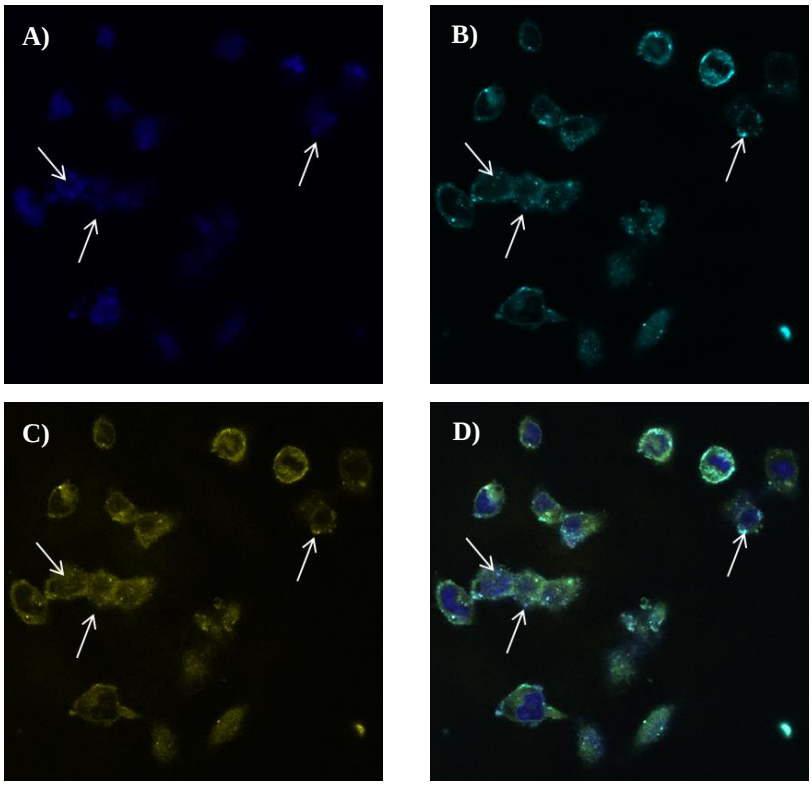

Figure 3.13: Confocal images of HeLa cells labelled with Cy5.5-9mer (3.29) (5 µM) for 30 minutes.
A) Nuclei staining using HOECHST-33342 (excitation laser 405 nm and emission filter 413-482 nm); B) Cellular labelling with Cy5.5-9mer (excitation laser 633 nm and emission filter 646-762 nm); C) Membrane staining with DilC 18 (excitation at 595 nm and emission filter 670-690 nm); D) Composite image. The arrows show the localisation of the Cy5.5-9mer inside the cells.

These confocal images clearly show that the Cy5.5-9mer (**3.29**) was inside the cells (appearing as blue dots), confirming cellular uptake of the peptoid within 30 minutes at a concentration of 5 µM.

3.4. In vivo studies (collaboration with Dr. Kevin Dhaliwal)

The first step in the design of new anti-inflammatory treatments is a greater understanding of the migration and trafficking of immune cells (such as macrophages and neutrophils). Macrophages are a type of white blood cells that are crucial in microbial defence. They orchestrate the subsequent innate response. In the case of lung infection due to bacteria, macrophages create 'early' interactions with the pathogens that will command the clearance of bacteria within the lung.[182] Neutrophils are another type of white blood cells. They are known as circulating granulocytes, filled with neutrally-staining granules (sacs of enzymes) that are involved in the killing and digestion of microorganisms. Neutrophils are recruited to sites of acute inflammation and constitute the first line of cellular defence against bacterial infection. Although they are efficient phagocytes, they are also known to cause tissue damage as a result of an imbalance between neutrophil elastase and its inhibitor.[183] Given the potential of neutrophils to injure tissues, the inflammatory response has evolved to facilitate their efficient clearance once their phagocytic function has been completed. However in some instances, especially in response to certain infections, neutrophils may continue to be recruited and in the face of poor clearance of pathogens and toxic neutrophil products may perpetuate the inflammatory response.[184]

In order to obtain a better understanding of immune cells, primary cells were labelled with Cy7-9mer (**3.28**) or Cy5.5-9mer (**3.29**) before being followed inside murine bodies. Experiments were carried out on mice aged between 6 and 12 weeks old with all animal experiments were undertaken by Dr Kevin Dhaliwal with an approved licence from the Animal Scientific Procedure Division of the Home Office, London, U.K.

3.4.1. Cellular labelling of primary cells

Using the data obtained during the *in vitro* studies, the labelling capacity of both Cy7-9mer and Cy5.5-9mer was tested on immune cells. Cellular labelling of murine

marrow machrophages by Cy5.5-9mer (**3.29**) (10 minutes, 4.8 μM) was demonstrated by confocal microscopy.

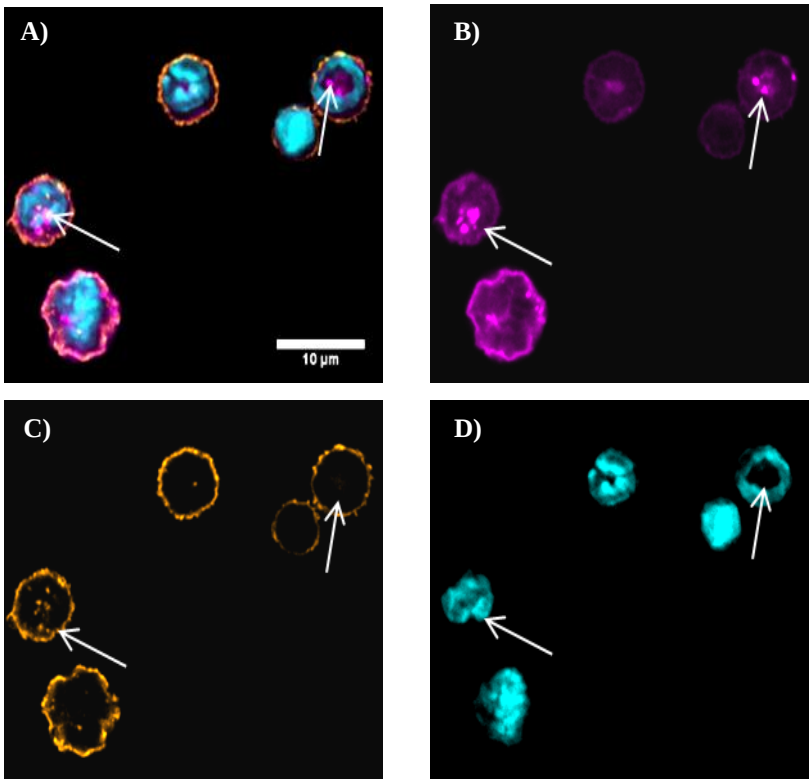

Figure 3.14: Confocal images of freshly-flushed murine marrow macrophages after cells labelled with Cy5.5-9mer (3.29) (4.8 μM) for 30 minutes.
A) Composite image; B) Cy5.5-9mer image (excitation laser 633 nm and emission filter 680-770 nm); C) Actin staining with Alexa^{555} (excitation laser 543 nm and emission filter 550-590 nm); D) Nuclei staining using DAPI (excitation laser 405 nm and emission filter 415-490 nm). Data courtesy of Dr. Kevin Dhaliwal from MRC (Medical Research Council) Centre for Inflammation Research, Queen's Medical Research Centre, University of Edinburgh.

The images (**Figure 3.14**) showed clearly the intracellular accumulation of the peptoids. Similar experiments were carried out by Niel MacDonald on monocytes and murine neutrophils and comparable results were obtained.[173]

3.4.2. Toxicity assays

In order to study the optical accessibility of Cy7 labelled peptoids *in vivo* and to evaluate the functional viability of peptoids-treated cells, primary murine macrophages were labelled *in vitro* for 10 minutes with Cy7-9mer (**3.28**) and

simultaneously transfected with a replication-deficient adenovirus encoding *luciferase*. The cells were then instilled (via spontaneously breathing leading in high concentration of light around the head) into the murine lung and imaged 24 hours later using IVIS SPECTRUM. The Cy7 (**Figure 3.15-A**) allowed tracking of the macrophage while the production of bioluminescence monitored the cell viability (**Figure 3.15-B**).

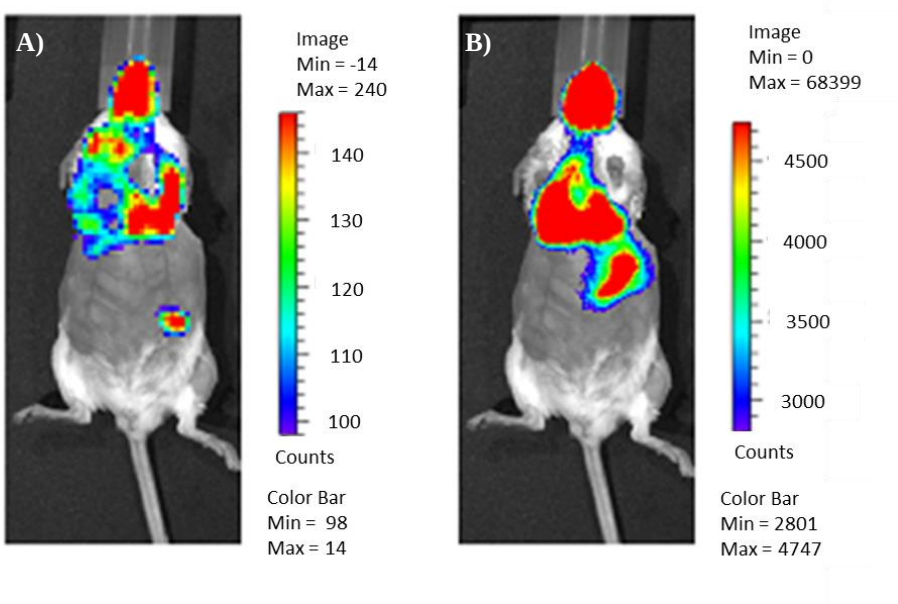

Figure 3.15: *In vivo* imaging of primary murine macrophages labelled with Cy7-9mer (3.28) (also transfected with adenovirus encoding luciferase) and instilled in murine lungs.
A) Image shows fluorescence imaging with Cy7 filters; B) Luminescence imaging of the same animal after intraperitoneal luciferin administration. Images captured on the Xenogen Spectrum. Data courtesy of Dr. Kevin Dhaliwal from MRC (Medical Research Council) Centre for Inflammation Research, Queen's Medical Research Centre, University of Edinburgh.

As expected, Cy7-9mer labelled cells could be easily visualised, thanks to fluorescence imaging and were localised in the lungs (**Figure 3.15-A**). To demonstrate the non-toxicity of the Cy7-9mer peptoid (**3.28**), luciferin was intraperitonealy injected. As the cells were transfected with adenovirus encoding firefly luciferase, the presence of luciferin would allow the generation of luminescence in the same region as the Cy7-9mer (**Figure 3.15-B**). These images showed the bioluminescence and labelling of the macrophages. Therefore, these results demonstrated that *in vivo* the Cy7-9mer (**3.28**) labelling was retained and did not affect cell viability of the macrophages as the cells generated bioluminescence.

3.4.3. Tracking of cells to inflammation sites

In vivo studies were extended to assess the dynamic migration and functional viability of labelled cells during inflammation over several days. Lipopolysaccharides (LPS) were instilled into the lungs of a healthy mouse. The presence of LPS generated an inflammation of the murine lungs. Bone marrow-derived macrophages (BMDMs) were isolated and treated with Cy7-9mer peptoids (**3.28**) (10 minutes). After incubation, BMDMs were washed and injected into the murine tail. Migration of the labeled BMDMs was monitored over two days (**Figure 3.16**).

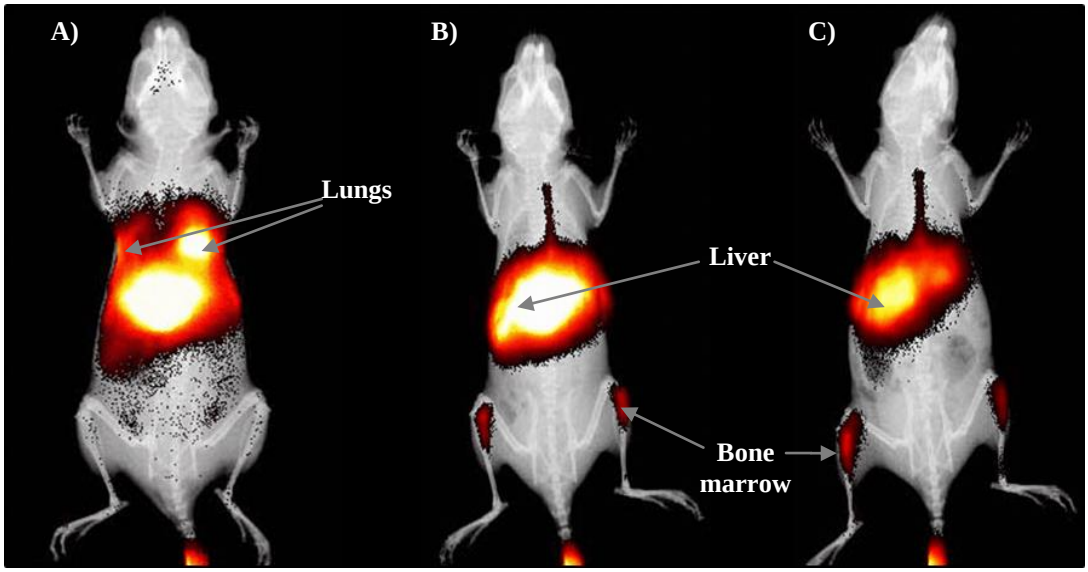

Figure 3.16: Tracking of Cy7-9mer (3.28) labelled BMDMs (Bone Marrow-Derived Macrophages) on 2 days of LPS injury.
X-ray superimposed on reflectance fluorescent images on Kodak Multispectral FX Pro (excitation 745nm, emission 820nm); A) Image after injection day 0; B) Image at day 1; C) Image at day 2. Data courtesy of Dr. Kevin Dhaliwal from MRC (Medical Research Council) Centre for Inflammation Research, Queen's Medical Research Centre, University of Edinburgh.

Figure 3.16-A was taken on the day of the cell injection. Labelled primary cells were easily localised in the lungs (where the inflammation took place) and in the liver. Once the inflammation ended the BMDMs cell migrated the from the inflammation site (lungs) to the liver and to the hips (the bone marrow) (**Figure 3.16-B**). This result was confirmed on the image taken two days after LPS injury (**Figure 3.16-C**). This last image showed clearly the localisation of Cy7-9mer (**3.28**) labelled cells into

the liver and the bone marrow. Furthermore, the intensity of fluorescence inside the liver decreased between day 1 (Image B) and day 2 (Image C). This diminution could be associated with the degradation of the BMDMs and thus of the Cy7 dye.

So far, *in vivo* studies showed that using the cyanine-9mer peptoids, primary cells could be tracked in lung tissues where the inflammation takes places. Furthermore, the cell movements were followed over several days and up to the liver and the bone marrow, where macrophages can be regenerated and/or degraded.

3.5. Conclusions

Cyanine-9mer peptoids, Cy7-9mer (**3.28**) and Cy5.5-9mer (**3.29**), have shown rapid and efficient cellular labelling of various cell lines (HeLa, B16F10 and HEK293T cells) and primary immune cells (macrophages and neutrophils) without cytotoxicity. *Ex vivo* labelling of primary cells by peptoids did not affect their prime functions, their movement and their efficiency. Furthermore, thanks to the proteolytic resistance of peptoids, cell imaging was possible over a few days. These experiments and the cell-labelling characteristics (including remarkably low cytotoxicity) described the NIR-labelled 9mer peptoids as a highly attractive tool for optical imaging.

The next step of this project could be the study of the stability of the peptoid and the NIR-infrared dye *in vitro* and *in vivo*. This experiment could be carried out using longer cell tracking analysis and/or cell lysis. Once lysed, the intracellular content could be separated, the peptoid recovered and analysed by HPLC and MS to determinate any possible degradation.

Another perspective could lead to introducing a specific sequence to the peptoid to enable cell selectivity. Indeed, one of the main limitations of this cellular penetrating system is its poor selectivity to different cells. If this project works, the peptoid could be injected intravenously and label only the desired cells.

CHAPTER 4 : MACROMOLECULE DELIVERY

When coupled to dyes, 9mer peptoids have been shown to rapidly, efficiently and without cytotoxicity penetrate multiple cell lines including primary cells. Furthermore, the peptoids have demonstrated to be applicable for both *in vitro* and *in vivo* studies. In this chapter, the capacity of the 9mer peptoid was evaluated for its ability to deliver macromolecules (peptides, proteins and DNA) into cells.

4.1. Peptide delivery

4.1.1. Previous cellular delivery of peptides using CPPs and peptoids

Cellular delivery of exogenous macromolecules is essential in several scientific fields of research as well in the treatment of diseases. Delivery of biologically active peptides has been carried out, *in vitro* and *in vivo*, using Antennapedia and TAT peptides (**Table 1.1**: peptide strucutre). These two CPPs are known to rapidly and efficiently enter cells including non-dividing primary cells.[185] The peptides of interest can be coupled to the CPPs through either ionic or more normally covalent bonding. For covalent coupling the conjugates are typically synthesised using solid-phase peptide synthesis. An important range of peptides have been delivered into various cell lines such as cancer cells (HeLa, E49 and BMRPA1), blood cells (monocytes and neutrophils), muscle cells and neurons. These biologically active peptide-CPPs have been studied for several applications (**Table 4.1**) including initiation of cellular apoptosis,[186] cancer vaccines[187] and modulation of asthma[188] and inflammation.[189, 190]

Peptide of interest	CPPs used	Aim and Cellular response
Bcl-2 homology (BH3) domain of Bcl-2 associated death promoter (BAD) H-NLWAAQRYGRE LRRMSDEFVD-OH	Penetratin	Binding to Bcl-2 leading to apoptosis of malignant cells[186]
Putative signalling mediator (PSM) amino terminal Pro-rich region H-FPSPPALPPPPPPSWQ-OH	Penetratin	Positive stimulation of PDGF/ IGF/ insulin signalling (SH3 domain) leading to DNA synthesis and proliferation of cells[191]
β3-integrin cytoplasmic tail Tyrosine 747: H-ANNPL**Y**KEATS-OH Tyrosine 759: H-FTNIT**Y**RGT-OH	TAT	Inhibition of PI3K leading to no PMNs transmatrix migration[189]
N-terminal influenza hemagglutinin peptide derivative: H-LFEAIEGFI-OH	Polylysine	Creation of cancer vaccines[187] Binding to MHC class I haplotype H2-K leading to immune system recognition and tumour cell aptosis
NEMO-binding domain (NBD) peptide H-TALDWSWLQTE-OH	Penetratin	Inhibition of NF- κB and blockage of osteoclastogenesis[192]
p53C' peptide H-GSRAHSSHLKSK KGQSTSRHKK-OH	TAT	Induce apoptosis by activating wild-type p53 protein[193]

Table 4.1: CPP-mediated peptide delivery.
MHC: major histocompatibility complex; PDGF: platelet-derived growth factor; PI3K: phosphoinositide 3-OH kinase; PKI: protein kinase inhibito peptide; PMNs: polymorphonuclear leukocytes.

In 2008, polylysine-like peptoids (five and nine units) were covalently coupled to a nuclear localizing sequence (NLS, PKKKRKV).[194] After incubating the fluorescein labelled peptide-peptoid hybrid (9mer-NLS: **4.1** and 5mer-NLS: **4.2**, **Figure 4.1**) with cells (HeLa and 16HBE14o-), flow cytometry analysis demonstrated efficient cellular delivery, while confocal microscopy showed co-localization of the fluorescent probes and the HOECHST-33342 stained nuclei.[104]

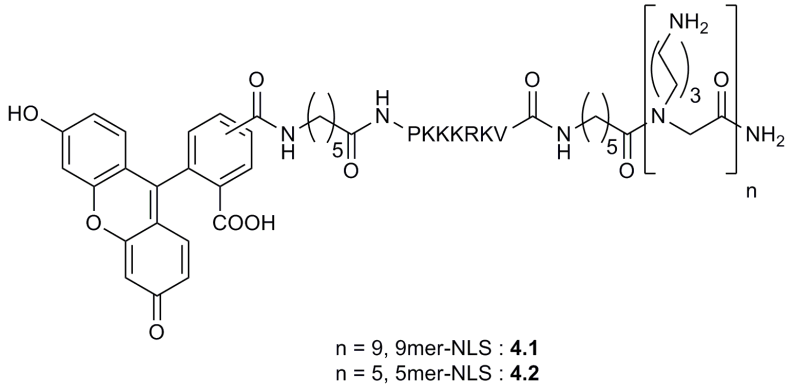

Figure 4.1: NLS peptide delivery constructs.

The hormone α-MSH (α-melanocyte stimulating hormone, Ac-SYSMEHFRWGKPV-NH_2) is a 13 amino acid peptide that binds to the melanocortin 1 receptor expressed on the surface of melanocytes and melanoma cells.[195] *In vitro* studies have shown α-MSH stimulated pigmentation of melanocytes and melanoma cells. Once the hormone binds to melanocortin 1 receptor (MC1R), it generates a succession of steps leading to an increased production of eumelanin (one of the two type of melanin produced by mammalian melanocytes).[196] Using the peptoid delivery system, two α-MSH peptide-peptoids (**4.3** and **4.4**, **Figure 4.2**) were synthesised. The 7mer peptoid successfully delivered the hormone into skin and cells (confirmed by confocal microscopy and flow cytometry analysis). *Ex-vivo* mouse, pig and human skin model studies demonstrated the skin penetration of the compounds **4.3** and **4.4** within these three different skin types. Furthermore, pigmentation analysis showed that the conjugation of α-MSH-peptide with the peptoid did not affect the activity of the hormone.[131]

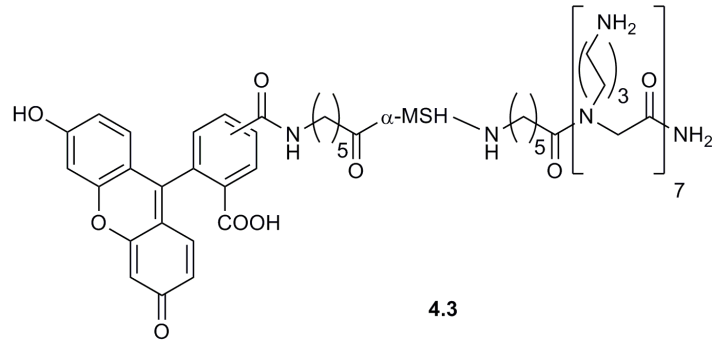

4.3

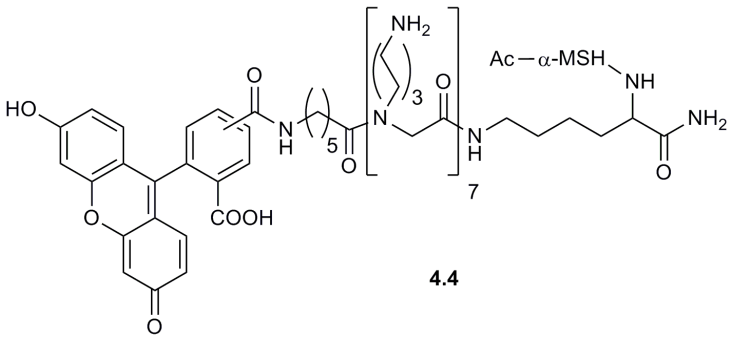

4.4

Figure 4.2: α-MSH (α-melanocyte stimulating hormone) delivery system
α-MSH = SYSMEHFRWGKPV

4.1.2. Cellular delivery of peptide inhibitor of MDM2-E3 activity : synthesis

4.1.2.1. Background

In cancer research, one short-lived transcription factor has been extensively studied: p53. This tumour suppressor protein recognises DNA damage (stand breaks and single stranded gaps). Once activated p53 can lead to various biological outcomes namely; cell repair or oncogene-induced senescence (growth arrest) or apoptosis. p53 is mainly controlled by a multidomain nuclear phosphoprotein, MDM2 (murine double minute 2 gene). Human MDM2 (**Figure 4.3**) is a RING-type E3 ubiquitin ligase of 491 amino acids that is divided in four regions. Two of these regions allow the control p53 through two distinct mechanisms. On one hand, MDM2 (its N-terminal region) can directly bind to the N-terminus of p53 leading to an inhibition of its transcriptional activational function. On the other hand, MDM2 RING finger (C terminus) can promote the proteasomal degradation of p53 through its E3 ubiquitin activity. [197, 198, 199]

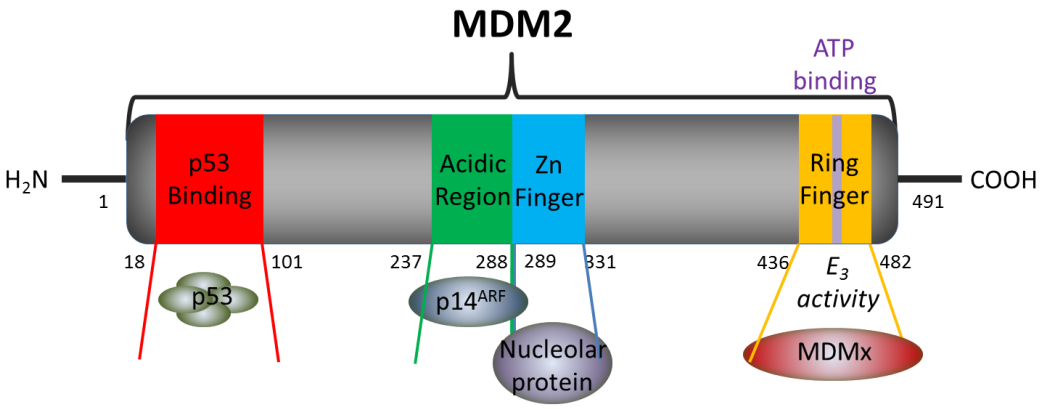

Figure 4.3: Human MDM2 with its four regions.[199, 201]
p53 binding site on the N-terminus; Acidic and Zn finger in the middle section are binding sites of several regulatory factors (including $p14^{ARF}$ an alternate reading frame that hinibits MDM2); Ring finger on the C-terminus that includes ATP and MDMx binding sites. E_3 ubiquitin ligase activity of MDM2 is located in this region.

The Ball group,[200] which works on the regulation of the E3 ubiquitin ligase activity of MDM2,[201] has isolated a twelve amino acids peptide (KEIQLVIKVFIA) that binds to the Ring domain of MDM2. Therefore, the interaction between p53 and MDM2 could not occur leading to the inhibition of E3 ubiquitin ligase activity and of the proteasomal degradation of p53. However, this peptide is unable to cross the cell membrane on its own thus the polylysine-like peptoid was coupled to it with a flurorescein dye attached (in order to analyse cellular uptake).

For this project four peptide-peptoid hybrids were synthesised based on two 12 amino acids sequences defined by the Ball group:

- sequence 1 (KEIQLVIKVFIA): peptide of interest (**4.16** and **4.18**, **Scheme 4.3**) that could bind to MDM2
- sequence 2 (KEIQLVIKVAAA): negative control (**4.17** and **4.19**, **Scheme 4.3**) that should not bind to the multidomain nuclear phosphoprotein.

Both of these peptides were prepared using solid-phase synthesis with either an acid group (**4.16** and **4.17**) or an amide group at the C-terminus (**4.18** and **4.19**).

4.1.2.2. Synthesis of the fluorescein peptide-peptoid hybrids

The synthesis of the fluorescein peptide-peptoid hybrids (**4.16**, **4.17**, **4.18** and **4.19**) began with the synthesis of the supported peptides.

The 2-chlorotrityl linker is known to be very sensitive to moisture leading to a substitution of the chloride by a hydroxy group (**4.6**).[202] The 2-chlorotrityl chloride polystyrene resin (**4.5**) was first activated in dry DCM in the presence of an excess of thionyl chloride (**Scheme 4.1**).[203].

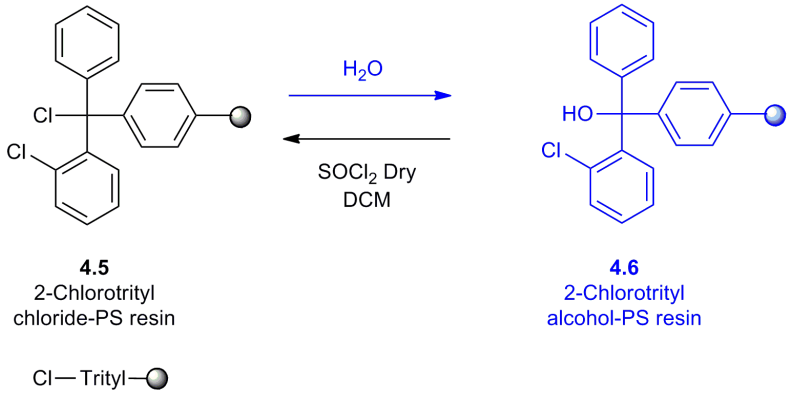

Scheme 4.1: Activation of hydrolysed 2-chlorotrityl chloride polystyrene resin (4.5).

The 2-chlorotrityl chloride polystyrene resin (**4.5**) was loaded with Fmoc-Ala-OH (**4.7**) in presence of DIPEA. For all the peptide sequences of this project, the first amino acid was alanine. The Fmoc-Ala-2-chlorotrityl polystyrene resin **4.8** was Fmoc deprotected (20% piperidine in DMF) to give the H-Ala-2-chlorotrityl polystyrene resin (**4.9**, **Scheme 4.2**).

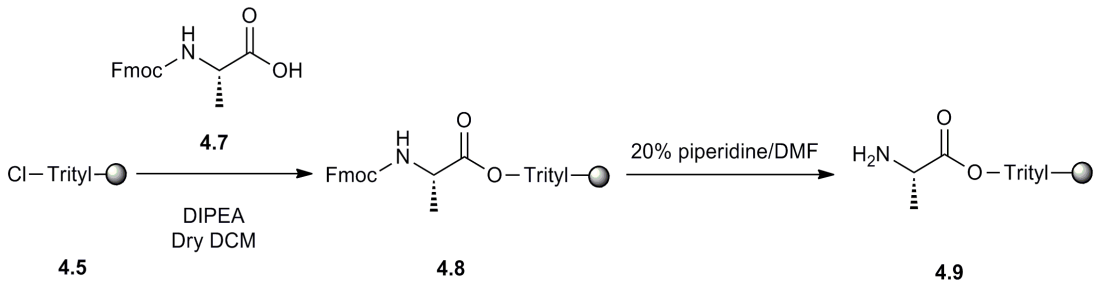

Scheme 4.2: Preparation of the H-Ala-2-chlorotrityl polystyrene resin (4.9).

The peptides **4.10** and **4.11** on solid support were synthesised manually from the resin **4.9** using a DIC/HOBt microwave assisted technique. Peptide couplings were performed using three equivalents of protected amino acids, DIC and HOBt in DMF (0.2 M) and under microwave irradiation at 60°C for 20 minutes. Fmoc deprotections were carried out at room temperature (2 cycles of 10 minutes). The resins **4.12** and **4.13** were also prepared using the same microwave assisted SPPS on the Rink amide polystyrene resin (**2.28**).

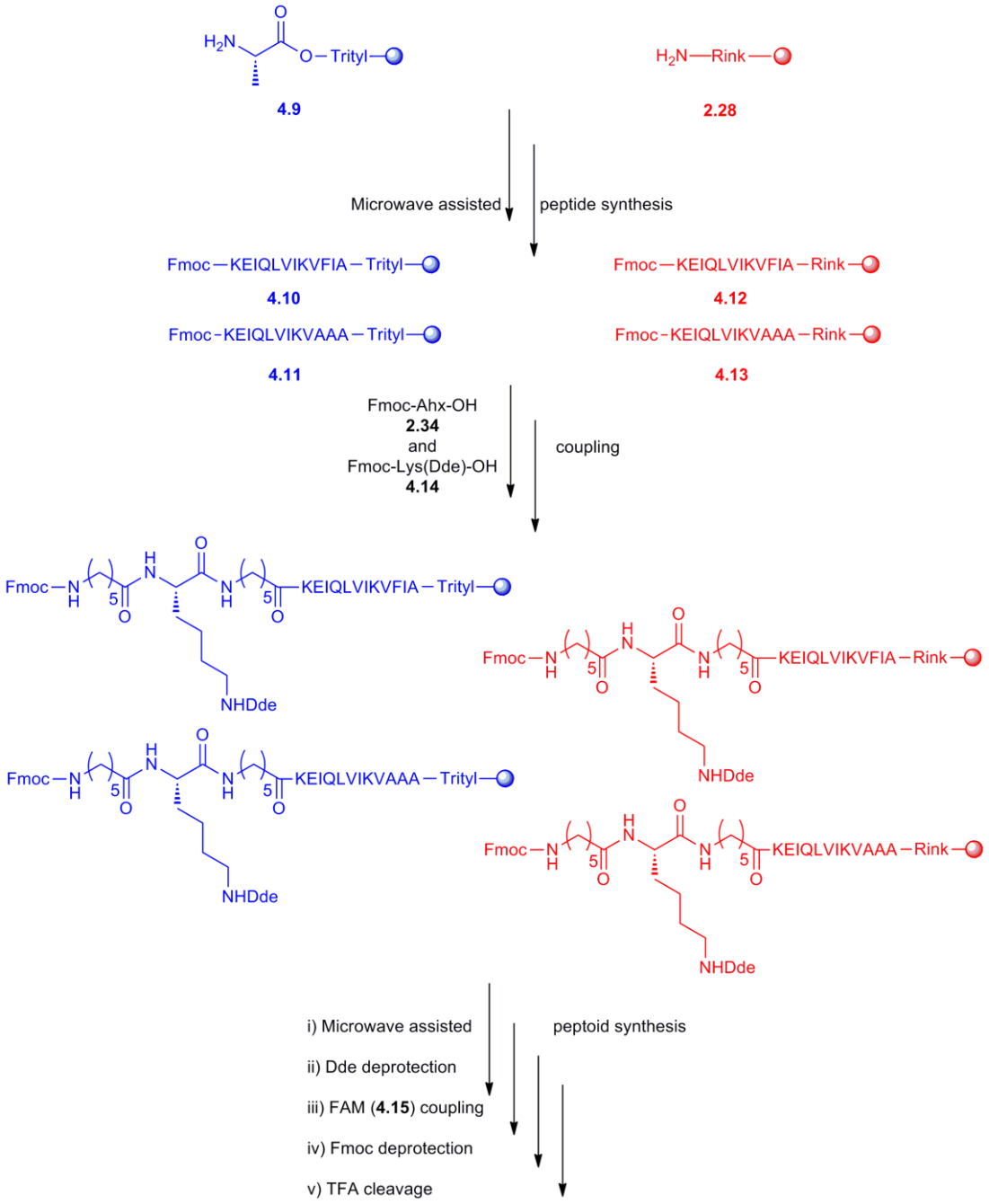

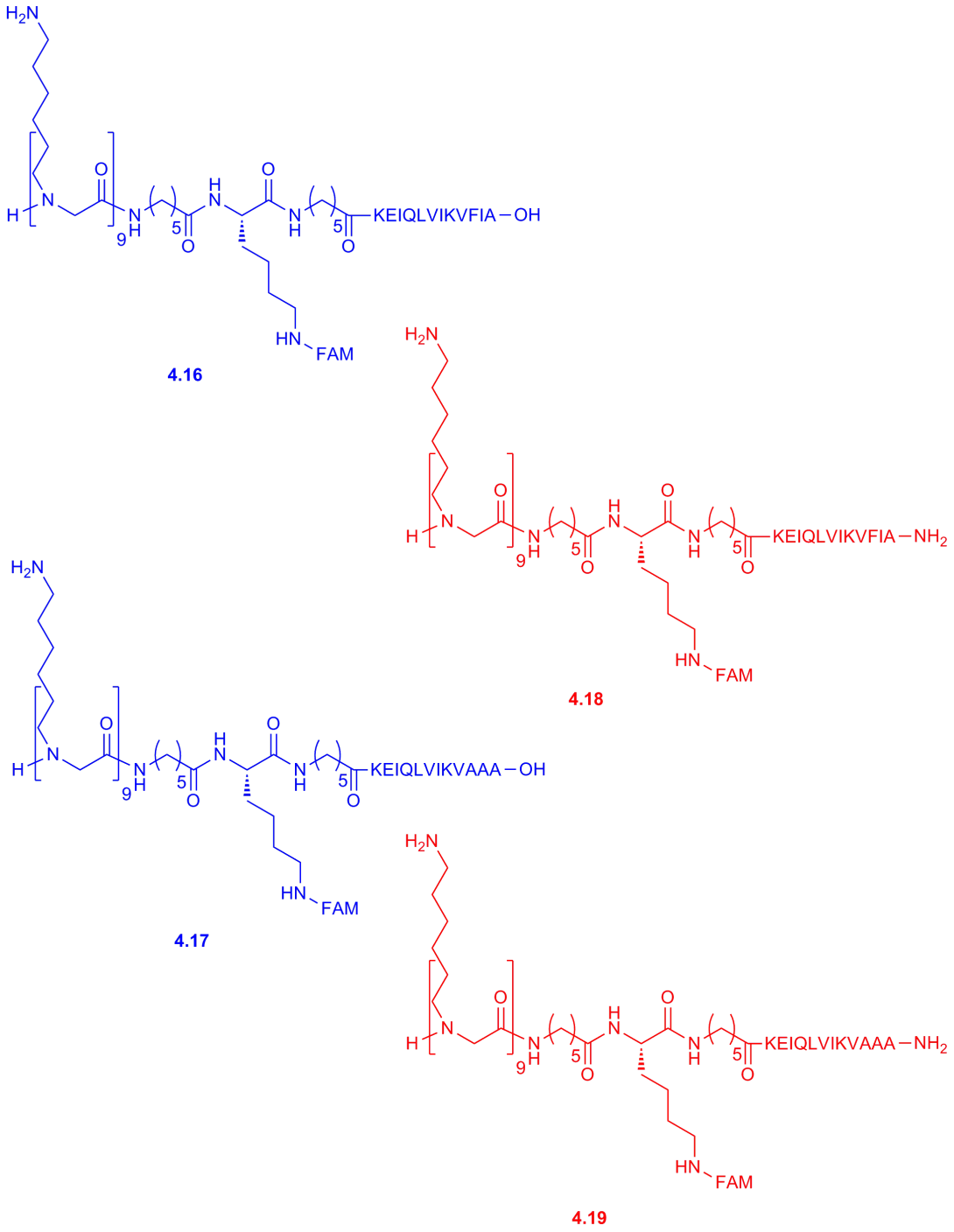

Scheme 4.3: Synthesis of the Fluorescein peptide-peptoid hybrids (4.16, 4.17, 4.18 and 4.19). Acid peptide-peptoid synthesis in blue using Trityl PS resin and amide peptide-peptoid synthesis in red using Rink amide PS resin. *Reagents and conditions:* Coupling of amino acids, Fmoc-Ahx-OH (**2.34**), Fmoc-Lys(Dde)-OH (**4.14**) and peptoid monomer (**2.22**): Acid (3 eq), HOBt (3 eq), DIC (3 eq) in DMF (0.2 M), µw 20 minutes, 60°C; Fmoc deprotection: 20% piperidine in DMF, 2 cycles of 10 minutes, rt; Selective Dde deprotection: $NH_2OH.HCl$/imidazole in NMP/CH_2Cl_2, 3 hours, rt; Coupling of 5(6)-carboxyfluorescein (**4.15**): FAM (5 eq), HOBt (5 eq), DIC (5 eq) in DMF (0.2 M), 4 hours, rt followed by washings with 20% piperidine in DMF; Cleavage and deprotection: For **4.16** and **4.17**, TFA/DCM/TIS (90: 5: 5), 2 hours, rt; For **4.18** and **4.19**, TFA/TIS/H_2O (95: 2.5: 2.5), 4 hours, rt.

The peptide sequence and the cell penetrable peptoid were separated from each another using two units of the aminohexanoic acid spacer (Fmoc-Ahx-OH, **2.34**) and one Fmoc-Lys(Dde)-OH (**4.14,** prepared from Fmoc-Lys-OH and DdeOH **4.20**) which was used as the attachment point for the 5(6)-carboxyfluorescein (**4.15, Scheme 4.3)**. The nine units of lysine-like N-substituted glycine were coupled using the monomer **2.22**.

The 5(6)-carboxyfluorescein **4.15** was attached to the side chain of the Lys spacer. The Dde group was deprotected using a mixture of hydroxylamine ($NH_2OH.HCl$)/imidazole in *N*-methyl-2-pyrrolidone (NMP)/DCM.[204] The 5(6)-carboxyfluorescein coupling was carried out over 4 hours using 5 equivalents of **4.15**, DIC and HOBt in DMF (0.2 M). The excess of dye and Fmoc group were removed by an hour treatment of the resin with 20% piperidine in DMF.[205]

The fluorescein peptide-peptoid hybrids were cleaved and deprotected using TFA/TIS/DCM (90: 5: 5) for 2 hours (**4.16** and **4.17**) or TFA/TIS/H_2O (90: 2.5: 2.5) for 4 hours (**4.18** and **4.19)**. After precipitation in cold diethylether, they were purified by preparative HPLC (**Table 4.2**).

Peptide-peptoid hybrids	Yield (%)	Purity (%)
4.16	58	99
4.17	69	98
4.18	79	100
4.19	75	100

Table 4.2: Yields and purities of the peptide-peptoid hybrids.
Yields were calculated from the loading of respectively the resin **4.10, 4.11, 4.12** and **4,13**; Purities were measured by HPLC (ELSD).

4.1.3. *In vitro* delivery and cytotoxicity assays of the peptide-peptoid hybrids

The cellular uptake of the fluorescein peptide-peptoid hybrids was tested in HeLa cells. For comparison, the peptide **4.21** (synthesis from the resin **4.10**, **Figure 4.4,**

yield = 66%, purity ELSD = 99%) was used as negative control, while the peptoid **4.22** (Fluo-9mer**, Figure 4.4**)[104] as positive control.

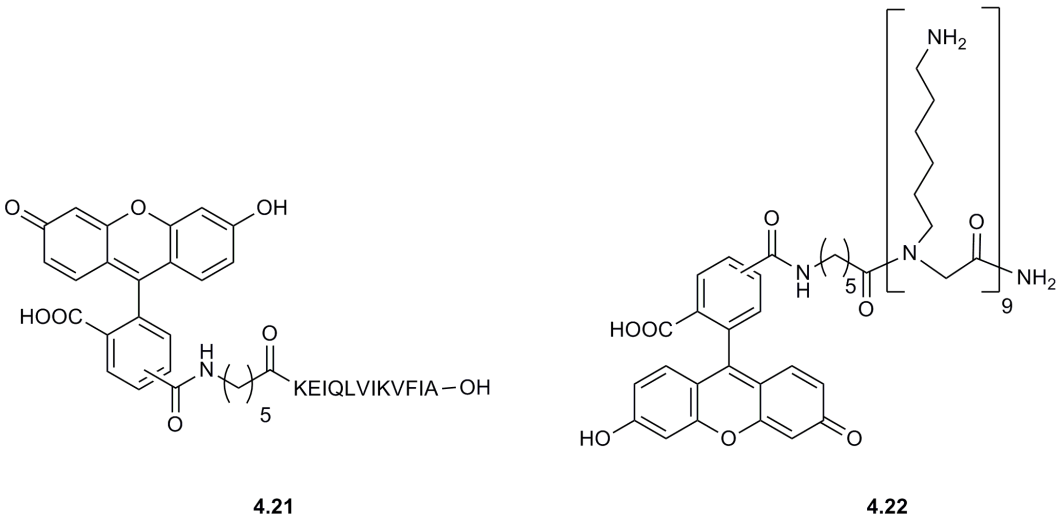

Figure 4.4: Structure of the peptide 4.21 and the peptoid 4.22 (Fluo-9mer).

The peptoids **4.16**, **4.17**, **4.18, 4.19** and **4.22** were dissolved in PBS while the negative control **4.21** was dissolved using 10% of DMSO in PBS. Each probe was incubated with HeLa cells at a concentration of 10 µM. Incubations were run over 2 and 24 hours (**Graph 4.1**).

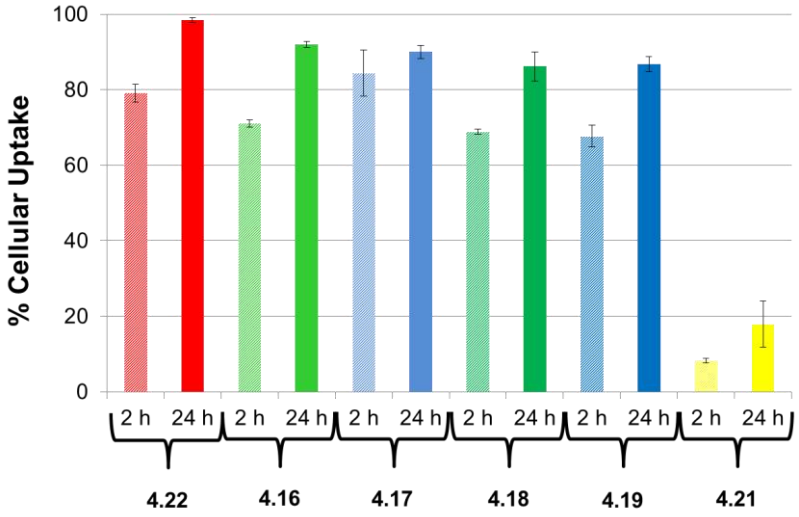

Graph 4.1: Uptake of the Fluorescein peptide-peptoid hybrids.
% uptake measured for peptide-peptoid hybrids (**4.16**, **4.17**, **4.18** and **4.19**), the peptide (**4.21**) and the Fluo-9mer (**4.22**). The % of cells with a fluorescent emission exceeding untreated cells as 0% uptake. The cells were treated with 10 µM of the desired compound for 2 and 24 hours prior to analysis. The errors bar represents the standard error of the average (n = 3).

Uptake was found to be high for the peptide-peptoid hybrids and the positive control **4.22** with at least 69% of labelled cells during the two first hours of incubation with the hybrids **4.19**. As expected, the cellular uptake was dependent on incubation time with longer incubation times resulting in higher uptake (85% after 24 hours with the hybrid **4.18)**. Results were confirmed by microscopy (**Figure 4.5**). Unsurprisingly, the negative control **4.21** penetrated very poorly into the cells.

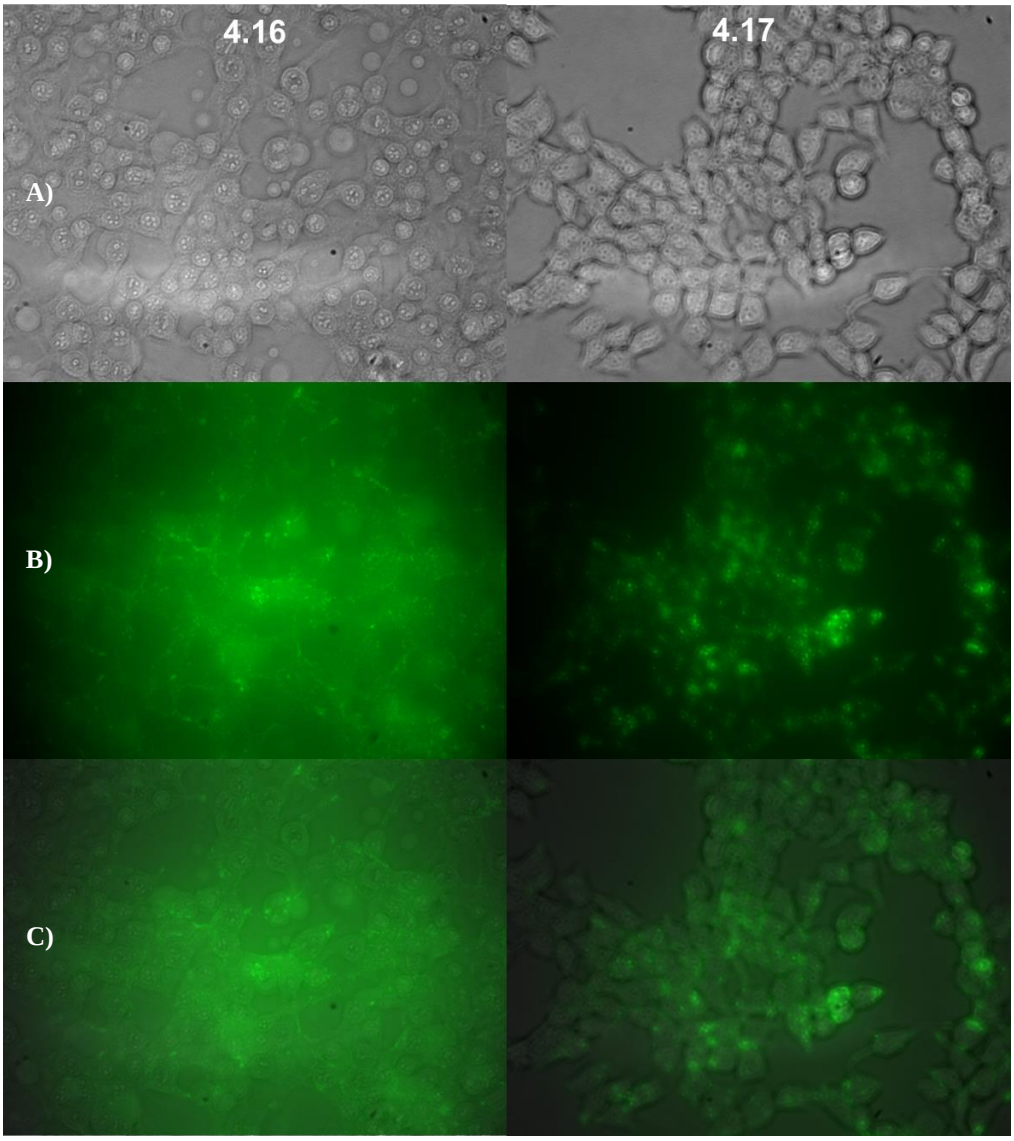

Figure 4.5: Live HeLa cells imaging.
These images were taken after incubation of the HeLa cells for 4 hours at 37°C with 10 µM of peptoid-peptide hybrids **4.16** and **4.17**. A) Brightfield image; B) Fluorescent image (Fluorescein excitation 450-490 nm); C) Fluorescence image merge with brightfield.

Graph 4.2 summarises, the effect of various concentrations (5, 10 and 20 µM) of peptoid-peptide hybrids **4.16**, **4.17**, **4.18, 4.19** and Fluo-9mer (**4.22)** on the health of HeLa cells. After 24 hours of incubation, only compound **4.18** showed any noticeable cytotoxicity but only at 20 µM with 75% of cells still viable. **4.16** showed some reduction in cell viability, but this was within experimental error. These results were unsurprising as the binding of the peptide should lead to cell apoptosis. Indeed, if as expected the peptide binds with the C-terminus of MDM2 (Ring finger), the E3 ubiquitin ligase activity is inhibited and the p53 is not degraded anymore, therefore, the amount of p53 increases.

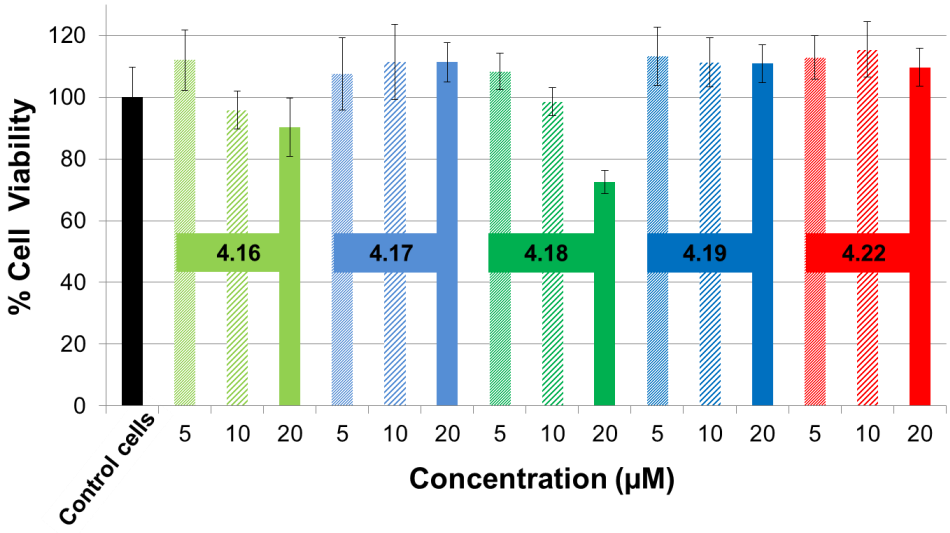

Graph 4.2: MTT assays to evaluate the cytotoxicity of peptoid-peptide hybrids and Fluo-9mer peptoid.
HeLa cells in presence of 5, 10 and 20 µM of **4.16**, **4.17**, **4.18**, **4.19** and **4.22** for 24 hours. The errors bar represents the standard error of the average (n = 6).

4.1.4. Conclusions

The four fluorescein peptide-peptoid hybrids (**4.16**, **4.17**, **4.18** and **4.19**) were successfully synthesised via solid-phase microwave assisted synthesis with a yield between 59% and 79%. The cellular uptake of these probes was shown by flow cytometry and microscopy. These results demonstrated and confirmed the ability of the 9mer peptoid as a cellular transporter for peptides. As the delivery of this specific peptide-sequence was never published, the comparison with another delivery system cannot be done. Nevertheless, the peptide-peptoid showed a cellular uptake

equivalent to the one of the Fluo-9mer peptoid, which contained a smaller cargo. The probes were transferred to the Ball group where they are being analysed to test their binding effects with the Ring domain of MDM2. Assays (cellular uptake and apoptosis study) are being carried out on a selection of cell lines derived from the human tumour cell line (NCI 60 panel).

4.2. Green Fluorescent Protein delivery

4.2.1. Green Fluorescent Protein: discovery and applications

Green fluorescent protein (GFP) is a chemiluminescent protein, which was first described in 1962 by Shimomura. GFP, a 238 amino acids protein, was isolated from the *Aequorea* jellyfish. When exposed to light (~ 400 nm), GFP emits bright green fluorescence with an emission at 508 nm.

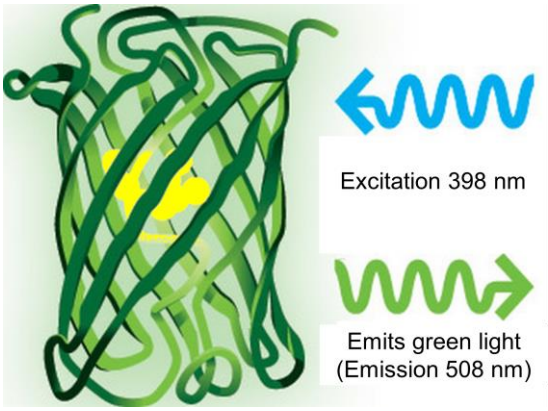

Figure 4.6 : GFP, 3D structure.
3D structure of GFP in which the yellow component corresponds to the chromophore.
[Modified with permission, **Appendix 1**]

The fluorescence was identified to come from a chromophore located in the 11-strand β-barrel. The 4-(*p*-hydroxybenzylidene)-imidazolid-5-one chromophore (**4.23**) is formed, in the presence of oxygen, by the intramolecular autocatalytic cyclisation of 65Ser-Tyr-Gly67 (formation of the imidazolidone moiety by backbone condensation of the amide nitrogen of Gly67 and the amide carbonyl of Ser65).[206]

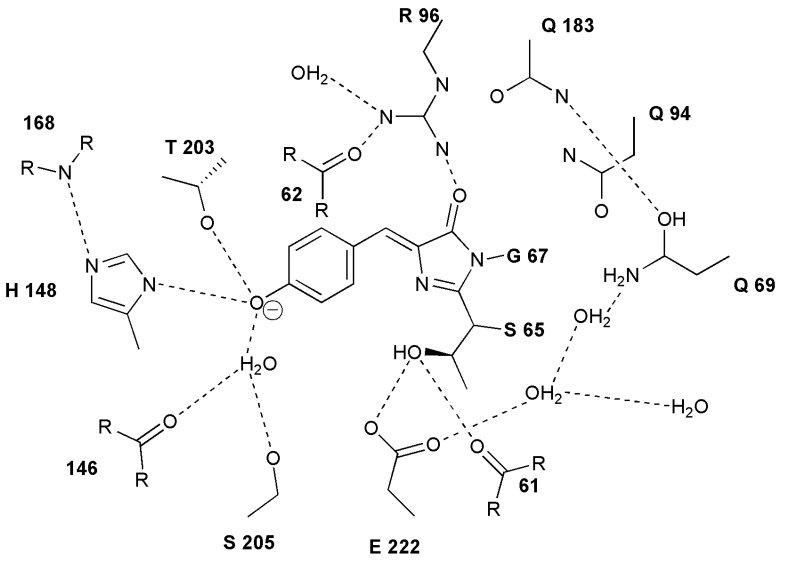

Figure 4.7: GFP, chromophore structure.
Chemical structure of GFP chromophore **4.23** (one-letter code and number for side chains amino acid and number alone for main chain).[207]

Nowadays, GFP is a common tool in molecular biology, medicine and cell biology, as a: [207, 208]

- Protein tag to visualise and locate proteins of interest within living organism,
- Flurorophore for FRET systems to study cellular mechanism (e.g. lipid metabolism),
- Gene reporter to analyse the activity of a specific gene,
- Biomarker of tumour cells to track their migrations.

The importance of this protein was acknowledged by the Nobel Prize in Chemistry 2008 for O. Shimomura, M. Chalfie and R. Y. Tsien.[209]

4.2.2. Previous GFP delivery

For several applications of GFP, it is essential to take the protein inside cells. One way to achieve this could be by using cell penetrating peptides. These carriers could directly deliver the protein or the DNA (plasmid) encoding GFP. eGFP is a popular synthetic version of the original protein in which the Ser65 was substituted with a Thr, Ala or Gly resulting in an increase of the excitation from ~400 nm to ~ 488

nm.[207] In 2007, eGFP was delivered into HeLa cells using a mixture a polyarginine and lipids. The principle of this technique was based on the delivery of nucleic acids such as plasmid DNA using multifunctional envelope-type nano device (MEND).[210] The eGFP was delivered into cells after formation of 3 layers particles around the protein. The eGFP was first condensed thanks to stearyl-R_8. This first layer interacted with the protein via electrostatic interactions between the positive charges of the poly-arginine and the negative charges of the protein (aspartic and glutamic acid) while the stearyl acid, with hydrophobic character formed a lipid layer. The second layer, a mixture of DOPE/CHEMS (1,2-dioleoyl-*sn*-glycero-3-phosphoethanolamine (**Figure 1.8**)/cholesteryl hemisuccinate **4.24 (Figure 4.8)**, 9:2) was used to form the MEND. However, this structure cannot cross the cell membrane without a positively charge surface made by a final treatment on stearyl-R_8 (third layer). The nanoparticles were delivered into HeLa cells with cellular uptake confirmed via Western blot analysis and confocal laser scanning microscopy.[211]

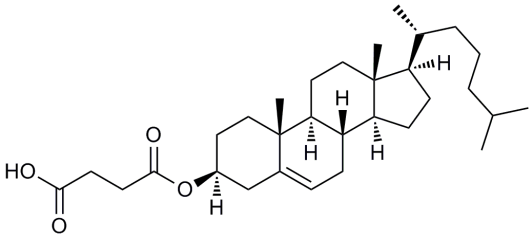

4.24

Figure 4.8: Structure of CHEMS (4.24) used for the GFP-R_8-MEND (DOPE).

GFP was also delivered via protein transduction.[212] This technology, first described in 1988,[213] allows the internalisation of protein thanks to the synthesis of fusion proteins between a known protein or peptide being able to penetrate into cells (CPP or PTD) and the protein of interest. TAT-mediated GFP transduction was carried out in several cell types including primary brain cells,[214] mitochondria of breast cancer cells[215] and protozoan parasites.[216] The GFP-TAT proteins were prepared via expression of a modified vector. The TAT sequence was usually on the C-terminus while the purification sequence (hexahistidine-tag) was located on the N-terminus. In addition to the purification tag, the GFP-TAT protein could also be fused with

another protein or peptides. For instance, in a project aiming at labelling of mitochondria of breast cancer cells, the original GFP was modified with a mitochondrial targeting signal (MTS) on its N-terminus and the TAT sequence on its C-terminus.[215215] Even though, GFP transduction was mainly mediated by TAT, papers also reported the use of transportan,[217] penetratin[218] and others CPPs.[219]

As far as peptoid cellular transporters are concerned, only one GFP delivery device has been reported in the literature. The conjugation of the hexahistidine (His6) tag present on the protein to a heptalysine-like peptoid functionalised with two Ni^{2+} ligands (**4.25**, **Figure 4.9**). However only 8.6% (flow cytometry data) of B16F10 cells were labelled after 24 hours incubation using 10 µM of the heptapeptoid-Ni^{2+}-GFP complexes. The confocal microscopy images confirmed this result as most of the complexes were located in the membrane.[131]

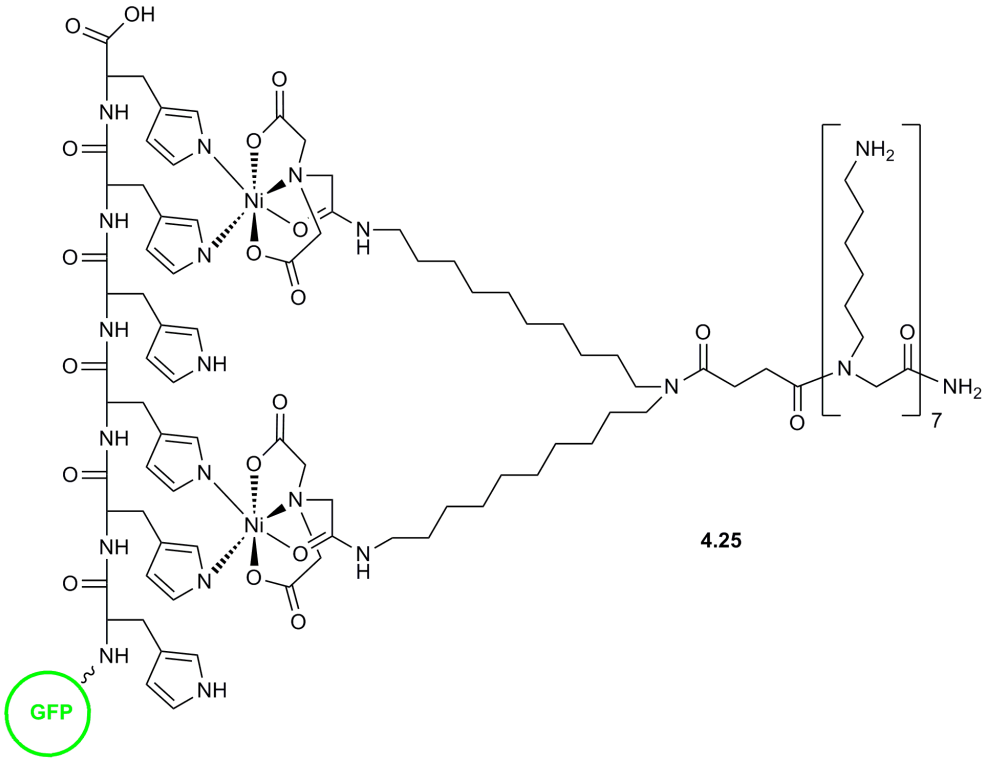

Figure 4.9: Structure of the heptapeptoid-Ni^{2+}-GFP complex.

So far, the cellular delivery of protein (GFP as a model) has not been tested using a covalent attached cell penetrating peptoid. Therefore, one of the aims was to deliver

GFP using a peptoid via the formation of two types of covalent bond a thiol-maleimide or an active ester.

4.2.3. GFP delivery via thiol-maleimide chemistry

4.2.3.1. Thiol-maleimide chemistry an efficient bioconjugation technique

For decades, maleimides **4.26** (maleic acid imides, **Scheme 4.4**) have been used as crosslinking agent (substance that allows the colavent bonding of two structures together) for protein modifications. Maleimides are the product of the reaction of maleic anhydride **4.27** and ammonia or any primary amine (**Scheme 4.5**). Since the middle of the 70s, this chemical structure has been used as an alkylation trap for sulfonyl groups. Even though, the maleimide can react with the amino group of peptides or imidazole of histidine, the nucleophilic attack on the double bond of the maleic acid imides by the thiolate anion of cysteine is 1000 times faster than by any amine. The optimal pH to create a thioether linkage using this agent is between 6.5 and 7.5. Above this pH, alkylation of the maleimide with an amine group tends to dominate.

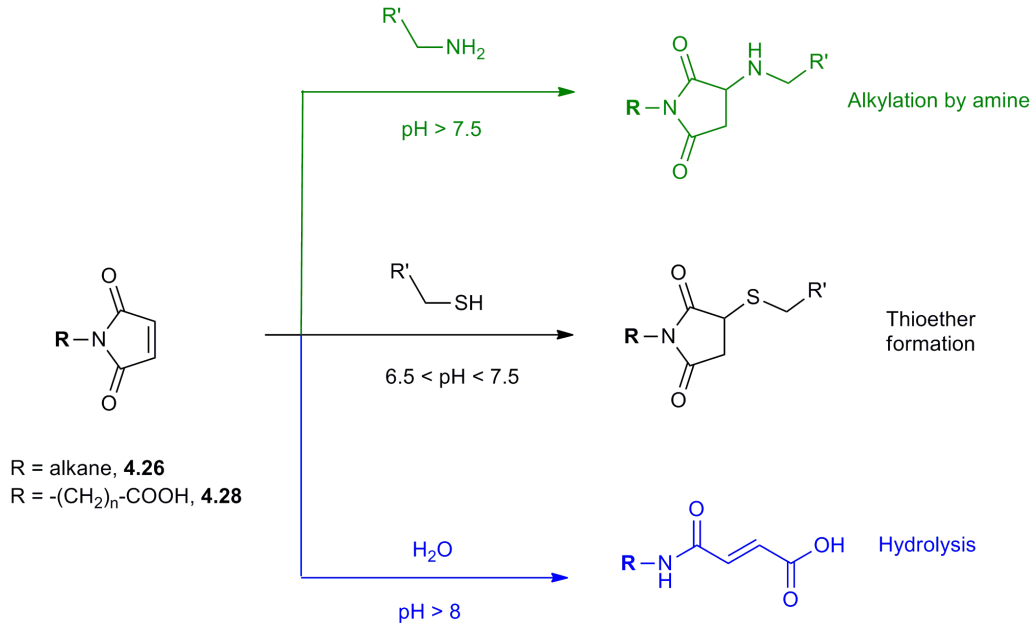

Scheme 4.4 : Reactivity of the maleimide compounds.

The reaction of the maleic anhydride with an aminoalkaloic acid, such as glycine or 4-aminobutanoic acid, produced an maleimidoalkanoic acids **4.28**. This type of crosslinking agent offers two orthogonal bonding spots. First, the activated carboxylic acid (via, for example, a *N*-hydroxysuccinimide ester) can react with primary or secondary amine group to create an amide bond and then the thiol can attack the double bond of the maleimide. Nevertheless, maleic acid imides have one major backdrawn, hydrolysis. Water can react with the compound leading to the opening of the heterocycle and to the loss of reactivity.[220, 221]

For this project, a Cys-GFP was used to couple to a nonalysine-like peptoid functionalised with a maleimidoalkanoic acid.

4.2.3.2. Cys-GFP expression

For this project, a modified GFP (Cys-GFP, **4.29**) was used and produced using recombinant DNA technology (rDNA). The plasmid for the His6-Cys-GFP (**4.30**) was prepared by Dr David Nagel (**Appendix 4-1**) and contained a His6 tag to purify the protein, a Asp-Asp-Asp-Asp-Lys enterokinase specific cleavage sequence (to remove the His6 tag)[222] and a final Cys on its N-terminal separated from the GFP by a $(Ser\text{-}Gly)_6$ spacer (**Appendix 4-2**)

The plasmid encoding His6-Cys-GFP (**4.30**) was transformed into BL21(RPS)DE3 (*E.Coli* strains) competent cells using a heat shock technique (succession of hot and cold shock to open the cell membrane). The modified GFP (**4.30**) was then expressed within the bacterial cells by the addition of isopropylthio-β-galactoside (ITPG, **4.31,** 1mM). IPTG binds to the *lac* repressor (*lacI*, from the *E. coli* genome of modified strains only) leading to the production of T7 RNA polymerase. This polymerase then binds with the T7 promoter on the pET system resulting in the transcription of the target DNA. The SDS-PAGE (sodium dodecyl sulfate - polyacrylamide gel electrophoresis) gel clearly showed the presence of the GFP (**Figure 4.11-A**, white circle line 2). The His6-Cys-GFP (**4.30**) was purified using Ni-NTA agarose beads. After purification, the protein **4.30** was released from the beads using a buffer rich in imidazole (250 mM) (**Figure 4.10**).

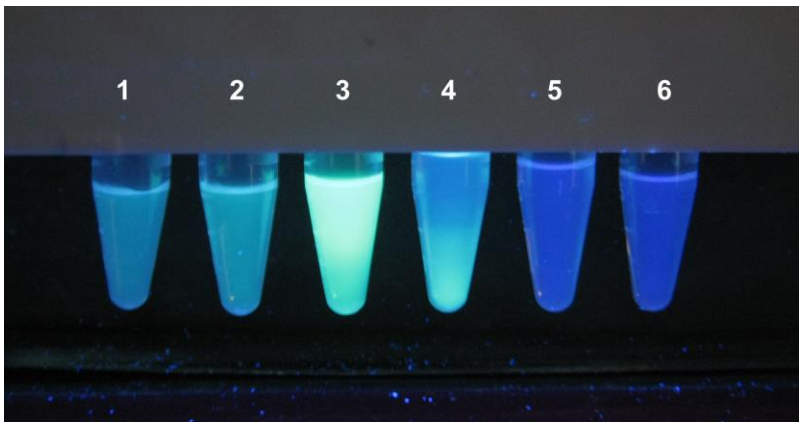

Figure 4.10: Images of the fractions of His6-Cys-GFP (4.30) eluted from the Ni-NTA beads. Picture taken under light of transilluminator (λ = 365 nm). Fractions 3 and 4 contained the protein **4.30**.

The His6 tag was cleaved from the protein using a protease which cleaves selectively after the Lys of this sequence Asp-Asp-Asp-Asp-Lys. Finally the Cys-GFP **4.29** protein was desalted using a PD 10 column and concentrated using an Amicon ultra-4 3000 Da centrifugal filter.

A)

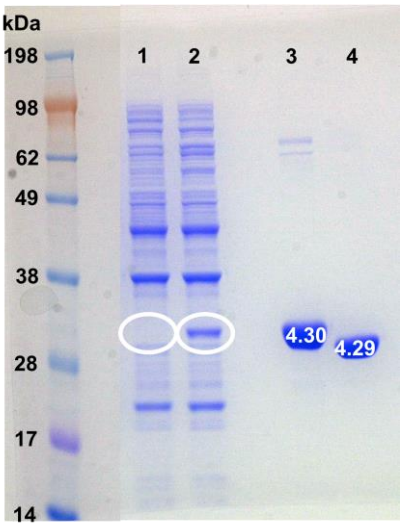

B)

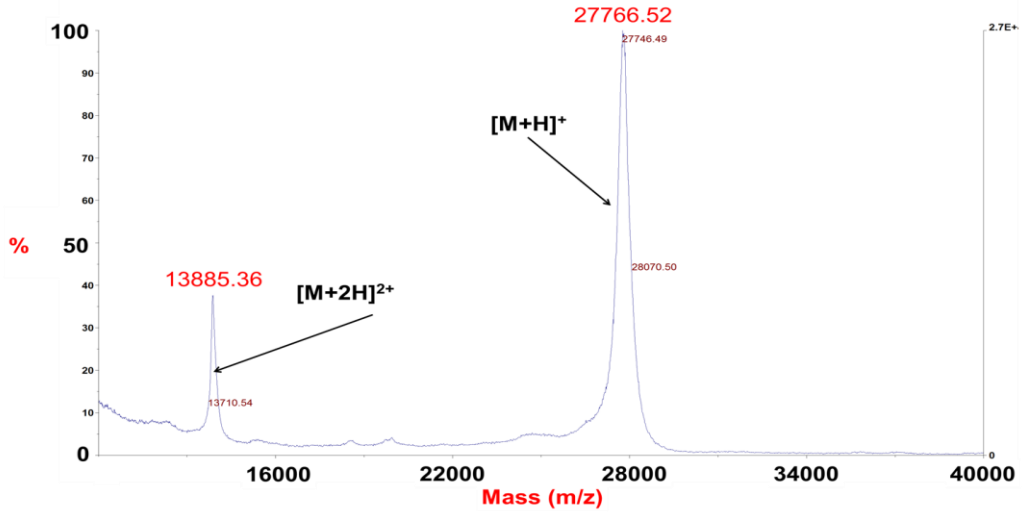

Figure 4.11: Analysis of the Cys-GFP protein (4.29).
A) SDS-PAGE analysis (lanes left to right): Marker See Blue® Plus 2 prestained; **1**. Products of cell lysis without IPTG induction, no GFP **4.30** band in the white circle; **2**. Product of cell lysis with IPTG induction, GFP **4.30** band in the white circle; **3**. His6-Cys-GFP **4.30** after purification; **4**. Cys-GFP **4.29** after cleavage of the His6 tag and final purification. B) MALDI-TOF spectrum of the Cys-GFP **4.29**.

The Cys-GFP **4.29** was analysed via SDS-PAGE and by MS (MALDI-TOF, **Figure 4.11**).

4.2.3.3. Synthesis of maleimide-9mer

Several synthesis of **4.34** (6-maleimidocaproic acid) have been described in the literature including the original by Rich[223] and its modified version by Marnett[224]

(**Scheme 4.5**). Only Christmann has published a large scale synthesis of maleimidoalkanoic acids **4.28**. In addition to the large scale production of the desired maleimide, this synthesis has the advantages of being carried out in one step and without chromatography purification. The 6-maleimidohexanoic acid **4.34** was synthesised using aminocaprioic acid (**4.32**) and the maleic anhydride (**4.27**) in acetic acid. The mixture was heated to reflux for 90 minutes. The desired maleimide **4.34** was isolated after aqueous work up and recrystallisation with a yield of 46% (**Scheme 4.5**).[225]

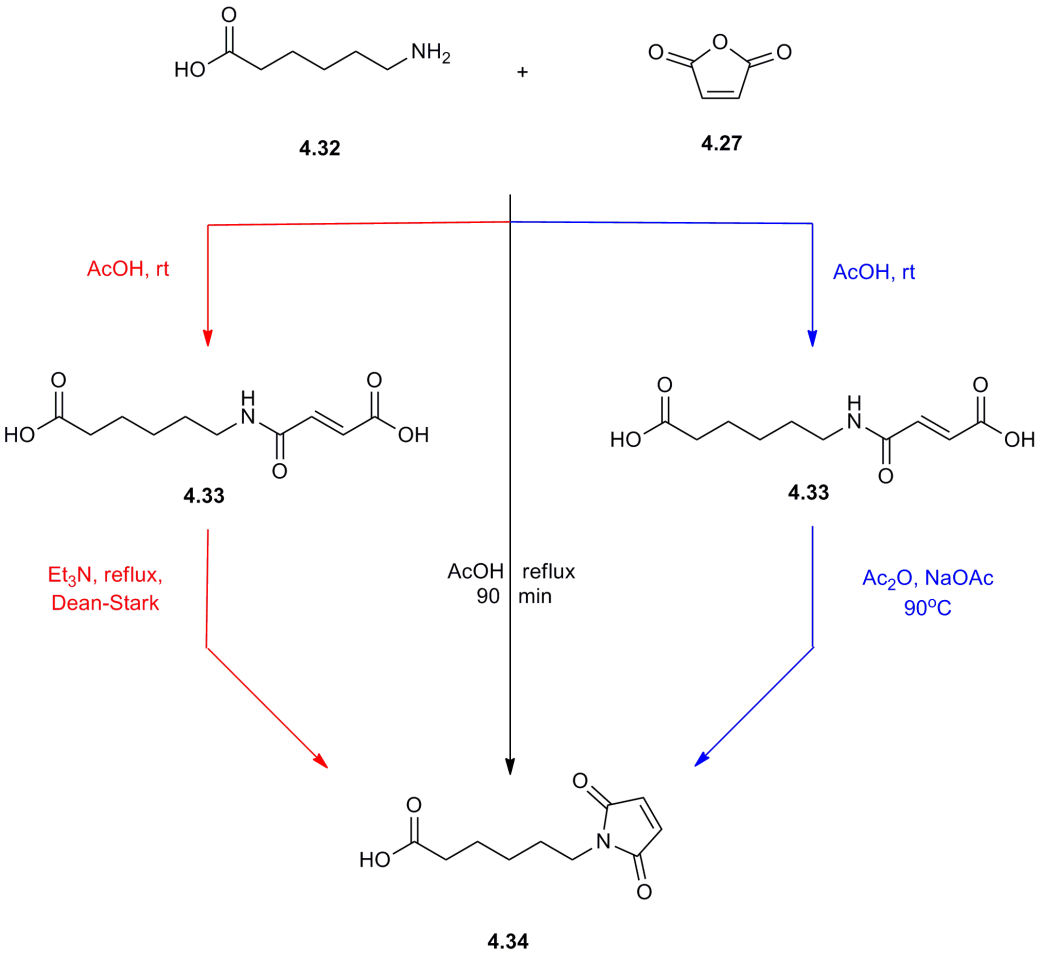

Scheme 4.5: Synthesis of 6-maleimidohexanoic acid, 4.34.
In red: Rich synthesis; In black: Christmann synthesis; In blue: Marnett synthesis.

The maleimide-9mer peptoid (Mal-9mer, **4.35**) was synthesised by coupling of 6-maleimidohexanoic acid **4.34** on the resin **2.35** previously Fmoc deprotected. The maleimide-9mer peptoid **4.35** (Mal-9mer) was released from the solid support by

treatment of the resin with TFA/TIS/H_2O, 95: 2.5: 2.5, (**Scheme 4.6**) with a yield of 92% and a purity of 98% (ELSD, **Figure 4.12**).

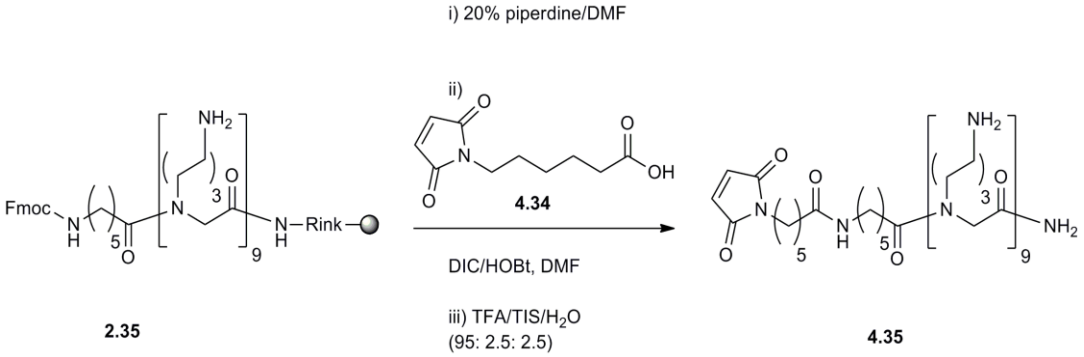

Scheme 4.6: Solid-phase synthesis of the maleimide-9mer, 4.35.

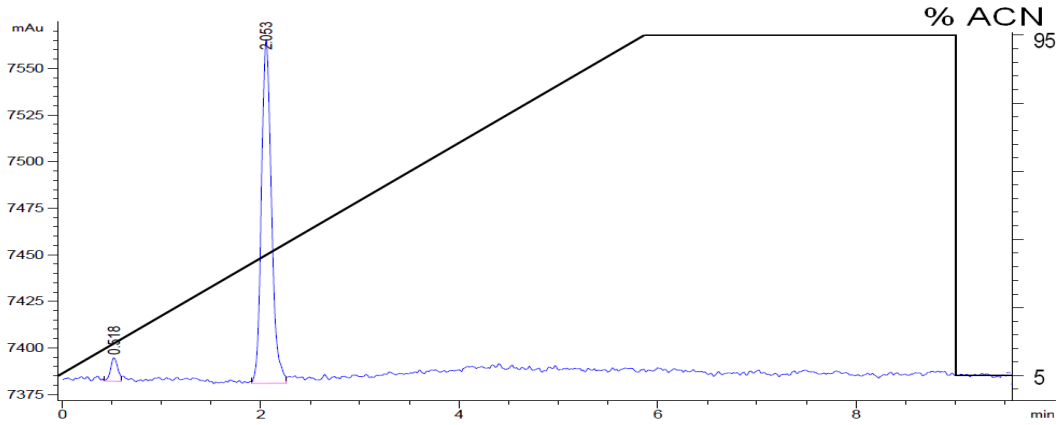

Figure 4.12: HPLC trace (ELSD) of the crude 4.35, purity 98%.

4.2.3.4. Preliminary coupling assays.

The capacity of the maleimide-9mer (**4.35**) to react with thiol compounds was tested using a modified rhodamine dye. 5-(6)-carboxyrhodamine **2.36** was functionalised with a thiol group using cysteamine (**4.36**) (**Scheme 4.7**). Cysteamine (5 equivalents) was coupled to 2-chlorotrityl chloride polystyrene resin (**4.5**) in the presence of DIPEA (5 equivalents) in DCM. The 5-(6)-carboxyrhodamine **2.36** was then attached to the primary amine of the resin **4.37** using a HOBt/DIC coupling and the thio-rhodamine **4.38** was cleaved from the solid support using TFA/DCM/TIS, 50: 45: 5 (yield = 82%, purity ELSD = 98%). The thio-rhodamine **4.38** was coupled to the

maleimide-9mer **4.35** in PBS (pH 7.0). For the coupling to work, it was essential to make sure that the pH of the peptoid solution was at 7.0. Indeed once the peptoid **4.35** was dissolved in PBS, the pH was measured as 3.6 therefore it was adjusted to pH 7.0 by addition of NaOH (1M). The thio-rhodamine was linked to the peptoid to give **4.39** (Rho-S-maleimide-9mer) with a yield of 96% (determined by HLPC analysis (ELSD), **Appendix 4-3**).

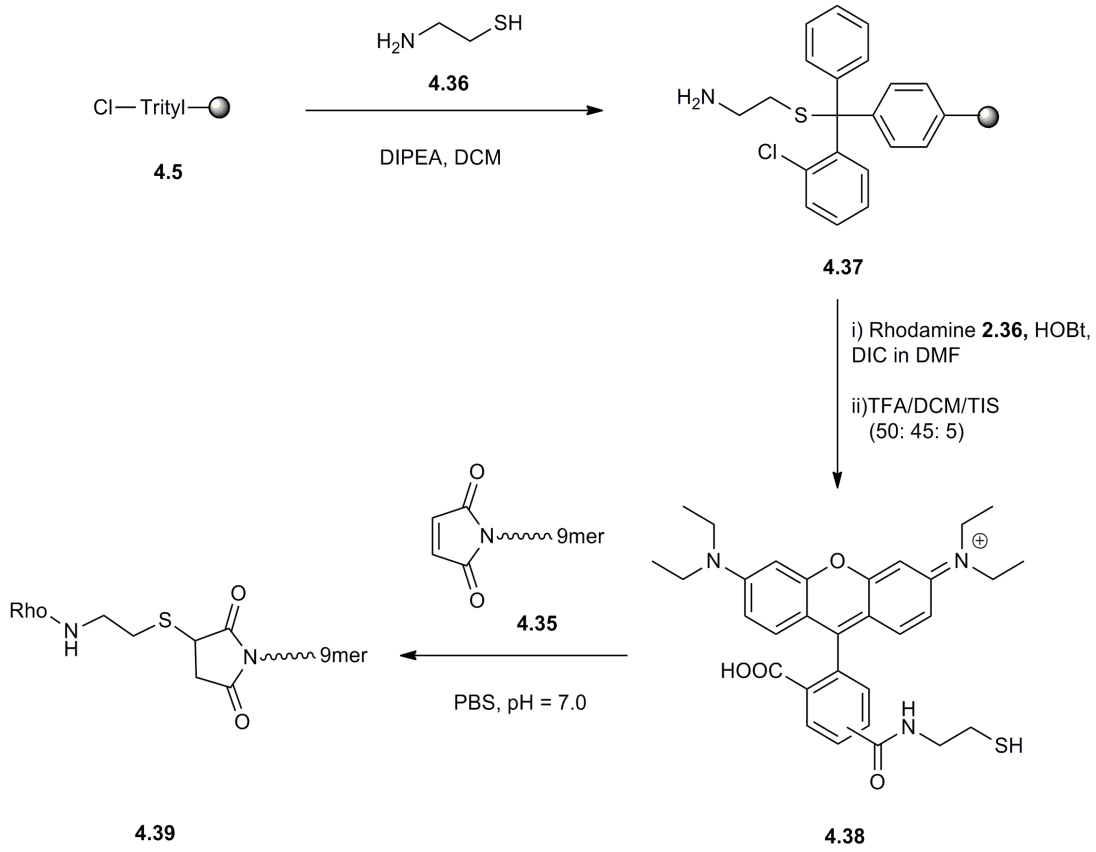

Scheme 4.7: Synthesis of the thiol-rhodamine (4.38) and test of its coupling with the maleimide-9mer (4.35).

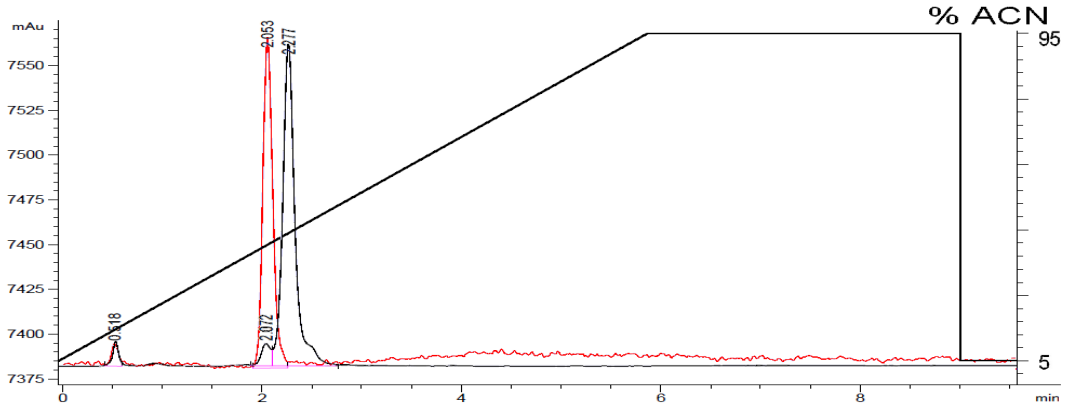

Figure 4.13: HPLC trace (ELSD) of the synthesis of the Rho-S-maleimide-9mer 4.39.
In red, the starting material (Mal-9mer, **4.39**); in black the reaction mixture after 16 hours at room temperature.

4.2.3.5. Cys-GFP delivery via single thiol-maleimide coupling

As the bio conjugation between the thio-rhodamine **4.38** and the maleimide-9mer **4.35** was a success, the previous protocol was repeated to link the GFP-SH **4.29** to the maleimide-peptoid (**Scheme 4.8**). However, the coupling did not work as analysed by SDS-PAGE gel and MS analysis (MALDI-TOF spectrum and SDS-PAGE gel, **Appendix 4-4**).

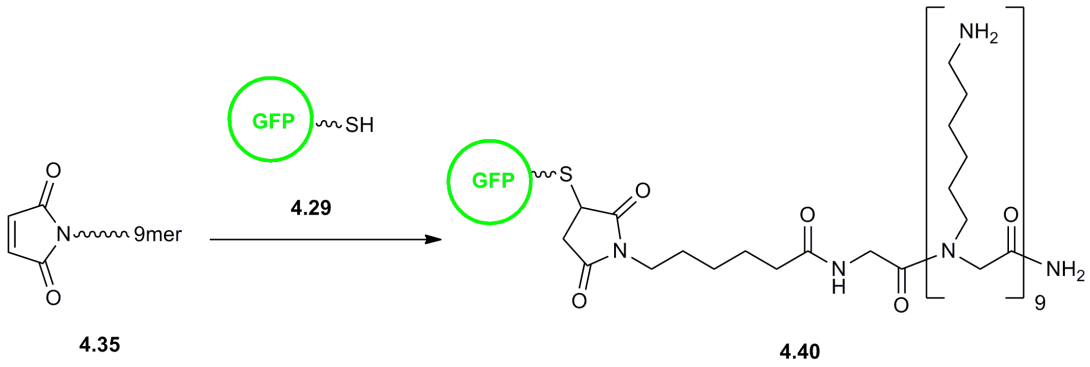

Scheme 4.8: Bioconjugation of the GFP-SH (4.29) with the maleimide-9mer (4.35).

The non-coupling of the Cys-GFP with the maleimide could be due to the formation of disulphide bonds between two molecules of Cys-GFP. Disulfide bonds can be completely reduced by dithiothreitol (DTT, **4.41**).[226, 227] For this project, the reducing conditions of the DTT must not denaturate the GFP.[207] Therefore, 10 equivalents of DTT were used at room temperature using a pH of 7.0. After

overnight reaction, the peptoid **4.35** was added to the reduced protein. An excess of 80 equivalents of maleimide-9mer was used to ensure maximum coupling (PBS, pH 7.0), as part of the maleimide would also be attacked by the unreacted DTT. However, the excess of peptoid leaded to precipitation of the protein. The precipitate was re-solubilised by the addition of PBS and the coupling was carried on for another ten hours. To remove uncoupled peptoid **4.35**, the coupling mixture was purified using two different techniques.

1. The reaction solution was placed in a dialysis tube with a molecular weight limit of 10 000 daltons. The comparison between the lane 2 (without purification) and 3 of the SDS-PAGE gel (**Figure 4.14-A**) clearly showed that this technique decreased the amount of free peptoid. Purification was incomplete.

2. The protein was purified using a SpinTrap G-25 (centrifugation, **Figure 4.14-B**). The SDS gel (**Figure 4.14-A**, lane 2 (without purification) and 4) proved that the majority of the unreacted peptoid was removed from the reaction. This technique offered several advantages; firstly the purification time was very short as the sample was centrifuged 4 × 5 minutes with addition of fresh PBS for each centrifugation cycle. Secondly, the loss of protein can easily be analysed. If the protein passed through the 5000 Da filter, the fluorescence was observed at the bottom of the tube. Finally, this technique allowed concentration of the protein to the desired volume. Using DTT and 80 equivalents of peptoids, the coupling product (**4.40**) was obtained. Indeed, the SDS-PAGE (**Figure 4.14-A**) showed the presence of a second band on top on the Cys-GFP. This result was confirmed by MS analysis (MALDI-TOF, **Figure 4.14-C**).

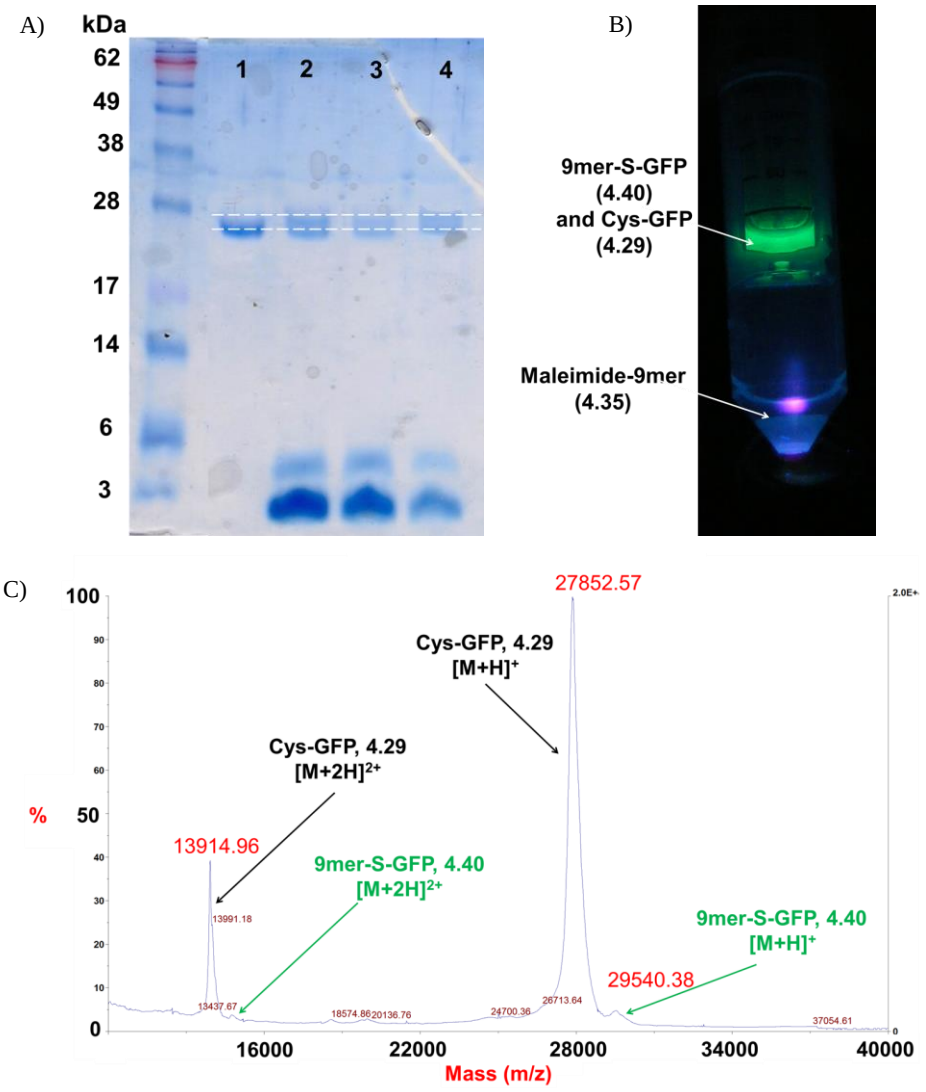

Figure 4.14: SDS-PAGE gel of the coupling with DTT and 80 equivalents of peptoid 4.35. A) SDS-PAGE analysis (lanes left to right): Marker See Blue® Plus 2 prestained; Lane **1:** untreated GFP **4.29**; **2:** Coupling reaction without purification of the peptoid excess; **3**: Coupling reaction with purification of the peptoid excess by dialysis; **4:** Coupling reaction with purification of the peptoid excess by centrifugation. B) Image of the purification of the protein using SpinTrap-25. The picture was taken after 4 cycles of centrifugation.

Even though, the coupling efficiency was very poor, the use of DTT (**4.41**) and a major excess of Mal-9mer (**4.35**) clearly played a role in the formation of the conjugate **4.40**. One parameter that could have decreased the formation of the thioether between the maleimide and the Cys-GFP might be the precipitation of the protein due to the large excess of peptoid. For the first attempt of coupling, 10 equivalents of peptoid **4.35** (C = 0.28 mM) did not crash out the protein while, in the second attempt, 80 equivalents (C = 45 mM) of the maleimide-9mer leaded to the

precipitation of the GFP. Using these previous data, the best coupling was obtained using first 10 equivalents of DTT. After overnight reduction, the excess of DTT was removed by centrifugation and 25 equivalent of peptoid **4.35** were used to couple the Cys-GFP **4.29** in PBS (pH 7.0). The bioconjugation was carried out at room temperature for 16 hours. The reaction was followed by size exclusion purification. The presence of the 9mer-S-GFP **4.40** was confirmed by SDS-PAGE gel with the presence of a second band on top of the GFP trace. This result was also observed using MS analysis (MALDI-TOF, **Appendix 4-5**).

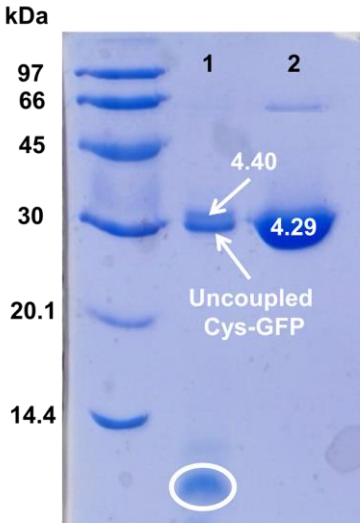

Figure 4.15: Analysis of the GFP bioconjugation with DTT and 25 equivalents of peptoid 4.35. SDS-PAGE analysis (lane left to right): LMW SDS marker; Lane **1**: Coupling reaction with purification of the peptoid excess by centrifugation; **2**: untreated GFP **4.29**

Although, the coupling efficiency was not optimal, the cellular uptake of the last attempt was tested. The coupling reaction (containing the bioconjugate **4.40**) purified from the excess peptoid was incubated for 24 hours with HeLa cells. As the 9mer-S-GFP (**4.40**) was not separated from the Cys-GFP (**4.29**), the uncoupled protein was also incubated with the cells as a negative control. The maleimide-9mer **4.35** was also used as a negative control.

A)

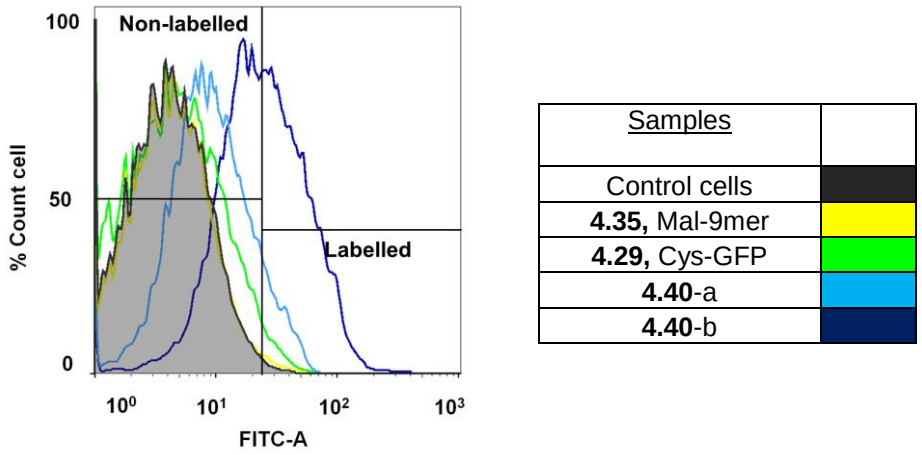

B)

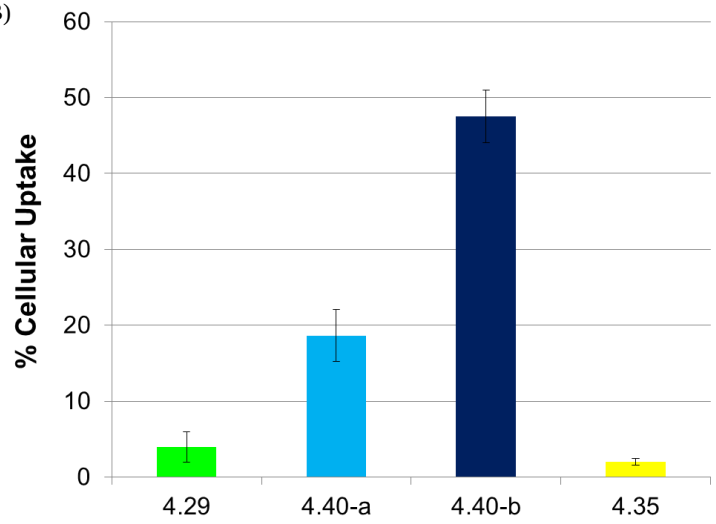

Figure 4.16: Flow analysis of cellular uptake of the bioconjugate 4.40 in HeLa cells.
A) Flow cytometry histogram of each sample after 24 hours; B) % uptake measured for the Cys-GFP (**4.29**, 6 µg/mL), 9mer-S-GFP bioconjugate (**4.40-a:** 2.7 µg/mL and **4.40-b:** 5.4 µg/mL) and maleimide-9mer (**4.35**, as negative control, 10 µM) as the % of cells with a fluorescent emission exceeding untreated control as 0% uptake (incubation time = 24 hours). The errors bar represents the standard error of the average (n = 6).

The flow cytometry analysis demonstrated cellular uptake of the bioconjugate with a maximum of 49% of labelled HeLa cells. For this experiment, the use of trypan blue to quench the external emission was essential as some of the bioconjugate and the uncoupled protein bound to the cell membrane. The cellular uptake of the bioconjugate (**4.40**) was confirmed using living cell microscopy after 24 hours (**Figure 4.17**). This result demonstrated the potential of the nonalysine-like peptoid as a cellular delivery device.

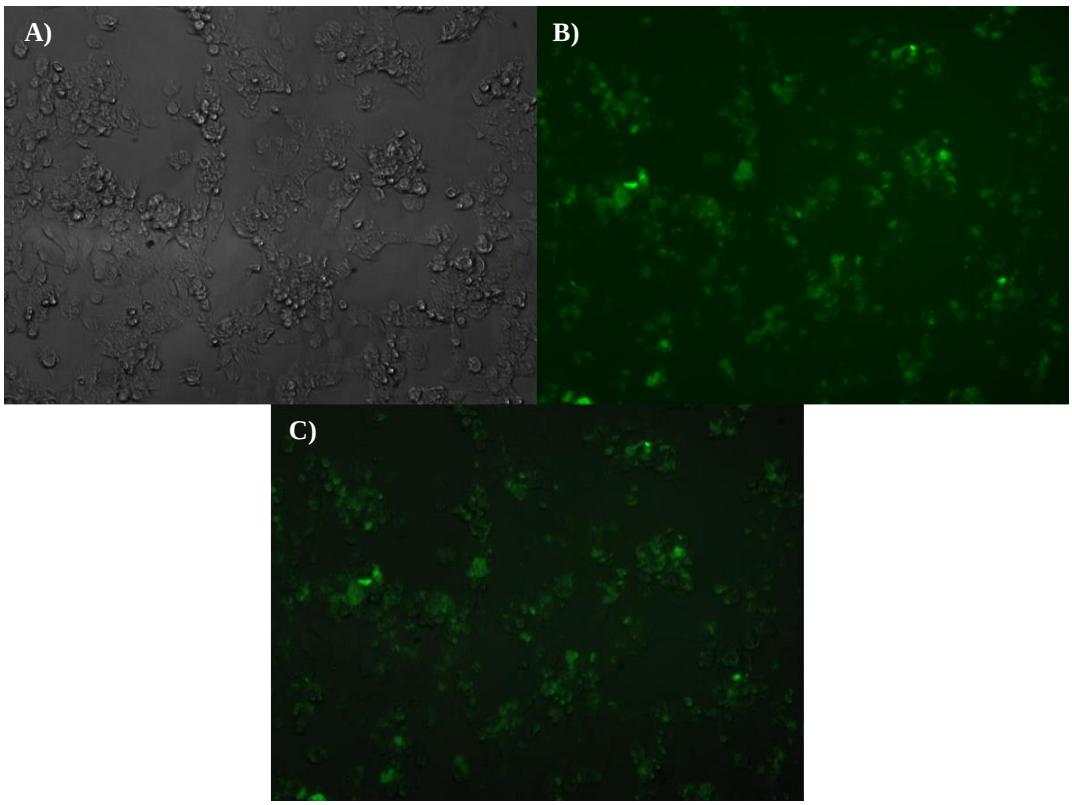

Figure 4.17: Fluorescence microscopy of HeLa cells.
These images were taken with a Leica fluorescent microscope after incubation of the HeLa cells for 24 hours at 37°C with the bioconjugate **4.40-b** (5.4 µg/mL). A) Brightfield image; B) GFP fluorescent image (excitation 450-490 nm); C) Fluorescence image merge with brightfield..

4.2.3.6. Cys-GFP delivery via multiple thiol-maleimide couplings

Although, cellular delivery of the Cys-GFP (**4.29**) was achieved using a single nonalysine-like peptoid, the cellular uptake remained under 50% mainly because of the poor bioconjugation of the protein with the cellular transporter. One solution could be to increase of the number of thiol groups within the protein.[228] Free sulfhydryl groups can be introduced to the first entity (protein) by reduction of disulphide bridges and/or thanks to a thiol generator.[229] A thiol generator is an organic compound that reacts with a free amine groups (e.g. a lysine side chain) resulting in the introduction of a new thiol. 2-iminothiolane (**4.42,** 2-IT, known as Traut's reagent) has been widely used to modify proteins and peptides[230] and was chosen as a thiolation agent. Thus Cys-GFP (**4.29**) was modified using 2-IT to increase the number of free sulfhydryl groups available. GFP contains 19 lysines which could potentially react with the 2-iminothiolane via a ring opening reaction to

create the modified GFP (**4.43**). Each sulfhydryl group could then form a thioether bond with one molecule of meleimide-9mer resulting in a new bioconjugate (**4.44,** $(9mer\text{-}S)_n$-GFP) (**Scheme 4.9**).

The first attempt began with the overnight modification of the Cys-GFP protein (**4.29**) with the 2-IT (**4.42**) at pH 7.4. The excess of thiolation agent was then removed and the buffer was exchanged for one at pH 7.0. The maleimide-9mer peptoid (**4.35**) was added and the overnight coupling reaction was analysed by SDS-PAGE gel and MS (**Appendix 4-6**). The analysis showed that none of the reactions worked (introduction of sulfhydryl groups via 2-IT reaction and coupling with the maleimide-9mer). The protein was not modified or at a very low level that could not be detected by any of these techniques (**Scheme 4.9**).

Studies have shown that the 2-IT modified 95% of ethanolamine in 100 minutes at pH 8 while 90% were thiolated in 6 hours at pH 6.5. Furthermore, Lambert et al. reported that the thiol adducts generated with 2-IT could be unstable.[230] The most efficient attempt was obtained when the thiolation reaction was carried out over 4 hours at room temperature. After removal of the excess of 2-IT, the protein was treated with DTT (**4.41**) for an hour. The protein was purified from the reducing agent and the maleimide-9mer (**4.35**) was added. After reaction, the reaction was analysed by SDS-PAGE and MS (**Figure 4.18**).

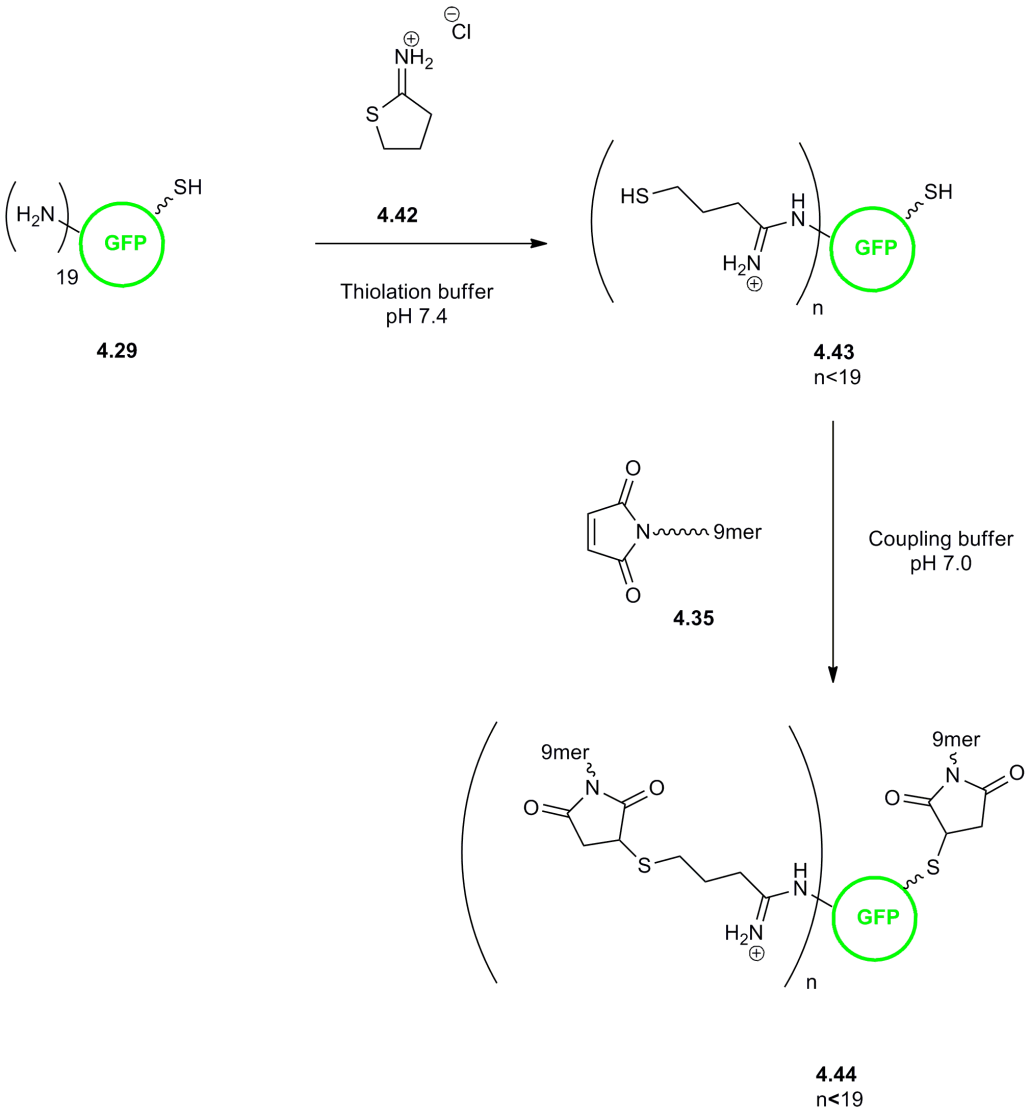

Scheme 4.9: Bioconjugation of the Cys-GFP (4.29) with peptoid (4.35) using 2-IT.HCl (4.42).

The SDS-PAGE gel (**Figure 4.18-A**) showed three bands for the reaction mixture. The lowest band corresponded to uncoupled Cys-GFP **4.29**, the middle one to the protein coupled with one unit of peptoid (**4.35**) and the highest one to the GFP bond to two entities of maleimide-9mer (**4.35**). The gel result was confirmed by the presence of the both peaks on the MALDI-TOF spectra (**Figure 4.18-B**).

- m/z = 27701, **4.29**;
- m/z = 29534, **4.44** with n = 1 (29534-27701 = 1833; expected + 1847);
- m/z = 31355, **4.44** with n = 2 (31355-27701 = 3654; expected + 3694).

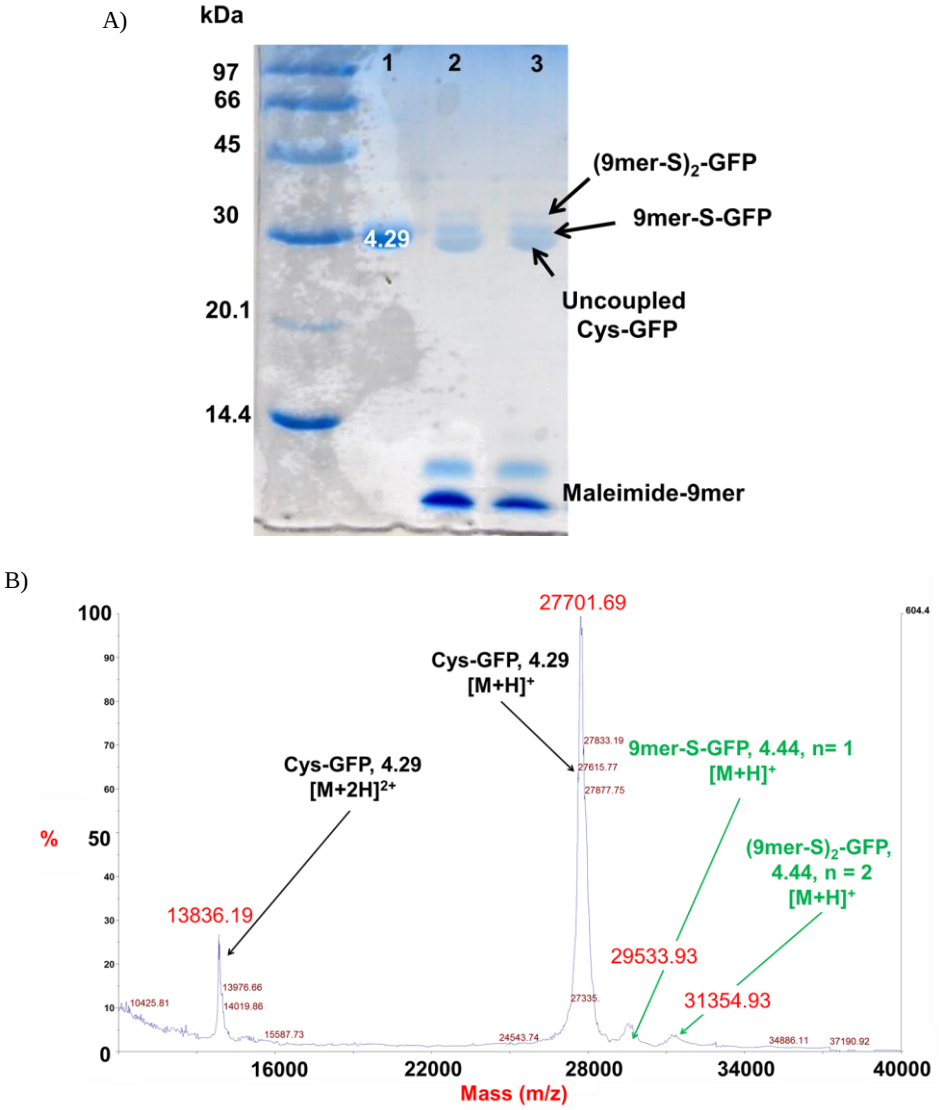

Figure 4.18: Analysis of the GFP bioconjugation with 2-IT and 25 equivalents of peptoid 4.35. A) SDS-PAGE analysis (lanes left to right): LMW SDS marker; Lane **1**: untreated GFP **4.29; 2**: Coupling reaction before purification of the peptoid excess by centrifugation; **3**: Coupling reaction after purification of the peptoid excess by centrifugation. B) MALDI-TOF spectra of the coupling reaction.

The cellular uptake of this bioconjugation (**4.44**) was tested in HeLa cells under the same conditions as previously described. The flow cytometry analysis showed a small amount a cellular uptake with a maximum of 15% of cells labelled after 24 hours of incubation (**Appendix 4-7**).

The cytotoxicity of the bioconjugates (**4.40** and **4.44**) was also assessed using MTT assay. The cell viability was not affected under any of the concentrations used for the project (**Appendix 4-8**).

4.2.3.7. Conclusions

A nonalysine-like peptoid was synthesised and functionalised with a maleimide using microwave assisted HOBt/DIC solid phase synthesis. Using a thio-rhodamine (**4.38**), the reactivity of the maleimide-9mer (**4.35**) was proven efficient and biocompatible. However, the coupling between the Cys-GFP (**4.29**) and the maleimide-9mer was not carried out with the same success. This could be due to the positively charged primary amine groups, which could interact with the protein and therefore not allow correct positioning of the maleimide leading to a poor coupling rate. In order to demonstrate this hypothesis the peptoid could be fully protected and the maleimide-thiol reaction re-tested. Nevertheless, flow cytometry, microscopy and cytotoxicity assays demonstrated positive and non-cytotoxic cellular delivery of the GFP in HeLa cells using a nonalysine-like peptoid. Therefore, the principle of coupling and the cellular delivery were demonstrated but there is still major room for improvement, mainly by increasing the coupling yield between the maleimide transporter and the protein. The analysis of the tertiary structure of the GFP could show that the lysine side chains are probably not available due to steric hindrance leading in the low reaction between the amine groups and the thiolation agent (2-IT).
In the future, after fixing the maleimide-thiol issues, the cellular uptake of GFP-peptoid should be compared to another cellular delivery system such as TAT or polyarginine. So far, the fusion TAT-GFP delivery is still much more efficient than this GFP-peptoid system. Nevertheless, it is important to remember that these carriers are known to be efficient but remain cytotoxic and very sensitive to proteases while the peptoid carrier did not show any cytotoxicity and is resistant to proteolytic degradations.

4.2.4. GFP delivery via active ester coupling chemistry

4.2.4.1. Aim and choice of protecting group

Another approach was to attach the peptoid to GFP via formation of an amide bond.[220] However, the nonalysine-like peptoid contains nine primary amines that can be very reactive depending on the pH (pKb around 10.5). These primary amines are mainly under the form of protonated amine at low pH (under 8) generating some

aggregations. At pH>10, the amines are not protonated and very reactive. Therefore, in this new approach the side chains of the peptoids were kept protected and the protein was coupled to the protected peptoid via an active ester. Once the protein was coupled, the side chain would need to be deprotected under physiological conditions.

The choice of the side chains protecting group was dictated by several requirements:

1. Being resistant to the final acidic cleavage from the solid support,
2. Being orthogonal to Fmoc group, that protects the α-secondary amine of the peptoid chain,
3. Allowing being deprotection under physiological conditions.

The Dde protecting group seemed an interesting choice. The only doubt being if deprotection could occur under physiological conditions. In 2006, S-acetylated thiopropionul residues were deprotected *in situ* using hydroxylamine (500 mM) without degradation of the antibody[231] while Dde can be deprotected by hydroxylamine (300 mM) with imidazole.[204] Based on these two publications, the following deprotecting solution was prepared with hydroxylamine.HCl (500 mM), EDTA dipotassium (25 mM) and sodium phosphate dibasic (50 mM) at pH 7.5.
The deprotection solution was tested on the compound Fmoc-Lys(Dde)-OH **4.14.**

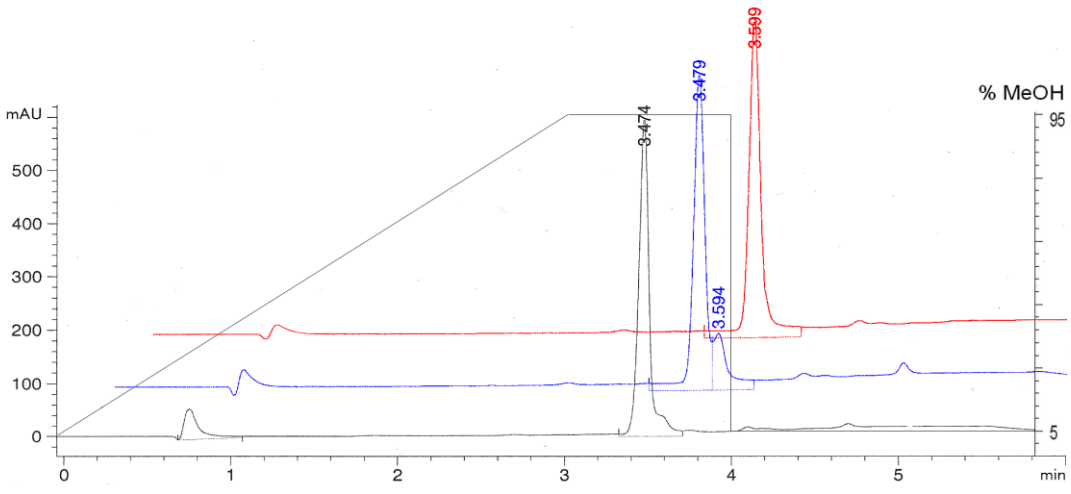

Figure 4.19: HPLC trace (λ = 240 nm) of the Dde deprotection under physiological conditions.
In red, the starting material (Fmoc-Lys(Dde)-OH); in blue, the reaction mixture after 4 hours at room temperature; in black the reaction mixture after 6 hours at room temperature.

HPLC analysis (**Figure 4.19**) showed transformation of the starting material (Fmoc-Lys(Dde)-OH, **4.14**, retention time 3.6 minutes) to the non-protected Fmoc-Lys-OH (retention time 3.5 minutes). Thus, due to the good deprotection of the Dde group under physiological conditions, its orthogonality to the Fmoc group and its stability under acidic cleavage, a peptoid monomer was prepared with the side chain protected with a Dde (instead of a Boc) group and the α-amine group with an Fmoc group.

4.2.4.2. Dde monomer synthesis

The Dde monomer **4.48** was synthesised based on the synthesis of the Boc monomer (**2.22**, described in ***CHAPTER 2***) (**Scheme 4.10**). The Dde monoprotection was first carried out using the same protocol than for the Boc monoprotection, using 8 equivalents of 1,6-diaminohexane (**2.18**) and 1 equivalent of DdeOH (**4.20**). However, analysis of the crude reaction revealed the presence of unprotected, mono-protected and di-protected amine. Furthermore, the washing step to remove the excess of diamine (**2.18**) resulted on the degradation of the desired Dde mono-protected compound (**4.45**). Previously, in the Bradley group, other diamine compounds were monoprotected using DdeOH with the synthesis carried out using a 1:1 molar ratio of the diamine and the DdeOH. This protocol was repeated here.

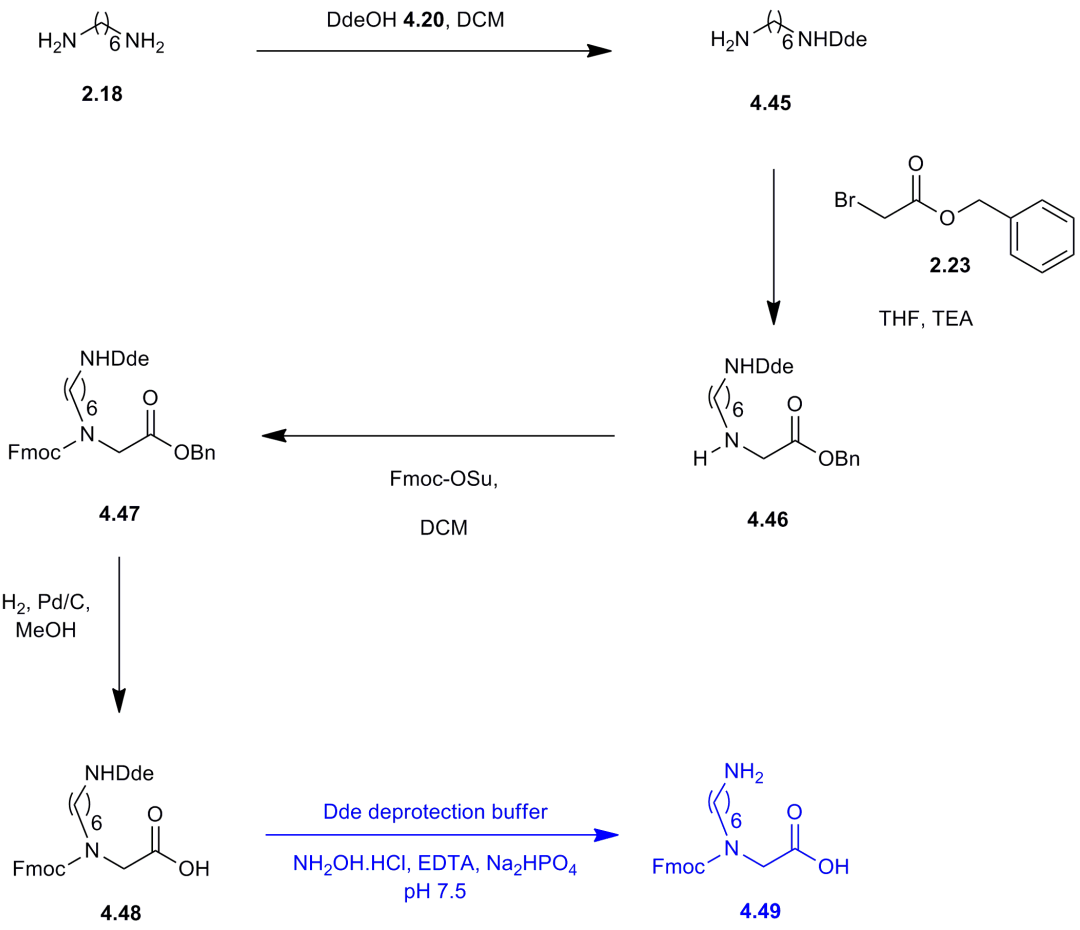

Scheme 4.10: Synthesis of the Dde protected lysine-like peptoid monomer 4.48 and its Dde deptrotected analogue 4.49.
The synthesis corresponded to the synthesis of the Dde protected lysine-like peptoid monomer **4.48** and the selective Dde deprotection of the monomer **4.48** under physiological conditions (blue).

The free primary amine was monoalkylated with benzyl-2-bromoacetate (**2.23**) to obtain the desired N-substituted glycine protected by a benzyl ester and a Dde group (**4.46**). Compound **4.46** was isolated by column chromatography in 32% yield over the first two steps (calculated from **4.20**). This low yield was mainly due to the poor stability of **4.45**. The non-protected secondary amine group was then protected by an Fmoc group using Fmoc-OSu. After purification by chromatography, **4.47** was obtained in a 98% yield (calculated from **4.46**). Benzyl group deprotection was carried out using Pd/C as a catalyst under H_2 and the Dde monomer **4.48** was obtained in a 80% yield.

Before synthesising a fully Dde protected peptoid, the Dde deprotection at physiologic pH was also tested on the monomer **4.48** (**Scheme 4.10**). The Dde removal assay was carried out in a biphasic mixture composed with DCM (to dissolve the monomer) and the Dde deprotection solution (500 mM of $NH_2OH.HCl$, 25 mM of EDTA dipotassium, 50 mM of anhydrous sodium phosphate dibasic, pH 7.5). As expected the Dde protected monomer **4.48** was deprotected to form **4.49** (**Figure 4.20**). The synthesis of the protected peptoid was then started.

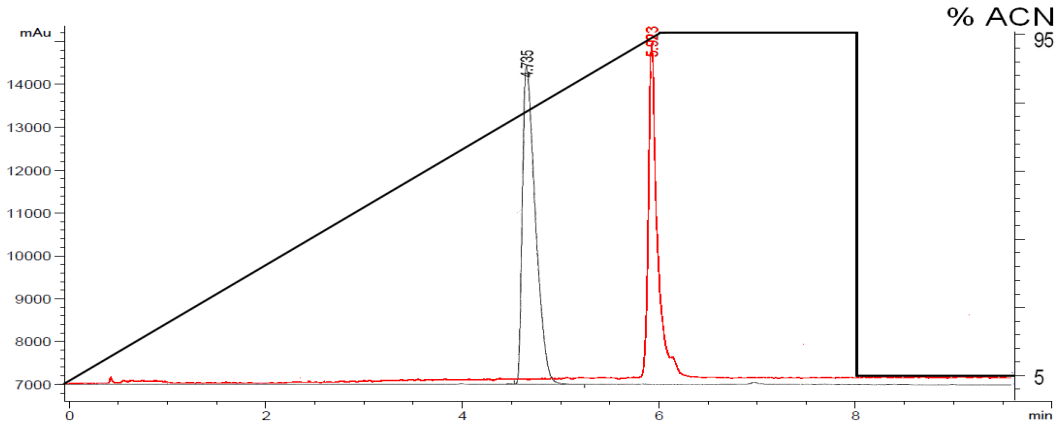

Figure 4.20: HPLC trace (ELSD) of the Dde deprotection of the Dde monomer 4.48 under physiological conditions.
In red, the starting material (Dde monomer **4.48**); in black the reaction mixture with the formation of the compound **4.49** after 6 hours at room temperature.

4.2.4.3. Synthesis of the fully protected peptoid

The fully Dde protected peptoid was synthesised using the previously described (***CHAPTER 2***) solid-phase synthesis protocol used for the synthesis of the non-protected peptoid using a Rink amide polystyrene resin (**2.28**), the Dde monomer **4.48** and an HOBt/DIC microwave assisted coupling protocol. The Fmoc-9mer$(Dde)_9$-NH_2 peptoid **4.51** was released from the solid support by treatment of the resin (**4.50**) with TFA (TFA/TIS/H_2O, 95: 2.5: 2.5) (**Scheme 4.6**) in a purity of 67% (ELSD) before purification. The synthesis of this peptoid was more complicated (a few couplings had to be repeated) than the synthesis of the Boc-protected analogue and less pure. The product **4.51** was isolated after reverse phase chromotography in an overall yield of 51%.

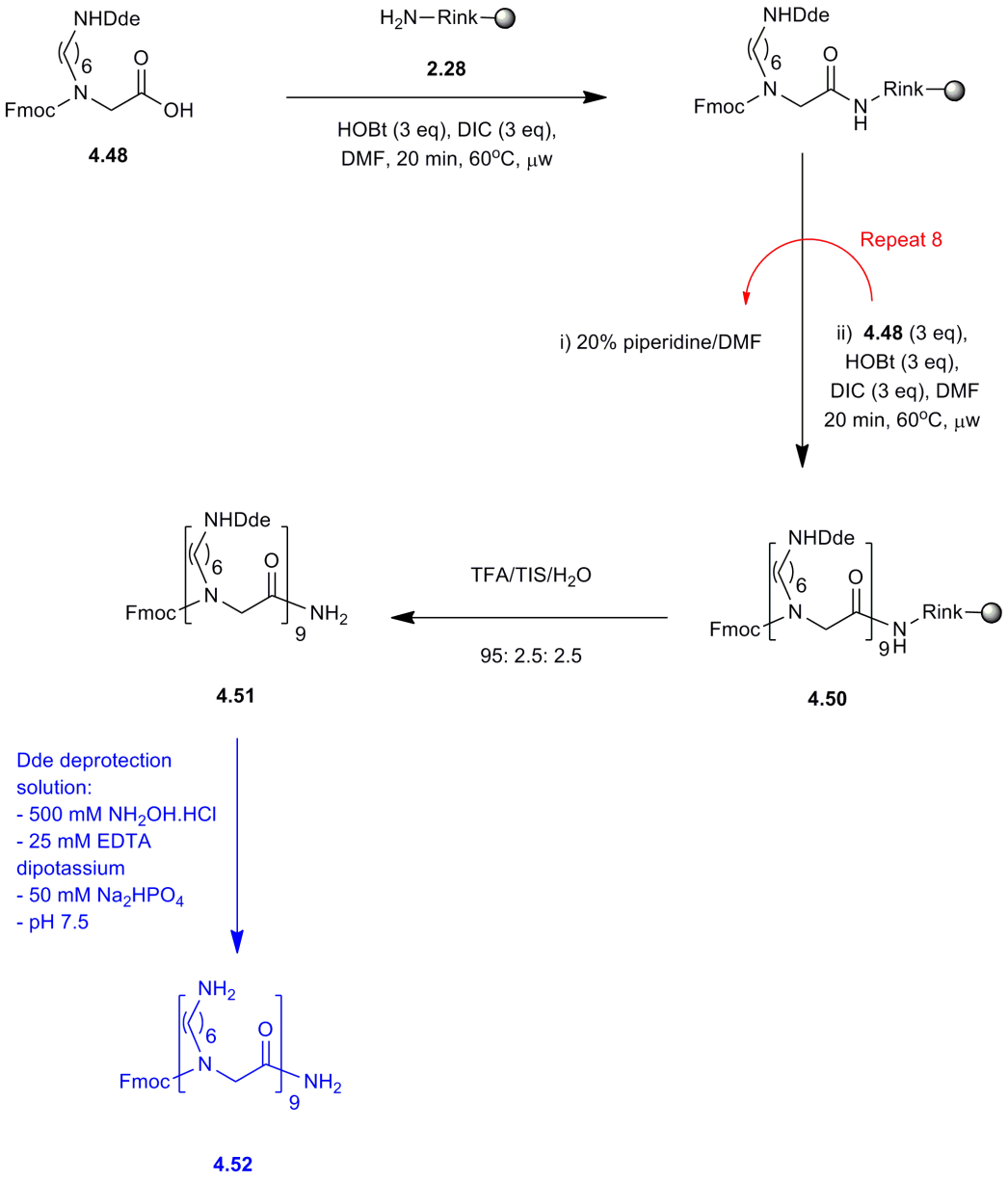

Scheme 4.11: HOBt/DIC microwave assisted solid-phase synthesis of Fmoc-9mer(Dde)$_9$-NH$_2$ peptoid (4.51) and formation of the Fmoc-9mer peptoid (4.52) by physiologic Dde deprotection.

Before carrying on any further in the project, it was essential to confirm that the Dde deprotection buffer was also efficient for the deprotection of the purified Fmoc-9mer(Dde)$_9$-NH$_2$. The Fmoc-9mer(Dde)$_9$-NH$_2$ was treated with the Dde deprotection solution. Once the water was removed, the crude was precipitated in cold diethyl ether.

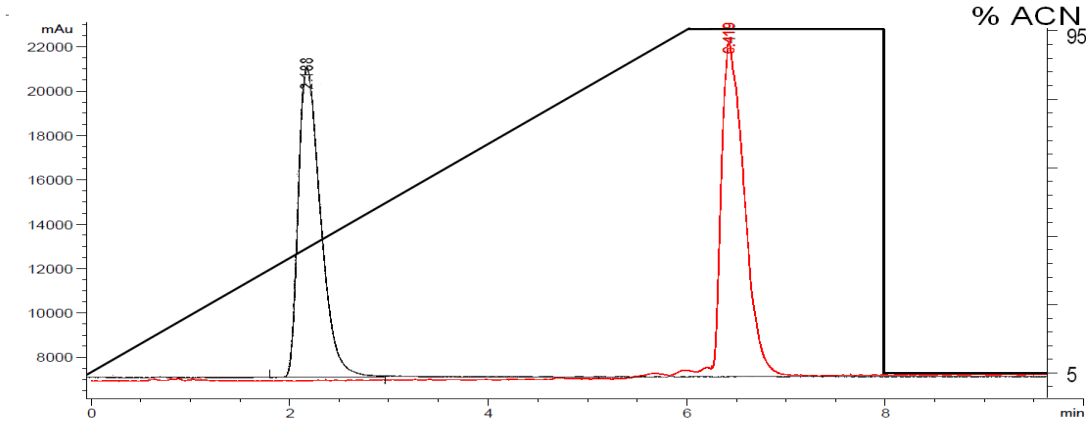

Figure 4.21: HPLC trace (ELSD) of the Dde deprotection of the protected peptoid 4.54 under physiological conditions.
In red, the pure starting material (Fmoc-9mer(Dde)$_9$-NH$_2$, **4.51**); in black the reaction mixture with the formation of the compound **4.52** (Fmoc-9mer-NH$_2$) after overnight reaction at room temperature.

After precipitation the reaction was analysed and the HPLC trace showed 100% of conversion from the fully protected peptoid (**4.51**) to the nonprotected 9mer (**4.52**). The result was confirmed by comparison with Fmoc-9mer peptoid (**4.52**) synthesised using the same protocol as the peptoid **4.51** but using the Boc monomer (**2.22**) instead of the Dde monomer (**4.48**).

4.2.4.4. Choice of the active ester

After synthesising the Dde protected peptoid, work focused on the choice of the active ester. The best synthetic route would be to couple the active ester on the peptoid while it was still on the solid support and to purify everything as one. In order to do so, the active ester has to be stable under the acidic conditions used to cleave the protected peptoid from the Rink amide polystyrene resin. The *N*-hydroxysuccinimide active ester (NHS) is the most commonly used for bioconjugation however it is easily hydrolysed below pH 2. The NHS ester has a half-life of a few hours at pH 7-8. The fluorophenyl esters, including pentafluorophenyl (OPfp or PFP), tetrafluorophenyl and sulfo-tetrafluorophenyl ester, are another famous family that react with amine containing biomolecules (e.g. proteins) to give an amide bond. This family of active esters has the same reactivity than NHS esters with a better stability toward hydrolysis making these esters a potential contender for this project.[220]

Commercially available Fmoc-Leu-OPf (**4.53**) was treated for different time periods with different TFA concentrations (1, 5, 10, 25 and 50% TFA in DCM). The stability of the active ester was monitored using HPLC (ELSD) and MS after neutralisation (with triethyamine).

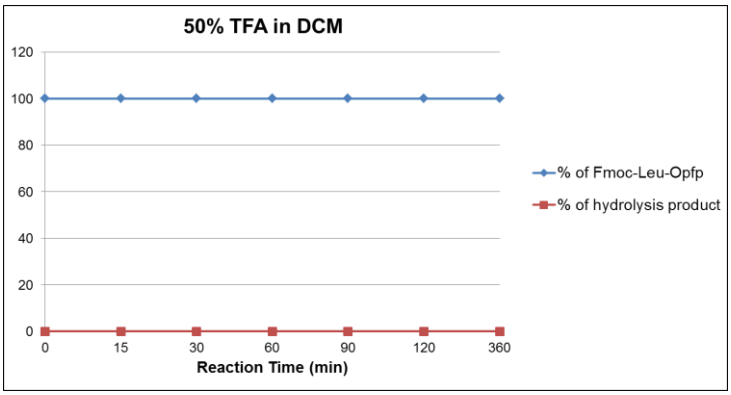

Graph 4.3: Stability assay of the OPfp ester with 50% TFA in DCM.

None of the concentrations of TFA tested caused the hydrolysis of the OPfp ester independent of the reaction time (**Graph 4.3** and **Appendix 4-9**). These results validated the choice of the pentafluorophenyl ester for this project.

4.2.4.5. Results and discussion

Fmoc-9mer(Dde)$_9$-resin (**4.50, Scheme 4.11**) was Fmoc deprotected and coupled to the cyclised 3, 6, 9 trioxaudecanedioic acid **4.54** in DCM. The cyclisation reaction was carried out in DCM in presence of DCC before being added to the resin without purification.[232] As the chloranil test was negative (no sign of free secondary amine), the formation of the active ester was activated using pentafluorophenol (**4.56**) and DCC in DCM.[233] After overnight reaction, the resin was treated with 50% TFA in DCM to cleave the expected peptoid **4.60**. Unfortunately, the analysis of the crude revealed that the synthesis had not worked. The HPLC showed a very unpure cleavage product that, once purified, was mainly the Fmoc deprotected version of the peptoid **4.51**. The synthesis was repeated with PEG coupling step repeated twice. However, the same result was observed. The coupling with the **4.54** may have failed due to a steric hindrance. One alternative could be to couple first an Fmoc-Ahx-OH

spacer (**2.34**) and then the cyclised PEG (**4.54**). Unfortunatly, this hypothesis could not be tested due to lack of time.

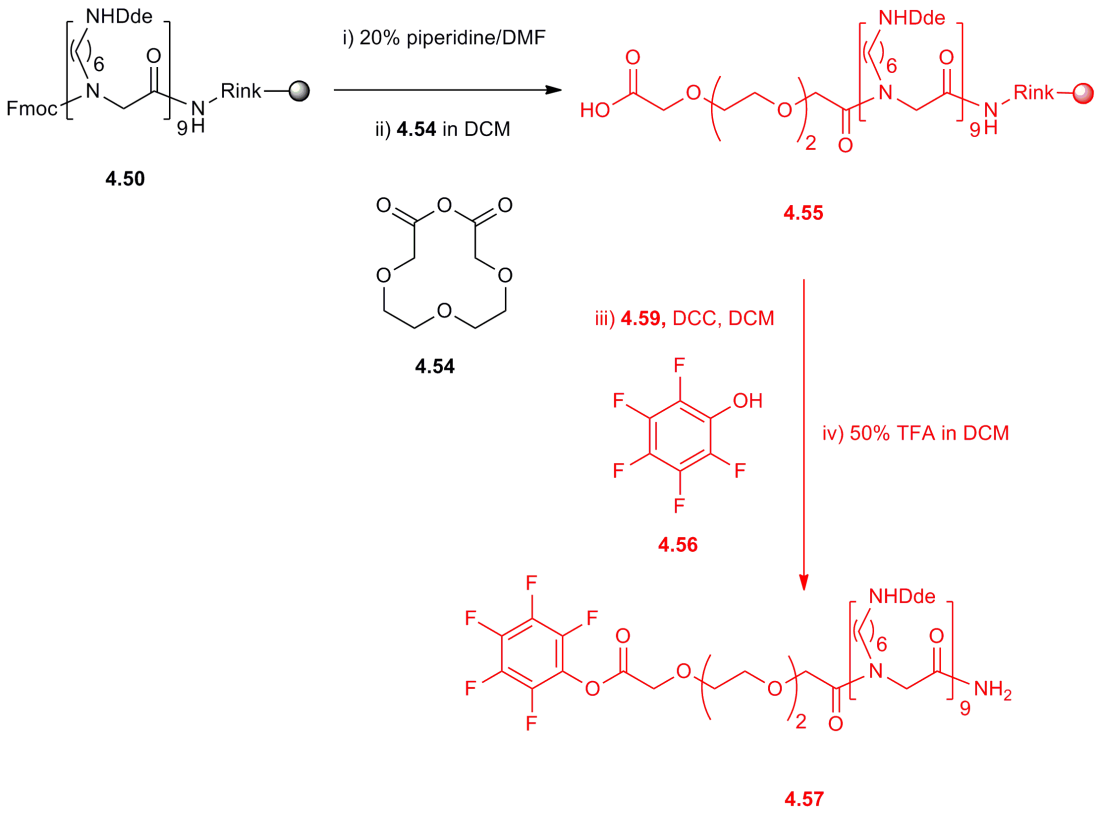

Scheme 4.12: Tested synthesis of the OPfp activated protected peptoid 4.57.
In black, the part of the synthesis that worked; in red, the part that did not work. The compound **4.54** was cyclised before being added to the resin.

4.3. eGFP DNA plasmid delivery

4.3.1. Introduction

Efficient cellular delivery of DNA, commonly known as transfection, is a key technique for numerous biomedical sciences leading, potentially, to the treatment of countless diseases. In the past decade, new technologies have been developed to overcome the major barriers of this technique (permeability of the cell membrane to DNA and specific targeting). New cellular carriers are very diverse in shapes, chemical structures and DNA binding methodologies, for instance nanodevices,[234] quantum dots,[235] cationic lipids (such as Lipofectamine, ***Paragraph 1.2.3***) and derivates,[236] micropsheres[237] and cell penetrating peptides.[238] Thanks to the negative

charges of the phosphate deoxyribose DNA backbone, the DNA can be encapsulated via electrostatic interactions by positive charged molecules such as poly-lysine or poly-arginine (**Figure 4.22**).[239]

In 2007, Davis published a paper in which DNA containing nanoparticles were prepared by encapsulation of the DNA with polyethylene glycol (PEG) substituted cysteine-polylysine peptides (PEG-CK_{30}).[240] In order to track the nanoparticles inside the cells, the compacted DNA/polylysines were labelled with rhodamine dye. Previously in this thesis was described the synthesis and the efficient cellular uptake without cytotoxicity of the Rho-9mer peptoid (**2.37**) in several cell lines. Although, the peptoid **2.37** was shorter than the PEG-CK_{30} compound,[240] its nine positive charges should interact strongly with the anionic phosphates of DNA. The complexation of the eGFP plasmid (pEGFP) was first evaluated with the Rho-9mer peptoid (**2.37**) and then with a PEG-peptoid (**4.61**).

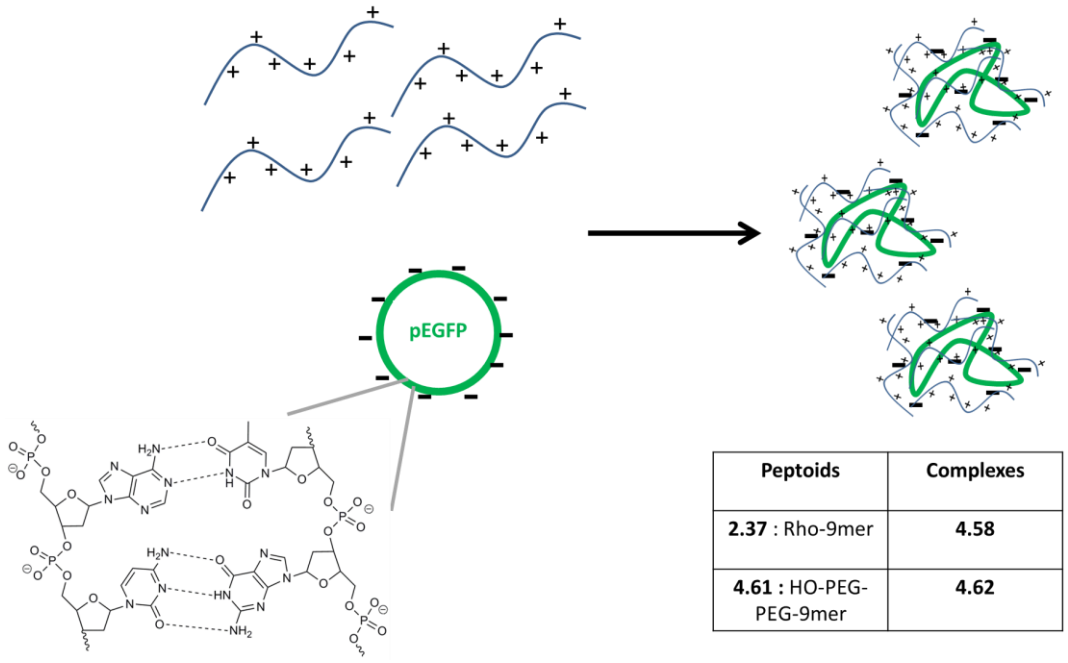

Peptoids	Complexes
2.37 : Rho-9mer	**4.58**
4.61 : HO-PEG-PEG-9mer	**4.62**

Figure 4.22: Electrostatic encapsulation of DNA with cationic molecules including the nonalysine-like peptoids.

4.3.2. Cellular delivery of pEGFP by complexation with the Rho-9mer

4.3.2.1. Formation of the pEGFP/Rho-9mer complex

The Rho-9mer synthesis was described earlier in this thesis (***CHAPTER 2***). The first step of this project was the evaluation of the complexation power of the peptoid Rho-9mer (**2.37**). The amount of peptoid used was calculated from the number of negative charges on the plasmid. The eGFP plasmid (pEGFP-C1) contained 4731 bases. Each base was composed of one molecule phosphate deoxyribose therefore the plasmid used had 4731 negatives charges. The Rho-9mer **2.37** has a maximum of nine positive charges thanks to its primary amines, therefore to obtain a charge ratio of 1:2 between the DNA and the peptoid, 1052 molecules of nonalysine-like peptoid were required.

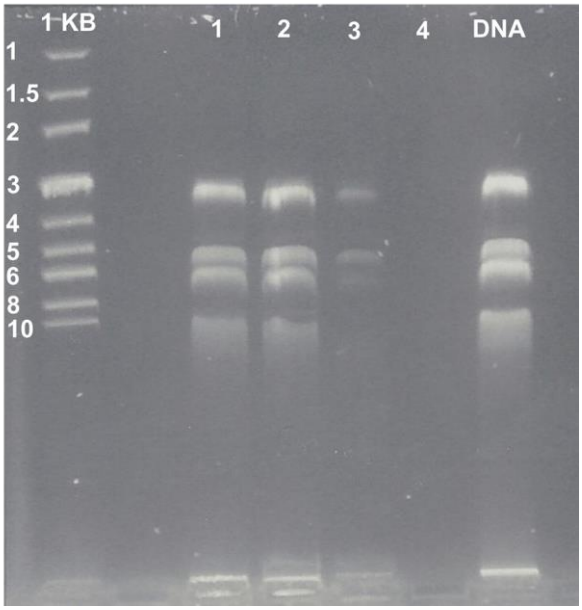

Figure 4.23: Electrophoresis gel of the binding of pEGFP-C1 with the Rho-9mer peptoid (2.37). Lanes left to right: Marker 1 kilobase (KB), Lane **1**: charge ratio pEGFP/Rho-9mer = 1: 2, **2**: charge ratio pEGFP/Rho-9mer = 1: 5, **3**: charge ratio pEGFP/Rho-9mer = 1: 10, **4**: charge ratio pEGFP/Rho-9mer = 1: 20.

The eGFP plasmid was mixed at room temperature with different amounts of Rho-9mer (**2.37**) but with the same DNA concentration (0.01 µg/µL). Several charge ratios pEGFP-peptoid were tested and the results were summarised below (**Figure 4.23**).

- Lane 1, 1: 2: bands were very intense but decreased compare to the untreated DNA,
- Lane 2, 1: 5: almost as intense as the first ratio,
- Lane 3, 1: 10: intensity of the bands decreased but there was still some uncomplexed plasmid,
- Lane 4, 1: 20: all DNA trapped within peptoid complexes.

From the previous data, cellular delivery in HEK293T cells was tested using a charge ratio of 1: 20, pEGFP/Rho-9mer.

4.3.2.2. Cellular delivery of the pEGFP/Rho-9mer complex

The cellular delivery of the pEGFP-C1 was assessed by production of green fluorescent protein. Lipofectamine™ 2000 (L2000, **Figure 1.8**) was used as a positive control and uncomplexed pEGFP-C1 and untreated cells as a negative control. After 24 and 48 hours, cells were analysed by flow cytometry (**Figure 4.24**) and microscopy (live cells microscopy: **Figure 4.25**; confocal microscopy: **Figure 4.26**).

Using the rhodamine, the cellular penetration of the complex was confirmed. Flow cytometry analysis showed that the pEGFP/Rho-9mer complex **4.58** penetrated as easily as the free Rho-9mer **2.37** (**Figure 4.24-A**) with almost 100% of cell labelled after 24 hours of incubation with the complex **4.61** and the uncomplexed peptoid **2.37**. After 48 hours, the whole population was highly labelled. As expected the Lipofectamine/pEGFP complex was not detected after 24 and 48 hours using the rhodamine filter. The presence of the peptoid was also confirmed by microscopy (**Figure 4.25-B**). Direct GFP expression was analysed using the FITC filter via flow cytometry (**Figure 4.24-B**). After 24 hours of incubation, no GFP expression was detected in the cells transfected with the pEGFP/peptoid complexes (**4.58**). As far as the positive control was concerned (Lipofectamine™2000/DNA), 10% of the treated cells showed GFP expression. After 48 hours, the cells treated with the complexes **4.58** clearly expressed GFP (**Figure 4.25-C**) and this result was confirmed with flow analysis (**Figure 4.24**). The pEGFP/Rho-9mer peptoid **4.58** was not as efficient as the Lipofectamine complex with only 20% of cell labelling (expression of GFP) for

the peptoid complex while the commercially available reagent achieved a cellular labelling of 52%.

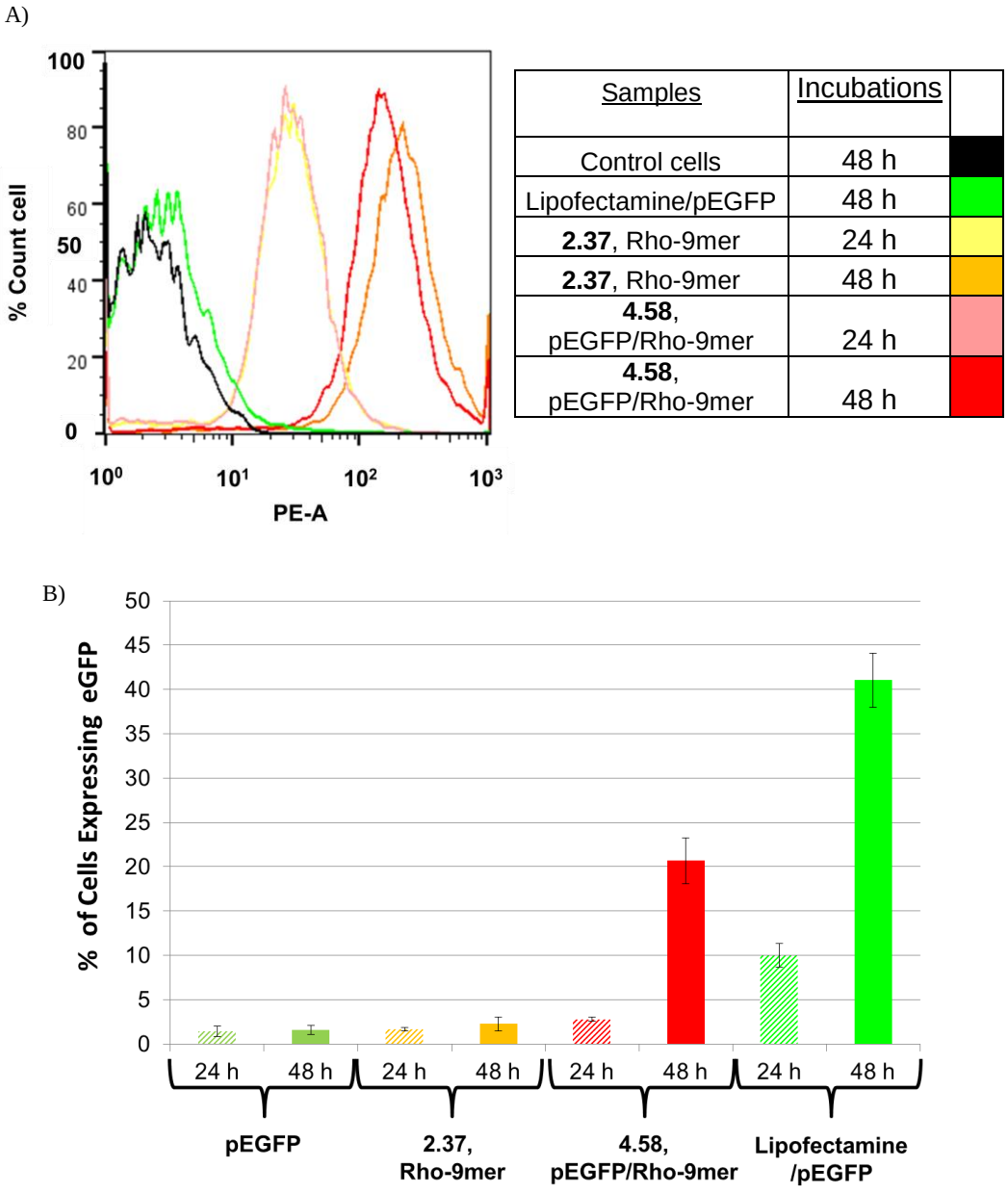

Figure 4.24: Flow analysis of cellular uptake of the pEGFP/Rho-9mer complexes (4.58) in HEK293T cells.

A) Histogram showing the cellular uptake based on the rhodamine. PE axis: Rhodamine fluorescence intensity; B) % uptake measured for the direct expression of GFP using pEGFP/Rho-9mer complexes **4.58** (0.5 µg of DNA/well), Rho-9mer (**2.37**, 13 µM) and Lipofectamine™ 2000 (0.5 µg of DNA/well) as the % of cells with a fluorescent emission exceeding untreated control as 0% uptake (incubation time = 24 (hatched columns) and 48 hours (plain columns)). The errors bar represents the standard error of the average (n=3).

After 24 hours, even though live cell microscopy (**Figure 4.25**) shown that the DNA complex **4.58** or the free peptoids (**2.37**) penetrated the cells (red colour within the HEK293T cells), no GFP fluorescence was detectable. These results were similar to the data obtained via flow cytometry. However after 48 hours, direct GFP expression was clearly observed.

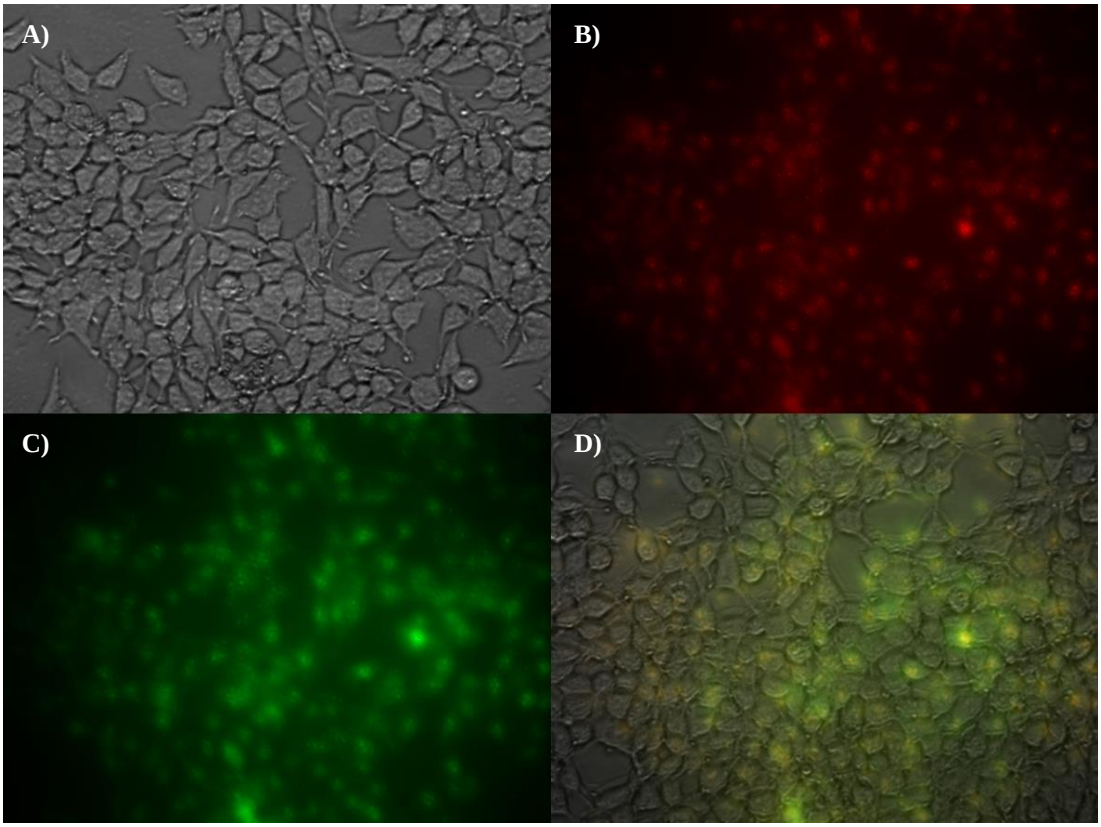

Figure 4.25: Microscopy analysis of the cellular delivery of DNA/Rho-9mer complexes (4.58). These images were taken after incubation of the HEK293T cells for 48 hours at 37^{o}C with 0.5 µg of eGFP plasmid complexed with Rho-9mer (**2.37**)**.** A) Brightfield image; B) Rhodamine fluorescent image, Rho-9mer detection (excitation 515-560 nm); C) GFP fluorescent image (excitation 450-490 nm); D) Fluorescence image merge with brightfield.

Confocal microscopy (**Figure 4.26**) showed the presence of rhodamine peptoid inside cells. The expressed GFP protein was observed, as expected, in the cytoplasm only.

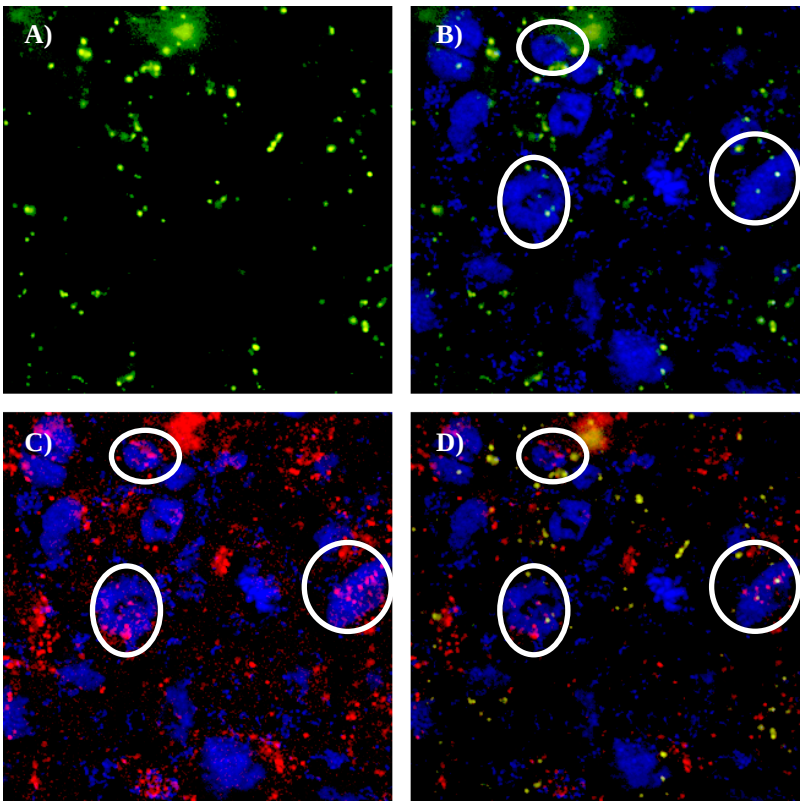

Figure 4.26: Confocal microscopy of the DNA/Rho-9mer complexes (4.58) delivery. These images were taken after incubation of the HEK293T cells for 24 hours at 37°C with **4.58** (2.5 µg of DNA/well). A) GFP fluorescent image (excitation laser 490 nm and emission filter 528-550 nm); B) Rhodamine fluorescent image, Rho-9mer **2.37** (excitation laser 561 nm and emission filter 567-630 nm) and nuclei staining using HOECHST-33342 (excitation at 405 nm and emission filter 413-482 nm); C) GFP fluorescent image (excitation laser 490 nm and emission filter 528-550 nm) and nuclei staining using HOECHST-33342 (excitation at 405 nm and emission filter 413-482 nm); D) Composite image. The circles showed the co-localisation of the peptoid (in red) in the nucleus while the green colour of the GFP protein was localised in the cytoplasm.

4.3.2.3. Delivery of the pEGFP/Rho-9mer complex into active T-cells (collaboration with Dr. Stefano Caserta)

In the ***CHAPTER 2***, the Rho-9mer (**2.37**) peptoid was shown to penetrate without cytotoxicity primary cell lines. Therefore, the cellular delivery of DNA via peptoid complexation was also tested in T-cells.

All experiments carried out in T-cells were performed by Dr. Stefano Caserta from Prof. Zamoyska's group at the Institute of Immunology and Infection Research, School of Biological Sciences in Edinburgh University.

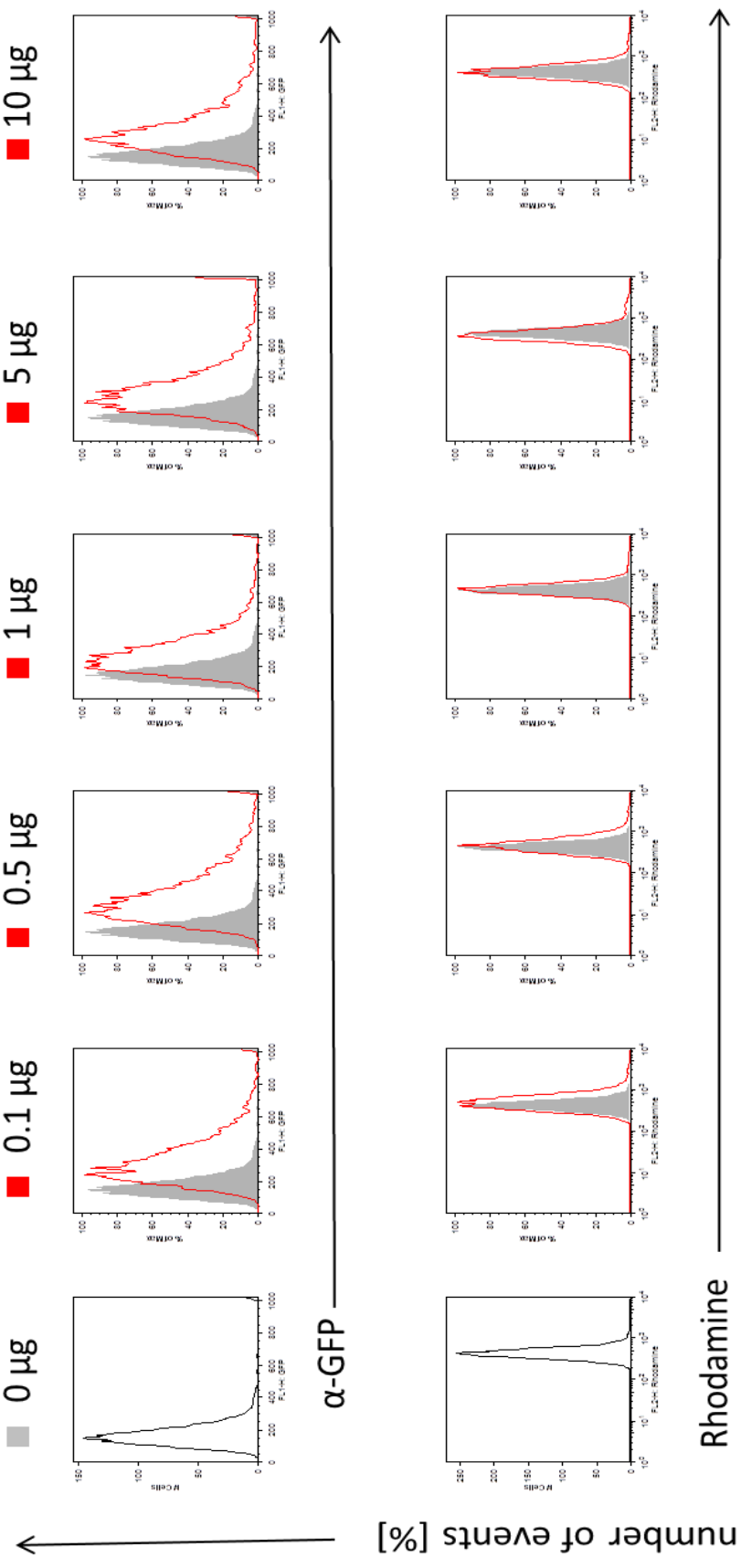

Figure 4.27: Flow cytometry analysis of DNA delivery in lymph node cells using Rho-9mer (2.37).

The cells were analysed on day 4 of incubation with complex GFP-plasmid & Rho-9mer (**2.37**, 10µM). The top row corresponds to the detection of the anti-GFP antibody fluorescence function of the amount of DNA used. The bottom row corresponds to the rhodamine detection function of the amount of DNA used. Data courtesy of Dr. Stefano Caserta from the Institute of Immunology & Infection Research (Prof. Rose Zamoyska) at the University of Edinburgh.

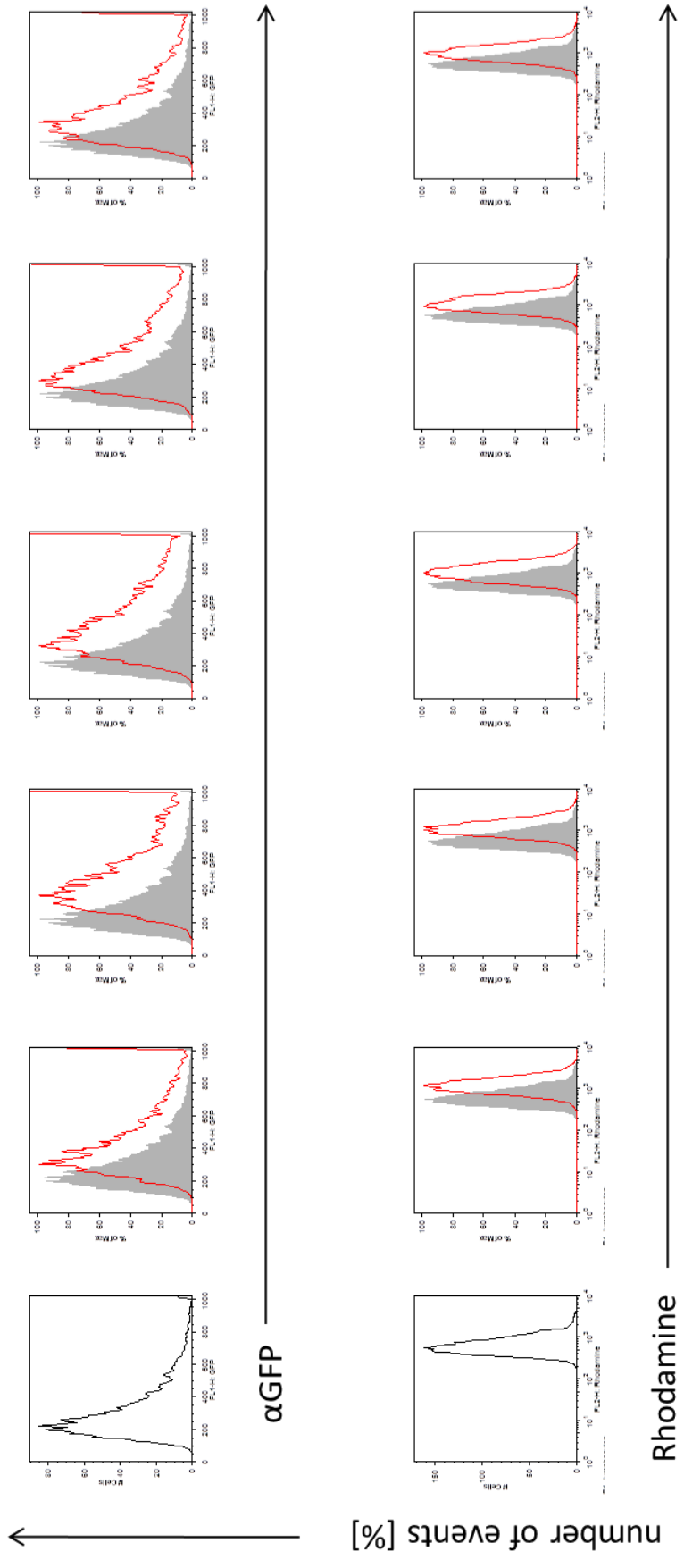

Figure 4.28 : Flow cytometry analysis of DNA delivery in lymph node cells using Rho-9mer (2.37).

The cells were analysed on day 4 of incubation with complex GFP-plasmid & Rho-9mer (**2.37**, 20 µM). The top row corresponds to the detection of the anti-GFP-antibody fluorescence function of the amount of DNA used. The bottom row corresponds to the rhodamine detection function of the amount of DNA used. Data courtesy of Dr. Stefano Caserta from the Institute of Immunology & Infection Research (Prof. Rose Zamoyska) at the University of Edinburgh.

The first flow cytometry analysis (**Appendix 4-10**) was carried out on the direct detection of the eGFP expression and on the detection of the rhodamine. The data showed the presence of rhodamine inside the cells, therefore the peptoids penetrated. However, no trace of eGFP was observed. These results could have several explanations:

1. complex **4.58** was degraded before its cellular penetration in the cells resulting to the penetration of the peptoid only,
2. complex **4.58** was taken up by the cells but it was too stable and the DNA was not released,
3. complex **4.58** was able to penetrate in the cytoplasm, but could not access the nucleus (trap in endosomes), therefore the DNA could not be expressed in proteins.

In order to confirm the presence of the DNA in the cells, the second detection of eGFP expression was carried out with an anti-GFP-antibody. Anti-GFP-antibody binds specifically to eGFP protein and is commonly used for the low detection of protein.[241] The flow cytometry analysis showed a clear increase of the antibody fluorescence intensity (**Figure 4.27** and **Figure 4.28**). A higher concentration of peptoid did not affect the percentage of cells expressing eGFP. However, the high concentration of peptoid gave broader cell populations (**Figure 4.28**). This result might be due to some interactions between the peptoid and the antibody as the control population (no DNA just Rho-9mer and antibody) was already quite disperse. This could correspond to an aggregation of peptoid within the cell membrane.

4.3.3. Cellular delivery of pEGFP by complexation with PEG-9mer

The DNA delivery was also tested with a dye-free peptoid to confirm the previous results and to try to improve the cellular uptake. Polyethylene glycol (PEG) is a polymer known to be non-toxic, non-immunogenic and non-antigenic. PEGylation, the process to functionalise proteins, peptides or drugs with one or several units of PEG, have demonstrated several advantages including an increase of hydrophilicity, of proteolytic resistance and an decrease or elimination of immunogenicity.[242] PEGylation was also reported to improve the cellular uptake of nanoparticle formed between polycationic polymer (peptides or lipids) and DNA by increasing their stability.[243]

For this project, the PEGylation of the nonalysine-like peptoid could compensate the loss of positive charges and stabilise the DNA/peptoid complexes leading to a higher transfection.

4.3.3.1. Synthesis of HO-PEG-PEG-9mer-NH_2

As previously described in ***CHAPTER 2***, the PEG nonalysine-like peptoid **4.61** was prepared on a Rink amide polystyrene resin using the Boc monomer **2.22** and an HOBt/DIC microwave assisted coupling protocol. The cellular penetrating peptoid was first functionalised with the Fmoc-PEG-OH (**4.59**) spacer. After Fmoc deprotection (20% piperidine in DMF), the resin **4.60** was coupled at room temperature with the cyclised 3, 6, 9 trioxaudecanedioic acid **4.54** in DCM.[232] The HO-PEG-PEG-9mer-NH_2 (**4.61**) was deprotected and cleaved from the solid support by treatment of the resin with TFA (TFA/TIS/H_2O, 95: 2.5: 2.5) (**Scheme 4.13**) with a purity of 96% (ELSD).

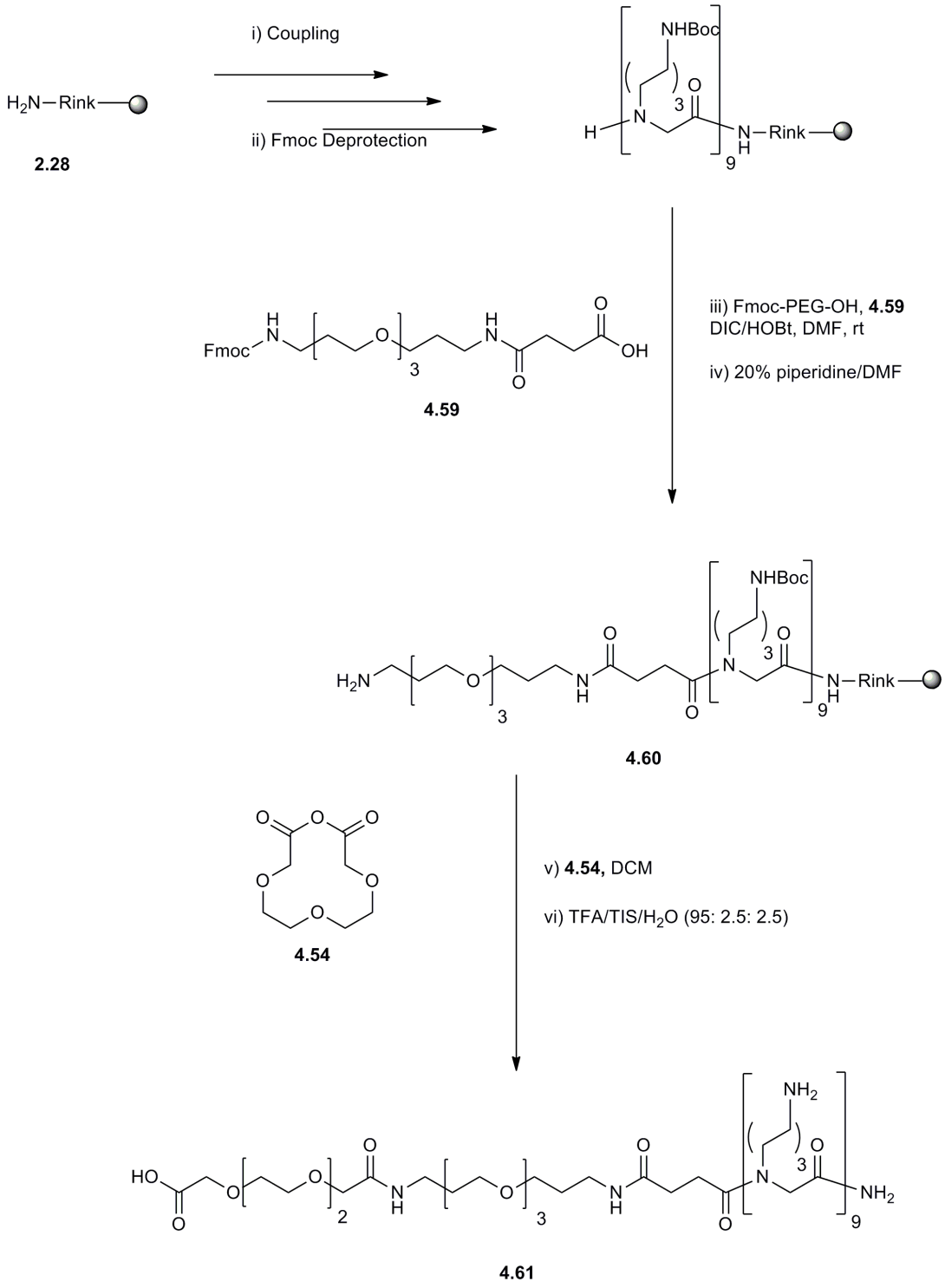

Scheme 4.13: Solid-phase synthesis of the HO-PEG-PEG-9mer peptoid (4.61).
Peptoid monomer couplings were carried using 3 equivalents of the Fmoc, Boc protected monomer **2.22**, HOBt and DIC in DMF for 20 minutes at 60^{o}C µw; Fmoc deprotection were carried over 2 cycles of 10 minutes using 20% piperidine in DMF.

4.3.3.2. Formation of the pEGFP/PEG-9mer complex

The DNA was encapsulated within the PEG-peptoid **4.61** was carried out using the same protocol as previously used with the Rho-9mer (**2.37**). The complexation was confirmed by electrophoresis. As expected, a DNA/peptoid charge ratio of 1:20 was sufficient to have 100% of complexation. Therefore, the complex DNA/PEG-9mer **4.62** was prepared using the ratio 1: 10 for the *in vitro* cellular delivery assays.

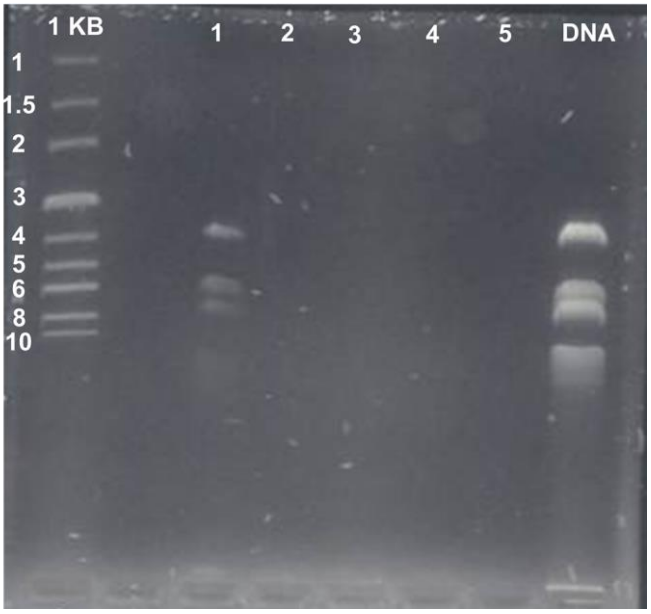

Figure 4.29: Electrophoresis gel of the binding of pEGFP-C1 with the PEG-9mer peptoid (4.61). Lanes left to right: Marker 1 kilobase (KB), Lane **1**: charge ratio DNA/peptoid = 1: 10, **2**: charge ratio DNA/peptoid = 1: 20, **3**: charge ratio DNA/peptoid = 1: 30, **4**: charge ratio DNA/peptoid = 1: 40, **5**: charge ratio DNA/peptoid = 1: 50.

4.3.3.3. Cellular delivery of the pEGFP/PEG-9mer complex

The delivery was then tested on HEK293T cells using the Lipofectamine^{TM} 2000 (L2000, **Figure 1.8**) as positive control and uncomplexed pEGFP-C1 and untreated cells as negative control. Direct GFP expression was only analysed after 48 hours and, as expected, similar results to DNA/Rho-9mer complex were obtained. The complex **4.62** achieved 27% of cellular labelling. This result was still lower than the one obtained with the Lipofectamine^{TM}2000 (48%).

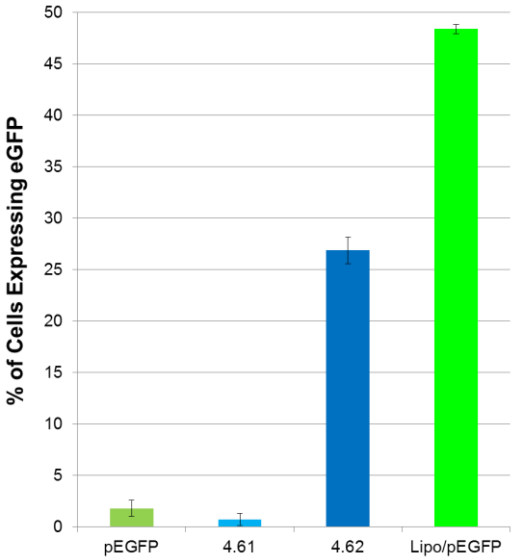

Graph 4.4: Flow analysis of cellular uptake of the DNA complexation with HO-PEG-PEG-9mer peptoid (4.61) in HEK293T cells.
% uptake measured for the direct expression of GFP using eGFP plasmid (0.5 µg of DNA/well), Lipofectamine™ 2000 (0.5 µg of DNA/well), HO-PEG-PEG-9mer (**4.61**, 13 µM) and DNA/ HO-PEG-PEG-9mer complex **4.62** (0.5 µg of DNA/well) as the % of cells with a fluorescent emission exceeding untreated control as 0% uptake (incubation time = 48 hours). The errors bar represents the standard error of the average (n = 3).

The direct expression of the GFP was confirmed by live cells microscopy (**Figure 4.30**), where the direct GFP expression can be easily monitored. Unfortunately, the images were not as good as expected. Indeed after washing most of the cells were detached due to a too high confluence of the cells. Indeed, the cells were plated for 3 days before being analysed and the confluence of the cells was 85% at day 1. To ensure that it was just a problem of confluence, the cytotoxicity of the DNA/peptoid complexes was assessed using MTT assays.

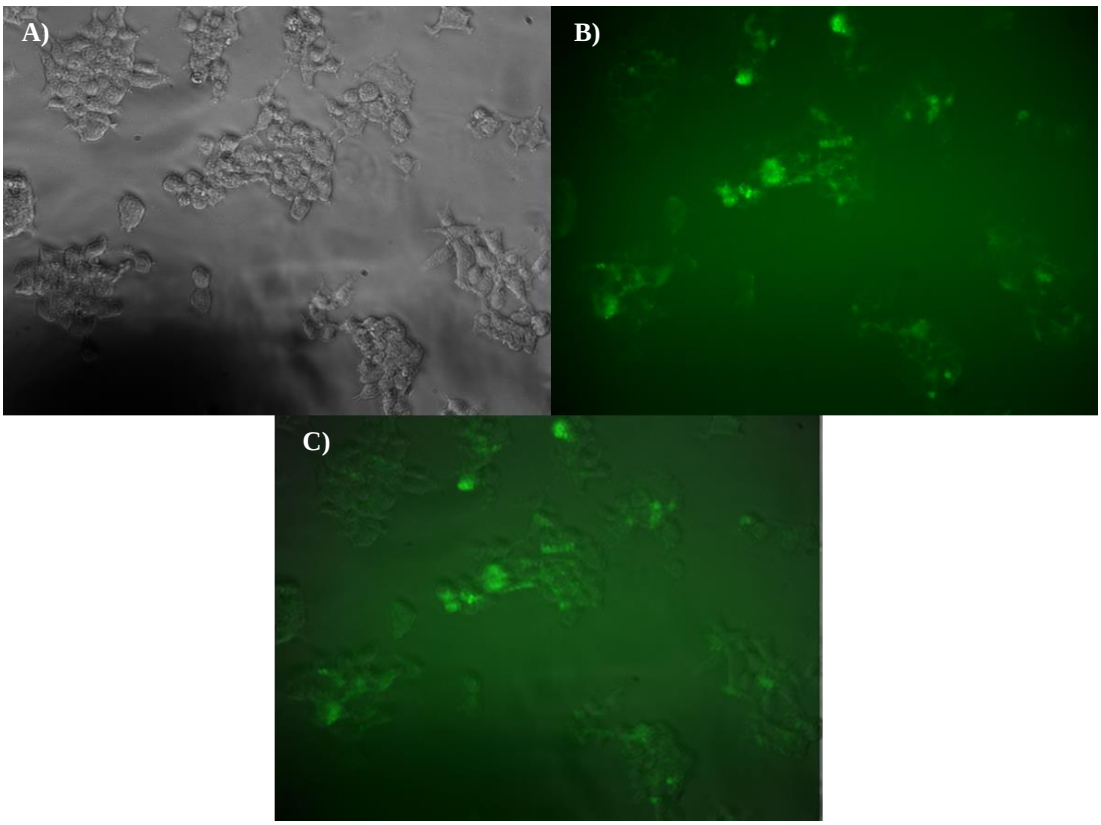

Figure 4.30: Microscopy of the cellular delivery of DNA/HO-PEG-PEG-9mer complex, 4.62. These images were taken after incubation of the HeLa cells for 48 hours at 37^{o}C with the complex **4.62.** A) Brightfield image; B) eGFP fluorescent image (excitation 450-490 nm); C) Fluorescence image merge with brightfield.

4.3.4. Cytotoxicity assays of the DNA/pepoid complexation

The MTT assay was carried out using 85% of confluency on the day on the injection of the several compounds to test. At the concentrations and time of incubation used none of the peptoids (**2.37** and **4.61**) and their DNA/peptoids complexes shown cytotoxicity towards HEK293T cells (**Graph 4.5**).

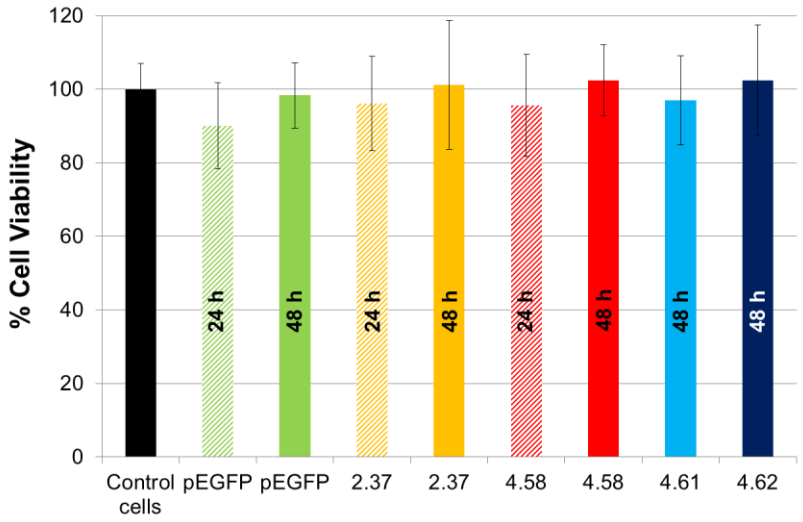

Graph 4.5: MTT analysis of the several pEGFP/peptoid complexes in HEK293T cells. HEK293T cells incubated with pEGFP (0.1 µg of DNA/well), pEGFP/Rho-9mer (**4.58,** 0.1 µg of DNA/well), Rho-9mer (**2.37**, 13 µM), HO-PEG-PEG-9mer (**4.61**, 13 µM) and pEGFP/PEG-9mer (**4.62,** 0.1 µg of DNA/well), for 24 and/or 48 hours before being treated with MTT. Healthy cells corresponded to 100% cell viability. The errors bar represents the standard error of the average (n = 8).

4.3.5. Conclusions

The nonalysine-like peptoid was able to complex the eGFP plasmid and to deliver it into the nucleus of HEK293T. Once inside the nucleus, the DNA was released and was transformed into RNA before being translated in the cytoplasm into eGFP. Both peptoids **2.37** and **4.61** enabled transfection without cytotoxicity. Although, the DNA delivery obtained with the peptoids was lower than the ones with the Lipofectamine™ 2000, the peptoids showed no cytotoxicity in various cell lines and allowed a delivery of the DNA into T cells. To increase the cellular labelling, studies could be carried out on the stability of the complex and on the capacity of the complex to access the nucleus. As the complex DNA/peptoid is not cytotoxic, longer incubation time (72 hours) could also be tested. Also, studies on the cellular uptake mechanism could be carried out allowing a better understanding of the poor eGFP expression. Indeed, use of lysosome/endosome trackers could show if the complex is isolated and, therefore, unable to be released to the cytoplasm for expression of the DNA. The presence of the DNA inside the cells could also be confirmed by labelling the DNA prior to complexion with the peptoid.

CHAPTER 5 : UNLABELLED NONALYSINE-LIKE PEPTOID AS AN ANTIBIOTIC (COLLABORATION WITH DR. KEVIN DHALIWAL)

5.1. Small peptides and peptoids as antimicrobial agents

5.1.1. Bacteria-Introduction

Bacteria are prokaryotic cells with a size range from 0.1 up to 10 micrometers (linear dimension). These microorganisms possess a simple structure. The cytoplasm is protected by a tough protective coat, the so-called cell wall. In comparison to eukaryotes, prokaryotic organisms are devoid of a specific defined cell nucleus. Indeed, the genetic material of the organism, circular DNA contained within the so-called nucleoid, which is located into the cytoplasmic compartment, as well as the RNA, proteins and several small molecules.[244]

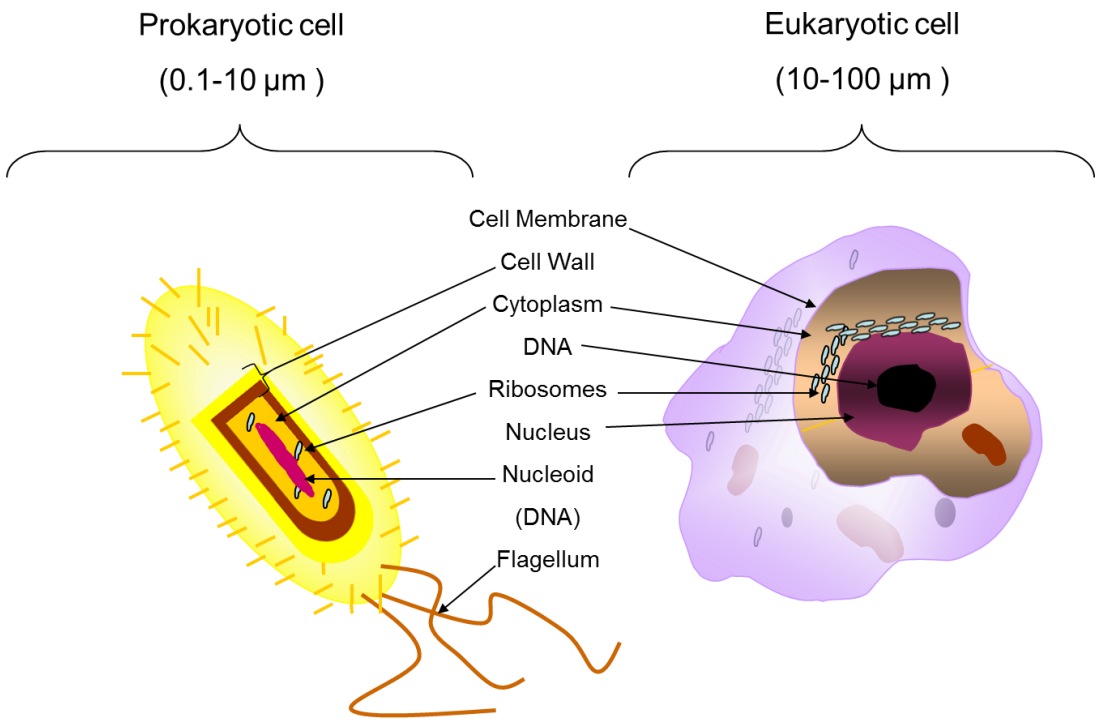

Figure 5.1: Schematic representation of both types of cells, prokaryotic on the left and eukaryotic on the right.

Bacteria are characterised using two major criteria. The first is the morphology of the bacteria (size, shape and organisation), namely rod-like, spherical and spiral (helical). The second criterion is based on the cell wall structure. The bacteria cell wall is composed of liposaccharides, proteins and peptidoglycans. Using the Gram's method or Gram staining, bacteria can be sorted as a function of their percentage of peptidoglycans present in the cell wall.[245] This colorimetric technique, based on crystal violet, was published in 1884 by Hans Christian Gram.[246] Using this protocol, bacteria are readily separated into two large groups: Gram positive (stains purple) and Gram negative (stains pink) bacteria. **Gram positive** bacteria (e.g. Staphylococcus aureus) have a thick cell wall consisting of three layers, which are (going from the exterior to the inside) peptidoglycans (at least 50% of the whole cell wall), periplasmic space and the plasma membrane (lipid bilayer). **Gram negative** (e.g. Escherichia coli) have a thinner cell wall composed by five layers starting outside with outer membrane (lipopolysaccharides and proteins), periplasmic space, peptidoglycans (10% of the whole cell wall), periplasmic space and finishing inside by the plasma membrane.

Bacteria are present everywhere[247] including in Human body with 10^{13} bacteria in the human gut,[248] therefore all the bacteria are not harmful. Nevertheless, several species are known to cause severe infections. For instance, cholera (*Vibrio cholerae*),[249] syphilis (*Treponema pallidum*)[250] and Lyme disease (*Borrelia burgdorferi*)[251] are human illnesses mediated by bacteria. In developed countries, a major concern is community-acquired pneumonia. This infection contracted during hospitalisation is mainly caused by three bacteria: *Streptococcus pneumoniae*, *Haemophilus influenzae* and *Moraxella catarrhalis*.[252] Meanwhile worldwide the most fatal bacterial malady is tuberculosis (*Mycobacterium tuberculosis*), with 9.3 million new cases in 2007 leading to 1.3 million deaths (it also causes 23% of all HIV/AIDS deaths).[253]

5.1.2. Antibiotics

Antibiotics are, by definition, substances that work against bacteria by killing them or inhibiting their growth. The first modern antibiotic, penicillin **5.1** was discovered in 1929 by Alexander Fleming, with the clinically useful antibiotic benzylpenicillin isolated by Chain (**Figure 5.2**)[254, 255] but nowadays many antibiotics are known and

used daily. They are often classified according to their target. For instance, quinolones (e.g. nalidixic acid **5.2**) inhibit DNA gyrase and therefore DNA replication,[256] while aminoglycosides (e.g. streptomycin **5.3**) block the synthesis of proteins by binding to a ribosomal subunit preventing the translocation of mRNA to proteins.[257] As far as the penicillin family (penicillin and cephalosporin) is concerned, it prevents the cross-linking of peptidoglycans.[258] Peptidic chains of peptidoglycans are cross-linked together by a transpeptidase to form a strong, rigid cell wall.[259]

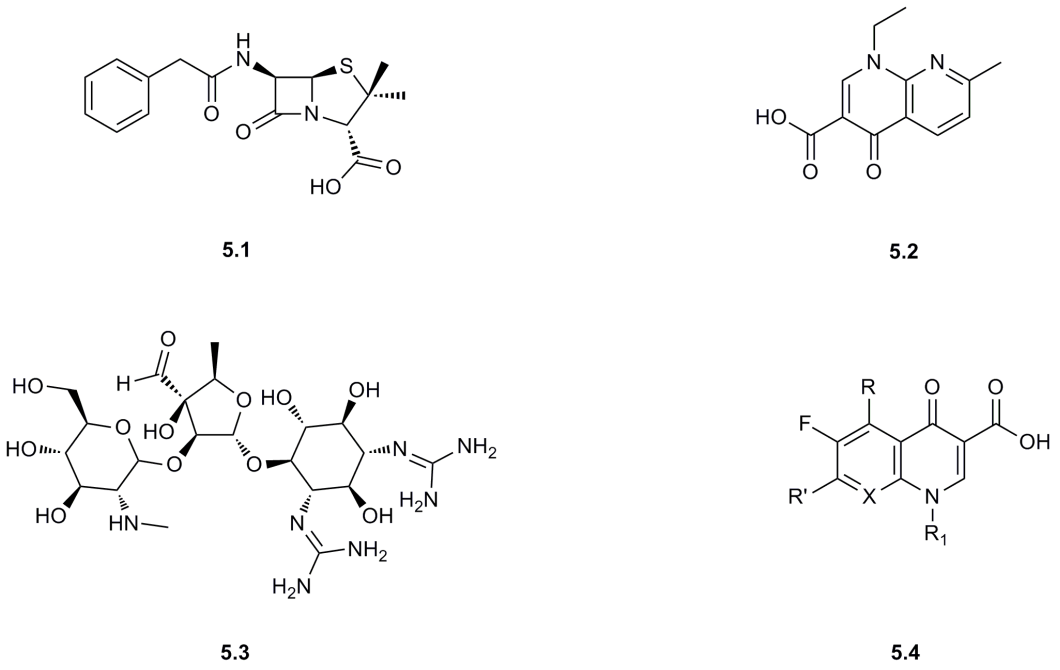

Figure 5.2: Structures of some common antibiotics.
5.1: penicillin G (benzylpenicillin), **5.2**: nalixidic acid, **5.3**: streptomycin and **5.4**: general structure of fluoroquinolones.

Even though antibiotics have proven their worth (estimated in 2002 to up to 200 000 tonnes of antibiotics per year), their excessive use is partially responsible for a problem known as antibacterial resistance.[260] This medical issue is not new as it was first observed in a military hospital in 1938.[261] Bacteria thus protect themselves from antibiotic treatments thanks to one or several genetic modifications. These changes are manifold and may allow decreasing the cell wall permeability, blocking the drug binding site or deactivation of the drug.[262] Unfortunately, antibacterial resistance has kept increasing generating major concerns within the medical community leading to

complications and numerous fatal outcomes, and warnings of a return to the pre-antibiotic era.

Antibacterial resistance is not the only issue to this treatment. Side effects, low efficiency and low bioavailability[263] at sites of chronic infection are known problems linked to antimicrobial cure. For instance, fluoroquinolones (**5.4, Figure 5.2**) are often associated with adverse gastrointestional reactions, central nervous system disorders or photo-toxicity.[264] Another limitation to antibiotic treatment is access to the intracellular niche.[265] These intracellular niches are small pockets located in the eukaryotic cells. These niches can contain bacteria inactive or duplicating without affecting the cells. Later on, these "dormant" bacteria can get released into healthy cells and generate infection. *Helicobacter pylori*, as an example, are bacteria involved in peptic ulcer disease, have shown the ability to penetrate epithelial cells and to survive inside macrophages and neutrophils.[266] Even if the bacteria within these sites are often non-multiplying, they act like a reserve, from where multiplying bacteria can easily emerge and generate chronic infections.[267] One solution to this issue could be based on the study of the antibacterial potential of natural compounds known to cross both eukaryotic and prokaryotic cell membranes like peptides.

5.1.2.1. Antimicrobial peptides (AMPs)

In 1925, Gratia reported that some peptides were toxic to certain strains of *Escherichia coli*.[268] These peptides were the bacteriocins, synthesised ribosomally but with extensive post-translational modifications. The most famous of these peptides, nisin **5.5** (**Figure 5.3**) was discovered in 1933 by Whitehead[269] and isolated in 1947 by Mattick and Hirsch.[270] This 34 amino acid polycyclic peptide was produced by fermentation of the bacterium *Lactococcus lactis*.[271]

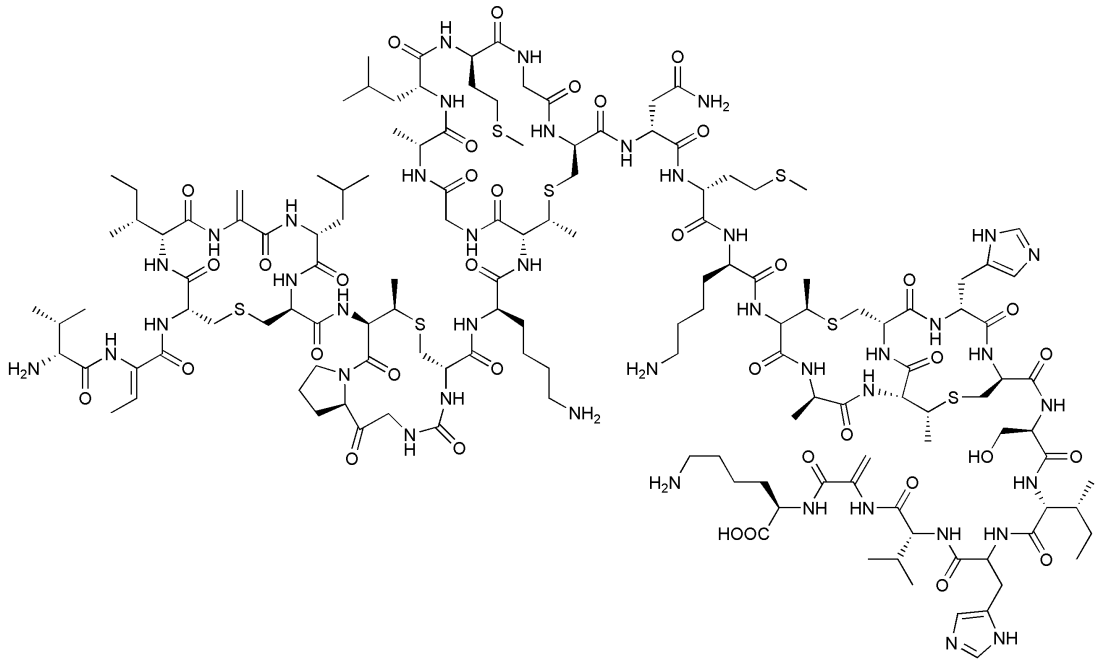

Figure 5.3: Structure of the commercial nisin (5.5).

Nevertheless bacteriocin peptides were not the only class of molecules to gain the attention of scientists. For more than 50 years, peptides have been described in the literature for being able to penetrate the bacterial cell wall.[272] At first, most of these peptides did not seem to possess any other activity than being bacteria's nutriments. Nevertheless, in the early 1980's, cationic peptides possessing antibacterial activities were discovered in the cecropia moth.[273] Since this discovery, any peptide with toxic effects on bacteria has been termed as antimicrobial peptide (AMP). This breakthrough continued with the publication of a family of cationic peptides, termed the Magainins (e.g. magainin-1, 23 AAs), which was isolated from the skin of a Sub-Saharian frog, *Xenopus laevis*.[274] This group of AMPs is composed of 23-27 amino acids that organize themself into amphipathic α-helices able to penetrate the cell-wall.[275] Defensins (e.g. Human Beta-Defensin 1, HBD1, 68 AAs) are another famous family of AMPs. These cationic peptides often contain 6 to 8 cysteines that generate disulfide bridges and form β-sheets. The killing process of defensins is based on the permeabilisation of the bacterial cell wall allowing the uncontrolled penetration and efflux of small molecules into the cytoplasm. Once within the bacteria, these small compounds can inhibit RNA, DNA and protein synthesis leading to the death of the microorganisms.[276]

Nowadays, more than 850 eukaryotic and prokaryotic AMPs have been listed in databases[277] and some of them are commercially available, such as Nisin[278] (**5.5**, **Figure 5.3**) and Gramicidin[279] (**5.6**, **Figure 5.4**).

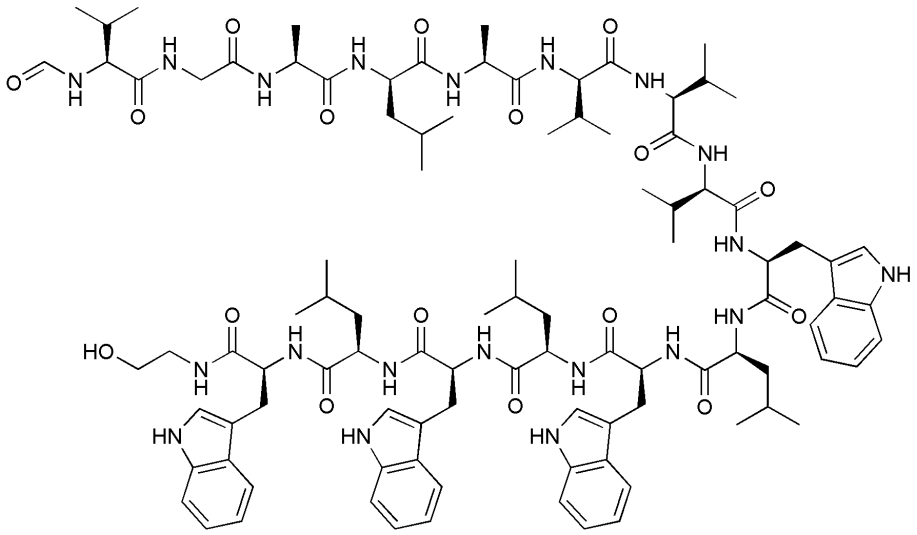

Figure 5.4: Structure of the gramicidin A (5.6).[279]

In Nature, a large diversity of antimicrobial peptides (sequences and structures) exists preventing or delaying antimicrobial resistance. At this time, even if some papers described some examples of antibiotic resistance towards some AMPs,[280, 281] they remain the type of antimicrobial treatment having so far demonstrated the smallest resistance while showing potent effects.[282, 283] Nevertheless, as for the CPPs (***CHAPTER 1***) and peptides in general (except for instance cyclic peptides,[284] proline and D-amino acids based peptides[285]), antibacterial peptides can be very sensitive to proteolytic degradation and, therefore, have limited *in vivo* application.[286, 287]

The use of analogues of theses peptides can be considered allowing them to retain biological activity while increasing the resistance against proteases and controlling the cytotoxicity to the host cell.

5.1.2.2. Use of peptoids as antibacterial agents

N-substituted glycines have been reported to be an efficient peptidomimetics of various biologically active peptides such as CPPs and lung protein surfactants.[288]

Thanks to their structure (N-substituted rather than α-carbon-substituted glycine), peptoids have demonstrated a higher resistance to proteolysis compared to the analogous peptides, while remaining similar biological activity.[289]

Peptoids as antibacterial agents were first reported by Goodson in 1999.[290, 291] Using combinatorial chemistry, a library of trimer peptoids was synthesised and screened for antibacterial activity. Trimers were tested using a growth inhibition assay against *Staphylococcus aureus* (gram positive) and *Escherichia coli* (gram negative).[291] Using these data, a series of peptoids containing DHAA (dehydroabiethylamine, **5.7**, **Figure 5.5**) was identified. DHAA possesses antibacterial activity and is structurally similar to totarol (**5.8**, **Figure 5.5**), a natural compound with anti-staphylococcal activity.

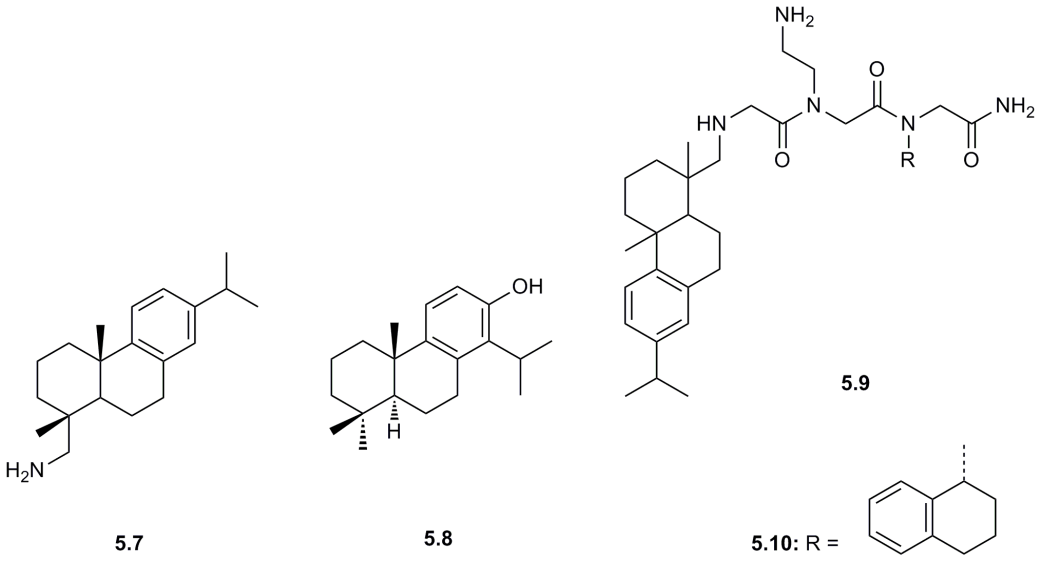

Figure 5.5: Structure of DHAA (5.7), totarol (5.8) and DHAA-trimer peptoids (5.9 and 5.10).

DHAA-trimer peptoids (**5.9**) were shown to have efficient *in vitro* bactericidal activities against various bacteria (gram positive and gram negative). *In vivo* studies demonstrated 100% survival of mice infected with *S. aureus* after treatment with 30 mg/kg of trimer **5.10** (**Figure 5.5**).[292] Although these results were very promising and demonstrated the potential of peptoid as antibiotic, the next paper based on a peptoid as an antibacterial agent was published four years later by Messeguer.[292] Using a submonomer approach, the synthesis of 10648 peptoids was carried out. These N-substituted glycine trimers were screened against six bacterial strains (including

Staphyloccocus aureus (gram positive) and *Pseudomonas aeruginosa* (gram negative)). From this study, one potential trimer peptoid (**Figure 5.6**, **5.11**) was isolated. Surprisingly, this hit (**5.11**) had a similar structure to Goodson's agent (**5.7**) but with a lower efficiency (similar MIC data but at least 2.5 less potent for MBC assays). The same year, 2003, two new classes of antibacterial peptoids were synthesised. The first class was made with at least three N-substituted glycine units and mimicked natural or non-natural AMPs. The family of compounds, published by Barron, were named as AmPetoids, or anti-microbial peptoid oligomers.[293] After publishing a paper with Zuckermann on the synthesis of stable α-helical peptoids,[294, 295] Barron reported the design and the antibacterial character of a peptoid series that mimicked the antibiotic Magainin-2-amide.[293] All these oligomer structures were composed with *N*-lysine and N-α-chiral side chains, such as *N*-phenylethyl. These two kinds of N-substitution were used to generate an amphipathic α-helical secondary structure. The highest antibacterial efficiency was achieved by a 12mer (**5.12**) made of *N*-(4-aminobutyl)glycine (NLys) and (*S*)-*N*-(1-phenylethyl)glycine (Nspe) residues only (**Figure 5.6, 5.12**). This analogue showed the lowest MIC against both gram positive (0.82 ± 0.14 μg/mL) and gram negative (5.4 ± 0.9 μg/mL) bacteria. Furthermore, using these MIC concentrations, peptoid **5.12** did not demonstrate haemolytic activity below 10 μg/mL.

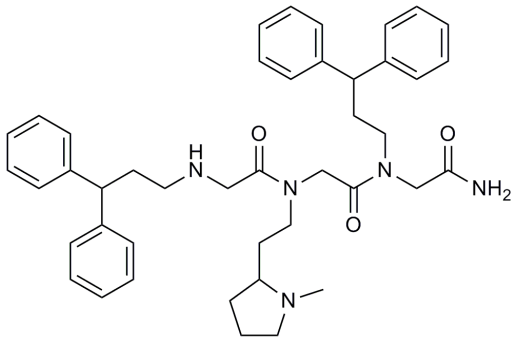

5.11

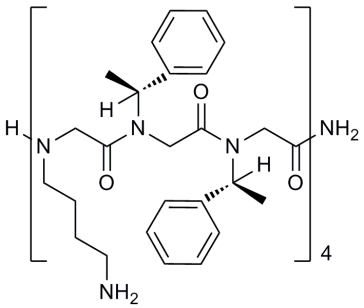

5.12

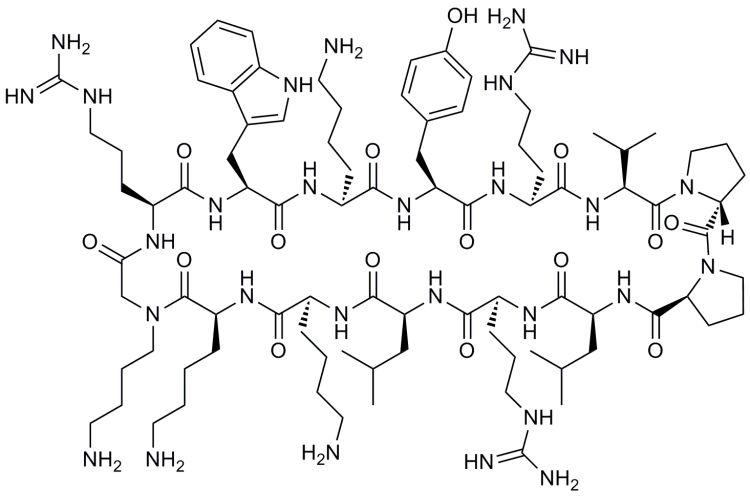

5.13

Figure 5.6: Representation of antibiotics containing a peptoid structure.
5.11: [*N*-(3,3-Diphenylpropyl)glycyl]-[*N*-[2-(2-(1-methylpyrrolidinyl))ethyl]glycyl]-*N*-(3,3-diphenylpropyl)glycinamide ,[292] **5.12**: 12mer peptoid mimicking magainin-2-amide based on NLys and Nspe units,[293] **5.13**: hybrid protegrin-I mimic.[296]

Another class are the hybrid or mixed peptide-peptoids. Robisson was pioneer in this area with the synthesis of hybrid protegrin-I mimics.[296] They substituted into their lead peptide mimic[297] one or more lysines and arginines by at least one NLys peptoid residue. One of these hybrids (**Figure 5.6**, **5.13**) showed a higher efficiency compared to the lead peptide (up to 2 times more efficient for MIC assays) against both gram bacteria but was less potent compared to protegrin (16 fold less potent in MIC assays). The hybrid (**5.13)** showed almost no hemolysis (0.5%) while the natural antibiotic hemolysed 37% of the human red blood cells at 100 mg/mL. Some antibacterial studies have been carried out using β-peptoids, but so far β-peptoids have not shown a good efficiency-toxicity ratio (toward red blood cell).[298] Hybrids have been also studied by Shin.[299] His work consisted of the substitution of a few key amino acids inside a known peptide by a N-substituted glycine, for instance of a proline unit was replaced by an *N*-alanine (NAla).[300] Hansen isolated a peptoid lead (**Figure 5.7**, **5.14**) that was composed by three different N-substituted glycines.[301] Using these results, 20 new peptoid-peptide hybrids were prepared by introducing one or several lysine units (up to six Lys, outside **5.15** or mixed **5.16**) to the peptoid lead core (**5.14**). These both hybrid matched the MIC values of the peptoid **5.14**

(MIC values for *S. aureus*: **5.14** and **5.15** = 2 and **5.16** = 5 μM) while decreasing dramatically hemolysis (from 100% for **5.14** down to 4% for **5.15** and 6% for **5.16** at 50 μM). Nevertheless none of these hybrids have been tested *in vivo*. Many papers on peptoid oligomers as antibiotics have been published by the Barron group, such as helical peptoids (based on **5.12**)[302] and lipopeptoids (peptoid structure containing DOPA units).[303]

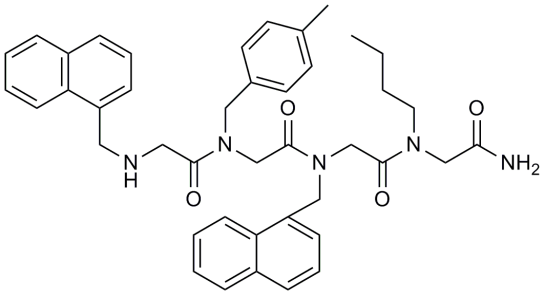

5.14

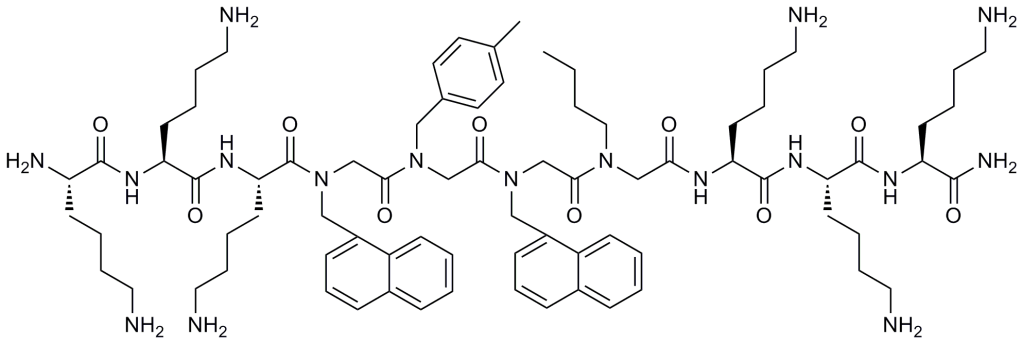

5.15

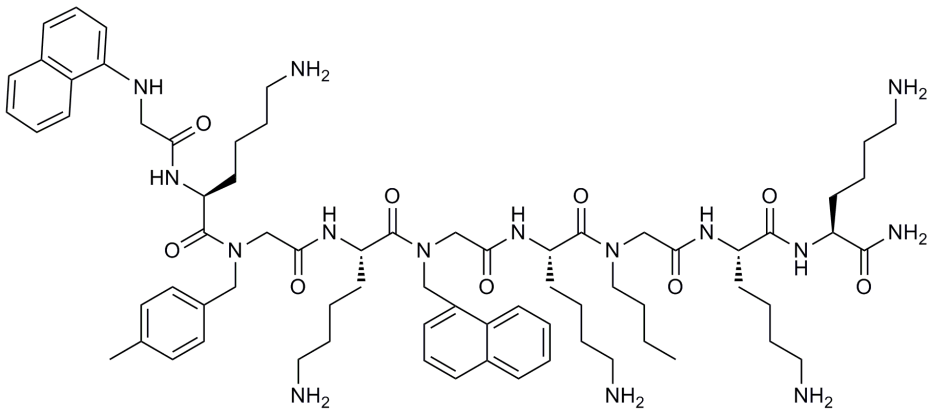

5.16

Figure 5.7: Structure of Hansen peptoid (5.14) and lysine-peptoid hybrids (5.15 and 5.16).[301]

In this chapter, the naked 9mer, termed nonalysine-like peptoid, (NLLP, **Figure 5.8**, **5.17**) was studied as an antibacterial agent. The term NLLP was used to emphasise the difference between the labelled peptoid and the non-labelled one.

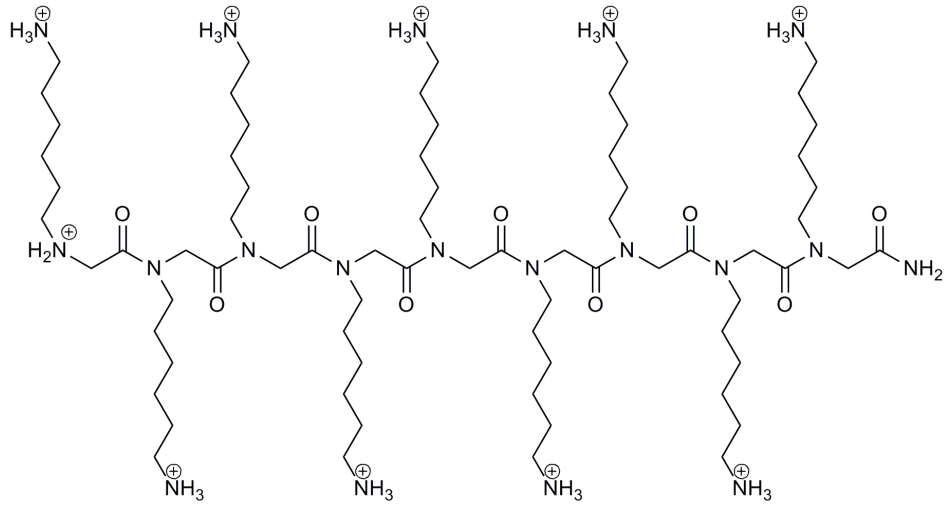

5.17

Figure 5.8: Structure of NLLP (nonalysine-like peptoid) 5.17.

This peptoid core has already been reported (***CHAPTER 2*** and ***CHAPTER 3***) as an efficient and non-toxic cellular penetrating compound in both *in vitro* and *in vivo.* Here its antimicrobial properties were explored.

5.2. Synthesis, purification and quantification of the nonalysine-like peptoid (NLLP)

5.2.1. Solid-phase synthesis and analysis of the NLLP before purification

As described in the ***CHAPTER 2*** (**Scheme 2.12**), the peptoid **5.17** was prepared using a monomer strategy followed by a microwave assisted solid-phase synthesis. However, at the time of this project (between July 2008 and December 2010) the use of the coupling reagent HOBt was restricted.[304,305] Thus, the solid-phase synthesis couplings were carried out in the same conditions than HOBt/DIC but HOBt was replaced by oxyma (**Figure 5.9**, **5.18**)[306] using 3 equivalent of reagents at 60°C for 20

minutes (microwave) and a concentration of 0.2 M. Coupling completion was confirmed using ninhydrin[129] or chloranil tests.[130]

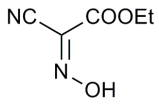

5.18

Figure 5.9: Structure of the coupling reagent oxyma (ethyl 2-cyano-2-(hydroxyimino)acetate, 5.18).

Once the nine units of N-Fmoc-N-(6-N'-Boc-aminohexyl)-glycine (**2.22**) were coupled on to the Rink amide polystyrene resin, the Fmoc group was removed and NLLP **5.17** was Boc-deprotected and cleaved from the resin. NLLP peptoid (**5.17**) was analysed by ^{1}H-NMR, MS (**Appendix 5-2**) and HPLC (**Figure 5.10**).

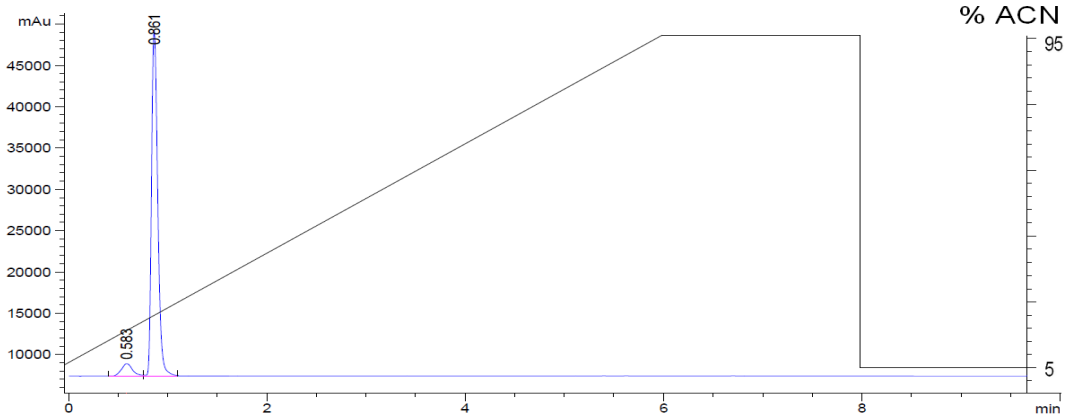

Figure 5.10: HPLC trace (ESLD) of the unpured NLLP (5.17).

The synthesis of the peptoid **5.17** was a success, however, the exact yield of this reaction was difficult to calculate due to the high hygroscopic character of the NLLP (based on the theoretical loading capacity (**Equation 6.2**)[307], the mass was superior to what was expected).

In addition due to its nature it eluted very rapidly by HPLC (**Figure 5.10**). An exact quantification of the NLLP peptoid and its purification were essential before starting any biological assays. Therefore, a solution was required to be able to separate and isolated the NLLP from the other materials (e.g. 8mer, 7mer, etc…).

5.2.2. Purification of the NLLP

5.2.2.1. Design of the purification protocol

In order to separate the several peptoids (9mer, 8mer,…), one solution was to the decrease the hydrophilicity of the peptoids thanks to protecting groups. During the SPPS of the NLLP, amino groups on the side chains were protected with Boc groups. The initial idea was to keep the Boc groups during the cleavage of the NLLP from the Rink amide polystyrene resin. Until now, the only publication dealing with selective deprotection between Boc protective group and the Rink amide linker describes the deprotection of the *tert*-butyloxycarbonyl while the peptides were still attached on the resin.[308] Therefore, a new method allowing the cleavage of the peptoid from the Rink amide polystyrene resin without deprotection of the Boc side chains was required. Before investigating the peptoid cleavage from the resin, the stability of the Boc group against TFA was determined using Fmoc-Lys(Boc)-OH and different concentrations of TFA. The reactions were monitored after neutralisation (using Et_3N) by HPLC and MS.

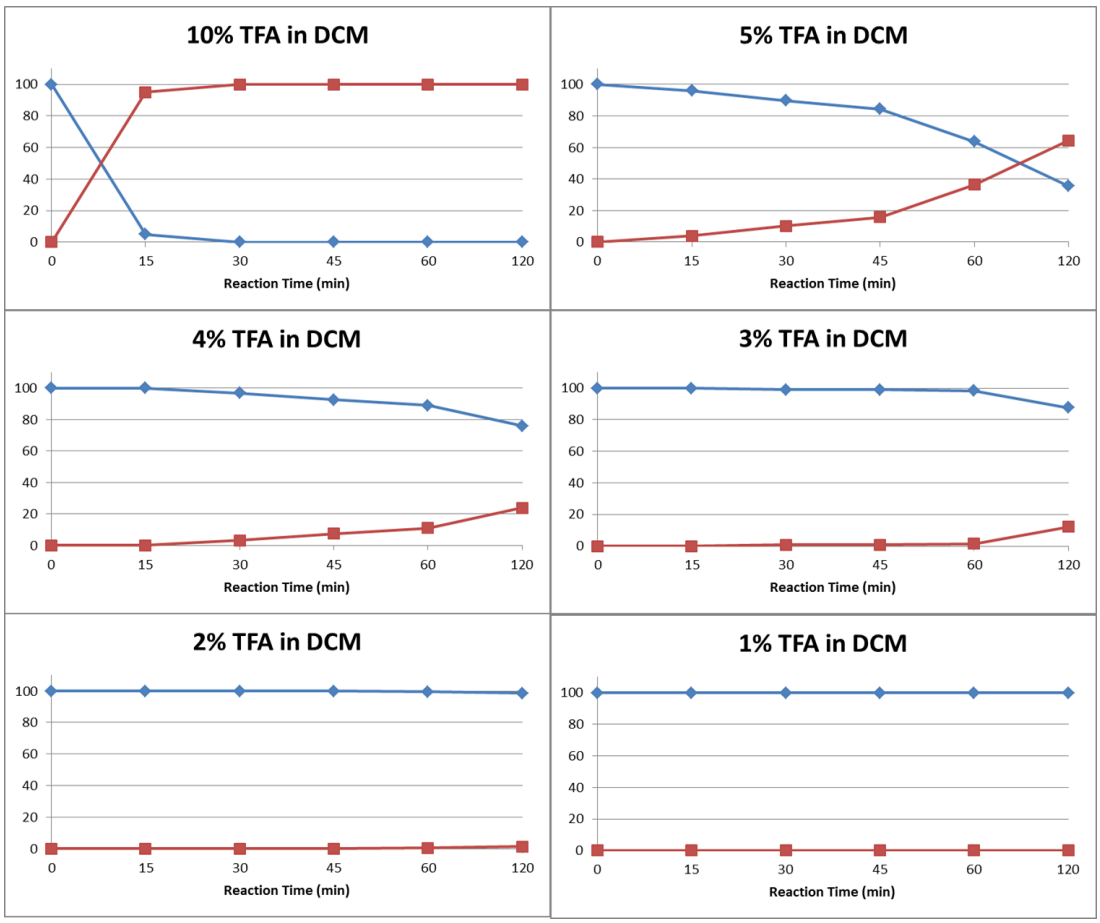

Graph 5.1: Boc group stability against TFA in DCM.
Blue line: % of Fmoc-Lys(Boc)-OH; Red line: % of Fmoc-Lys-OH calculated from the HPLC trace (ELSD).

Graph 5.1 showed that the Boc group was stable in solutions containing up to 3% TFA. A 10% TFA solution fully removed the Boc group in less than 30 minutes.

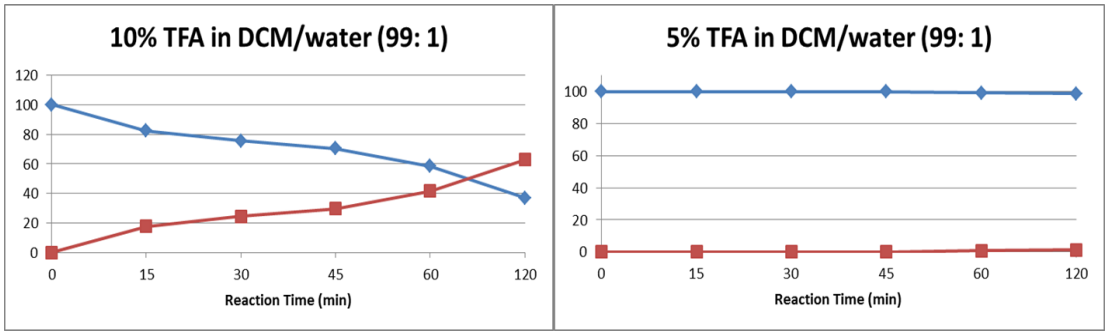

Graph 5.2: Boc group stability against TFA in DCM/water (99:1).
Blue line: % of Fmoc-Lys(Boc)-OH; Red line: % of Fmoc-Lys-OH calculated from the HPLC trace (ELSD).

Secondly, the effect of TFA in presence of water (1% in DCM) on Boc stability was also tested (**Graph 5.2**). For 10% TFA in DCM/water (99: 1), the addition of water clearly slowed down Boc removal and in 5% TFA in DCM/water, the Boc group was stable, even after 2 hours. Using these data, the cleavage of Rink amide linker will need to be carried out using a maximum of 5% TFA in DCM/H_2O (99: 1).

In order to cleave the Rink amide linker while keeping the amines protected, two strategies were tested: a traditional cleavage protocol and a flow band approach. Both techniques were applied on the trimer model (**5.19**, **Figure 5.11-A**).

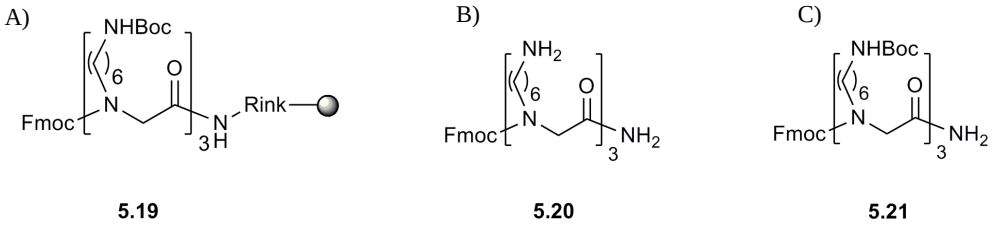

5.19 **5.20** **5.21**

Figure 5.11: Structure of the 3mer lysine-like peptoids.
A) Fmoc and Boc protected 3mer peptoid on Rink amide polystyrene resin (**5.19**); B) Fmoc-3mer peptoid (**5.20**); C) Fmoc and Boc protected 3mer (**5.21**).

Strategy 1: traditional cleavage protocol.

The first test was inspired by Brown's paper.[309] In this publication, small alkylated molecules were prepared on the Rink amide polystyrene resin. The cleavage of these amide materials from the solid support was achieved over two 20 minutes treatments using a mixture DCM/TFA/H_2O (95: 5: 1). For the first assay of this method, the same cleavage solution (DCM/TFA/H_2O, 95: 5: 1) was applied onto the resin **5.19**. Previously, data showed that the Boc group started to be deprotected after 15 minutes using 5% of TFA in DCM. The resin **5.19** was treated with TFA solution (DCM/TFA/H_2O, 95: 5: 1) for 4 × 10 minutes cycle with the filtrate collected in 3% triethylamine (DCM) and analysed by HPLC and MS. The change of the resin colour was also monitored. For this first cleavage, the colour of the polystyrene beads has changed from yellowish to reddish and to very dark red (corresponding to the formation of a carbocation (**Scheme 2.10**, ***CHAPTER 2***)). HPLC and MS analysis (**Figure 5.12** and **Appendix 5-3**) of the filtrate revealed the presence of three

compounds: the fully unprotected, the mono Boc-protected and the di Boc-protected compounds.

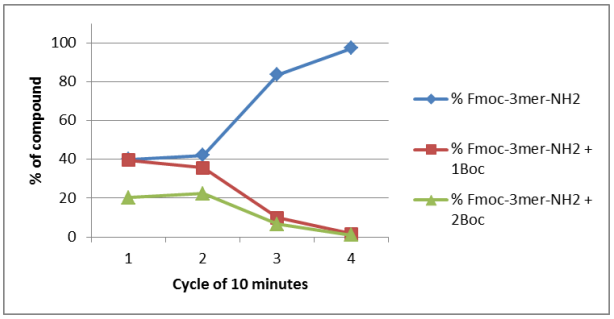

Graph 5.3 : Percentage of each product present at the end of each cleavage cycle.
Treatment of the resin **5.19** with DCM/TFA/H_2O (95: 5: 1), 4 cycles of 10 minutes. The percentage of products was calculated from the area of each peak by HPLC (ELSD).

Graph 5.3 summarised the percentage of each product present in each cycle filtrate. From the third cycle of cleavage, only the fully deprotected compound was recovered in the filtrate.

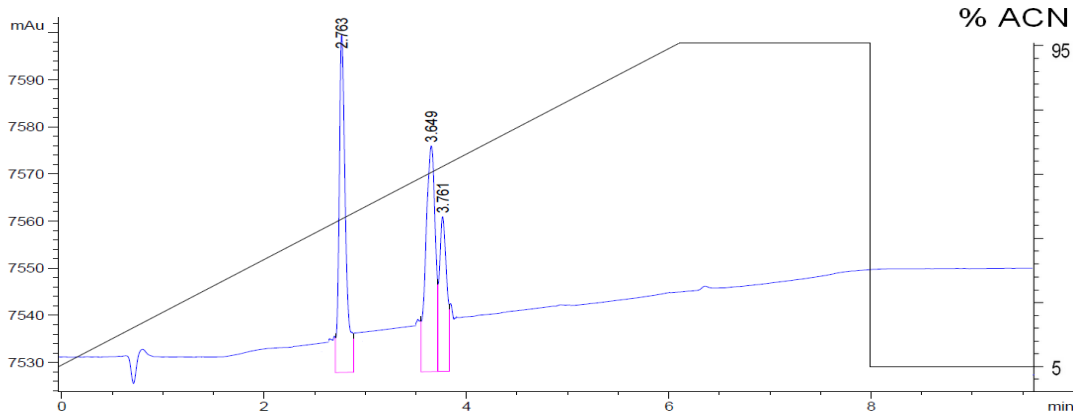

Figure 5.12: HPLC trace (ELSD) of the first cycle filtrate.
t_R = 2.8 min corresponded to Fmoc-3mer-NH_2 (**5.20**); t_R = 3.6 min corresponded to Fmoc-3mer-NH_2 + 1 Boc; t_R = 3.6 min corresponded to Fmoc-3mer-NH_2 + 2 Boc.

Having three different Boc protected peptoids clearly did not help the purification process. To solve this problem, various conditions were tested, in which the percentage of TFA and the reaction time were changed (***CHAPTER 6***, **6.6.4.1**). The peak corresponding (m/z = 1008.42 $[M+H]^+$) to the protected 3mer peptoid **5.21** was only detected by MS analysis (**Appendix 5-4**) using DCM/TFA/H_2O (96: 3: 1) for 2 hours. Unfortunately, the quantity of protected peptoid **5.21** recovered was tiny and

unpure (mixture of protected and non-protected 3mer). Treatment of the orange remaining resin with 95% TFA in DCM showed that more than 90% of product (**5.20**) was still attached to the solid support.

Strategy 2: Flow chemistry.

A flow cleavage was carried out.[310] A continuous flow of TFA solution was passed through the resin **5.19** before being collected into a solution of TEA (3% in DCM). The filtrate was analysed by HPLC and MS while the resin colour and the formation of precipitate (in diethylether) were also observed.

From the previous experiments, the addition of water clearly slows down the deprotection of the Boc group. Initially, solutions containing between 2 and 5% TFA in DCM/water (99: 1) were tested. As no cleavage product was detected or observed (resin color and precipitation), the percent of TFA was increased up to 10%. Only from 8% TFA were cleavage products observed, but once again it was a mixture of peptoid fully or partially deprotected.

As neither of these two methods allowed selective cleavage of the Rink amide polystyrene resin, another approach was applied. The principle was to fully deprotect the peptoid (including the terminal Fmoc group) and then reprotect each amino group with a Boc group.

5.2.2.2. Synthesis and purification of Boc-9mer(Boc)$_9$-NH$_2$

The 9mer peptoid resin **2.33** was Fmoc deprotected (20% piperidine in DMF) and then Boc deprotected and cleaved from the solid using TFA/TIS/H_2O (95: 2.5: 2.5). The peptoid isolated **5.17** was precipitated in cold ether before being Boc protected.

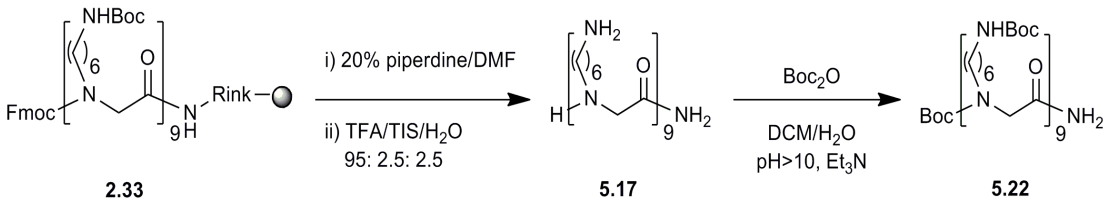

Scheme 5.1: Synthesis of Boc-9mer(Boc)$_9$-NH$_2$ peptoid (5.22).

The peptoid **5.17** unpure was dissolved in water with triethylamine (pH>10) before addition of the di-*tert*-butyl dicarbonate. The reaction was mixed for 2 hours at 30°C.[311] Once Boc-protected, the peptoid started to precipitate out of the solvent leading to a mixture of partially protected and fully protected peptoids. In order to solve this issue, the peptoid **5.17** was first dissolved in water with triethylamine as above (pH>10). A solution of Boc_2O (11 equivalents) in dichloromethane was then added to the aqueous solution of peptoid. The biphasic system was mixed for an hour. This version of Boc protection offered an easy isolation of the compounds with fully protected peptoid (**5.22**) automatically transferred into the organic phase. The Boc protection was carried out with 100% conversion calculated by HPLC analysis (**Figure 5.13**) (MS data: **Appendix 5-5**).

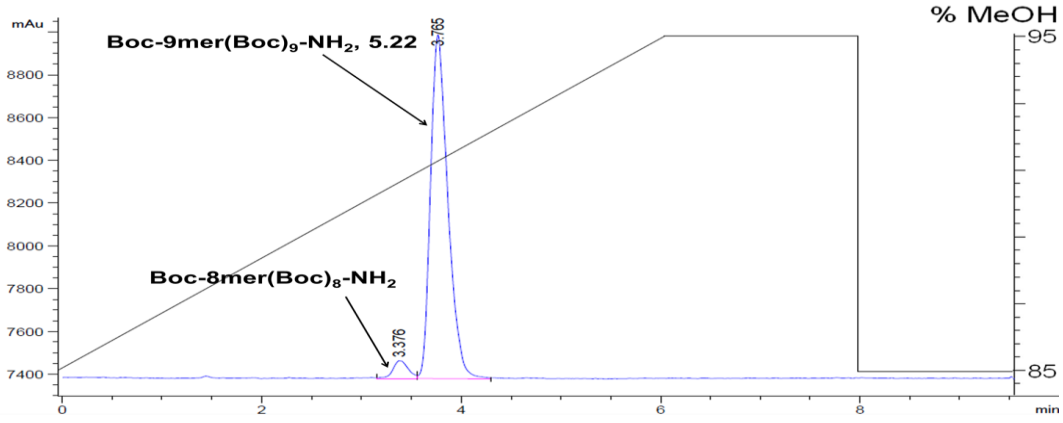

Figure 5.13: HPLC trace (ELSD) of crude Boc-9mer(Boc)$_9$-NH$_2$ peptoid (5.22).

The several peptoids were separated using preparative HPLC and the Boc-9mer(Boc)$_9$-NH$_2$ was isolated in a final yield of 80% (calculated from the theoretical loading of the resin **2.33**, HPLC: **Figure 5.14** and MS: **Appendix 5-6**).

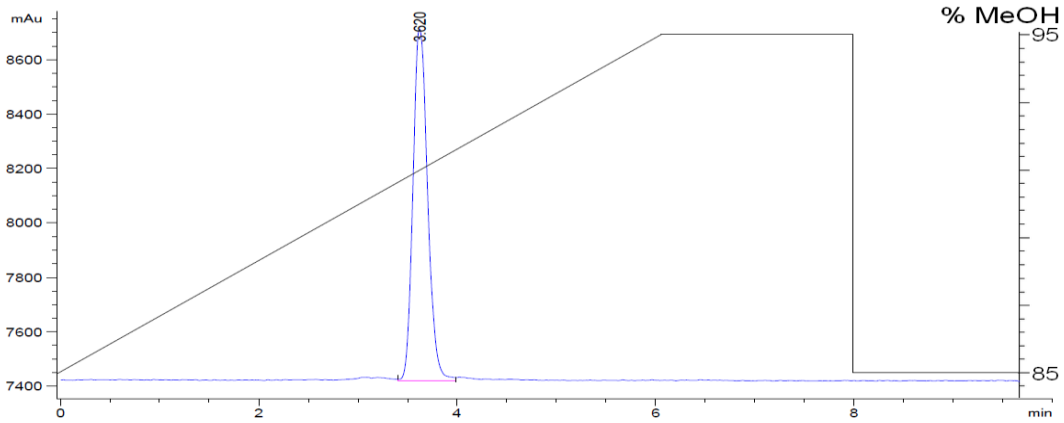

Figure 5.14: HPLC trace (ELSD) pure Boc-9mer(Boc)$_9$-NH$_2$ peptoid (5.22).

5.2.3. Quantification by NMR

Usually, the concentration of the peptoid solution was calculated using UV or weight. However, due to the highly hydroscopic character of the NLLP, the concentration was calculated using quantitative NMR (qNMR). NMR is typically used for qualitative purpose but can also be used as a quantitative analytical tool (quantitative NMR (qNMR)) and can be applied to all atoms possessing a nuclear spin. In the literature, qNMR refers to proton quantitative NMR. The interest in this quantitative technique has increased continuously over the past 40 years, especially thanks to the work of Turczan.[312] Several studies have demonstrated the power of this technique and its small error (0.5 to 2% range). In order to achieve a reproducible quantitative analysis, quantitative experimental conditions, post-acquisition processing and the choice of internal standard are three crucial factors.[313]

Efficient quantitative proton NMR required several parameters to be modified by the user:

- D1: relaxation delay in seconds,
- NS: number of scans,
- AQ: acquisition time in seconds.

For the following experiments, the temperature was fixed at 298 K and the samples were not spun. Spinning samples are usually used to improve the line shapes. This eliminates the need to adjust manually shims (shims are adjusted to have the

narrowest and most uniform line shape possible). Once all the shim axes are set up, all the other parameters can be modified.

Before starting a quantitative NMR experiment, the choice of an appropriate internal standard is essential. Efficient internal standard must possess all the following criterions:

- high purity,
- stable and chemically inert,
- non volatile, but with a boiling point allowing removal by evaporation,
- non hygroscopic,
- soluble in the NMR solvent,
- non interfering signal with the analyte ones.[313, 314]

Several organic compounds have already proven their efficiency as internal standard, such as hexamethyldisiloxane (**5.23**, HMDS),[315] 1,4-dioxane (**5.24**)[316] or 2,5-dimethylfuran (**5.25**).[314]

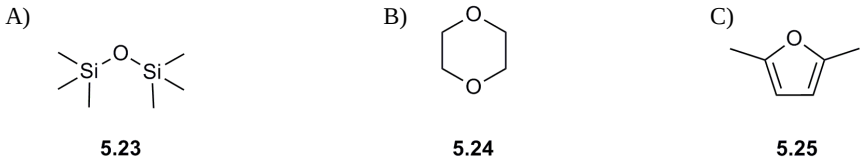

5.23 **5.24** **5.25**

Figure 5.15: Structure of internal standards for quantitative NMR.
A) hexadimethyldisiloxane, **5.23**; B) 1,4-dioxane, **5.24**; C) 2,5-dimethylfuran, **5.25**.

For the quantitative NMR of **5.22**, HMDS (**5.23**, **Figure 5.15-B**) was first thought. This internal standard has a singlet at 0.09 ppm (18H) corresponding to its six methylene groups and was previously used for quantitative NMR of β-peptoids.[315] HMDS possess all the criterion for a good internal standard (boiling point 101°C) and its signal does not interfere with the protons of Boc-9mer$(Boc)_9$-NH_2. However, the ^{1}H-NMR of **5.22** was run in deuterated chloroform ($CDCl_3$) and this solvent contained some trimethylsilane (TMS). All the protons of TMS and HMDS have same chemical shifts at 0.09 ppm and overlap. Therefore, the integration of HMDS would not be accurate resulting in an incorrect and non-precise quantitative NMR.

In literature, the control of another criterion, the ratio between signal and noise, was described as crucial for a quantitative NMR analysis. The use of an internal standard with two signals allows a good calibration of the instrument (internal relaxation standard) and thus a good control of the ratio noise/signal. 2,5-dimethylfuran (2,5-DMFu, **5.25**, **Figure 5.15-C**) possesses two types of protons and all the conditions to be an efficient internal standard for qNMR (boiling point 92-97°C). The methyl protons (s, 6H, 2 × CH_3) appear as a singlet at 2.27 ppm while the two heterocyclic hydrogens (s, 2H, 2 × CH) have a chemical shift of 5.85 ppm (**Appendix 5-7**). The quantitative NMR assay was carried out using 2,5-dimethylfuran as internal standard. The best relaxation delay (D1) was evaluated. From a previous paper, it was demonstrated that the best D1 for the 2,5-DMFu was 30 seconds.[314] This result was confirmed with ^{1}H NMR of **5.22** containing 2,5-DMFu (**5.25**) (**Table 5.1** and **Appendix 5-7**). In this experiment, the integration of the two heterocyclic protons (C*H*=C*H*) was fixed at 2 and the integration of the methylene hydrogens were measured. The best D1 for 2,5-DMFu (30 seconds) was obtained when the ratio between the two signals (CH_3 and C*H*) was equal to 1.00 to 3.00. The error with a D1 of one second was equal to 5.7% with little error observed with a D1 of 10 (error = 0.7%) or more seconds.

Relaxation delay (seconds)	Integration CH=CH (δ_H = 5.85 ppm)	Integration 2 × CH_3 (δ_H = 2.27 ppm)	Ratio between the two signals
1	2	6.34	1 : 3.17
10	2	6.04	1 : 3.02
30	2	6.00	1 : 3.00

Table 5.1: Relaxation delay assays on 2,5-dimethylfuran.
^{1}H NMR parameters used for this experiment: NS = 16, AQ = 2 sec, no spin, 400 MHz.

Relaxation time (T1) and relaxation delay (D1, D1 = 5 × T1) are inversely proportional to molecular weight.[314] The 2,5-DMFu (**5.25**) has a molecular weight (96.1 g/mol) much lower than the protected peptoid **5.22** (2422.7 g/mol), therefore a D1 of ten seconds should be enough for obtaining a relaxation of the peptoid protons. This theory was proved by measurement of integration of two types of peptoid

hydrogens (NCH_2O, δ_H = 4.12 ppm and CH_2CH_2N, δ_H = 3.32 ppm). The ratio between these two protons must be 1 to 1 (18H each).

Relaxation delay (seconds)	Integration CH_2CH_2N (δ_H = 3.32 ppm)	Integration NCH_2O (δ_H = 4.12 ppm)	Ratio between the two signals
1	10.14	10.20	1 : 1.005
10	9.04	9.09	1 : 1.005
30	9.03	9.09	1 : 1.006

Table 5.2: Relaxation delay assays for the peptoid 5.22.
^{1}H NMR parameters: NS = 16, AQ = 2 sec, no spin, 400 MHz.

As expected, the Boc-9mer$(Boc)_9$-NH_2 peptoid (**5.22**) with a higher molecular weight was less sensitive to the relaxation time delay than 2,5-DMFu. In order to have a good ratio for the internal standard and a fair experiment time, the following spectra were acquired using a D1 of 10 seconds.

Once the relaxation delay was set up, the next parameters to be adjusted were the number of scans (NS) and the acquisition time (AQ). Both factors were modified (NS tested = 16, 32, 64 and 128; AQ = 2, 16 and 32 seconds) without affecting the ratio N/S neither between two integrations (***6.6.6.2***). Therefore, the NMR parameters for the quantitative assays were the following: NS = 16, AQ = 2 seconds, D1 = 10 seconds, T = 298 K, $CDCl_3$ as solvent and 400 MHz (irradiation frequency).

Now that the experimental parameters were defined, the effect of concentrations was studied. In case of one of the both concentrations is much higher than the other, the ratio N/S for the lower concentrated compound will not be correct. In order to simply the process, commercially available Fmoc-Lys(Boc)-OH was used. One solution with a precise concentration was prepared in $CDCl_3$ for each compound (analyte: Fmoc-Lys(Boc)-OH and internal standard: 2,5-DMFu). The both solution were mixed together in order to increase the concentration of the internal standard in comparison to the one of the analyte. Once mixed, each sample was analysed and the integration of one type of proton for each molecules were recorded. To ensure a good quantification, the peaks chosen must have a good baseline and not overlap with

another signal. From these two criterions the following protons were used for the quantification:

- Analyte: d, δ_H = 7.75 ppm, 2H, ArC*H*-Fmoc;
- Internal standard: s, δ_H = 5.87 ppm, 2H, C*H*.

From the integrations and the concentration of the internal standard, the concentration of the analyte was calculated for each sample. In the **Table 5.3**, the ratio between the both concentrations was calculated from the expected concentration with the analyte as 1.

Concentration expected Fmoc-Lys(Boc)-OH (mM)	Concentration calculated Fmoc-Lys(Boc)-OH (mM)	Error between both concentrations of Fmoc-Lys(Boc)-OH (%)	Ratio concentration standard/analyte
0.8	2.56	68.7	53.5 : 1
1.4	4.26	67.1	27 : 1
1.6	4.52	64.6	20 : 1
3.73	3.95	5.5	4.5 : 1
4.2	4.17	0.7	3 : 1
4.8	4.77	0.6	1.5 : 1

Table 5.3: Effect of the concentration variation between the internal standard and the analyte by qNMR.
Internal standard: 2,5-dimethylfuran (**5.25**); analyte: Fmoc-Lys(Boc)-OH. Concentration expected was calculated from the mass of Fmoc-Lys(Boc)-OH used for each sample. Concentration calculated was determined by qNMR.

The data obtained during these concentration experiments (**Table 5.3**) clearly shown that the highest the concentration of the standard increased was compared to the analyte concentration, the bigger was the error. The best results were obtained when the concentration ratio was two to one for the standard compared to analyte.

Quantification by ^{1}H NMR of the protected peptoid Boc-9mer(Boc)$_9$-NH$_2$

Peptoid **5.22** (concentration estimated at 6 mM by weight) and 12 mM of 2,5-DMFu (**5.25**) in $CDCl_3$ were analysed by NMR using the following parameters: 400 MHz (irradiation frequency), NS = 16, AQ = 2 seconds, D1 = 10 seconds, T = 298 K.
The calculated concentration was 5.86 mM with an error of 2.9%. The quantified protected peptoid **5.22** was then deprotected before being evaluated as an antimicrobial agent.

5.2.4. NLLP via *N-tert*-butyloxycarbonyl deprotection

The peptoid **5.22** (Boc protected) was deprotected under acidic to give the NLLP **5.17**.

5.2.4.1. Boc deprotection using 1,4-dioxane/HCl (4N)

4 N HCl in 1,4-dioxane allowed efficient and rapid Boc deprotection at room temperature in 1 hour.[317] Although this method was efficient for the Boc removal, it was difficult to eliminate all the traces of the dioxane. Purification was achieved by multiple lyophilisations (10 times) of the NLLP (**5.17**). 72 mg of the final compound **5.17** were isolated. This mass was greater to what was expected (by quantitative NMR) due to the remaining traces of 1,4-dioxane (estimated by ^{1}H NMR to 2.7 mg, **Appendix 5-8**) that could not be totally removed. In addition, the hygroscopic property of the NLLP-HCl salt lead to an increase in weight. This Boc deprotection was time consuming and did not allow the isolation of clean pure peptoid.

5.2.4.2. Boc deprotection using trifluoroacetic acid

Full deprotection of the peptoid was carried out at room temperature using 20% TFA in dichloromethane. After an hour, all the Boc groups on the peptoid **5.22** were removed. The DCM and TFA were rapidly removed under vacuum and the pure NLLP (**5.17**) did not require any further treatment. The mass of the final compound (59 mg, expected 50 mg) was still greater than expected due to the hygroscopic property of the peptoid (**5.17**).

5.2.4.3. Boc deprotection using diethylether/HCl

Unprotected peptides or peptoids precipitate in cold diethylether, allowing direct isolation of the compound. Boc removal of **5.22** was carried out using 1 M HCl in diethylether. The NLLP-HCl salt **5.17** was isolated after one hour of reaction. Once again the mass (65 mg) was higher than expected mass. Initial NMR analysis showed some remaining traces of diethylether but those were removed after several days under vacuum.

5.2.5. Conclusions

The NLLP **5.17** was successfully synthesised, purified, analysed (HPLC, MS (**Appendix 5-9**) and NMR (**Appendix 5-10** and **5-11**)) with a final yield of 75%. For this project the use of quantification by NMR was essential to know the exact concentration of NLLP as the pure peptoid was to be tested for its antimicrobial activity. However after purification the peptoid is highly hygroscopic, so after purification of the fully protected peptoid **5.22,** its quantification was carried out using the internal standard 2,5-dimethylfuran (**5.25**). This internal standard allowed the optimisation of the relaxation delay which is a crucial parameter for efficient qNMR. In order to removal the acid labile protective group, the most efficient, clean and rapid technique was the use of 20% TFA in DCM. The pure peptoid was then tested for its antimicrobial activity.

5.3. Antibacterial activity of the NLLP

The antibacterial efficiency was evaluated in association with Jagath Kasturiarachchi (Ph.D. student in the Dr Kevin Dhaliwal group). All animal experiments were undertaken by Kevin Dhaliwal with an approved licence from the Animal Scientific Procedure Division of the Home Office, London, U.K..

5.3.1. Cellular labelling and NLLP cytotoxicity

Efficient cellular penetration and non-cytotoxicity of labelled peptoids have been demonstrated in the previous chapters (***CHAPTER 2*** for Rho-9mer **2.37** and ***CHAPTER 3*** for Cy7-9mer **3.28** and Cy5.5-9mer **3.29**). This cellular carrier allowed

accessing to the cytoplasm of various cells lines such as HeLa, B16F10 and HEK293T and primary cells like monocytes and neutrophils.

As the NLLP is a non-labelled compound, the efficiency of its cellular uptake is difficult to assess. As the core of the peptoid remained the same, the protonation of the labelled and non-labelled peptoid should be very similar. In addition previous data on cellular delivery carried out using labelled peptoid showed clear cell penetration. Thus, it was hypothetised that non-fluorescent NLLP (**5.17**), should have the same cellular penetration as its labelled homologues.

Before applying the NLLP for bacteria killing, it is essential to prove its non-cytotoxicity towards eukaryotic cells. **Graph 5.4** showed that the NLLP was not toxic for all the tested cell lines and at all the tested concentrations.

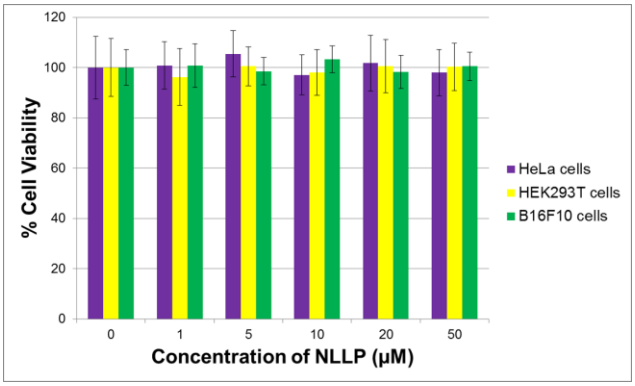

Graph 5.4: MTT assays of NLLP 5.17 in HeLa, HEK293T and B16F10 cells.
HeLa, HEK293T and B16F10 cells incubated with peptoid **5.17** (1, 5, 10, 20 and 50 µM) for 24 hours before being treated with MTT. Healthy cells corresponded to 100 % cell viability. The errors bar represents the standard error of the average (n = 14).

5.3.2. *In vitro* antibacterial activity of NLLP

Bacteria contained within the eukaryotic intracellular niche multiply very slowly.[267, 318] In this study, the pathogens used were all shown to persist in the intracellular niche[265, 319] and are also major causes of morbidity and mortality. Pathogens within the *Bcc* complex (*Burkholderia cepacia* complex) are inherently resistant to all known antibiotics.[320] The following bacteria were tested with the NLLP:

- *S.aureus* (*Staphylococcus aureus):* gram positive bacteria.

- *MRSA: Methycillin-resistant Staphylococcus Aureus*
- *MSSA: Methicillin-sensitive Staphylococcus aureus*

- *B.cepacia* (*Burkholderia cepacia* complex): gram negative bacteria.
- *P.aeuriginosa* (*Pseudomonas aeruginosa):* gram negative bacteria.

The non-dividing cultures of bacteria were left untreated in PBS or treated with NLLP (6.5, 12.5, 25, 50 or 100 μM) and the $O.D._{600}$ was measured using a spectrophotometer every hour over a 6 hour time period.

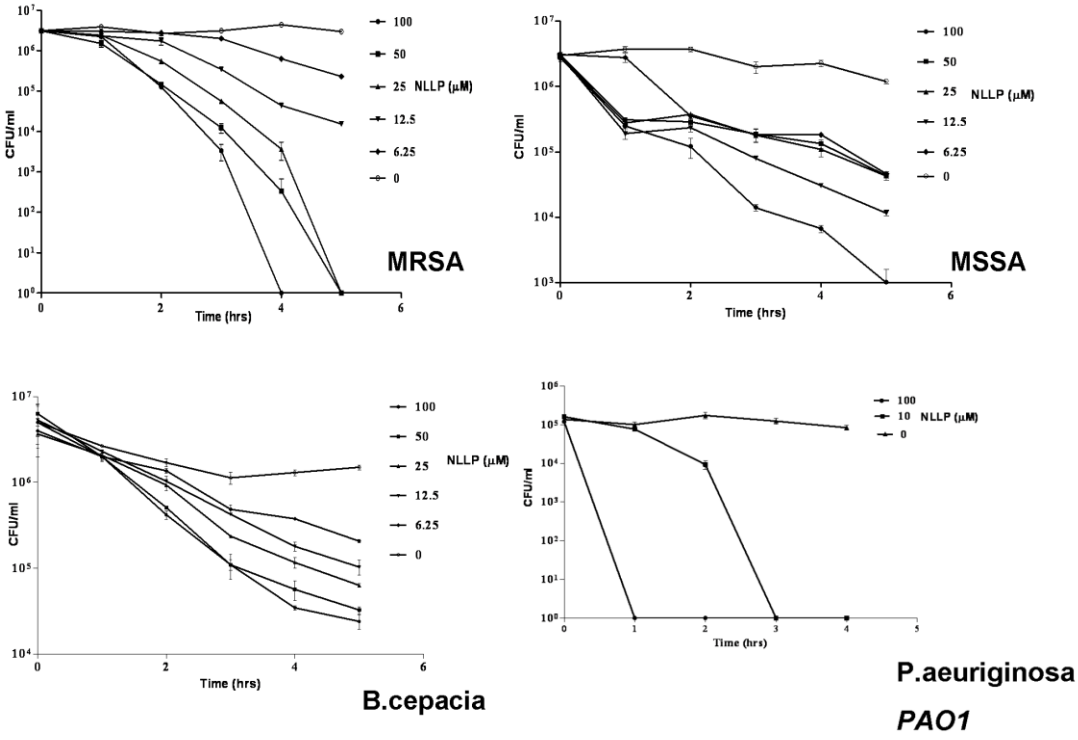

Graph 5.5: Curves showing the killing activity of the NLLP against 4 non-multiplying bacteria.
Data courtesy of Dr. Kevin Dhaliwal from MRC (Medical Research Council) Centre for Inflammation Research, Queen's Medical Research Centre, University of Edinburgh.

Under these conditions, NLLP displayed dose dependent antibacterial activity with a complete kill of *MRSA*, *MSSA* and *P.aeuriginosa* and a 1 to 3 log kill of *Bcc*.

Transmission electron microscopy was used to analyse cell morphology. The experiment was carried out on *P.aeuriginosa* (*PAO1*) and *S.aureus* (*RN6390*) under non-multiplying conditions. Images (**Figure 5.16**) clearly showed major disturbances in their membranes after treatment by the peptoid. These images did not allow

defining an exact mechanism of action but the images of the colonies demonstrated the loss of filaments between the cells and a total disorganisation. The images of *S.aureus* cell showed that the septum was well defined in the case of healthy bacteria, whilst it was distorted under NLLP treatment. The distortion of the septum will play a major role in the malformation of the two progeny bacteria. As eukaryotic and prokaryotic cell membranes do not possess the same properties, the cationic charges on the peptoid could more affect the prokaryotic cell wall while mainting the eukaryotic cell integrity.

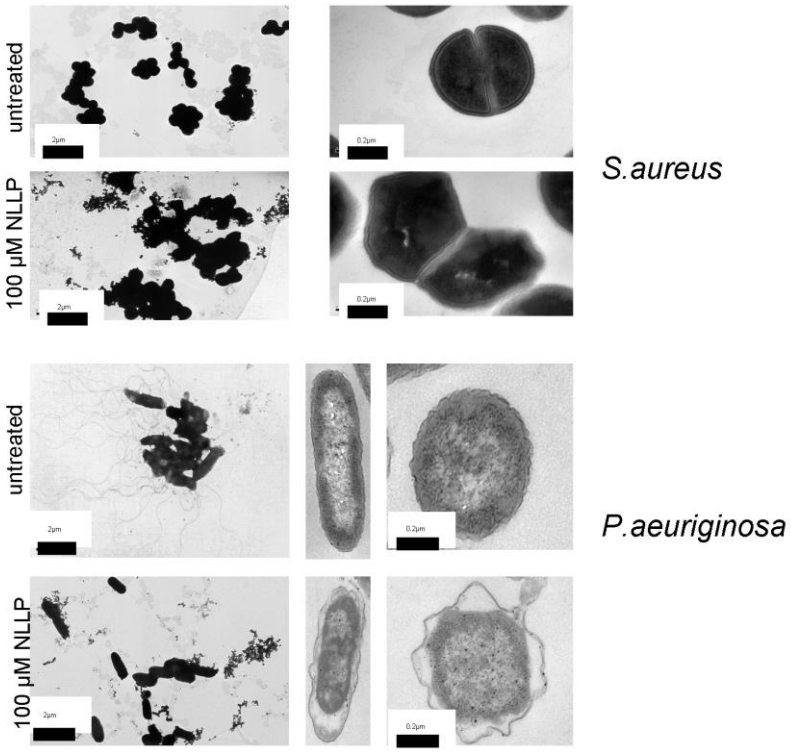

Figure 5.16: Transmission electron microscopy of NLLP treated bacteria (*P.aeuriginosa* and *S.aureus*).
Non-multiplying batecria treated with 100 µM of NLLP (**5.17**). Data courtesy of Dr. Kevin Dhaliwal from MRC (Medical Research Council) Centre for Inflammation Research, Queen's Medical Research Centre, University of Edinburgh.

In order to evaluate the real antimicrobial potential of the NLLP peptoid, it was important to determine the minimum inhibitory concentration (MIC). MIC determination was carried out using the same bacteria than in the non-multiplying test, growing in Mueller Hinton Broth (MHB).[321] The absorbance was measured

every 15 minutes and at the end of an overnight experiment, bacteria cultures were plated for CFU determination to confirm kill effects. (n = 3 independent experiments). NLLP displayed a MIC_{100} against *MSSA* (400 µM) and *MRSA* (300 µM) under these conditions. In comparison to the slow growth experiments, the MIC_{100} for these multiplying bacteria was obtained using higher concentrations of NLLP. The growth of *Bcc* also decreased, but MIC_{100} was not reached. Similar results were obtained for *P.aeuriginosa*. NLLP clearly inhibited the growth of these both gram negative cells without achieving a MIC_{100} at the concentrations used in this study.

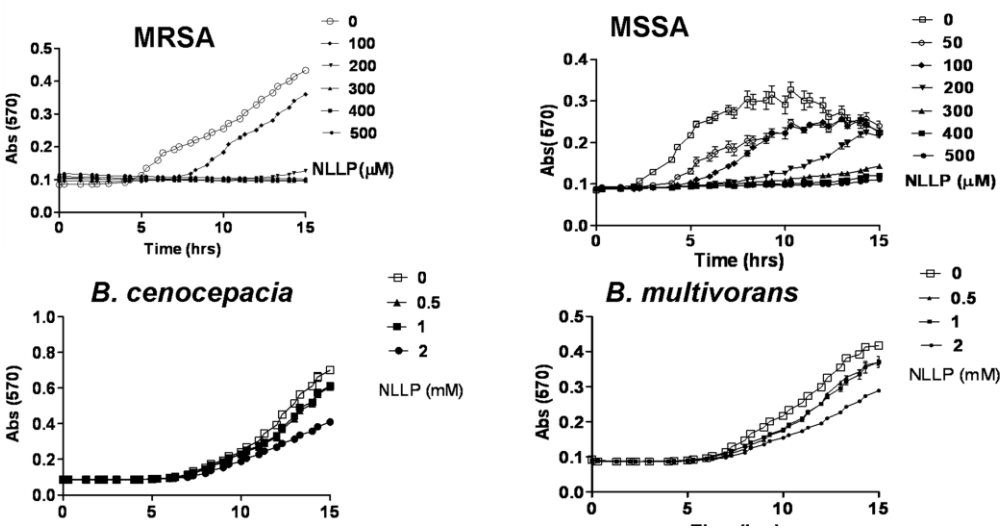

Graph 5.6: Curves showing the killing activity of the NLLP on 4 multiplying bacteria.
Data courtesy of Dr. Kevin Dhaliwal from MRC (Medical Research Council) Centre for Inflammation Research, Queen's Medical Research Centre, University of Edinburgh.

Even though the concentrations of NLLP required to completely kill multiplying bacteria were 3 fold greater than in non-multiplying conditions, the absence of any significant haemolysis at 60 fold higher concentrations (20 mM) than used in the MIC assays (300 µM) generates a favourable selectivity ratio (S.R.) for the clinical application of the NLLP.

Although promising results were obtained for *in vitro* studies, *in vivo* experiments after show very often different data than the ones obtained *in vitro*. Therefore, it was essential to evaluate the *in vivo* activity of the NLLP.

5.3.3. *In vivo* antibacterial activity of NLLP

In order to determine whether the NLLP retained therapeutic antibacterial activity *in vivo*, a model of *PAO1* pneumonic infection was developed. Mice received 10^7 *PAO1 lux* (with intrinsic bioluminescence) via intratracheal instillation.[322] 30 minutes later, NLLP (2 mg/kg) was instilled into the murine lung. Whole body bioluminescence of the mice (9 hours after *PAO1 lux* administration) revealed the presence of the bacteria in the lungs and in all the airways (**Figure 5.17, Control**). Imaging clearly showed a decrease in luminescence intensity in the mice that were treated with NLLP. Almost no trace of bacteria was observed in the nose of mice which received the peptoid. These observations indicated the killing process of the bacteria.

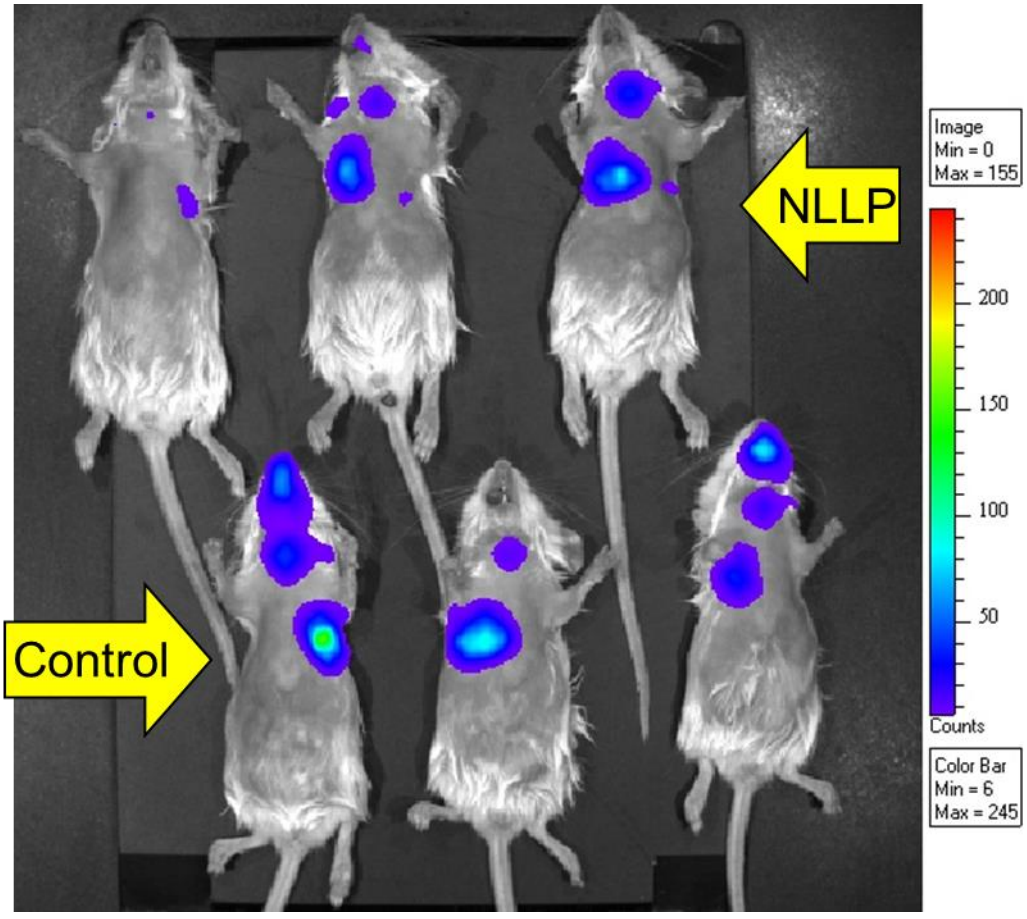

Figure 5.17: Luminescence capture of light using a *in vivo PAO1 lux* pneumonia model following treatment with NLLP (5.17).
Data courtesy of Dr. Kevin Dhaliwal from MRC (Medical Research Council) Centre for Inflammation Research, Queen's Medical Research Centre, University of Edinburgh.

The efficiency of the NLLP as antibiotic was thus demonstrated for *in vivo*.

5.4. Conclusions

In summary, the NLLP peptoid offers a new antibiotic approach. Although, this peptidomimetic does not possess a specific secondary structure or clear amphipathic properties, it demonstrated promising antibacterial activity. NLLP was able to kill both, non-growing and growing, bacteria. In addition, to its low cytotoxicity, this peptoid remains active during *in vivo* studies. All these findings suggest that the NLLP could offer a new direction in antimicrobial reagents.

Even if these results are promising, the amount for peptoid used is still too high to be applied for clinical applications.[323] In comparison with the antibiotic **5.12** (ampetoid), the NLLP is less efficient (MIC of 5.4 µM against Gram negative and 0.84 µM against Gram positive for the compound **5.12**).[293] The efficiency of the peptoid as antibiotic could be increased, for instance, by forcing α-helix secondary structure or by creating a proper amphipathic property via longer side chain, for example. This conformation change could be carried by introducing chiral centres or benzene ring. The helical structure could be obtained by π-interactions of several benzene rings. Finally, mechanical studies of the killing mechanism of the peptoid could be carried out for a better understanding and improvement for the peptoid as an antibiotic.

CHAPTER 6 : EXPERIMENTAL SECTION

6.1. General information

All solvents and reagents were obtained from commercial suppliers and used without purification, unless otherwise stated.

Thin-layer chromatography (TLC) was carried out using silica gel 60 F_{250} plates with a thickness of 0.25 mm. TLC plates were visualised by ultra-violet light (254 nm) and/or with ninhydrin staining (0.3% ninhydrin and 3% acetic acid in *n*-butanol). Column chromatography was carried out on Silica gel 60 (mesh 0.040-0.063 mm) (Merck).

^{1}H NMR spectra were recorded in the solvents indicated at 298 K on Bruker ARX250, DPX360, AVA400 or DMX500 spectrometers operating at 250, 360, 400 and 500 MHz, respectively. **^{13}C NMR** spectra were recorded in the solvents indicated at 298 K on Bruker ARX-250, DPX360, or DMX500 spectrometers operating at 63, 90 and 126 MHz, respectively. Chemical shifts for proton and carbon spectra are reported on the δ scale in ppm and were referenced to residual non-deuterated solvent. All coupling constants (*J* values) were measured in Hz.

Low resolution electrospray mass spectra (ES/MS) were recorded on an Agilent Technologies LC/MSD 1100 Quadrupole Mass Spectrometer (QMS) with an electrospray ion source.

Matrix assisted laser desorption ionisation-time of flight (MALDI-TOF) mass spectra were performed using an Applied Biosystems Voyager-DE™ STR instrument and analysed with the Voyager Instrument Control Panel software. For peptoid and protein analysis, sinapic acid was used as a matrix and positive ion mass spectra were reported.

High resolution mass spectrometry (HRMS) was recorded by the MS Section of the University of Edinburgh on a Finnigan MAT 900 XLP high resolution, double-focussing mass spectrometer.

Fourier transform ion cyclotron resonance mass spectrometry (FT-ICR MS) was recorded by the SIRCAMS (School of Chemistry, Edinburgh) on a Bruker Daltonics 12T SolariX Fourier Transform Ion Cyclotron Resonance mass spectrometer.

Microwave reactions were carried out using a Biotage Initiator instrument in sealed (vial caps, Biotage AB) heavy-walled Pyrex tubes (Biotage AB, size 2 mL or 5 mL).

UV/Vis spectrophotometry was performed on an Agilent 8453 spectrophotometer using a 1 cm path length disposable cuvette (Fisherbrand).

Fluorescence measurements were performed on a Jobin Yvon Spex Fluoromax spectrofluorometer or a FS900 spectrofluorometer.

Infrared (IR) spectra were obtained on a Fourier transform IR Bruker Tensor 27 Spectrometer (FTS) fitted with a Specac single reflection diamond attenuated total reflection (ATR) Golden Gate. All samples were run neat and frequencies are reported in cm^{-1} and only frequencies corresponding to significant functional groups are reported.

Melting points (Mp) were determined using a Gallenkamp melting point apparatus.

High pressure liquid chromatography (HPLC) analyses were performed using the following eluents:

A: H_2O + 0.1% FA;

B: MeOH + 0.1% FA;

C: H_2O + 0.1% TFA;

D: MeCN + 0.04% TFA;

E: MeCN + 0.1% TFA.

Analytical HPLC were performed on an Agilent 1100 analytical system with a Supelco Discovery® C18, 5 μm, 5 cm column coupled to a Polymer laboratories 100 ES evaporative light scattering detector (ELSD). HPLC grade eluents were employed, at a flow rate of 1 mL/min with samples filtered prior to injection. The following methods were used:

- Method 1 (eluents A and B): 5 to 95% B over 3 min, then 95% B for 1 min.
- Method 2 (eluents A and B): 5 to 95% B over 6 min, then 5% B for 3 min.
- Method 3 (eluents C and D): 5 to 95% D over 6 min, then 5% D for 3 min.
- Method 4 (eluents A and B): 85 to 95% B over 6 min, then 95% B for 3 min.

Preparative reverse phase-HPLC purifications were performed on an Agilent Technologies HP1100 Chemstation eluting on a Waters X-Terra RP18 preparative column (150 mm x 19 mm, 5 μm), at a flow rate of 2.5 mL/min. Detection was

carried out at 214, 254 nm and at the wavelength of the specific dye. The following gradients were used:

- Gradient 1: 5 to 95 % E over 20 min, 95% E for 5 min.
- Gradient 2: 85 to 95% E over 18 min, 95% E for 9 min.
- Gradient 3: 15 to 55% E over 20 min, 55 to 95% E over 10 min, 95% B for 5 min.
- Gradient 4: 75 to 95% B over 18 min, 95% B for 9 min.

Cell cultures were performed in a HERAcell 150 incubator from Heraeus.

Cell experiments were carried out in a HERAsafe KS 18 class II negative-flow cabinet from Heraeus.

Cell viability was assessed using a Bio-Rad microplate reader (Version 1.15) measuring absorbance at 570 nm.

Flow cytometry was performed on a BD FACS Aria® System using the BD FACS Diva® software. The data were analysed using the software Flowjo® 7.5.

Live cells were imaged on a Leica fluorescence microscope (DM IRB) under brightlight and the desired excitation wavelength (Filter I3 (450-490 nm) for GFP and FITC, Filter N2.1. (515-560 nm) for Rhodamine).

Confocal microscopy was performed on a Leica SP5 Confocal. Zeiss 510 Meta software was used for digital acquisition. Deconvolution was carried out using the software AutoQuant X.

For *in vivo* analysis:

All animal procedures were performed by Dr. Kevin Dhaliwal with ethical review and licences. CD1 inbred mice aged between 6-12 weeks old were used.

***In vivo* optical imaging** was performed on the Xenogen Spectrum (Caliper LS) and a Visen FMT 2500.

Histology images were taken on a Zeiss microscope and images acquired using Openlab software.

6.2. General methods

6.2.1. Chemistry

6.2.1.1. Qualitative ninhydrin test[129]

The test was carried out on a few resin beads by the addition of 3 drops of reagent A and 1 drop of reagent B. The mixture was heated at 100°C for 5 minutes. A blue solution indicated the presence of free amine on the resin while a yellow solution corresponded to no free amine.

Preparation of ninhydrin solutions A and B:

Reagent A:

Solution 1: Reagent grade phenol (40 g, 0.43 mol) was added to absolute ethanol (10 mL) and the mixture was heated until complete dissolution of the phenol. Amberlite mixed-bed resin MB-3 (4 g) was added to the solution and stirred for 45 minutes and filtered.

Solution 2: KCN (65 mg, 1 mmol) was dissolved in water (100 mL). The KCN solution (2 mL) was diluted to 100 mL with pyridine (freshly distilled from ninhydrin). Amberlite mixed-bed resin MB-3 (4 g) was added, stirred for 45 minutes and filtered. Solution 1 and 2 were mixed.

Reagent B: Ninhydrin (2.5 g, 14 mmol) was dissolved in absolute ethanol (50 mL).

6.2.1.2. Quantitative ninhydrin test[324]

A known mass of resin (5 mg) was placed in a small test tube and 6 drops of reagent A (**6.2.1.1**) and 2 drops of reagent B (**6.2.1.1**) were added. The mixture was heated at 100°C for 5 minutes. The test tube was placed in a cold water bath, 60% aqueous ethanol (2 mL) was added and mixed thoroughly. The resin was removed by filtration through cotton wool and the deep blue filtrate collected in a 25 mL volumetric flask. The resin was washed with a solution of Et_4NCl (0.5 M in DCM, 2 x 0.5 mL) and the sample made up to 25 mL with 60% aqueous ethanol. The absorbance at 570 nm was measured three times against a blank solution and the average value was used. The level of amine present was calculated using the following equation (**Equation 6.1**):

$$\text{Amount of primary amine (mmol/g)} = [(A_{570} \times V) / (\varepsilon_{570} \times m)] \times 10^3$$

Equation 6.1: Amount of primary amine residues (mmol/g), where A_{570} is the recorded absorbance at 570 nm, V is the final volume (mL), ε_{570} is an extinction coefficient suitable for most peptides (1.5×10^4 M^{-1} cm^{-1}) and m is the mass of resin (mg).

6.2.1.3. Qualitative chloranil test[130]

The test was carried out on a few resin beads by the addition of 1 drop of solution A and 1 drop of solution B. The mixture is shacked at room temperature for 3 minutes. Blue resin beads indicated free secondary amine group, whilst colourless resin beads correspond to no free secondary amine group.

Chloranil solutions A and B:

Solution A: 2% of acetaldehyde in DMF

Solution B: 2% of chloranil in DMF

6.2.1.4. Preparation of samples for MALDI-TOF MS.

1 µL of compound solution (0.01 M in HPLC solvent) was loaded onto the MALDI plate. 1 µL of the specific matrix solution was added on top of the compound and mixed up and down. The plate was allowed to dry at room temperature for 10 minutes prior to analysis. Sinapic acid matrix solution was used and prepared by dissolution of 15 mg of sinapic acid in 1 mL of 70% of H_2O and 30% of ACN with 0.1% of TFA.

6.2.1.5. Calculation of the theoretical loading

Theoretical loading of a resin after a reaction was calculated using the Equation 6.2.

$$\text{New theoretical loading (mmol/g of resin)} = \frac{\text{SR loading}}{[1 + (\text{SR loading} * \text{Difference of Mw})/1000]}$$

Equation 6.2: Theoretical loading, where: "SR loading" is the loading of the starting resin (mmol/g) and Difference of Mw refers to the difference of formular weight between the product and the starting resin (g/mol).

6.2.1.6. Solid-phase synthesis: generalities

All peptoids were prepared on polystyrene resin (1% DVB, loading = 1.6 mmol/g) functionalised with a Rink amide linker. The functionalization of the solid support is described in section **6.3.5**. The ratio of solvent-resin used for coupling washes was 15 mL of solvent for 1 g of dry resin. The resin (100 mg) must be swollen for 20 minutes at room temperature in DCM (1.5 mL). Fmoc deprotection and final Boc deprotection/resin cleavage steps were carried out in solid-phase extractor (SPE), polypropylene syringe equipped with a frit and a valve.
All the following protocols are described for 100 mg of dry resin.

6.2.1.7. Soli-phase synthesis coupling of monomer units, amino acids and dyes at room temperature

The Fmoc-protected monomer unit, amino acid or dye (3 equiv., 0.2 M) and HOBt (3 equiv., 0.2 M) were dissolved in DMF (0.2 M). DIC (3 equiv., 0.2 M) was then added to the solution and the mixture was stirred for 10 minutes at room temperature. The solution was added to the Fmoc deprotected pre-swollen resin and the mixture was mixed for 4 hours. The resin was then washed with three times with DMF (1.5 mL) and DCM (1.5 mL). Coupling completion was monitored using the appropriate qualitative colorimetric tests (qualitative ninhydrin test for detection of primary amines (**6.2.1.1**) and qualitative chloranil test for detection of secondary amines (**6.2.1.3**)) and repeated if unsatisfactory.

6.2.1.8. Solid-phase coupling of monomer units and amino acids under microwave irradiation

The Fmoc-protected monomer unit or amino acid was activated as described earlier (**6.2.1.7**). The solution of monomer, DIC and HOBt in DMF (0.2 M) was added to the Fmoc deprotected pre-swollen resin and the mixture transferred into a 2.5 mL microwave vial containing a small stir bar. The Pyrex tube was capped with an aluminium crimp cap fitted with a silicon septum and introduced into the single-mode microwave. The mixture was subjected to microwave irradiation at a temperature of 60°C for 20 minutes under magnetic stirring. The resin was then

transferred to a solid-phase extractor (SPE) and washed with DMF (3 x 1.5 mL) and DCM (3 x 1.5 mL). Couplings were monitored using the appropriate qualitative colorimetric test (qualitative ninhydrin test for detection of primary amines (**6.2.1.1**) and qualitative chloranil test for detection of secondary amines (**6.2.1.3**)) and repeated if unsatisfactory.

6.2.1.9. Fmoc deprotection

Fmoc deprotection was carried out by suspending the resin in 20% piperidine in DMF (1.5 mL) and shaking for 10 minutes. The resin was then filtered, washed with DMF (3 x 1.5 mL), DCM (3 x 1.5 mL). The treatment of the resin by 20% piperidine in DMF (1.5 mL) was repeated for another 10 minutes after which time the resin was washed with DMF (3 x 1.5 mL) and DCM (3 x 1.5 mL).

6.2.1.10. TFA cleavage/deprotection and cold ether precipitation

The resin containing the acid-labile protected peptoids, peptides or peptoid-peptide hybrids was washed with DMF (3 x 1.5 mL), DCM (3 x 1.5 mL), MeOH (3 x 1.5 mL), Et_2O (3 x 1.5 mL) and dried *in vacuo* on the manifold for 30 minutes. Once washed and dry, the resin was suspended in 2.5 mL of a mixture of TFA/TIS/H_2O (95: 2.5: 2.5, or other specific mixture) and stirred for 4 hours (unless stated otherwise). After cleavage, the resin was separated from the solution by filtration and washed with 2.5 mL of TFA solution (25 mL per gram of resin). The TFA filtrates were collected and concentrated *in vacuo* (1 mL ca.). The concentrated mixture was then added dropwised in a centrifuge tube containing cold Et_2O (12 mL). The precipitated peptoid was then sonicated and recovered by centrifugation. The solid was then washed with cold ether (12 mL) and centrifuged three times. After the last cycle of washes/centrifugation, the peptoid was dried overnight in a vacuum oven at 40^{o}C.

6.2.1.11. General Dde deprotection

Dde deprotection was carried out by suspending the resin in 2% N_2H_4 in DMF (1.5 mL) and shaking for 30 minutes. The resin was then filtered, washed with DMF (3 x

1.5 mL), DCM (3 x 1.5 mL) and re-suspended in 2% NH_2OH-H_2O in DMF (1.5 mL) and shaken for a further 30 minutes after which time the resin was washed with DMF (3 x 1.5 mL) and DCM (3 x 1.5 mL).

6.2.1.12. Selective Dde deprotection in presence of Fmoc group[204]

1.25 g (1.80 mmol) of $NH_2OH.HCl$ and 0.92 g (1.35 mmol) of imidazole were suspended in NMP (5 mL) and the mixture was sonicated until complete dissolution. Just before reaction, 1 mL of this solution was diluted with 0.2 mL of DCM. Selective Dde deprotection was carried out by suspending the resin in 1.2 mL of the freshly prepared mixture and shaking it for 3 hours at room temperature. The resin was filtered and washed with DMF (3 x 1.5 mL) and DCM (3 x 1.5 mL).

6.2.2. Biology

6.2.2.1. Cell culture

All cells were cultured at 37°C/5% CO_2 in the appropriate culture medium (Roswell Park's Memorial Institute (RPMI-1640, Sigma-Aldrich) medium for HEK293T, B16F10 and Dulbecco's Modified Eagle Medium (DMEM, Sigma-Aldrich) for HeLa) supplemented with 10% of foetal bovine serum (FBS, Gibco), 100 U/mL penicillin and streptomycin and 4mM L-glutamine (Gibco). Cells were grown in T-25 flask coated with 0.1% gelatine/PBS until 80-90% confluency. Old media was removed and cells were washed with PBS and were harvested via trypsination (0.5 mL) (trypsin/EDTA, Gibco) at 37°C/5% CO_2 for 5 minutes. The detached cells were suspended in fresh growth media. A 20% aliquot was re-seeded to a T-25 flask for re-growth.

6.2.2.2. Haemocytometry

Cell densities were determined by haemocytometry. An aliquot (10 µL) of cells detached from a T-25 flask and collected in growth media (total volume: 5 mL) was mixed with 0.2% trypan blue (40 µL, Sigma-Aldrich) and pipetted into a Bright Line™ haemocytometer (an etched glass device with an H-shaped moat forming two

cell-counting areas (with 4 quadrants in each area), with surface features enhanced by Neubauer rulings, Sigma-Aldrich). Cell concentration and the densities required for experiments were determined by **Equation 6.3** and **Equation 6.4** respectively.

$$\text{Concentration (cell/mL)} = (N / Q) \times 5\times10^{4}$$

Equation 6.3: Concentration of cell/mL by haemocytometry, where 'N' is the total number of cells counted and 'Q' is the number of quadrants counted.

$$V_{Exp}\ (mL) = (V_{Tot} \times C_{Well}) \times (1000 / V_{Well}) / C_{Tot}$$

Equation 6.4: Volume of cells detached from T-75 flask (V_{Exp}) required in an experiment a total medium volume of V_{Tot} and a concentration per well of C_{Well}. V_{Well} is the volume required per well and C_{Tot} is the concentration of cells/mL as calculated in Equation 6.3.

6.2.2.3. Cell labelling and flow cytometry analysis

Detached cells in fresh media were seeded at appropriated density onto polystyrene well-plates (Nunc, **Table 6.1**). Cells were incubated (37°C/5% CO_2) for 24 hours prior to peptoid treatment at the desired concentration (μM). After the desired incubation time, the old media was removed and cells washed with PBS. Cells were detached by trypsination at 37°C (trypsin/EDTA, 80 μL per well) and collected in 2% FBS/PBS with or without 0.2% of trypan blue (final volume per well of 300 μL). Samples were analysed by flow cytometry using the appropriate filters according to the dyes under investigation (**Table 6.2**) using the BD Biosciences FACSDiva software. Results were analysed and histograms produced using the software FlowJo (see raw data on the attached CD-ROM).

Well plate	Density of cells per well	Volume of media per well
6	1×10^{5}	2 mL
12	6×10^{4}	800 μL
24	3×10^{4}	350 μL
96	1×10^{4}	100 μL

Table 6.1: Well plate characteristic for cell experiment

Laser Wavelengths (nm)	Band Pass Filters	Dyes
633	780/60 (APC-Cy7-A)	Cy7
561	670/14 (PE-Cy5)	Cy5.5
488	530/30 (FITC-A) 585/42 (PE-A) 616/23 (PE-Texas Red-A)	Fluorescein and eGFP Rhodamine B PI
375	450/20	DAPI/HOECHST Blue

Table 6.2: BD Biosciences FACSAria® system specifications (lasers and band pass filters) and corresponding fluorophores.

6.2.2.4. MTT assays

Cells were seeded into 96-well plates at a density of 1×10^4 cells/well (100 µL per well). The last row of the well plate was used as a blank (no cells). Cells were incubated (37°C/5% CO_2) for 24 hours prior to peptoid treatment at the desired concentrations. After the desired incubation time, the old media was removed and replaced with fresh phenol-red free medium (90 µL). 10 µL of 3-(4,5-dimethylthiazol-2-yl)-2,5-diphenyltetrazolium bromide (MTT, Sigma-Aldrich) at concentration of 5 mg/mL in PBS buffer were added to the fresh media. Cells were incubated for 3 hours (37°C/5% CO_2) prior dissolving the formed formazan using 100 µL of the solubilising solution (10% TRITON X-100, 0.1 N HCl in isopropanol) and gentle shaking for 1 hour. The 96-well plate was read on a microplate reader at 570 nm and cellular viability was calculated according to the **Equation 6.5**.

$$\% \text{ of cellular viability} = (\text{Abs}_{570\ \text{exp}} / \text{Abs}_{570\ \text{control}}) \times 100$$

Equation 6.5: Viability of cells as determined by a MTT assay, where "$\text{Abs}_{570\ \text{exp}}$" refers to the absorbance at 570 nm of cells treated with peptoids and "$\text{Abs}_{570\ \text{control}}$" refers to the absorbance at 570 nm of untreated control cells.

6.2.2.5. Confocal miscroscopy

Cells were seeded onto 24 mm glass coverslips at a density of 1×10^5 cells/coverslip (volume of culture media per well: 2 mL). Cells were incubated (37°C/5% CO_2) for 24 hours prior to peptoid treatment at the desired concentrations. After the desired incubation time with the peptoids, cells were washed with PBS (3 times). Cells were fixed with 4% formaldehyde in PBS for 30 minutes. Nuclei were stained by treatment with a 10 μg/mL solution of HOECHST-33342 in media in 5 minutes at 37°C. After PBS washes (3 × 2 mL), the membrane was stained using 1 nM of 1, 1'-dioctadecyl-3, 3, 3', 3'-tetramethylindocarbocyanine perchlorate (DilC 18) in Hank's buffered salt solution (HBSS) (30 minutes), followed by six PBS washes (2 mL). The glass coverslip was mounted on a Leica SP5 microscope and cells were imaged confocally. DilC 18 was excited using a 595 nm excitation laser and collecting emission using a 670-690 nm band-pass filter. HOECHST-33342 was excited using an excitation laser at 405 nm and collecting emission using a 413-482 nm band-pass filter. Zeiss 510 Meta software was used for digital acquisition. Deconvolution was carried out using the software AutoQuant X.

6.3. Experimental for Chapter 2

6.3.1. Synthesis of 1,6-diamino-*N*-*tert*-butyloxycarbonylhexane (**2.19**) [114]

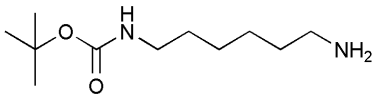

Di-*tert*-butyl carbonate (10.0 g, 46 mmol) in DCM (100 mL) was added drop-wise to 1,6-diaminohexane (**2.18**) (42.5 g, 367 mmol) in DCM (150 mL) and the reaction was stirred for 3 hours. The solvent was evaporated under vacuum and the white solid was dissolved in H_2O (200 mL). The aqueous phase was extracted using DCM (3 × 150 mL). The combined organic phase was then washed with brine (2 × 100 mL), dried over $MgSO_4$, and concentrated *in vacuo* to give pale yellow oil. The crude compound (**2.19**) was analysed and used for the next step without any further purification (7.2 g, 72%).

Analysis:

m/z (ES^+): $C_{11}H_{24}N_2O_2$ calculated 216.2; found 217.1 $[M+H]^+$ (100%), 533.3 $[M+2H]^{2+}$ (29.6%).

HPLC (Method 1): t_R = 2.9 min, purity = 95% (ELSD).

^{1}H NMR ($CDCl_3$, 250 MHz): δ = 1.27-1.35 (m, 4H, BocNHCH$_2$CH$_2$C*H*$_2$C*H*$_2$CH$_2$ CH$_2$NH$_2$) 1.37-1.52 (m, 13H, BocNHCH$_2$C*H*$_2$CH$_2$CH$_2$C*H*$_2$CH$_2$NH$_2$ and C(C*H*$_3$)$_3$), 1.89 (br sg, 2H, CH$_2$N*H*$_2$), 2.68 (m, 2H, CH$_2$C*H*$_2$NH$_2$), 3.14 (m, 2H, BocNHC*H*$_2$), 4.57 (br sg, 1H, BocN*H*CH$_2$).

^{13}C NMR ($CDCl_3$, 63 MHz): δ = 26.5, 26.6 (BocNH(CH$_2$)$_2$*C*H$_2$*C*H$_2$CH$_2$), 28.4 (C(*C*H$_3$)$_3$), 30.4 (*C*H$_2$CH$_2$NH$_2$), 33.1 (BocNHCH$_2$*C*H$_2$), 40.5 (*C*H$_2$NH$_2$), 41.9 (BocNH*C*H$_2$CH$_2$), 79.0 (*C*(CH$_3$)$_3$), 156.0 (*C*=O-Boc).

6.3.2. Synthesis of benzyl-(6-*tert*-butoxycarbonylamino-hexylamino)-acetate (**2.24**)[104]

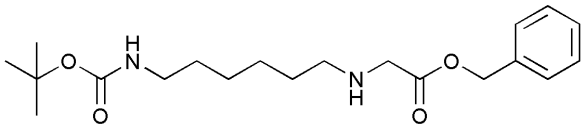

A solution of benzyl-2-bromacetate (**2.23**) (5.3 mL, 33 mmol) in THF (25 mL) was added drop-wise to a stirred solution of *N*-Boc-1,6-hexanediamine (**2.19**) (7.2 g, 33 mmol) and triethylamine (14 mL, 99 mmol) in THF (50 mL) over 2 hours. The reaction was stirred for a further 2 hours. The THF was removed *in vacuo*. The white solid was suspended in Et_2O (100 mL) and filtered. The solution was concentrated *in vacuo* and the crude product was purified by column chromatography (silica gel) using ethyl acetate as an eluent to yield compound **2.24** as a pale yellow oil (11.4 g, 68%, two steps, based on di-tertbutyl carbonate).

Analysis:

m/z (ES^+): $C_{20}H_{32}N_2O_4$ calculated 364.2; found 365.1 $[M+H]^+$ (100%), 387.1 $[M+Na]^+$ (10.1%).

Rf: 0.36 (EtOAc).

HPLC (Method 1): t_R = 3.4 min, purity = 100% (ELSD).

^{1}H NMR ($CDCl_3$, 250 MHz): δ = 1.11-1.43 (m, 17H, BocNHCH$_2$(C*H*$_2$)$_4$CH$_2$ and C(C*H*$_3$)$_3$), 1.56 (br s, 1H, CH$_2$N*H*CH$_2$), 2.53 (t, *J* = 7.30 Hz, 2H, CH$_2$C*H*$_2$NHCH$_2$), 3.00-3.08 (m, 2H, BocNHC*H*$_2$), 3.36 (s, 2H, NC*H*$_2$CO), 4.46 (br sg, 1H, BocN*H*CH$_2$), 5.08 (s, 2H, COOC*H*$_2$), 7.26-7.43 (m, 5H, ArC*H*).

^{13}C NMR ($CDCl_3$, 63 MHz): δ = 26.8, 26.6 (BocNH(CH$_2$)$_2$*C*H$_2$*C*H$_2$CH$_2$, 27.5 (C(*C*H$_3$)$_3$), 31.5, 32.8 (BocNHCH$_2$*C*H$_2$(CH$_2$)$_2$*C*H$_2$), 41.5 (BocNH*C*H$_2$), 52.3 (CH$_2$*C*H$_2$NHCH$_2$), 61.5 (N*C*H$_2$CO), 66.8 (NCH$_2$COO*C*H$_2$), 72.7 (*C*(CH$_3$)$_3$), 128.6, 128.4, 128.3 , 134.8 (Ar*C*H), 135.0 (Ar*C*), 156.0 (*C*=O-Boc), 177.6 (*C*OOBn).

6.3.3. Synthesis of benzyl-[(6-*tert*-butoxycarbonylamino-hexyl)-(9*H*-fluoren-9-ylmethoxy carbomyl)-amino]-acetate (**2.25**)[104]

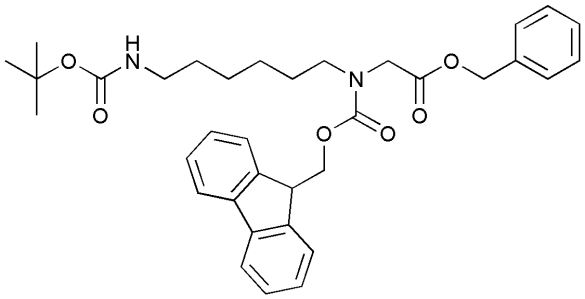

Fmoc-OSu (10.5 g, 31 mmol) was added to a solution of **2.24** (11.3 g, 31 mmol) in DCM (100 mL). The reaction was stirred and monitored by TLC until completion (2 hours). The solvent was removed *in vacuo* and the crude product was purified by column chromatography (silica) eluting with EtOAc/Hexane (1: 1) to yield **2.25** as a light yellow oil (17.1 g, 94%).

Analysis:

m/z (ES^+): $C_{35}H_{42}N_2O_6$ calculated 586.7 ; found 609.2 $[M+Na]^+$ (100%), 487.2 $[M-Boc+H]^+$ (17.3%), 587.3 $[M+H]^+$ (4.6%).

Rf: 0.39 (EtOAc/Hexane, 1: 1).

HPLC (Method 2): t_R = 6.9 min, purity = 99% (ELSD).

^{1}H NMR ($CDCl_3$, 500 MHz): two rotamers δ = 1.15-1.53 (m, 17H, $BocNHCH_2(CH_2)_4CH_2$ and $C(CH_3)_3$), 3.21 and 3.50 (m, 4H, $BocNHCH_2$ and $FmocNCH_2CH_2$), 3.99 and 4.03 (s, 2H, NCH_2CO), 4.16 and 4.30 (t, J = 6.10 Hz, 1H, C*H*-Fmoc), 4.41 and 4.50 (d, J = 6.15 Hz, 2H, CH_2-Fmoc)), 4.55 (br sg, 1H, $BocNHCH_2$), 5.19 and 5.21 (s, 2H, $COOCH_2$), 7.29-7.45 (m, 9H, ArC*H*-Fmoc and Ph), 7.58-7.65 (m, 2H, ArC*H*-Fmoc), 7.69-7.72 (m, 2H, ArC*H*-Fmoc).

^{13}C NMR ($CDCl_3$, 126 MHz): two rotamers δ = 26.2, 26.4 ($BocNH(CH_2)_2CH_2CH_2CH_2$), 26.5, 27.8 ($CH_2CH_2NCH_2$), 28.3 ($C(CH_3)_3$), 28.5, 30.0 ($BocNHCH_2CH_2$), 40.5 ($BocNHCH_2$), 47.3 (*C*H-Fmoc), 48.8 , 48.9 ($CH_2CH_2NCH_2$), 49.2 (NCH_2CO), 66.9 (NCH_2COOCH_2), 67.0 (CH_2-Fmoc), 79.1 ($C(CH_3)_3$), 120.0, 124.8, 125.0, 127.1, 127.7, 128.3, 128.6 (ArCH-Fmoc and ArCH-

Ph), 135.3, 135.4 (Ar*C*-Ph), 141.3, 141.4 (Ar*C*-Fmoc), 144.0 (Ar*C*-Fmoc), 155.9, 156.0, 156.4 (*C*=O-Boc and *C*=O-Fmoc), 169.5 and 169.6 (*C*OOBn).

6.3.4. Synthesis of [(6-*tert*-butoxycarbonylamino-hexyl)-(9*H*-fluoren-9-ylmethoxy carbomyl) -amino]-acetic acid (**2.22**)[114]

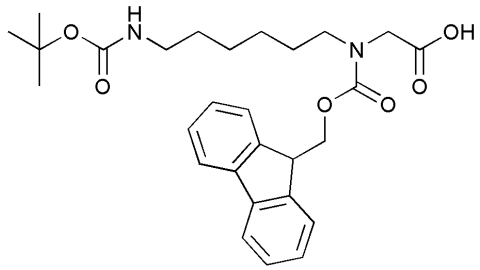

Pd/C 10% (0.24 g) was added to a solution of **2.25** (8 g, 13.6 mmol) in ethanol (150 mL). The air was purged with N_2. N_2 was removed by suction (vacuum) and H_2 was slowly added thanks to a tap. The reaction was stirred under an atmosphere of H_2 for 4 hours. The reaction mixture was filtered through celite to remove the catalyst and the filtrate concentrated *in vacuo*. The product was purified by column chromatography (silica, eluting with DCM/MeOH, 1: 1) to yield **2.22** as a white solid (5.3 g, 80%).

Analysis:

m/z (ES^+): $C_{28}H_{36}N_2O_6$ calculated 496.3; found 397.0 $[M\text{-Boc}+H]^+$ (100%), 519.1 $[M+Na]^+$ (74.3%), 497.1 $[M+H]^+$ (4.6%).

Rf: 0.42 (DCM/MeOH, 10: 1).

HPLC (Method 2): t_R = 5.9 min, purity = 100% (ELSD).

^{1}H-NMR ($CDCl_3$, 500 MHz): two rotamers δ = 1.03-1.36 (m, 17H, BocNHCH_2 (CH_2)$_4$CH_2 and C(CH_3)$_3$), 2.97 and 2.99 (two br m, 4H, BocNCH_2 and FmocNCH_2CH_2), 3.20 and 3.25 (br sg, 2H, NCH_2CO), 4.02 (m, 1H, C*H*-Fmoc), 4.40 and 4.46 (two m, 2H, CH_2-Fmoc), 4.58 (br sg, 1H, BocN*H*CH_2), 7.23 (m, 2H, ArC*H*-Fmoc), 7.31 (m ,2H, ArC*H*-Fmoc), 7.49 (d, *J* = 7.00 Hz, 2H, ArC*H*-Fmoc), 7.68 (d, *J* = 7.05 Hz,2H, ArC*H*-Fmoc).

^{13}C-NMR ($CDCl_3$, 126 MHz): two rotamers δ = 26.0, 26.3 (BocNH(CH_2)$_2$*C*H$_2$*C*H$_2$CH$_2$), 27.8 (*C*H$_2$CH$_2$NCH$_2$), 28.1 (C(*C*H$_3$)$_3$), 28.4, 29.4 (BocNHCH$_2$*C*H$_2$), 40.4 (BocNH*C*H$_2$), 47.3 (*C*H-Fmoc), 48.5 (CH$_2$*C*H$_2$NCH$_2$), 51.4 (N*C*H$_2$CO), 67.4 (NCH$_2$COO*C*H$_2$), 68.9 (*C*H$_2$-Fmoc), 78.9 (*C*(CH$_3$)$_3$), 120.0, 124.8, 127.0, 127.6 (Ar*C*H-Fmoc), 141.3, 143.9 (Ar*C*-Fmoc), 156.0, 157.5 (*C*=O-Boc and *C*=O-Fmoc), 167.6 and 168.2 (*C*OOH).

6.3.5. Functionalisation of the aminomethyl-PS with Rink amide linker (**2.28**)

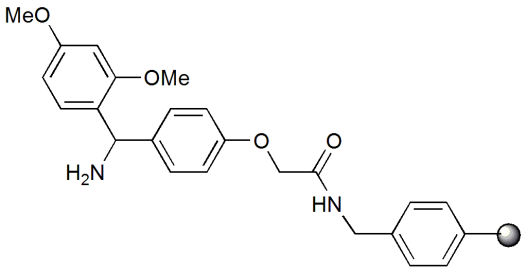

Fmoc-Rink linker (**2.26**, 4.3 g, 8 mmol) was coupled to aminomethyl polystrene resin (**2.27**, 1 g, 1.6 mmol) using the protocol **6.2.1.7**. After coupling, the solid support was Fmoc deprotected using 20% piperidine in DMF (**6.2.1.9**). A new loading of the resin **2.28** was calculated using a quantitative ninhydrin test **6.2.1.2** (0.86 mmol/g).

6.3.6. Synthesis of the resin Fmoc-Ahx-9mer (**2.35**)

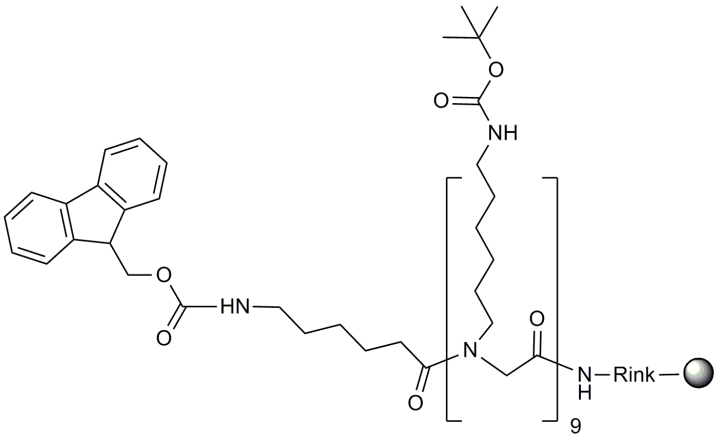

2.35 was synthesised on **2.28** and using the monomer **2.22**. The resin (50 mg, 0.043 mmol) was first swollen in DCM (0.75 mL) for 20 minutes. Each peptoid monomer unit (65 mg, 0.130 mmol) was coupled using the protocol **6.2.1.8** followed by Fmoc deprotection **6.2.1.9**. These reactions corresponded to one coupling cycle. This coupling cycle was repeated 8 times in order to obtain the desired oligomer of the required length. The first monomer coupling was monitored by a qualitative ninhydrin test (**6.2.1.1**), while the following Fmoc deprotections and couplings were controlled using the chloranil test (**6.2.1.3**). The solid supported 9mer peptoid (**2.33,** 0.27 mmol/g) was Fmoc deprotected and then coupled to Fmoc-aminohexanoic acid spacer **2.34** (46 mg, 0.130 mmol) using the coupling procedure **6.2.1.8** (monitored by chloranil test **6.2.1.3**). The resin was washed with DMF, DCM, MeOH and Et_2O (3 × 1 mL) before being dried overnight at 40°C in a vacuum oven (299 mg). The new theoritical loading (**6.2.1.5**) calculated from the measured Rink amide resin (**6.3.5**) was 0.28 mmol/g.

*Characteristation of the resin **2.35***

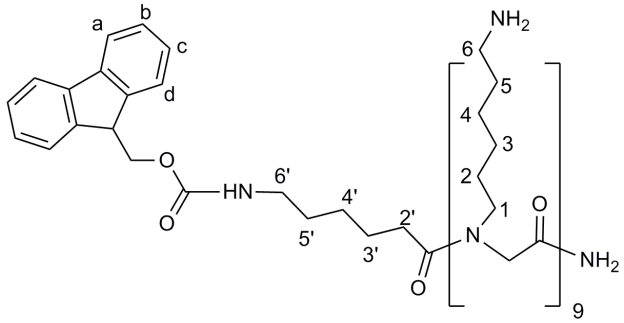

20 mg of the resin **2.35** was cleaved using a TFA/TIS/DCM (95: 2.5: 2.5) solution (500 µL) for 4 hours and treated as described in **6.2.1.10**.

m/z (ES^+) $C_{93}H_{168}N_{20}O_{12}$ calculated 1757.3, found 440.34 $[M+4H]^{4+}$ (20.2%), 352.5 $[M+5H]^{5+}$ (100%), 293.9 $[M+6H]^{6+}$ (80.1%), 252.2 $[M+7H]^{7+}$ (13.9%).
m/z (MALDI-TOF) $C_{93}H_{168}N_{20}O_{12}$ calculated 1757.32, found 1758.47 $[M+H]^+$ (100%).
m/z (FT-MS) $C_{93}H_{168}N_{20}O_{12}$ calculated $[M+2H]^{2+}$ 879.66535, found 879.67800.

HPLC (Method 4): t_R = 2.8 min; purity = 100% (ELSD, 254 nm)

^{1}H NMR (500 MHz, D_2O, eSpresat water suppression) δ = 1.58-1.72 (m, 78H, 72H for $NH_2CH_2(CH_2)_4CH_2$-9mer ($H_{2,3,4,5}$), 6H for $CH_2(CH_2)_3CH_2$-Ahx ($H_{3', 4', 5'}$)), 2.1-2.21 (m, 2H, $COCH_2$-Ahx, $H_{2'}$), 2.88 (m, 18H, NH_2CH_2-9mer, H_6), 3.23 (m, 20H, 18H for $CH_2CH_2NCH_2$-9mer (H_1), 2H for CH_2NH-Ahx ($H_{6'}$)), 3.76-4.42 (m, 21H, 18H for NCH_2CO, 1H for C*H*-Fmoc, 2H for CH_2-Fmoc), 7.34 (t, *J* = 7.15 Hz, 2H, ArC*Hc*-Fmoc), 7.42 (m, 4H, 2H for ArC*Hb*-Fmoc, 2H for $CONH_2$), 7.62 (d, *J* = 6.20 Hz, 2H, ArC*Hd*-Fmoc), 7.75 (m, 2H, ArC*Ha*-Fmoc).

^{13}C NMR (D_2O, 126 MHz) δ = 25.2, 25.3, 25.4, 25.5, 25.6, 25.7, 26.2, 26.3, 26.4, 26.5, 26.7, 26.8, 27.1, 27.2, 27.3, 27.5 ($NH_2CH_2(CH_2)_4CH_2$-9mer and $CH_2(CH_2)_3CH_2$-Ahx), 32.4 (CH_2CO-Ahx), 39.3, 39.4, 39.5 (NH_2CH_2-9mer), 46.7, 47.0, 47.2, 47.5, 47.8, 48.0, 48.2, 48.3, 48.4, 48.5, 48.6, 49.1, 49.2 ($CH_2CH_2NCH_2$-9mer, CH-Fmoc, NCH_2CO), 64.2 (CH_2-Fmoc), 120.2 (ArCH-Fmoc, Cd), 120.5 (ArCH-Fmoc, Ca), 127.5, 127.6 (ArCH-Fmoc, Cc), 128.0, 128.1 (ArCH-Fmoc, Cb), 143.7, 143.8, 144.5, 145 (ArC-Fmoc), 159.1 (C=O-Fmoc), 162.4, 162.7, 162.8, 163.0, 163.1, 163.3 (C=O-9mer), 170.0 (C=O-Ahx).

6.3.7. Preparation and analysis of 5(6)-carboxy-*N,N,N',N'*-tetraethylrhodamine (**2.36**, Rho)

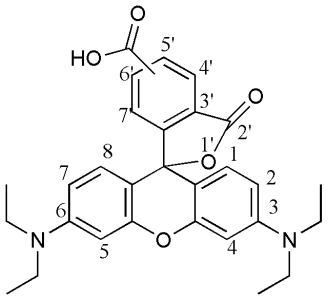

10 mL of rhodamine WT (from Keystone) were acidified by addition of 0.15 mL of HCl 2 M. The red solution was frozen in a mixture of acetone and dry ice and lyophilised overnight in the dark to protect the dye.

Tetraethylrhodamine **2.36** was isolated as a purple powder (3.2 g).

Analysis:

m/z (ES^+): $C_{29}H_{31}N_2O_5^+$ calculated 487.2; found 487.1 $[M]^+$ (100%), 488.1 $[M+H]^+$ (35.4%), 509.1 $[M+Na]^+$ (26.8%).

HPLC (Method 3): t_R = 4.0 (isomer 6') and 4.2 (isomer 5') min, purity = 97% (ELSD).

^{1}H-NMR (D_2O, 500 MHz, eSpresat water suppression): δ = 0.98-1.18 (m, 12H, CH_2CH_3), 3.26-3.52 (m, 8H, NCH_2CH_3), 6.55 (d, *J* = 7.95 Hz, 2H, ArC*H*, H_5 and H_4), 6.72 (dd, *J* = 7.05 Hz, *J* = 7.95 Hz, 2H, ArC*H*, H_7 and H_2), 7.03 (dd, *J* = 7.00 Hz, *J* = 7.90 Hz, ArC*H*, 2H, H_8 and H_1), 7.51 (d , *J* = 6.90 Hz, 0.66H, ArC*H*, $H_{7'}$ for isomer 5'), 7.80 (d, *J* = 7.25 Hz, 0.33H, ArC*H*, $H_{5'}$ for isomer 6'), 8.08 (d, *J* = 7.30 Hz, 0.33H, ArC*H*, $H_{4'}$ for isomer 6'), 8.14 (d, *J* = 6.90 Hz, 0.66H, ArC*H*, $H_{6'}$ for isomer 5), 8.18 (s, 0.33H, ArC*H*, $H_{7'}$ for isomer 6'), 8.21 (s, 0.66H, ArC*H*, $H_{4'}$ for isomer 5').

^{13}C-NMR (D_2O, 126 MHz): δ = 12.0 (CH_2CH_3), 45.6 (CH_2CH_3), 96.0 (Ar*C*H, C_5 and C_4), 112.5, 113.7 (Ar*C*H, C_2 and C_7), 128.7 (Ar*C*H, $C_{5'}$ for isomer 6'), 128.9, 129.1 (Ar*C*H, $C_{7'}$ for isomer 6' and $C_{6'}$ for isomer 5'), 130.1 (Ar*C*H, $C_{7'}$ for isomer 5'), 130.3 (Ar*C*H, $C_{4'}$ for isomer 6'), 130.5 (Ar*C*H, $C_{4'}$ for isomer 5'), 131.1, 133.2 (Ar*C*H, C_1 and C_8), 133.2, 137.6, 138.0, 140.4, 142.1, 155.2, 156.9, 157.5 (Ar*C*), 173.5, 174.2 (*C*OOH).

UV (MeOH) λ_{abs} = 550 nm.

6.3.8. Synthesis of Rhodamine-9mer peptoid (Rho-9mer, **2.37**)

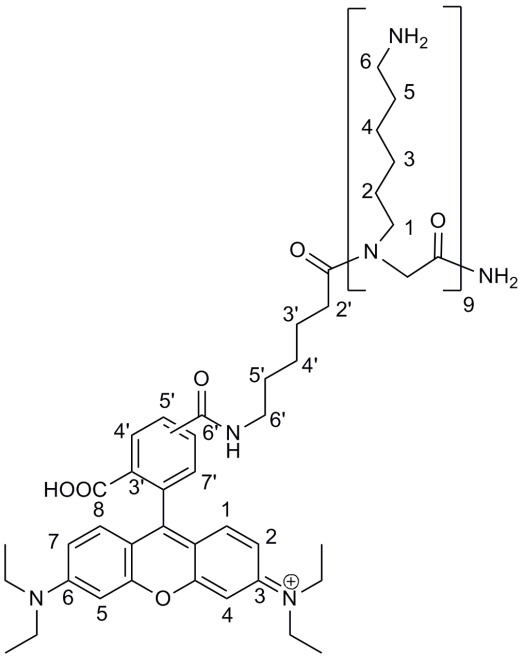

The Rho-9mer peptoid **2.37** was synthesised on the resin **2.34**. The resin (150 mg, 0.043 mmol) was first swollen in DCM (1.5 mL) for 20 minutes. The Fmoc group was deprotected with 20% piperidine in DMF (**6.2.1.9)** and **2.36** (63 mg, 0.130 mmol) was conjugated to the solid supported peptoid using method **6.2.1.7**. The coupling was monitored by a qualitative ninhydrin test (**6.2.1.1**). Finally, the resin bound Rho-9mer was deprotected and cleaved from the solid support using the cleavage protocol (**6.2.1.10**). Rho-9mer **2.37** was obtained as a red powder (80 mg, 0.040 mmol, 94%).

Analysis:

m/z (ES^+): $C_{107}H_{187}N_{22}O_{14}^+$ calculated 2004.5, found 502.0 $[M+4H]^{4+}$ (18.5%), 401.8 $[M+5H]^{5+}$ (100%), 335.0 $[M+6H]^{6+}$ (75.9%), 287.3 $[M+7H]^{7+}$ (26.9%).

m/z (MALDI-TOF): $C_{107}H_{187}N_{22}O_{14}^+$ calculated 2004.46, found 2004.64 $[M]^+$ (100%).

m/z (FT-MS): $C_{107}H_{187}N_{22}O_{14}^+$ calculated $[M+2H]^{2+}$ 669.15306, found 669.16793

HPLC (Method 3): t_R = 3.6 (Rho^6-9mer) and 3.8 (Rho^5-9mer) min, purity > 98% (220 and 540 nm).

^{1}H-NMR (D_2O, 500 MHz, eSpresat water suppression): δ = 1.15-1.69 (m, 90H, 12H for CH_2CH_3-Rho, 6H for CH_2-Ahx ($H_{3', 4' \text{ and } 5'}$) and 72H for CH_2-9mer ($H_{2, 3, 4 \text{ and } 5}$)), 2.04-2.26 (m, 2H, CH_2CO-Ahx, $H_{2'}$), 2.89 (m, 18H, CH_2NH_2-9mer, H_6), 3.24 (m, 18H, CH_2N-9mer, H_1), 3.37-3.46 (m, 2H, CH_2NH-Ahx, $H_{6'}$), 3.57 (m, 8H, NCH_2CH_3-Rho), 3.87-4.43 (m, 18H, NCH_2CO), 6.91 (m, 4H, ArCH, H_2, H_4, H_5 and H_7), 7.03 (dd, J = 11.65 Hz, J = 8.85 Hz, ArCH, 2H, H_8 and H_1), 7.45 (br s, 2H, $CONH_2$), 7.63 (m, 0.66H, ArCH, $H_{7'}$ for isomer 5'), 7.76 (m, 0.33H, ArCH, $H_{5'}$ for isomer 6'), 7.85 (m, 0.33H, ArCH, $H_{4'}$ for isomer 6'), 8.05 (d, J = 6.90 Hz, 0.66H, ArCH, $H_{6'}$ for isomer 5'), 8.16 (s, 0.33H, ArCH, $H_{7'}$ for isomer 6'), 8.42 (s, 0.66H, ArCH, $H_{4'}$ for isomer 5').

^{13}C-NMR (D_2O, 126 MHz): δ = 11.8 (CH_2CH_3-Rho), 25.3, 25.4, 25.5, 25.6, 25.7, 26.0, 26.3, 26.6, 26.7, 27.2, 27.3, 27.4 and 27.5 (CH_2,$C_{3', 4', 5'}$,$C_{2, 3, 4, 5}$), 31.9 (CH_2, $C_{2'}$), 39.2, 39.3, 39.4, 39.5 (CH_2, C_6), 45.7 (CH_2CH_3-Rho), 47.3, 47.4, 47.5, 47.7, 47.8, 48.2, 48.3, 48.4, 48.5, 48.6 (CH_2, CH_2NH-Ahx, NCH_2CO and C_1), 96.3 (ArCH, C_5 and C_4), 112.4, 113.8 (ArCH, C_2 and C_7), 128.7 (ArCH, $C_{5'}$ for isomer 6'), 129.2, 129.8 (ArCH, $C_{7'}$ for isomer 6' and $C_{6'}$ for isomer 5'), 130.2 (ArCH, $C_{7'}$ for isomer 5'), 130.4 (ArCH, $C_{4'}$ for isomer 6'), 130.6 (ArCH, $C_{4'}$ for isomer 5'), 131.1, 133.3 (ArCH, C_1 and C_8), 134.9, 137.5, 138.1, 140.5, 142.1, 154.9, 156.6, 157.4 (ArC), 162.7, 162.8, 163.0, 163.3 (CO-9mer), 173.8 (CO-Ahx).

UV (MeOH) λ_{abs} = 525 nm, λ_{em} = 584 nm.

6.3.9. Cellular uptake of Rho-9mer peptoid (**2.37**)

Cells (HeLa, B16F10 and HEK293T) were labelled 35 µL of Rho-9mer peptoid (**2.37**) (100 µM) or 35 µL of free Rhodamine dye (**2.36**) (100 µM) in PBS were placed into three random wells (final concentration 10 µM). Cellular uptake was analysed after 5, 30 minutes, 2, 4 and 24 hours of incubation by flow cytometry in 2% FBS in PBS with 0.2% of trypan blue (**6.2.2.3**).

HeLa cells

	Incubation time	Average (%)	Error (%)
Untreated cells		0.6	0.2
2.37	5 min	68.5	6.5
	30 min	96.1	2.3
	2 h	99.0	0.1
	4 h	99.4	0.1
	24 h	99.9	0.1

Table 6.3: Cellular uptake of Rho-9mer (2.37, 10 µM) in HeLa cells (n = 3).

	Incubation Time	Average (arb. units)	Error (arb. units)
Untreated cells		76.7	6.7
2.36	5 min	410.7	13.5
	30 min	424.3	4.5
	2 h	535.3	5.1
	4 h	518.7	13.5
	24 h	322.7	17.0
2.37	5 min	305.0	124.5
	30 min	942.0	75.5
	2 h	1539.3	67.0
	4 h	2006.7	104.8
	24 h	4005.1	163.7

Table 6.4: Fluorescence intensity of HeLa cells (arbitrary units) labelled with Rho (2.36, 10 µM) and Rho-9mer (2.37, 10 µM) (n = 3).

B16F10 cells

	Incubation time	Average (%)	Error (%)
Untreated cells		0.4	0.3
2.37	5 min	10.2	5.0
	30 min	31.6	1.6
	2 h	80.7	1.1
	4 h	90.4	0.7
	24 h	93.6	1.1

Table 6.5: Cellular uptake of Rho-9mer (2.37, 10 µM) in B16F10 cells (n = 3).

	Incubation Time	Average (arb. units)	Error (arb. units)
Untreated cells		95.3	7.1
2.36	5 min	221.7	45.6
	30 min	202.7	22.5
	2 h	270.0	51.0
	4 h	290.3	44.9
	24 h	375.3	14.0
2.37	5 min	192.0	22.6
	30 min	319.3	9.0
	2 h	630.3	20.6
	4 h	936.7	61.8
	24 h	2530.3	36.1

Table 6.6: Fluorescence intensity of B16F10 cells (arbitrary units) labelled with Rho (2.36, 10 µM) and Rho-9mer (2.37, 10 µM) (n = 3).

HEK293T cells

	Incubation Time	Average (%)	Error (%)
Untreated cells		0.5	0.2
2.37	5 min	33.8	3.0
	30 min	57.8	3.6
	2 h	93.3	0.4
	4 h	97.7	0.8
	24 h	99.6	0.2

Table 6.7: Cellular uptake of Rho-9mer (2.37, 10 µM) in HEK293T cells (n = 3).

	Incubation Time	Average (arb. units)	Error (arb. units)
Untreated cells		78.3	14.9
2.36	5 min	417.7	41.1
	30 min	446.7	22.2
	2 h	569.3	36.3
	4 h	541.0	23.3
	24 h	432.7	20.5
2.37	5 min	382.3	103.5
	30 min	913.0	59.4
	2 h	1780.3	125.8
	4 h	3795.3	66.7
	24 h	10220.7	496.2

Table 6.8: Fluorescence intensity of HEK293T cells (arbitrary units) labelled with Rho (2.36, 10 µM) and Rho-9mer (2.37, 10 µM) (n = 3).

6.3.10. Microscopy of Rho-9mer peptoid (**2.37**) into cells

Cells were seeded onto a 12-well plate at a density of 6×10^4 cells/well (volume of culture media per well: 800 µL). After 24 hours, 80 µL of Rho-9mer peptoid (**2.37**) (100 µM) in PBS were added to three random wells. After 4 hours of incubation with the peptoids, cells were washed with PBS and microscopy was performed in 2% FBS in PBS without further staining.

6.3.11. Confocal microscopy of Rho-9mer peptoid (**2.37**) into HeLa cells

HEK293T cells were seeded, stained and analysed as described in **6.2.2.5**. The cells were labelled for 24 hours with 200 µL of Rho-9mer peptoid (**2.37**) (100 µM) prior to imaging. The rhodamine dye on the Rho-9mer peptoids **2.37** was excited using a 561 nm excitation laser and collecting emission using a 567-630 nm band-pass filter.

6.3.12. Temperature effect on cellular uptake

HeLa and HEK293T cells were seeded onto a 24-well plate. After 24 hours, 35 µL of Rho-9mer peptoid (100 µM, **2.37**) in PBS were placed in three wells. Cells were incubated for 3 hours at 37, 20 or 4ºC prior to washing, trypsination and flow cytometry as described in the general procedures (**6.2.2.3**).

HeLa cells

	Temperature (°C)	Average (%)	Error (%)
Untreated cells	4	0.6	0.1
	20	0.6	0.3
	37	0.4	0.2
2.37	4	23.6	3.6
	20	94.7	3.2
	37	98.6	0.9

Table 6.9: Effect of temperature on the cellular uptake of Rho-9mer (2.37, 10 µM) in HeLa cells (n = 6).

HEK293T cells

	Temperature (°C)	Average (%)	Error (%)
Untreated cells	4	0.7	0.3
	20	0.5	0.2
	37	0.3	0.1
2.37	4	18.6	1.5
	20	71.7	6.3
	37	96.4	1.3

Table 6.10: Effect of temperature on the cellular uptake of Rho-9mer (2.37, 10 µM) in HEK293T cells (n = 6).

6.3.13. Temperature effect on cellular uptake: Microscopy

HeLa and HEK293T cells were seeded onto a 12-well plate at a density of 6×10^4 cells/well (volume of culture media per well: 800 µL). After 24 hours, 80 µL of Rho-9mer peptoid (100 µM, **2.37**) in PBS were added in three wells. Cells were incubated for 3 hours at 37, 20 or 4ºC prior to PBS washing. Microscopy of the cells was performed in 2% FBS/PBS without further staining.

6.3.14. Effect on sodium azide on cellular uptake[114]

HeLa and HEK293T cells were seeded onto a 24-well plate at a density of 3×10^4 (volume of culture media per well: 350 µL). After 24 hours, 50% of the cells were treated with sodium azide (20 mM, Sigma-Aldrich) in serum-free culture media for 30 minutes prior to treatment the peptoids. Cells (treated with NaN_3 anduntreated) were incubated with 35 µL of Rho-9mer peptoid (100 µM, **2.37**) in PBS. Cells were incubated for 3 hours at 37ºC prior to washing, trypsination and flow cytometry as described in the general procedures (**6.2.2.3**).

HeLa cells

	Average (%)	Error (%)
Untreated cells	0.4	0.2
2.37	99.6	0.5
2.37, NaN_3	36.3	2.7

Table 6.11: Effect of sodium azide on the cellular uptake of Rho-9mer (2.37, 10 µM) in HeLa cells (n = 6).

HEK293T cells

	Average (%)	Error (%)
Untreated cells	0.6	0.2
2.37	97.5	0.7
2.37, NaN_3	23.2	3.7

Table 6.12: Effect of sodium azide on the cellular uptake of Rho-9mer (2.37, 10 µM) in HEK293T cells (n = 6).

6.3.15. Cytotoxicity assays

MTT cytotoxicity assays were carried out as according to the general procedures (**6.2.2.4**). Cells were treated with 1, 5, 10 or 20 µL of Rho-9mer (**2.37**) 100 µM in order to obtain a final concentration of 1, 5, 10 or 20 µM, respectively. After 24 hours of incubation at 37^{o}C, the wells were read on a microplate reader.

HeLa cells

	Concentration (µM)	Average (arb. units)	Error (arb. units)	Average (%)	Error (%)
Untreated cells		1.110	0.086	100.0	7.8
2.37	1	1.126	0.097	101.4	8.7
	5	1.200	0.058	108.1	5.2
	10	1.218	0.087	109.7	7.8
	20	1.129	0.111	101.7	9.9

Table 6.13: Percentage of cell vailability (HeLa cells) after 24 hours of incubation with Rho-9mer (2.37) at different concentrations (n = 10).

B16F10 cells

	Concentration (μM)	Average (arb. units)	Error (arb. units)	Average (%)	Error (%)
Untreated cells		0.844	0.066	100.0	7.8
2.37	1	0.861	0.097	102.0	11.5
	5	0.844	0.079	100.0	9.3
	10	0.823	0.073	97.6	8.6
	20	0.855	0.050	101.2	5.9

Table 6.14: Percentage of cell vailability (B16F10 cells) after 24 hours of incubation with Rho-9mer (2.37) at different concentrations (n = 10).

HEK293T cells

	Concentration (μM)	Average (arb.units)	Error (arb. units)	Average (%)	Error (%)
Untreated cells		1.339	0.138	100.0	10.3
2.37	1	1.360	0.135	101.6	10.1
	5	1.311	0.120	97.9	8.9
	10	1.331	0.102	99.4	7.6
	20	1.343	0.150	100.3	11.2

Table 6.15: Percentage of cell vailability (HEK293T cells) after 24 hours of incubation with Rho-9mer (2.37) at different concentrations (n = 10).

6.4. Experimental for Chapter 3

6.4.1. Synthesis of *tert*-butyl 4-hydroxyphenylcarbamate PS (**3.15**)[163]

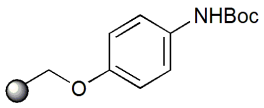

A mixture of *tert*-butyl 4-hydroxy-phenylcarbamate **3.14** (6.27 g, 30 mmol), Cs_2CO_3 (9.78 g, 30 mmol), KI (0.17 g, 1 mmol) and 1% DVB cross-linked chloromethyl polystyrene **3.13** (5 g, 10 mmol) in acetone (35 mL) was heated at 70°C for 16 hours. After reaction, the resin **3.15** was isolated by filtration, washed with water, DMF, DCM, Et_2O and dried overnight *in vacuo* at 40°C to give the product as a grey resin (7.45 g).

Analysis:

IR (neat): 3361 (w, ν_{N-H}), 2977 (m, ν_{C-H}), 2879 (m, ν_{C-H}), 1687 (s, $\nu_{C=O}$), 1513 (s, $\nu_{C=O}$), 1159 (s, ν_{C-O}) cm^{-1}.

Colorimetric test for the detection of chloromethyl groups in Merrifield resin[325]

A 75 mM solution of 4-(4-nitrobenzyl)pyridine in toulene with 5% of triethylamine (1 mL) was added to 2 mg of resin **3.15**. No coloration was observed by naked eyes on the resin. As a positive control the colorimetric test was repeated on 2 mg of Merrifield resin **3.13** (1% DVB, 2 mmol Cl/g). The resin turned pink.

6.4.2. Synthesis of 4-aminophenol PS (**3.16**)[163]

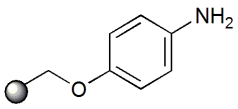

Resin **3.15** (5 g, 7.5 mmol) was shaken at room temperature with a 20% solution of TFA in DCM (75 mL) for 2 hours. At the end of the reaction time, the deprotected

resin was filtered and washed with DCM (3 × 50 mL). The resin was then shaken with a 10% solution of triethylamine in DCM (75 mL) for 15 minutes at room temperature, filtered, washed with DCM (5 × 50 mL), and dried overnight a vacuum oven at 40°C to give **3.16** as a beige resin (4.76 g). The presence of free primary amine was confirmed by a qualitative ninhydrin test (**6.2.1.1**).

Analysis:

IR (neat): 3363 (w, ν_{N-H}), 1509 (s, $\nu_{C=C}$), 1221 (m, ν_{C-N}), 1015 (m, ν_{C-O}) cm^{-1}.

6.4.3. Synthesis of 1,2,3,3-tetramethyl-3*H*-indolium iodide (**3.28**) [163]

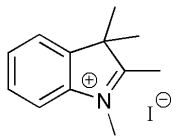

A mixture of 2,3,3-trimethyl-3*H*-indole (0.5 mL, 3.2 mmol) and methyl iodide (1.2 mL, 19.2 mmol) in acetonitrile (2 mL) was heated in a sealed vial at 150°C for 30 minutes, by microwave irradiation. After cooling, the pink precipitate was collected by filtration, washed with Et_2O, ethanol and then dried *in vacuo* to yield **3.28** as a white/pink solid (912 mg, 92%).

Analysis:

m/z (ES^+): $C_{25}H_{27}N_2O^+$ calculated 371.2, found 371.1 $[M]^+$ (100%), 372.1 $[M+H]^+$ (28%).

Rf : 0.45 (DCM/MeOH, 9: 1).

HPLC (Method 2): t_R = 4.5 min, purity = 100% (ELSD).

IR (neat): 3013 (m, ν_{C-H}), 2964 (m, ν_{C-H}), 1630 (s, $\nu_{C=C}$), 1480 (s, ν_{C-H}) cm^{-1}.

^{1}H NMR (DMSO-d_6, 250 MHz): δ = 1.45 (s, 6H, C(C*H*$_3$)$_2$), 2.70 (s, 3H, N=CC*H*$_3$), 3.90 (s, 3H, NC*H*$_3$), 7.55-7.60 (m, 2H, ArC*H*), 7.76-7.80 (m, 1H, ArC*H*), 7.85-7.90 (m, 1H, ArC*H*).

^{13}C NMR (DMSO-d_6, 63 MHz): δ = 14.1 (C(CH_3)$_2$), 24.6 (C(CH_3)$_2$), 36.2 (N=CCH_3), 54.8 (C(CH$_3$)$_2$), 116.9, 122.9, 129.0, 129.7 (ArCH), 141.9, 143.6 (ArC), 197.6 (C=N).

Mp: 217-219 °C.

6.4.4. Synthesis of 2-[(1*E*,3*E*,5*E*)-6-(acetylanilino)-1,3,5-hexatrienyl]-1,3,3-trimethyl-3*H*-indolium iodide (**3.17**) [163]

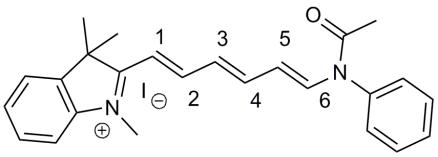

A suspension of 1,2,3,3-tetramethyl-3*H*-indolium iodide **3.28** (1.42 g, 4.13 mmol) and *N*-[(*E*,2*E*,4*E*)-5-anilino-2,4-pentadienylidene]aniline hydrochloride **3.27** (1 g, 3.44 mmol) in a (1: 1) mixture of acetic acid and acetic anhydride (15 mL) was heated at 120°C for 2.5 hours. The reaction was carefully monitored by UV-visible spectrometry (the hemicyanine intermediate and symmetrical dicarboxylic acid cyanine dye have an absorption maximum around 489 and 750 nm, respectively). At the end of the reaction time, the reaction mixture was cooled down and the solvent was evaporated *in vacuo*. The resulting red dark solid was dissolved in DCM (10 mL) and repeatedly washed with water (5 × 10 mL). After removal of the solvent *in vacuo*, the crude product was precipitated in Et_2O (addition of 5 mL of cold Et_2O), sonicated and collected by filtration. After vacuum drying, **3.17** was yieled as a dark red solid (950 mg, 75%).

Analysis:

m/z (ES$^+$): $C_{25}H_{27}N_2O^+$ calculated 371.2, found 371.1 $[M]^+$ (100%), 372.1 $[M+H]^+$ (28%).

Rf : 0.38 (DCM/MeOH, 9: 1).

HPLC (Method 2): t_R = 4.7 min, purity = 93 % (ELSD).

IR (neat): 2973 (m, ν_{C-H}), 2863 (m, ν_{C-H}), 1684 (s, $\nu_{C=O}$), 1596 (s, $\nu_{C=C}$), 1440 (m, ν_{C-H}) cm^{-1}.

^{1}H NMR ($CDCl_3$, 250 MHz) δ = 1.37 (s, 6H, C(CH_3)$_2$), 1.70 (s, 3H, COCH_3), 3.67 (s, 3H, NCH_3), 6.57 (dd, *J* = 14.20 Hz, *J* = 11.45 Hz, 1H, C*H*, H_3), 6.90-6.94 (m, 2H, C*H*, H_3 and H_5), 7.08-7.36 (m, 9H, ArC*H*), 7.90 (dd, *J* = 14.90 Hz, *J* = 11.42 Hz, 1H, C*H*, H_4), 8.10-8.13 (m, 1H, C*H*, H_2), 8.15 (d, *J* = 14.00 Hz, 1H, C*H*, H_6).
UV (MeOH): λ_{abs} = 489 nm.

6.4.5. Synthesis of 2-[(1*E*,3*E*,5*E*)-6-(hydroxyanilino)-1,3,5-hexatrienyl]-1,3,3-trimethyl-3*H*-indolium iodide PS **(3.18)** [163]

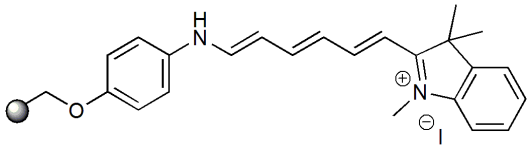

4-aminophenol PS **3.16** (0.5 g, 0.8 mmol) was swollen for 10 minutes in DCM (0.75 mL). A solution of compound **3.17** (0.9 g, 1.8 mmol) in DCM (5 mL, C = 0.4M) was added to the resin **3.16**. The mixture was stirred for 1 hour. After reaction, the resin was isolated by filtration, washed extensively with DMF (5 × 5 mL), MeOH (5 × 5 mL), DCM (5 × 5 mL) to remove the symmetrycal dye and dried *in vacuo* to yield **3.18** as a dark resin (0.87 g). The reaction was confirmed by a qualitative ninhydrin test (**6.2.1.1**).

Analysis:
IR (neat): 3026 (w, ν_{N-H}), 2918 (w, ν_{C-H}), 1481 (s, $\nu_{C=C}$) , 1146 (m, $\nu_{C-O)}$ cm^{-1}.

6.4.6. Synthesis of 1-(5-carboxypentyl)-2,3,3-trimethyl-3H-indolium bromide (**3.19**) [163]

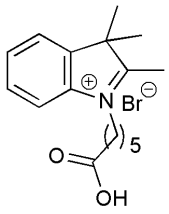

A mixture of 2,3,3-trimethyl-3*H*-indole (0.25 mL, 1.6 mmol) and 6-bromoexanoic acid (936 mg, 4.8 mmol) in acetonitrile (1 mL) was heated in a sealed vial at 150°C for 1 hour under microwave irradiation. The reaction was left to cool, the solvent was evaporated and the residue obtained was suspended in Et_2O and filtered. The solid was extensively washed with Et_2O and DCM several times (5 × 2 mL with each solvent) until all starting material had been removed. After drying overnight in a vacuum oven (40°C), the compound **3.19** was yield as a white-grey solid (449 mg, 80%).

Analysis:

m/z (ES^+): $C_{17}H_{24}NO_2^+$ calculated 274.1, found 274.2 $[M]^+$ (100%).

Rf: 0.28 (DCM/MeOH, 3:2).

HPLC (Method 1): t_R = 3.7 min, purity = 100% (ELSD).

^{1}H NMR (DMSO-d_6, 250 MHz): δ = 1.56-1.77 (m, 10H, $CH_2CH_2CH_2CH_2COOH$, $C(CH_3)_2$), 2.01-2.09 (m, 2H, CH_2COOH), 2.46 (t, 2H, *J* = 7.30 Hz, $NCH_2CH_2CH_2$), 3.94 (s, 3H, CH_3), 4.72 (t, 2H, *J* = 7.35 Hz, $NCH_2CH_2CH_2$), 7.85-7.90 (m, 2H, ArCH) , 8.08-8.11 (m, 1H, ArCH), 8.19-8.22 (m, 1H, ArCH).

^{13}C NMR (DMSO-d_6, 63 MHz) δ = 14.4, 23.4 ($C(CH_3)_2$), 24.2 , 25.7, 27.0, 33.5 (CH_2), 35.8 ($N{=}CCH_3$), 48.1 (CH_2), 55.0 ($C(CH_3)_2$), 117.0, 123.1, 129.0, 129.7 (ArCH), 142.0, 144.1, (ArC), 173.9 (C=O), 197.6 (C=N).

IR (neat): 3450 (s, ν_{O-H}), 1689 (s, $\nu_{C=O}$), 1459 (m, ν_{C-H}), 1294 (s, ν_{O-H}), 1178 (w, ν_{C-O}) cm^{-1}.

Mp: 136-137.5°C.

6.4.7. Synthesis 2-{(1*E*,3*E*,5*E*,7*E*)-7-[1-(5-carboxypentyl)-3,3-dimethyl-1,3-dihydro-3*H*-indol-2-ylidene]-1,3,5-heptatrienyl}-1,3,3-trimethyl-3*H*-indolium inner salt (**3.20,** carboxy-Cy7) [163]

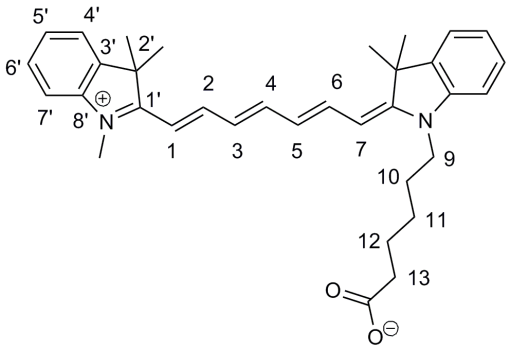

To PS-bound Hemicyanine **3.18** (250 mg, 0.19 mmol) were added dry pyridine (1.5 mL), Ac_2O (0.18 mL, 1.9 mmol) and 1-(5-carboxypentyl)-2,3,3-trimethyl-3*H*-indolium bromide (12 mg, 0.035 mmol) **3.19**. The mixture was stirred for 2 hours under N_2. Afterwards, the resin was isolated by filtration and washed with DCM (2 × 3 mL). The reaction was repeated using the same conditions as described above. The filtrates were then combined and evaporated and the resulting solid was dissolved in DCM (5 mL) and washed several times with water (5 × 5 mL). The solvent was removed *in vacuo*. The crude was precipitated by addition of cold Et_2O (2 mL), sonicated and recovered by centrifugation. The product was washed with Et_2O (3 × 2 mL) and dried *in vacuo* to yield **3.20** as a green solid (33 mg, 92%).

Analysis:

m/z (ES^+): $C_{34}H_{41}N_2O_2^+$ calculated 509.7, found 509.5 $[M]^+$ (100%), 510.5 $[M+H]^+$ (37.6%), 511.5 $[M+2H]^+$(8.2%).

Rf : 0.32 (DCM/MeOH, 9: 1).

HPLC (Method 2): t_R = 5.9 min, purity = 97% (ELSD).

^{1}H NMR (MeOD, 500 MHz): δ = 1.44-1.55 (m, 2H, C*H*$_2$, H_{11}), 1.64-1.69 (m, 2H, C*H*$_2$, H_{12}), 1.72 (s, 12H, C*H*$_3$), 1.85 (m, 2H, C*H*$_2$, H_{10}), 2.31 (t, 2H, *J* = 7.45 Hz, C*H*$_2$, H_{13}), 3.61 (s, 3H, C*H*$_3$), 4.09 (t, 2H, *J* = 7.50 Hz, C*H*$_2$, H_9), 6.26 (t, 2H, *J* = 13.10 Hz, C*H*, H_1 and H_7), 6.56 (t, 1H, *J* = 12.50 Hz, C*H*, H_3), 6.60 (t, 1H, *J* = 12.60 Hz, C*H*,

H_5), 7.23-7.27 (m, 4H, ArCH, $H_{6'}$ and $H_{8'}$), 7.39 (dd, 2H, *J* = 7.65 Hz, *J* = 1.13 Hz, ArC*H*, $H_{7'}$), 7.48 (dd, 2H, *J* = 7.55 Hz, *J* = 1.77 Hz, ArC*H*, $H_{5'}$), 7.62 (t, 1H, *J* = 12.15 Hz, C*H*, H_4), 7.97 (t, 2H, *J* = 12.90 Hz, C*H*, H_6 and H_2).

^{13}C NMR (MeOD, 126 MHz): δ = 25.9 (*C*H_2, C_{11}), 26.2 (*C*H_2, C_{10}), 26.3 (*C*H_2, C_{12}), 26.8, 26.9 (C(*C*H_3)$_2$), 29.8 (N*C*H_3), 33.7 (*C*H_2, C_{13}), 43.2 (*C*H_2, C_9), 47.5, 47.7, 47.9, 48.1, 48.3 (*C*(CH$_3$)$_2$), 103.7, 104.5 (*C*H=CH, $C_{1,\ 7}$), 114.3 (*C*H=CH, C_3), 121.8 (Ar*C*H, $C_{5'}$), 124.4, 124.5 (Ar*C*H, $C_{6',\ 8'}$), 126.0 (*C*H=CH, C_5), 128.2 (Ar*C*H, $C_{7'}$), 133.2 (*C*H=CH, C_4), 139.4, 140.8, 141.6, 142.4, 143.2 (Ar*C*), 151.5, 151.9 (*C*H=CH, $C_{2,\ 6}$), 171.8 (*C*OOH), 173.8, 174.2 (*C*=N).

IR (neat): 2970 (w, $\nu_{C\text{-}H}$), 2862 (w, $\nu_{C\text{-}H}$), 1719 (m, $\nu_{C=O}$), 1392 (s, $\nu_{C=C}$), 1193 (w, $\nu_{C\text{-}O}$) cm^{-1}.

UV/vis (MeOH): λ_{abs} = 745 nm, λ_{em} = 765 nm.

6.4.8. Synthesis of 4-{[(*E*,2*E*)-3-methoxy-2-propenylidene]amino}phenol PS (**3.22**) [163]

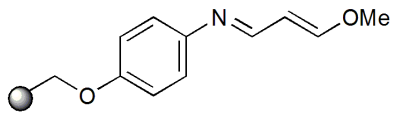

To 4 aminophenol PS **3.16** (1.5 g, 2.51 mmol) was added a solution of 1,1,3,3-tetramethoxypropane **3.21** (5.6 mL, 33.9 mmol) and BF3.OEt$_2$ (0.344 mL, 2.79 mmol) in dry DCM (6.75 mL) and the solution stirred at room temperature for 6 hours. Dry DIEA (0.71 mL, 4.1 mmol) was added and the mixture stirred for 5 minutes. The resin was isolated by filtration, washed several times with DCM (15 mL), and dried *in vacuo* to yield the product **3.22** as a dark blue-black resin (1.6 g). The reaction was confirmed by a qualitative ninhydrin test (**6.2.1.1**).

Analysis:

IR (neat): 3024 (w, $\nu_{C\text{-}H}$), 2916 (w, $\nu_{C\text{-}H}$), 1624 (s, $\nu_{C=C}$), 1451 (s, $\nu_{C\text{-}H}$), 1220 (m, $\nu_{C\text{-}O}$) cm^{-1}.

6.4.9. Synthesis of 1,2,3,3-tetramethyl-3*H*-benzo[*e*]indolium iodide (**3.23**) [163]

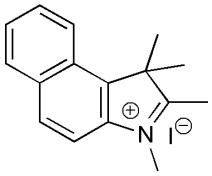

A mixture of 2,3,3-trimethyl-3*H* -benz[e]indole (27.6 g, 0.13 mol) and methyl iodide (20.50 mL, 0.33 mol) in acetonitrile (125 mL) was heated under reflux for 2 hours. At the end of the reaction time, the solution was cooled to room temperature and the sovent was removed under vacuum. The residue obtained was washed with Et_2O several times (5 × 20 mL) and then with ethanol (5 × 20 mL) until removal of the starting material. The residue was dried *in vacuo* and **3.23** isolated as a white/yellow solid (35.4 g, 75%).

Analysis:

m/z (ES^+): $C_{16}H_{18}N^+$ calculated 224.1; found 224.2 $[M]^+$ (100%), 225.1 $[M+H]^+$ (19.5%).

Rf: 0.33 (DCM/MeOH, 9:1).

HPLC (Method 1): t_R = 4.1 min, purity = 100% (ELSD).

^{1}H NMR (DMSO-d_6, 250 MHz) δ = 1.80 (s, 6H, C(C*H*$_3$)$_2$), 2.95 (s, 3H, N=CC*H*$_3$), 4.15 (s, 3H, NC*H*$_3$), 7.70-7.85 (m, 2H, ArC*H*) , 8.10 (d, 1H, *J* = 8.90 Hz, ArC*H*), 8.22 (dd, 1H, *J* = 8.15 Hz, *J* = 1.4 Hz, ArC*H*), 8.32 (d, 1H, *J* = 8.92 Hz, ArC*H*), 8.40 (d, 1H, *J* = 8.25 Hz, ArC*H*).

^{13}C NMR (DMSO-d_6, 63 MHz): δ = 14. 5, 22.6 (C(*C*H$_3$)$_2$), 35.9 (N=C*C*H$_3$), 55.3 (*C*(CH$_3$)$_2$), 112.9, 124.1, 127.5, 128.7, 129.1, 130.7(Ar*C*H), 136.9, 142.0, 144.1 (Ar*C*), 197.6 (C=N).

IR (neat): 2983(w, ν_{C-H}), 1637 (s, $\nu_{C=C}$), 1462 (s, ν_{C-H}) cm^{-1}.

Mp: 221-223 °C.

6.4.10. Synthesis of 2-[(1*E*,3*E*)-4-(4-hydroxyanilino)-1,3-butadienyl]-1,3,3-trimethyl-3*H*-benzo[*e*]indolium iodide PS (**3.24**) [163]

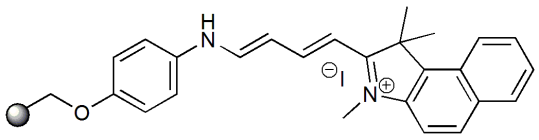

To 4-{[(*E*,2*E*)-3-methoxy-2-propenylidene]amino}phenol PS **3.22** (0.5 g, 0.78 mmol) and

1,2,3,3-tetramethyl-3H-indolium iodide **3.23** (1.4 g, 3.9 mmol) was added DMF (4 mL) and the mixture stirred at 120°C for 15 minutes under microwave irradiation. After reaction, The mixture was cooled and the resin was isolated by filtration, washed with DMF (3 × 10 mL) and DCM (3 × 10 mL). After overnight drying in a vacuum oven at 40°C, **3.24** was obtained as a blue-black resin (0.53 g).

Analysis:

IR (neat): 3025 (w, ν_{N-H}), 2918 (m, ν_{C-H}), 1507 (s, $\nu_{C=C}$), 1170 (m, ν_{C-O}) cm^{-1}.

6.4.11. Synthesis of 1-(5-carboxypentyl)-2,3,3-trimethyl-3*H*-benzo[*e*]indolium bromide (**3.25**) [163]

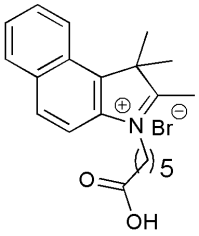

A mixture of 2,3,3-trimethyl-3*H*-benz[e]indole (7.9 g, 37.7 mmol) and 6-bromoexanoic acid (15.0 g, 94.5 mmol) in acetonitrile (25 mL) was heated at reflux for 2 days. The solution was cooled and the solvent was evaporated *in vacuo*. The dark residue obtained was washed with Et_2O and DCM several times (5 × 10 mL for

each solvent) until removal of the starting material. After drying under vacuum, **3.25** was isolated as a pink-grey solid (12.2 g, 80%).

Analysis:

m/z (ES^+): $C_{21}H_{26}NO_2^+$ calculated 324.2; found 324.3 $[M]^+$ (100%), 325.2 $[M+H]^+$ (35%).

Rf: 0.13 (DCM/MeOH, 3:2).

HPLC (Method 1): t_R = 3.1 min, purity = 100% (ELSD).

^{1}H NMR (DMSO-d_6, 250 MHz,): δ = 1.56-1.70 (m, 10H, $CH_2CH_2CH_2CH_2COOH$, $C(CH_3)_2$), 1.99-2.07 (m, 2H, CH_2COOH), 2.30 (t, 2H, *J* = 7.10 Hz, $NCH_2CH_2CH_2$), 3.03 (s, 3H, CH_3), 4.65 (t, 2H, *J* = 7.18 Hz, $NCH_2CH_2CH_2$), 7.77-7.90 (m, 2H, ArCH) , 8.26 (d, 1H, *J* = 8.90 Hz, ArCH), 8.30 (dd, 1H, *J* = 8.75 Hz, *J* = 1.46 Hz, ArCH), 8.37 (d, 1H, *J* = 8.95 Hz, ArCH), 8.46 (d, 1H, *J* = 8.20 Hz, ArCH).

^{13}C NMR (DMSO-d_6, 63 MHz): δ = 14.6, 21.9 ($C(CH_3)_2$), 24.6, 25.8 (CH_2), 27.7 (CH_2COOH), 33.6 (NCH_2CH_2), 36.1 (CH_3), 48.2 (NCH_2), 55.3 ($C(CH_3)_2$), 114.1, 124.3, 127.5, 128.5, 129.6, 130.7 (ArCH), 135.9 , 137.4 , 138.9 (ArC), 174.7 (COOH), 197. 6 (C=N).

IR (neat): 2964 (w, ν_{C-H}), 1707 (s, $\nu_{C=O}$), 1474 (m, ν_{C-H}), 1389, 1156 (m, ν_{C-O}) cm^{-1}.

Mp: 233-234.5°C.

6.4.12. Synthesis of 2-{(1*E*,3*E*,5*E*)-5-[3-(5-carboxypentyl)-3,3-dimethyl-1,3-dihydro-3*H*-benzo[*e*]indol-2-ylidene]-1,3-pentadienyl}-1,1,3-trimethyl-1*H*-benzo [*e*] indolium inner salt (**3.26**, carboxy-Cy5.5) [163]

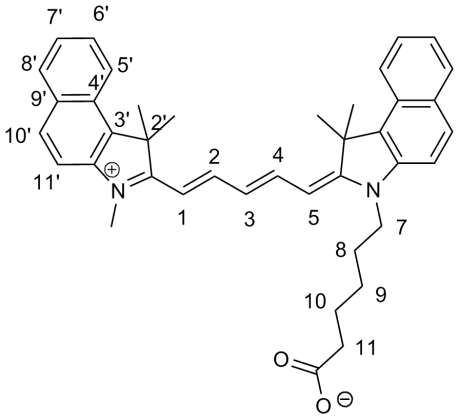

To PS-bound hemicyanine **3.24** (0.7 g, 0.75 mmol) were added dry pyridine (5.5 mL), DIEA (1.3 mL, 7.50 mmol), Ac_2O (0.7 mL, 7.50 mmol) and 1-(5-carboxypentyl)-2,3,3- trimethyl-3*H*-indolium bromide **3.25** (40 mg, 0.10 mmol). The mixture was stirred in the dark for 2 hours under N_2. The resin was isolated by filtration and washed several times with DCM (5 × 7.5 mL). The filtrates were combined and evaporated under vacuum. The resulting blue-green solid was dissolved in DCM (5 × 10 mL) and washed several times with water (10 mL). The organic layer was dried over $MgSO_4$ and filtered. After removal of the solvent *in vacuo*, the crude product was precipitated by addition of cold Et_2O (5 mL). After sonication and centrifugation, the blue solid was washed several times with Et_2O (5 × 5 mL) and then purified by column chromatography (silica, eluting with DCM to DCM/MeOH, 1:1) to yield **3.26** (carboxy-Cy5.5) as a dark blue-green solid (52 mg, 90%).

Analysis:

m/z (ES^+): $C_{40}H_{43}N_2O_2^+$ calculated 583.3; found 583.5 [M^+] (100%), 584.5 $[M+H]^+$ (45%).

Rf: 0.36 (DCM/MeOH, 9:1).

HPLC (Method 2): t_R = 5.4 min, purity = 100% (ELSD and 675 nm).

^{1}H NMR (MeOD, 500 MHz): δ = 1.52-1.60 (m, 2H, C*H*$_2$, H_9), 1.69-1.79 (quin, 2H, *J* = 9.65 Hz, *J* = 8.35 HZ, C*H*$_2$, H_{10}), 1.88-1.95 (m, 2H, C*H*$_2$, H_8), 2.06 (s, 12H, C(C*H*$_3$)$_2$), 2.23 (t, 2H, *J* = 9.10 Hz, C*H*$_2$, H_{11}), 3.77 (s, 3H, NC*H*$_3$), 4.26 (t, 2H, *J* = 9.15 Hz, C*H*$_2$, H_7), 6.34 (d, 1H, *J* = 14.75 Hz, C*H*, H_5), 6.39 (d, 1H, *J* = 14.95 Hz, C*H*, H_1), 6.71 (t, 1H, *J* = 16.00 Hz, C*H*, H_3), 7.51 (dd, 2H, *J* = 8.90 Hz , *J* = 3.65 Hz, ArC*H*, $H_{7'}$), 7.59-7.71 (m, 4H, ArC*H*, $H_{10'}$ and $H_{6'}$), 8.02 (d, 2H, *J* = 11.35 Hz, ArC*H*, $H_{8'}$), 8.05 (d, 2H, *J* = 11.25 Hz, ArC*H*, $H_{11'}$), 8.28 (d, 2H, *J* = 10.75 Hz, ArC*H*, $H_{5'}$), 8.37 (t, 2H, *J* = 17.80 Hz, C*H*, H_2 and H_4).

^{13}C NMR (MeOD, 126 MHz): δ = 25.4 (*C*H$_2$, C_9), 25.6 (*C*H$_2$, C_{10}), 25.9, 26.1 (C(*C*H$_3$)$_2$), 26.3 (*C*H$_2$, C_8), 31.2 (N*C*H$_3$), 34.3 (*C*H$_2$, C_{11}), 45.0 (*C*H$_2$, C_7), 47.8, 48.4 (*C*(CH$_3$)$_2$), 103.2, 103.9 (*C*H=CH, $C_{1,\ 5}$), 114.0 (*C*H=CH, C_3), 122.1 (Ar*C*H, $C_{11'}$), 122.9 (Ar*C*H, $C_{5'}$), 124.4, 124.5 (Ar*C*H, $C_{6',\ 10'}$), 128.6 (Ar*C*H, $C_{7'}$), 130.4 (Ar*C*H,

$C_{8'}$), 133.4, 134.9, 135.1, 140.9, 141.6 (Ar*C*), 153.5, 154.0 (*C*H=CH, $C_{2,4}$), 172.6 (*C*OOH), 175.8 (C=N), 176.4 (C=N).

IR (neat): 2971 (w, ν_{C-H}), 2862 (w, ν_{C-H}), 1684 (m, $\nu_{C=O}$), 1454(s, $\nu_{C=C}$), 1092 (w, ν_{C-O}) cm^{-1}.

UV/vis (MeOH): λ_{abs} = 678 nm, λ_{em} = 704 nm.

6.4.13. Synthesis of Cy7-9mer (**3.28**)

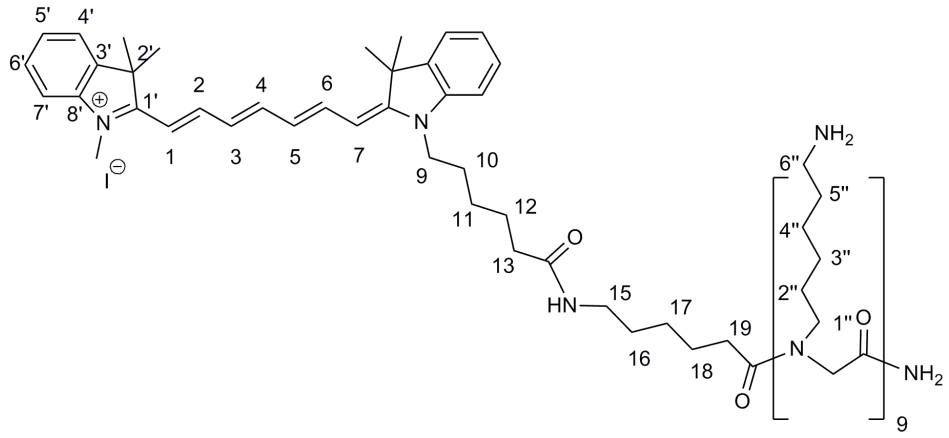

The Cy7-9mer peptoid **3.28** was coupled to the resin **2.35** previously Fmoc deprotected (50 mg, 0.015 mmol). The carboxy-Cy7 **3.20** was first activated in solution before being added to the solid support.

Method 1: NHS-Cy7

The Cy7 **3.20** (23 mg, 0.045 mmol) was activated under nitrogen in the presence of N-N'-Disuccinimidylcarbonate (17 mg, 0.0675 mmol) with a solution of anhydrous DMF/pyridine (1: 1) (2 mL) at 35°C for 3 hours (reaction was followed by TLC and MS). The solvent was evaporated under vacuum and the residue was precipitated by the addition of 3 mL of cold Et_2O (solid recovered by centrifugation) before being dried in a vacuum oven (m/z = 606.33 M^+).

The ester succinimide Cy7 was dissolved in a minimum of DMF (0.8 mL) and mixed with the Fmoc deprotected **2.35**. The mixture was stirred overnight in the dark. The resin was isolated by filtration and the filtrate recycled and reused (3 times) using the same conditions as described above until completion of the coupling (negative ninhydrin test, **6.2.1.1**).

Finally, the resin bound peptoid was deprotected and cleaved from the solid support by treatment with a mixture of TFA/TIS/H_2O (95: 2.5: 2.5) for 2 hours and precipitated in cold Et_2O (**6.2.1.10**) to give **3.28** as a blue solid. It was purified by semi-preparative HPLC (Gradient 1) (18 mg, 60% based on **2.35,** purity 98% (ELSD)).

Method 2: OBt-Cy7

The Cy7 **3.20** (23 mg, 0.045 mmol) and HOBt (6 mg, 0.045 mmol) were dissolved in DMF (1.25 mL). DIC (6.6 µL) was added to the solution and mixed for 15 minutes. The OBT ester Cy7 was added to **2.35** (Fmoc deprotected). The mixture was stirred overnight in the dark. After reaction the resin was isolated by filtration and washed with DMF, DCM, MeOH (5 × 1 mL for each solvent) until the filtrate was colourless. The completion of the coupling was monitored by a ninhydrin test (**6.2.1.1**).

Finally, the resin bound peptoids were deprotected and cleaved from the solid support as previously decribed (Method 1, protocol **6.2.1.10**) to give **3.28** as a blue solid. After overnight drying, the compound was isolated in a 94% final yield (29 mg, purity = 98%).

Analysis:

m/z (ES^+): $C_{112}H_{197}N_{22}O_{11}^+$ calculated 2026.6; found m/z: 507.5 $[M+4H]^{4+}$ (14.3%), 406.2 $[M+5H]^{5+}$ (100%), 338.7 $[M+6H]^{6+}$ (56.7%), 290.4 $[M+7H]^{7+}$ (12.2%).

m/z (MALDI-TOF): $C_{112}H_{197}N_{22}O_{11}^+$ calculated 2026.55; found 2026.19 $[M]^+$ (100%).

m/z (FT-MS): $C_{112}H_{197}N_{22}O_{11}^+$ calculated $[M+3H]^{3+}$ 676.52538; found 676.53027.

HPLC (Method 3): t_R = 4.9 min; purity > 98% (750 nm).

^{1}H NMR (D_2O, 500 MHz, eSpresat water suppression): δ = 1.22-1.71 (m, 94H, 12H for 2×C(C*H*$_3$)$_2$-Cy7, 72H for C*H*$_2$ ($H_{2'', 3'', 4'', 5''}$), 10H for C*H*$_2$ ($H_{11, 12, 16, 17, 18}$)), 1.79-1.90 (m, 2H, C*H*$_2$, H_{10}), 2.37-2.45 (m, 2H, C*H*$_2$CO, H_{19}), 2.47-2.56 (m, 2H, C*H*$_2$CO, H_{13}), 2.89-3.09 (m, 20H, 18H for C*H*$_2$NH$_2$ ($H_{6''}$) and 2H for C*H*$_2$NH (H_{15})), 3.21-

3.46 (m, 18H, C*H*$_2$N, H$_{1''}$), 3.54-3.60 (m, 3H, CH$_3$-Cy7), 3.93-4.53 (m, 20H, 18H for NC*H*$_2$CO and 2H for C*H*$_2$N (H$_9$)), 6.21-6.32 (m, 2H, C*H*-Cy7, H$_1$ and H$_7$), 6.48-6.62 (m, 2H, C*H*-Cy7, H$_3$ and H$_5$), 7.24-7.34 (m, 4H, ArC*H*, H$_{5'}$ and H$_{7'}$), 7.40-7.48 (m, 2H, ArC*H*, H$_{6'}$), 7.50-7.65 (m, 3H, 2H for ArC*H* (H$_{4'}$) and 1H for C*H*-Cy7, (H$_4$)), 7.83-7.92(m, 2H, C*H*-Cy7, H$_2$ and H$_6$), 7.94 (s, 2H, CON*H*$_2$).

^{13}C NMR (D$_2$O, 126 MHz): δ = 21.7, 21.9, 22.1, 24.1, 25.0, 25.1, 25.3, 25.4, 25.5, 25.8, (CH$_2$*C*H$_2$CH$_2$), 26.4 (*C*H$_2$, C$_{10}$), 26.6 (*C*H$_2$, C$_{19}$), 26.7, 26.9, 27.7, 27.8 (C(*C*H$_3$)$_2$), 30.0 (N*C*H$_3$), 35.1 (*C*H$_2$, C$_{13}$), 39.0, 39.1, 39.2, 39.3 (*C*H$_2$, C$_{6'', 15}$), 47.2, 47.3, 47.4, 47.5, 47.6, 47.8, 47.9, 48.0, 48.1, 48.2, 48.4 (N*C*H$_2$ (C$_9$), *C*H$_2$N (C$_{1''}$), NCH$_2$CO, (*C*(CH$_3$)$_2$), 103.3, 104.0 (*C*H=CH, C$_{1, 7}$), 115.3 (*C*H=CH, C$_3$), 120.7 (Ar*C*H, C$_{4'}$), 122.3, 122.5 (Ar*C*H, C$_{5', 7'}$), 123.4 (*C*H=CH, C$_5$), 129.1 (Ar*C*H, C$_{6'}$), 135.6 (*C*H=CH, C$_4$), 139.9, 141.1, 141.9, 143.3, 143.6 (Ar*C*), 149.1, 150.9 (*C*H=CH, C$_{2, 6}$), 162.4, 162.7, 163.0, 163.2 (N*C*O-9mer), 169.8, 170.1 (*C*O), 172.9, 173.4 (*C*=N).

UV/vis (MeOH): λ_{abs} = 744 nm, λ_{em} = 777 nm.

UV/vis (H$_2$O): λ_{abs} = 693 nm, λ_{em} = 779 nm.

6.4.14. <u>Synthesis of Cy5.5-9mer (**3.29**)</u>

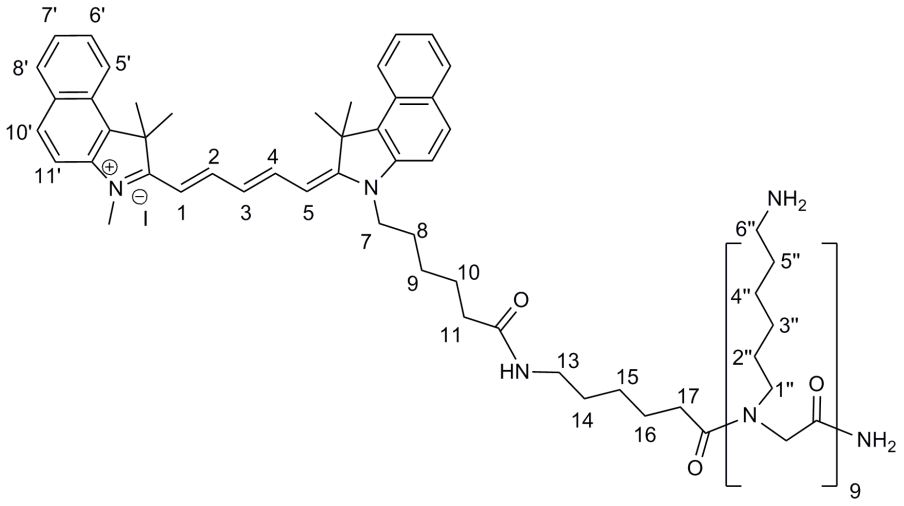

Cy5.5 **3.26** (26 mg, 0.045 mmol) was coupled to the Fmoc deprotected peptoid **2.35** (50 mg, 0.015 mmol), as previously described in **6.4.14**. The ***Method 2*** was used to

activate the fluorophore. After cleavage and deprotection, **3.29** was isolated as a blue solid (27 mg, 87% based on **2.35**).

Analysis:

m/z (ES^+): $C_{118}H_{199}N_{22}O_{11}^+$ calculated 2100.6; found m/z: 700.9 $[M+3H]^{3+}$ (8.4%), 526.0 $[M+4H]^{4+}$ (100%), 421.0 $[M+5H]^{5+}$ (88.5%), 351.1 $[M+6H]^{6+}$ (12.1%).

m/z (MALDI-TOF): $C_{118}H_{199}N_{22}O_{11}^+$ calculated 2100.57; found 2101.28 $[M+H]^+$ (100%).

m/z (FT-MS): $C_{118}H_{199}N_{22}O_{11}^+$ calculated $[M+3H]^{3+}$ 701.19727; found 701.20514.

HPLC (Method 3): t_R = 4.1 min, purity > 98% (675 nm).

^{1}H NMR (D_2O, 500 MHz, eSpresat water suppression): δ = 1.10-1.71 (m, 82H, 10H for C*H*$_2$ ($H_{9, 10, 14, 15, 16}$), 72H for C*H*$_2$ ($H_{3'', 4'', 5''}$)), 1.84 (m, 2H, C*H*$_2$, H_8), 1.89 (s, 12H, C(C*H*$_3$)$_2$), 2.07-2.14 (m, 4H, C*H*$_2$CO, H_{11} and H_{17}), 2.79-2.98 (m, 18H, C*H*$_2$NH$_2$, $H_{6''}$), 3.06-3.41 (m, 20H, 2H for NHC*H*$_2$ (H_{13}), 18H for C*H*$_2$N ($H_{1''}$)), 3.63 (s, 3H, NC*H*$_3$), 3.85-4.46 (m, 20H, 2H for NC*H*$_2$ (H_7), 18H for NC*H*$_2$CO), 6.27 (m, 2H, C*H*, H_1 and H_5), 6.56 (m, 1H, C*H*, H_3), 7.47 (m, 2H, ArC*H*, $H_{7'}$), 7.55 (d, *J* = 8.40 Hz, 2H, ArC*H*, $H_{10'}$), 7.62 (m, 2H, ArC*H*, $H_{6'}$), 7.94 (m, 2H, *J* = 6.20 Hz, ArC*H*, $H_{8'}$), 7.96-8.02 (m, 4H, ArC*H*, $H_{11'}$ and CONH$_2$), 8.12 (m, 2H, C*H*, H_2 and H_4), 8.23 (d, 2H, *J* = 8.05 Hz, ArC*H*, $H_{5'}$).

^{13}C NMR (D_2O, 126 MHz): δ = 25.2, 25.3, 25.4 25.5, 25.6, 25.8 (CH$_2$*C*H$_2$CH$_2$), 26.1, 26.2, 26.3 (C(*C*H$_3$)$_2$), 26.6, 26.7, 28.8 (CH$_2$*C*H$_2$CH$_2$), 31.4 (N*C*H$_3$), 35.1 (*C*H$_2$, C_{11} and C_{17}), 46.7, 48.4, 48.5, 48.6, 49.5 (*C*H$_2$, $C_{7, 13, 1''}$ and N*C*H$_2$CO), 52.7 (*C*(CH$_3$)$_2$), 103.4, 104.1 (*C*H=CH, $C_{1, 5}$), 115.2 (*C*H=CH, C_3), 122.3 (Ar*C*H, $C_{11'}$), 123.2 (Ar*C*H, $C_{5'}$), 124.8, 125.1 (Ar*C*H, $C_{6', 10'}$), 128.8 (Ar*C*H, $C_{7'}$), 130.4 (Ar*C*H, $C_{8'}$), 133.5, 134.8, 141.0, 141.6 (Ar*C*), 153.8, 154.2 (*C*H=CH, $C_{2, 4}$), 162.7, 162.8, 163.1 (N*C*O-9mer and NH*C*O), 172.5 (*C*=N).

UV/vis (MeOH): λ_{abs} = 678 nm, λ_{em} = 710 nm.

UV/vis (H_2O): λ_{abs} = 623 nm, λ_{em} = 710 nm.

6.4.15. Synthesis of the resin **3.33**

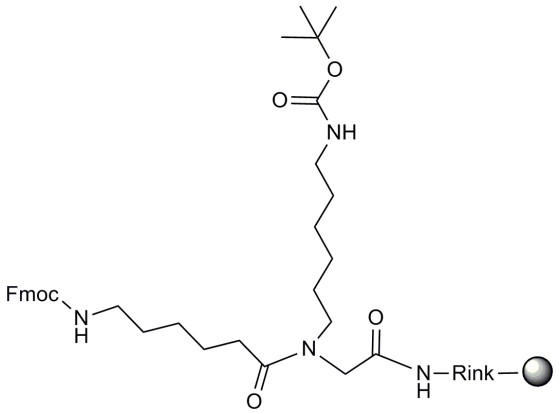

One peptoid monomer unit **2.22** (65 mg, 0.130 mmol) was coupled to **2.28** (50 mg, 0.043 mmol) using the protocol **6.2.1.6** followed by Fmoc deprotection (**6.2.1.7**). Fmoc-Ahx-OH spacer **2.34** (46 mg, 0.130 mmol) was coupled using HOBt/DIC in DMF (**6.2.1.6**). A new loading of the resin **3.33** was calculated using a quantitative ninhydrin test **6.2.1.2** (0.57 mmol/g).

6.4.16. Synthesis of Cy7-1mer (**3.30**)

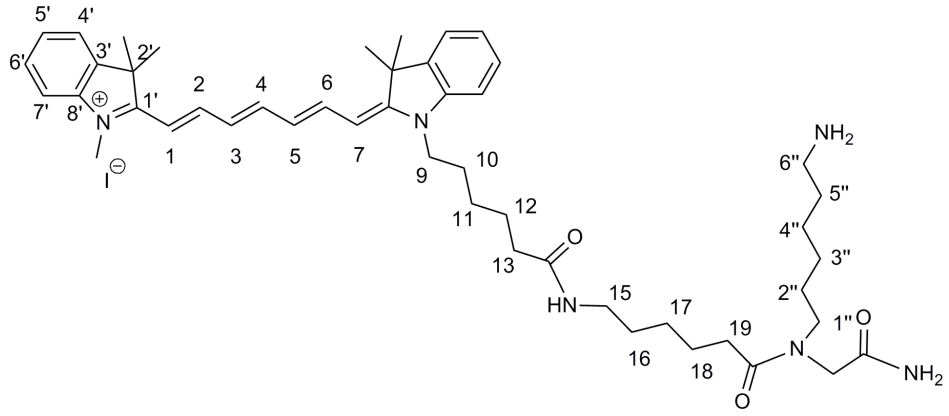

Cy7 (22 mg, 0.043 mmol) was activated and coupled to **3.33** (75 mg, 0.043 mmol) previously Fmoc deprotected using the ***Method 2*** described earlier (**6.4.14**). The coupling was repeated 3 times with recycling the carboxy-Cy7 (controlled by a ninhydrin test, **6.2.1.1**). Cy7-1mer was deprotected and cleaved from the solid

support (**6.2.1.10,** 2 hours at room temperature using TFA/TIS/H_2O, 95: 2.5: 2.5) to give **3.30** as a blue solid (32 mg, 97% based on **3.33**).

Analysis:

m/z (ES^+): $C_{48}H_{69}N_6O_3^+$ calculated 777.5; found 389.5 $[M+H]^{2+}$ (100%), 777.4 $[M]^+$ (78.4%).

m/z (HRMS, ES^+): $C_{48}H_{69}N_6O_3^+$ calculated $[M]^+$ 777.54257; found 777.54315.

HPLC (Method 3): t_R = 4.6 min, purity = 97% (ELSD).

^{1}H NMR (D_2O, 500 MHz, eSpresat water suppression): δ = 1.09-1.38 (m, 8H, C*H*$_2$, $H_{3'', 4'', 11, 17}$), 1.39-1.73 (m, 22H, 12H for 2 × C(C*H*$_3$)$_2$-Cy7, 10H for C*H*$_2$ ($H_{2'', 5'', 12, 16, 18}$)), 1.78 (m, 2H, C*H*$_2$, H_{10}), 2.14-2.24 (m, 2H, C*H*$_2$CO, H_{19}), 2.33-2.40 (m, 2H, C*H*$_2$CO, H_{13}), 2.82-3.02 (m, 4H, C*H*$_2$NH$_2$ ($H_{6''}$) and C*H*$_2$NH, (H_{15})), 3.27-3.36 (m, 2H, C*H*$_2$N, $H_{1''}$), 3.50 (s, 3H, CH_3-Cy7), 3.90-3.94 (two s, 2H, NC*H*$_2$CO), 3.98-4.07 (m, 2H, C*H*$_2$N, H_9), 6.13-6.24 (m, 2H, C*H*-Cy7, H_1 and H_7), 6.38-6.54 (m, 2H, C*H*-Cy7, H_3 and H_5), 7.04-7.11 (m, 1H, C*H*-Cy7, H_4), 7.17-7.28 (m, 4H, ArC*H*, $H_{5'}$ and $H_{7'}$), 7.33-7.43 (m, 2H, ArC*H*, $H_{6'}$), 7.44-7.48 (m, 2H, ArC*H*, $H_{4'}$), 7.77-7.88 (m, 2H, C*H*-Cy7, H_2 and H_6), 8.38 (s, 2H, CON*H*$_2$).

^{13}C NMR (D_2O, 126 MHz): δ =22.0, 23.1, 24.4, 25.1, 25.3, 25.6, 25.7, 26.0 (CH_2*C*H_2CH_2), 26.5 (*C*H_2, C_{10}), 26.7 (*C*H_2, C_{19}), 27.7, 27.8 (C(*C*H_3)$_2$), 30.1 (N*C*H_3), 35.2 (*C*H_2, C_{13}), 38.9, 39.1 (*C*H_2, $C_{6'', 15}$), 47.3, (*C*H_2N, $C_{1''}$), 48.0, 48.1, 48.4 (N*C*H_2 (C_9), N*C*H_2CO), 49.8, 50.1 (*C*(CH_3)$_2$), 103.1, 103.6 (*C*H=CH, $C_{1, 7}$), 115.2 (*C*H=CH, C_3), 120.8 (Ar*C*H, $C_{4'}$), 122.4, 122.6 (Ar*C*H, $C_{5', 7'}$), 123.4 (*C*H=CH, C_5), 128.9 (Ar*C*H, $C_{6'}$), 135.4 (*C*H=CH, C_4), 141.6, 142.9, 143.6 (Ar*C*), 148.7, 149.2 (*C*H=CH, $C_{2, 6}$), 163.1 (N*C*O-9mer), 170.0, 170.4 (*C*O), 173.1, 173.3 (*C*=N).

UV/vis (MeOH): λ_{abs} = 743 nm, λ_{em} = 779 nm.

6.4.17. Synthesis of Cy5.5-1mer (**3.31**)

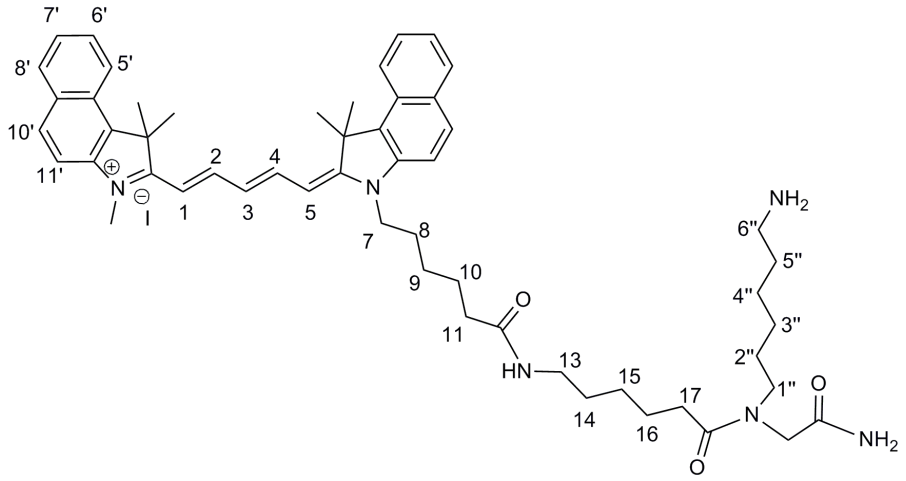

The Cy5.5-1mer peptoid **3.31** was synthesised as for **3.30** above (**6.4.16)** using 75 mg of **3.33** (0.043 mmol). **3.31** was isolated after ether precipitation and overnight vacuum drying to yield 34 mg of a blue solid (94% based on **3.33**)

Analysis:

m/z (ES^+): $C_{54}H_{71}N_6O_3^+$ calculated 851.6; found 851.5 $[M]^+$ (100%), 426.2 $[M+H]^{2+}$ (56.3%).

m/z (HRMS, ES^+): $C_{54}H_{71}N_6O_3^+$ calculated $[M]^+$ 851.55822; found 851.55605.

HPLC (Method 3): t_R = 4.9 min, purity = 95% (ELSD).

^{1}H NMR (D_2O, 500 MHz, eSpresat water suppression): δ = 1.16-1.30 (m, 10H, CH_2, $H_{3'', 4'', 5'', 9, 15}$), 1.53-1.63 (m, 2H, CH_2, H_{14}), 1.71 (quin, 2H, *J* = 5.30 Hz, *J* = 6.20 HZ, CH_2, H_{10}), 1.85 (m, 4H, CH_2, H_8 and $H_{2''}$), 1.99 (s, 12H, C(CH_3)$_2$), 2.08-2.17 (m, 4H, CH_2CO, H_{11} and H_{17}), 2.74-2.83 (m, 2H, CH_2NH_2, $H_{6''}$), 3.09 (t, *J* = 5.61 Hz, 2H, NHCH_2, H_{13}), 3.64 (s, 3H, NCH_3), 3.66-3.71 (m, 2H, CH_2N, $H_{1''}$), 3.80-3.90 (2 s, 2H, NCH_2CO), 4.18 (m, 2H, CH_2, H_7), 6.22 (d, 2H, *J* = 14.05 Hz, C*H*, H_1 and H_5), 6.51 (t, 1H, *J* = 12.80 Hz, C*H*, H_3), 7.43 (m, 2H, ArC*H*, $H_{7'}$), 7.55 (d, *J* = 9.05 Hz, 2H, ArC*H*, $H_{10'}$), 7.61 (td, *J* = 12.80 Hz, *J* = 1.55 Hz, 2H, ArC*H*, $H_{6'}$), 7.94 (d, 2H, *J* = 6.20 Hz, ArC*H*, $H_{8'}$), 8.00 (2 d, 2H, *J* = 9.20 Hz, ArC*H*, $H_{11'}$), 8.06 (td, 2H, *J* = 13.55 Hz, *J* = 2.30 Hz, C*H*, H_2 and H_4), 8.21 (d, 2H, *J* = 8.55 Hz, ArC*H*, $H_{5'}$), 8.38 (s, 2H, CONH_2).

^{13}C NMR (D_2O, 126 MHz): δ = 24.9, 25.0, 25.1, 25.3, 25.4 25.5, 25.6 ($CH_2CH_2CH_2$, $C3'', 4'', 5'', 9, 15$), 25.9 (CH_2, C_{14}), 26.2, 26.4 ($C(CH_3)_2$), 26.8 (CH_2, C_{10}) , 28.6, 28.8 (CH_2, $C_{8,\ 2''}$), 31.5 (NCH_3), 35.0, 35.2 (CH_2, C_{11} and C_{17}), 46.6 , 46.8 (CH_2, $C_{6''}$),48.3, 48.4, 48.7, (CH_2, $C_{13,\ 1''}$ and NCH_2CO), 49.7 (CH_2, C_7), 50.2, 50.4 ($C(CH_3)_2$), 104.6, 105.0 (CH=CH, $C_{1,\ 5}$), 114.7 (CH=CH, C_3), 117.8 (ArCH, $C_{11'}$), 123.3 (ArCH, $C_{5'}$), 124.7, 125.2 (ArCH, $C_{6',\ 10'}$), 127.9 (ArCH, $C_{7'}$), 129.6 (ArCH, $C_{8'}$), 142.3, 143.8, 143.9, 141.5 (ArC), 153.7, 154.0 (CH=CH, $C_{2,\ 4}$), 162.5, 162.8, 163.1 (NCO-9mer and NHCO), 172.8 (C=N).

UV/vis (MeOH): λ_{abs} = 675 nm, λ_{em} = 710 nm.

6.4.18. Cellular uptake of Cy-peptoid in HeLa, B16F10 and HEK293T cells

Cells were seeded into a 24-well plate. After 24 hours, 35 µL of Cy7-9mer (**3.28**), Cy5.5-9mer (**3.29**), Cy7-1mer (**3.30**) or Cy5.5-1mer (**3.31**) (100 µM) in PBS were adde in three random wells. Cellular uptake was analysed after 5, 30 minutes, 2, 4 and 24 hours of incubation by flow cytometry in 2% FBS in PBS with 0.2% of trypan blue (**6.2.2.3**).

HeLa cells

	Incubation time	Average (%)	Error (%)
Untreated cells		0.3	0.1
3.28	5 min	63.6	3.1
	30 min	82.9	3.1
	2 h	98.4	0.6
	4 h	99.5	0.2
	24 h	99.8	0.1

Table 6.16: Cellular uptake of Cy7-9mer (3.28, 10 µM) in HeLa cells (n = 6).

	Incubation time	Average (%)	Error (%)
Untreated cells		0.3	0.1
3.29	5 min	77.2	2.1
	30 min	98.3	0.4
	2 h	99.0	0.8
	4 h	99.7	0.2
	24 h	100.0	0.1

Table 6.17: Cellular uptake of Cy5.5-9mer (3.29, 10 µM) in HeLa cells (n = 6).

	Incubation time	Average (%)	Error (%)
Untreated cells		0.2	0.1
3.30	5 min	8.9	0.3
	30 min	14.0	1.5
	2 h	29.8	7.8
	4 h	38.0	1.1
	24 h	45.2	1.6
3.31	5 min	9.4	0.4
	30 min	16.3	2.0
	2 h	38.0	1.3
	4 h	43.9	1.1
	24 h	48.2	1.0

Table 6.18: Cellular uptake of Cy7-1mer (3.30, 10 µM) and Cy5.5-1mer (3.31, 10 µM) in HeLa cells (n = 3).

B16F10 cells

	Incubation time	Average (%)	Error (%)
Untreated cells		0.4	0.2
3.28	5 min	35.4	1.3
	30 min	60.3	2.0
	2 h	92.3	1.0
	4 h	98.0	0.7
	24 h	99.9	0.1

Table 6.19: Cellular uptake of Cy7-9mer (3.28, 10 µM) in B16F10 cells (n = 6).

	Incubation time	Average (%)	Error (%)
Untreated cells		0.3	0.1
3.29	5 min	25.2	0.9
	30 min	65.7	1.2
	2 h	90.0	1.0
	4 h	97.5	1.0
	24 h	99.9	0.1

Table 6.20: Cellular uptake of Cy5.5-9mer (3.29, 10 µM) in B16F10 cells (n = 6).

	Incubation time	Average (%)	Error (%)
Untreated cells		0.3	0.1
3.30	5 min	3.0	0.1
	30 min	4.9	0.2
	2 h	11.2	1.2
	4 h	20.9	2.1
	24 h	32.4	0.6
3.31	5 min	2.3	0.6
	30 min	5.4	0.6
	2 h	13.9	0.9
	4 h	26.6	1.6
	24 h	34.8	1.7

Table 6.21: Cellular uptake of Cy7-1mer (3.30, 10 µM) and Cy5.5-1mer (3.31, 10 µM) in B16F10 cells (n = 3).

HEK293T cells

	Incubation time	Average (%)	Error (%)
Untreated cells		0.4	0.2
3.28	5 min	80.7	1.9
	30 min	94.8	2.3
	2 h	97.9	1.1
	4 h	99.6	0.4
	24 h	100.0	0.1

Table 6.22: Cellular uptake of Cy7-9mer (3.28, 10 µM) in HEK293T cells (n = 6).

	Incubation time	Average (%)	Error (%)
Untreated cells		0.4	0.2
3.29	5 min	86.5	5.1
	30 min	94.4	3.7
	2 h	97.3	1.9
	4 h	99.2	0.7
	24 h	100.0	0.1

Table 6.23: Cellular uptake of Cy5.5-9mer (3.29, 10 µM) in HEK293T cells (n = 6).

	Incubation time	Average (%)	Error (%)
Untreated cells		0.2	0.2
3.30	5 min	9.0	0.8
	30 min	12.3	0.6
	2 h	20.8	0.7
	4 h	28.3	1.0
	24 h	39.4	0.9
3.31	5 min	9.9	2.3
	30 min	16.9	0.6
	2 h	26.4	0.8
	4 h	32.1	1.8
	24 h	48.2	1.9

Table 6.24: Cellular uptake of Cy7-1mer (3.30, 10 µM) and Cy5.5-1mer (3.31, 10 µM) in HEK293T cells (n = 3).

6.4.19. MTT assays of Cy-peptoid in HeLa, B16F10 and HEK293T cells

MTT cytotoxicity assays were carried out as according to the general procedures (**6.2.2.4**). Cells were treated with 1, 5, 10 or 20 µL of Cy7-9mer (**3.28**), Cy5.5-9mer (**3.29**), Cy7-1mer (**3.30**) or Cy5.5-1mer (**3.31**) 100 µM in order to obtain a final concentration of 1, 5, 10 or 20 µM, respectively. After 24 hours of incubation at 37^{o}C, the cells were prepared to be read on the microplate reader.

HeLa cells

	Concentration (μM)	Average (arb. units)	Error (arb. units)	Average (%)	Error (%)
Untreated cells		1.110	0.086	100.0	7.8
3.28	1	1.173	0.088	105.7	7.9
	5	0.838	0.115	75.4	10.3
	10	0.634	0.161	57.1	14.5
	20	0.489	0.125	44.1	11.2
3.29	1	1.129	0.083	101.7	7.5
	5	0.975	0.053	87.8	4.8
	10	0.831	0.076	74.9	6.8
	20	0.639	0.132	57.6	11.9
3.30	1	1.127	0.062	101.5	5.6
	5	0.954	0.068	85.9	6.1
	10	0.741	0.038	66.8	3.4
	20	0.575	0.088	51.8	7.9
3.31	1	1.112	0.069	100.1	6.2
	5	1.095	0.071	98.6	6.4
	10	0.886	0.043	79.8	3.9
	20	0.752	0.085	67.7	7.6

Table 6.25: Percentage of cell vailability (HeLa cells) after 24 hours of incubation with Cy7-9mer (3.28), Cy5.5-9mer (3.29), Cy7-1mer (3.30) and Cy5.5-1mer (3.31) at different concentrations (n = 5).

B16F10 cells

	Concentration (μM)	Average (arb. units)	Error (arb. units)	Average (%)	Error (%)
Untreated cells		0.872	0.064	100.0	7.4
3.28	1	0.879	0.074	100.8	8.5
	5	0.619	0.055	70.9	6.3
	10	0.490	0.068	56.2	7.8
	20	0.348	0.061	40.0	7.0
3.29	1	0.883	0.074	101.3	8.5
	5	0.664	0.100	76.1	11.5
	10	0.508	0.064	58.3	7.3
	20	0.405	0.097	46.5	11.1
3.30	1	0.885	0.050	101.5	5.7
	5	0.749	0.053	85.9	6.1
	10	0.581	0.030	66.7	3.5
	20	0.451	0.065	51.8	7.4

3.31	1	0.909	0.030	104.3	3.4
	5	0.771	0.053	88.4	6.1
	10	0.609	0.029	69.9	3.4
	20	0.517	0.066	59.3	7.6

Table 6.26: Percentage of cell vailability (B16F10 cells) after 24 hours of incubation with Cy7-9mer (3.28), Cy5.5-9mer (3.29), Cy7-1mer (3.30) and Cy5.5-1mer (3.31) at different concentrations (n = 5).

HEK293T cells

	Concentration (μM)	Average (arb. units)	Error (arb. units)	Average (%)	Error (%)
Untreated cells		1.037	0.080	100.0	7.8
3.28	1	1.025	0.049	98.9	4.8
	5	0.914	0.040	88.1	3.9
	10	0.598	0.034	57.6	3.3
	20	0.453	0.052	43.7	5.0
3.29	1	1.081	0.056	104.3	5.4
	5	0.956	0.054	92.2	5.2
	10	0.672	0.066	64.8	6.4
	20	0.545	0.042	52.6	4.0
3.30	1	1.024	0.073	98.7	7.1
	5	0.884	0.048	85.2	4.6
	10	0.789	0.026	76.1	2.5
	20	0.719	0.059	69.3	5.7
3.31	1	1.140	0.059	110.0	5.7
	5	0.992	0.040	95.7	3.9
	10	0.921	0.048	88.8	4.6
	20	0.749	0.069	72.2	6.6

Table 6.27: Percentage of cell vailability (HEK293T cells) after 24 hours of incubation with Cy7-9mer (3.28), Cy5.5-9mer (3.29), Cy7-1mer (3.30) and Cy5.5-1mer (3.31) at different concentrations (n = 5).

6.4.20. Synthesis of H-Ahx-9mer (**3.32**)

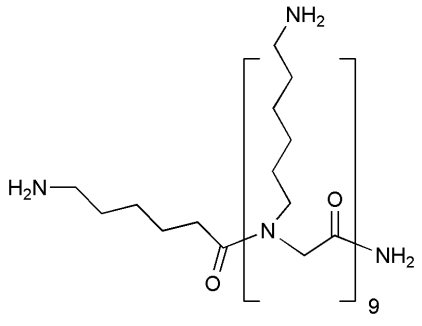

The H-Ahx-9mer peptoid **3.32** was obtained after Fmoc deprotection (**6.2.1.9**) and cleavage (**6.2.1.10**) from the previously prepared Fmoc-Ahx-9mer resin **2.35** (50 mg, 0.014 mmol). After precipitation in cold Et_2O and overnight drying, the **3.32** was isolated as a white solid in 95% final yield (20 mg).

Analysis:

m/z (ES^+): $C_{78}H_{158}N_{20}O_{10}$ calculated 1535.3, found 768.7 $[M+2H]^{2+}$ (32.6%), 512.8 $[M+3H]^{3+}$ (100%), 384.8 $[M+4H]^{4+}$ (62.4%),308.1 $[M+5H]^{5+}$ (18.7%).

m/z (MALDI-TOF): $C_{78}H_{158}N_{20}O_{10}$ calculated 1535.25; found 1536.37 $[M+H]^+$ (100%).

m/z (FT-MS): $C_{78}H_{158}N_{20}O_{10}$ calculated $[M+2H]^{2+}$ 768.63132, found 768.63587.

HPLC (Method 4): t_R = 1.0 min, purity >98% (ELSD).

^{1}H NMR (D_2O, 500 MHz, eSpresat water suppression): δ = 1.48-1.68 (m, 78H, 72H for $NH_2CH_2(CH_2)_4CH_2$-9mer, 6H for $CH_2(CH_2)_3CH_2$-Ahx), 2.09-2.18 (m, 2H, $COCH_2$-Ahx), 2.69 (m, 20H, 18H for NH_2CH_2-9mer, 2H for CH_2NH_2-Ahx), 3.18 (m, 18H, $CH_2CH_2NCH_2$), 3.82-4.47 (m, 18H for NCH_2CO-9mer).

^{13}C NMR (D_2O, 126 MHz): δ = 24.9, 25.0, 25.1, 25.3, 25.5, 25.6, 26.1, 26.2, 26.3, 26.5, 26.7, 26.8, 27.0, 27.1, 27.2, 27.3 ($NH_2CH_2(CH_2)_4CH_2$-9mer and $CH_2(CH_2)_3CH_2$-Ahx), 32.1 (CH_2CO-Ahx), 39.2, 39.3 (NH_2CH_2-9mer), 47.0,47.1, 47.2, 47.5, 48.0, 48.1 48.2, 48.3, 48.4, 48.5, 48.7, 49.1, 49.2, 49.3 ($CH_2CH_2NCH_2$-9mer, NCH_2CO), 162.5, 162.6, 162.7, 162.8, 163.0, 163.1, 163.3 (NCO-9mer), 170.4 (C=O-Ahx).

6.4.21. MTT assays of H-Ahx-9mer (**3.32**) in HeLa, B16F10 and HEK293T cells

MTT cytotoxicity assays were carried out as according to the general procedures (**6.2.2.4**). Cells were treated with 1, 5, 10, 20 or 50 µL of H-Ahx-9mer (**3.32**) 100 µM in order to obtain a final concentration of 1, 5, 10, 20 or 50 µM, respectively. After 24 hours of incubation at 37°C, the cells were prepared to be read on the microplate reader.

HeLa cells

	Concentration (μM)	Average (arb. units)	Error (arb. units)	Average (%)	Error (%)
Untreated cells		1.130	0.128	100.0	11.4
3.32	1	1.123	0.101	99.4	8.9
	5	1.218	0.095	107.8	8.4
	10	1.107	0.113	97.9	10.0
	20	1.139	0.100	100.8	8.8
	50	1.118	0.109	99.0	9.6

Table 6.28: Percentage of cell vailability (HeLa cells) after 24 hours of incubation with H-Ahx-9mer (3.32) at different concentrations (n = 5.)

B16F10 cells

	Concentration (μM)	Average (arb. units)	Error (arb. units)	Average (%)	Error (%)
Untreated cells		0.880	0.063	100.0	7.1
3.32	1	0.905	0.074	102.9	8.5
	5	0.883	0.055	100.4	6.3
	10	0.904	0.045	102.7	5.1
	20	0.871	0.045	99.0	5.1
	50	0.880	0.060	100.0	6.8

Table 6.29: Percentage of cell vailability (B16F10 cells) after 24 hours of incubation with H-Ahx-9mer (3.32) at different concentrations (n = 5).

HEK293T cells

	Concentration (μM)	Average (arb. units)	Error (arb. units)	Average (%)	Error (%)
Untreated cells		1.137	0.127	100.0	11.2
3.32	1	1.117	0.104	98.3	9.2
	5	1.143	0.117	100.5	10.3
	10	1.127	0.091	99.2	8.0
	20	1.143	0.121	100.5	10.6
	50	1.144	0.106	100.6	9.3

Table 6.30: Percentage of cell vailability (HEK293T cells) after 24 hours of incubation with H-Ahx-9mer (3.32) at different concentrations (n = 5).

6.4.22. *In vitro* MTT assays for *in vivo* studies (HeLa and HEK293T cells)

MTT cytotoxicity assays were carried out as according to the general procedures (**6.2.2.4**). Cells were treated with 5 µM of Cy7-9mer (**3.28**), Cy5.5-9mer (**3.29**), Cy7-1mer (**3.30**) or Cy5.5-1mer (**3.31**) 100 µM in order to obtain a final concentration of 5 µM. After 15 and 30 minutes of incubation at 37^{o}C, the cells were prepared to be read on the microplate reader.

HeLa cells

	Incubation time	Average (arb. units)	Error (arb. units)	Average (%)	Error (%)
Control cells		0.849	0.103	100.0	8.3
	30 min	0.874	0.063	102.9	7.4
3.28	15 min	0.859	0.075	101.1	8.8
	30 min	0.843	0.101	99.3	11.9
3.29	15 min	0.849	0.056	100.0	6.6
	30 min	0.867	0.054	102.1	6.3
3.30	15 min	0.839	0.069	98.8	8.1
	30 min	0.853	0.042	100.5	5.0
3.31	15 min	0.885	0.036	104.3	4.3
	30 min	0.850	0.067	100.2	7.9
3.32	15 min	0.818	0.071	96.4	8.3

Table 6.31: Percentage of cell vailability (HeLa cells) after 15 and 30 minutes of incubation with 5 µM of Cy7-9mer (3.28), Cy5.5-9mer (3.29), Cy7-1mer (3.30), Cy5.5-1mer (3.31) and H-Ahx-9mer (3.32) (n = 5).

HEK293T cells

	Incubation time	Average (arb. units)	Error (arb. units)	Average (%)	Error (%)
Untreated cells		1.130	0.128	100.0	8.0
	30 min	1.157	0.110	102.4	9.7
3.28	15 min	1.155	0.079	102.2	7.0
	30 min	1.139	0.066	100.8	5.8
3.29	15 min	1.143	0.100	101.1	8.9
	30 min	1.132	0.092	100.2	8.1
3.30	15 min	1.175	0.053	103.9	4.7
	30 min	1.163	0.067	102.9	5.9
3.31	15 min	1.127	0.075	99.7	6.6
	30 min	1.167	0.075	103.3	6.7
3.32	15 min	1.123	0.101	99.4	9.0

Table 6.32: Percentage of cell vailability (HEK293T cells) after 15 and 30 minutes of incubation with 5 µM of Cy7-9mer (3.28), Cy5.5-9mer (3.29), Cy7-1mer (3.30), Cy5.5-1mer (3.31) and H-Ahx-9mer (3.32) (n = 5).

6.4.23. *In vitro* cellular uptake of Cy7-9mer and Cy5.5-9mer for *in vivo* studies (HeLa and HEK293T cells)

Cells were seeded onto a 24-well plate at a density of 3×10^4 cells/well (volume of culture media per well: 350 µL). After 24 hours, 17.5 µL of Cy7-9mer (**3.28**) or Cy5.5-9mer (**3.29**) (100 µM) in PBS were injected in three random wells. Cellular uptake was analysed after 15 and 30 minutes of incubation by flow cytometry in 2% FBS in PBS with 0.2% of trypan blue (**6.2.2.3**).

HeLa cells

	Incubation time	Average (%)	Error (%)
Untreated cells		0.2	0.1
	15 min	80.5	3.2
3.28	30 min	95.0	3.4
	15 min	80.8	2.1
3.29	30 min	97.4	1.6

Table 6.33: Cellular uptake of Cy7-9mer (3.28, 5 µM) and Cy5.5-9mer (3.29, 5 µM) in HeLa cells (n = 6).

HEK293T cells

	Incubation time	Average (%)	Error (%)
Untreated cells		0.2	0.1
3.28	15 min	98.8	1.3
	30 min	99.8	0.2
3.29	15 min	99.8	0.1
	30 min	99.8	0.4

Table 6.34: Cellular uptake of Cy7-9mer (3.28, 5 µM) and Cy5.5-9mer (3.29, 5 µM) in HEK293T cells (n = 6).

6.4.24. Confocal microscopy of HeLa cells labelled with Cy5.5-9mer (**3.29**)

HeLa cells were prepared and stained as previously described in **6.2.2.5.** Cells were labelled with 200 µL of Cy5.5-9mer peptoid (**3.29,** 100 µM) for 24 hours. The Cy5.5 on the Cy5.5-9mer peptoids was excited using a 633 nm excitation filter and collecting emission using a 646-762 nm band-pass filter.

6.5. Experimental for Chapter 4

6.5.1. Experimental for peptide delivery

6.5.1.1. Preparation of the 2-chlorotrityl chloride resin (**4.5**)[203]

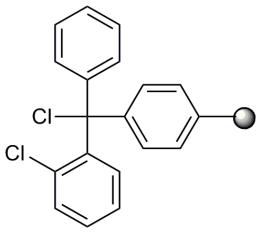

2-chlorotrityl chloride resin **4.5** containing 2-chlorotrityl alcohol resin **4.6** (600 mg, loading 1.49 mmol/g) was swollen in DCM (60 mL) for 20 minutes. The DCM was filtered off and the resin was washed 3 times with DMF (60 mL) and then with dry DCM (3 × 60 mL). The resin was treated with thionyl chloride (1 mL, 13.5 mmol) in dry DCM (60 mL). The mixture was stirred for 1 hour at room temperature before being filtered. The resin was washed twice with DMF (60 mL) and 3 times with DCM (60 mL). The resin **4.5** was dried under vacuum and stored at -18^{o}C under N_2.

6.5.1.2. Preparation of the preloaded 2-chlorotrityl-alanine resin (**4.9**)

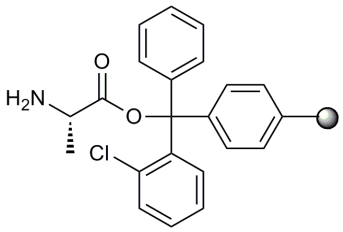

The activated resin **4.5** (250 mg, 0.38 mmol) was swollen in dry DCM (5 mL) for 30 minutes. Fmoc-Ala-OH **4.7** (140 mg, 0.45 mmol) was dissolved in dry DCM (2.5 mL) in the presence of DIPEA (0.315 mL, 1.80 mmol). The amino acid solution was added to the filtered resin **4.5** the mixture was stirred for 3 hours. The loaded resin was filtered and washed 3 times with a solution of DCM/MeOH/DIPEA (17: 2: 1, 5 mL), then with DCM (3 × 5 mL), DMF (3 × 5 mL) and DCM again (3 × 5 mL).The

Fmoc group was removed from the resin **4.8** using the protocol **6.2.1.9** (comfirmed by a ninhydrin test, **6.2.1.1**). The white resin **4.9** was then dried *in vacuo* at 40°C for 16 hours.

Analysis:

Quantitative ninhydrin test (6.2.1.2): loading 1.02 mmol/g.

IR (neat): 3387 (w, ν_{N-H}), 1738 (s, $\nu_{C=O}$), 1632 (m, $\nu_{C=C}$), 1144 (m, ν_{C-O}) cm^{-1}.

6.5.1.3. Synthesis of Fmoc-K(Boc)-E(OtBu)-I-Q(Trt)-L-V-I-K(Boc)-V-F-I-A-2-chlorotrityl resin (**4.10**)

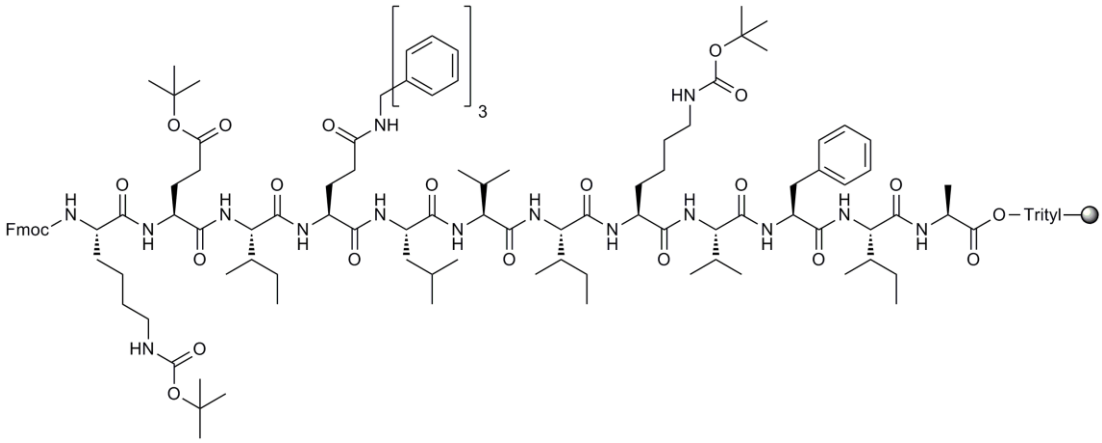

The supported protected Fmoc acid peptide (**4.10**) was synthesised on the preloaded 2-chlorotrityl-alanine resin **4.9** (70 mg, 0.07 mmol) using DIC/HOBT microwave assisted SPPS. The resin was first swollen in DCM (0.7 mL) for 20 minutes. Each Fmoc-AA-OH (0.21 mmol, **Table 6.35**) was dissolved in DMF (1.05 mL, 0.2 M) in presence of DIC/HOBt (0.21 mmol) and coupled to the resin **4.9** using the protocol **6.2.1.8** (μw, 20 minutes at 60°C). Each amino acid coupling was followed by Fmoc deprotection using 20% piperidine in DMF (**6.2.1.9**). Each step (coupling and Fmoc deprotection) was monitored by a qualitative ninhydrin test (**6.2.1.1**). The final Fmoc group was deprotected. The resin was washed with DMF (3 x 0.7 mL), DCM (3 x 0.7 mL), MeOH (2 x 0.7 mL) and DCM (2 x 0.7 mL) before being dried *in vacuo* at 40°C for 16 hours.

Reagent	Mw (g/mol)	Mass (mg)
HOBt (monohydrate)	153.1	32
DIC	126.2 (d = 0.81)	26.5 (32.7 µL)
Fmoc-Ala-OH	311.3	65
Fmoc-Ile-OH	353.4	74
Fmoc-Phe-OH	387.4	82
Fmoc-Val-OH	339.4	71
Fmoc-Lys(Boc)-OH	468.5	89
Fmoc-Leu-OH	353.4	74
Fmoc-Gln(Trt)-OH	610.7	128
Fmoc-Glu(OtBu)-OH	425.5	90

Table 6.35: Quantity of reagent used per coupling for SPPS of resin 4.10 and 4.11.

Analysis:

Theoretical loading (6.2.1.5): loading 0.38 mmol/g.

Characterisation: a small sample of resin **4.10** was cleaved using a TFA/TIS/DCM (90: 5: 5) solution (500 µL) for 2 hours at room temperature.

m/z (ES+): $C_{68}H_{117}N_{15}O_{16}$ mass expected 1621.9, mass found 812.2 $[M+2H]^{2+}$ (100%), 541.7 $[M+3H]^{3+}$ (14.9%).

m/z (MALDI-TOF): $C_{83}H_{127}N_{15}O_{18}$ calculated 1621.94 (correspond to Fmoc-KEIQLVIKVFIA-OH), found 1621.86 $[M+H]^{+}$ (100%), 1644.87 $[M+Na]^{+}$ (47.1%).

HPLC (Method 2): t_R = 6.2 min, purity = 84% (ELSD).

6.5.1.4. Synthesis of Fmoc-K(Boc)-E(OtBu)-I-Q(Trt)-L-V-I-K(Boc)-V-A-A-A-2-chlorotrityl resin (**4.11)**

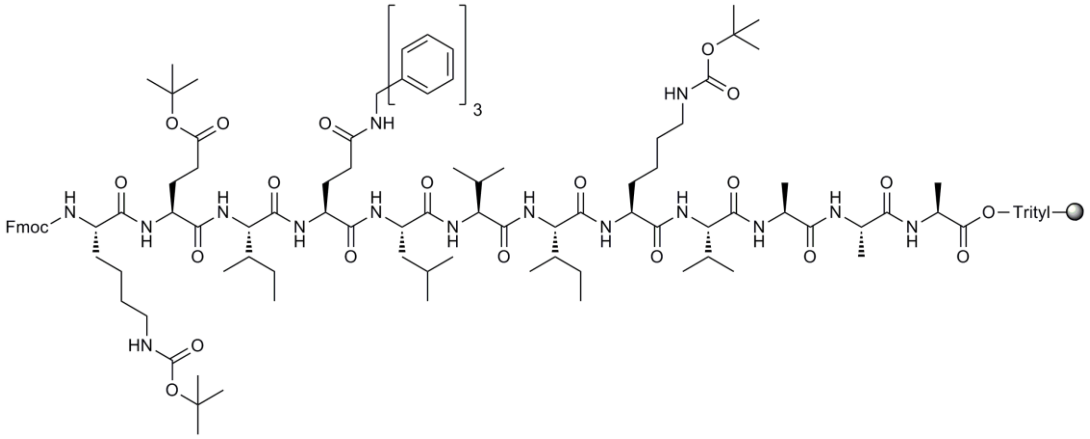

The supported protected Fmoc acid peptide (**4.10**) was synthesised on the preloaded 2-chlorotrityl-alanine resin **4.9** (70 mg, 0.07 mmol) using DIC/HOBt microwave assisted SPPS as previously decribed for the resin **4.11** (**6.5.1.3**).

Analysis:

Theoretical loading (6.2.1.5): loading 0.41 mmol/g.

Characterisation: a small sample of resin **4.11** was cleaved (before final Fmoc-deprotection) using a TFA/TIS/DCM (90: 5: 5) solution (500 µL) for 2 hours at room temperature.

m/z (ES+): $C_{74}H_{117}N_{15}O_{18}$ mass expected 1503.9, mass found 753.0 $[M+2H]^{2+}$ (100%), 502.4 $[M+3H]^{3+}$ (9.4%).

m/z (MALDI-TOF): $C_{74}H_{117}N_{15}O_{18}$ calculated 1503.87 (correspond to Fmoc-KEIQLVIKVAAA-OH), found 1504.92 $[M+H]^{+}$ (100%), 1527.00 $[M+Na]^{+}$ (51.6%).

HPLC (Method 2): t_R = 6.0 min, purity = 78% (ELSD).

6.5.1.5. Synthesis of Fmoc-K(Boc)-E(OtBu)-I-Q(Trt)-L-V-I-K(Boc)-V-F-I-A-Rink amide resin (**4.12**)

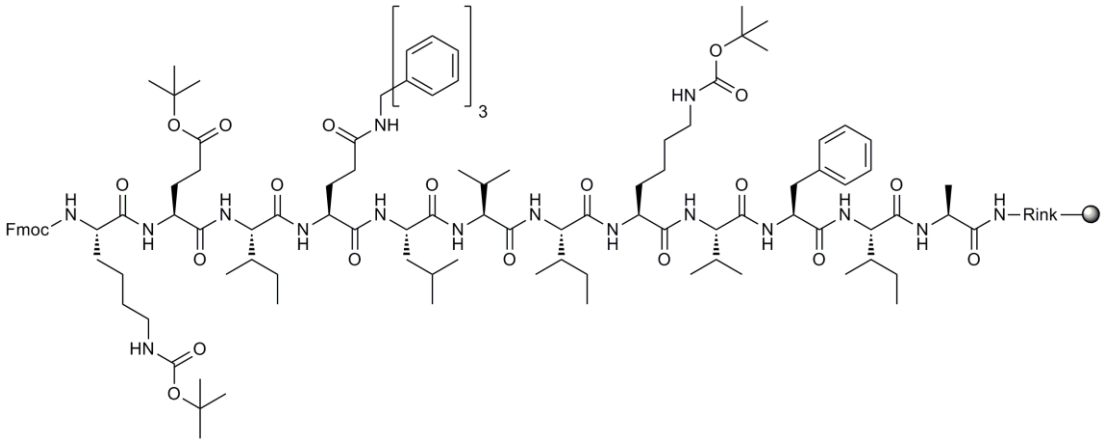

The supported protected amide peptide (**4.12**) was synthesised on aminomethyl polystyrene resin functionalized with a Rink amide linker (**2.28**) (200 mg, 0.16 mmol) using DIC/HOBT microwave assisted SPPS as above (**6.5.1.3**).

Reagent	Mw (g/mol)	Mass (mg)
HOBt	135.5	65
DIC	126.2 (d = 0.81)	60.6 (74.7 µL)
Fmoc-Ala-OH	311.3	149
Fmoc-Ile-OH	353.4	170
Fmoc-Phe-OH	387.4	186
Fmoc-Val-OH	339.4	163
Fmoc-Lys(Boc)-OH	468.5	204
Fmoc-Leu-OH	353.4	170
Fmoc-Gln(Trt)-OH	610.7	293
Fmoc-Glu(OtBu)-OH	425.5	204

Table 6.36: Quantity of reagent used per coupling for SPPS of resin 4.12 and 4.13.

Analysis:

Theoretical loading (6.2.1.5): loading 0.38 mmol/g.

Characterisation: a small sample of resin **4.12** was cleaved using a TFA/TIS/DCM (95: 2.5: 2.5) solution (500 µL) for 4 hours at room temperature.

m/z (ES^+): $C_{83}H_{128}N_{16}O_{17}$ calculated 1621.0, found 811.5 $[M+2H]^{2+}$ (100%), 541.3 $[M+3H]^{3+}$ (19.5%).

m/z (MALDI-TOF): $C_{83}H_{128}N_{16}O_{17}$ calculated 1621.04 (correspond to Fmoc-KEIQLVIKVFIA-NH_2), found 1622.41 $[M+H]^+$ (100%).

HPLC (Method 2): t_R = 6.3 min, purity = 86% (ESLD).

6.5.1.6. Synthesis of H-K(Boc)-E(OtBu)-I-Q(Trt)-L-V-I-K(Boc)-V-A-A-A-Rink amide resin (**4.13**)

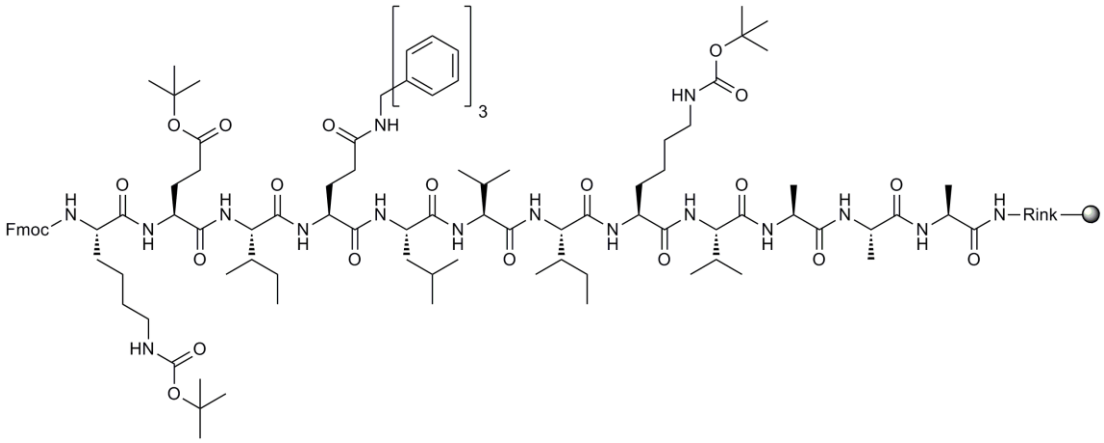

The supported protected amide peptide (**4.13**) was synthesised on aminomethyl polystyrene resin functionalized with a Rink amide linker (**2.28**) (200 mg, 0.16 mmol) as above **6.5.1.3** (**Table 6.36** for quantities).

Analysis:

Theoretical loading (6.2.1.5): loading 0.38 mmol/g.

Characterisation: a small sample of resin **4.13** was cleaved using a TFA/TIS/DCM (95: 2.5: 2.5) solution (500 µL) for 4 hours at room temperature.

m/z (ES+): $C_{74}H_{118}N_{16}O_{17}$ calculated 1502.8, found 752.4 $[M+2H]^{2+}$ (100%), 501.9 $[M+3H]^{3+}$ (27.4%).

m/z (MALDI-TOF): $C_{74}H_{118}N_{16}O_{17}$ calculated 1502.82 (correspond to Fmoc-KEIQLVIKVFIA-OH), found 1526.11 $[M+Na]^+$ (100%).

HPLC (Method 2): t_R = 6.1 min, purity = 83% (ELSD).

6.5.1.7. Synthesis of 2-acetyldimedone (DdeOH, **4.20**)[326]

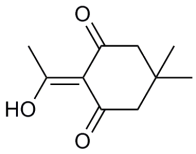

Dimedone (20 g, 143 mmol) was dissolved in DMF (350 mL) with acetic acid (8.17 mL, 143 mmol), dicyclohexylcarbodiimide (DCC) (29.5 g, 143 mmol) and 4-di(methylamino)pyridine (DMAP) (1.8 g, 14.3 mmol). The solution was stirred for 36 hours at room temperature. The reaction was followed by TLC. Precipitating dicyclohexylurea (DCU) was filtered. The solvent was evaporated and the residue was dissolved in ethyl acetate. DCU was filtered again and the organic layer was washed with a solution of 1N KHSO4 (3 × 150 mL), dried with MgSO4 and filtered. The solvent was evaporated and crude product was purified by column chromatography, using DCM/EtOAc (97: 3) as eluting phase, to yield compound **4.20** as a yellow solid (22.1 g, 85%).

Analysis:

m/z (ES+): $C_{10}H_{14}O_3$ calculated 182.1, found 183.1 $[M+H]^+$ (100%), 205.0 $[M+Na]^+$ (36.4%).

Rf: 0.68 (EtOAc/DCM, 5: 95).

HPLC (Method 1): t_R = 3.4 min, purity = 98% (ELSD).

^{1}H NMR ($CDCl_3$, 250 MHz): δ = 1.01 (s, 6H, C(C*H*$_3$)$_2$), 2.29 (s, 2H, C*H*$_2$), 2.46 (s, 2H, C*H*$_2$), 2.54 (s, 3H, C*H*$_3$).

^{13}C NMR ($CDCl_3$, 63 MHz): δ = 28.2 (C(*C*H$_3$)$_2$), 28.5 (C*C*H$_3$), 30.6 (*C*(CH$_3$)$_2$), 46.5 (*C*H$_2$), 52.4 (*C*H$_2$), 112.3 (*C*), 195.1 (*C*=O), 197.8 (*C*=O), 202.4 (*C*).

6.5.1.8. Synthesis of Fmoc-Lys(Dde)-OH (**4.14**)[327]

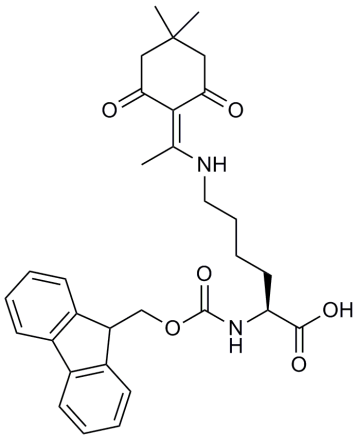

Fmoc-Lys-OH (1.6 g, 4.2 mmol) and DdeOH **4.20** (2.3 g, 12.5 mmol) were suspended in ethanol (35 mL) then TFA (32 µL, 0.4 mmol) was added dropwise. The mixture was refluxed for 72 hours. Once all the Fmoc-Lys-OH was consumed (monitored by TLC), the solvent was removed under vacuum and the resulting orange sticky residue was dissolved in EtOAc (30 mL). The organic phase was washed with 1 M $KHSO_4$ (3 x 80 mL) before being dried over $MgSO_4$ and concentrated *in vacuo*. The crude was purified by column chromatography (silica, eluting with DCM/MeOH, 8:1) to afford Fmoc-Lys(Dde)-OH **4.14** as a brown yellow solid (1.63 g, 74%).

Analysis:

m/z (ES^+): $C_{31}H_{36}N_2O_6$ calculated 532.3, found 533.3 $[M+H]^+$ (100%).

Rf: 0.21 (DCM/MeOH, 2:1).

HPLC (Method 1): t_R = 3.6 min, purity = 100% (254 nm).

^{1}H NMR ($CDCl_3$, 500 MHz): δ = 1.05 (s, 6H, C(C*H*$_3$)$_2$-Dde), 1.46-1.60 (m, 2H, C*H*$_2$-Lys), 1.73-2.01 (m, 4H, C*H*$_2$-Lys), 2.32 (m, 3H, C*H*$_3$-Dde), 2.50 (s, 4H, C*H*$_2$-Dde), 3.33 (m, 2H, C*H*$_2$-NH-Lys), 4.17 (d, *J* = 7.06 Hz, 2H, C*H*$_2$-Fmoc), 4.33 (t, *J* = 7.01 Hz, 1H, C*H*-Fmoc), 4.44 (m, 1H, C*H*), 5.84 (br sg, 1H, N*H*), 7.27 (t, *J* = 7.48 Hz, 2H, ArC*H*-Fmoc), 7.36 (t, *J* = 7.38 Hz, 2H, ArC*H*-Fmoc), 7.57 (t, *J* = 8.11 Hz, 2H, ArC*H*-Fmoc), 7.73 (d, *J* = 7.50 Hz, 2H, ArC*H*-Fmoc), 13.26 (br sg, 1H, COO*H*).

^{13}C NMR ($CDCl_3$, 126 MHz): δ = 18.0 (*C*H_3-Dde), 22.5 (*C*H_2 -Lys), 28.1 (C(*C*H_3)$_2$-Dde), 30.0 (C(*C*H_3)$_2$-Dde), 31.8 (*C*H_2-Lys), 36.6 (*C*H_2-Lys), 43.2 (*C*H_2NH), 50.6 (*C*H-Fmoc), 52.4 (2 x *C*H_2-Dde), 54.0 (*C*H-Lys), 67.0 (*C*H_2-Fmoc), 107.8 (*C*=CNH), 119.9, 125.1, 127.0, 127.7 (Ar*C*H-Fmoc), 141.2, 143.7 (Ar*C*-Fmoc), 156.4 (*C*OO-Fmoc), 173.9 (C=*C*NH-Dde), 175.8 (*C*OOH), 198.1 (*C*=O-Dde).

6.5.1.9. Synthesis of H-9mer-Ahx-Lys(FAM)-Ahx- KEIQLVIKVFIA-OH **4.16**

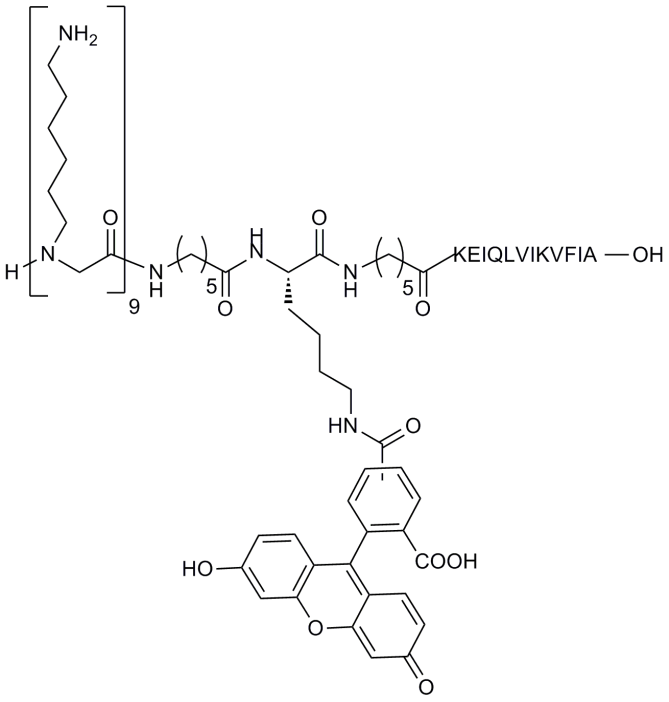

The acid peptide-peptoid hybrid (**4.16**) was synthesised from the resin **4.10** (50 mg, 0.019 mmol) using DIC/HOBT microwave assisted SPPS (unless stated otherwise, **6.2.1.8,** for quantities see **Table 6.37**). Once every spacer and monomer unit were coupled, the Dde group was selectively deprotected using a mixture of hydroxylamine and imidazole in NMP/DCM (**6.2.1.12**). The deprotection was monitored by qualitative ninhydrin test (**6.2.1.1**). 5(6)-Carboxyfluorescein **4.15** (34 mg, 0.095 mmol) was coupled with the side chain of the Lys over 4 hours using a HOBt/DIC (13 mg/15.1 µL, 0.095 mmol) activation in DMF (0.48 mL, 0.2 M) (**6.2.1.7**). The coupling was confirmed by a negative qualitative ninhydrin test

(**6.2.1.1**). The resin was then washed with DCM, DMF and MeOH (3 × 0.5 mL). In order to remove the excess of fluorescein and to deprotect the final Fmoc group, the resin was mixed with 20% piperidine in DMF (0.5 mL) for 1 hour.[328] Afterwards, the resin was washed with DMF (3 × 0.5 mL) and the basic treatement (20% piperidine, 0.5 mL) in DMF was repeated for 10 minutes. As the washing solution was still fluorescent, the resin was left to stir under these basic conditions for another hour. The resin was then washed with DMF, DCM, MeOH and Et_2O (3 × 0.5 mL). The Fluorescein peptide-peptoid was deprotected and cleaved from the resin using TFA/TIS/DCM (90: 5: 5) solution (1.25 mL) for 2 hours at room temperature (**6.2.1.10**). The peptide-peptoid **4.16** was isolated after drying (*in vacuo* at 40°C for 16 hours) and purification (preparative reverse phase-HPLC, Gradient 3) as a yellow solid (39 mg, 58 % based on **4.10**).

Reagent	Mw (g/mol)	Mass (mg)
HOBt	135.5	8
DIC	126.2 (d = 0.81)	8.9 µL
Fmoc-Ahx-OH (**2.34**)	353.4	20
Fmoc-Lys(Dde)-OH (**4.14**)	532.3	30
Peptoid monomer (**2.22**)	496.3	28

Table 6.37: Quantity of reagent used per coupling for the synthesis of acid peptide-peptoid 4.16.

Analysis:

m/z (ES^+): $C_{179}H_{305}N_{37}O_{34}$ calculated 3519.3, found 880.5 $[M+4H]^{4+}$ (10.2%), 704.8 $[M+5H]^{5+}$ (34.9%), 587.5 $[M+6H]^{6+}$ (100%), 503.7 $[M+7H]^{7+}$ (62.2%), 441.1 $[M+8H]^{8+}$ (9.2%).

m/z (MALDI-TOF): $C_{179}H_{305}N_{37}O_{34}$ calculated 3519.33, found 3520.18 $[M+H]^+$ (100%).

m/z (FT-MS): $C_{179}H_{305}N_{37}O_{34}$ calculated $[M+4H]^{4+}$ = 880.89112, found 880.86172.

HPLC (Method 3): t_R = 3.0 min; purity ≥ 99% (ELSD and 475 nm).

UV (Tris buffer pH 7.8): λ_{abs} = 498 nm.

6.5.1.10. Synthesis of H-9mer-Ahx-Lys(FAM)-Ahx-KEIQLVIKVAAA-OH **4.17**

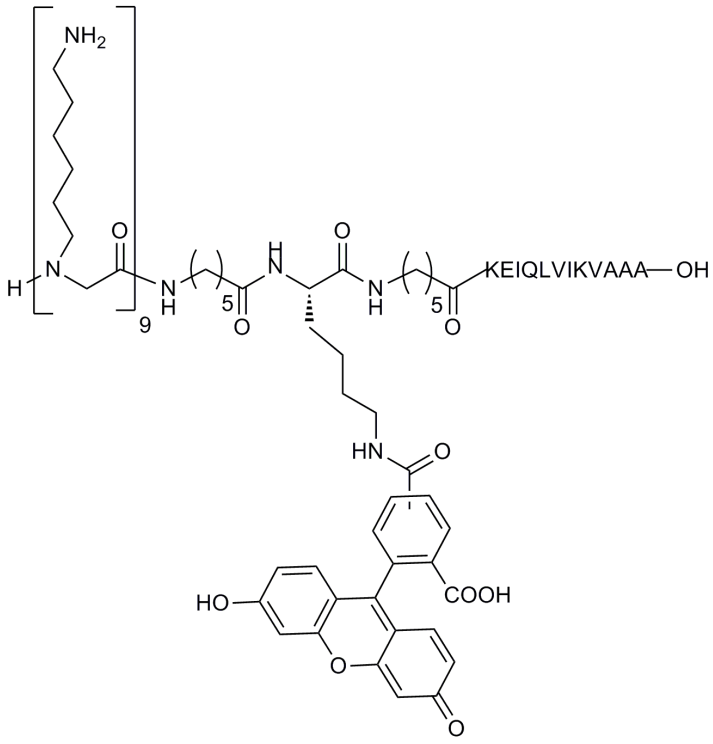

The acid peptide-peptoid hybrid (**4.17**) was synthesised on the resin **4.11** (50 mg, 0.021 mmol) using the same protocol as for **4.16**. The peptide-peptoid **4.17** was isolated as a yellow solid (47 mg, 69% based on **4.11**) after preparative reverse-phase purification (Gradient 3).

Reagent	Mw (g/mol)	n (mmol)	Quantity (mg)
HOBt	135.5	0.062	8
DIC	126.2 (d = 0.81)	0.062	9.7 µL
DMF	73.1 (d = 0.95)	Conc 0.15 M	0.42 mL
Fmoc-Ahx-OH (**2.34**)	353.4	0.062	22
Fmoc-Lys(Dde)-OH (**4.14**)	532.3	0.062	33
Peptoid monomer (**2.22**)	496.3	0.062	31
5(6)-Carboxyfluorescein (**4.15**)	356.3	0.103	36

HOBt (FAM coupling)	135.5	0.103	14
DIC (FAM coupling)	126.2 (d = 0.81)	0.103	16.1 µL
DMF (FAM coupling)	73.1 (d = 0.95)	Conc 0.2 M	0.52 mL

Table 6.38: Quantities of reagent used per coupling for the synthesis of acid peptide-peptoid 4.17.

Analysis:

m/z (ES^+): $C_{170}H_{295}N_{37}O_{34}$ calculated 3401.4, found 851.2 $[M+4H]^{4+}$ (34.9%), 681.1 $[M+5H]^{5+}$ (100%), 567.8 $[M+6H]^{6+}$ (82.3%), 486.6 $[M+7H]^{7+}$ (25.4%).

m/z (MALDI-TOF): $C_{170}H_{295}N_{37}O_{34}$ calculated 3401.39, found 3402.04 $[M+H]^+$ (100%).

m/z (FT-MS): $C_{107}H_{187}N_{22}O_{14}^+$ calculated $[M+3H]^{3+}$ = 1134.79629, found 1134.79673.

HPLC (Method 3): t_R = 2.7 min, purity = 98% (ELSD).

UV (Tris buffer pH 7.8): λ_{abs} = 498 nm.

6.5.1.11. Synthesis of H-9mer-Ahx-Lys(FAM)-Ahx-KEIQLVIKVFIA-NH_2 **4.18**

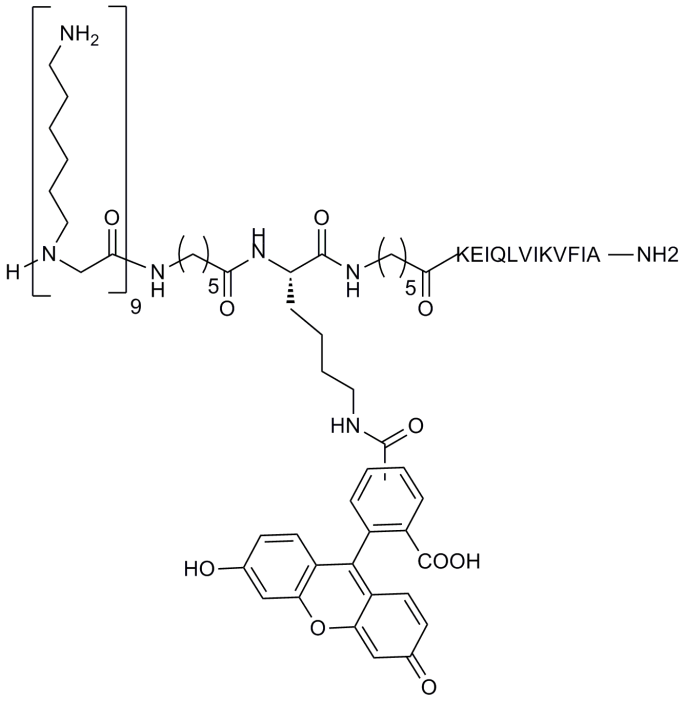

The amide peptide-peptoid hybrid (**4.18**) was synthesised on the resin **4.12** (70 mg, 0.025 mmol) using the same protocol as for **4.16**. The peptide-peptoid **4.18** was isolated as a yellow solid (66 mg, 79% based on **4.12**) after preparative reverse-phase purification (Gradient 3).

Reagent	Mw (g/mol)	n (mmol)	Quantity
HOBt	135.5	0.075	10
DIC	126.2 (d = 0.81)	0.075	11.7 µL
DMF	73.1 (d = 0.95)	Conc 0.15 M	0.50 mL
Fmoc-Ahx-OH (**2.34**)	353.4	0.075	27
Fmoc-Lys(Dde)-OH (**4.14**)	532.3	0.075	40
Peptoid monomer (**2.22**)	496.3	0.075	37
5(6)-Carboxyfluorescein (**4.15**)	356.3	0.125	45
HOBt (FAM coupling)	135.5	0.125	17
DIC (FAM coupling)	126.2 (d = 0.81)	0.125	19.5 µL
DMF (FAM coupling)	73.1 (d = 0.95)	Conc 0.2 M	0.63 mL

Table 6.39: Quantity of reagent used per coupling for the synthesis of acid peptide-peptoid 4.18.

Analysis:

m/z (ES^+): $C_{179}H_{306}N_{38}O_{33}$ calculated 3518.6, found 880.5 $[M+4H]^{4+}$ (58.2%), 704.6 $[M+5H]^{5+}$ (100%), 587.3 $[M+6H]^{6+}$ (60.8%), 503.7 $[M+7H]^{7+}$ (27.0%).

m/z (MALDI-TOF): $C_{179}H_{306}N_{38}O_{33}$ calculated 3518.56, found 3519.88 $[M+H]^+$ (100%).

m/z (FT-MS): $C_{179}H_{306}N_{38}O_{33}$ calculated $[M+3H]^{3+}$ = 1179.85991, found 1173.86023.

HPLC (Method 3): t_R = 3.1 min, purity = 100% (ELSD and 475 nm).

UV (Tris buffer pH 7.8): λ_{abs} = 499 nm.

6.5.1.12. Synthesis of H-9mer-Ahx-Lys(FAM)-Ahx-KEIQLVIKVAAA-NH_2 **4.19**

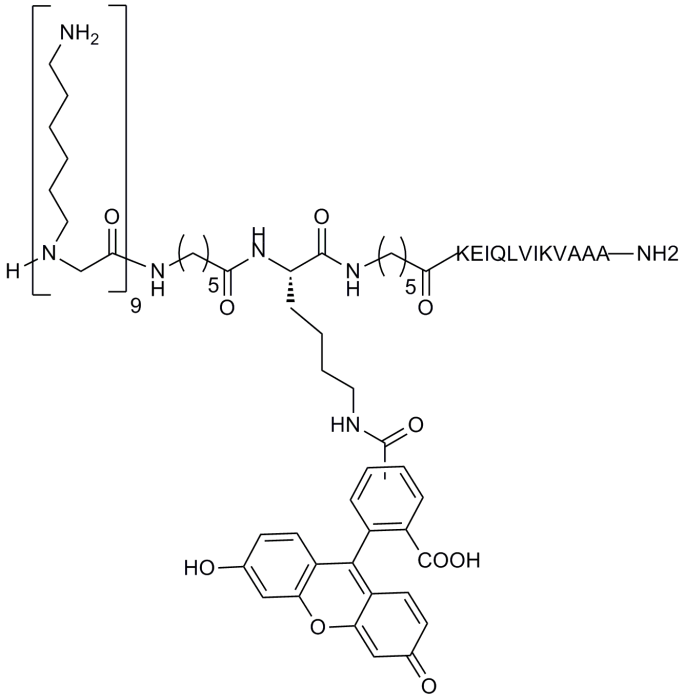

The amide peptide-peptoid hybrid (**4.19**) was synthesised on the resin **4.13** (50 mg, 0.0185 mmol) using the same protocol as for **4.16**. The peptide-peptoid **4.19** was isolated as a yellow solid (47 mg, 75% based on **4.13**) after preparative reverse-phase purification (Gradient 3).

Reagent	Mw (g/mol)	n (mmol)	Quantity
HOBt	135.5	0.056	8
DIC	126.2 (d = 0.81)	0.056	8.7 µL
DMF	73.1 (d = 0.95)	Conc 0.15 M	0.38 mL
Fmoc-Ahx-OH (**2.34**)	353.4	0.056	20
Fmoc-Lys(Dde)-OH (**4.14**)	532.3	0.056	30
Peptoid monomer (**2.22**)	496.3	0.056	28
5(6)-Carboxyfluorescein (**4.15**)	356.3	0.093	33

HOBt (FAM coupling)	135.5	0.093	13
DIC (FAM coupling)	126.2 (d = 0.81)	0.093	14.5 µL
DMF (FAM coupling)	73.1 (d = 0.95)	Conc 0.2 M	0.47 mL

Table 6.40: Quantity of reagent used per coupling for the synthesis of acid peptide-peptoid 4.19.

Analysis:

m/z (ES^+): $C_{170}H_{296}N_{38}O_{33}$ calculated 3400.4, found 851 $[M+4H]^{4+}$ (13.2%), 680.9 $[M+5H]^{5+}$ (42.5%), 567.6 $[M+6H]^{6+}$ (100%), 486.6 $[M+7H]^{7+}$ (54.6%).

m/z (MALDI-TOF): $C_{170}H_{296}N_{38}O_{33}$ calculated 3400.40, found 3401.36 $[M+H]^+$ (100%).

m/z (FT-MS): $C_{170}H_{296}N_{38}O_{33}$ calculated $[M+2H]^{2+}$ = 669.15306, found 669.16793

HPLC (Method 3): t_R = 2.8 min, purity = 100% (ELSD and 475 nm).

UV (Tris buffer pH 7.8): λ_{abs} = 498 nm.

6.5.1.13. Synthesis of Fluo-Ahx- KEIQLVIKVFIA-OH (**4.21**)

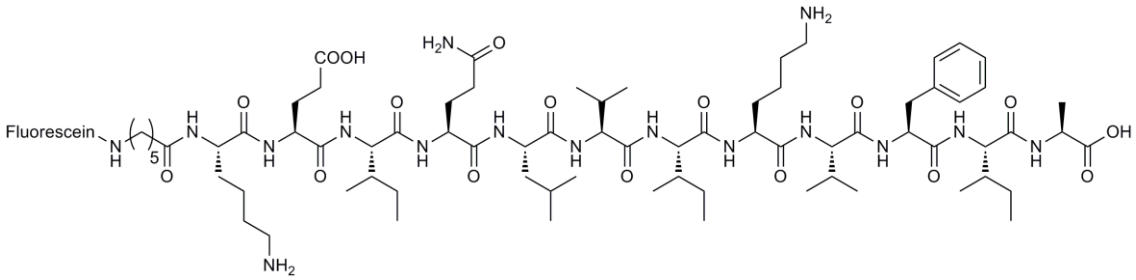

The peptide **4.21** was synthesised from resin **4.10** (50 mg, 0.019 mmol). The Fmoc-Ahx-OH **2.34** (20 mg, 0.057 mmol) and 5(6)-carboxyfluorescein **4.15** (41 mg, 0.15 mmol) were coupled to **4.10** using the protocol **6.2.1.7**. Excess of fluorescein and Fmoc group were removed by basic treatment (as described in **6.5.1.9**). The Fluorescein peptide was deprotected and cleaved from the resin using TFA/TIS/DCM (90: 5: 5) solution (1.25 mL) for 2 hours (**6.2.1.10**). The peptide **4.21** was isolated after precipitation, drying and purification (preparative reverse phase-HPLC, Gradient 3) as a yellow solid (24 mg, 66% based on **4.10**)

Analysis:

m/z (ES^+): $C_{95}H_{138}N_{16}O_{23}$ calculated 1871.0, mass 936.6 $[M+2H]^{2+}$ (100%), 624.6 $[M+3H]^{3+}$ (18.7%).

m/z (MALDI-TOF): $C_{95}H_{138}N_{16}O_{23}$ calculated 1871.01, found 1872.28 $[M+H]^+$ (100%).

m/z (FT-MS): $C_{95}H_{138}N_{16}O_{23}$ calculated $[M+2H]^{2+}$ = 936.50603, found 936.50658.

HPLC (Method 2): t_R = 5.6 min, purity = 99% (ELSD).

UV (MeOH): λ_{abs} = 500 nm.

6.5.1.14. Synthesis of Fluorescein-Ahx-9mer (Fluo-9mer, **4.22**)[104]

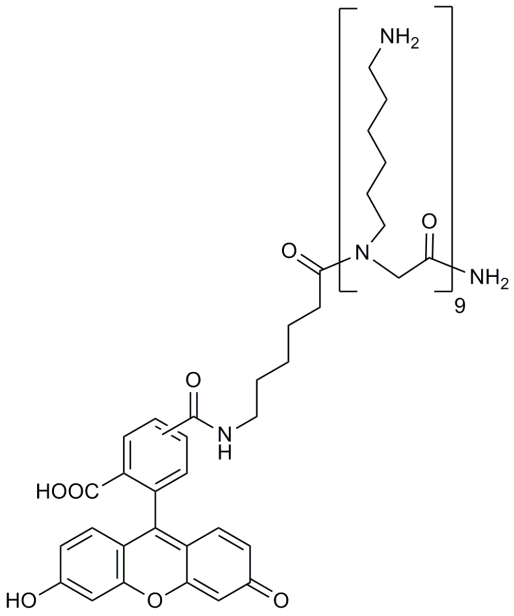

The Fluorescein-Ahx-9mer peptoid (**4.22**) was synthesised on the resin Fmoc-Ahx-9mer **2.35** (50 mg, 0.014 mmol). 5(6)-Carboxyfluorescein **4.15** (25 mg, 0.07 mmol) was then coupled to the Fmoc deprotected resin over 4 hours using a HOBt/DIC (10 mg/10.9 µL, 0.07 mmol) activation in DMF (0.35 mL, 0.2 M) (**6.2.1.7**). The resin was mixed with 20% piperidine in DMF (0.5 mL) to remove the Fmoc group and excess of fluorescein.[328] The resin was then washed with DMF, DCM, MeOH and Et_2O (3 × 0.75 mL). The Fluorescein peptoid **4.23** was deprotected and cleaved from the resin using the protocol **6.2.1.10** to yield a yellow solid (25 mg, 96% based on **2.35**) after drying (*in vacuo* at 40°C for 16 hours).

Analysis:

m/z (ES^+): $C_{99}H_{168}N_{20}O_{16}$ calculated 1894.5, mass found 948.2 $[M+2H]^{2+}$ (21.5%), 632.5 $[M+3H]^{3+}$ (100%), 474.7 $[M+4H]^{4+}$ (74.3%), 380.0 $[M+5H]^{5+}$ (24.8%).

m/z (MALDI-TOF): $C_{99}H_{168}N_{20}O_{16}$ calculated 1894.52, found $[M+H]^+$ 1895.35 (100%).

HPLC (Method 3): t_R = 2.6 min, purity > 98% (ELSD).

UV (Tris buffer pH 7.8): λ_{abs} = 498 nm.

6.5.1.15. Cellular delivery of **4.16**, **4.17, 4.18**, **4.19, 4.21** and **4.22** into HeLa cells

Cells were seeded onto a 24-well plate at a density of 3×10^4 cells/well (volume of culture media per well: 350 µL). After 24 hours, 35 µL of **4.16**, **4.17, 4.18**, **4.19, 4.22** (100 µM in PBS) and **4.21** (100 µM in PBS with 8% of DMSO) were injected in three random wells (final concentration 10 µM). Cellular uptake was analysed after 2 and 24 hours of incubation by flow cytometry in 2% FBS in PBS with 0.2% of trypan blue (**6.2.2.3**).

	Incubation time	Average (%)	Error (%)
Untreated cells		0.7	0.1
4.22	2 h	79.1	2.4
	24 h	98.5	0.7
4.16	2 h	71.1	0.9
	24 h	92.0	0.9
4.17	2 h	84.3	6.1
	24 h	90.0	1.8
4.18	2 h	68.8	0.7
	24 h	86.2	3.9
4.19	2 h	67.7	2.9
	24 h	86.8	2.0
4.21	2 h	8.3	0.6
	24 h	17.9	6.1

Table 6.41: Cellular uptake of Fluo-9mer (4.22, 10 µM), peptide-peptoids (4.16, 4.17, 4.18 and 4.19, 10 µM) and peptide (4.21, 10 µM) in HeLa cells (n = 3).

6.5.1.16. Microscopy of **4.16**, **4.17** into HeLa cells

Cells were seeded onto a 24-well plate at a density of 3×10^4 cells/well (volume of culture media per well: 800 µL). After 24 hours, 35 µL of **4.16**, **4.17** (100 µM in PBS) were injected in three random wells (final concentration 10 µM). After 4 hours of incubation with the peptoids, cells were washed with PBS and microscopy was performed in 2% FBS in PBS without further staining.

6.5.1.17. MTT assays of **4.16**, **4.17, 4.18**, **4.19** and **4.22** in HeLa cells

MTT cytotoxicity assays were carried out as according to the general procedures (**6.2.2.4**). In order to obtain a final concentration of 5, 10 and 20 µM, cells were treated respectively with 5, 10 and 20 µL of the compound **4.16**, **4.17, 4.18**, **4.19** and **4.22** at a starting concentration of 100 µM (in PBS). After 24 hours of incubation at 37°C, the wells were read on a microplate reader.

	Concentration (µM)	Average (arb. units)	Error (arb. units)	Average (%)	Error (%)
Untreated cells		0.167	0.016	100.0	9.7
4.16	5	0.189	0.016	112.0	9.8
	10	0.161	0.010	95.7	6.2
	20	0.152	0.016	90.2	9.5
4.17	5	0.181	0.020	107.6	11.7
	10	0.188	0.021	111.3	12.2
	20	0.188	0.011	111.3	6.4
4.18	5	0.183	0.010	108.3	5.8
	10	0.166	0.008	98.5	4.6
	20	0.122	0.006	72.6	3.7
4.19	5	0.191	0.016	113.2	9.5
	10	0.188	0.013	111.3	7.9
	20	0.187	0.010	110.8	6.1
4.22	5	0.190	0.012	112.8	7.1
	10	0.195	0.015	115.4	8.9
	20	0.185	0.010	109.6	6.2

Table 6.42: Percentage of cell vailability (HeLa cells) after 24 hours of incubation with peptides-peptoid (4.16, 4.17, 4.18 and 4.19) and Fluo-9mer (4.22) at different concentrations. (n = 6)

6.5.2. Experiment for GFP protein delivery

6.5.2.1. Cys-GFP protein (**4.29**) expression

The His6-Cys-GFP plasmid (pET 19b-His6-GFP) was prepared and donated by Dr David Nagel. (**Appendix 4-1**) Cys-GFP protein was modified on its N-terminal with a spacer composed by six successions of Ser-Gly and the Cys as final amino acid. In order to purify the protein, a His-tag (and a cleavage site) was introduced in the protein sequences. (**Appendix 4-2**)

6.5.2.1.1. Sodium Dodecyl Sulfate - Polyacrylamide gel electrophoresis (SDS-PAGE)

Gel:
Precast polyacrylamide NuPAGE® Bis-Tris gels from Invitrogen were used.

Running buffer, 1X MOPS (3-(N-morpholino)propanesulfonic acid) buffer:
For 1 L, 200 mL of 5X MOPS buffer were mixed with 800 mL of deionised water.

5X MOPS buffer:
250 mM MOPS (52.33 g)
250 mM Tris-HCl (30.28 g)
5 mM EDTA (1.86 g)
0.5% SDS (50 mL of 10%)
Dissolved in distilled water and adjusted to a final volume of 1 L.

Coomassie staining solution:
450 mL water
450 mL Methanol
100 mL of GAA (Glacial acetic acid)
2.5 g/L of brillant blue

Destaining solution:

1 hour: 10% GAA and 45% MeOH in water

Overnight: 10% GAA and 10% MeOH in water

Marker:

Marker See Blue® Plus2 Prestained Standard (1X) by Invitrogen.

Protocol:

The desired volume of each sample (0.5 mg/mL of protein) was mixed with a required amount of 2X SDS. The mixture was then boiled for 5 minutes and then centrifuged at maximum speed for 2 minutes. The blue solution was then loaded into the gel.

The gel was run at 200V for 70 minutes in 1X MOPS buffer. Afterwards, the gel was transferred into the staining solution for 1 hour and decoloured using the destaining solution.

6.5.2.1.2. Transformation step and amplification

For the transformation step, competent cells (BL21(RPS)DE3 E.coli strains) from Stratagene were used :

- **Specie:** E. coli,
- **Cell line:** BL21(RPS)DE3 (Stratagene),
- **Genotype:** *E. coli* B F^- *dcm ompT hsdS*(r_B^- m_B^-) gal λ(DE3)
- **Application:** Transformation, expression host.

LB (Luria Bertani) Broth media:

10 g/L Tryptone

5 g/L Yeast extract

10 g/L NaCl

Dissolved in 1 L distilled water, adjusted to pH 7.5 and autoclaved during 20 minutes at 120°C.

Protocol:

The His-tag thiol-GFP plasmid was transformed using heat shock and BL21(RPS)DE3 competent cells. Plasmid DNA (2 μL) was added to BL21(DE3) competent cells (50 μL) and incubated for 15 minutes on ice. The cells were then heat shocked for 30 seconds at 42°C. The mixture was incubated on ice for 15 minutes. The cells were then heat shocked at 42°C for 45 seconds before being incubated on ice for a further 1 minute. LB broth (400 μL) was added and the cells were shaked (250 rpm) for 40 minutes at 37°C. Subsequently, the cells (50 μL) were spread on a LB containing ampicillin (100 μg/mL, Sigma) and chloramphenicol (34 μg/mL, Sigma) and incubated overnight at 37°C.

6.5.2.1.3. Induction step

Four colonies of transformed cells were picked into a sterile tube containing 3 mL of LB media and antibiotics (100 μg/mL ampicillin and 34 μg/mL chloramphenicol) and grown overnight at 37^{o}C. The optical density at 600 nm (OD_{600}) was measured (~2.0). The cultures were stored at room temperature for 4 hours. 12 samples were prepared by dilution of 0.5 mL of overnight cell culture with 5 mL of fresh LB media. The cells were grown again for 4 hours at 37^{o}C to obtain an OD_{600} 0.9. Then in each 50 mL cell culture was added IPTG to give a final concentration of 1 mM. IPTG (**4.31**) was not added to one of the 5mL mixture. This tube was used for non-induction comparison. All cell cultures were grown overnight at 27^{o}C and then stored on ice.

6.5.2.1.4. Cell lysis

Cell lysis buffer:

300 mM NaCl (60 mL of 5 M solution)

15 mM imidazole (15 mL of 1 M solution)

50 mM Tris-HCl (pH 8) (25 mL of 2 M solution)

10% mM glycerol (125 mL of 80% solution)

10 mM 2-mercaptoethanol (0.7 mL of 14.3 M solution)

1 protease inhibitor tablet (Complete EASYpack)

Dissolved and mixed in sterile water to obtain a final volume of 1 L.
Just before use, 1X of PMSF (2.5 mL from a 400X starting solution in isopropanol) were added to the mixture.

Protocol:

Induced cell cultures were mixed into 50 mL centrifuge tubes. Induced (A+) and non-induced solutions were spin down at 5000 rpm for 10 minutes at 4^{o}C. The supernatant was removed. The pellets were detached and washed with 20 mL of PBS. Samples were centrifuged again using the same conditions. The His6-Cys-GFP (**4.30)** gave a green pellet. The supernatant was removed by suction and the pellet was resuspended into 10 mL of cold cell lysis buffer (4 tubes). Once cells were suspended into this buffer, tubes were transferred from ice into dry ice. The cells were frozen for 30 minutes. After this step, cells were warm up under hot water to defreeze them while keeping them cold. Each defrost tube was put into ice with 0.5 mL of lysozyme (Lysozyme from chicken egg white, 20 mg/mL, Sigma-Aldrich) to give a final concentration of 1 mg/mL. The lysozyme was left to react during 45 minutes on ice. At the end of the incubation time, each tube, kept on ice, was sonicated for 5 minutes (Soniprep 150, MSE)). 0.5 mL of triton-x 0.1% was added to each tube which was then again spin down (16000g for 15 minutes at 4^{o}C). The clear supernatant of each tube was removed, mixed and transferred into a 50 mL centrifuge tube on ice (40 mL). In case of the pellets were still green, 10 mL of supernatant were used to resuspend them. Sonication, centrifugation and transfer steps were repeated. 200 µL of A+ supernatant and of A- supernatants were taken and small aliquots were analysed by SDS-PAGE gel to confirm the presence of protein **4.30**.

6.5.2.1.5. His-Tag purification

In order to purify the protein, Ni-NTA agarose beads from QIAGEN were used.

Washing buffer:

300 mM NaCl (60 mL of 5 M solution)
20 mM imidazole (20 mL of 1 M solution)

50 mM Tris-HCl (pH 8) (25 mL of 2 M solution)
10% mM glycerol (125 mL of 80% solution)
10 mM 2-mercaptoethanol (0.7 mL of 14.3 M solution)
Dissolved and mixed in sterile water to obtain a final volume of 1 L.
Just before use, 1X of PMSF (2.5 mL from a 400X starting solution in isopropanol) were added to the mixture.

Elution buffer:
300 mM NaCl (60 mL of 5 M solution)
250 mM imidazole (250 mL of 1 M solution)
50 mM Tris-HCl (pH 8) (25 mL of 2 M solution)
10 mM 2-mercaptoethanol (0.7 mL of 14.3 M solution)
Dissolved and mixed in sterile water to obtain a final volume of 1 L.
Just before use, 1X of PMSF (2.5 mL from a 400X starting solution in isopropanol) were added to the mixture.

Protocol:
Ni-NTA agarose beads (10 mL) were added to 30 mL of PBS, mixed and then centrifuged 2000 rpm for 2 minutes. The washing with PBS was repeated twice. Once the beads ready, they were mixed with the His6-Cys-GFP protein (**4.30**, 40 mL) for 1 hour. After reaction, the clear supernatant was removed. 25 mL of washing buffer were added to the beads and mixed. The mixture was centrifuge 2000 rpm for 2 minutes at 4^{o}C. The washing step was repeated 3 times. The beads were suspended in 10 mL of washing buffer and transferred into a SPE column. The washing buffer was eluted until the edge of the beads and 10 mL of elution buffer were added. The solution was collected as 20 fractions of 0.5 mL. The aliquots were passed under the transilluminator (UVP TM 40 Dual intensity Ultraviolet transilluminator from Ultra Violet Products) to detect the fractions containing the GFP. The fluorescent aliquots were mixed together.

6.5.2.1.6. His-Tag cleavage

Once purified, the His-tag was cleaved from the GFP **4.30** using an Enterokinase (light chain, BioLabs, 2 µg/mL), that specifically cleaves the protein after lysine in the sequence Asp-Asp-Asp-Asp-Lys.

Reaction buffer:
50 mM NaCl (1 mL of 5 M solution)
20 mM Tris-HCl (pH 8) (1 mL of 2 M solution)
2 mM CaCl (0.1 mL of 2 M solution)
Dissolved and mixed in sterile water to obtain a final volume of 100 mL.

Protocol:
1.5 mL of His6-Cys-GFP (**4.30**, 1755 µg) was mixed with 30 µL of entrokinase and 1.5 mL of reaction buffer for 16 hours at 25^{o}C, 700 rpm on a Thermomixer comfort (Eppendorf). After digestion and its SDS-PAGE confirmation (Cys-GFP, **4.29**), the entrokinase was removed using a large excess trypsin inhibitor agarose (Glycine max, soybean, Sigma-Aldrich). 30 µL of inhibitor beads were prepared by mixing with reaction buffer and centrifuging (room temperature, 2 minutes, 2000 rpm). This step was repeated twice. The beads were added to the entrokinase-GFP **4.29** solution and mixed for 2 hours at room temperature.

6.5.2.1.7. Protein desalting and concentration

The protein **4.29** was desalted using a PD 10 column (GE Healthcare, exclusion limit 5000 Da, 2.5 mL) and the reaction buffer (**6.5.2.1.6**). The GFP was concentrated using Amicon ultra-4 3000 Da centrifugal filter devices (Millipore) for 10 minutes at 4000g (concentrate down from 4 mL to 0.5 mL). The location of the protein in the upper level of the device was confirmed by transilluminator.

6.5.2.1.8. Analysis

The final concentration of the Cys-GFP was calculated using Beer-Lambert law (55000 $M^{-1}cm^{-1}$) after measurement of the absorption at 390 nm using a SmartSpec 3000 (Biorad):

A = 0.428 at 390 nm

Concentration of Cys-GFP (**4.29**) = 77 µM

$C_{\mathbf{4.29}}$ mg/mL = 2.16 mg/mL.

m/z (MALDI-TOF): calculated 27767.7, found 27766.5 $[M+H]^+$ (100%), 13885.4 $[M+2H]^{2+}$ (37.9%).

6.5.2.2. Synthesis of 6-(2,5-dioxo-2,5-dihydro-1H-pyrrol-1-yl)hexanoic acid (**4.34**)[225]

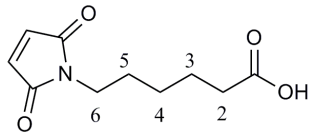

A suspension of maleic anhydride **4.27** (4.9 g, 50 mmol) and aminohexanoic acid **4.32** (6.58 g, 50 mmol) in acetic acid (37.5 mL) was heated to reflux for 90 minutes. The solution was then cooled down and the solvent was removed *in vacuo*. Residual AcOH was removed by azeotrope with toluene (2 × 50 mL). The white residue was dissolved in water (50 mL). The aqueous phase was extracted with EtOAc (3 × 50 mL). The organic phases were combined, dried over $MgSO_4$, filtred and concentrated under vacuum. The crude was crystallized in EtOAc (10 mL, overnight at 4°C). Clear crystals of **4.34** were obtained, filtered, washed with cold EtOAc (3 × 5 mL) and dried *in vacuo* (4.6 g, 46%).

Analysis:

m/z (ES^+): $C_{10}H_{13}NO_4$ calculated 211.0, found 234.0 $[M+Na]^+$ (100%), 212.1 $[M+H]^+$ (9.8%).

Rf: 0.63 (EtOAc**).**

HPLC (Method 1): t_R = 3.3 min, purity = 100% (ELSD).

^{1}H NMR ($CDCl_3$, 360 MHz): δ = 1.21-1.30 (m, 2H, CH_2, C_4), 1.53-1.62 (m, 4H, CH_2, C_3 and C_5), 2.28 (t, *J* = 7.42 Hz, 2H, CH_2, C_2), 3.45 (t, *J* = 7.27 Hz, 2H, CH_2, C_6), 6.62 (s, 2H, *H*C=C*H*).

^{13}C NMR ($CDCl_3$, 90 MHz): δ = 23.7 (C_3), 25.8 (C_4), 27.8 (C_5), 33.3 (C_2), 37.2 (C_6), 133.8 (2C, *C*=*C*), 170.5 (2C, *C*=O), 178.9 (*C*OOH).

IR (neat): 1690 (s, $\nu_{C=C}$), 1446 (m, ν_{C-H}), 1408 (m, ν_{O-H}), cm^{-1}.

Mp: 77.9-78.7°C.

6.5.2.3. Synthesis of maleimide-9mer (**4.35**)

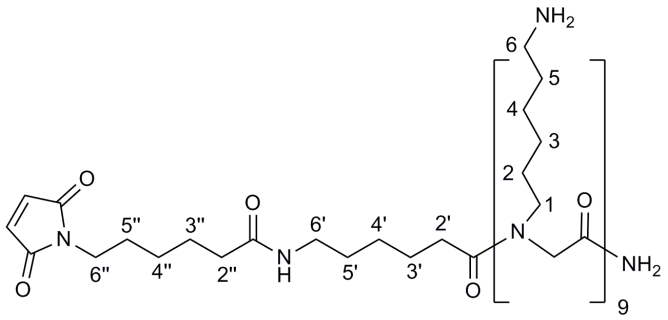

The maleimide-9mer peptoid **4.35** was synthesised from the resin **2.28** (50 mg, 0.043 mmol) and the monomer **2.22** (65 mg, 0.13 mmol) using the protocols **6.2.1.8** and **6.2.1.9.**

After coupling of Fmoc-Ahx-OH (**2.34**, 45.9 mg, 0.13 mmol), the maleimide spacer **4.34** (27 mg, 0.13 mmol) was conjugated to the solid supported peptoid using a DIC/HOBt (20.3 µL/18 mg, 0.13 mmol) activation in DMF (0.65 mL, 0.2 M, **6.2.1.7**). Finally, the resin bound maleimide-9mer peptoid was deprotected and cleaved from the solid support using a solution TFA/TIS/H_2O (95: 2.5: 2.5, 2.5 mL) (**6.2.1.10**). Maleimide-9mer **4.35** was isolated after overnight drying (vacuum oven, 40^{o}C) as a white powder (68 mg, 92% based on **2.28**).

Analysis:

m/z (ES^+): $C_{88}H_{169}N_{21}O_{13}$ calculated 1729.4, found 865.5 $[M+2H]^{2+}$ (18.7%), 577.3 $[M+3H]^{3+}$ (72.3%), 433.2 $[M+4H]^{4+}$ (100%), 346.8 $[M+5H]^{5+}$ (11.0%).

m/z (MALDI-TOF): $C_{88}H_{169}N_{21}O_{13}$ calculated 1729.42, found 1752.47 $[M+Na]^+$ (100%), 1730.47 $[M+H]^+$ (80.7%).

m/z (FT-MS): $C_{107}H_{187}N_{22}O_{14}^+$ calculated $[M+3H]^{3+}$ = 577.47212, found 577.45354.

HPLC (Method 3): t_R = 2.0 min, purity > 98% (ELSD).

^{1}H NMR (D_2O, 500 MHz, presat water suppression): δ = 1.12-1.37 (m, 40H, 4H for C*H*$_2$ (H $_{4'}$ and $H_{4''}$) and 36H for C*H*$_2$ (H $_3$ and H_4)) , 1.37-1.68 (m, 44H, 8H for C*H*$_2$ (H $_{3', 5', 3'' \text{ and } 5''}$) and 36H for C*H*$_2$ (H $_2$ and H_5)), 2.07-2.17 (m, 2H, C*H*$_2$, $H_{2'}$), 2.40 (t, *J* = 7.20 Hz, 2H, C*H*$_2$, $H_{2''}$), 2.91 (m, 18H, C*H*$_2$NH_2, H_6), 2.98-3.14 (m, 2H, C*H*$_2$, $H_{6'}$), 3.28 (m, 18H, C*H*$_2$N, H_1), 3.42 (t, *J* = 6.85 Hz, 2H, C*H*$_2$, $H_{6''}$), 3.89-4.42 (m, 18H, NC*H*$_2$CO), 6.77 (s, 2H, *H*C=C*H*), 7.47 (br sg, 2H, CON*H*$_2$).

^{13}C NMR (D_2O, 126 MHz): δ = 22.1 (*C*H$_2$, $C_{3''}$), 24.9 (*C*H$_2$, $C_{4''}$), 25.2, 25.3, 25.4, 25.5, 25.6, 26.1, 26.2, 26.3, 26.4, 26.6, 26.7, 27.1, 27.2, 27.3, 27.5 and 27.6 (*C*H$_2$, $C_{5''}$,$C_{2', 4', 5'}$,$C_{2, 3, 4, 5}$), 31.8 (*C*H$_2$, $C_{2''}$), 35.4 (*C*H$_2$, $C_{2'}$), 37.2 (*C*H$_2$, $C_{6''}$), 39.1, 39.4, 39.5, 39.6 (*C*H$_2$, C_6),47.3, 47.4, 47.5, 47.7, 47.8, 47.9, 47.9, 48, 481, 48.2, 48.3, 48.4, 48.5 (*C*H$_2$, NC*H*$_2$CO and C_1), 134.3 (H*C*=*C*H), 162.4, 162.7, 162. 9, 163.3 (*C*=O-9mer), 169.9, 170.1, 170.2, 170.3 (*C*=O- 9mer and spacer), 173.3 (*C*=O-maleimide).

6.5.2.4. Preparation of the 2-chlorotrityl-cysteamine resin **4.37**

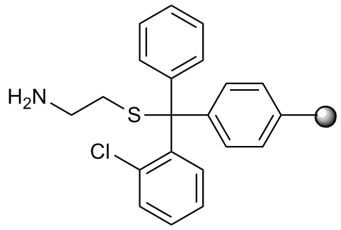

The preactivated 2-chlorotrytil chloride resin **4.5** (500 mg, 0.75 mmol) was swollen for 20 minutes at room temperature in DCM (5 mL). The resin was then mixed with cysteamine **4.36** (289 mg, 0.75 mmol) and DIPEA (0.65 mL, 3.75mmol) in 6 mL of DCM. The mixture was stirred overnight. The resin was filtered and washed with DCM and DMF (3 × 5 mL each). The coupling was confirmed by a qualitative ninhydrin test (**6.2.1.1**). After overnight drying in a vacuum oven (40^{o}C), the resin **4.37** was isolated as a beige solid (625 mg).

Analysis:

Quantitative ninhydrin test (6.2.1.2): loading 0.75 mmol/g.

IR (neat): 3024 (m, ν_{C-H}), 1600 (m, ν_{C-H}), 1448 (s, ν_{C-H}) cm^{-1}.

6.5.2.5. Synthesis of 5(6)-(N) thioethyltetraethylrhodaminamide **4.38**

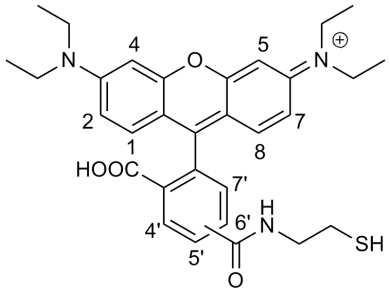

The resin **4.37** (100 mg, 0.075 mmol) was swollen in DCM (1 mL) for 20 minutes at room temperature. Rhodamine **2.36** (183 mg, 0.375 mmol) and HOBt (51 mg, 0.375 mmol) were dissolved in DMF (1.9 mL, 0.2 M). DIC (58.4 µL, 0.375 mmol) was added to the solution that was stirred for 15 minutes. The activated solution was added to the resin and the mixture was shaked overnight. The resin was isolated by filtration and was washed with DMF, DCM, MeOH and Et_2O (3 × 5 mL each). The modified rhodamine **4.38** was finally released from the solid support by a 2 hour treatment with a mixture of TFA/DCM/TIS (50: 45: 5, 2.5 mL). The red solution was filtered off, and the resin was washed twice with 1 mL of cocktail solution and DCM (3 × 1 mL). The solvent was evaporated and the remaining product was precipitated in cold Et_2O (2 x 15 mL). After the centrifugation and overnight drying *in vacuo* at 40°C, the dye **4.42** was obtained as a red/purple powder (33 mg, 82%).

Analysis:

m/z (ES^+): $C_{31}H_{36}N_3O_4S^+$ calculated 546.2, found 546.2 $[M]^+$ (100%), 547.1 $[M+H]^+$ (38.7%).

m/z (HRMS, ES^+): $C_{31}H_{36}N_3O_4S^+$ calculated 546.24210, found 546.24337.

HPLC (Method 3): t_R = 4.8 min, purity > 98% (ELSD)

^{1}H NMR (D_2O, 500 MHz, presat water suppression): δ = 1.13 (t, *J* = 8.40 Hz, 12H, 4 × C*H*$_3$), 2.75 (t, *J* = 7.85 Hz, 2H, C*H*$_2$SH), 3.47 (q, *J* = 8.55 Hz, *J* = 8.90 Hz, 8H,

C*H*$_2$CH$_3$), 3.57 (t, *J* = 7.70 Hz, 2H, C*H*$_2$NH), 6.65 (s, 2H, Ar*H*, H_5 and H_4), 6.76 (d, *J* = 11.75 Hz, 2H, Ar*H*, H_7 and H_2), 7.02 (d, *J* = 11.75 Hz, 2H, Ar*H*, H_8 and H_1), 7.31 (d , *J* = 9.65 Hz, 0.5H, Ar*H*, $H_{7'}$ for isomer 5'), 7.85 (m , 0.5H, Ar*H*, $H_{5'}$ for isomer 6'), 7.92 (d, *J* = 9.45 Hz, 0.5H, Ar*H*, $H_{6'}$ for isomer 5'), 8.15 (m, 0.5H, Ar*H*, $H_{4'}$ for isomer 6'), 8.33 (s, 1H, Ar*H*, $H_{4'}$ for isomer 5' and $H_{7'}$ for isomer 6').

^{13}C-NMR (D_2O, 126 MHz): δ = 12.3 (CH_2CH_3), 31.0 (CH_2SH), 39.3 (CH_2NH), 45.4 (CH_2CH_3), 96.7 (ArCH, C_5 and C_4), 112.7, 113.6 (ArCH, C_2 and C_7), 128.7 (ArCH, $C_{5'}$ for isomer 6'), 129.1, 129.3 (ArCH, $C_{7'}$ for isomer 6' and $C_{6'}$ for isomer 5'), 130.8 (ArCH, $C_{7'}$ for isomer 5'), 131.3 (ArCH, $C_{4'}$ for isomer 6'), 131.6 (ArCH, $C_{4'}$ for isomer 5'), 132.1, 133.4 (ArCH, C_1 and C_8), 135.2, 137.7, 138.2, 140.5, 142.6, 155.8, 157.6, 158.3 (ArC), 163.8 (CONH), 174.3 (COOH).

UV (MeOH): λ_{abs} = 560 nm, λ_{em} = 589 nm.

IR (neat): 3450 (s, ν_{O-H}), 3190 (w, ν_{N-H}), 1689 (s, $\nu_{C=O}$), 1178 (s, ν_{O-H}) cm^{-1}.

Mp: 178-180.5°C

6.5.2.6. Synthesis of **4.39** via coupling between the maleimide-9mer **4.35** and the thio-rhodamine **4.38**

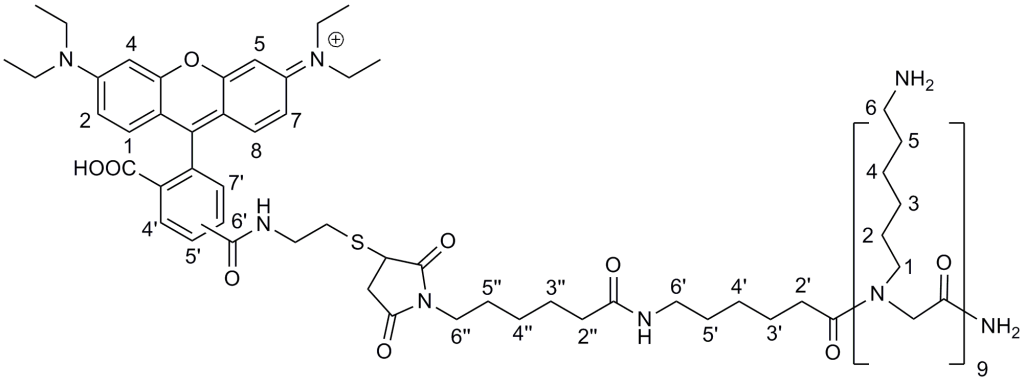

Maleimide-9mer **4.35** (10 mg, 5.7 µmol) was dissolved in PBS (1 mL) and the pH was adjusted at 7.0 using 1 M NaOH. The thio-rhodamine **4.38** (3 mg, 5.7 µmol) was added and the solution was mixed for 16 hours. The solution was lyophilised and the crude was precipated in cold Et_2O (1 mL) using TFA (100 µL). After centrifugation and drying, **4.39** was isolated as a red solid. A small amount of the crude was analysed by MS and HPLC without purification in order to know the

efficiency of the couplage. After purification by preparative HPLC (Gradient 1), the pure **4.39** (10 mg, 79%) was analysed.

Analysis of the crude:

m/z (ES^+): $C_{119}H_{205}N_{24}O_{17}S^+$ calculated 2276.1, 570.0 $[M+4H]^{4+}$ (5.7%), 456.2 $[M+5H]^{5+}$ (58.6%), 380.3 $[M+6H]^{6+}$ (100%), 326.4 $[M+7H]^{7+}$ (22.1%).

m/z (MALDI-TOF): $C_{119}H_{205}N_{24}O_{17}S^+$calculated 2276.12, found 2276.12 $[M+H]^+$ (100%).

HPLC (Method 3): t_R = 2.3 min, purity > 96% (ELSD).

*Analysis of the pure **4.39**:*

m/z (FT-MS): $C_{119}H_{205}N_{24}O_{17}S^+$calculated $[M+4H]^{4+}$ 569.64857, found 569.66215.

HPLC (Method 3): t_R = 2.3 min, purity = 100% (ELSD).

^{1}H NMR (D_2O, 500 MHz, presat water suppression): δ = 1.07 (t, *J* = 6.55 Hz, 12H, 4 × C*H*$_3$), 1.19-1.44 (m, 40H, 4H for C*H*$_2$ (H $_{4'}$ and H$_{4''}$) and 36H for C*H*$_2$ (H $_3$ and H$_4$)) , 1.44-1.71 (m, 44H, 8H for C*H*$_2$ (H $_{3', 5', 3'' \text{ and } 5''}$) and 36H for C*H*$_2$ (H $_2$ and H$_5$)), 2.19 (t, *J* = 7.20 Hz, 2H, C*H*$_2$, H$_{2'}$), 2.46 (t, *J* = 7.50 Hz, 2H, C*H*$_2$, H$_{2''}$), 2.79 (t, , *J* = 7.45 Hz 2H, C*H*$_2$S-Rho), 2.97 (m, 18H, C*H*$_2$NH$_2$, H$_6$), 3.03 and 3.06 (2 dd, *J* = 6.70 Hz, *J* = 1.05 Hz, 2H, COC*H*$_2$CHS-succinimidyl), 3.25-3.43 (m, 18H, C*H*$_2$N, H$_1$), 3.46 (t, *J* = 7.82 Hz, 2H, C*H*$_2$NH-Rho), 3.48 (t, *J* = 6.65 Hz, 2H, C*H*$_2$, H$_{6'}$), 3.53 (t, *J* = 6.65 Hz, 2H, C*H*$_2$, H$_{6''}$), 3.68 (q, *J* = 6.55 Hz, *J* = 6.50 Hz, 8H, C*H*$_2$CH$_3$), 4.00-4.46 (m, 18H, NC*H*$_2$CO), 4.66 (m, 1H, C*H*S-succinimidyl), 6.82 (s, 2H, ArC*H*, H$_5$ and H$_4$), 6.88 (d, *J* = 9.55 Hz, 2H, ArC*H*, H$_7$ and H$_2$), 7.10 (d, *J* = 9.85 Hz, 2H, ArC*H*, H$_8$ and H$_1$), 7.52 (d, *J* = 7.50 Hz, 0.5H, ArC*H*, H$_{7'}$ for isomer 5'), 7.66 (m, 0.5H, ArC*H*, H$_{5'}$ for isomer 6'), 7.99 (d, *J* = 8.15 Hz, 0.5H, ArC*H*, H$_{6'}$ for isomer 5'), 8.10 (m, 0.5H, ArC*H*, H$_{4'}$ for isomer 6'), 8.21 (s, 1H, ArC*H*, H$_{4'}$ for isomer 5' and H$_{7'}$ for isomer 6').

^{13}C NMR (D_2O, 126 MHz): δ = 12.3, 12.4 (CH_2CH_3), 22.1 (*C*H$_2$, *C*$_{3''}$), 25.0 (*C*H$_2$, *C*$_{4''}$), 25.3, 25.4, 25.5, 25.6, 26.1, 26.2, 26.3, 26.4, 27.0, 27.1, 27.2, 27.3, 27.5, 27.6, 27.8, 27.9 (*C*H$_2$, *C*$_{5''}$,*C*$_{2', 4', 5'}$,*C*$_{2, 3, 4, 5}$), 31.9 (*C*H$_2$, *C*$_{2''}$), 35.4 (*C*H$_2$, *C*$_{2'}$), 36.2 (*C*H$_2$S-Rho), 37.2 (*C*H$_2$, *C*$_{6''}$), 39.1, 39.4, 39.5, 39.6, 39.8, 40.0, 41.2 (*C*H$_2$ (*C*$_6$), *C*H$_2$NH-

Rho, COC*H*$_2$CHS-succinimidyl), 45.5 (*C*H$_2$CH$_3$), 47.2, 47.3, 47.5, 47.7, 47.8, 47.9, 47.9, 48, 48.1, 48.2, 48.3, (*C*H$_2$, NCH$_2$CO and *C*$_1$), 54.5 (C*H*S-succinimidyl), 96.7 (Ar*C*H, C$_5$ and C$_4$), 112.8, 113.6 (Ar*C*H, C$_2$ and C$_7$), 128.5 (Ar*C*H, C$_{5'}$ for isomer 6'), 129.0, 129.3 (Ar*C*H, C$_{7'}$ for isomer 6' and C$_{6'}$ for isomer 5'), 130.8 (Ar*C*H, C$_{7'}$ for isomer 5'), 131.2 (Ar*C*H, C$_{4'}$ for isomer 6'), 131.6 (Ar*C*H, C$_{4'}$ for isomer 5'), 132.1, 133.3 (Ar*C*H, C$_1$ and C$_8$), 137.9, 138.1, 140.5, 142.7, 156.0, 157.6, 158.3 (Ar*C*), 162.4, 162.7, 163.0, 163.3 (*C*=O-9mer), 170.1, 170.2 (*C*=O-spacer), 173.3 (*C*=O-maleimide).

UV (H$_2$O): λ_{abs} = 560 nm, λ_{em} = 586 nm.

6.5.2.7. Preparation and analysis of the 9mer-Cys-GFP **4.40**

6.5.2.7.1. SDS-PAGE gel protocol

SDS-PAGE gels were carried out using a Mini-Protean® Tetra Cell from BioRad.

Gel preparation:

SDS-PAGE was carried out using a SDS-Tris system with 15% polyacrylamide gel. Two gels were prepared: the running gel (bottom) containing 15% acrylamide and the stacking gel (top) containing 4% acrylamide.

Compound	Running gel	Stacking gel
H$_2$O	3.5 mL	6.15 mL
Acrylamide BIS (40%)	3.75 mL	1.01 mL
Tris buffer	2.5 mL (1.5 M, pH 8.8)	2.5 mL (0.5 M, pH 6.8)
SDS 10%	100 µL	100 µL
APS (50 mg/mL) Ammonium peroxodisulfate	200 µL	200 µL

TEMED	15 µL	15 µL

Table 6.43: Quantities used to prepare one SDS gel.

SDS loading buffer (2X):

1.5 mL 1.5 M TrisBuffer pH 8.0

2.0 mL 10% Glycerol

2.0 mL 0.05% Bromophenol blue

1.0 mL 10% SDS

0.4 mL β-Mercapoethanol

Running buffer, TGS (Tris-Glycine-SDS) buffer:

25 mM Tris

192 mM Gycine

0.1% SDS (w/v)

pH 8.3

Coomassie staining solution:

450 mL water

450 mL Methanol

100 mL of GAA (Glacial acetic acid)

2.5 g of brillant blue

Marker:

LMW calibration kit for SDS electropherisis from GE Healthcare. The marker is unstained, so it was prepared as a sample (10 µL of marker + 10 µL of SDS loading buffer).

Preparation of samples, staining and destaining were the same as described in section **6.5.2.1.1.**

6.5.2.7.2. Preparation of the bioconjugation 9mer-S-GFP (**4.40**)

8 µL of Cys-GFP (**4.29**, 0.62 nmol) were mixed with 0.5 mL of DTT (**4.41,** 6.2 nmol, 10 equiv., 12.4 µM) in PBS pH 7.0. The solution was mixed overnight at 20^{o}C using the Thermomixer (700 rpm). Excess of DTT was removed using PD SpinTrap G-25. The protein mixture was centrifuged 4 times at 800 g and washed with PBS (pH 7.0) and concentrated down to 100 µL. The protein was dissolved in 345 µL of PBS (pH 7.0) and 155 µL of maleimide-9mer **4.35**(15.5 nmol, 25 equiv., 100 µM) solution in PBS (pH 7.0) was mixed with the reduced protein. The solution was mixed overnight in the Thermomixer (20^{o}C, 700 rpm). The excess of peptoid was removed by centrifugation (PD SpinTrap G-25). The protein mixture was centrifuged 4 times at 800g and washed with PBS (pH 7.0). The protein was concentrated down to 160 µL (1 µg of **4.40** per 10 µL).The sample was analysed using MALDI-TOF and SDS-PAGE.

Analysis:

m/z (MALDI-TOF): found **4.29** = 27852.6 $[M+H]^{+}$ (100%) and 13915 $[M+2H]^{2+}$ (40%); **4.40** = 29540.4 $[M+H]^{+}$ (13%)

SDS-PAGE: two bands corresponding to Cys-GFP (**4.29**) and 9mer-S-GFP (**4.40**).

6.5.2.7.3. Cellular delivery of the bioconjugate **4.40** and **4.44** into HeLa cells

Cells were seeded onto a 24-well plate at a density of 3 × 10^{4} cells/well (volume of culture media per well: 350 µL). After 24 hours, 10 µL (**4.40-a** and **4.44-a**) and 20 µL of (**4.40-b** and **4.44-b)** of **4.40** and **4.44** (100 µg/mL), 35 µL of **4.35** (100 µM in PBS) and 3.5 µL of **4.29** (0.6 mg/mL) were injected in three random wells. Cellular uptake was analysed 24 hours of incubation by flow cytometry in 2% FBS in PBS with 0.2% of trypan blue (**6.2.2.3**).

*Cellular uptake of **4.40***

	Concentration per well	Average (%)	Error (%)
Untreated cells		0.6	0.6
4.29	6 µg/mL	4.0	2.0
4.40-a	2.7 µg/mL	18.6	3.4
4.40-b	5.4 µg/mL	47.5	3.5
4.35	10 µM	2.0	0.5

Table 6.44: Cellular uptake of Cys-GFP (4.29), 9mer-S-GFP (4.40) and Mal-9mer (4.35) after 24 hours of incubation in HeLa cells (n = 6).

*Cellular uptake of **4.44***

	Concentration per well	Average (%)	Error (%)
Untreated cells		0.8	0.2
4.29	6 µg/mL	0.9	0.1
4.44-a	2.7 µg/mL	8.8	1.2
4.44-b	5.4 µg/mL	14.8	3.3
4.35	10 µM	1.1	0.6

Table 6.45: Cellular uptake of Cys-GFP (4.29), 9mer-S-GFP (4.44) and Mal-9mer (4.35) after 24 hours of incubation in HeLa cells (n = 3).

6.5.2.7.4. Microscopy of the bioconjugate **4.40** into HeLa cells

Cells were seeded onto a 24-well plate at a density of 3×10^4 cells/well (volume of culture media per well: 350 µL). After 24 hours, 20 µL of **4.40** (5.4 µg/mL) were injected in random wells. After 24 hours of incubation with the peptoids, cells were washed with PBS and microscopy was performed in 2% FBS in PBS without further staining.

6.5.2.7.5. MTT assays of the bioconjugate **4.40** and **4.44** in HeLa cells

MTT cytotoxicity assays were carried out as according to the general procedures (**6.2.2.4**). The cells were treated respectively with 3 and 6 µL of **4.40** and **4.44** (1 µg/10 µL), 10 µL of **4.35** (100 µM in PBS) and 1 µL of **4.29** (0.6 mg/mL) were injected. After 24 hours of incubation at 37°C, the wells were read on a microplate reader.

	Concentration per well	Average (arb. units)	Error (arb. units)	Average (%)	Error (%)
Control cells		1.146	0.044	100.0	3.9
4.29	6 µg/mL	1.093	0.054	95.4	4.7
4.40-a	2.7 µg/mL	1.059	0.086	92.4	7.5
4.40-b	5.4 µg/mL	1.084	0.079	94.6	6.9
4.44-a	2.7 µg/mL	1.060	0.125	100.1	11.8
4.44-b	5.4 µg/mL	1.030	0.173	97.3	16.4
4.35	10 µM	1.143	0.085	99.8	7.4

Table 6.46: Percentage of cell vailability (HeLa cells) after 24 hours of incubation with Cys-GFP (4.29), 9mer-S-GFP (4.40) and (9mer-S)$_n$-GFP (4.44) and Mal-9mer (4.35) (n = 8).

6.5.2.8. Preparation and analysis of the bioconjugate (9mer-S)$_n$-GFP **4.44**

6.5.2.8.1. Bioconjugation buffers[329]

Thiolation reaction buffer:

100 mM sodium phosphate

1 mM EDTA

water

Adjusted to pH 7.4 with 1 N NaOH

Bioconjugation buffer:

10 mM sodium phosphate

1 mM EDTA

150 mM NaCl

water

Adjusted to pH 7.0 with 1 N NaOH

6.5.2.8.2. Preparation of the bioconjugation (9mer-S)$_n$-GFP (**4.44**)

8 µL of Cys-GFP (**4.29**, 0.62 nmol) were added to 0.5 mL of 2-iminothiolane (**4.42**, 15.5 nmol, 31 µM) in thiolation reaction buffer. The solution was mixed for 4 hours and then the excess of thiolation agent was removed using a PD SpinTrap G-25 and PBS (pH 7.0). The thiolated Cys-GFP (**4.43**) was mixed with 0.5 mL of DTT solution (**4.41,** 6.2 nmol, 10 equiv., 12.4 µM) in PBS pH 7.0. The solution was mixed overnight using the Thermomixer (700 rpm, 20^{o}C). Excess of DTT was removed

purified using a PD SpinTrap G-25. The protein mixture was centrifuged 4 times at 800g and washed with bioconjugation buffer and concentrated down to 100 µL. The protein was dissolved in 345 µL of PBS (pH 7.0) and 155 µL of maleimide-9mer **4.35** (15.5 nmol, 25 equiv., 100 µM) solution in PBS (pH 7.0) was mixed with the protein. The solution was shaked overnight. The excess of peptoid was removed using a PD SpinTrap G-25. The protein mixture was centrifuge 4 times at 800g and washed with PBS (pH 7.0). The protein was concentrated down to 160 µL (1 µg of protein per 10 µL).The sample was analysed using MALDI-TOF and SDS-PAGE.

Analysis:

m/z (MALDI-TOF): found **4.29** = 27701.2 $[M+H]^+$ (100%) and 13836.1 $[M+2H]^{2+}$ (27%); **4.44 ((9mer-S)$_n$-GFP, n = 1)** = 29534.4 $[M+H]^+$ (8%) and **4.44 ((9mer-S)$_n$-GFP, n = 2)** = 31355.8 $[M+H]^+$ (4%)

SDS-PAGE: three bands corresponding to Cys-GFP (**4.29**), (9mer-S)$_n$-GFP (**4.44, n = 1**) and (9mer-S)$_n$-GFP (**4.44, n = 2**).

6.5.2.9. Via fully protected peptoid

6.5.2.9.1. Physiologic deprotection of the Dde group on Fmoc-Lys(Dde)-OH **4.14**

Dde deprotection solution:

500 mM of hydroxylamine.HCl
25 mM of EDTA Dipotassium
50 mM of sodium phosphate dibasic
water
Adjusted to pH 7.5 with 4M NaOH.

Reaction and analysis:

50 mg of Fmoc-Lys(Dde)-OH (**4.14**, 94.9 mmol) were dissolved in 1 mL of deprotection solution and mixed for 6 hours. The solvent was removed under vacuum. The crude of the reaction was analysed by HPLC, MS and ^{1}H-NMR.

	Fmoc-Lys(Dde)-OH, **4.14**	Crude after deprotection
HPLC (Method 1, min, λ = 240 nm)	3.6 (100%)	3.5 (95%)
MS (ES^+)	532.2	369.1 (Fmoc-Lys-OH)

^{1}H NMR of the crude (500 MHz, $CDCl_3$): δ = 1.51 (m, 4H, C*H*$_2$-Lys), 1.70-2.04 (m, 2H, C*H*$_2$-Lys), 3.17 (m, 2H, C*H*$_2$-NH-Lys), 4.25 (d, *J* = 5.75 Hz, 2H, C*H*$_2$-Fmoc), 4.41 (t, *J* = 5.85 Hz, 1H, C*H*-Fmoc), 4.67 (m, 1H, C*H*), 5.66 (br sg, 1H, N*H*), 7.32 (t, *J* = 6.80 Hz, 2H, ArC*H*-Fmoc), 7.41 (t, *J* = 6.85 Hz, 2H, ArC*H*-Fmoc), 7.62 (m, 2H, ArC*H*-Fmoc), 7.78 (d, *J* = 7.25 Hz, 2H, ArC*H*-Fmoc).

6.5.2.9.2. Synthesis of 1,6-diamino-*N*-(4,4-dimethyl-2,6-dioxocyclo hexylidene)-hexane **4.45**

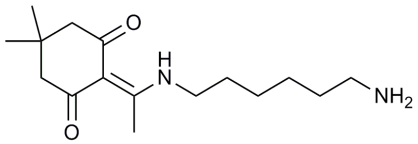

1,6-diaminohexane **2.18** (6.4 g, 0.056 mol) and DdeOH **4.20** (10 g, 0.056 mol) were dissolved in DCM (140 mL) and the reaction was stirred 2 hours. The solvent was evaporated and the yellow crude **4.45** (16.2 g) was used for the next step without further purification as it was unstable.

Analysis:

m/z (ES^+): $C_{16}H_{28}N_2O_2$ calculated 280.2 , found 281.1 $[M+H]^+$ (100%), 303.1 $[M+Na]^+$ (10.7%).

Rf: 0.21 (EtOAc).

HPLC (Method 1): t_R = 3.0 min, purity = 66% (ELSD).

6.5.2.9.3. Synthesis of benzyl-(6-(4,4-dimethyl-2,6-dioxocyclohexylidene) - hexylamino)-acetate **4.46**

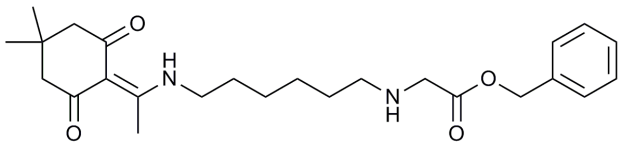

4.45 was dissolved in THF (80 mL) with TEA (23.3 mL, 0.165 mol). To this solution was added, drop-wise, a solution of benzyl 2-bromacetate **2.23** (8.9 mL, 0.056 mol) in THF (40 mL) over 2 hours, then the reaction was stirred for another 2 hours at room temperature. The THF was removed *in vacuo*. The white solid was suspended in Et_2O (200 mL) and then filtered. The solution was concentrated *in vacuo* and the crude product was purified by column chromatography (silica, eluting with EtOAc) to yield **4.46** as a pale yellow oil (7.6 g, 32% based on **4.20**).

Analysis:

m/z (ES^+): $C_{25}H_{36}N_2O_4$ calculated 428.3, found 429.1 $[M+H]^+$ (100%), 451.1 $[M+Na]^+$ (8.9%).

m/z (HRMS, ES^+): $C_{25}H_{36}N_2O_4$ calculated $[M+H]^+$ 429.27478, found 429.27471.

Rf: 0.05 (EtOAc).

HPLC (Method 3): t_R = 3.5 min; purity = 100% (ELSD).

^{1}H NMR ($CDCl_3$, 250 MHz): δ = 1.04 (s, 6H, 2×C*H*$_3$-Dde), 1.39-1.64 (m, 9H, DdeNHCH$_2$(C*H*$_2$)$_4$CH$_2$ and CH$_2$N*H*CH$_2$), 2.29 (s, 4H, 2×C*H*$_2$-Dde), 2.48 (s, 3H, C*H*$_3$-Dde); 2.53 (t, *J* = 6.90 Hz, 2H, CH$_2$C*H*$_2$NHCH$_2$), 3.27-3.36 (m, 2H, DdeNHC*H*$_2$), 3.38 (s, 2H, NHC*H*$_2$CO), 5.1 (s, 2H, C*H*$_2$-Bn), 7.37 (m, 5H, ArC*H*-Bn).

^{13}C NMR ($CDCl_3$, 63 MHz) δ = 17.9 (*C*H$_3$-Dde), 26.7 (DdeNH(CH$_2$)$_2$*C*H$_2$*C*H$_2$CH$_2$, 28.2, 28.9 (C(*C*H$_3$)$_2$-Dde), 29.7, 30.1 (DdeNHCH$_2$*C*H$_2$(CH$_2$)$_2$*C*H$_2$), 43.3 (DdeNH*C*H$_2$), 49.3 (CH$_2$*C*H$_2$NHCH$_2$), 50.9 (N*C*H$_2$CO), 66.5 (NCH$_2$COO*C*H$_2$), 107.8 (*C*=CNH), 128.3, 128.4, 128.6 (Ar*C*H), 135.6 (Ar*C*), 173.4 (C=*C*NH-Dde).

IR (neat): 3341 (w, ν_{N-H}), 2959 (w, ν_{C-H}), 2872 (w, ν_{C-H}), 1696 (s, $\nu_{C=O}$), 1256 (m, ν_{C-O}) cm^{-1}.

6.5.2.9.4. Synthesis of benzyl-[(6-(4,4-dimethyl-2,6-dioxocyclo hexylidene)-hexyl)-(9*H*-fluoren-9-ylmethoxycarbomyl)-amino]-acetate **4.47**

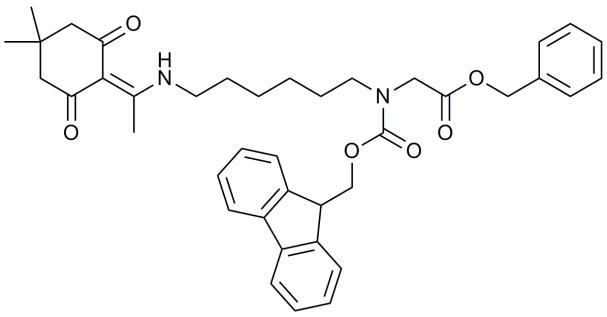

Fmoc-OSu (3.2 g, 9.3 mmol) was added to a solution of **4.46** (4.0 g, 9.3 mmol) in DCM (30 mL). The reaction was stirred at room temperature and monitored by TLC (EtOAc, Rf: 0.63) until completion (2 hours). The solvent was removed *in vacuo* and the crude product was purified by column chromatography (silica, eluting with EtOAc/Hexane, 2: 1) to yield **4.47** as a light yellow oil (6.15 g, 98%).

Analysis:

m/z (ES^+): $C_{40}H_{46}N_2O_6$ calculated 650.3, found 651.2 $[M+H]^+$ (100%), 673.3 $[M+Na]^+$ (10.1%).

m/z (HRMS, ES^+): $C_{25}H_{36}N_2O_4$ calculated $[M+H]^+$ 651.34286, found 651.34258.

Rf: 0.49 (EtOAc**).**

HPLC (Method 3): t_R = 7.2 min, purity = 97% (ELSD)

^{1}H NMR ($CDCl_3$, 500 MHz) two rotamers δ = δ 1.05 (s, 6H, 2 × C*H*$_3$-Dde), 1.10-1.73 (m, 8H, DdeNHCH$_2$(C*H*$_2$)$_4$CH$_2$), 2.39 (s, 4H, 2 × C*H*$_2$-Dde); 2.57 (s, 3H, C*H*$_3$-Dde), 3.17 (m, 2H, DdeNHC*H*$_2$), 3.37 (m, 2H, CH$_2$C*H*$_2$NCH$_2$), 3.96 and 4.03 (two s, 2H, NC*H*$_2$CO), 4.15 and 4.27 (two t, *J* = 8.25 Hz, 1H, C*H*-Fmoc), 4.40 and 4.55 (two d, *J* = 8.25 Hz, 2H, C*H*$_2$-Fmoc), 5.14 and 5.18 (two s, 2H, C*H*$_2$-Bn), 7.26-7.37 (m, 7H, ArC*H*-Bn and ArC*H*-Fmoc), 7.41 (m, 2H, ArC*H*-Fmoc), 7.56 (m, 2H, ArC*H*-Fmoc), 7.77 (m, 2H, ArC*H*-Fmoc), 13.45 (br sg, 1H, N*H*-Dde).

^{13}C NMR ($CDCl_3$, 126 MHz): two rotamers δ = 18.0 (*C*H$_3$-Dde), 26.2, 26.3 (DdeNH(CH$_2$)$_2$*C*H$_2$*C*H$_2$CH$_2$), 28.1, 28.3 (C(*C*H$_3$)$_2$-Dde), 28.9, 29, 29.7 (DdeNHCH$_2$*C*H$_2$(CH$_2$)$_2$*C*H$_2$), 43.4 (DdeNH*C*H$_2$), 47.2, 47.3 (*C*H-Fmoc), 48.8, 48.9

($CH_2CH_2NCH_2$), 49.2 (NCH_2CO), 52.8 (2 x CH_2-Dde), 67.0 (NCH_2COOCH_2), 67.3, 67.6 (CH_2-Fmoc), 107.8 (*C*=CNH), 120.0, 124.8, 124.9, 127.1, 127.7, 128.3, 128.4, 128.5, 128.6 (Ar*C*H-Bn and Ar*C*H-Fmoc), 135.3, 135.4 (Ar*C*-Bn), 141.3, 141.4 (Ar*C*-Fmoc), 143.9, 144 (Ar*C*-Fmoc), 156.5 (*C*=O-Fmoc), 159.0 (*C*OO), 169.5, 169.6 (NCH_2CO), 173.5 (C=*C*NH-Dde), 198.0 (*C*=O-Dde).

IR (neat): 2938 (w, ν_{C-H}), 2859 (w, ν_{C-H}), 1688 (w, $\nu_{C=O}$), 1573 (s, ν_{N-H}), 1244 (m, ν_{C-O}) cm^{-1}.

6.5.2.9.5. Synthesis of [(6-(4,4-dimethyl-2,6-dioxocyclo hexylidene)-hexyl)-(9*H*-fluoren-9-yl methoxycarbomyl)-amino]-acetic acid **4.48**

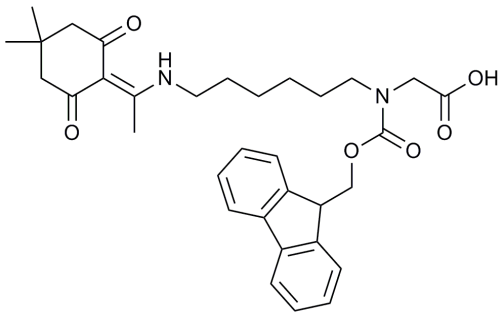

Pd/C 10% (315 mg) was added to a solution of **4.47** (6.15 g, 9.45 mmol) in ethanol (120 ml). The air was purged with N_2 for 30 minutes. N_2 was removed by suction (vacuum) and H_2 was slowly added thanks to a tap. The reaction was stirred under an atmosphere of H_2 for 4 hours. The reaction mixture was filtered through celite and the filtrate concentrated *in vacuo*. The product was filtrated through silica gel (DCM/MeOH, 10: 1) to yield **4.48** as a sticky white solid (2.71 g, 80%).

Analysis:

m/z (ES^+): $C_{33}H_{40}N_2O_6$ calculated 560.3, found 561.2 $[M+H]^+$ (100%), 583.2 $[M+Na]^+$ (58.8%), 599.2 $[M+K]^+$ (22.1%).

m/z (HRMS, ES^+): $C_{33}H_{40}N_2O_6$ calculated $[M+H]^+$ 561.29591, found 561.29578.

Rf: 0.25 (DCM/MeOH, 10: 1**).**

HPLC (Method 3): t_R = 5.9 min, purity = 98% (ELSD)

^{1}H NMR ($CDCl_3$, 500 MHz): two rotamers δ = 1.01 (s, 6H, 2 × C*H*$_3$-Dde), 1.09-1.69 (m, 8H, DdeNHCH$_2$(C*H*$_2$)$_4$CH$_2$), 2.33 (s, 4H, 2 × C*H*$_2$-Dde), 2.49 (s, 3H, C*H*$_3$-Dde),

3.16 (m, 2H, DdeNHCH_2), 3.38 (m, 2H, $CH_2CH_2NCH_2$), 3.97 (s, 2H, NCH_2CO), 4.15 and 4.23 (m, 1H, C*H*-Fmoc), 4.42 and 4.52 (two d, *J* = 6.72 Hz, 2H, CH_2-Fmoc), 7.31 (m, 2H, ArC*H*-Fmoc), 7.39 (m, 2H, ArC*H*-Fmoc), 7.58 (m, 2H, ArC*H*Fmoc), 7.75 (m, 2H, ArC*H*-Fmoc), 13.35 (br sg, 1H, N*H*-Dde).

^{13}C NMR ($CDCl_3$, 126 MHz): two rotamers δ = 18.0 (CH_3-Dde), 26.1, 26.6 ($DdeNH(CH_2)_2CH_2CH_2CH_2$), 28.1, 28.3 ($C(CH_3)_2$-Dde), 28.9, 30.0 ($DdeNHCH_2CH_2(CH_2)_2CH_2$), 43.4 ($DdeNHCH_2$), 47.1, 47.2 (*C*H-Fmoc), 48.4 ($CH_2CH_2NCH_2$), 48.9 (NCH_2CO), 52.7 (2 x CH_2-Dde), 67.8 (CH_2-Fmoc), 107.7 (*C*=CNH), 119.9, 124.8, 125.2, 127, 127.1, 127.6, 127.7 (Ar*C*H-Fmoc), 141.2, 141.3 (Ar*C*-Fmoc), 143.9, 144.0 (Ar*C*-Fmoc), 156.2 (*C*=O-Fmoc), 163.0 (NCH_2COOH), 173.6 (C=*C*NH-Dde), 198.1 (*C*=O-Dde).

IR (neat): 3354 (m, ν_{O-H}), 2963 (w, ν_{C-H}), 2864 (w, ν_{C-H}), 1696 (m, $\nu_{C=O}$), 1572 (s, ν_{N-H}), 1368 (m, ν_{C-O}) cm^{-1}.

Mp: 72.5-74 ^oC

6.5.2.9.6. Synthesis of [(6-aminohexyl)-(9*H*-fluoren-9-yl methoxy carbomyl)-amino]-acetic acid **4.49**

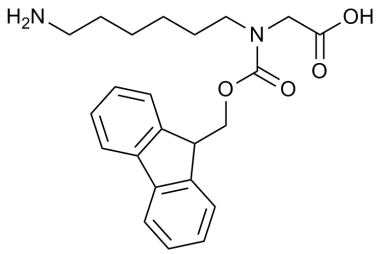

50 mg of **4.48** (89.2 mmol) were dissolved in 1 mL of DCM and 1 mL of Dde deprotection solution (**6.4.2.9.1**) was added to the monomer. The mixture was stirred for 6 hours at room temperature. The solvents were removed under vacuum. The crude of the reaction was analysed by HPLC, MS and ^{1}H-NMR.

	Dde monomer, **4.48**	Crude after deprotection
HPLC (Method 3, min, ELSD)	5.9 (99%)	4.7 (100%)
MS (ES^+)	561.2	397.2 (**4.49**)

^{1}H NMR of the crude ($CDCl_3$, 500 MHz): two rotamers δ = 1.12-1.25 (m, 4H, $CH_2CH_2CH_2CH_2CH_2CH_2NH_2$), 1.32-1.47 (m, 4H, $CH_2CH_2CH_2CH_2CH_2CH_2NH_2$), 1.78 (s, 2H, CH_2NH_2), 2.63 (m, 2H, $CH_2CH_2NH_2$), 3.31 (m, 2H, $CH_2CH_2NCH_2$), 3.94 (s, 2H, NCH_2CO); 4.13 and 4.19 (m, 1H, C*H*-Fmoc), 4.39 and 4.50 (two d, *J* = 6.75 Hz, 2H, CH_2-Fmoc), 7.36 (m, 2H, ArC*H*-Fmoc), 7.44 (m, 2H, ArC*H*-Fmoc), 7.62 (m, 2H, ArC*H*-Fmoc); 7.79 (m, 2H, ArC*H*-Fmoc).

6.5.2.9.7. Synthesis of the Fmoc-9mer(Dde)$_9$ resin **4.50**

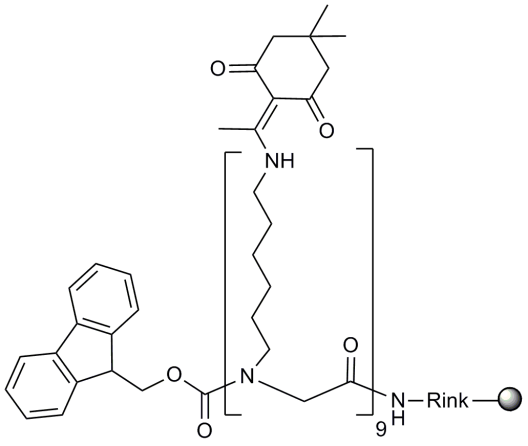

The Fmoc-9mer(Dde)$_9$-resin **4.50** was synthesised on aminomethyl polystyrene resin functionalized with a Rink amide linker (**2.28**) using the Dde monomer **4.48**. The resin (100 mg, 0.086 mmol) was first swollen in DCM (1 mL) for 20 minutes. Each peptoid monomer unit (146 mg, 0.26 mmol) was coupled using DIC/HOBt (40.6 µL/35 mg, 0.26 mmol) in DMF (1.3 mL, 0.2 M) coupling (**6.2.1.8**). The first monomer coupling was monitored by qualitative ninhydrin test (**6.2.1.1**), while the following Fmoc deprotections and couplings were controlled using chloranil test (**6.2.1.3**). After coupling, Fmoc deprotection was carried out using 20% piperidine in DMF (**6.2.1.9**). These reactions corresponded to one coupling cycle. This coupling cycle was repeated 8 other times in order to obtain the desired oligomer. It was essential to control each coupling very carefully before moving on with the Fmoc deprotection. Each slightly blue chloranil test leaded to a new coupling. The final N-terminal Fmoc group was not deprotected. The resin was washed with DMF, DCM, MeOH and Et_2O (3 × 1.5 mL) before

being dried over night at 40°C under vacuum (645 mg, new theoretical loading = 0.19 mmol/g).

6.5.2.9.8. Synthesis of Fmoc-9mer(Dde)$_9$ peptoid **4.51**

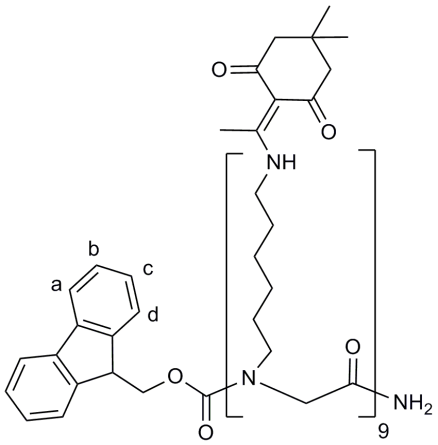

The Fmoc-9mer(Dde)$_9$ peptoid **4.51** was cleaved from the previously prepared solid support **4.50** (100 mg, 0.019 mmol) using a solution TFA/TIS/H_2O (95: 2.5: 2.5, 2.5 mL) (**6.2.1.10**). Fmoc-9mer(Dde)$_9$-NH_2 **4.51** was isolated after purification (preparative reverse phase-HPLC, Gradient 4) as a clear yellowish solid (30 mg, 51%).

Analysis:

m/z (MALDI-TOF): $C_{177}H_{265}N_{19}O_{29}$ calculated 3120.98, found 3144.25 $[M+Na]^+$ (100%), 3122.29 $[M+H]^+$ (51.2%).

m/z (FT-MS): $C_{177}H_{265}N_{19}O_{29}$ calculated $[M+4H]^{4+}$ = 781.25396, found 781.25408.

HPLC (Method 3): t_R = 6.5 min, purity > 98% (ELSD).

^{1}H NMR ($CDCl_3$, 500 MHz) δ = δ 1.02 (s, 54H, C(C*H*$_3$)$_2$-Dde), 1.58-1.72 (m, 72H, DdeNHCH$_2$(C*H*$_2$)$_4$CH$_2$), 2.34 (s, 36H, 2 × C*H*$_2$-Dde), 2.40 (s, 27H, C*H*$_3$-Dde), 3.03 (t, *J* = 5.60 Hz, 18H, CH$_2$C*H*$_2$NCH$_2$), 3.22-3.44 (m, 18H, DdeNHC*H*$_2$), 3.85-4.28 (m, 21H, 18H for NC*H*$_2$CO, 1H for C*H*-Fmoc, 2H for C*H*$_2$-Fmoc), 7.29 (td, *J* = 7.55 Hz, *J* = 1.10 Hz, 2H, ArC*Hc*-Fmoc), 7.37 (td, *J* = 7.45 Hz, *J* = 1.05 Hz, 2H, ArC*Hb*-

Fmoc), 7.68 (dt, *J* = 7.45 Hz, *J* = 0.75 Hz, 2H, ArC*Hd*-Fmoc), 7.75 (dt, *J* = 7.50 Hz, *J* = 0.80 Hz, 2H, ArC*Ha*-Fmoc), 13.38 (br sg, 9H, N*H*-Dde).

^{13}C NMR ($CDCl_3$, 126 MHz) δ = 17.6 (*C*H_3-Dde), 22.7, 23, 23.2, 25.7, 26.2, 26.6 (DdeNHCH$_2$(CH$_2$)$_4$*C*H$_2$), 28.1, 28.2, 29.1 (C(*C*H$_3$)$_2$-Dde), 43.3, 43.4 (DdeNH*C*H$_2$), 44.7 (CH$_2$*C*H$_2$NCH$_2$), 47.9 (*C*H-Fmoc), 48.8, 49.2, 49.7, 50.3 (N*C*H$_2$CO), 50.9, 51.5, 52.3, 52.8 (2 x *C*H$_2$-Dde), 56.2 (*C*H$_2$-Fmoc), 107.7, 107.8 (*C*=CNH), 119.6(Ar*C*H-Fmoc, Cd), 120.9 (Ar*C*H-Fmoc, Ca), 126.9 (Ar*C*H-Fmoc, Cc), 128.7 (Ar*C*H-Fmoc, Cb), 138.0, 140.1, 143.2 (Ar*C*-Fmoc), 156.2 (*C*=O-Fmoc), 162.0, 162.2, 162.5, 162.6, 162.8 (NH*C*O-peptoid), 173.4, 173.5, 173.6 (C=*C*NH-Dde), 195.8, 196.4 (*C*=O-Dde).

6.5.2.9.9. Synthesis Fmoc-9mer **4.52** via physiologic Dde deprotection of the peptoid **4.51**

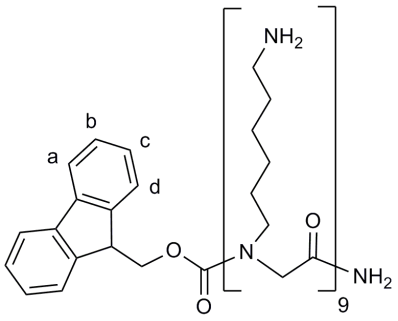

The peptoid **4.51** (20 mg, 0.006 mmol) was mixed overnight in 1 mL of the Dde deprotection solution (**6.4.2.9.1**). The water was removed *in vacuo* and the crude was dissolved in a minimum of TFA (150 µL) and precipitated in cold Et_2O (1.5 mL). The Fmoc-9mer peptoid (**4.55**) was dried at 40°C under vacuum and was isolated as a slightly sticky white solid (10 mg, 94%).

Analysis:

m/z (ES^+): $C_{87}H_{157}N_{19}O_{11}$ calculated 1644.23, found 823.0 $[M+2H]^{2+}$ (6.7%), 549.1 $[M+3H]^{3+}$ (54.3%), 412.0 $[M+4H]^{4+}$ (100%), 329.8 $[M+5H]^{5+}$ (39.3%).

m/z (MALDI-TOF): $C_{87}H_{157}N_{19}O_{11}$ calculated 1644.23, found 1644.1 $[M+H]^+$ (100%), 1667.0 $[M+Na]^+$ (48.5%).

HPLC (Method 3): t_R = 2.2 min, purity = 100% (ELSD).

6.5.2.9.10. Synthesis of the Fmoc-9mer peptoid **4.52**

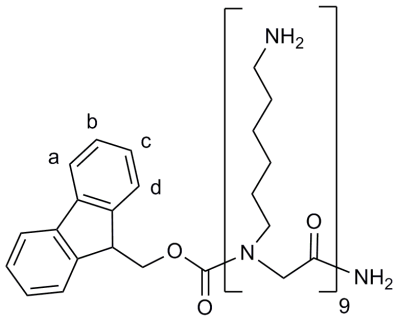

Fmoc-9mer-NH_2 **4.55** was isolated from the resin **2.33** (50 mg, 0.04 mmol, **6.3.6**) by TFA treatment (**6.2.1.10**) as a sticky white solid (63 mg, 95%).

Analysis:

m/z (ES^+): $C_{87}H_{157}N_{19}O_{11}$ calculated 1644.23, found 823.0 $[M+2H]^{2+}$ (6.7%), 549.1 $[M+3H]^{3+}$ (54.3%), 412.0 $[M+4H]^{4+}$ (100%), 329.8 $[M+5H]^{5+}$ (39.3%).

m/z (MALDI-TOF): $C_{87}H_{157}N_{19}O_{11}$ calculated 1644.23, found 1645.6 $[M+H]^+$ (100%), 1666.5 $[M+Na]^+$ (37.8%).

m/z (FT-MS): $C_{87}H_{157}N_{19}O_{11}$ calculated $[M+3H]^{3+}$ 549.44031, found 549.42374.

HPLC (Method 3): t_R = 2.2 min; purity = 98% (ELSD).

^{1}H NMR (D_2O, 500 MHz, presat water suppression): δ = 1.00-1.70 (m, 72H, $NCH_2(CH_2)_4CH_2NH_2$) , 2.90 (m, 18H, CH_2NH_2), 3.11-3.37 (m, 2H, NCH_2), 3.82-4.47 (m, 21H, 3H for C*H*-Fmoc and CH_2-Fmoc, and 18H for NCH_2CO), 7.35 (m, 2H, ArC*H*-Fmoc, Hc), 7.43 (m, 2H, ArC*H*-Fmoc, Hb), 7.59 (m, 2H, ArC*H*-Fmoc, Hd), 7.80 (m, 2H, ArC*H*-Fmoc, Ha), 7.84 (br sg, 2H, $CONH_2$).

^{13}C NMR (D_2O, 126 MHz): δ = 25.2, 25.3, 25.4, 25.5, 25.6, 25.7, 25.8, 26.5, 26.6, 26.7, 26.8 ($NCH_2(CH_2)_4CH_2NH_2$), 39.3, 39.4, 39.5, 39.6 (CH_2NH_2), 46.6, 47.3, 47.4, 47.5, 47.7, 47.8, 47.9, 47.9, 48.0, 481, 48.2, 48.3, 48.4, 48.5 (*C*H-Fmoc, CH_2-Fmoc, NCH_2CO and NCH_2CH_2), 120.1 (ArCH-Fmoc, Ca), 124.7 (ArCH-Fmoc, Cd), 127.5 (ArCH-Fmoc, Cc), 127.8 (ArCH-Fmoc, Cb), 141.0, 141.3, 141.7 (ArC-Fmoc), 153.2 (*C*=O-Fmoc), 162.7, 163.0, 163.3 (*C*=O-9mer).

6.5.2.9.11. Stability of the OPfp ester

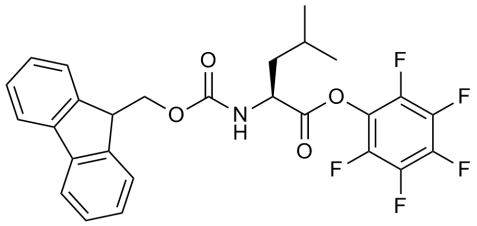

50 mg of Fmoc-Leu-OPfp **4.53** (0.096 mmol) was dissolved in 1 mL of DCM and the appropriate solution of TFA in DCM was added:

- 1% of TFA: 0.02 mL of TFA in 0.98 mL of DCM,
- 5% of TFA: 0.10 mL of TFA in 0.90 mL of DCM,
- 10% of TFA: 0. 20 mL of TFA in 0.80 mL of DCM,
- 25% of TFA: 0.50 mL of TFA in 0.50 mL of DCM,
- 50% of TFA: 1 mL of TFA.

After 15, 30, 60, 90, 120 minutes and 6 hours of stirring, 0.2 mL of each solution was collected and mixed with 1 mL of Et_3N in DCM. Each collection sample was analysised by HPLC (ELSD) and mass spectroscopy.

Analysis:

Starting materiel:

m/z (ES^+): $C_{27}H_{22}FNO_4$ calculated 519.1, found 520.2 $[M+H]^+$ (100%).

HPLC (Method 1): t_R = 5.1 min, purity = 100% (ELSD).

Fmoc-Leu-OH (without active ester):

m/z (ES^+): $C_{21}H_{23}NO_4$ calculated 353.2, found 354.1 $[M+H]^+$ (14.6%), 376.1 $[M+Na]^+$ (100%).

HPLC (Method 1): t_R = 4.6 min, purity = 100% (ELSD).

Reaction analysis:

All the reactions gave the same results (Full data and graph: **Appendix 4-9**):

m/z (ES^+): $C_{27}H_{22}FNO_4$ calculated 519.1, found 520.2 $[M+H]^+$ (100%).

HPLC (Method 1): t_R = 5.1 min, purity = 100% (ELSD).

6.5.2.9.12. Cyclisation of the 3,6,9 trioxaudecanedioic acid **4.54**[330]

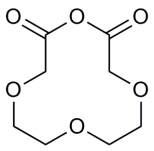

5 g of 3,6,9 trioxaudecanedioic acid (22.5 mmol) were dissolved in 100 mL of DCM before adding the DCC (4.6 g, 22.5 mmol). The solution was stirred for 6 hours. The reaction mixture was then filtered and concentrated *in vacuo* down to a volume of 15 mL. The required volume of solution of **4.54** was directly added onto the desired solid support without further purification.

6.5.2.9.13. Synthesis tested for OPfp-PEG-9mer(Dde)$_9$ **4.57**

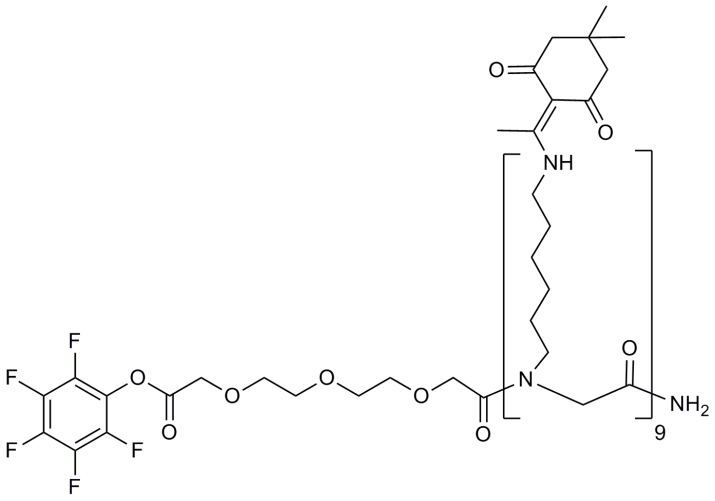

Resin **4.50** (50 mg, 9.5 µmol) was swollen in DCM for 20 minutes. The Fmoc group was deprotected (**6.2.1.9,** confirmed by a chloranil test **6.2.1.3**) and the cyclised PEG **4.54** (0.5 mL, 750 µmol) in 0.5 mL of DCM was added to the resin. The mixture was stirred for 16 hours. DCC (6 mg, 28.5 µmol) in DCM (0.5 mL) was first mixed with the resin for 30 minutes before adding the pentafluorophenol **4.56** (5 mg) in DCM (0.5 mL). The mixture was stirred for 6 hours. The peptoid was then

cleaved from the solid support using a 4 hour treatment of 50% of TFA in DCM. After the TFA treatment, the solvent was removed *in vacuo* and the crude analysed. The product isolated corresponded to H-9mer(Dde)$_9$-NH$_2$.

Analysis:

m/z (MALDI-TOF): $C_{176}H_{266}N_{19}O_{33}$ calculated 3268.9, found 2900.2 $[M+H]^+$ (100%) H-9mer(Dde)$_9$-NH$_2$, 3122.3 $[M+H]^+$ (9.8%).

HPLC (Method 1): t_R = 4.6 min; purity = 98% (ELSD) corresponding to H-9mer(Dde)$_9$-NH$_2$.

6.5.3. Experimental for eGFP plasmid delivery

The eGFP DNA plasmid (pEGFP-C1) was prepared by members of the Bradley group (0.4 µg/µL in TE buffer, 4.7 kb, 1534 kDa calculated from average Mw base = 327.0 g/mol).

6.5.3.1. Preparation of agarose gel (0.7%) for electrophoresis analysis

Gel preparation and running conditions:

0.245 g of agarose type I-B was mixed with 35mL of TEB (pH 7.5). The agarose was diluted by heating the mixture at 60°C (water bath) for 20 minutes. 2.5 µL of ethidium bromide (10 mg/mL in water, Sigma-Aldrich) were added to the solubilised agarose. The solution was heated for 15 minutes in a boiling water batch (100°C) before being poured into a electrophoresis casting mould containing the desired comb. The gel was left to set for 45 minutes at room temperature and the comb was carefully removed. Each well was filled with the sample to analyse. The gel was then covered with TBE buffer and ran for 56 minutes at 90 V. The gels were viewed and photographed under UV-light.

Sample preparation:

Maker: Ladder 1KB from New England Biolab 10 µL + 10 µL of water.

Sample: 5 µL of reaction (0.05 µg of DNA) + 15 µL of water + 5 µL of bromophenol blue. Each sample was quickly mixed using a Vortex.

6.5.3.2. Determination of the DNA/peptoid ratio by gel retardation assays

Each solution was prepared as described in **Table 6.47**. Both peptoid **2.37** (Rho-9mer) and **4.61** (HO-PEG-PEG-9mer) were dissolved in PBS to a final concentration of 100 µM.

The DNA (pEGFP-C1) was first mixed with the PBS (pH 7.4) and the peptoid was added. The solution was quickly mixed using a vortex before being stirred for 30 minutes at 25°C, 1400 rpm (Thermonix). The mixtures were analysed via electrophoresis.

Charge ratio DNA/peptoid	Volume DNA (µL) (0.4 µg/µL)	Volume of peptoid (**2.37** or **4.61**, 100 µM)	Volume of PBS
1: 2	2.5 µL	3.4 µL	94.1 µL
1: 5	2.5 µL	8.5 µL	89.0 µL
1: 10	2.5 µL	17.0 µL	80.5 µL
1: 20	2.5 µL	34.0 µL	63.5 µL
1: 30	2.5 µL	51.0 µL	46.5 µL
1: 40	2.5 µL	68.0 µL	29.5 µL
1: 50	2.5 µL	85.0 µL	12.5 µL

Table 6.47: Volumes of reagents used for the DNA complexation assays.

6.5.3.3. Cells assays of DNA/peptoid complex in HEK293T cells

Lipofection with Lipofectamine™ 2000:

For each tranfection sample (triplicate), 2 µL eGFP plasmid (0.8 µg, 0.4 µg/µL) were diluted in 50 µL of Opti-MEM® medium and gently mixed. 2 µL of Lipofectamine™ 2000 was gently mixed with 20 µL of Opti-MEM® medium and then incubated for 5 minutes at 25°C. The diluted DNA was combined with the transfecting agent, mixed gently and incubated for 20 minutes at 25°C to allow complex formation to occur. This solution was added to cells.

Cells were seeded onto a 24-well plate at a density of 3×10^4 cells/well in growth media (DMEM, volume of culture media per well: 350 µL). Once the cell confluence was between 70 and 90% (usually 24 hours), the growth media was removed, the cells were washed with PBS and new fresh serum- and antibiotic free Opti-MEM® medium was added (500 µL). The well plate was incubated (37°C/5% $CO_{2)}$ for one hour before addition of the DNA/lipofectamine complexes. Cells were incubated for 24 and 48 hours prior to analysis by flow cytometry.

Transfection using peptoid:

4 µL of eGFP plasmid (1.6 µg, 1 pmol) was diluted with 14 µL pf PBS (pH 7.4). 102 µL of Rho-9mer **2.37** or HO-PEG-PEG-9mer-NH_2 (**4.61**) (100 µM, 10.46 nmol) were added and the solution was quickly vortexed before being stirred for 30 minutes at 25°C (Thermomix, 1400 rpm). This solution was then added to cells (one third, 40 µL of complex solution per well plate).

Cells were seeded onto a 24-well plate at a density of 3×10^4 cells/well in growth media (DMEM, volume of culture media per well: 350 µL). Once the cell confluence was between 70 and 90% (usually 24 hours), the DNA/peptoid complexes were added (0.5 µg of DNA/well). Cells were incubated for 24 and 48 hours prior to analysis by flow cytometry and microscopy (for **4.58** after 48 hours).

Results:

*Cellular uptake of **4.58***

	Incubations	Average (%)	Error (%)
Untreated cells		0.3	0.2
pEGFP	24 h	1.4	0.6
	48 h	1.6	0.5
2.37, Rho-9mer	24 h	1.7	0.2
	48 h	2.3	0.8
4.58, pEGFP/Rho-9mer	24 h	2.8	0.3
	48 h	20.7	2.6
Lipofectamine/pEGFP	24 h	10.0	1.4
	48 h	41.0	3.1

Table 6.48: Cellular uptake of HEK293T cells transfected (for 24 and 48 hours) with plasmid pEGFP-C1 using Rho-9mer (4.58) and lipofectamine as positive control (n = 3).

*Cellular uptake of **4.62***

	Average (%)	Error (%)
Untreated cells	0.4	0.2
pEGFP	1.8	0.8
4.61, PEG-9mer	0.7	0.6
4.62, pEGFP/PEG-9mer	26.9	1.3
Lipofectamine/pEGFP	48.4	0.5

Table 6.49: Cellular uptake of HEK293T cells transfected (for 48 hours) with plasmid pEGFP-C1 using PEG-9mer (4.62) and lipofectamine as positive control (n = 3).

6.5.3.4. Confocal microscopy in HEK293T using the DNA/Rho-9mer complex **4.58**

6.3 µL of eGFP plasmid (2.5 µg, 1.6 pmol) was diluted with 14 µL pf PBS (pH 7.4). 160 µL of Rho-9mer **2.37** (100 µM) were added and the solution was quickly vortexed before being stirred for 30 minutes at 25°C (Thermomix, 1400 rpm). This solution was then added to cells.

HEK293T cells were seeded on a 6-well plate, stained and analysed as described in **6.2.2.5**. The cells were labelled for 24 hours with 180 µL of DNA/Rho-9mer complex (**4.61**) prior to imaging (2.5 µg of DNA/well). The rhodamine dye on the Rho-9mer peptoids **2.37** was excited using a 561 nm excitation laser and collecting emission using a 567-630 nm band-pass filter. GFP was excited using a 490 nm excitation laser and collecting emission using a 528-550 nm band-pass filter.

6.5.3.5. DNA delivery in lymph node cells (collaboration with Dr. Stefano Caserta)

Complexation:

10 and 20 µL of Rho-9mer (**2.37**, 100 µM) were mixed (vortex) with respectively 90 and 80 µL of PBS. The desired amount of DNA (0.4 µg/µL, 0.1, 0.5, 1, 5 and 10 µg) was then added to the peptoid solution before being vortexed. The DNA/peptoid solutions were gently mixed (Thermonix, 600 rpm) at 4°C for 30 minutes. Afterwards, the solutions were directly added to the cells.

Cellular uptake

Lymph node cells were seeded at a density of 2×10^6 cells/well ((cultured with cytokines, volume of culture RPMI per well: 350 µL). Once cells settled as a monolayer, the DNA/peptoid solutions were added. T cells were stimulated with plate-bound 5 µg/mL anti-CD3 (145-2C11, BD Pharmingen) and 2 µg/mL anti-CD28 (37.51, BD Pharmingen) for 24 hours during incubation with the peptoids. After 4 days of incubation with the complexes, cells were washed with PBS and analysed using a flow cytometer (LSR II, BD).

6.5.3.6. Synthesis of the HO-PEG-PEG-9mer **4.61**

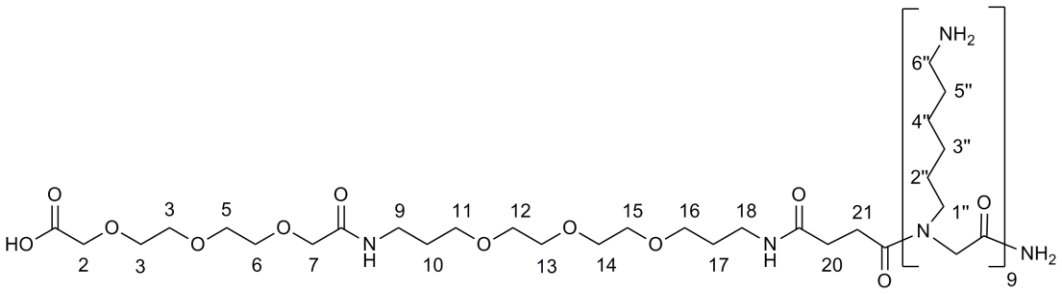

The HO-PEG-PEG-9mer peptoid **4.61** was synthesised on aminomethyl polystyrene resin functionalized with a Rink amide linker (**2.28**) using the monomer **2.22** as described in ***6.3.6***. The solid supported 9mer peptoid was then coupled to the Fmoc-PEG-spacer **4.62** (Sigma-Aldrich) (71 mg, 0.13 mmol) using the coupling procedure **6.2.1.8** (DIC: 20.3 µL, HOBt: 18 mg, 0.13 mmol; DMF: 0.65 mL, 0.2 M). The success of the coupling was controlled by a chloranil test (**6.2.1.3**). Afterwards, the Fmoc group was deprotected with 20% piperidine in DMF (**6.2.1.9)** and controlled by qualitative ninhydrin test (**6.2.1.1**). The cyclised PEG **4.57** (1 mL, 1.5 mmol) in DCM (1 mL) was added to the solid supported peptoid and mixed overnight at room temperature. The final coupling was monitored by qualitative ninhydrin test (**6.2.1.1**). Finally, the HO-PEG-PEG-9mer peptoid was deprotected and cleaved from the solid support using a solution TFA/TIS/H_2O (95: 2.5: 2.5, 2.5 mL) (**6.2.1.10**). HO-PEG-PEG-9mer **4.64** was isolated after ON drying (vacuum oven, 40^oC) as a sticky clear product in 92% yield (73 mg).

Analysis:

m/z (ES^+): $C_{94}H_{185}N_{21}O_{20}$ calculated 1929.6, found 644.0 $[M+3H]^{3+}$ (51.2%), 483.3 $[M+4H]^{4+}$ (100%), 396.9 $[M+5H]^{5+}$ (13.3%).

m/z (MALDI-TOF): $C_{94}H_{185}N_{21}O_{20}$ calculated 1929.60, found 1953.05 $[M+Na]^+$ (100%), 1930.69 $[M+H]^+$ (43.1%).

m/z (FT-MS): $C_{107}H_{187}N_{22}O_{14}^+$ calculated $[M+3H]^{3+}$ = 644.20852, found 644.20811.

HPLC (Method 3): t_R = 0.6 min. purity > 98% (ELSD).

^{1}H NMR (D_2O, 500 MHz, eSpresat water suppression): δ = 1.25-1.50 (m, 36H, C*H*$_2$, H $_{3''}$ and H$_{4''}$), 1.51-1.79 (m, 40H, 36H for C*H*$_2$ (H $_{2''}$ and H$_{5''}$) and 4H for C*H*$_2$ (H $_{10}$ and H$_{17}$)), 2.34-2.45 (m, 2H, C*H*$_2$, H$_{20}$), 2.48-2.60 (m, 2H, C*H*$_2$, H$_{20}$), 3.00-3.16 (m, 18H, C*H*$_2$NH$_2$, H$_{6''}$), 3.18-3.38 (m, 22H, 18H for C*H*$_2$N (H$_{1''}$), 4H for C*H*$_2$NH (H$_9$ and H$_{18}$)), 3.40-3.66 (m, CH$_2$O, H$_{3, 4, 5, 6, 11, 12, 13, 14, 15, 16}$), 3.72-4.36 (m, 22H, 18H for NC*H*$_2$CO (H$_\alpha$), 4H for OC*H*$_2$CO (H$_2$ and H$_7$), 7.52 (br sg, 2H, CON*H*$_2$).

^{13}C NMR (D_2O, 126 MHz): δ = 24.8, 25.0, 25.1, 25.2, 25.3, 25.4, 25.5, 26.2, 26.3, 26.4, 26.5, 26.6, 27.0, 27.1, 27.2, 27.3, 27.4 (*C*H$_2$, *C*$_{2'', 3'', 4'', 5'', 10, 17}$), 37.7, 37.9 (*C*H$_2$, C$_{20, 21}$), 39.1, 39.2, 39.3, 39.4, 39.5, 39.7 (*C*H$_2$, *C*$_{6'', 9,}$ 18), 47.2, 47.3, 47.4,47.5, 47.6, 48.4, 48.5, 48.6, 48.7 (*C*H$_2$, N-*C*H$_2$-CO and *C*$_{1''}$), 69.7, 69.8, 71.2, 71.4, 71.5 (*C*H$_2$O, H$_{3, 4, 5, 6, 11, 12, 13, 14, 15, 16}$), 158.9, 162.4, 162.7, 163.0, 163.3, 169.5, 169.6, 170, 174.5 (*C*=O-9mer and PEG), 176.2 (*C*OOH).

6.5.3.7. MTT assays of DNA/peptoid complex in HEK293T cells

MTT cytotoxicity assays were carried out as according to the general procedures (**6.2.2.4**).

Cells were seeded onto a 96-well plate. Once the cell confluence was between 70 and 90% (usually 24 hours), the cells were treated with 10.8 µL of **4.58** and **4.62** (0.1 µg of DNA /well), 13 µL of Rho-9mer (**2.37**, 100 µM, final concentration 13 µM) and of PEG-9mer (**4.61**, 100 µM, final concentration 13 µM) and 2.5 µL of eGFP plasmid (0.04 µg/µL, 0.1 µg of DNA/well) in 8 random wells. At day 2, 10.8 µL of **4.61** (0.1 µg of DNA/well), 13 µL of Rho-9mer (**2.37**, 100 µM, final concentration 13 µM) and 2.5 µL of eGFP plasmid (0.04 µg/µL, 0.1 µg of DNA/well) were

injected in 8 random wells. At day 3, the wells were treated and read on a microplate reader.

	Average (arb. units)	Error (arb. units)	Average (%)	Error (%)
Untreated cells	1.097	0.077	100.0	7.0
pEGFP, 24 hours	0.988	0.129	90.1	11.7
pEGFP, 48 hours	1.078	0.098	98.3	8.9
2.37, Rho-9mer, 24 hours	1.054	0.141	96.1	12.9
2.37, Rho-9mer, 48 hours	1.110	0.193	101.2	17.5
4.58, pEGFP/Rho-9mer, 24 hours	1.048	0.152	95.6	13.8
4.58, pEGFP/Rho-9mer, 48 hours	1.123	0.107	102.4	9.7
4.61, PEG-9mer, 48 hours	1.063	0.134	97.0	12.2
4.62, pEGFP/PEG-9mer, 48 hours	1.124	0.166	102.5	15.1

Table 6.50: Percentage of cell vailability (HEK293T cells) after 24 and 48 hours of incubation with the DNA/peptoid complexes (n = 8).

6.6. Experimental for Chapter 5

6.6.1. Preparation of the Fmoc-9mer(Boc) resin (**2.33**) using the oxyma reagent.

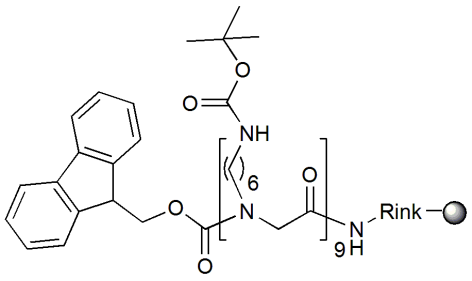

The 9mer peptoid resin **2.33** was prepared as previously described in ***6.3.6*** but in this synthesis the HOBt was substituted with Oxyma. New theoretical loading (**6.2.1.5**) calculated from the measured Rink amide resin (**6.3.5**) was 0.27 mmol/g.

6.6.2. Synthesis of the NLLP (**5.17**) without purification

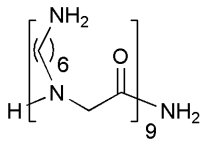

The resin **2.32** (**6.6.1**, 300 mg, 0.081 mmol from theoretical loading) was deprotected using 20% piperidine in DMF (**6.2.1.9**) and then fully deprotected and cleaved from its support by treatment of the cleavage mixture TFA/TIS/ H_2O (95: 2.5: 2.5, 7.5 mL) and precipitated in cold Et_2O (**6.2.1.10**). The compound **5.17** was isolated as a very hydroscopic white solid 201 mg.

Analysis:

m/z (ES^+): $C_{72}H_{147}N_{19}O_9$ calculated 1422.2, found 712.2 $[M+2H]^{2+}$ (32.5 %), 475.2 $[M+3H]^{3+}$ (100%), 356.6 $[M+4H]^{4+}$ (71.8%), 285.5 $[M+5H]^{5+}$ (8.9%). Peaks of the 8mer: 634.0 $[M+2H]^{2+}$ (9.7%), 317.5 $[M+3H]^{3+}$ (41.9%), 423.0 $[M+4H]^{4+}$ (18.4).

m/z (MALDI-TOF): $C_{72}H_{147}N_{19}O_9$ calculated 1422.16, found 1423.48 $[M+H]^+$ (100%), 1445.47 $[M+Na]^+$ (38.7%). Peaks of the others peptoids: 8mer 1288.40 $[M+H]^+$ (47.2%), 7mer 1109.91 $[M+H]^+$ (14.3%), 6mer 953.83 $[M+H]^+$ (8.4%).

HPLC (Method 3): t_R= 0.84 min, purity > 98% (ELSD).

6.6.3. Stability of Boc under TFA conditions on solution phase: Test on the Fmoc-Lys(Boc)-OH

The stability of the Boc group was tested in solution phase against TFA using Fmoc-Lys(Boc)-OH.

Protocol

25 mg of (0.021 mmol) of Fmoc-Lys(Boc)-OH were dissolved in DCM (0.5 mL) and the following volumes of DCM, H_2O and TFA were added (**Table 6.51**). The mixture was mixed at room temperature for 2 hours. Every 15 minutes, a sample of 15 µL was collected and added in 100 µL of MeOH containing 3% of Et_3N (to neutralise the TFA). Each sample was then analysed by HPLC and MS.

Solution	Volume added (mL)		
	DCM	H_2O	TFA
1% TFA/DCM	0.5	0	0.01
2% TFA/DCM	0.5	0	0.02
3% TFA/DCM	0.5	0	0.03
4% TFA/DCM	0.5	0	0.04
5% TFA/DCM	0.5	0	0.05
10% TFA/DCM	0.5	0	0.10
15% TFA/DCM	0.5	0	0.15
20% TFA/DCM	0.5	0	0.20
1% TFA in DCM/H_2O (99:1)	0	0.5	0.01
2% TFA in DCM/H_2O (99:1)	0	0.5	0.02

3% TFA in DCM/H_2O (99:1)	0	0.5	0.03
4% TFA in DCM/H_2O (99:1)	0	0.5	0.04
5% TFA in DCM/H_2O (99:1)	0	0.5	0.05
10% TFA in DCM/H_2O (99:1)	0	0.5	0.10
15% TFA in DCM/H_2O (99:1)	0	0.5	0.15
20% TFA in DCM/H_2O (99:1)	0	0.5	0.20

Table 6.51: Preparation of the various TFA solution used for the Boc stability study.

Results

Analysis of Fmoc-Lys(Boc)-OH as a positive control:

m/z (ES^+): $C_{26}H_{32}N_2O_6$ calculated 468.2, found 369.1 $[M\text{-}Boc+H]^+$ (100%), 491.1 $[M+Na]^+$ (53.8%), 469.1 $[M+H]^+$ (17.3%).

HPLC (Method 1): t_R = 4.5 min, purity = 100% (ELSD).

Analysis of Fmoc-Lys-OH as a negative control:

m/z (ES^+): $C_{21}H_{24}N_2O_4$ calculated 368.2, found 369.0 $[M+H]^+$ (100%), 391.0 $[M+Na]^+$ (10.2%).

HPLC (Method 1): t_R = 3.6 min, purity > 98% (ELSD).

Solution	% of Fmoc-Lys-OH formed	
	30 minutes	2 hours
1% TFA/DCM	0	0
2% TFA/DCM	0	1
3% TFA/DCM	1	12
4% TFA/DCM	3	24
5% TFA/DCM	10	65
10% TFA/DCM	100	-
15% TFA/DCM	100	-
20% TFA/DCM	100	-
1% TFA in DCM/H_2O (99:1)	0	0
2% TFA in DCM/H_2O (99:1)	0	0
3% TFA in DCM/H_2O (99:1)	0	0
4% TFA in DCM/H_2O (99:1)	0	0
5% TFA in DCM/H_2O (99:1)	0	5
10% TFA in DCM/H_2O (99:1)	25	63
15% TFA in DCM/H_2O	63	90

(99:1)		
20% TFA in DCM/H_2O (99:1)	95	100

Table 6.52: Results of the Boc group stability against TFA.
Method 1, ESLD. (Full data: **Appendix 5-1**)

6.6.4. Preparation of the Fmoc-3mer(Boc)$_3$ resin (**5.19**)

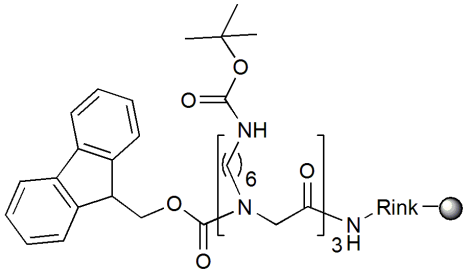

The Fmoc-3mer(Boc)$_3$ resin **5.19** was prepared as previously described for **2.33** using oxyma (3 couplig cycles). The final Fmoc deprotection was not carried out. The resin was washed with DMF (3 x 3 mL), DCM (3 x 3 mL), MeOH (3 x 3 mL), Et_2O (3 x 3 mL) and dried *in vacuo* for 30 minutes. The resin (321 mg) was stored under N_2 at -4^{o}C. The loading of the resin **5.19** was calculated using the quantitative ninhydrin test (0.46 mmol/g, **6.2.1.2**).

Characteristion of Fmoc-3mer-NH_2 peptoid (**5.20**)

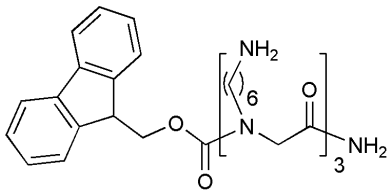

The compound **5.20** was isolated as 16 mg (95.4%) after cleavage and deprotection of **5.19** (50 mg, 0.023 mmol) (**6.2.1.10**).

Analysis:

m/z (ES^+): $C_{39}H_{61}N_7O_5$ calculated 707.5, found 708.5 $[M+H]^+$ (60.3%), 354.8 $[M+2H]^{2+}$ (100%).

m/z (MALDI-TOF): $C_{39}H_{61}N_7O_5$ calculated 707.47, found 708.46 $[M+H]^+$ (100%).

m/z (HMRS, ES^+): $C_{39}H_{61}N_7O_5$ calculated $[M+H]^+$ 708.48124, found 708.48131.

HPLC (Method 3): t_R = 2.6 min, purity > 97% (ELSD).

^{1}H NMR (D_2O, 500 MHz, eSpresat water suppression) δ = 1.25-1.40 (m, 12H, C*H*$_2$, H $_{3''}$ and H$_{4''}$), 1.40-1.68 (m, 12H, C*H*$_2$, H $_{2''}$ and H$_{5''}$), 2.93 (m, 6H, C*H*$_2$NH$_2$, H$_{6''}$), 3.29 (m, 6H, C*H*$_2$N, H$_{1''}$), 3.83-4.00 (m, 6H, NC*H*$_2$CO, H$_\alpha$), 4.32 (t, *J* = 7.05 Hz, 1H, C*H*-Fmoc), 4.45 (d, *J* = 7.50 Hz, 2H, C*H*$_2$-Fmoc), 7.60 (m, 2H, ArC*H*), 7.71 (m, 2H, ArC*H*), 7.81 (d, J = 8.65 Hz, 2H, ArC*H*), 7.89 (d, *J* = 8.95 Hz, 2H, ArC*H*).

^{13}C NMR (D_2O, 126 MHz) δ = 25.1, 25.4, 25.5, 25.6, 26.4, 26.5, 27.1, 27.2, 27.3 (*C*H$_2$, *C*$_{2, 3, 4, 5}$), 39.2, 39.3, 39.4 (*C*H$_2$, *C*$_6$), 47.4, 47.5, 47.7, 48.4, 48.5, 48.6, 48.7 (*C*H$_2$ (N*C*H$_2$CO and *C*$_1$) and *C*H-Fmoc), 68.3 (*C*H$_2$-Fmoc), 120.0, 124.7, 127.4, 127.8 (Ar*C*H), 141.0, 141.2, 141.7 (Ar*C*), 162.4, 162.7, 162.8, 163.3, 169.5, 169.6, 170.0 (*C*=O-3mer), 178.2 (*C*=O-Fmoc).

6.6.5. Synthesis of the Fmoc-3mer(Boc)$_3$-NH$_2$ peptoid (**5.21**)

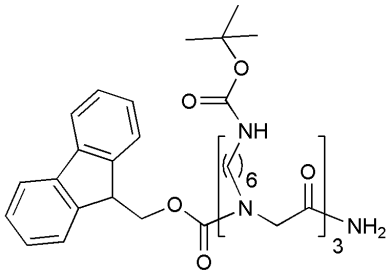

6.6.5.1. Strategy 1 : Selective Rink amide cleavage using low TFA conditions.

All the following experiments were carried out on 50 mg (0.023 mmol) of **5.19**. The resin was used dried and was mixed with 1.25 mL (25 mL/g of dry resin) of one of the following cleavage mixture. Two methods were tested:

- *Cycle*: the resin was treated at room temperature with the TFA solution (1.25 mL, **Table 6.54**) for 10 minutes. The resin was filtered, washed with DCM (3 × 1 mL) and a fresh solution was added to the resin. The filtrate was collected in 5 mL of DCM containing 3% of TEA. This cycle was repeated as needed (more details below). After each cycle, the filtrate was concentrated *in vacuo* and was analysed by HPLC and MS. The colour change of the resin was observed.

- *Constant*: the resin was treated with the TFA solution for 2 hours and a sample of the solution (50 µL) was collected after 30 minutes and 2 hours. Each sample was diluted in 1 mL of DCM containing 3% of TEA. Each sample was analysed by HPLC and MS. The colour change of the resin was observed and recorded.

Correspondance analysis/product:

Product	HPLC (ELSD) (Method 3, min)	MS (MALDI-TOF)
Fmoc-3mer-NH_2, **5.20**	2.6	708.46 $[M+H]^+$
Fmoc-3mer$(Boc)_1$-NH_2	3.6	808.52 $[M+H]^+$
Fmoc-3mer$(Boc)_2$-NH_2	3.7	908.35 $[M+H]^+$
Fmoc-3mer$(Boc)_3$-NH_2, **5.21**	4.2	1008.42 $[M+H]^+$

Table 6.53: Analysis of the several Boc protected 3mer peptoids.

Results for the method “cycle”:

Solution	Cycles	HPLC (ESLD) (Method 3, min)	MS (MALDI-TOF)	Resin colour
	1	2.7 (40%) 3.6 (39.5%) 3.7 (20.3%)	708.29 (11.9%) 808.32 (100%) 908.35	Yellow-orange

DCM/TFA/H_2O 95: 5: 1			(24.6%)	
	2	2.7 (42.1%) 3.6 (35.6%) 3.7 (22.3)	708.37 (18.4%) 808.41 (100%) 908.44 (32.8%)	Orange
	3	2.7 (83.6%) 3.6 (9.9%) 3.7 (6.5%)	708.46 (43.1%) 808.52 (100%) 908.57 (33.4%)	Reddish
	4	2.7 (97.3%) 3.6 (1.6%) 3.7 (1.0%)	708.51 (100%) 808.55 (82.7%) 908.60 (14.8%)	Dark red
DCM/TFA/H_2O 95: 4: 1	1	2.7 (41.3%) 3.6 (58.7%)	808.70 (74.5%) 908.77 (100%)	Yellow
	2	2.7 (1.5%) 3.6 (51.4%) 3.7 (47.1%)	708.67 (4.9%) 808.72 (100%) 908.80 (30.1%)	Yellow
	3	2.7 (7.8%) 3.6 (65.7%) 3.7 (28.5%)	708.63 (9.8%) 808.72 (100%) 908.79 (27.6%)	Orange
	4	2.7 (13.7%) 3.6 (65.8%) 3.7 (21.5%)	708.64 (10.0%) 808.72 (100%) 908.80 (50.1%)	Orange deep

	5	2.7 (18.1%) 3.6 (60.4%) 3.7 (21.5%)	708.51 (16.7%) 808.55 (100%) 908.82 (19.6%)	Reddish
	6	2.7 (26.9%) 3.6 (57.7%) 3.7 (15.4%)	708.65 (27.1%) 808.73 (100%) 908.82 (81.1%)	Reddish
DCM/TFA/H_2O 96: 3: 1	1	Nothing	Nothing	Yellow
	2	Nothing	Nothing	Yellow
	3	Nothing	Nothing	Yellow
	4	Nothing	Nothing	Yellow
	5	3.6 (50.1 %) 3.7 (49.9%)	808.48 (93.1%) 908.51 (100%)	Yellow
	6	2.7 (4.7 %) 3.6 (49.6%) 3.7 (45.7%)	708.51 (15.4%) 808.55 (100%) 908.60 (84.8%)	Yellow- Orange

Table 6.54: Results for the Rink amide cleavage carried out using the method "cycle".

Results for method “constant”:

Solution	Samples	HPLC (ELSD) (Method 3, min) (ESLD, min)	MS (MALDI-TOF)	Resin colour
DCM/TFA 98: 2	30 minutes	Nothing	Nothing	Yellow
	2 hours	Nothing	Nothing	Yellow
DCM/TFA 97: 3	30 minutes	Nothing	Nothing	Yellow
	2 hours	2.6 (35.6%) 3.6 (56.5%) 3.7 (7.9%)	708.11 (100%) 808.11 (100%) 908.10 (28.7%)	Orange
DCM/TFA 96: 4	30 minutes	2.6 (47.9%) 3.6 (37.4%) 3.7 (14.7%)	708.24 (100%) 808.27 (64.7%) 908.21 (12.3%)	Orange
	2 hours	2.6 (98.2%) 3.6 (1.8%)	708.31 (100%) 808.32 (24.5%)	Red
DCM/TFA/H_2O 97: 2: 1	30 minutes	Nothing	Nothing	Yellow
	2 hours	Nothing	Nothing	Yellow

DCM/TFA/H_2O 96: 3: 1	30 minutes	Nothing	Nothing	Yellow
	2 hours	3.6 (48.4%) 3.7 (51.6%)	808.70 (74.8%) 908.77 (100%) 1008.72 (11.3%)	Yellow
DCM/TFA/H_2O 95: 4: 1	30 minutes	3.6 (36.1%) 3.7 (48.7%) 4.2 (13.5%)	808.27 (64.7%) 908.21 (100%) 1008.42 (8.7%)	Yellow/orange
	2 hours	2.7 (81.0%) 3.6 (10.8%) 3.7 (8.2%)	708.68 (57.1%) 808.63 (100%) 908.59 (27.3%)	Reddish

Table 6.55: Results for the Rink amide cleavage carried out with the method "constant".

6.6.5.2. Strategy 2: Selective Rink amide cleavage using continous flow

Protocol

The resin was transferred in a solid-phase extractor (a polypropylene syringe equipped with a frit and a valve) and a solution of TFA/DCM/H_2O (**Table 6.56**) was passed through it for an hour under gravity. Over an hour, 5 mL of TFA solution were used at a continuous flow. The solution was collected into 10 mL DCM containing 3% of TEA. At the end of the reaction time (1 hour), the resin was washed three times with DCM (1 mL) and the DCM mixture was concentrated *in*

vacuo. The crude was then analysed by HPLC, MS and precipitation (described below). The resin was also tested using a qualitative ninhydrin test (**6.2.1.1**).

Test of precipitation in cold Et_2O

The filtrates containing the peptoid were collected and concentrated *in vacuo* (0.2 mL). The concentrated mixture was then added dropwised in a centrifuge tube containing cold Et_2O (2.5 mL). The precipitated peptoid was then sonicated and collected by centrifugation.

Results

Solution	HPLC (ELSD) (Method 3, min)	MS (MALDI-TOF)	Precipitation	1. Colour resin 2. Ninhydrin test
DCM/TFA/H_2O 97:2:1	Nothing	Nothing	Nothing	1. Yellow 2. Yellow
DCM/TFA/H_2O 96:3:1	Nothing	Nothing	Nothing	1. Yellow 2. Yellow
DCM/TFA/H_2O 95:4:1	Nothing	Nothing	Nothing	1. Yellow 2. Yellow
DCM/TFA/H_2O 94:5:1	Nothing	Nothing	Nothing	1. Yellow 2. Light blue
DCM/TFA/H_2O 93:6:1	Nothing	Nothing	Nothing	1. Yellow 2. Light blue
DCM/TFA/H_2O 92:7:1	Nothing	Nothing	Small precipitate	1. Yellow 2. Blue
DCM/TFA/H_2O 91:8:1	2.7 (6.9%) 3.6 (60.6%) 3.7 (32.5%)	708.44 (18.8%) 808.51 (100%) 908.57	White precipitate	1. Orange 2. Blue

		(77.4%)		
DCM/TFA/H_2O 90:9:1	2.7 (49.4%) 3.6 (35.2%) 3.7 (15.4%)	708.72 (16.7%) 808.75 (100%) 908.78 (19.6%)	White precipitate	1. Reddish 2. Blue
DCM/TFA/H_2O 89:10:1	2.7 (58.7%) 3.6 (30.9%) 3.7 (10.4%)	708.63 (32.5%) 808.59 (100%) 908.61 (24.9%)	White precipitate	1. Reddish 2. Blue

Table 6.56: Results for the Rink amide cleavage carried out by continuous flow.
Colour of the resin interpretation: Yellow: no formation of cationic species, no cleavage; Orange to red: formation of cationic species, cleavage.
Ninhydrin test interpretation: Yellow: no free NH_2 on the resin; Blue: free NH_2 on the resin.

6.6.6. Synthesis of Boc-9mer(Boc)-NH_2 (**5.22**)

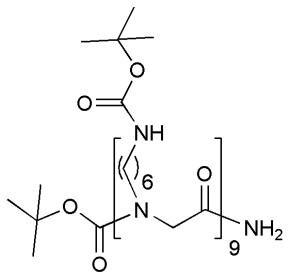

500 mg (0.135 mmol calculated from the theoretical loading) of resin **2.33** (**6.6.1**) were swollen in DCM (5 mL) for 20 minutes before being Fmoc deprotected (**6.2.1.9**). Once the Fmoc group was removed, the resin was Boc deprotected and cleaved (**6.2.1.10**). The cleaved peptoid (**5.17**) was dissolved in water (3 mL) and the solution was basified by slow addition of TEA (0.4 mL, pH > 10). To the 9mer solution (**5.17**) was added di-*tert*-butyl carbonate (665 mg, 2.02 mmol) in DCM (3

mL). The mixture was mixed for 1 hour. After reaction, the aqueous phase was isolated and washed with 2 mL of DCM (3 times). The organic layers were combined and concentrated *in vacuo*. The Boc-9mer$(Boc)_9$-NH_2 was purified by preparative HPLC (Gradient 2). After freeze drying, the Boc-peptoid was isolated as a white solid (261 mg, 80% based on the theoretical loading of **2.33**).

Analysis:

m/z (ES^+): $C_{122}H_{227}N_{19}O_{29}$ calculated 2422.7, found 606.6 $[M+4H]^{4+}$ (10.9%), 485.5 $[M+5H]^{5+}$ (68.1%), 404.7 $[M+6H]^{6+}$ (100%), 347.1 $[M+7H]^{7+}$ (23.4 %).

m/z (MALDI-TOF): $C_{122}H_{227}N_{19}O_{29}$ mass calculated 2422.7, mass found 2446.6 $[M+Na]^+$ (100%), 2462.5 $[M+K]^+$ (92%).

m/z (FT-MS): $C_{122}H_{227}N_{19}O_{29}$ calculated $[M+4H]^{4+}$ 606.67963, found 606.65079.

HPLC (Method 4): t_R = 3.8 min; purity > 98% (ELSD).

^{1}H NMR ($CDCl_3$, 500 MHz): δ = 1.25-1.40 (m, 36H, C*H*$_2$, H_3 and H_4), 1.41-1.53 (m, 126H, 36H for C*H*$_2$ (H_2 and H_5)) and 90H for C*H*$_3$-Boc), 3.11 (m, 18H, C*H*$_2$NHBoc, H_6), 3.32 (m, 18H, C*H*$_2$N, H_1), 3.95-4.23 (m, 18H, NC*H*$_2$CO).

^{13}C NMR ($CDCl_3$, 126 MHz): δ = 26.2, 26.3, 26.4, 26.5, 26.6, 26.7 (*C*H_2, $C_{3, 4}$), 27.6, 27.7, 27.8 (C(*C*H_3)$_3$), 28.3, 28.4, 28.5, 28.6 (*C*H_2, $C_{2, 5}$), 40.2, 40.3, 40.4, 40.5 (*C*H_2, C_6), 46.7, 46.8, 46.9, 47.1, 47.6, 47.7, 47.9, 48, 48.1, 48.4, 48.6, 48.8, 48.9 (*C*H_2, N*C*H_2CO and C_1), 78.8, 78.9, 79, 79.7 (*C*$(CH_3)_3$), 155.9, 156.0, 156.1, 156.2, 156.3 (*C*=O-Boc), 162.4, 162.5, 162.7 (*C*=O-9mer).

6.6.7. qNMR

6.6.7.1. Formulae to calculate the concentration of an unknown analyte[314]

$$[\text{analyte}] = \frac{\text{Integration for 1 analyte proton}}{\text{Integration for 1 standard proton}} \times [\text{standard}]$$

Equation 6.6: Calculation of the analyte concentration.
Concentration in mM.

Integration for 1 proton was calculated by dividing the integration on the spectrum by the number of proton expected for this signal.

6.6.7.2. qNMR with 2,5-dimethylfuran (2,5-DMFu)

Relaxation delay

In order to have a good reproducibility, the experiments were carried out in the same tube. The NMR tube was prepared with 2,5-DMFu (12 mM,) and peptoid **5.22** (6 mM estimated) in $CDCl_3$. The spectra were obtained at 400 MHz, after 16 scans (acquisition time 2 seconds).
Integration measurements were the same for all spectra and were measured between the following ppm values:

- C*H*$_3$ for 2,5-DMFu (**5.25**): 2.239 -2.302 ppm (measured),
- C*H*=C*H* for 2,5-DMFu (**5.25**): 5.833 -5.872 ppm (fixed).
- C*H*$_2$N for the peptoid **5.22**: 3.202 -3.488 ppm
- NC*H*$_2$CO for the peptoid **5.22**: 3.804-4.364 ppm.

Effect of number of scans and of the acquisition time

The NMR tube was prepared with 2,5-DMFu (12 mM) and peptoid **5.22** (6 mM estimated) in $CDCl_3$. The spectra were obtained at 400 MHz using D1 = 10 seconds. The ratio was calculated using the same protons as for the relaxation delay experiments.

Number of scans	Acquisition time (seconds)	Ratio 2,5-DMFu proton C*H*:C*H*$_3$	Ratio peptoid proton CH_2N:NCH_2CO
16	2	1 : 3.01	1 : 1.005
16	16	1 : 3.02	1 : 1.005
16	32	1 : 3.01	1 : 1.006
32	2	1 : 3.01	1 : 1.005
64	2	1 : 3.02	1 : 1.006
128	2	1 : 3.01	1 : 1.005

Table 6.57: Effect of the number of scans and of the aquisition time on the NMR spectrum.

Effect of concentrations

A solution of Fmoc-Lys(Boc)-OH was prepared in $CDCl_3$ (5.6 mM). A solution of 2,5-DMFu was prepared in $CDCl_3$ (50 mM).

Conc 2,5-DMFu (mM)	Vol 2,5-DMFu (mL)	Integration 2,5-DMFu	Conc analyte (mM)	Vol analyte (mL)	Integration analyte
7.15	0.1	3.0	4.8	0.6	2
12.5	0.2	6.0	4.2	0.6	2
16.6	0.3	8.4	3.73	0.6	2
42.8	0.6	33.4	0.8	0.1	2
37.5	0.6	17.6	1.4	0.2	2
33.3	0.6	14.8	1.6	0.3	2

Table 6.58: Preparation of the NMR solutions for study of the concentration effects.
Integration of 2,5-DMFu was measured at δ = 5.87 ppm (s, 2H, CH) and the integration of the analyte, Fmoc-Lys(Boc)-OH, was measured at δ = 7.75 ppm (d, 2H, ArCH-Fmoc).

A known volume of each solution was transferred into a NMR tube. Volumes used and expected concentration were summarised in the **Table 6.58**. ^{1}H NMR of the mixture was recorded at 400 MHz (NS = 16, D1 = 10 seconds, AQ = 2 seconds and 298 K). The calculated concentration was obtained using the equation 1.

*Quantification of protected peptoid Boc-9mer(Boc)$_9$-NH$_2$, **5.22***

A solution containing an estimated concentration of 6 mM (246 mg in 17 mL of $CDCl_3$) of protected peptoid **5.22** and 12 mM of 2,5-DMFu (**5.25**) in $CDCl_3$ was prepared. The NMR spectrum was recorded three times on a 400 MHz spectrometer using the following parameters:

- NS = 16,
- AQ = 2 seconds,
- D1 = 10 seconds,
- T = 298 K.

Once recorded, the spectrum was treated in order to obtain the best signals (base line and phase correction). The concentration was **5.22** calculated using the equation 1 and the average of the 3 spectrum integrations. The integrations were measured with the heterocyclic 2,5-DMFu proton normalised at 1 and the peptoid proton were measured for H_1, H_6 and H_α. This was defined due to the non-satisfying integrations between 2 and 1 ppm.

Results:

Integration per peptoid proton: 0.4883.

Concentration of peptoid: 5.86 mM ± 0.17 mM.

6.6.8. Synthesis of NLLP **5.17**: Boc deprotection using 1,4-dioxane/HCl 4N

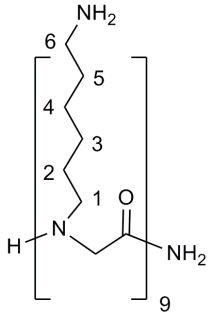

The peptoid **5.22**(85.2 mg, 0.035 mmol) was dissolved in DCM (2 mL) and 3 mL of 1,4-dioxane/HCl 4N were added. The solution was mixed for an hour before removing the solvent *in vaccuo.* However 1,4-dioxane was still present in the NMR spectrum. 10 lyophilisations using 5 mL of water were carried out. The mass (white sticky solid) was 72 mg (mass exact using qNMR 50 mg). The ratio 1,4-dioxane (CH_2, 3.75 ppm) / proton 9mer (CH_2N, 3.28 ppm) was 0.8 therefore the amount of 1,4-dioxane left after lyophilisations was 2.7 mg.

Analysis:

m/z (ES^+): $C_{72}H_{147}N_{19}O_9$ calculated 1422.2, found 712.2 $[M+2H]^{2+}$ (23.7 %), 475.2 $[M+3H]^{3+}$ (100%), 356.6 $[M+4H]^{4+}$ (68.2%), 285.5 $[M+5H]^{5+}$ (5.3%).

m/z (MALDI-TOF): $C_{72}H_{147}N_{19}O_9$ calculated 1422.16, found 1423.25 $[M+H]^+$ (26.2%), 1445.24 $[M+Na]^+$ (100%), 1461.21 $[M+K]^+$ (35.9%).

m/z (FT-MS): $C_{72}H_{147}N_{19}O_9$ calculated $[M+3H]^{3+}$ 475.06213, found 475.06471.

HPLC (Method 3): t_R = 0.82 min, purity = 100% (ELSD).

^{1}H NMR (D_2O, 500 MHz, eSpresat suppression water): δ = 1.29-1.46 (m, 36H, C*H*$_2$, H $_3$ and H_4), 1.47-1.73 (m, 36H, C*H*$_2$, H $_2$ and H_5), 2.99 (m, 18H, C*H*$_2$NH$_2$, H_6), 3.23-3.51 (m, 18H, C*H*$_2$N, H_1), 3.93-4.53 (m, 18H, NC*H*$_2$CO) 7.56 (br sg, 2H, CON*H*$_2$).

^{13}C NMR (D_2O, 126 MHz): δ = 25.1, 25.2, 25.3, 25.4, 25.5, 25.6, 26.4, 26.5, 26.6, 27, 27.1, 27.2, 27.3 and 27.4 (*C*H$_2$, *C*$_{2, 3, 4, 5}$), 39.2, 39.3, 39.4 (*C*H$_2$, *C*$_6$), 47.4, 47.5, 47.7, 48, 4, 48.5, 48.6, 48.7 (*C*H$_2$, NC*H*$_2$CO and *C*$_1$), 162.4, 162.7, 162.99, 163.3, 169.5, 169.6, 170 (*C*=O- 9mer).

6.6.9. Synthesis of NLLP **5.17**: Boc deprotection using TFA

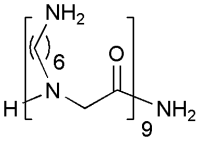

The peptoid **5.22** (85.2 mg, 0.035 mmol) was dissolved in DCM with 20% TFA (3 mL). The solution was mixed for an hour before removing the solvent *in vaccuo*. The mass was 59 mg (mass exact using qNMR 50 mg).

Analysis:

m/z (MALDI-TOF): $C_{72}H_{147}N_{19}O_9$ calculated 1422.16, found 1423.60 $[M+H]^+$ (17.3%), 1445.62 $[M+Na]^+$ (100%), 1461.55 $[M+K]^+$ (72.5%).

HPLC (Method 3): t_R = 0.83 min; purity = 100% (ELSD).

(**m/z** and **NMR** identical to the one reported for **5.17** in section **6.6.7**).

6.6.10. Synthesis of NLLP **5.17**: Boc deprotection using Et_2O/ HCl 1M

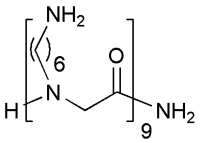

The peptoid **5.22** (85.2 mg, 0.035 mmol) was dissolved in a minimum of Et_2O (3 mL) and transferred in a centrifuge tube. 10 mL of Et_2O/HCl 1M were added and the

mixture was shaken for an hour. The formation of unprotected NLLP **5.17** was observed by the formation of a white precipitate. The mixture was cooled down, centrifuged and the product washed with cold Et_2O (10 mL) three times. The white sticky solid was dried under N_2. The NMR showed remaining traces of Et_2O that were removed after 3 days under vacuum. The mass was 65 mg (mass exact using qNMR 50 mg).

Analysis:

m/z (MALDI-TOF): $C_{72}H_{147}N_{19}O_9$ calculated 1422.16, found 1423.69 $[M+H]^+$ (44.9%), 1445.68 $[M+Na]^+$ (100%), 1461.66 $[M+K]^+$ (48.7%).

HPLC (Method 3): t_R = 0.85min, purity = 100% (ELSD).

(**m/z** and **NMR** identical to the one reported for **5.17** in section **6.6.7**).

6.6.11. MTT assays of the NLLP in cell lines

MTT cytotoxicity assays were carried out on HeLa, HEK293T and B16F10 cells according to the general procedures (**6.2.2.4**). Cells were treated with 1, 5, 10, 20 or 50 µL of 100 µM NLLP (**5.17**) solution in PBS in order to obtain a final concentration of 1, 5, 10, 20 or 50 µM, respectively. After 24 hours of incubation at 37°C, the cells were prepared to be read on the microplate reader.

HeLa cells

	Concentration (µM)	Average (arb. units)	Error (arb. units)	Average (%)	Error (%)
Untreated cells		1.123	0.139	100.0	12.4
5.17	1	1.133	0.107	100.9	9.5
	5	1.185	0.104	105.5	9.2
	10	1.091	0.089	97.1	8.0
	20	1.144	0.125	101.8	11.1
	50	1.101	0.105	98.0	9.3

Table 6.59: Percentage of cell vailability (HeLa cells) after 24 hours of incubation with NLLP (5.17) at different concentrations (n = 14).

B16F10 cells

	Concentration (µM)	Average (arb. units)	Error (arb. units)	Average (%)	Error (%)
Untreated cells	0	0.872	0.062	100.0	7.1
5.17	1	0.879	0.075	100.8	8.6
	5	0.860	0.048	98.6	5.5
	10	0.901	0.047	103.3	5.4
	20	0.857	0.058	98.3	6.6
	50	0.876	0.048	100.5	5.6

Table 6.60: Percentage of cell vailability (B16F10 cells) after 24 hours of incubation with NLLP (5.17) at different concentrations (n = 14).

HEK293T cells

	Concentration (µM)	Average (arb. units)	Error (arb. units)	Average (%)	Error (%)
Untreated cells		1.137	0.131	100.0	11.5
5.17	1	1.094	0.129	96.3	11.3
	5	1.142	0.087	100.5	7.7
	10	1.114	0.103	98.0	9.1
	20	1.143	0.120	100.6	10.6
	50	1.139	0.108	100.3	9.5

Table 6.61: Percentage of cell vailability (HEK293T cells) after 24 hours of incubation with NLLP (5.17) at different concentrations (n = 14).

APPENDIX 1:

PERMISSION

Figure 1.1: Modified with permission from Molecular biology of the cell;

Figure 1.2: Modified with permission from Molecular biology of the cell;

Figure 1.3: Modified with permission from Molecular biology of the cell;

Figure 1.4: Modified with permission from Molecular biology of the cell;

Figure 1.11: Modified from "Cell-Penetrating Peptides—Mechanisms of Cellular Uptake and Generation of Delivery Systems" (Figure 1) with permission from Prof. Maria C. Pedroso de Lima;

Figure 3.2: Adapted with permission from "Bright ideas for chemical biology". Copyright 2012 American Chemical Society.

Figure 4.6: Modified with permission from nobelprize.org; http://www.nobelprize.org/nobel_prizes/chemistry/laureates/2008/illpres.html.

APPENDIX 2:

DATA FOR CHAPTER 2

1. Expansion of the HPLC trace (λ = 580 nm, Method 3) and measurement of the area of each peak for the Rho-9mer (**2.37**)

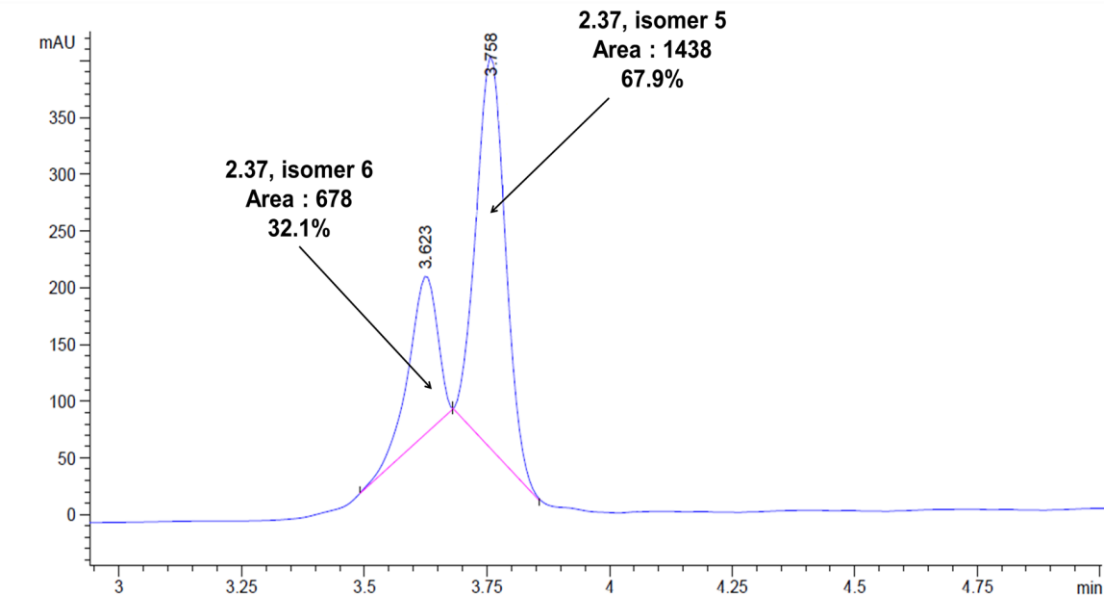

2. TO-PRO-3 analysis of primary immune cells.

a. S2 Drosophila cells

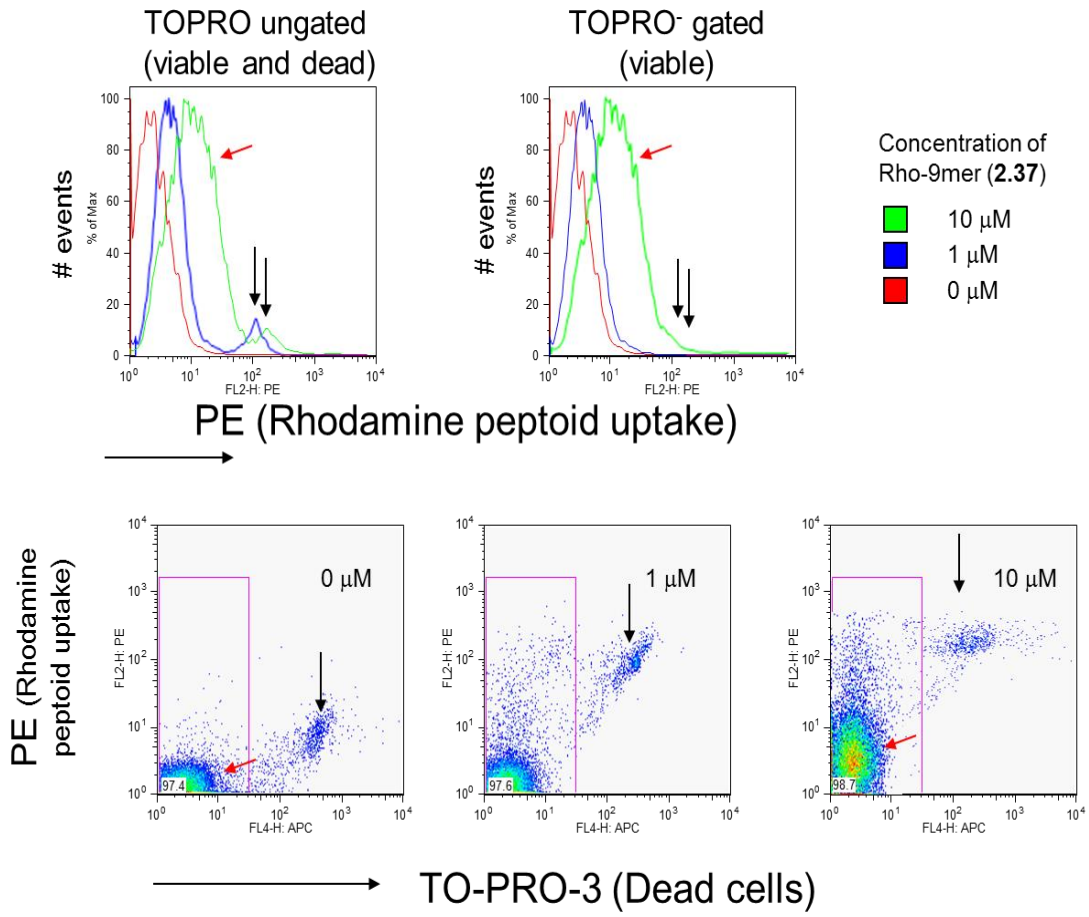

Figure 6.1 : TO-PRO-3 analysis of primary S2 Drosophila cell viability.

Cells were treated with 0, 1 and 10 µM for one hour prior TO-PRO-3 analysis. A) Histogram plotting the rhodamine fluorescence (X axis) against the number of event (Y axis) before gating; B) Histogram plotting the rhodamine fluorescence (X axis) against the number of event after gating; C) Gating of the histogram plotting the TO-PRO-3 fluorescence (X axis) against rhodamine fluorescence (Y axis) for untreated cell; D)) Gating of the histogram plotting the TO-PRO-3 fluorescence (X axis) against rhodamine fluorescence (Y axis) for cells treated with 1 µM of Rho-9mer (**2.37**) ; E)) Gating of the histogram plotting the TO-PRO-3 fluorescence (X axis) against rhodamine fluorescence (Y axis) for cells treated with 10 µM of Rho-9mer (**2.37**). The red arrows show the Intact cells, while the black ones point the dead cells. Data courtesy of Dr. Stefano Caserta from the Institute of Immunology & Infection Research (Prof. Rose Zamoyska) at the University of Edinburgh.

b. Mouse F5 hybridoma cells

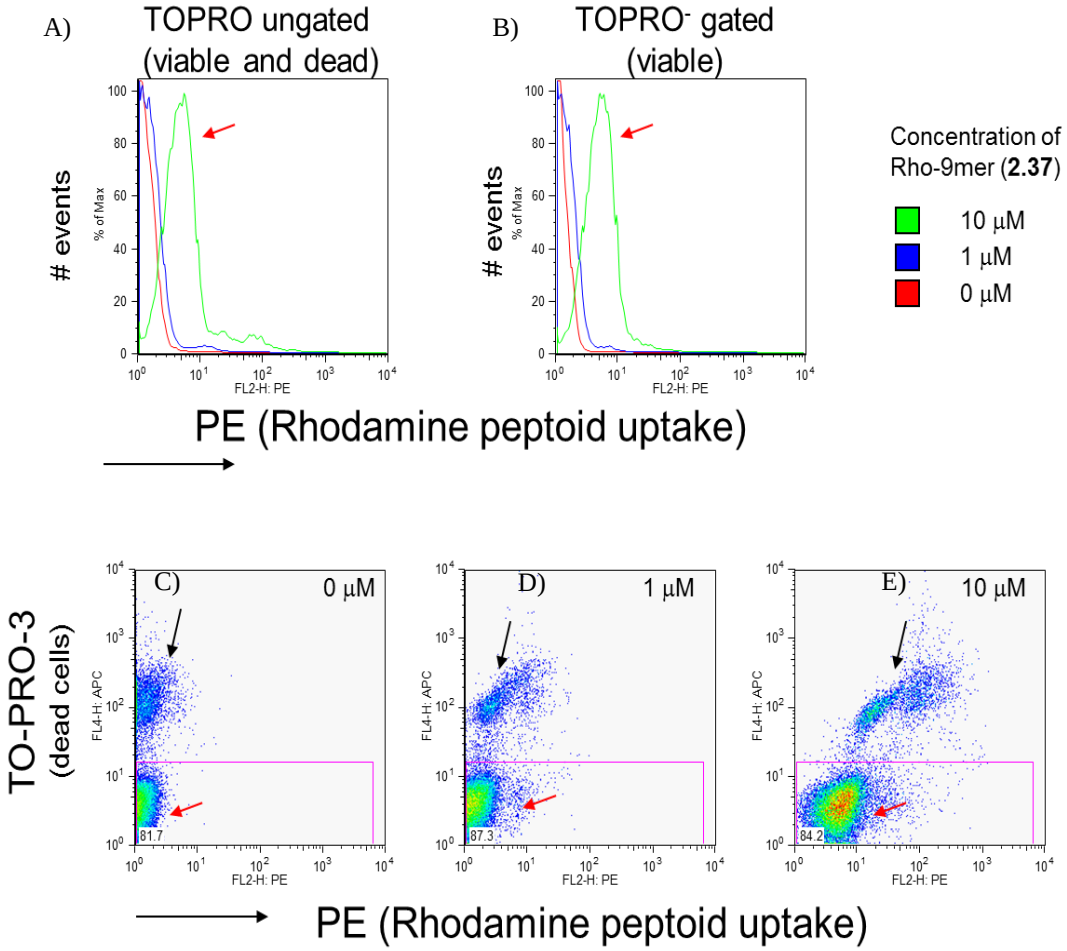

Figure 6.2 : TO-PRO-3 analysis of primary Mouse F5 hybridoma cell viability.
Cells were treated with 0, 1 and 10 µM for one hour prior TO-PRO-3 analysis. A) Histogram plotting the rhodamine fluorescence (X axis) against the number of event (Y axis) before gating; B) Histogram plotting the rhodamine fluorescence (X axis) against the number of event after gating; C) Gating of the histogram plotting the rhodamine fluorescence (X axis) against TO-PRO-3 fluorescence (Y axis) for untreated cell; D)) Gating of the histogram plotting the rhodamine fluorescence (X axis) against TO-PRO-3 fluorescence (Y axis) for cells treated with 1 µM of Rho-9mer (**2.37**) ; E)) Gating of the histogram plotting the rhodamine fluorescence (X axis) against TO-PRO-3 fluorescence (Y axis) for cells treated with 10 µM of Rho-9mer (**2.37**). The red arrows show the Intact cells, while the black ones point the dead cells. Data courtesy of Dr. Stefano Caserta from the Institute of Immunology & Infection Research (Prof. Rose Zamoyska) at the University of Edinburgh.

APPENDIX 3:

DATA FOR CHAPTER 3

Cellular uptake of Cy1-9mer (3.30) and Cy5.5-1mer (3.31).

HeLa, B16F10 and HEK293T cells incubated with 10 μM of peptoids (Cy7-1mer (**3.30**) and Cy5.5-1mer (**3.31**)) for 5, 30 minutes, 2, 4 and 24 hours at 37°C. The errors bar represents the standard error of the average (n = 3).

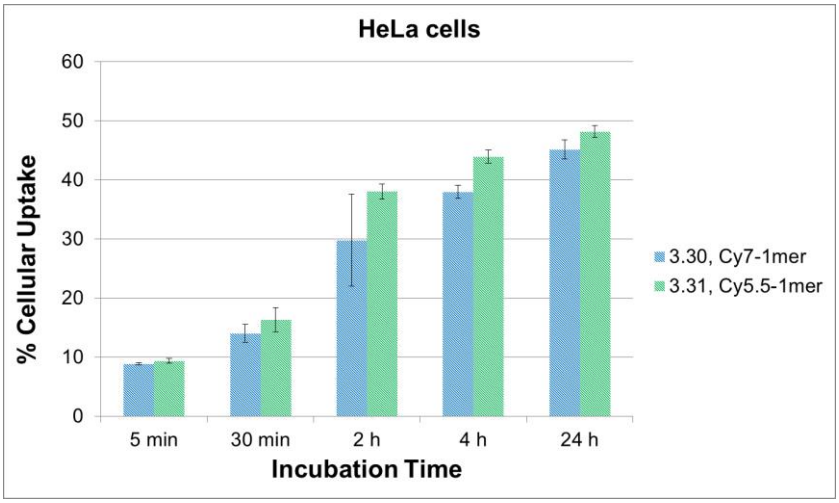

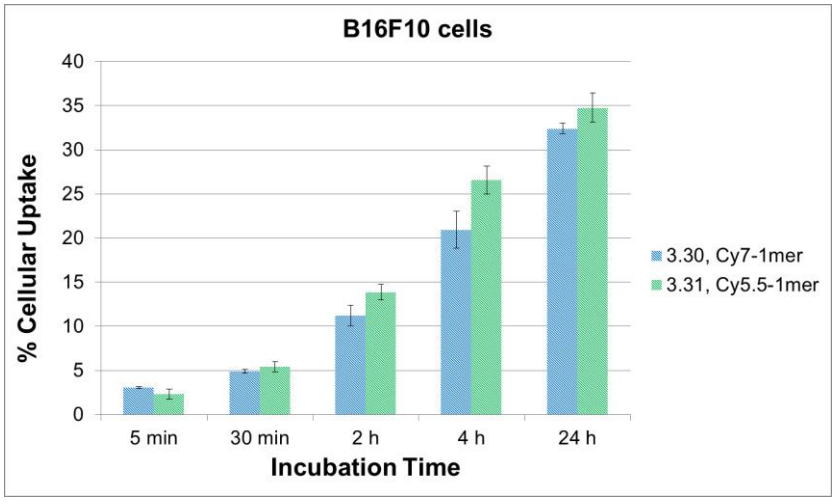

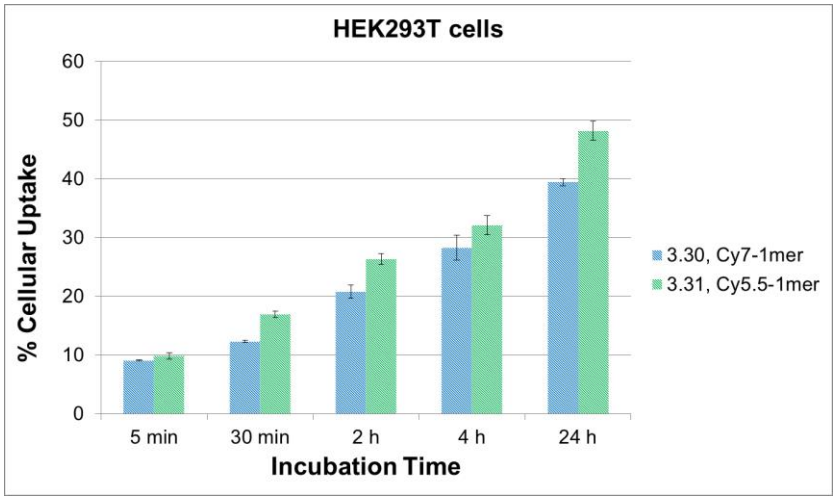
HEK293T cells
% Cellular Uptake
60
50
40
30
20
10
0
5 min
30 min
2 h
4 h
24 h
Incubation Time
3.30, Cy7-1mer
3.31, Cy5.5-1mer

APPENDIX 4:

DATA FOR CHAPTER 4

1. Map of the Cysteine modified GFP plasmid prepared and given by Dr David Nagel.

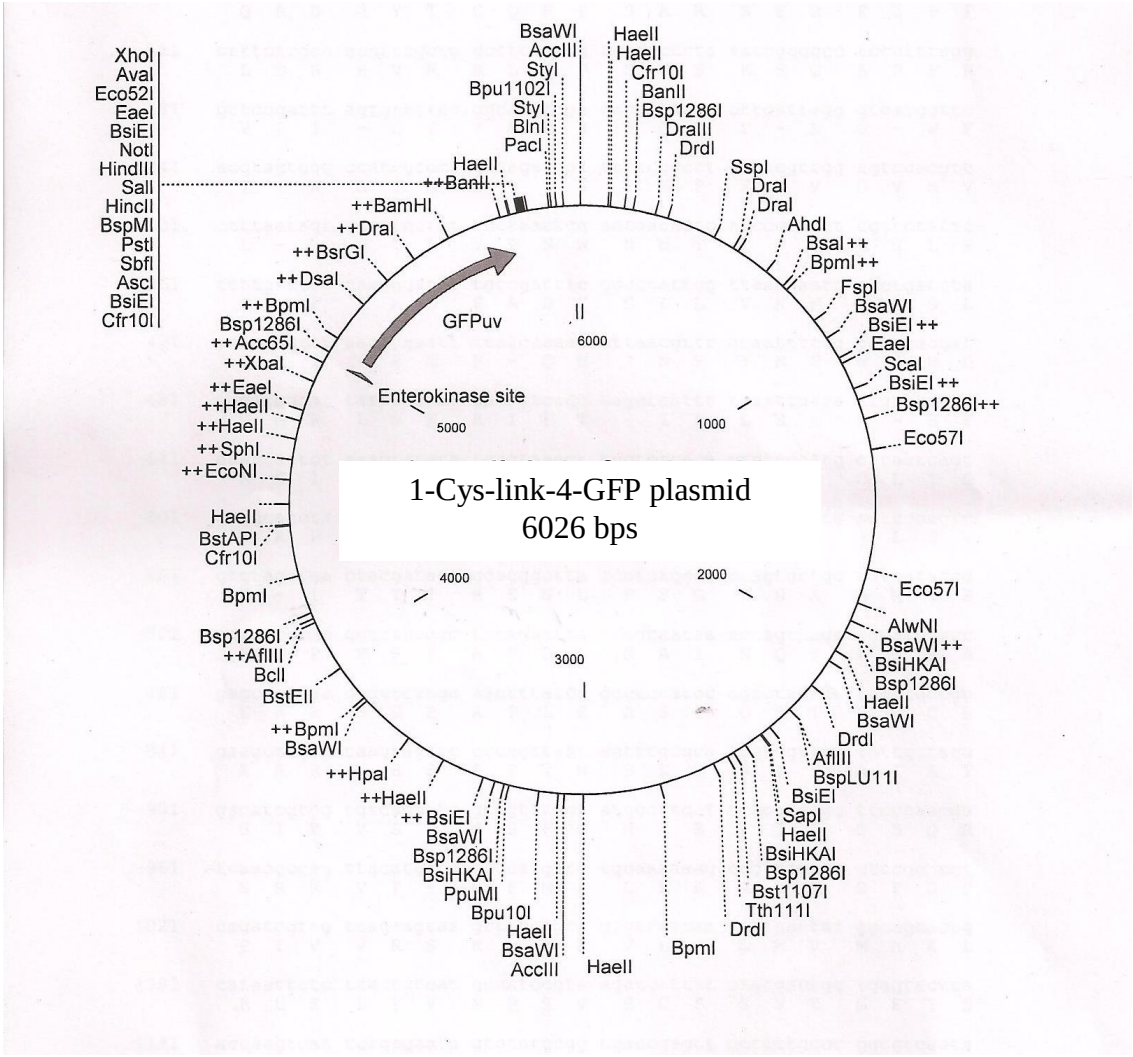

2. His6-tag-Cys-GFP (**4.30**) sequence data


PspXI
XhoI
Bst1107I
541 acaaactcga gtacaactat aactcacaca atgtatacat cacggcagac aaacaaaaga
tgtttgagct catgttgata ttgagtgtgt tacatatgta gtgccgtctg tttgttttct
>.....GFP.....>
h k l e y n y n s h n v y i t a d k q k
BamHI
601 atggaatcaa agctaacttc aaaattcgcc acaacattga agatggatcc gttcaactag
taccttagtt tcgattgaag ttttaagcgg tgttgtaact tctacctagg caagttgatc
>.....GFP.....>
n g i k a n f k i r h n i e d g s v q l
BtgZI
MunI
661 cagaccatta tcaacaaaat actccaattg gcgatggccc tgtcctttta ccagacaacc
gtctggtaat agttgtttta tgaggttaac cgctaccggg acaggaaaat ggtctgttgg
>.....GFP.....>
a d h y q q n t p i g d g p v l l p d n
DrdI
721 attacctgtc gacacaatct gccctttcga aagatcccaa cgaaaagcgt gaccacatgg
taatggacag ctgtgttaga cgggaaagct ttctagggtt gcttttcgca ctggtgtacc
>.....GFP.....>
h y l s t q s a l s k d p n e k r d h m
BsiHKAI
SacI
GsaI
BpuEI
BseYI
Eco53kI
781 tccttcttga gtttgtaact gctgctggga ttacacatgg catggatgag ctctacaaat
aggaagaact caaacattga cgacgaccct aatgtgtacc gtacctactc gagatgttta
>.....GFP.....>
v l l e f v t a a g i t h g m d e l y k
PstI
SbfI
SfcI
MmeI
AscI
EcoRI
HaeII
BssHII
BspMI
841 aatgaattcc aactgagcgc cggtcgctac cattaccaac ttgtggcgcg cctgcaggtc
ttacttaagg ttgactcgcg gccagcgatg gtaatggttg aacaccgcgc ggacgtccag
>> GFP

3. Expansion of the HPLC trace (ESLD) and measurement of the area of each peak for the Rho-S-maleimide-9mer (**4.39**)

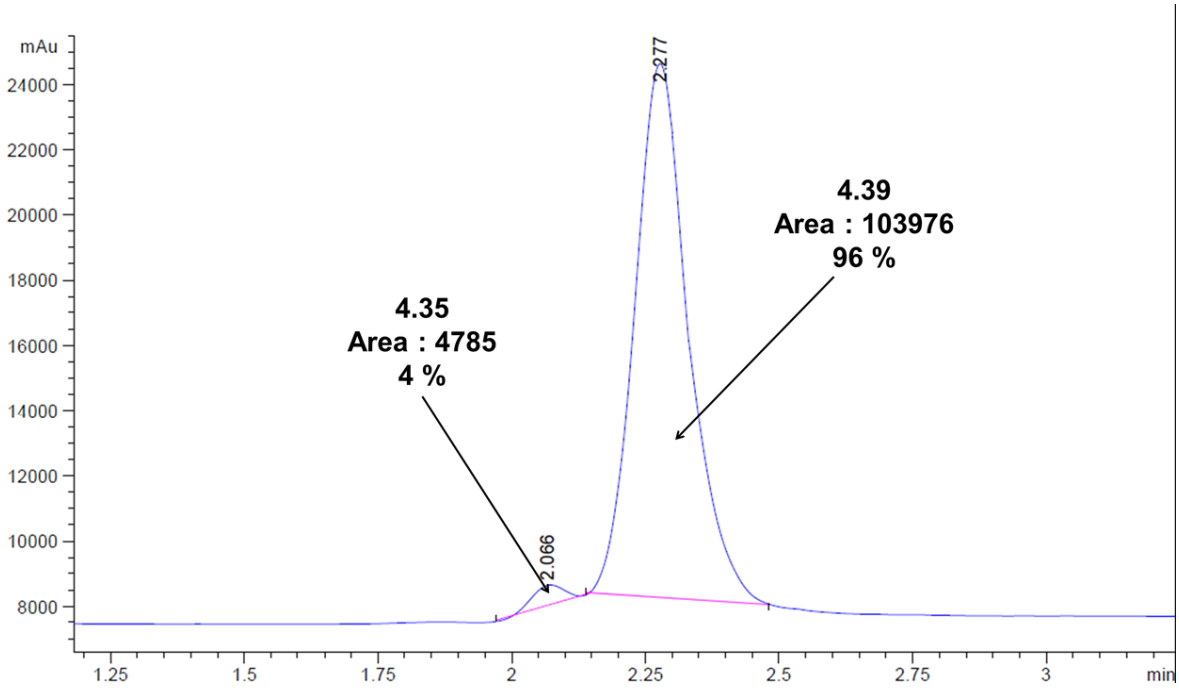

4. Analysis of the first coupling assay via single thiol-maleimide coupling (the coupling did not work)

a. MALDI-TOF spectrum

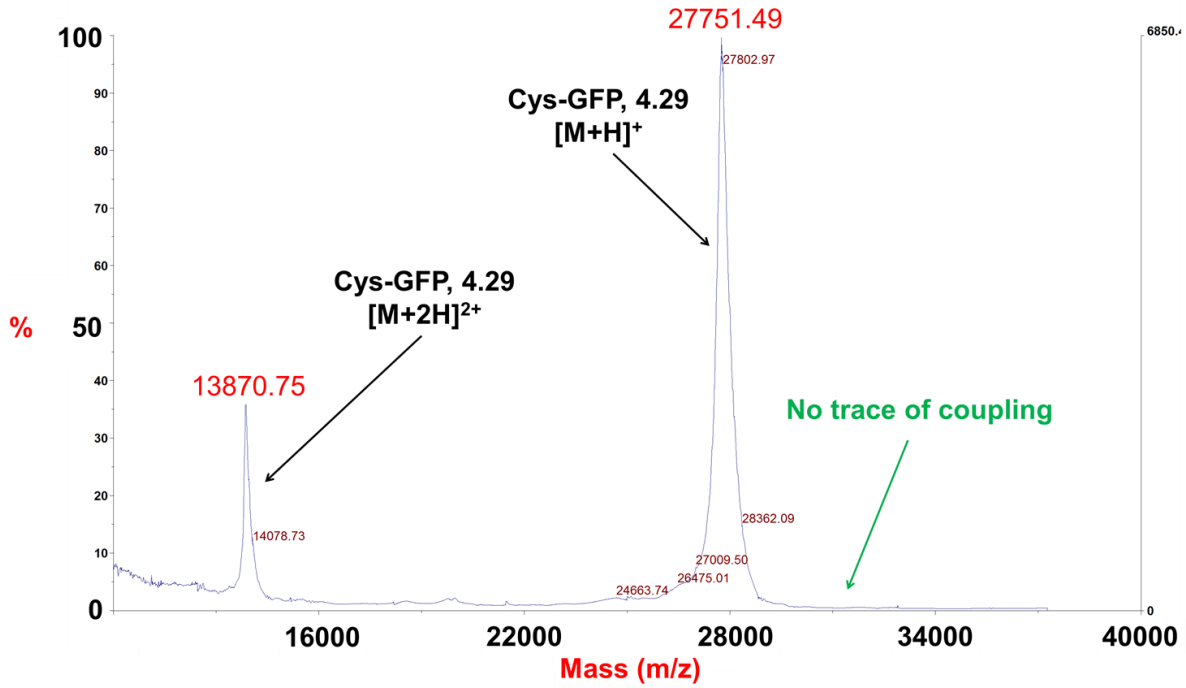

b. SDS-PAGE gel

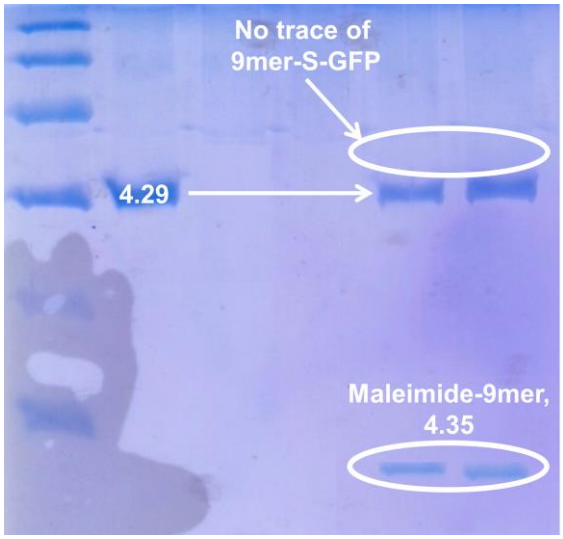

5. MALDI-TOF analysis of the Cys-GFP bioconjugation with 10 equivalents of DTT and 25 of **4.35**.

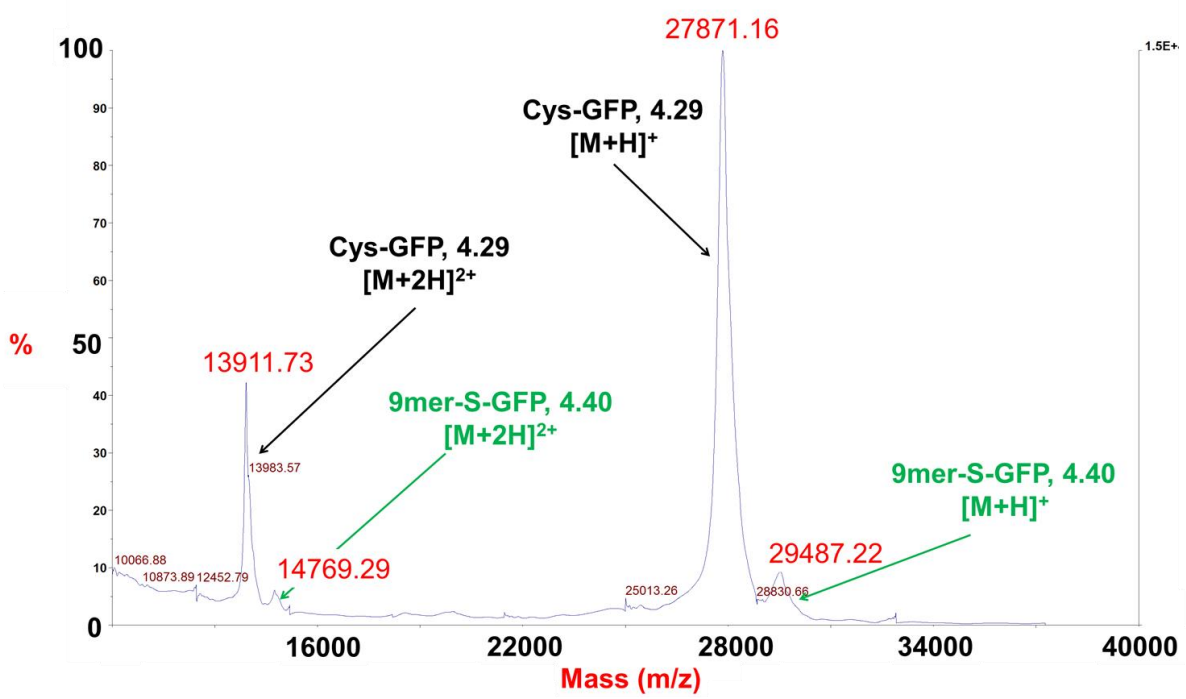

6. Analysis of the first coupling assay via multiple thiol-maleimide coupling (the coupling did not work)

a. MALDI-TOF spectrum after reaction

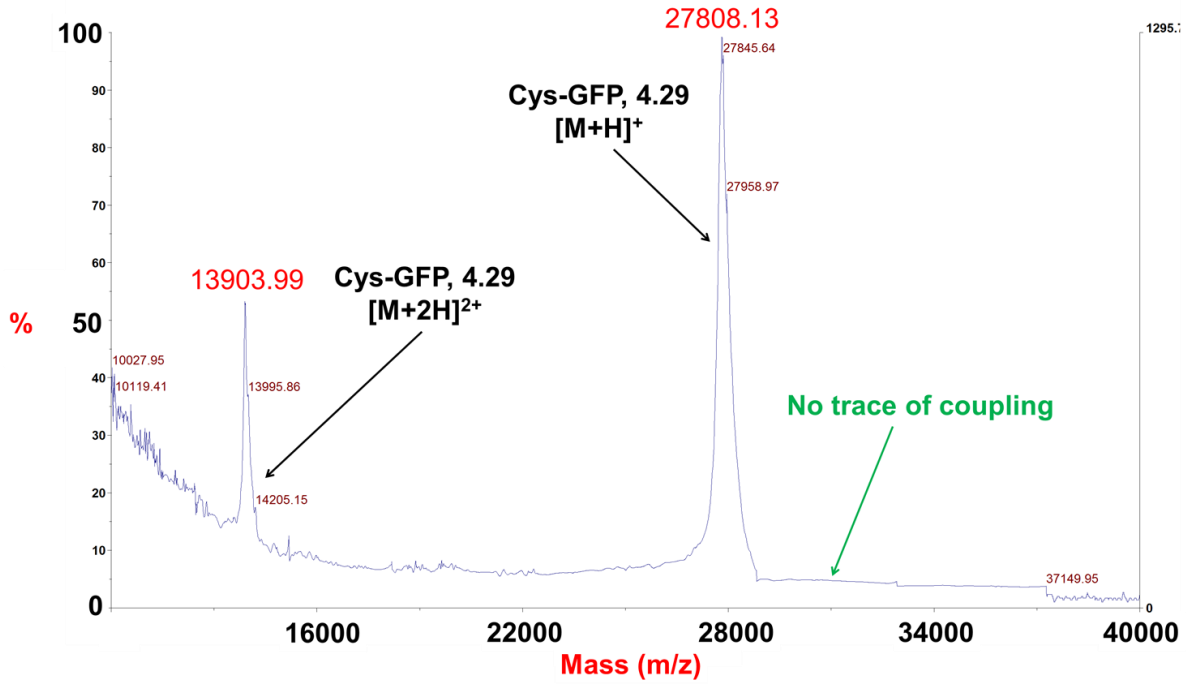

b. SDS-PAGE gel

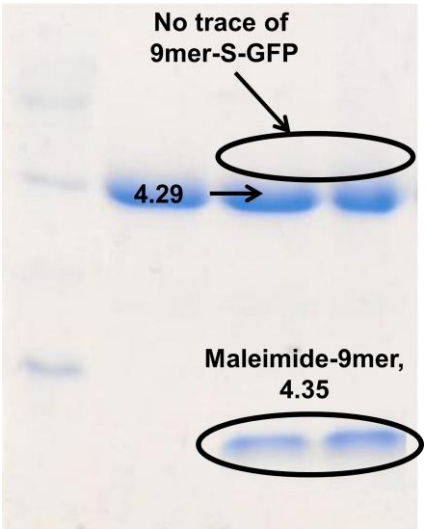

7. Cellular uptake of the bioconjugate **4.44 ((**9mer-S)$_n$-GFP) in HeLa cells

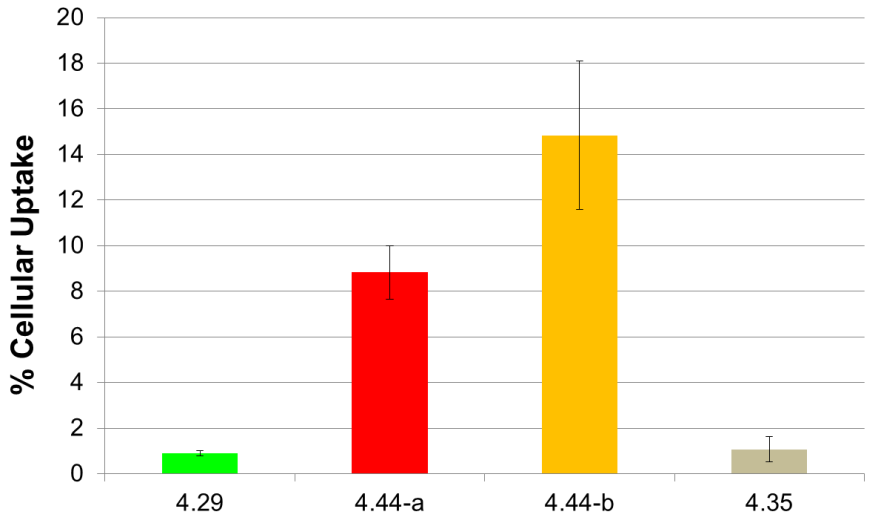

Graph 6.1 : Cellular uptake of the bioconjugate 4.44.
% uptake measured for the Cys-GFP (**4.29**, 6 µg/mL), (9mer-S)$_n$-GFP bioconjugate (**4.44-a**: 2.7 µg/mL and **4.44-b**: 5.4 µg/mL) and maleimide-9mer (**4.35**, as negative control, 10 µM) as the % of cells with a fluorescent emission exceeding untreated control as 0% uptake (incubation time = 24 hours). The errors bar represents the standard error of the average (n = 3).

8. MTT analysis of the 9mer-S-GFP bioconjugate (**4.40** and **4.44**) in HeLa cells.

HeLa cells were incubated with Cys-GFP (**4.29**, 6 µg/mL), 9mer-S-GFP bioconjugate (**4.40** and **4.44, a**: 2.7 µg/mL and **b**: 5.4 µg/mL) and maleimide-9mer (**4.35**, as negative control, 10 µM) for 24 hours before being treated with MTT. Healthy cells corresponded to 100% cell viability. The errors bar represents the standard error of the average (n = 8).

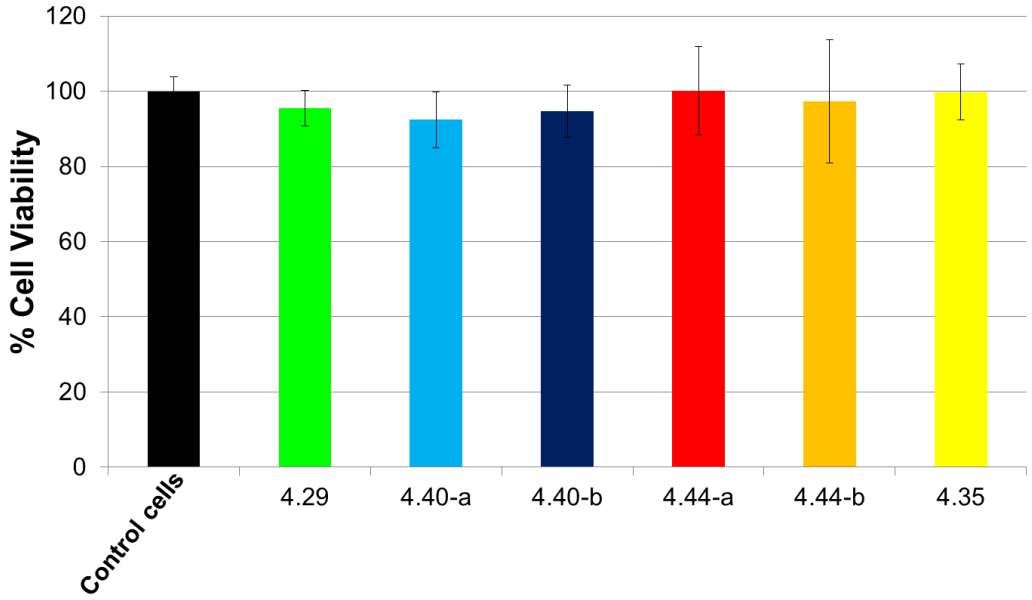

9. Data for the stability of the OPfp ester against TFA.

The % of each compound was calculated via the area of each HPLC (ELSD) peak.

1 % of TFA	% of Fmoc-Leu-Opfp	% of hydrolysis product
0 min	100	0
15 min	100	0
30 min	100	0
60 min	100	0
90 min	100	0
120 min	100	0
360 min	100	0

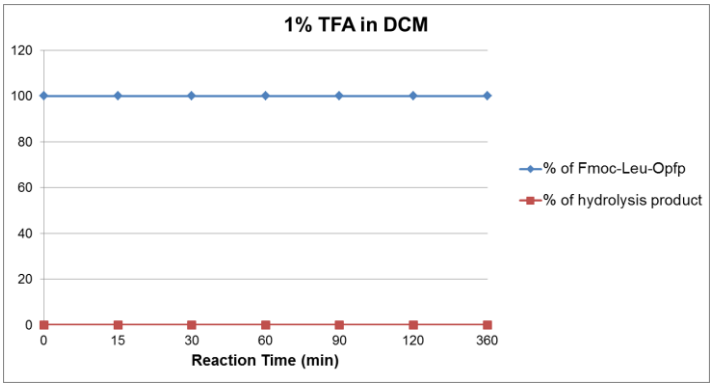

5 % of TFA	% of Fmoc-Leu-Opfp	% of hydrolysis product
0 min	100	0
15 min	100	0
30 min	100	0
60 min	100	0
90 min	100	0
120 min	100	0
360 min	100	0

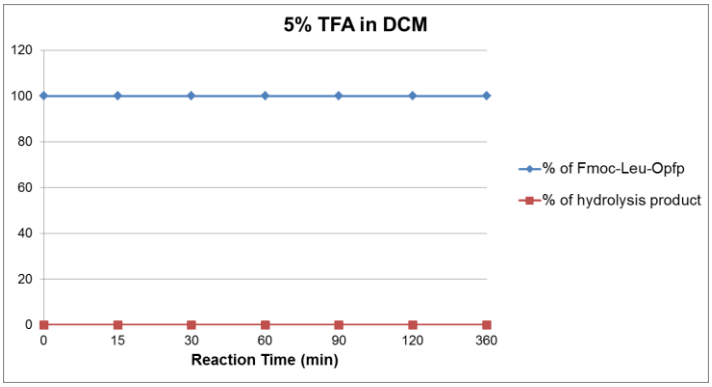

10 % of TFA	% of Fmoc-Leu-Opfp	% of hydrolysis product
0 min	100	0
15 min	100	0
30 min	100	0
60 min	100	0
90 min	100	0
120 min	100	0
360 min	100	0

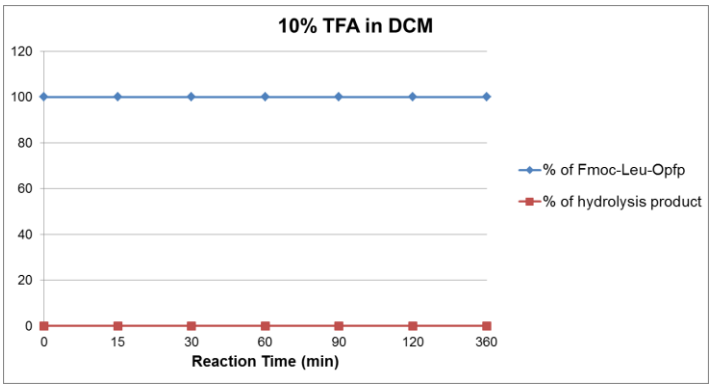

25 % of TFA	% of Fmoc-Leu-Opfp	% of hydrolysis product
0 min	100	0
15 min	100	0
30 min	100	0
60 min	100	0
90 min	100	0
120 min	100	0
360 min	100	0

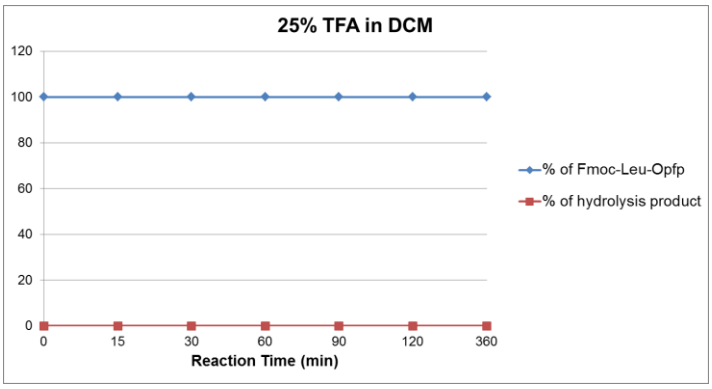

50 % of TFA	% of Fmoc-Leu-Opfp	% of hydrolysis product
0 min	100	0
15 min	100	0
30 min	100	0
60 min	100	0
90 min	100	0
120 min	100	0
360 min	100	0

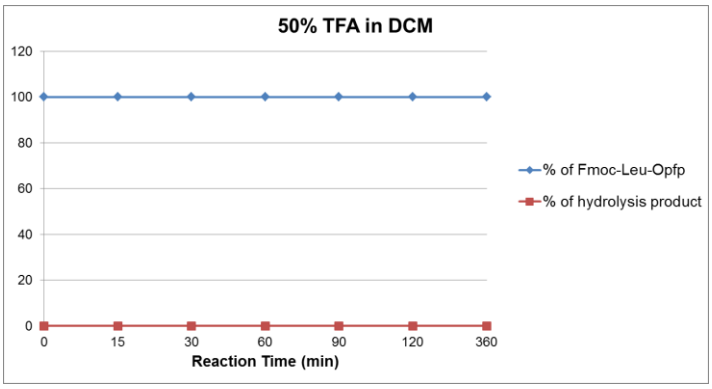

10. Direct GFP expression in lymph node cells following peptoid mediated DNA delivery.

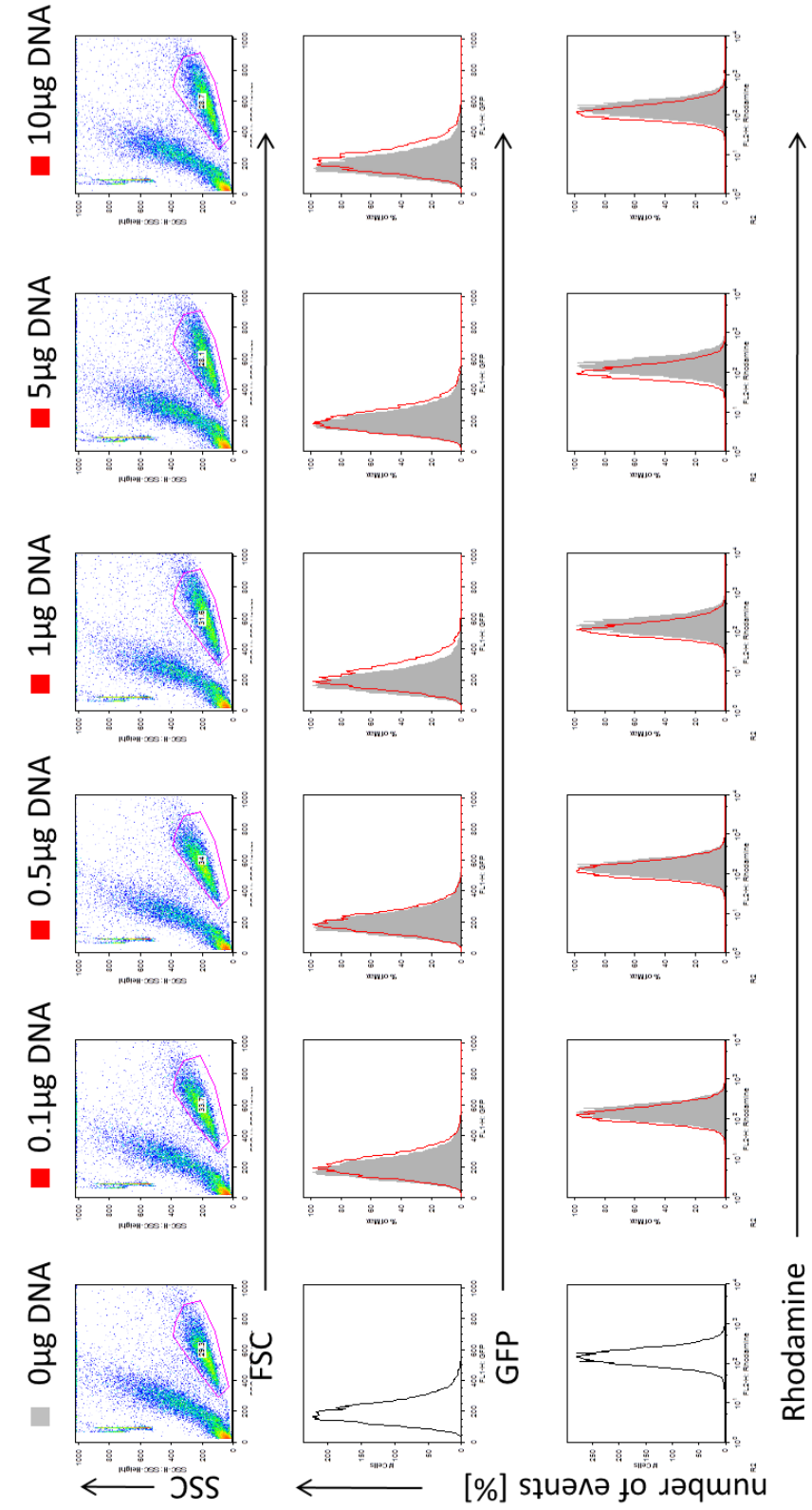

Flow cytometry analysis of peptoid (Rho-9mer, 2.37) mediated DNA delivery in lymph node cells . Direct GFP fluorescence

The cells were analysed on day 4 of incubation with complex GFP-plasmid & Rho-9mer (**2.37**, 10µM). The top row corresponds to the detection of the GFP expression (GFP fluorescence) as a function of the amount of DNA used. The bottom row corresponds to the Rhodamine detection function of the amount of DNA used. Data courtesy of Dr. Stefano Caserta from the Institute of Immunology & Infection Research (Prof. Rose Zamoyska) at the University of Edinburgh.

APPENDIX 5:

DATA FOR CHAPTER 5

1. Table of the stability Boc group in solution phase:

Solution	% of Fmoc-Lys-OH formed			
	15 minutes	30 minutes	45 minutes	60 minutes
1% TFA/DCM	0	0	0	0
2% TFA/DCM	0	0	0	1
3% TFA/DCM	0	0.9	1	2
4% TFA/DCM	0	3	7	11
5% TFA/DCM	4	10	16	36
10% TFA/DCM	99	100	100	100
15% TFA/DCM	100	100	100	100
20% TFA/DCM	100	100	100	100
1% TFA in DCM/H_2O (99:1)	0	0	0	0
2% TFA in DCM/H_2O (99:1)	0	0	0	0
3% TFA in DCM/H_2O (99:1)	0	0	0	0
4% TFA in DCM/H_2O (99:1)	0	0	0	0
5% TFA in DCM/H_2O (99:1)	0	0	0	1
10% TFA in DCM/H_2O (99:1)	18	25	30	42

15% TFA in DCM/H_2O (99:1)	53	63	70	75
20% TFA in DCM/H_2O (99:1)	89	95	99	100

Solution	% of Fmoc-Lys-OH formed			
	75 minutes	90 minutes	105 minutes	120 minutes
1% TFA/DCM	0	0	0	0
2% TFA/DCM	1	1	1	2
3% TFA/DCM	4	6	10	12
4% TFA/DCM	15	17	20	24
5% TFA/DCM	45	51	59	65
10% TFA/DCM	-	-	-	-
15% TFA/DCM	-	-	-	-
20% TFA/DCM	-	-	-	-
1% TFA in DCM/H_2O (99:1)	0	0	0	0
2% TFA in DCM/H_2O (99:1)	0	0	0	0
3% TFA in DCM/H_2O (99:1)	0	0	0	0
4% TFA in DCM/H_2O (99:1)	0	0	0	0
5% TFA in DCM/H_2O (99:1)	1	1	1	1
10% TFA in DCM/H_2O (99:1)	46	53	57	63

15% TFA in DCM/H_2O (99:1)	80	84	88	90
20% TFA in DCM/H_2O (99:1)	100	100	100	100

2. MALDI-TOF spectrum of the unpurified NLLP **5.17**.

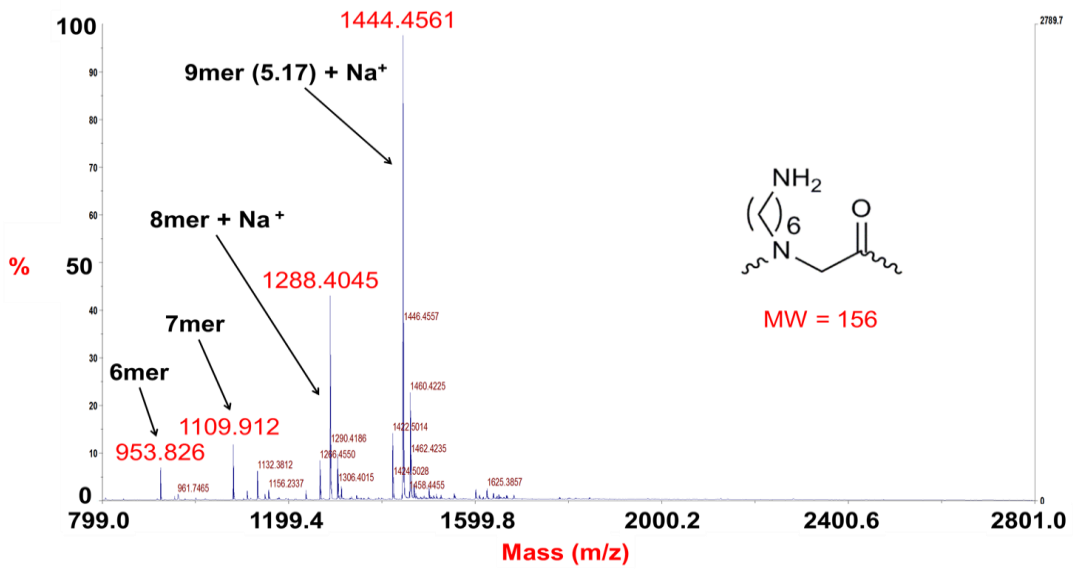

3. Analysis of the products obtained after cleavage of the resin **5.19** using DCM/TFA/H_2O (95: 5: 1) for 4 cycles of 10 minutes: MS and HPLC analysis of the cycle 2, 3 and 4.

a. MALDI-TOF spectrum of material recovered at the first cycle cleavage

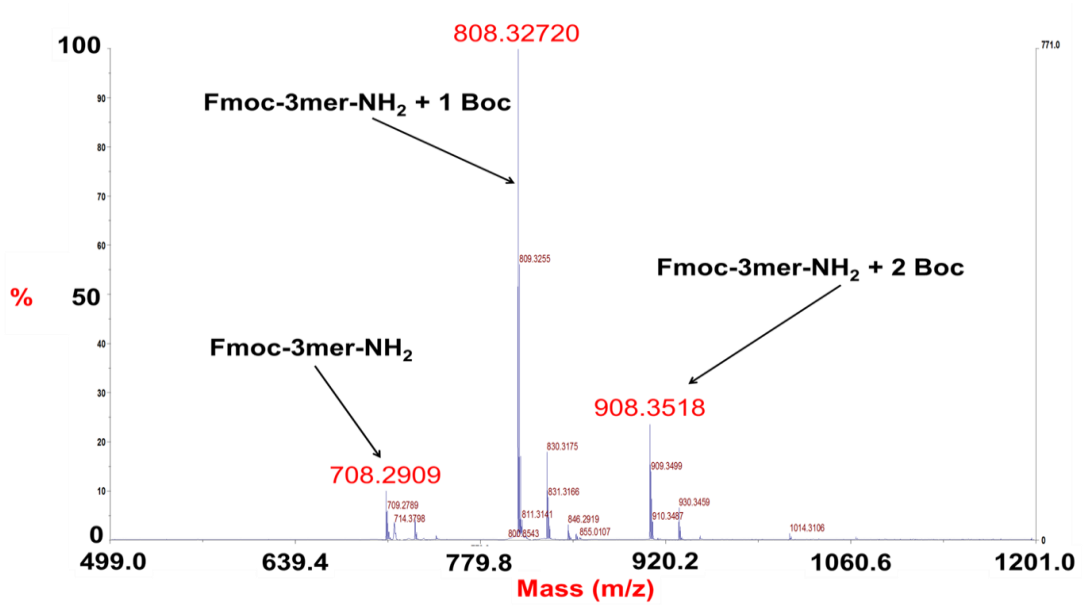

b. MALDI-TOF spectrum and HPLC (ELSD) trace of material recovered at the second cycle cleavage

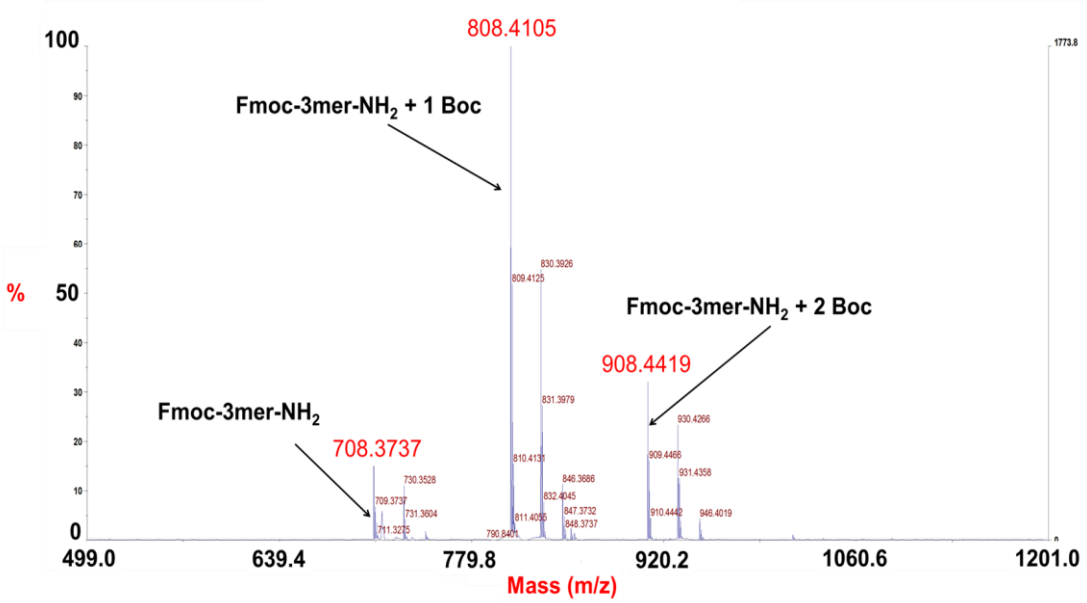

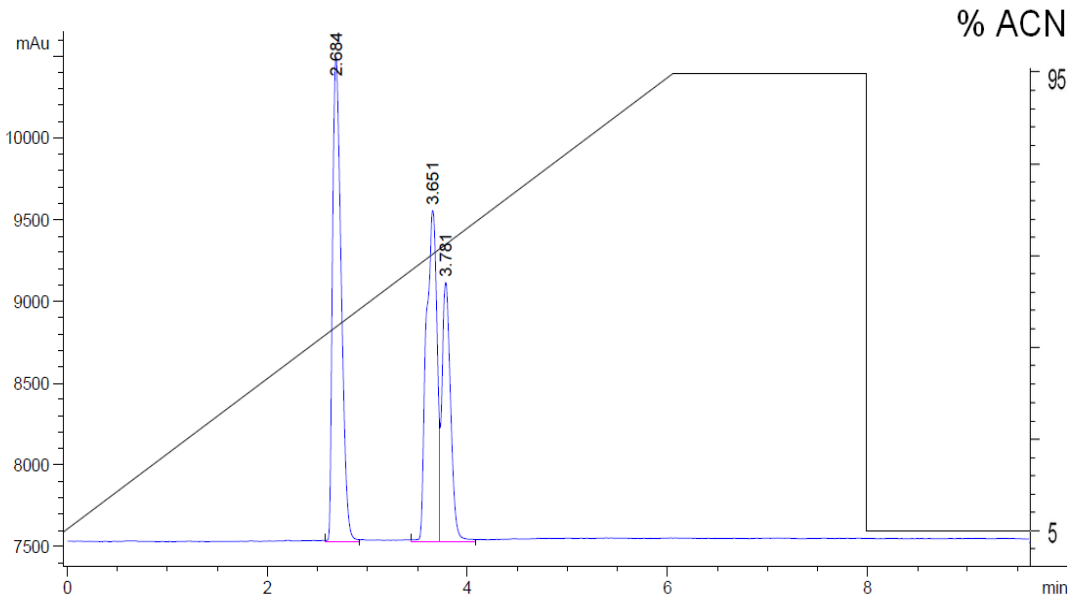

c. MALDI-TOF spectrum and HPLC (ELSD) trace of material recovered at the third cycle cleavage

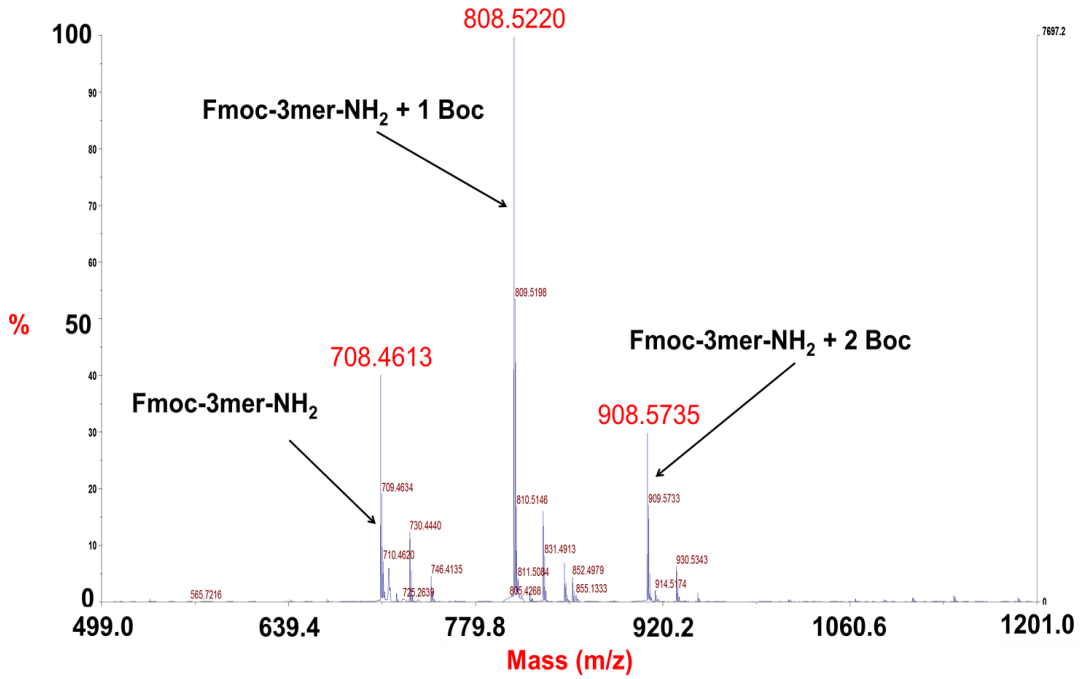

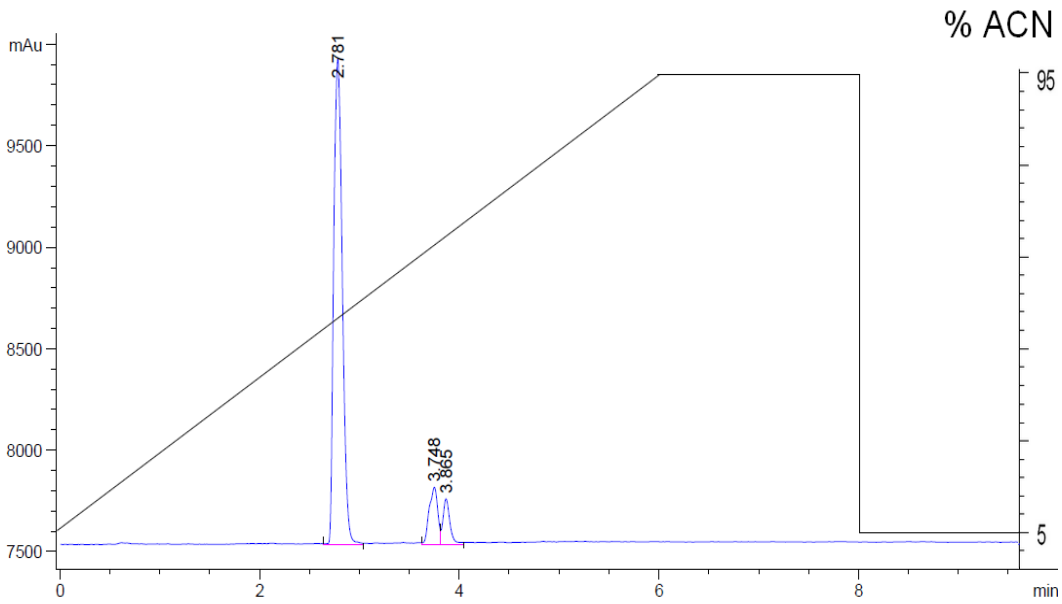

d. MALDI-TOF spectrum and HPLC (ELSD) trace of the material recovered at the forth cycle cleavage

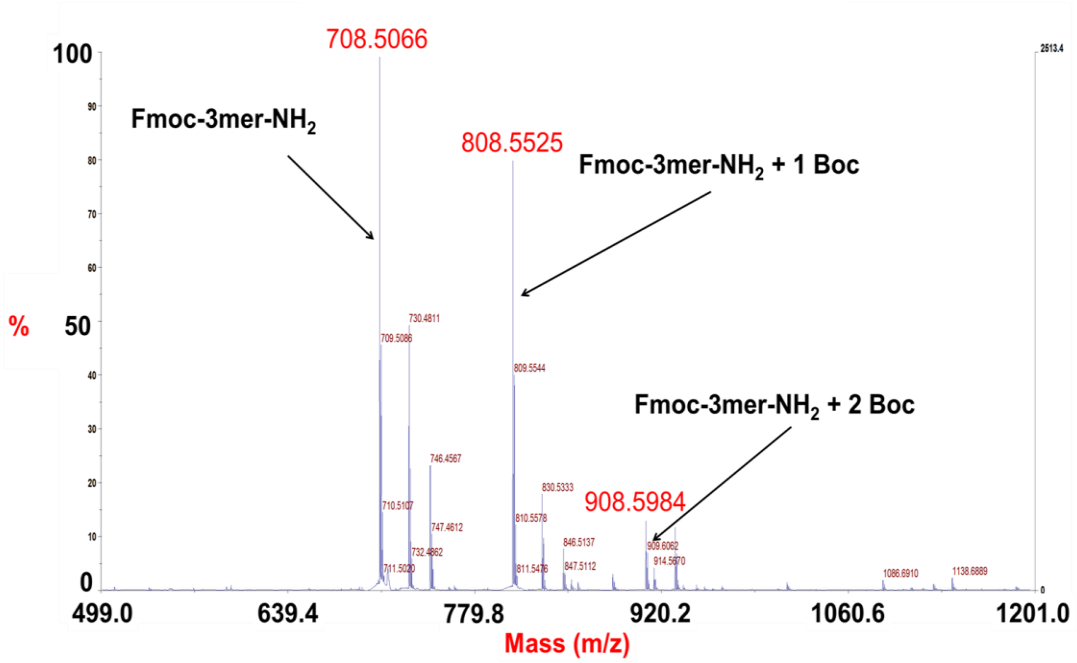

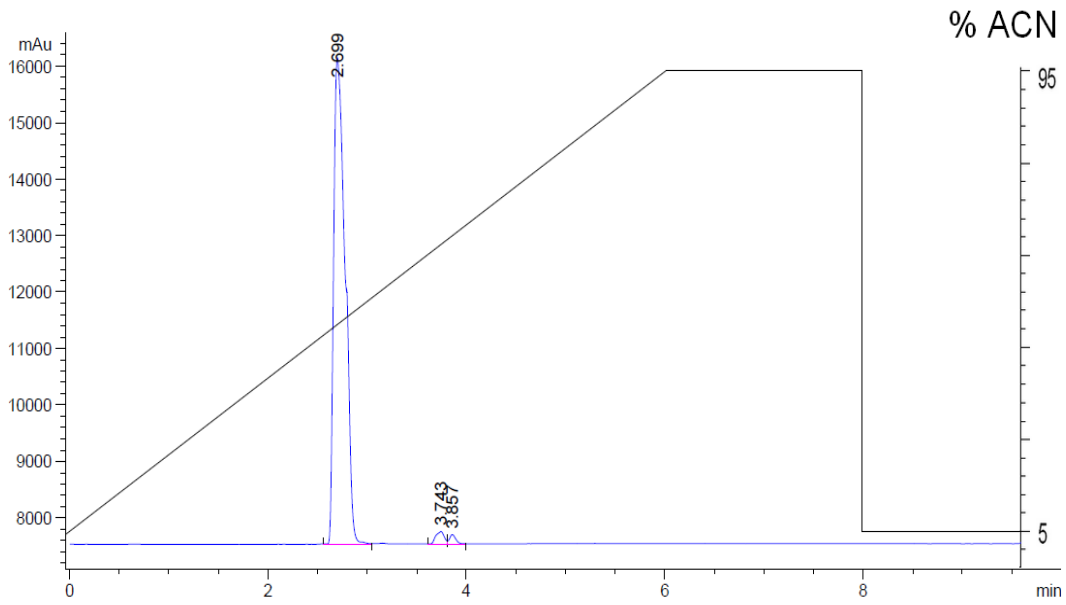
% ACN
mAu
16000
15000
14000
13000
12000
11000
10000
9000
8000
2.699
3.743
3.857
95
5
0
2
4
6
8
min

4. MALDI-TOF spectrum of the products obtained after cleavage of the resin **5.19** using DCM/TFA/H_2O (96: 3: 1) for 2 hours at room temperature.

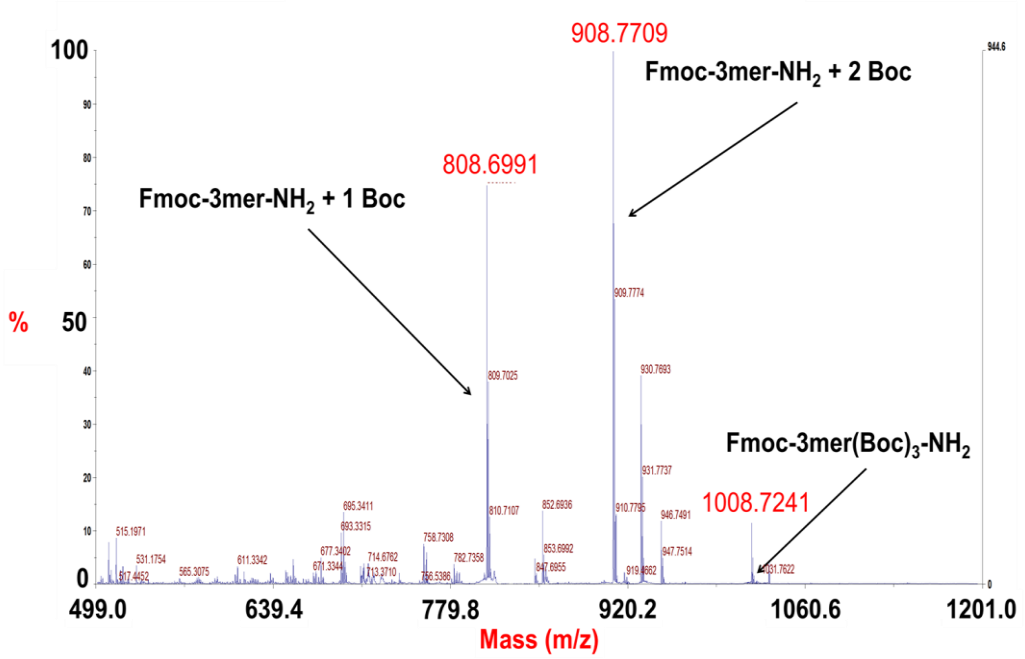

5. MALDI-TOF spectrum of the crude of Boc-9mer(Boc)$_9$-NH$_2$ (**5.22**) synthesis

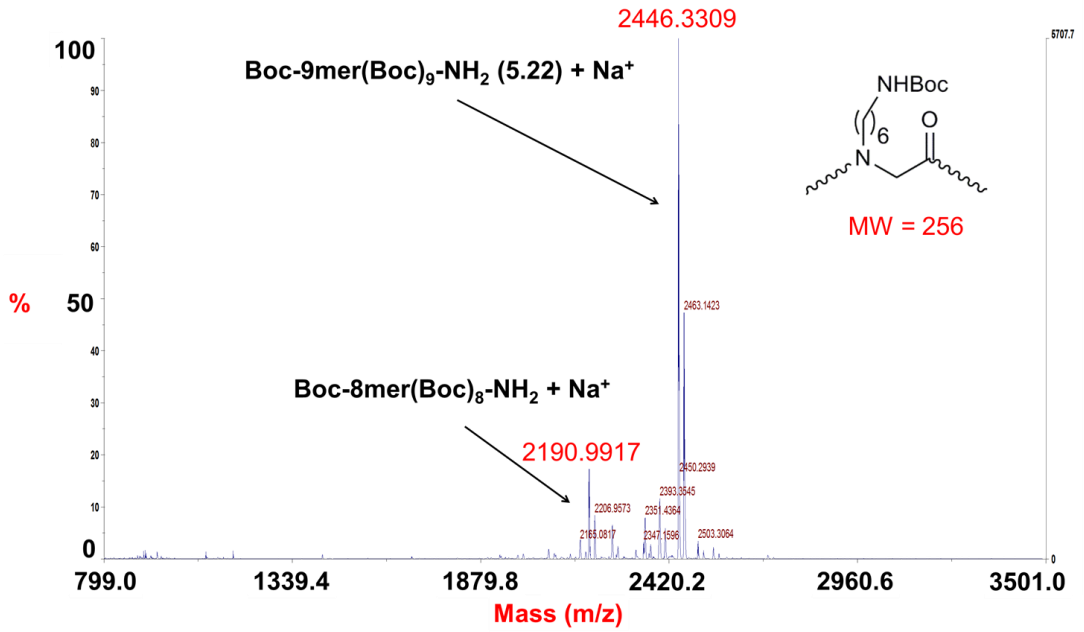

6. MALDI-TOF spectrum of the pure Boc-9mer(Boc)$_9$-NH$_2$ (**5.22**)

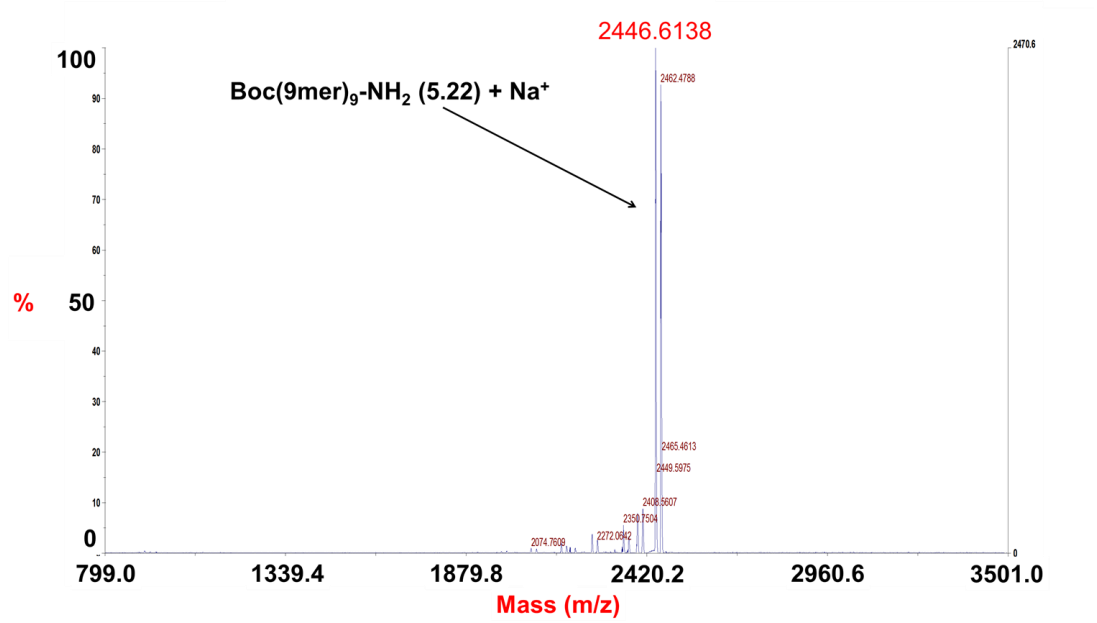

7. Relaxation delay assay: ^{1}H NMR spectrum (zoom between 6.2 and 2.0 ppm) of Boc-9mer(Boc)$_9$-NH$_2$ peptoid (**5.22**) in presence of 2,5-DMFu in $CDCl_3$, 400 MHz.

a. D1 = 1 second

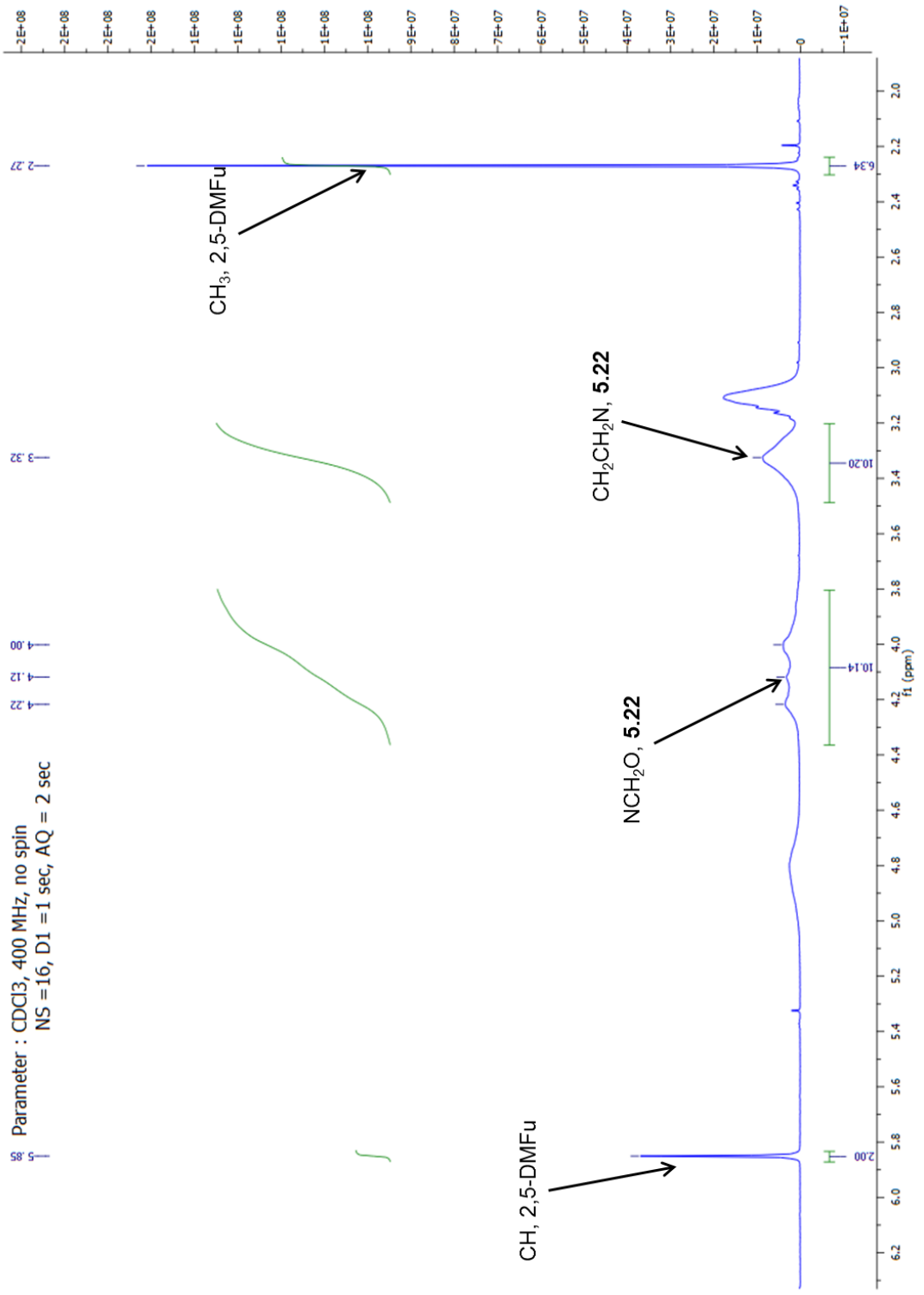

b. D1 = 10 seconds

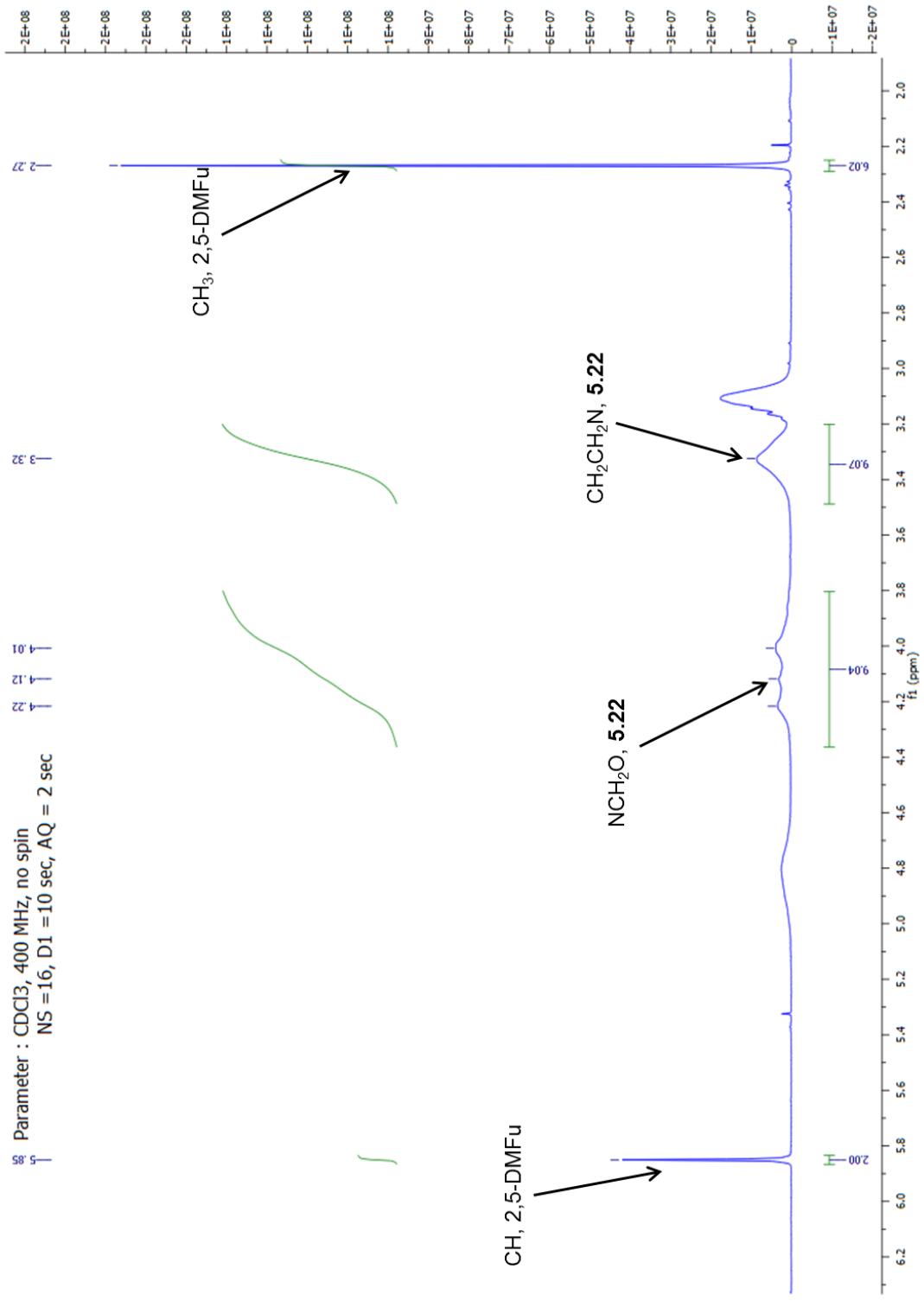

c. D1 = 30 seconds

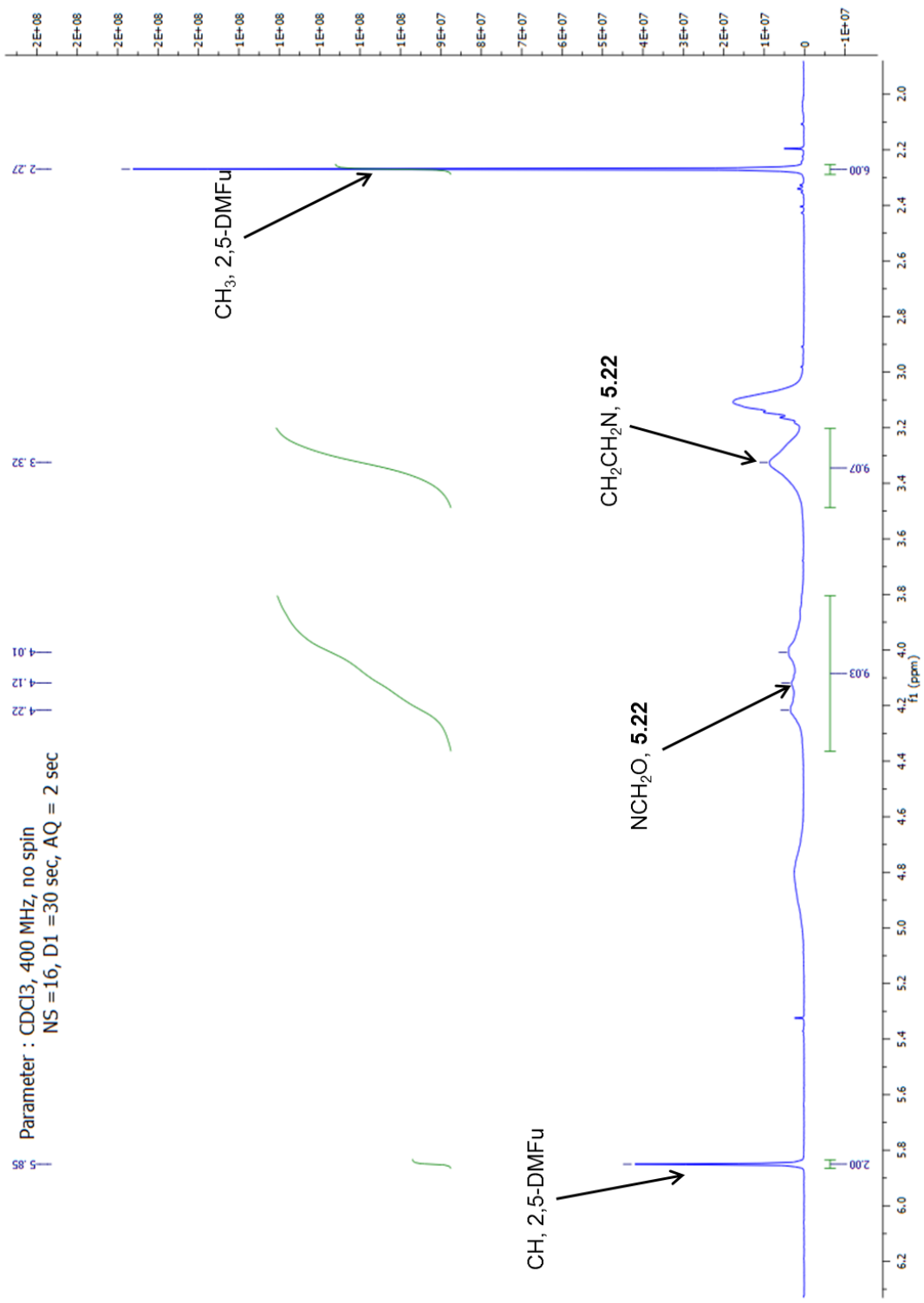

8. Suppression of 1,4-dioxane xignals in the 9mer **5.17** after Boc deprotection of the protected peptoid **5.22** using 1,4-dioxane/HCl (4M):

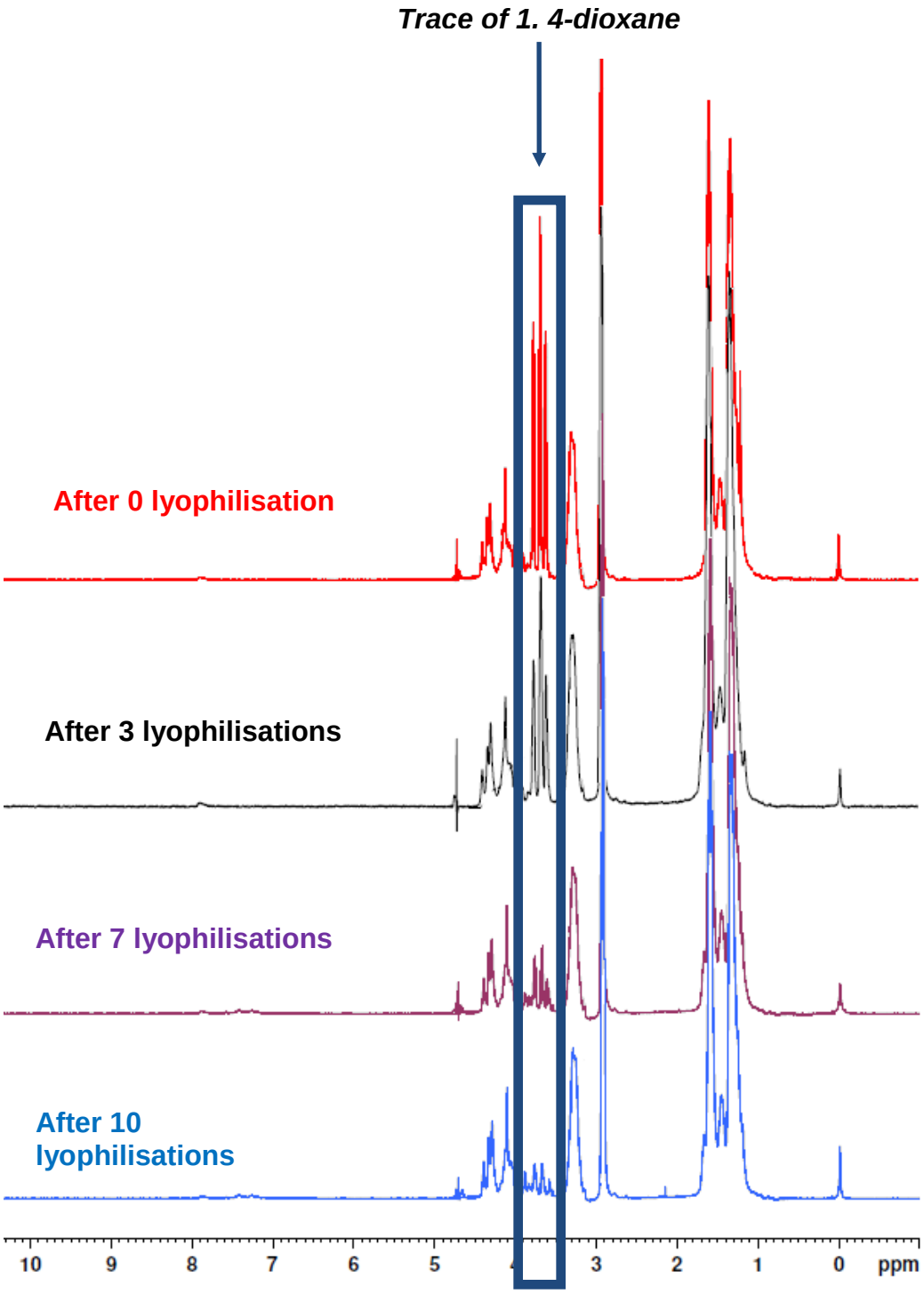

9. Analysis of the pure NLLP **5.17**

The spectra were obtained after deprotection of **5.22** with 20% TFA in DCM. The others deprotections gave very similar analytical spectrum.

a. MALDI-TOF spectrum

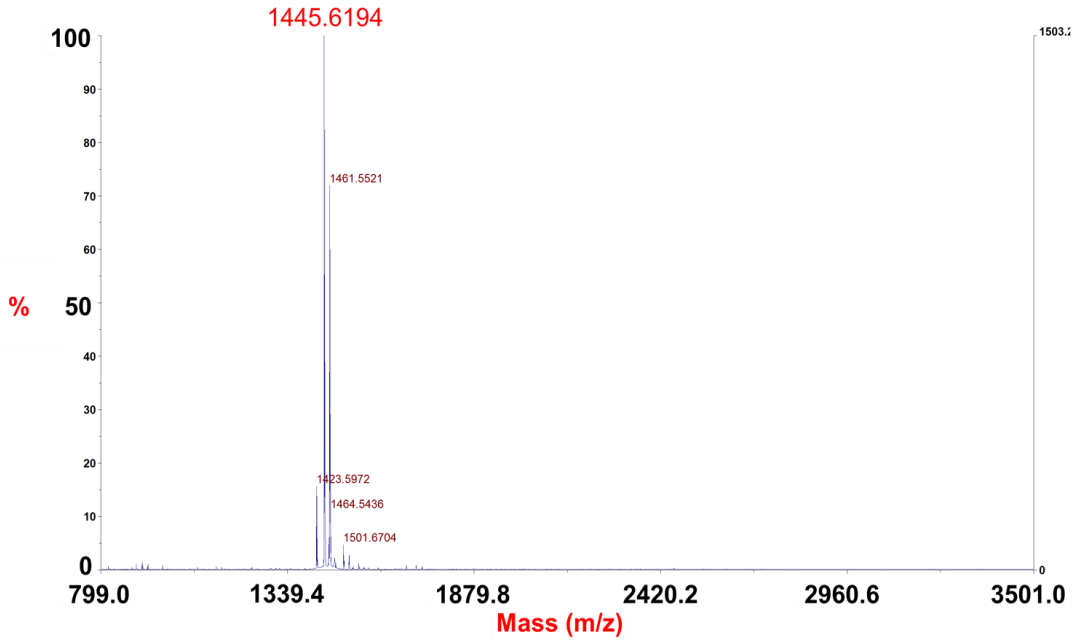

b. HPLC trace (ELSD)

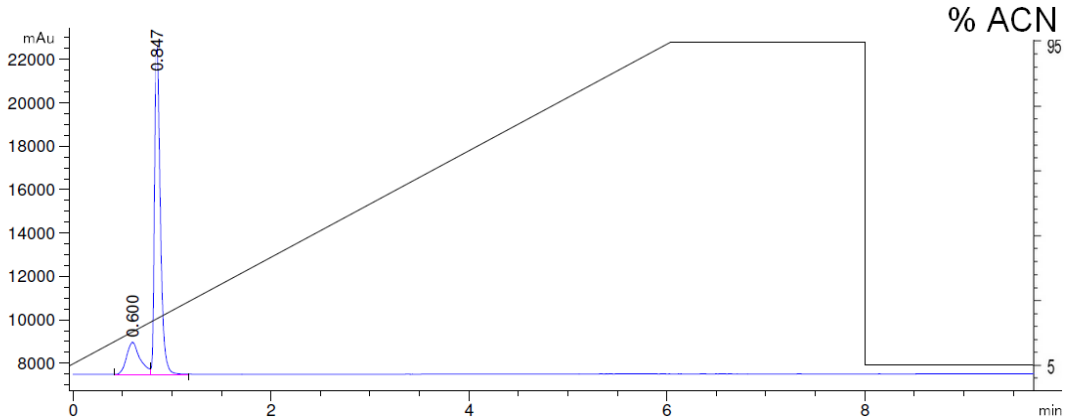

10. ^{1}H NMR of the 9mer peptoid **5.17**, 500 Hz, D_2O, eSpresat water suppression.

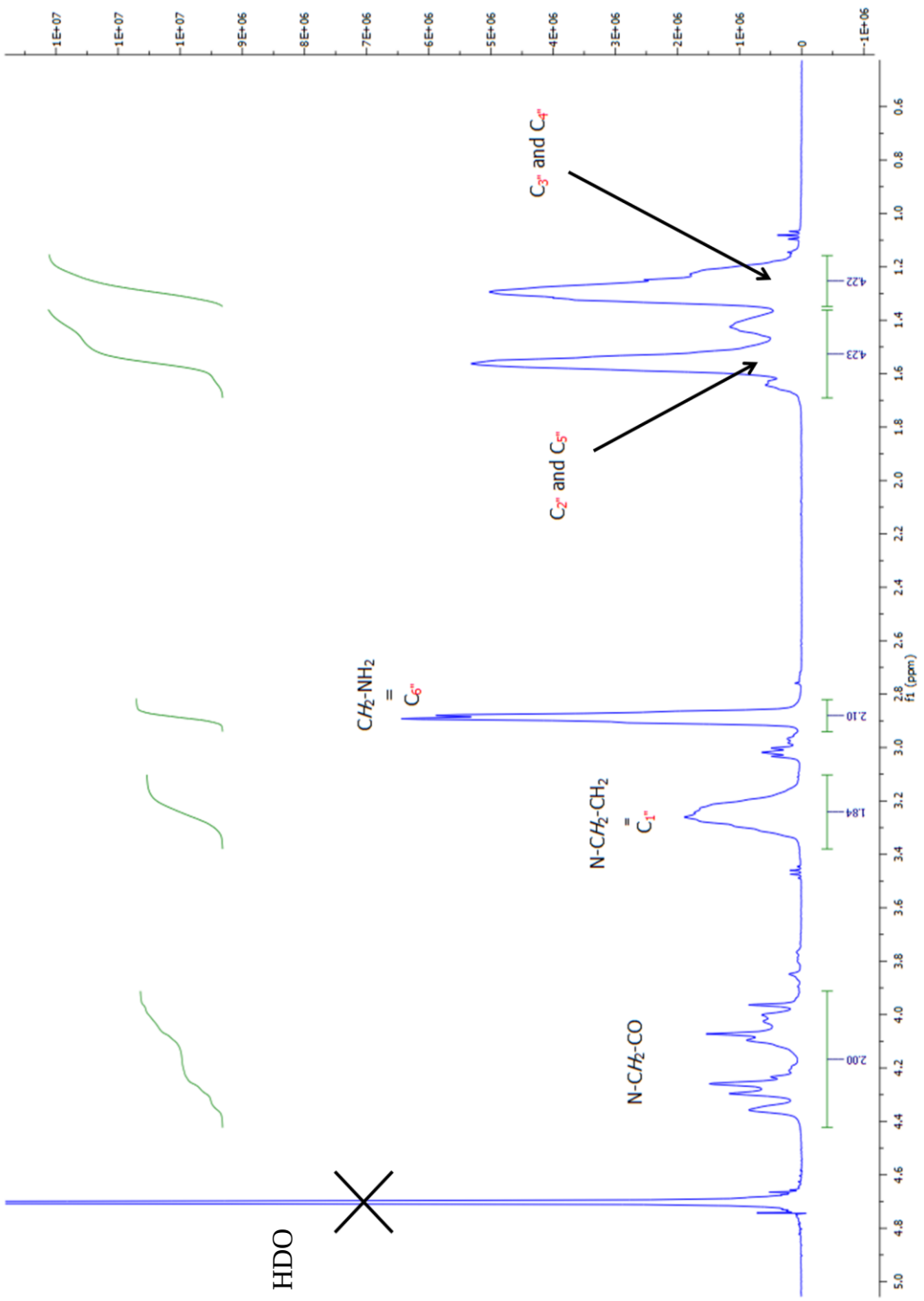

11. COSY NMR spectrum of the NLLP **5.17** (D_2O, 500 MHz)

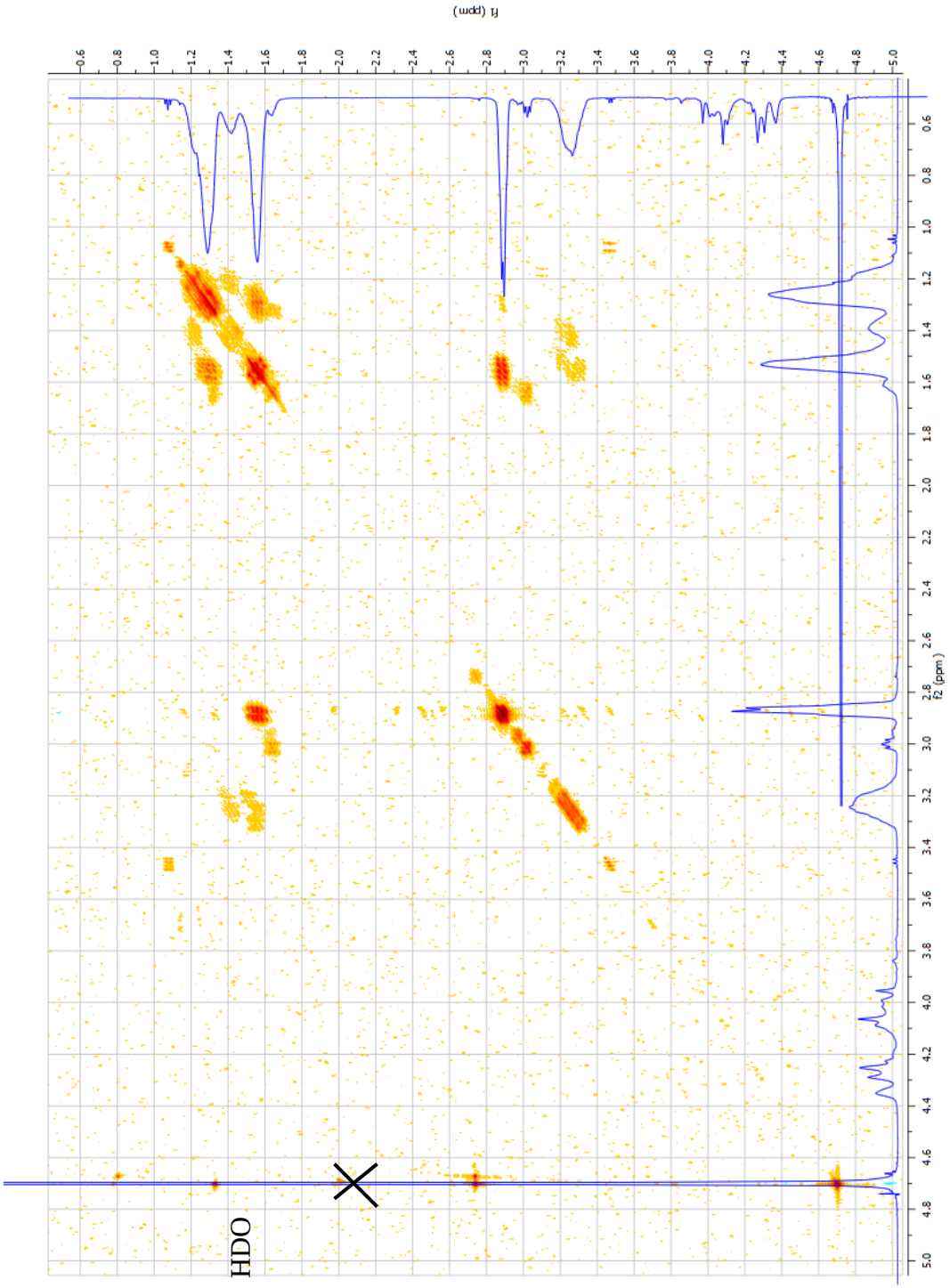

APPENDIX 6: PUBLICATIONS

PAPER www.rsc.org/faraday_d | Faraday Discussions

Multi-modal molecular imaging approaches to detect primary cells in preclinical models†

Kevin Dhaliwal,*[a] Lois Alexander,[b] Geraldine Escher,[b] Asier Unciti-Broceta,[b] Maurits Jansen,[a] Neil Mcdonald,[a] Juan M. Cardenas-Maestre,[b] Rosario Sanchez-Martin,[b] John Simpson,[a] Chris Haslett,[a] and Mark Bradley*[b]

Received 1st June 2010, Accepted 5th July 2010
DOI: 10.1039/c005410k

The need to understand cellular trafficking *in vivo in situ* requires the development and application of novel methodologies for cellular labeling and cell tracking. Here we applied new technologies associated with advances in molecular imaging to demonstrate the feasibility of labeling primary immune cells. We demonstrate the utility of fluorescently tagged polystyrene microspheres, MRI susceptible emulsions and cell entry peptoids. The adaptation of these labeling agents will permit cell specific delivery, diagnostic sensing and the delivery of therapeutic agents to sites of inflammation and infection.

Introduction

Molecular imaging (MI) is a rapidly expanding field. It can be described as a broad technological approach by which molecular events and pathways can be observed and defined *in vivo in situ* (and in real-time) without perturbation and pathological sampling of the process. The technological platforms by which imaging contrast is generated and detected have been extensively reviewed and compared for sensitivity and depth penetration.[1] Modalities include computerised tomography (CT), magnetic resonance imaging (MRI), positron emission tomography (PET), single photon emission computerised tomography (SPECT) and optical molecular imaging (OMI).

The principal clinical MI modalities historically have been PET and SPECT.[2] MRI and CT have also been used for MI approaches but the paucity of specific molecular probes and low sensitivity have limited their clinical application.

OMI remains the most utilised modality in preclinical MI and is a rapidly advancing field with potential to revolutionise near patient testing and theranostics. The detection of light deep within living tissues has been made possible by the dramatic advances in both fluorophores and physical systems able to excite and detect photons.[3] Photons can be detected at both the macroscopic and microscopic level *in vivo in situ* using instruments that are now commercially available. Preclinically on a whole-body level, OMI platforms exist that are able to perform both epi and transillumination. These platforms employ varying forms of excitation sources coupled with extremely sensitive charge coupled device (CCD) detection systems.

[a]*MRC Centre for Inflammation Research, Queen's Medical Research Centre, University of Edinburgh, 47 Little France Crescent, Edinburgh, UK. E-mail: kdhaliwa@staffmail.ed.ac.uk*
[b]*School of Chemistry, Joseph Black Building, Kings Buildings, West Mains Road, Edinburgh, UK. E-mail: mark.bradley@ed.ac.uk*

† All animal experimentation had local ethical committee approval and Home Office licence authorisation.

The accurate detection of fluorophores within tissue are limited to approximately three centimetres for epiillumination platforms, whilst transillumination approaches may be extended deeper utilising near-infrared (NIR) fluorophores.[4]

However, the lack of clinical grade molecular probes have hindered translational implementation of OMI, highlighting the need for multidisciplinary interactions for the development of *chemical* probes in *biological* systems that can be detected by *physical* systems. There is thus a pressing need for the concerted global clinical development and application of MI methodologies and solutions to provide fundamental answers to biological processes that remain poorly defined.

The need to detect the recruitment and trafficking of cells is a major area of interest in preclinical and clinical arenas in the context of both developing a better understanding of the temporal kinetics of cell recruitment in inflammation and also in the application of cell-based therapies. Optical imaging approaches permit the rapid, economical and multiplexed ability to delineate such trafficking in a whole-body scenario in preclinical imaging and also potentially in macroscopic and microscopic resolution in man. The choice of fluorophore is dictated primarily by the detection system to be used. In the context of whole-body imaging, NIR fluorophores are used to enable tissue penetration and overcome the extensive tissue absorption of light that occurs with wavelengths less than 600 nm.

Requirements for labeling cells for *in vivo* imaging include: speed, low toxicity, uniform labeling and intracellular targeting to ensure no label is easily transferred between live cells. We describe in this discussion report varying approaches: using optically encoded polystyrene microspheres, dual-modality perfluoropolyether (PFPE) emulsions for MRI and cell entry peptoids. We present data demonstrating labeling of primary murine macrophages and *in vivo* imaging in preclinical models. Table 1 summarises the *in vitro* data of toxicity, speed of labeling and efficiency of the three approaches for labeling primary murine macrophages.

Microspheres as cell tracking reagents

We have previously described the synthesis of robust, biocompatible, functionalised cross-linked polystyrene microspheres of highly defined sizes that can be highly-functionalised, with a range of cargos, ranging from fluorophores and proteins to sensors and small interfering ribonucleic acid (siRNA).[5,6] We have reported their efficient entry into a range of cell lines and primary cells *in vitro*.[7] Here we report their synthesis and use in *ex vivo* labeling of primary murine leucocytes and subsequent adoptive transfer by intravenous administration into animals with established inflammation.

Briefly, 0.5 μm polystyrene microspheres synthesised as previously were coupled to in-house synthesised Cy5.5 *via* an aminohexanoic spacer.[7,8] Primary murine macrophages were isolated by obtaining femurs of mice and flushing the bones with ice-cold Hank's Balanced Salt Solution (HBSS), triturating through a 19 gauge needle and then growing the cells under adherent conditions at 37 °C/5% CO_2 for 5 days in macrophage colony-stimulating factor enriched media as previously described.[9] Day 5 murine macrophages were then exposed to microspheres (86 μg mL^{-1}) in complete buffer at 37 °C/5% CO_2 (Dulbelco's Modified Eagle's Medium (DMEM) plus 10% fetal calf serum (FCS))

Cell viability was assessed by propidium iodide incorporation measured on flow cytometry (FACScan, BD). Confocal analysis with co-staining for the nucleus (DAPI) and cell membrane (actin) (cells labeled in adherent conditions on coverslips, washed extensively and then fixed for 15 min followed by confocal imaging) ensured intracellular localisation of microspheres. Flow cytometry of macrophages (FACSdiva) in fluorescent quenching solution (0.4% trypan blue in HBSS) ensuring that only internalised microspheres could be detected, confirmed over 65% labeling after 4 h. Fig. 1 demonstrates the intracellular accumulation of microspheres in primary macrophages. Direct intratracheal intubation of mice and single lung

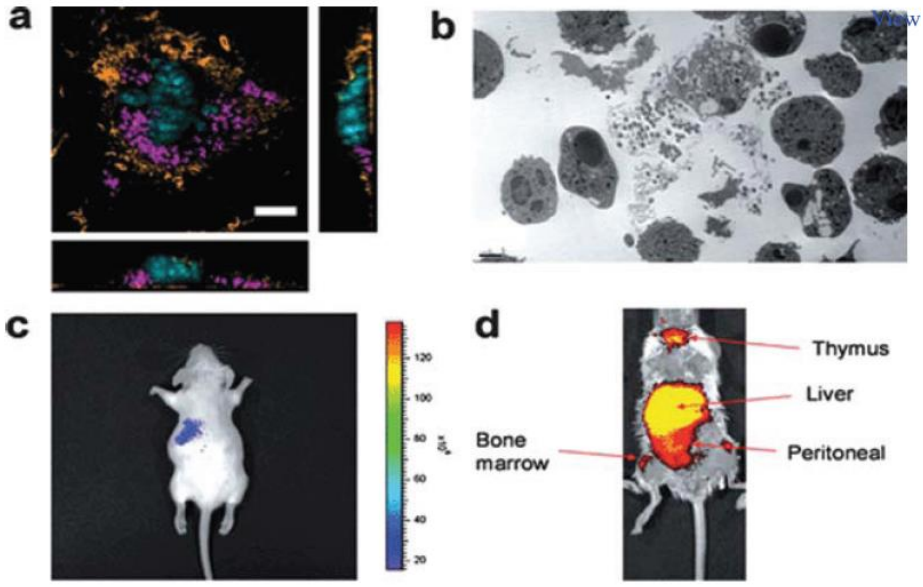

Fig. 1 Microsphere labeling of cells. (a) Merged confocal image of murine macrophages with microspheres (magenta), nuclei (DAPI, excitation 405 nm) and actin (phalloidin, excitation 543 nm). Scale bar 10 μm. (b) Apoptotic primary human neutrophils releasing intact microspheres. (c) Single lung instillation of 0.25×10^6 Cy 5.5 microspheres, imaged post instillation with a Xenogen IVIS Spectrum (excitation 675 nm, emission 720 nm). (d) 10×10^6 Cy7-microsphere labeled macrophages intravenously administered to mouse that had established peritoneal inflammation. Imaged with a Xenogen Spectrum (excitation 745 nm, emission 820 nm). Image shows cells recruited to liver and bone marrow but also to peritoneal space.

instillation of 0.5×10^6 labeled macrophages showed ability to detect microsphere labeled cells *in vivo in situ*. Extending the *in vivo* experiments, 10×10^6 Cy7 microsphere labeled cells were administered to mice that had an intraperitoneal injection of zymosan using methods described.[10] Mice were imaged the following day showing recruitment of cells to the peritoneal space. Control animals showed no peritoneal recruitment. Further, the ability of the microspheres to resist cellular degradation was tested by loading primary human neutrophils with microspheres and allowing the neutrophils to age overnight. Aged necrotic and apoptotic neutrophils were then fixed and imaged using scanning electron microscopy to demonstrate that the microspheres remained intact. Hence it is likely that any protracted imaging of cell fate *in vivo in situ* with fluorescently tagged microspheres may be difficult to interpret as cell-free microspheres may contribute to the signal/contrast. Nevertheless, the electron microscopy imaging confirmed that the polystyrene microspheres resist the proteolytic repertoire of the neutrophil, and suggest that further studies to use the neutrophil as a potential 'Trojan horse' are warranted.

Fluorescent perfluoropolyether nanoemulsions as MRI cell tracking agents

Cell tracking utilising MRI has received much interest with a number of iron-based contrast reagents.[11] Iron loading of cells with superparamagnetic iron oxide (SPIO) or ultrasmall superparamagnetic iron oxide (USPIO) results in signal dephasing due to magnetic field inhomogeneity leading to a signal 'void' or hypointensity on T2 and T2* weighted scans in the vicinity of cell localisation. An example of this is demonstrated in Fig. 2 where primary murine macrophages were isolated as described above and either:

(a) incubated with 100 μg ml^{-1} Feridex™ (SPIO) for 4 h in DMEM plus 10% FCS at 37 °C/5% CO_2; or

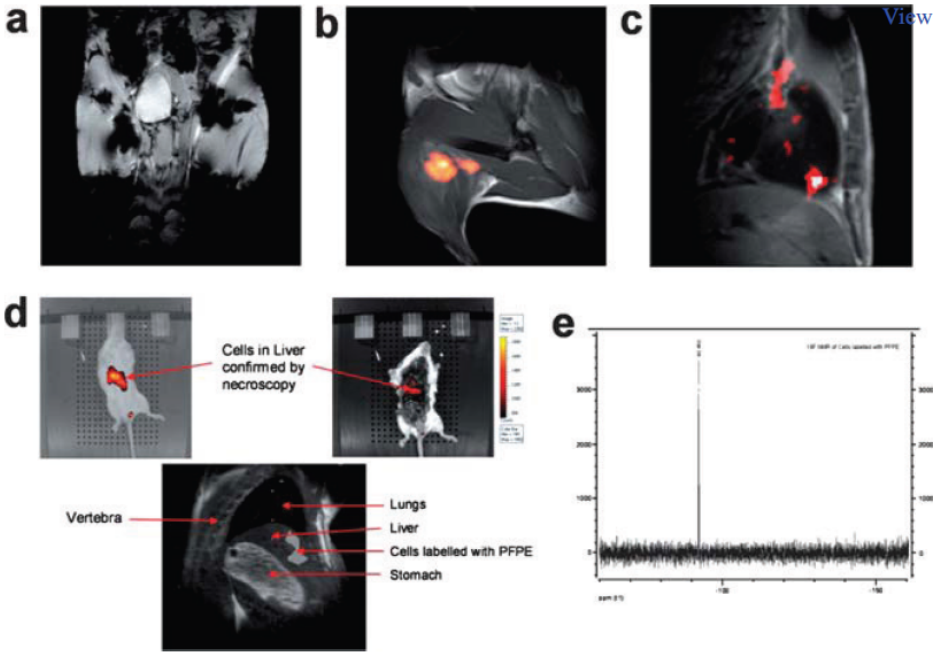

Fig. 2 MRI imaging of PFPE emulsions loaded into cells. (a) T2 weighted image of lower thighs of mice showing 'voids' of signal in the right thigh from 5×10^6 Cd11b Miltenyi Biotec microbead labeled macrophages and void in the left thigh from 5×10^6 Feridex labeled macrophages. (b) ^{19}F MRI imaging of 5×10^6 labeled macrophages injected directly into the the right thigh superimposed on a ^{1}H image for structure. (c) ^{19}F MRI of 5×10^6.macrophages labeled with PFPE directly instilled into the murine lung. (d) 5×10^6 Cy7-PFPE labeled macrophages homing to the murine liver. Optical images were acquired with a 3 s exposure with excitation filter 745 nm, emission filter 820 nm with a Xenogen Spectrum. MRI image of upper torso of the same mouse showing ^{19}F labeled cells in liver. Image acquisition was over one hour. (e) *In vitro* nuclear magnetic resonance (NMR) of labeled cells showing a single specific resonance for ^{19}F measured in a Brucker 400 MHz NMR.

(b) labeled with CD11b microbeads (Miltenyi Biotec) according to the manufacturers instructions.

5×10^6 cells were injected into each thigh of a mouse and imaged on a Varian 7 Tesla MRI DirectDrive system using a gradient echo scan (matrix size 256 × 256, FOV 40 × 40 mm, TR 423 ms, TE 10 ms, flip angle 30°, slice thickness 1 mm (30 slices), number of averages 2). Despite the localised injection of the cells, a considerable 'volume or blooming' effect was observed. This highlights some of the challenges in using paramagnetic iron for tracking cells with MRI using T2 weighted sequences in that the local signal void makes it impossible to perform quantification. Additionally, signal voids depend on the contrast that is inherently present in the tissue and inflammatory events may themselves cause signal dephasing due to iron-rich red cell extravasation.

One approach to overcome this problem is the ability to multiplex MRI using ^{1}H imaging for structural resolution alongside ^{19}F imaging for the localisation of labeled cells. This results in a positive contrast MRI cell labeling technique. We hence generated ^{19}F nanoemulsions using similar methods described previously.[12] PFPE emulsions were prepared using a 1 : 1 molar ratio of perfluoropolyethelene glycol (molecular weight 1750, Exfluor) and sterile filtered Pluronic (Sigma-Aldrich) with emulsification by sonication giving an average particle diameter of 150 nm (as measured by laser diffraction). In addition NIR fluorescent PFPE emulsion particles were prepared by mixing the PFPE emulsion with Cy7.

Primary murine macrophages (isolated as described above) were incubated (25μl mL^{-1} final concentration of ^{19}F nanoemulsions) for four hours in DMEM

with 10% FCS at 37 °C/5% CO_2 prior to extensive washing. 5×10^6 cells were then injected into the thigh of a mouse. ^{19}F Images were acquired on a Varian 7T DirectDrive MRI system using a 20 mm surface coil tuned to the ^{19}F resonance frequency. ^{1}H images were acquired with the same coil tuned to the ^{1}H resonance frequency and similar MRI parameters to serve as anatomical reference. Sequential images of the mouse were acquired using a respiratory-gated fast spin echo sequence (echo train length 8) with a matrix size of 256 × 256 and a field of view of 40 mm × 40 mm. The TR was 1000 ms and the TE was 10 ms. Slices were acquired with 2 mm thickness (8 slices) and the total number of averages was 512.

The ability to detect the cells within the thigh using this approach then led us to test if it would be possible to detect ^{19}F labeled primary macrophages in the lungs of a mouse. Cells were labeled as previously described and anaesthetised mice intubated with a 19 gauge needle. 5×10^6 cells were instilled in a 50 μl volume of PBS and the mouse allowed to recover prior to MRI imaging. Fig. 2 shows the distribution of labeled cells within the murine thorax. The integration time for scanning for ^{19}F labeled cells was over one hour. Imaging animals for this duration of time is fraught with anaesthetic concerns with the potential to modify the underlying inflammatory process. Hence we dual labeled our nanoemulsions by incorporating Cy7 during the emulsification process. Murine macrophages were injected intravenously into mice which allowed the dual detection with MRI and reflectance optical imaging and localisation of the cells within the liver. Optical imaging using the Xenogen Spectrum required only a one second exposure on large binning compared to over one hour with MRI, highlighting the sensitivity, speed and economical utility of preclinical optical imaging.

Cell entry peptoids as cell tracking agents

The description of HIV TAT as an efficient protein transduction domain heralded the development of peptide facilitated cell delivery.[13] Despite the widespread realisation of HIV TAT as an efficient means to potentiate cell entry, it remains only 50–60% efficient in delivering some NIR dyes into primary cells while also showing some cellular toxicity.[14] Hence based on our recent description of cell entry peptoids with nine lysine-containing repeating units as efficient tools for cell entry, we attached a NIR fluorophore to our nonalysine-like peptoid (NLLP) (Fig. 3).[15] (NLLPs were generated by using a highly-optimised microwave-based solid-phase synthesis route as detailed previously with the NIR dye coupled by using the *N*-hydroxysuccinimidyl ester of the Cy5.5 or Cy7 dye).[8] Cy5.5 and Cy7 tagged peptoids displayed no detectable toxicity at any of the concentrations used in this study and achieved rapid cell entry with 100% efficiency in primary murine macrophages. Washing and fixing at time points up to 30 min demonstrated efficient labeling within minutes. Intracellular incorporation was confirmed in all primary cells by confocal microscopy. Inflammatory cytokine liberation from primary murine macrophages loaded with Cy5.5-NLLP was not elevated compared to controls. Imaging of mice that had lipopolysaccharide (50 μg *Escherichia coli* LPS intratracheally instilled 24 h earlier) lung injury demonstrated recruitment of Cy7-NLLP labeled cells to the lung. The facile, non-toxic nature of this primary cell labeling technique for cell tracking and cell delivery opens up promising therapeutic applications.

Discussion

The ability to rapidly and safely deliver cargoes into cells and optically detect these cargoes will be of major interest in clinical applications to either use cells as 'Trojan horses', to deliver therapeutic payloads or to use cell recruitment and behaviour as key cellular 'sensors' of disease initiation, progression and resolution.

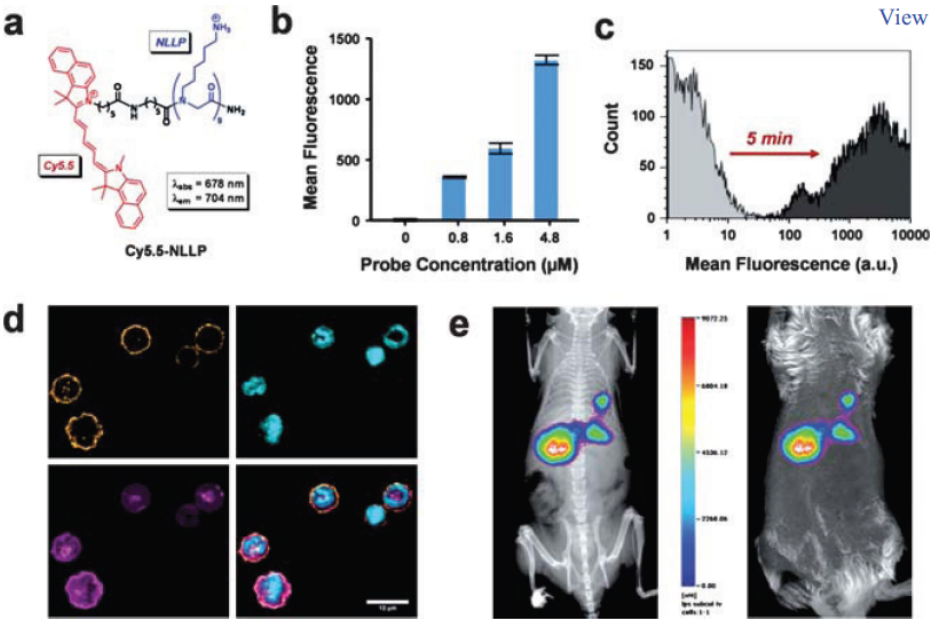

Fig. 3 (a) Chemical structure of the Cy5.5-NLLP. (b) Comparative uptake studies of Cy5.5-NLLP at various concentrations in primary murine macrophages as measured by flow cytometry analysis. (c) Representative cell population/fluorescence charts from primary murine macrophages: untreated cells (light grey) and cells after 5 min incubation with Cy5.5-NLLP (dark grey). (d) Confocal images of freshly-flushed murine marrow after 10 min incubation with 4.8 μM Cy5.5-NLLP: actin staining (543 nm excitation), DAPI nuclei staining (405 nm excitation), Cy5.5-NLLP labeling (633 nm excitation), and composite. (e) Tracking of Cy7-NLLP labelled murine macrophages to lipopolysaccharide induced pulmonary inflammation showing liver, spleen and lung recruitment. Image on left with X-ray superimposed on reflectance fluorescent images on Kodak Multispectral FX Pro (excitation 745 nm, emission 820 nm). Image on right showing the same mouse with just reflectance. Images show utility of using multimodal imaging with combined X-ray and fluorescent reflectance imaging to confirm localisation of cell recruitment.

The sensitivity, speed of imaging and anatomical resolution are all factors that need to be weighed up when determining the optimal modality for detection of cells *in vivo in situ*. Table 1 compares the three approaches used in this paper for tracking primary murine macrophages.

Microspheres represent a versatile platform for cell entry and cell tracking. Microspheres are easily functionalised and we have shown that they can be exploited to deliver proteins, siRNA, DNA and even pH and calcium sensors to the cell.[16] These remarkable facets of functional cellular delivery alongside other documented uses of microspheres as being scaffolds for the attachment and delivery of drugs such as antimicrobials emphasises their unique and effective versatility.[17]

^{19}F imaging permits positive contrast MRI and the ability to quantify labeled cells *in vivo in situ* and investigators have reported the ability to detect small numbers of cells using this methodology.[18] However, the current formulation of the nanoemulsions requires extended coincubation to gain intracellular entry. Further chemical modifications to improve cell entry and speed are required. Additionally ^{19}F MRI *in vivo in situ* requires prolonged image acquisition.

The NLLP represents the most efficient and versatile cell labeling tool discussed in this report. Five minutes incubation is all that is required for 100% cell labeling, with no toxicity demonstrated in cells or mice. The versatility of its chemical synthesis allows the decoration with a myriad of cargoes and opens up wide therapeutic possibilities that are currently being explored for theranostic applications *in vivo*.

Table 1 Summary of cell labeling characteristics of agents used to 'tag' primary murine marrow phages. Data represents means and standard error of means in brackets derived from three independent experiments in triplicate for labeling of 5×10^6 primary murine macrophages. Significance ($p < 0.05$) by Student's *t*-test.

Cell labeling agent	% cell death[a]	% labeling[b]	TNF secretion[c]	Speed of imaging/s[d]
Feridex	22 (6.2)	45 (7.2)	38 (8.2)	180
CD11b microbeads	9 (3.4)	85 (9.4)	10 (3.5)	180
Cy7 PFPE	17 (4.3)	55 (6.3)	17 (4.2)	40 800
Cy 5.5 microspheres	6 (1.4)	68 (6.7)	ns	1
Cy 5.5 and Cy 7-peptoid	ns	100	ns	1

[a] Increase over control of propidium iodide incorporation 4 h after labelling. [b] Prussian blue staining for Feridex and Cd11b microbeads and fluorescence intensity increase on flow cytometry for Cy7 and Cy5.5 over control. [c] Cytokine in cell free supernatants at 16 h corrected for total protein and expressed as percentage increase over control. [d] 5×10^6 cells injected directly into thigh of mice and time in seconds to acquire images.

With regard to cell labeling, whilst adoptive transfer techniques such as the ones illustrated above represent one approach, a more robust and accurate method for 'sensing' inflammatory cell recruitment is the direct intravenous administration of cell specific tags. Developing these methodologies is the focus of ongoing work.

OMI is now well established in preclinical models as a rapid, cost effective platform to assess disease processes *in vivo in situ*. OMI has versatility over other modalities due to the range of possible fluorophores that can be spectrally discriminated. With the advent of human optical imaging becoming a reality utilising both microscopic devices such as confocal microendoscopy and hand-held or boom-operated devices for theatre, OMI has the potential to become a point of care MI modality.[19,20] Additionally, the expanding portfolio of 'smart' molecular chemical probes permits the multiplexed detection of disease processes.[21] The recent description of the ability to detect nuclear sources using CCD devices opens up intriguing and versatile applications.[22]

Acknowledgements

This work was supported by the MRC, EPSRC and BBSRC.

References

1 F. A. Jaffer and R. Weissleder, *JAMA, J. Am. Med. Assoc.*, 2005, **293**, 855.
2 G. D. Luker and D. Piwnica-Worms, *Acad. Radiol.*, 2001, **8**, 4.
3 S. A. Hilderbrand and R. Weissleder, *Curr. Opin. Chem. Biol.*, 2010, **14**, 71.
4 F. Leblond, S. C. Davis, P. A. Valdes and B. W. Pogue, *J. Photochem. Photobiol., B*, 2010, **98**, 77.
5 R. Sanchez-Martin, M. Muzerelle, N. Chitkul, S. How, S. Mittoo and M. Bradley, *ChemBioChem*, 2005, **6**, 1341.
6 R. Sanchez-Martin, M. Cuttle, S. Mittoo and M. Bradley, *Angew. Chem., Int. Ed.*, 2006, **45**, 5472.
7 L. Alexander, K. Dhaliwal, J. Simpson and M. Bradley, *Chem. Commun.*, 2008, 3507.
8 M. Lopalco, E. M. Koini, J. K. Cho and M. Bradley, *Org. Biomol. Chem.*, 2009, **7**, 856.
9 T. S. Wilkinson, K. Dhaliwal, T. W. Hamilton, A. F. Lipka, L. Farrel, D. J. Davidosn, R. Duffin, A. C. Morris, C. Haslett, J. R. Govan, C. D. Gregory, J. M. Sallenave and A. J. Simspon, *Am. J. Pathol.*, 2009, **174**, 1338.
10 I. Bournazou, J. D. Pound, R. Duffin, S. Bournazos, L. A. Melville, S. B. Brown, A. G. Rossi and C. D. Gregory, *J. Clin. Invest.*, 2009, **119**, 20.
11 J. W. Bulte, *AJR, Am. J. Roentgenol.*, 2009, **193**, 314.

12 M. Srinivas, P. A. Morel, L. A. Ernst, D. H. Laidlaw and E. T. Ahrens, *Magn. Reson. Med.*, 2007, **58**, 725.
13 H. Brooks, B. LeBleu and E. Vives, *Adv. Drug Delivery Rev.*, 2005, **57**, 559.
14 C. Berger, H. U. Gremlich, P. Schmidt, C. Cannet, R. Kneuer, P. Hiestand, M. Rausch and M. Rudin, *J. Immunol. Methods*, 2007, **323**, 65.
15 A. Unciti-Broceta, F. Diezmann, C. Y. Ou-Yang, M. A. Fara and M. Bradley, *Bioorg. Med. Chem.*, 2009, **17**, 959.
16 R. Sanchez-Martin, L. Alexander and M. Bradley, *Ann. N. Y. Acad. Sci.*, 2008, **1130**, 207.
17 Y. I. Jeong, H. S. Na, J. W. Nah and H. C. Lee, *J. Pharm. Sci.*, 2009, **98**, 3659.
18 M. Srinivas, A. Heerschap, E. T. Ahrens, C. G. Figdor and I. J. Vries, *Trends Biotechnol.*, 2010, **28**, 363.
19 L. Thiberville, M. Salaün, S. Lachkar, S. Dominique, S. Moreno-Swirc, C. Vever-Bizet and G. Bourg-Heckly, *Eur. Respir. J.*, 2009, **33**, 974.
20 A. Da Silva, J. M. Dinten, J. L. Coll and P. Rizo, *Conf. Proc. IEEE Eng. Med. Biol. Soc.*, 2007, **2007**, 526.
21 A. Signore, S. J. Mather, G. Piaggio, G. Malviya and R. A. Dierckx, *Chem. Rev.*, 2010, **110**, 3112.
22 H. Liu, G. Ren, Z. Miao, X. Zhang, X. Tang, P. Han, S. S. Gambhir and Z. Cheng, *PLoS One*, 2010, **5**, e9470.

MedChemComm

www.rsc.org/medchemcomm

Volume 2 | Number 11 | November 2011 | Pages 1023–1126

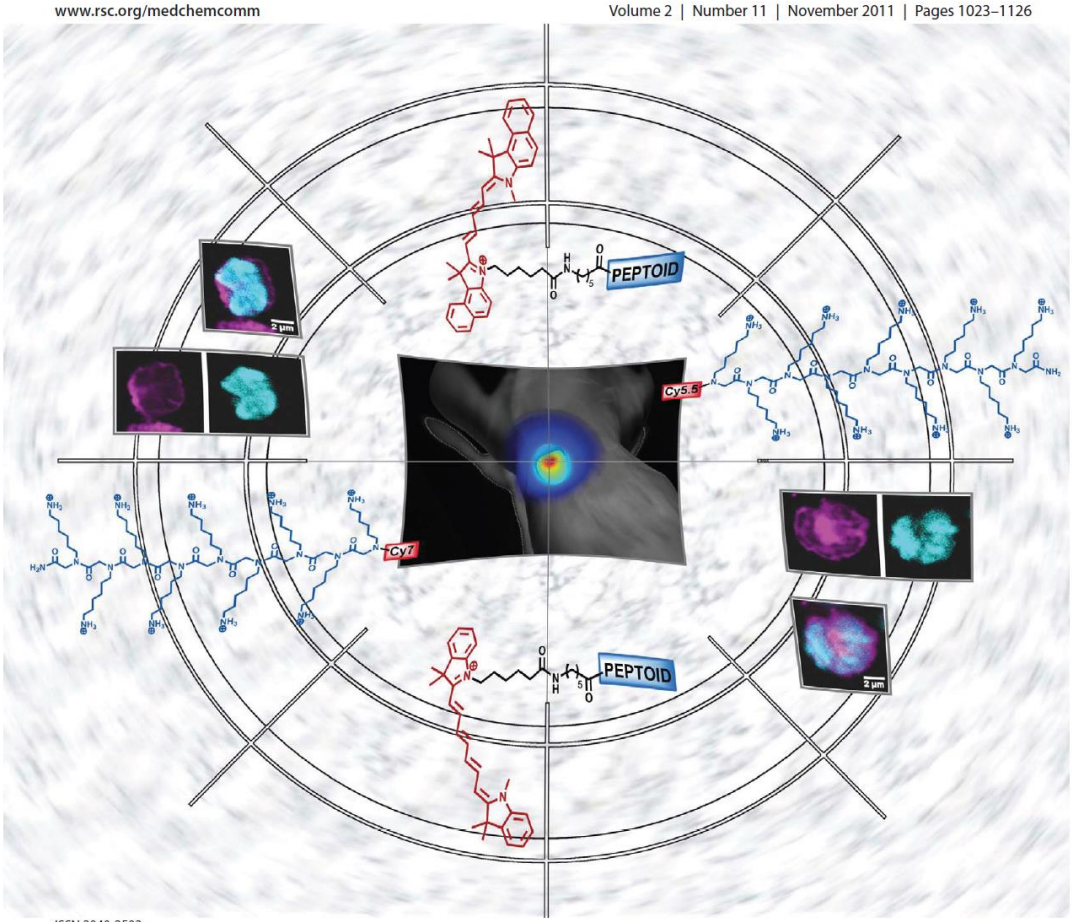

ISSN 2040-2503

RSC Publishing

EFMC European Federation for Medicinal Chemistry

2011 C CHEMISTRY International Year of CHEMISTRY 2011

2040-2503(2011)2:11;1-C

Cite this: *Med. Chem. Commun.*, 2011, **2**, 1050

www.rsc.org/medchemcomm

CONCISE ARTICLE

Far red and NIR dye-peptoid conjugates for efficient immune cell labelling and tracking in preclinical models†

Kevin Dhaliwal,[*a] Géraldine Escher,[b] Asier Unciti-Broceta,[c] Neil McDonald,[a] A. John Simpson,[d] Chris Haslett[a] and Mark Bradley[*b]

Received 1st July 2011, Accepted 30th July 2011
DOI: 10.1039/c1md00171j

Innate immune cell ingress into the site of inflammation is central for the efficient clearance of pathogens. However, in some circumstances the inflammatory response may become pathogenic to the host. Understanding the temporal ingress of innate immune cells is thus essential to predict both the defensive and adverse effects mediated by these cells in an infectious process and for developing novel therapeutic strategies. In this context, optical imaging has emerged as a powerful technique for the visualization of specific cellular events in preclinical models. Herein we describe a non-covalent tagging strategy to stably label innate immune cells using *in vivo*-traceable cell penetrating peptoids and their application in real-time imaging of cell migration in murine models, thereby providing a sensitive and cost effective way to visualize cellular recruitment in preclinical models of inflammation.

Introduction

Phagocytic cells such as monocytes, macrophages and neutrophils are white blood cells responsible for the host innate defense against infection.[1] Circulating monocytes differentiate into macrophages which are resident phagocytes involved in the orchestration of the innate response upon local pathogen recognition. Neutrophils are circulating granulocytes recruited to sites of acute inflammation and constitute the first line of cellular defense in bacterial infection.[2] However, although neutrophils are essential for the efficient clearance of intracellular and extracellular microbial pathogens, they also have the potential to cause tissue damage as a result of a dynamic imbalance between the levels of proteases and protective protease modulators.[3] Given the potential of neutrophils to injure tissues, the inflammatory response has evolved to facilitate their efficient removal after bacterial clearance. However, in some instances neutrophils may continue to be recruited and in the face of their poor clearance toxic neutrophil derived "products" may perpetuate the inflammatory response.[3,4] Understanding the migration and trafficking patterns of phagocytes is thus central to predict and control both the defensive and adverse effects mediated by these cells as well as to potentially devise novel immune cell-delivered therapeutic strategies.[5]

Optical imaging is widely used in preclinical research offering a number of practical advantages compared to other imaging modalities, specifically its sensitivity, moderate cost, non-invasiveness and direct cellular readout.[6,7] Among the possible chemical and biological strategies that can be employed to "optically" label primary cells (*e.g.* antibody labelling, genetic labelling – with bioluminescent or fluorescent GFP-like proteins–, and chemical labelling),[7–9] synthetic probes are probably the most cost-effective and straightforward, just requiring cell isolation, labelling with the probe of choice and subsequent infusion back into the host.[9,10] Nevertheless, due to the high sensitivity to inflammatory stimulation and short lifetime of immune cells,[11] probe labelling needs to have a number of essential features namely the ability to label cells rapidly (within minutes), lack of toxicity or alteration of normal cell behaviour, and be stably retained within the cells for long duration studies (days to weeks).

Currently four types of chemically-based fluorescent probes are used for *in vivo* cell tracking studies: (i) cell-permeable dyes which enter cells by difussion and bind strongly to intracellular structures by non-covalent interactions (*e.g.* DNA-binding dyes, membrane-inserting fluorescent dyes, *etc*);[12] (ii) labelling probes that covalently link to intracellular components,[13,14] with dyes such as 5-chloromethylfluorescein diacetate (also known as CellTracker Green) which has demonstrated high efficacy and delays the "label leaking" from the cells; and (iii) dye-labelled cell-penetrating probes, which enter cells by probe-mediated translocation and do not bind permanently to intracellular

[a]*MRC Centre for Inflammation Research, University of Edinburgh, 47 Little France Crescent, Edinburgh, UK. E-mail: kdhaliwa@staffmail.ed.ac.uk*
[b]*School of Chemistry, University of Edinburgh, West Mains Road, Edinburgh, UK. E-mail: mark.bradley@ed.ac.uk*
[c]*Edinburgh Cancer Research Centre, MRC Institute of Genetics and Molecular Medicine, University of Edinburgh, Crewe Road South, Edinburgh, UK*
[d]*Institute of Cellular Medicine, Medical School, Newcastle University, Newcastle upon Tyne, UK*

† Electronic supplementary information (ESI) available: Experimental description of the synthesis of compounds **5** and **6**, their characterization, and biological assays. See DOI: 10.1039/c1md00171j

structures (*e.g.* fluorescently-labelled cell-penetrating peptides (CPPs)),[15] and (iv) cell parenting micro and nanoparticles.[16] The first two kinds of labelling probes are particularly effective and have been widely used *in vivo*.[12–14] However, high levels of labelling equates to extensive protein or DNA modification which is undesirable as it may affect cell viability and normal cell behaviour. This risk can be circumvented by using reagents of the third category, fluorescently-labelled cell penetrating peptides, which are capable of translocating a wide range of covalently-linked cargoes across the plasma membrane.[17] However these are often susceptible to protease degradation, can be toxic and display lower labelling efficiency for primary cells.[18]

An attractive strategy to address these issues is the use of cell penetrating peptoids,[19–22] which are known to be resistant to proteolysis and have been shown by our group to offer some of the highest cell labelling/delivery efficacies known.[23] In particular the nona(*N*-aminohexyl)peptoid (9-mer) which display remarkable delivery properties, being able to efficiently label different cell lines within minutes (Fig. 1).[23] In this study we report the synthesis of peptoids conjugated to far red to near infra-red (NIR) dyes and their efficient application for *ex vivo* labelling and *in vivo* real-time tracking of primary phagocytes.

Results and discussion

Fluorescently-labelled cell penetrating peptoids were synthesized using microwave-assisted solid-phase synthesis as shown in Scheme 1. Peptoids were assembled following an Fmoc-based strategy on Rink amide-functionalized aminomethyl polystyrene resin **1** using orthogonally-protected lysine-like monomer **2**.[24,25] An in-house-optimized monomer-based synthesis was used[23,25] instead of the submonomer approach,[26] driven by the length of the desired product (9-mer) and the highly hydrophilic nature of the final conjugates that make purification of truncations problematic. Monomer assemblings were carried out using a two-step procedure: (i) piperidine-mediated Fmoc deprotection; (ii) followed by coupling with monomer **2** using HOBt/DIC. This procedure was repeated nine times to obtain the oligomer with desired length. The resulting resin **3** was Fmoc deprotected and, using the same procedure, coupled with a six carbon spacer (Fmoc-Ahx-OH) to give resin **4** (this spacer separates the dye from the peptoid and allows efficient conjugation of the dye). Finally, dyes were coupled onto the resin-bound peptoid **4** which was subsequently, Boc-deprotected and cleaved from the resin under acidic conditions to give **5** and **6**.

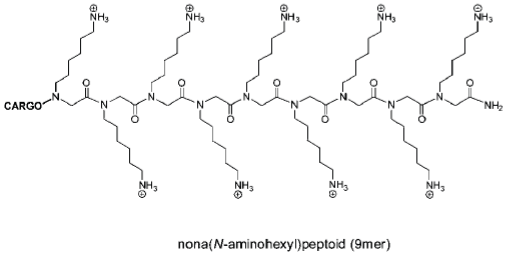

Fig. 1 Cell-penetrating peptoid.[23]

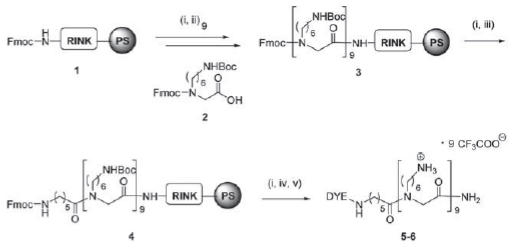

Scheme 1 Fmoc solid-phase synthesis of fluorescently-labelled cell penetrating peptoids. Reagents and conditions: (i) 20% piperidine in DMF, 10 min (×2); (ii) monomer **2** (3 equiv.), DIC (3 equiv.), HOBt (3 equiv.), DMF, μW, 60 °C, 20 min; (iii) Fmoc-Ahx-OH (3 equiv.), DIC (3 equiv.), HOBt (3 equiv.), DMF, μW, 60 °C, 20 min; (iv) activated dye (see ESI), DMF; (v) TFA/TIS/H_2O (95 : 2.5 : 2.5), 4 h.

The cyanine dyes are a group of fluorophores commonly used for optical imaging applications due to their tunable wavelengths (red to near infrared) and high extinction coefficients.[27] One of the most attractive subgroups are the indocyanine dyes that, in contrast with other cyanines dyes, avoid self-aggregation.[28] The polymethine indocyanine dyes (Cy) used to label the peptoid were readily generated by minor modifications to a generic synthetic procedure to allow conjugation to the peptoid.[29] As expected, dye-labelled peptoids **5** and **6** displayed emission maximum peaks in the far red (710 nm) and NIR (779 nm) region respectively (see Fig. 2a and ESI).

Assessment of the *ex vivo* labelling abilities of **5** and **6** was carried out with innate immune cells. Primary murine bone marrow monocytes and neutrophils were retrieved, incubated with dye-labelled peptoids **5** and **6** for 10 min and analyzed by

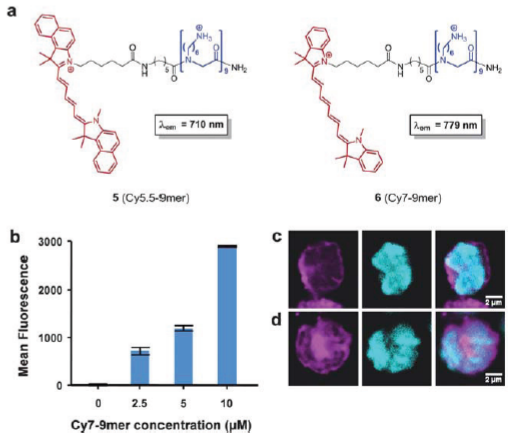

Fig. 2 (a) Structures of the dye-labelled peptoids **5** and **6**. (b) Comparative fluorescence intensity of labelled primary murine monocytes following 10 min incubation with Cy7-9-mer **6** at various concentrations as measured by flow cytometry. (c–d) Confocal images of (c) monocytes and (d) neutrophils after 10 min incubation with 5μM Cy5.5-9-mer **5**. Left: Cy5.5-9-mer **5** (633 nm excitation). Middle: DAPI nuclei staining (405 nm excitation). Right: composite image. Scale bar: 2 μm.

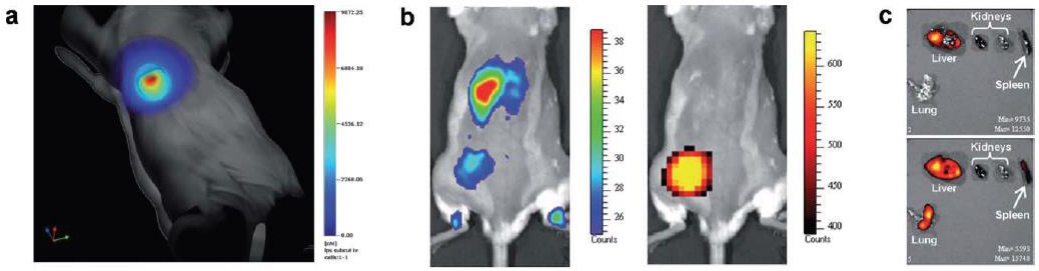

Fig. 3 Non-invasive optical imaging of mice with localized inflammation. (a) Tracking of Cy7-9-mer **6** labelled primary monocytes to LPS-induced subcutaneous inflammation using thoracic gated tomographic imaging. (b) Tracking of Cy5.5-9-mer **5** labelled primary neutrophils to subcutaneous inflammation induced by LPS-impregnated matrigel implanted in the left thigh of a mouse. Right panel: luminescence *in vivo* imaging after intraperitoneal administration of luminol showing myeloperoxidase activity in the site of inflammation. Left panel: fluorescence *in vivo* imaging of Cy5.5-9-mer **5** labelled neutrophils after intravenous infusion showing unilateral recruitment to the site of injury in the same mouse. (c) Dual channel fluorescent imaging of neutrophil recruitment to different organs after LPS-induced lung injury. Cy5.5-9-mer **5** labelled neutrophils were adoptively transferred 4 h after injury and Cy7-9-mer **6** labelled neutrophils 24 h after injury. 48 h after LPS lung injury, organs were removed and imaged under different channels (upper panel: ex/em 680/720 nm; lower panel: ex/em 745/820 nm), showing Cy5.5-9-mer **5** labelled neutrophil presence exclusively in liver while Cy7-9-mer **6** labelled neutrophils were present in liver, spleen and lungs of the same animal.

flow cytometry and confocal microscopy. Flow cytometry analyses showed 100% cell labelling, with a dose-dependent increase in fluorescence intensity (Fig. 2b) and no signs of cytotoxicity by MTT or TO-PRO-3 exclusion assays (see ESI). The cytoplasmic location of the labelled-peptoids was demonstrated by confocal microscopy (Fig. 2c, d), whilst inflammatory cytokines liberated from primary murine monocytes and neutrophils treated with Cy7-9-mer **6** were not elevated over controls.

The spectral properties of the dyes were optimal for live whole body, non-invasive biophotonic imaging in mice,[30] allowing investigation of dynamic migration and functional viability of labelled phagocytes which were infused intravenously into syngeneic mice that had localized subcutaneous inflammation.[31]

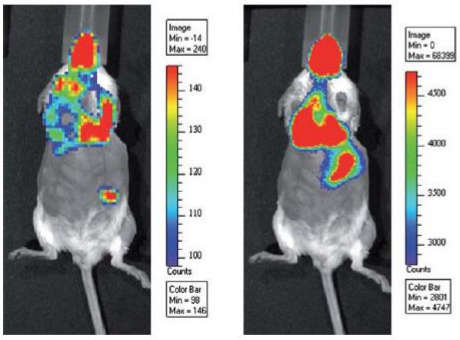

Fig. 4 *In vivo* functional viability study. Primary murine macrophages were chemically labelled with Cy7-9-mer **6** and labelled by transduction with an adenovirus encoding luciferase. These doubly-labelled macrophages were instilled into the murine lung and imaged 24 h later. Left panel shows fluorescence imaging under a Cy7 filter (ex/em 745/820 nm). Right panel shows luminescence imaging of the same animal after intraperitoneal luciferin administration. Images captured on a Xenogen Spectrum.

As shown in Fig. 3a, infused primary monocytes loaded with Cy7-9-mer **6** demonstrated tracking to sites of subcutaneous inflammation.

Further evidence for selective homing of innate immune cells was carried out utilising a recently described luminescent model[32] for imaging sites of inflamation based on the chemiluminescent oxidation of luminol due to reactive oxygen species produced by constitutive neutrophil myeloperoxidase. This model was used to identify an adoptive neutrophil-specific myeloperoxidase activity in a model of subcutaneous inflammation induced by lipopolysaccharide (LPS)-impregnated matrigel implanted in the left thigh of the mice. Cy5.5-9-mer **5** labelled neutrophils were infused intravenously in the injured mice and, after 4 h, luminol administered intraperitoneally. Optical imaging showed selective unilateral accumulation of Cy5.5-9-mer labelled neutrophils within the site of active inflammation with signal colocalisation with myeloperoxidase-mediated bioluminiscence of luminol (Fig. 3b).

The ability to spectrally unmix the far red and near infrared dyes and facilitate dual fluorescent channel imaging was exploited to delineate kinetic recruitment of adoptively transferred neutrophils to sites of inflammation. Two neutrophil populations were separately labelled with Cy5.5-9-mer **5** and Cy7-9-mer **6** and then infused intravenously at different time points after injury: 4h and 24 h after inducing lung injury, respectively. As shown in Fig. 3c, imaging of retrieved organs showed distinct time-dependent migration pattern, with only neutrophils infused 24 h after injury being efficiently recruited to the site of inflammation (lung).

Neutrophils and monocytes are primary cells recruited at the earliest stages of inflammation and their tracking has previously required the utilisation of radioisotopic methods due to difficulties in their rapid and non-toxic labelling.[33] Our data using optical agents is the first description of tracking monocytes and neutrophils *in vivo* utilising internalised non-covalent optical tracers as opposed to membrane dyes. Optimal cell isolation, labelling and injection into syngeneic mice was performed within

2 h of marrow harvest, with a total peptoid-cell incubation time of ten minutes. This speed of labelling being specifically facilitated by the nona(*N*-aminohexyl)peptoid (Fig. 1).

Finally, the *in situ* functional viability of peptoid-treated cells was demonstrated by labelling primary murine macrophages with Cy7-9-mer **6** and simultaneously transfecting with a replication-deficient adenovirus encoding luciferase. These cells were instilled directly into the murine lung and imaged 24 h later. Fluorescence imaging confirmed localisation in the lung, while intraperitoneal luciferin injection led to the generation of luminescence in the same region (Fig. 4), thus demonstrating the viability of labelled, adoptively transferred cells.

Conclusions

In summary, we have developed an efficient method to track innate immune cell migration *in vivo* using far red and NIR dye-labelled peptoids. Thanks to their proteolytic resistance and high labelling efficiency, neutrophils and monocytes were tracked for over three days, allowing the visualization of their recruitment to sites of inflammation. Their remarkably fast labelling, low toxicity and long-term stability, make the use of fluorescently-labelled peptoids highly attractive tools for *in vivo* optical imaging.

The authors would like to acknowledge funding from the EC FP6 (Marie Curie EST Fellowship to G.E.) and the MRC (K.D, C.H and M.B.). We also thank the MRC IGMM (A.U.B.) and Jules Thorne Trust (A.J.S.).

Notes and references

1 M. T. Silva, *J. Leukocyte Biol.*, 2009, **87**, 93–106.
2 T. S. Wilkinson, K. Dhaliwal, T. W. Hamilton, A. F. Lipka, L. Farrell, D. J. Davidson, R. Duffin, A. C. Morris, C. Haslett, J. R. W. Govan, C. D. Gregory, J.-M. Sallenave and A. J. Simpson, *Am. J. Pathol.*, 2009, **174**, 1338–1346.
3 A. G. Rossi, J. M. Hallett, D. A. Sawatzky, M. M. Teixeira and C. Haslett, *Biochem. Soc. Trans.*, 2007, **35**, 288–291.
4 S. Mandl, C. Schimmelpfennig, M. Edinger, R. S. Negrin and C. H. Contag, *J. Cell. Biochem.*, 2002, **87**, 239–248.
5 C. Haslett, *Am. J. Respir. Crit. Care Med.*, 1999, **160**, S5–11.
6 V. Ntziachristos, J. Ripoll, L. V. Wang and R. Weissleder, *Nat. Biotechnol.*, 2005, **23**, 313–320.
7 B. Isherwood, P. Timpson, E. J. McGhee, K. I. Anderson, M. Canel, A. Serrels, V. G. Brunton and N. O. Carragher, *Pharmaceutics*, 2011, **3**, 141–170.
8 H. Hong, Y. Yang, Y. Zhang and Weibo Cai, *Curr. Top. Med. Chem.*, 2010, **10**, 1237–1248.
9 K. M. Marks and G. P. Nolan, *Nat. Methods*, 2006, **3**, 591–596.
10 K. Dhaliwal, L. Alexander, G. Escher, A. Unciti-Broceta, M. Jansen, N. Mcdonald, J. M. Cardenas-Maestre, R. Sanchez-Martin, J. Simpson, C. Haslett and M. Bradley, *Faraday Discuss.*, 2011, **149**, 107–114.
11 E. L. Becker, *J. Leukocyte Biol.*, 1990, **47**, 378–89.
12 C. R. Parish, *Immunol. Cell Biol.*, 1999, **77**, 499–508.
13 F. K. Swirski, C. R. Berger, J.-L. Figueiredo, T. R. Mempel, U. H. v. Andrian, M. J. Pittet and R. Weissleder, *PLoS One*, 2007, **2**, e1075.
14 A. E. Foster, S. Kwon, S. Ke, A. Lu, K. Eldin, E. Sevick-Muraca and C. M. Rooney, *Appl. Opt.*, 2008, **47**, 5944–5952.
15 G. Tünnemann and M. C. Cardoso, in *Membrane-Active peptides: methods and results on structure and function*, ed. M. Castanho, IUL Publishers, La Jolla (US), pp. 331–362.
16 R. M. Sachez-Martin, M. Muzerelle, N. Chitkul, S. E. How, S. Mittoo and M. Bradley, *ChemBioChem*, 2005, **6**, 1341–1345.
17 J. S. Wadia and S. F. Dowdy, *Curr. Opin. Biotechnol.*, 2002, **13**, 52–56.
18 E. Koren, A. Apte, R. R. Sawant, J. Grunwald and V. P. Torchilin, *Drug Delivery*, 2011, **18**, 377–384.
19 P. A. Wender, D. J. Mitchell, K. Pattabiraman, E. T. Pelkey, L. Steinman and J. B. Rothbard, *Proc. Natl. Acad. Sci. U. S. A.*, 2000, **97**, 13003–13008.
20 I. Peretto, R. M. Sanchez-Martin, X. H. Wang, J. Ellard, S. Mittoo and M. Bradley, *Chem. Commun.*, 2003, 2312–2313.
21 R. N. Zuckermann and T. Kodadek, *Curr. Opin. Mol Ther.*, 2009, **11**, 299–307.
22 A. S. Culf and R. J. Ouellette, *Molecules*, 2010, **15**, 5282–5335.
23 A. Unciti-Broceta, F. Diezmann, C. Y. Ou-Yang, M. A. Fara and M. Bradley, *Bioorg. Med. Chem.*, 2009, **17**, 959–966.
24 D. Orain, J. Ellard and M. Bradley, Protecting groups in solid-phase organic synthesis, *J. Comb. Chem.*, 2002, **4**, 1–16.
25 M. A. Fara, J. J. Diaz-Mochon and M. Bradley, *Tetrahedron Lett.*, 2006, **47**, 1011–1014.
26 R. N. Zuckermann, J. M. Kerr, S. B. H. Kent and W. H. Moos, *J. Am. Chem. Soc.*, 1992, **114**, 10646–10647.
27 L. D. Lavis and R. T. Raines, *ACS Chem. Biol.*, 2008, **3**, 142–155.
28 J. V. Frangioni, *Curr. Opin. Chem. Biol.*, 2003, **7**, 626–634.
29 M. Lopalco, E. N. Koini, J. K. Cho and M. Bradley, *Org. Biomol. Chem.*, 2009, **7**, 856–859.
30 V. Ntziachristos, C. Bremer and R. Weissleder, *Eur. Radiol.*, 2003, **13**, 195–208.
31 Animal experimentation was approved by UK regulatory authorities (Project licence 60/3545 from UK Home Office).
32 S. Gross, S. T. Gammon, B. L. Moss, D. Rauch, J. Harding, J. W. Heinecke, L. Ratner and D. Piwnica-Worms, *Nat. Med.*, 2009, **15**, 455–461.
33 F. K. Swirski, M. J. Pittet, M. F. Kircher, E. Aikawa, F. A. Jaffer, P. Libby and R. Weissleder, *Proc. Natl. Acad. Sci. U. S. A.*, 2006, **103**, 10340–10345.

REFERENCES

1. Alberts, B., Bray, D., Lewis, J., Raff, M., Roberts, K., Watson, J.D., Molecular biology of the cell, *Third edition*, **1994,** Garland Publishing, New York.

2. Lodish, H., Berk, A., Zipursky, L.S., Matsudaira, P., Baltimore, D., Darnell, J., Transprort across cell membranes. *Molecular Cell Biology,* **2000,** *4th Edition,* W.H. Freeman and Company,

3. Jutras, I., Desjardins, M., Phagocytosis: at the crossroads of innate and adaptive immunity. *Annual Review of Cell and Developmental Biology,* **2005**, 21, 511-527.

4. Goldstein, J.L., Brown, M.S., Anderson, R.G., Russell, D.W., Schneider, W.J., Receptor-mediated endocytosis: concepts emerging from the LDL receptor system. *Annual Review of Cellular Biology,* **1985**, 1, 1-39.

5. Escriche, M., Burgueño, J., Ciruela, F., Canela, E.I., Mallol, J., Enrich, C., Lluís, C., Franco, R., Ligand-induced caveolae-mediated internalization of A1 adenosine receptors: morphological evidence of endosomal sorting and receptor recycling. *Experimental Cell Research,* **2003,** 285, (1), 72-90.

6. Ferrari, A., Pellegrini, V., Arcangeli, C., Fittipaldi, A., Giacca, M., Beltram, F., Caveolae-mediated internalization of extracellular HIV-1 tat fusion proteins visualized in real time. *Molecular Therapy, the journal of the American Society of Gene Therapy,* **2003**, 8, (2), 284-294.

7. Palmgren, M.G., Axelsen, K.B., Evolution of P-type ATPases. *Biochimica et Biophysica Acta,* **1998**, 1365, (1-2), 37-45.

8. Morth, J.P., Pedersen, B.P., Toustrup-Jensen, M.S., Sørensen, T.L., Petersen, J., Andersen, J.P., Vilsen, B., Nissen, P., Crystal structure of the sodium-potassium pump. *Nature,* **2007,** 450, (7172), 1043-1049.

9. Celis, J.E., Microinjection of somatic cells with micropipettes: comparison with other transfer techniques. *Biochem Journal,* **1984,** 223, (2), 281-291.

10. McNeil, P.L., Murphy, R.F., Lanni, F., Taylor, D.L., A method for incorporating macromolecules into adherent cells. *The Journal of Cell Biology*, **1984**, 98, (4), 1556-1564.

11. Chen, C., Smye, S.W., Robinson, M.P., Evans, J.A., Membrane electroporation theories: a review. *Medical & Biological Engineering Computing*, **2006,** 44, (1-2), 5-14.

12. Neumann, E., Kakorin, S., Toensing, K., Fundamentals of electroporative delivery of drugs and genes. *Bioelectrochemistry and Bioenergetics,* **1999**, 48, (1), 3-16.

13. Fechheimer, M., Boylan, J.F., Parker, S., Sisken, J.E., Patel, G.L., Zimmer, S.G., Transfection of mammalian cells with plasmid DNA by scrape loading and sonication loading. *Proceeding of the National Academy of Science of the United States of America,* **1987,** 84, (23), 8463-8467.

14. Hosokawa, Y., Ochi, H., Iino, T., Hiraoka, A., Tanaka, M., Photoporation of biomolecules into single cells in living vertebrate embryos induced by a femtosecond laser amplifier. *PLoS One,* **2011,** 6, (11),e27677.

15. Clark, I.B., Hanania, E.G., Stevens, J., Gallina, M., Fieck, A., Brandes, R., Palsson, B.O., Koller, M.R., Optoinjection for efficient targeted delivery of a broad range of compounds and macromolecules into diverse cell types. *Journal of Biomedical Optic,* **2006,** 11, (1), 014034.

16. Villemejane, J., Mir, L.M., Physical methods of nucleic acid transfer: general concepts and applications. *British Journal of Pharmacology,* **2009**, 157, (2), 207-219.

17. Vogel, U., Wanner, T., Bültmann, B., Extensive pectoral muscle necrosis after defibrillation: nonthermal skeletal muscle damage caused by electroporation. *Intensive Care Medicine,* **1998**, 24, (7), 743-745.

18. Kawai, S., Nishizawa, M., New procedure for DNA transfection with polycation and dimethyl sulfoxide. *Molecular and Cellular Biology,* **1984**, 4, (6), 1172-1174.

19. Bromberg, L.E., Klibanov, A.M., Detergent-enabled transport of proteins and nucleic acids through hydrophobic solvents. *Proceeding of the National Academy of Science of the United States of America,* **1994,** 91, (1), 143-147.

20. Yamashita, S., Furubayashi, T., Kataoka, M., Sakane, T., Sezaki, H., Tokuda, H., Optimized conditions for prediction of intestinal drug permeability using Caco-2 cells. *European Journal of Pharmaceutical Science,* **2000,** 10, (3), 195-204.

21. Uddin, S.N., Cationic lipids used in non-viral gene delivery systems. *Biotechnology and Molecular Biology Review*, **2007,** 2, (3),58-67.

22. Felgner, P.L., Gadek, T.R., Holm, M., Roman, R., Chan, H.W., Wenz, M., Northrop, J.P., Ringold, G.M., Danielsen, M., Lipofection: a highly efficient, lipid-mediated DNA-transfection. *Proceeding of the National Academy of Science of the United States of America,* **1987,** 84, (21), 7413-7417.

23. Liberska, A., Unciti-Broceta A., Bradley, M., Very long-chain fatty tails for enhanced transfection. *Organic & Biomolecular Chemistry*, **2009**, 7, (1), 61-68.

24. Zhang, S., Zhao, B., Jiang, H., Wang, B., Ma, B., Cationic lipids and polymers mediated vectors for delivery of siRNA. *Journal of Controlled Release,* **2007**, 123, (1), 1-10.

25. Floch, V., Le Bolc'h, G., Audrézet, M.P., Yaouanc, J.J., Clément, J.C., des Abbayes, H., Mercier, B., Abgrall, J.F., Férec, C., Cationic phosphonolipids as non viral vectors for DNA transfection in hematopoietic cell lines and CD34+ cells. *Blood Cells, Molecules & Diseases*, **1997**, 23, (1), 69-87.

26. Simberg, D., Hirsch-Lerner, D., Nissim, R., Barenholz, Y., Comparison of different commercially available cationic lipid-based transfection kits. *Journal of Liposome Research,* **2000**, 10, (1), 1-13.

27. Buchberger, B., Fernholz, E., vd Eltz H., Hinzpeter, M., DOSPER Liposomal Transfection Reagent: A Reagent with unique Transfection Properties. *Biochemica*, **1996**, 2, 7-10.

28. Zhao, M., Yang, H., Jiang, X., Zhou, W., Zhu, B., Zeng, Y., Yao, K., Ren, C., Lipofectamine RNAiMAX: an efficient siRNA transfection reagent in human embryonic stem cells. *Molecular Biotechnology,* **2008**, 40, (1), 19-26.

29. Lv, H., Zhang, S., Wang, B., Cui, S., Yan, J., Toxicity of cationic lipids and cationic polymers in gene delivery. *Journal of Controlled Release,* **2006,** 114, (1), 100-109.

30. Hirlekar, R., Yamagar, M., Garse, H., Vij, M., Carbon Nanotubes and its Applications: A Review. *Asian Journal of Pharmaceutical and Clinical Research,* **2009,** 2, (3), 17-27.

31. Shi Kam, N.W., Jessop, T.C., Wender, P.A., Dai, H., Nanotube molecular transporters: internalization of carbon nanotube-protein conjugates into Mammalian cells. *Journal of the American Chemical Society,* **2004,** 126, (22), 6850-6851.

32. Lacerda, L., Bianco, A., Prato, M., Kostarelos, K., Carbon nanotube cell translocation and delivery of nucleic acids in vitro and in vivo. *Journal of Materials Chemistry,* **2008,** 18, (1), 17-22.

33. Kam, N.W., Dai, H., Carbon nanotubes as intracellular protein transporters: generality and biological functionality. *Journal of the American Chemical Society,* **2005,** 127, (16), 6021-6026.

34. Firme, C.P., Bandaru, P.R., Toxicity issues in the application of carbon nanotubes to biological systems. *Nanomedicine: Nanotechnology, Biology, and Medicine,* **2010,** 6, (2), 245-256.

35. Smart, S.K, Cassady, A.I., Lu, G.Q., Martin, D.J., The biocompatibility of carbon nanotubes. *Carbon,* **2006,** 44, (6), 1034-1047.

36. Giovagnoli, S., Blasi, P., Ricci, M., Rossi, C., Biodegradable microspheres as carriers for native superoxide dismutase and catalase delivery. *AAPS PharmSciTech,* **2004,** 5, (4), e51, 1-9.

37. Sanchez-Martin, R.M., Muzerelle, M., Chitkul, N., How, S.E., Mittoo, S., Bradley, M., Bead-based cellular analysis, sorting and multiplexing. *ChemBioChem,* **2005**, 6, (8), 1341-1345.

38. Shi, M., Yang, Y.Y., Chaw, C.S., Goh, S.H., Moochhala, S.M., Ng, S., Heller, J., Double walled POE/PLGA microspheres: encapsulation of water-soluble and water-insoluble proteins and their release properties. *Journal of Controlled Release,* **2003,** 89, (2), 167-177.

39. Sanchez-Martin, R.M., Alexander, L., Muzerelle, M., Cardenas-Maestre, J.M., Tsakiridis, A., Brickman, J.M., Bradley, M., Microsphere-mediated protein delivery into cells. *ChemBioChem,* **2009,** 10, (9), 1453-1456.

40. Wang, C., Ge, Q., Ting, D., Nguyen, D., Shen, H.R., Chen, J., Eisen, H.N., Heller, J., Langer, R., Putnam, D., Molecularly engineered poly(ortho ester) microspheres for enhanced delivery of DNA vaccines. *Nature Materials,* **2004,** 3, (3), 190-196.

41. Bradley, M., Alexander, L., Duncan, K., Chennaoui, M., Jones, A.C., Sánchez-Martín, R.M., pH sensing in living cells using fluorescent microspheres. *Bioorganic and Medicinal Chemistry Letters,* **2008,** 18, (1), 313-317.

42. Dinarvand, R., Moghadam, S.H., Mohammadyari-Fard, L., Atyabi, F., Preparation of biodegradable microspheres and matrix devices containing naltrexone. *AAPS PharmSciTech,* **2003,** 4, (3), 45-54.

43. Varde, N.K., Pack, D.W., Microspheres for controlled release drug delivery. *Expert Opinion on Biological Therapy,* **2004,** 4, (1), 35-51.

44. Sinha, V.R., Trehan, A., Biodegradable microspheres for protein delivery. *Journal of Controlled Release,* **2003,** 90, (3), 261-280.

45. Boas, U., Heegaard, P.M., Dendrimers in drug research. *Chemical Society Reviews,* **2004,** 33, (1), 43-63.

46. Kukowska-Latallo, J.F., Bielinska, A.U., Johnson, J., Spindler, R., Tomalia, D.A, Baker, J.R. Jr, Efficient transfer of genetic material into mammalian cells using Starburst polyamidoamine dendrimers. *Proceeding of the National Academy of Science of the United States of America,* **1994,** 93, (10), 4897-4902.

47. Hussain, M., Shchepinov, M., Sohail, M., Benter, I.F., Hollins, A.J., Southern, E.M., Akhtar, S., A novel anionic dendrimer for improved cellular delivery of antisense oligonucleotides. *Journal of Controlled Release,* **2004,** 99, (1), 139-155.

48. Ke, W., Zhao, Y., Huang, R., Jiang, C., Pei, Y., Enhanced oral bioavailability of doxorubicin in a dendrimer drug delivery system. *Journal of Pharmaceutical Science,* **2008,** 97, (6), 2208-2216.

49. Deshayes, S., Morris, M.C., Divita, G., Heitz, F., Cell-penetrating peptides: tools for intracellular delivery of therapeutics. *Cellular and Molecular Life Sciences,* **2005,** 62, (16), 1839-1849.

50. Vives, E., Present and future of cell-penetrating peptide mediated delivery systems: « is the Trojan horse too wild to go only to Troy? ». *Journal of Controlled Release,* **2005**, 109, (1-3), 77-85.

51. Frankel, A.D., Bredt, D.S., Pabo, C.O., Tat protein from human immunodeficiency virus forms a metal-linked dimmer. *Science,* **1988,** 240, (4848), 70-73.

52. Loret, E.P., Vives, E., Ho, P.S., Rochat, H., Van Rietschoten, J., Johnson, W.C. Jr., Activating region of HIV-1 Tat protein: vacuum UV circular dichroism and energy minimization. *Biochemistry*, **1991**, 30, (24), 6013-6023.

53. Ruben, S., Perkins, A., Purcell, R., Joung, K., Sia, R., Burghoff, R., Haseltine, W.A., Rosen, C.A., Structural and functional characterization of human immunodeficiency virus tat protein. *Journal of Virology*, **1989,** 63, (1), 1-8.

54. a) Lundberg, P., El-Andaloussi, S., Sütlü, T., Johansson, H., Langel, Ü., Delivery of short interfering RNA using endosomolytic cell-penetrating peptides. *The Journal of the Federation of American Societies for Experimental Biology, Research communication*, **2007,** 21, (11), 2664-2671.
b) Turner, J.J., Ivanova, G.D., Verbeure, B., Williams, D., Arzumanov, A.A., Abes, S., Lebleu, B., Gait, M.J., Cell-penetrating peptide conjugates of peptide nucleic acids (PNA) as inhibitors of HIV-1 Tat-dependent trans-activation in cells. *Nucleic Acids Research*, **2005,** 33, 21, 6837-6849.

55. a) Gitton, Y., Tibaldi, L., Dupont, E., Levi, G., Joliot, A., Efficient CPP-mediated Cre protein delivery to developing and adult CNS tissues. *BMC Biotechnology*, **2009,** 9, 40.
b) Wadia, J.S., Dowdy, S.F., Transmembrane delivery of protein and peptide drugs by TAT-mediated transduction in the treatment of cancer. *Advanced Drug Delivery Reviews*, **2005,** 57, (4), 579-596.

56. a) Guo, Y.M., Liu, M., Yang, J.L., Guo, X.J., Wang, S.C., Duan, X.Y., Wang, P., Intercellular imaging by a polyarginine derived cell penetrating peptide labeled magnetic resonance contrast agent, diethylenetriamine pentaacetic acid gadolinium. *Chinese Medical Journal*, **2007**, 120, (1), 50-55.
b) Kersemans, V., Cornelissen, B., Targeting the Tumour: Cell Penetrating Peptides for Molecular Imaging and Radiotherapy. *Pharmaceuticals*, **2010,** 3, 600-620.

57. Brooks, H., Lebleu, B., Vivès, E., Tat peptide-mediated cellular delivery: back to basics. *Advanced Drug Delivery Reviews*, **2005,** 57, (4), 559-577.

58. Futaki, S., Membrane-permeable arginine-rich peptides and the translocation mechanisms. *Advanced Drug Delivery Reviews*, **2005,** 57, (4), 547-558.

59. Futaki, S., Suzuki, T., Ohashi, W., Yagami, T., Tanaka, S., Ueda, K., Sugiura, Y., Arginine-rich peptides. An abundant source of membrane-permeable peptides having potential as carriers for intracellular protein delivery. *The Journal of Biological Chemistry*, **2001,** 276, (8), 5836-5840.

60. a) Derossi, D., Joliot, A.H., Chassaing, A.G., Prochiantz, A., The third helix of the Antennapedia homeodomain translocates through biological membranes. *The Journal of Biological Chemistry,* **1994**, 269, (14), 10444-10450.
b) Derossi, D., Chassaing, G., Prochiantz, A., Trojan peptides: the penetratin system for intracellular delivery. *Trends in Cell Biology*, **1998,** 8, (2), 84-87.

61. Oehlke, J., Scheller, A., Wiesner, B., Krause, E., Beyermann, M., Klauschenz, E., Melzig, M., Bienert, M., Cellular uptake of an alpha-helical amphipathic model peptide with the potential to deliver polar compounds into the cell interior non-endocytically. *Biochimica et Biophysica Acta,* **1998,** 1414, (1-2), 127-139.

62. a) Zhao, Y., Brown, T.L., Kohler, H., Müller, S., MTS-conjugated-antiactive caspase 3 antibodies inhibit actinomycin D-induced apoptosis. *Apoptosis,* **2003,** 8, (6), 631-637.
b) Lin, Y.Z., Yao, S.Y., Veach, R.A., Torgerson, T.R., Hawiger, J., Inhibition of nuclear translocation of transcription factor NF-kappa B by a synthetic peptide containing a cell membrane-permeable motif and nuclear localization sequence. *Journal of Biological Chemistry,* **1995,** 270, (24), 14255-14258.
c) von Heijne, G., The signal peptide. *The Journal of Membrane Biology,* **1990,** 115, (3), 195-201.

63. Morris, M.C., Depollier, J., Mery, J., Heitz, F., Divita, G., A peptide carrier for the delivery of biologically active proteins into mammalian cells. *Nature Biotechnology,* **2001,** 19, 1173-1176.

64. Poogaa, M., llbrinka, M.H., Zorkoa, M., Langela, U., Cell penetration by transportan. *The Journal of the Federation of American Societies for Experimental Biology, Research communication,* **1998,** 12, 67-77.

65. Langel, Ü., Poogaa, M, Kairanec, C, Zilmerc, M., Bartfaia, T., A galanin-mastoparan chimeric peptide activates the Na+,K+-ATPase and reverses its inhibition by ouabain. *Regulatory Peptides,* **1996,** 62, (1), 47-52.

66. a) Deshayes, S., Gerbal-Chaloin, S., Morris, M.C., Aldrian-Herrada, G., Charnet, P., Divita, G., Heitz, F., On the mechanism of non-endosomial peptide-mediated cellular delivery of nucleic acids. *Biochimica et Biophysice Acta,* **2004,** 1667, (2), 141-147.
b) Gerbal-Chaloin, S., Gondeau, C., Aldrian-Herrada, G., Heitz, F., Gauthier-Rouvière, C., Divita, G., First step of the cell-penetrating peptide mechanism involves Rac1 GTPase-dependent actin-network remodelling. *Biology of the Cell,* **2007,** 99, (4), 223-238.

67.http://www.crbdiscovery.com/z_core/z_download/transporter-peptides.pdf, accessed 18th December 2012.

68. Simeoni, F., Morris, M.C., Heitz, F., Divita, G., Insight into the mechanism of the peptide-based gene delivery system MPG: implications for delivery of siRNA into mammalian cells. *Nucleic Acids Research,* **2003,** 31, (11), 2717-2724.

69. a) Morris, M.C., Vidal, P., Chaloin, L., Heitz, F., Divita, G., A new peptide vector for the efficient delivery of oligonucleotides into mammalian cells. *Nucleic Acids Research*, **1997**, 25, (14), 2730-2736.
b) Simeoni, F., Morris, M. C., Heitz, F., Divita, G., Insight into the mechanism of the peptide-based gene delivery system MPG: implications for delivery of siRNA into mammalian cells, *Nucleic Acids Research*, **2003**, 31, (11), 2717-2724.
c) http://www.panomics.com/downloads/DELIVERXBR_V1.pdf, accessed the 18th December 2012.

70. Temsamani, J., Rousselle, C., Rees, A.R., Scherrmann, J.M., Vector-mediated drug delivery to the brain. *Expert Opinion on Biological Therapy,* **2001,** 1, (5), 773-782.

71. Rousselle, C., Smirnova, M., Clair, P., Lefauconnier, J.M., Chavanieu, A., Calas, B., Scherrmann, J.M., Temsamani, J., Enhanced Delivery of Doxorubicin into the Brain via a Peptide-Vector-Mediated Strategy: Saturation Kinetics and Specificity. *The Journal of Pharmacology and Experimental Therapeutics*, **2001,** 296, (1), 124-131.

72. Derossi, D., Calvet, S., Trembleau, A., Brunissen, A., Chassaing, G., Prochiantz, A., Cell Internalization of the Third Helix of the Antennapedia Homeodomain Is Receptor-independent. *The Journal of Biological Chemistry*, **1996,** 271, (30), 18188-18193.

73. Suzuki, T., Futaki, S., Niwa, M., Tanaka, S., Ueda, K., Sugiura, Y., Possible existence of common internalization mechanisms among arginine-rich peptides. *The Journal of Biological Chemistry,* **2002,** 277, (4), 2437-2443.

74. Hällbrink, M., Florén, A., Elmquist, A., Pooga, M., Bartfai, T., Langel, U., Cargo delivery kinetics of cell-penetrating peptides. *Biochimica et Biophysica Acta,* **2001,** 1515, (2), 101-109.

75. Richard, J.P., Melikov, K., Vives, E., Ramos, C., Verbeure, B., Gait, M.J., Chernomordik, L.V., Lebleu, B., Cell-penetrating peptides. A reevaluation of the

mechanism of cellular uptake. *The Journal of Biological Chemistry,* **2003,** 278, (1), 585-590.

76. Drin, G., Cottin, S., Blanc, E., Rees, A.R., Temsamani, J., Studies on the Internalization Mechanism of Cationic Cell-penetrating Peptides. *The Journal of Biological Chemistry,* **2003,** 278, (33), 31192-31201.

77 . Henriques, S. T., Melo, M. N., Castanho, M. A. R. B., Cell-penetrating peptides and antimicrobial peptides: how different are they? *Biochemical Journal*, **2006,** 399, 1-7.

78. Huang, Y., Huang, J., Chen, Y., Alpha-helical cationic antimicrobial peptides: relationships of structure and function. *Protein & Cell,* **2010,** 1, (2), 143-152.

79. Yang, L., Harroun, T.A., Weiss, T.M., Ding, L., Huang, H.W., Barrel-stave model or toroidal model? A case study on melittin pores. *Biophysical Journal,* **2001,** 81, (3), 1475-1485.

80. Yang, L., Harroun, T. A., Weiss, T. M., Ding, L., Huang, H. W., Barrel-stave model or toroidal model? A case study on melittin pores. *Biophysical Journal*, **2001**, 81, (3), 1475-1485.

81. Matsuzaki, K., Magainins as paradigm for the mode of action of pore forming polypeptides. *Biochimica et Biophysica Acta,* **1998,** 1376, (3), 391-400.

82. Pouny, Y., Rapaport, D., Mor, A., Nicolas, P., Shai, Y., Interaction of antimicrobial dermaseptin and its fluorescently labeled analogues with phospholipid membranes. *Biochemistry,* **1992,** 31, (49), 12416-12423.

83. Trabulo, S., Cardoso, A.L., Mano, M., Pedroso De Lima, M.C., Cell-Penetrating Peptides - Mechanisms of Cellular Uptake and Generation of Delivery Systems. *Pharmaceuticals,* **2010,** 3, (4), 961-993.

84. Silverstein, S.C., Steinman, R.M., Cohn, Z.A., Endocytosis. *Annual Review of Biochemistry,* **1977,** 46, 669-722.

85. Fittipaldi, A., Ferrari, A., Zoppé, M., Arcangeli, C., Pellegrini, V., Beltram, F., Giacca, M., Cell membrane lipid rafts mediate caveolar endocytosis of HIV-1 Tat fusion proteins. *Journal of Biological Chemistry,* **2003,** 278, (36), 34141-34149.

86. Richard, J.P., Melikov, K., Brooks, H., Prevot, P., Lebleu, B., Chernomordik, L.V., Cellular Uptake of Unconjugated TAT Peptide Involves Clathrin-dependent

Endocytosis and Heparan Sulfate Receptors. *The Journal of Biological Chemistry,* **2005,** 280, (15), 15300-15306.

87. Gupta, B., Levchenko, T.S., Torchilin, V.P., Intracellular delivery of large molecules and small particles by cell-penetrating proteins and peptides. *Advanced Drug Delivery Reviews,* **2005,** 57, (4), 637-651.

88. Youngblood, D.S., Hatlevig, S.A., Hassinger, J.N., Iversen, P.L., Moulton, H.M., Stability of cell-penetrating peptide-morpholino oligomer conjugates in human serum and in cells. *Bioconjugate Chemistry,* **2007,** 18, (1), 50-60.

89. Goodman, M., Shao, H., Peptidomimetic building blocks for drug discovery: An overview. *Pure & Applied Chemistry,* **1996,** 68, (6), 1303-1308.

90. Tréhin, R., Merkle, H.P., Chances and pitfalls of cell penetrating peptides for cellular drug delivery. *European Journal of Pharmaceutics and Biopharmaceutics,* **2004,** 58, (2), 209-223.

91. Chauhan, A., Tikoo, A., Kapur, A.K., Singh, M., The Taming of the Cell Penetrating Domain of the HIV Tat: Myths and Realities. *Journal of Controlled Release,* **2007,** 117, (2), 148-162.

92. Funke, S.A., Willbold, D., Mirror image phage display - a method to generate D-peptide ligands for use in diagnostic or therapeutical applications. *Molecular BioSystems,* **2009,** 5, (8), 783-786

93. a) Wu, R.P., Youngblood, D.S., Hassinger, J.N., Lovejoy, C.E., Nelson, M.H., Iversen, P.L., Moulton, H.M., Cell-penetrating peptides as transporters for morpholino oligomers: effects of amino acid composition on intracellular delivery and cytotoxicity. *Nucleic Acids Research,* **2007,** 35, (15), 5182-5191.
b) Youngblood, D.S., Hatlevig, S.A., Hassinger, J.N., Iversen, P.L., Moulton, H.M., Stability of cell-penetrating peptide-morpholino oligomer conjugates in human serum and in cells. *Bioconjugate Chemistry,* **2007,** 18, (1), 50-60.

94. Cheng, R.P., Gellman, S.H., DeGrado, W.F., *β*-Peptides: From Structure to Function. *Chemical Reviews,* **2001,** 101, 3219-3232.

95. a) Frackenpohl, J., Arvidsson P.I., Schreiber J.V., Seebach D., The Outstanding Biological Stability of β- and γ-Peptides toward Proteolytic Enzymes: An In Vitro Investigation with Fifteen Peptidases. *ChemBioChem,* **2001,** 2, (6), 445-455.

b) Rueping, M., Mahajan, Y., Sauer, M., Seebach, D., Cellular uptake studies with beta-peptides. *ChemBioChem*, **2002,** 3, (2-3), 257-259.

96. a) Podlech, J., Seebach, D., The Arndt-Eistert Reaction in Peptide Chemistry: A Facile Access to Homopeptides. *Angewandte Chemie International Edition*, **1995,** 34, (4), 471-472.
b) Cole, D.C., Recent Stereoselective Synthetic Approaches to β-Amino Acids. *Tetrahedron*, **1994,** 50, (32), 9517-9582.
c) Wenzel, A.G., Jacobsen, E.N., Asymmetric catalytic Mannich reactions catalyzed by urea derivatives: enantioselective synthesis of beta-aryl-beta-amino acids. *Journal of the American Chemical Society*, **2002,** 124, (44), 12964-12965.

97. a) Shaw, R.A., Kollát, E., Hollósi, M., Mantsch, H.H., Hydrogen bonding and isomerization in thioamide peptide derivatives. *Spectrochimica Acta*, **1995,** 51, (8), 1399-1412.
b) Schutkowski, M., Neubert, K., Fischer, G., Influence on proline-specific enzymes of a substrate containing the thioxoaminoacyl-prolyl peptide bond. *European Journal of Biochemistry*, **1994,** 221, (1), 455-461.

98. Cava M.P., Levinson, M.L., Thionation Reactions of Lawesson's Reagents. *Tetrahedron*, **1985,** 41, (22), 5061-5087.

99. Farmer, P.S., Ariëns, E.J., Speculations on the design of nonpeptidic peptidomimetics. *Trends in Pharmacological Sciences*, **1982,** 3, 362-365.

100. Simon, R.J., Kania, R.S., Zuckermann, R.N., Huebner, V.D., Jewell, D.A., Banville, S., Ng, S., Wang, L., Rosenberg, S., Marlowe, C.K., Peptoids: a modular approach to drug discovery. *Proceeding of the National Academy of Science of the United States of America*, **1992,** 89, (20), 9367-9371.

101. Miller, S.M., Simon, R.J., Ng, S., Zuckermann, R.N., Kerr, J.M., Moos, W.H., Proteolytic studies of homologous peptide and N-substituted glycine peptoid oligomers. *Bioorganic & Medicinal Chemistry Letters*, **1994,** 4, (22), 2657-2662.

102. Elgersma, R. C., Mulder, G. E., Kruijtzer, J. A., Posthuma, G., Rijkers, D. T., Liskamp, R. M., Transformation of the amyloidogenic peptide amylin(20-29) into its corresponding peptoid and retropeptoid: access to both an amyloid inhibitor and template for self-assembled supramolecular tapes. *Bioorganic & Medicinal Chemistry Letters*, **2007**, 17, (7), 1837-1842.

103. Fowler, S.A., Blackwell, H.E., Structure-function relationships in peptoids: recent advances toward deciphering the structural requirements for biological function. *Organic & Biomolecular Chemistry,* **2009,** 7, (8), 1508-1524.

104. Unciti-Broceta, A., Diezmann, F., Ou-Yang, C.Y., Fara, M.A., Bradley, M., Synthesis, penetrability and intracellular targeting of fluorescein-tagged peptoids and peptide-peptoid hybrids. *Bioorganic & Medicinal Chemistry,* **2009,** 17, (3), 959-966.

105. Schröder, T., Niemeier, N., Afonin, S., Ulrich, A.S., Krug, H.F., Bräse, S., Peptoidic amino- and guanidinium-carrier systems: targeted drug delivery into the cell cytosol or the nucleus. *Journal of Medicinal Chemistry,* **2008,** 51, (3), 376-379.

106. Diaz-Mochon, J.J., Fara, M.A., Sanchez-Martin, R.M., Bradley, M., Peptoid dendrimers - microwave-assisted solid-phase synthesis and transfection agent evaluation. *Tetrahedron Letters,* **2008,** 49, (5), 923-926.

107. a) Chongsiriwatana, N.P., Patch, J.A., Czyzewski, A.M., Dohm, M.T., Ivankin, A., Gidalevitz, D., Zuckermann, R.N., Barron, A.E., Peptoids that mimic the structure, function, and mechanism of helical antimicrobial peptides. *Proceeding of the National Academy of Science of the United States of America,* **2008,** 105, (8), 2794-2799.
b) Patch, J.A., Barron, A.E., Helical Peptoid Mimics of Magainin-2 Amide. *Journal of the American Chemical Society,* **2003,** 125, (40), 12092-12093.

108. Kesavan, V., Tamilarasu, N., Cao, H., Rana, T.M., A new class of RNA-binding oligomers: peptoid amide and ester analogues. *Bioconjugate Chemistry,* **2002,** 13, (6), 1171-1175.

109. Lee, B.C., Chu, T.K., Dill, K.A., Zuckermann, R.N., Biomimetic nanostructures: creating a high-affinity zinc-binding site in a folded nonbiological polymer. *Journal of the American Chemical Society*, **2008**, 130, (27), 8847-8855.

110. Maayan, G., Ward, M.D., Kirshenbaum, K., Metallopeptoids. *Chemical Communications,* **2009,** (1), 56-58.

111. Mitchell, D.J., Kim, D.T., Steinman, L., Fathman, C.G., Rothbard, J.B., Polyarginine enters cells more efficiently than other polycationic homopolymers. *The Journal of Peptide Research,* **2000,** 56, (5), 318-325.

112. Ryser, H.J.P., Shen, W.C., Conjugation of methotrexate to poly(L-lysine) increases drug transport and overcomes drug resistance in cultured cells. *Proceedings*

of the National Academy of Sciences of the United States of America, **1978,** 75, (8), 3867-3870.

113. Wender, P.A., Mitchell, D.J., Pattabiraman, K., Pelkey, E.T., Steinman, L., Rothbard, J.B., The design, synthesis, and evaluation of molecules that enable or enhance cellular uptake: peptoid molecular transporters. *Proceedings of the National Academy of Sciences United States America*, **2000,** 97, (24), 13003-13008.

114. Peretto, I., Sanchez-Martin, R.M., Wang, X.H., Ellard, J., Mittoo, S., Bradley, M., Cell penetrable peptoid carrier vehicles: synthesis and evaluation. *Chemical Communications*, **2003,** (18), 2312-2313.

115. Kruijtzer, J.A.W., Liskamp, R.M.J., Synthesis in solution of peptoids using Fmoc-protected N-substituted glycines. *Tetrahedron Letters*, **1995,** 36, (38), 6969–6972.

116. Fara, M.A., Díaz-Mochón, J.J., Bradley, M., Microwave-assisted coupling with DIC/HOBt for the synthesis of difficult peptoids and fluorescently labelled peptides—a gentle heat goes a long way. *Tetrahedron Letters*, **2006,** 47, (6), 1011–1014.

117. Zuckermann, R.N., Kerr, J.M., Kent, S.B.H., Moos, W.H., Efficient method for the preparation of peptoids [oligo(N-substituted glycines)] by submonomer solid-phase synthesis. *Journal of the American Chemical Society*, **1992,** 114, (26), 10646-10647.

118. Kruijtzer, J.A.W., Hofmeyer, L.J.F., Heerma, W., Versluis, C., Liskamp, R.M.J., Solid-Phase Syntheses of Peptoids using Fmoc-Protected N-Substituted Glycines: The Synthesis of (Retro)Peptoids of Leu-Enkephalin and Substance P. *Chemistry – A European Journal*, **1998,** 4, (8), 1570-1580.

119. Schröder, T., Schmitz, K., Niemeier, N., Balaban, T.S., Krug, H.F., Schepers, U., Bräse, S., Solid-phase synthesis, bioconjugation, and toxicology of novel cationic oligopeptoids for cellular drug delivery. *Bioconjugate Chemistry*, **2007,** 18, (2), 342-354.

120. Zuckermann, R.N., Kerr, J.M., Siani, M.A., Banville, S.C., Design, construction and application of a fully automated equimolar peptide mixture synthesizer. *International Journal of Peptide and Protein Research*, **1992,** 40, (6), 497-506.

121. Olivos, H.J., Alluri, P.G., Reddy, M.M., Salony, D., Kodadek, T., Microwave-assisted solid-phase synthesis of peptoids. *Organic Letters,* **2002,** 4, (23), 4057-4059.

122. Nnanabu, E., Burgess, K., Cyclic semipeptoids: peptoid-organic hybrid macrocycles. *Organic Letters,* **2006,** 30, 8, (7), 1259-1262.

123. Gorske, B.C., Jewell, S.A., Guerard, E.J., Blackwell, H.E., Expedient synthesis and design strategies for new peptoid construction. *Organic Letters,* **2005,** 7, (8), 1521-1524.

124. Li, S., Bowerman, D., Marthandan, N., Klyza, S., Luebke, K.J., Garner, H.R., Kodadek, T., Photolithographic synthesis of peptoids. *Journal of the American Chemical Society,* **2004,** 126, (13), 4088-4089.

125. Van der Auwera, C., Anteunis, M.J.O., *N,N*'-bis(2-oxo-3-oxazolidinyl) phosphinic chloride (BOP-Cl); a superb reagent for coupling at and with iminoacid residues. *International Journal for Peptide and Protein Research,* **1987,** 29, 574-88.

126. a) Frérot, E., Coste, J., Pantaloni, A., Dufour, M.N., Jouin, P., PyBOP® and PyBroP: Two reagents for the difficult coupling of the α,α-dialkyl amino acid, Aib. *Tetrahedron,* **1991,** 47, (2), 259-270.
b) Coste, J., Le-Nguyen, D., Castro, B., PyBOP®: A new peptide coupling reagent devoid of toxic by-product. *Tetrahedron Letters,* **1990,** 31, (2), 205–208.

127. Zuckermann, R. N., Peptoid origins. *Biopolymers*, **2011**, 96, (5), 545-555.

128. Culf, A.S., Ouellette, R.J., Solid-Phase Synthesis of N-Substituted Glycine Oligomers (α-Peptoids) and Derivatives. *Molecules,* **2010,** 15, (8), 5282-5335.

129. Kaiser, E.; Colescot, R. L.; Bossinge, C. D.; Cook, P. I., Color Test for Detection of Free Terminal Amino Groups in Solid-Phase Synthesis of Peptides. *Analytical Biochemistry*, **1970**, 34, (2), 595-598.

130. Vojkovsky, T., Detection of secondary amines on solid-phase. *Peptide Research*, **1995**, 8, (4), 236-237.

131. Fara, M.A., Cell Penetrating Peptoid Carriers: Microwave Assisted Synthesis and Bioactive Molecules Delivery. *Ph.D. Thesis*, University of Edinburgh, **2008**.

132. Krapcho, A. P., Kuell, C. S., Mono-Protected Diamines. N-*tert*-Butoxycarbonyl-α,ω- alkanediamines from α,ω-Alkanediamines. *Synthetic Communications*, **1990**, 20, (16), 2559-2564.

133. Rink, H., Solid-phase synthesis of protected peptide fragments using a trialkoxy-diphenyl-methylester resin. *Tetrahedron Letters,* **1987,** 28, (33), 3787-3790.

134. Bernatowicz, M.S., Daniels, S.B., Köster, H., A comparison of acid labile linkage agents for the synthesis of peptide C-terminal amides. *Tetrahedron Letters,* **1989,** 30, (35), 4645-4648.

135. a) Giguere, R.J., Bray, T.L., Duncan, S.M., Majetich, G., Application of commercial microwave ovens to organic synthesis. *Tetrahedron Letters*, **1986**, 27, (41), 4945-4948.
b) Gedye, R., Smith, F., Westaway, K., Ali, H., Baldisera, L., Laberge, L., Rousell, J., The use of microwave ovens for rapid organic synthesis. Tetrahedron Letters, 1986, 27, (3), 279-282.

136. Yu, H.M., Chen, S.T., Wang, K.T., Enhanced coupling efficiency in solid-phase peptide synthesis by microwave irradiation. *The Journal of Organic Chemistry,* **1992,** 67, (18), 4781-4784.

137. Sánchez-Martín, R. M., Muzerelle, M., Chitkul, N., How, S. E., Mittoo, S., Bradley, M., Bead-Based Cellular Analysis, Sorting and Multiplexing. *ChemBioChem*, **2005**, 6, (8), 1341-1345.

138. Invitrogen tutorial: Introduction of Flow cytometry. http://probes.invitrogen.com/resources/education/tutorials/4Intro_Flow/player.html

139. Mosiman, V.L., Patterson, B.K., Canterero, L., Goolsby, C.L., Reducing cellular autofluorescence in flow cytometry: an in situ method. *Cytometry*, **1997**, 30, (3),151-156.

140. Loike, J.D., Silverstein, S.C., A fluorescence quenching technique using trypan blue to differentiate between attached and ingested glutaraldehyde-fixed red blood cells in phagocytosing murine macrophages. *Journal of Immunological Methods,* **1983,** 57, (1-3), 373-379.

141. a) Phillips, H.J., Terryberry, J.E., Counting actively metabolizing tissue cultured cells. *Experimental Cell Research,* **1957,** 13, (2), 341–347.

b) Tolnai, S., A method for viable cell count. *Methods in Cell Science,* **1975,** 1, (1), 37-38.

142. Silverstein, S.C., Steinman, R.M., Cohn, Z.A., Endocytosis. *Annual Review of Biochemistry*, **1977**, 46, 669-722.

143. Hall, J.M., Parrish, C.C., Thompson, R.J., Eicosapentaenoic acid regulates scallop (Placopecten magellanicus) membrane fluidity in response to cold. *The Biological Bulletin*, **2002**, 202, (3), 201-203.

144. Tsubaki, M., Fourier-transform infrared study of azide binding to the Fea3-CuB binuclear site of bovine heart cytochrome c oxidase: new evidence for a redox-linked conformational change at the binuclear site. *Biochemistry.* **1993,** 32, (1), 174-182.

145. Vives, E., Brodin, P., Lebleu, B., A truncated HIV-1 Tat protein basic domain rapidly translocates through the plasma membrane and accumulates in the cell nucleus. *Journal of Biological Chemistry,* **1997,** 272, (25), 16010–16017.

146. Mosmann, T., Rapid colorimetric assay for cellular growth and survival: application to proliferation and cytotoxicity assays. *Journal of Immunological Methods,* **1983,** 65, (1-2), 55-63.

147. Milanovich, N., Suh, M., Jankowiak, R., Small, G. J., Hayes, J. M., Binding of TO-PRO-3 and TOTO-3 to DNA: Fluorescence and Hole-Burning Studies. *Journal of the Physical Chemistry*, **1996**, 100, (21), 9181-9186.

148. Lee-MacAry, A. E., Ross, E. L., Davies, D., Laylor, R., Honeychurch, J., Glennie, M. J., Snary, D., Wilkinson, R. W., Development of a novel flow cytometric cell-mediated cytotoxicity assay using the fluorophores PKH-26 and TO-PRO-3 iodide. *Journal of Immunological Methods*, **2001**, 252, (1-2), 83-92.

149. Trollinger, D.R., Cascio, W.E., Lemasters, J.J., Mitochondrial calcium transients in adult rabbit cardiac myocytes: inhibition by ruthenium red and artefacts caused by lysosomal loading of Ca($^{2+}$)-indicating fluorophores. *Biophysical Journal,* **2000**, 79, (1), 39-50.

150. a) Mayor, S., Sabharanjak, S., Maxfield, F.R., Cholesterol-dependent retention of GPI-anchored proteins in endosomes. *The EMBO Journal*, **1998**, 17, (16), 4626-4638.
b) Kilsdonk, E.P., Yancey, P.G., Stoudt, G.W., Bangerter, F.W., Johnson, W.J., Phillips, M.C., Rothblat, G.H., Cellular cholesterol efflux mediated by cyclodextrins. *The Journal of Biological Chemistry*, **1995**, 270, (29), 17250-17256.

c) Zuhorn, I.S., Kalicharan, R., Hoekstra, D., Lipoplex-mediated transfection of mammalian cells occurs through the cholesterol-dependent clathrin-mediated pathway of endocytosis. *The Journal of Biological Chemistry*, **2002**, 277, (20), 18021-18028.

151. a) Orlandi, P.A., Fishman, P.H., Filipin-dependent inhibition of cholera toxin: Evidence for toxin internalisation and activation through caveolae-like domains. *The Journal of Cell Biology*, **1998**, 141, (4), 905-915.
b) Pelkmans, L., Püntener, D., Helenius, A., Local actin polymerisation and dynamin recruitment in SV40-induced internalisation of caveolae. *Science*, **2002**, 296, (5567), 535-539.

152. Willmann, J. K., van Bruggen, N., Dinkelborg, L. M., Gambhir, S.S., Molecular imaging in drug development. *Nature Reviews Drug Discovery*, **2008**, 7, (7), 591-607.

153. Knight, J. C., Edwards, P. G., Paisey, S. J., Fluorinated contrast agents for magnetic resonance imaging; a review of recent developments. *RSC Advances*, **2011**,1, (8), 1415-1425.

154. Langer, A., A systematic review of PET and PET/CT in oncology: a way to personalize cancer treatment in a cost-effective manner? *BMC Health Services Research*, **2010**, 8, (10), 283.

155 . Lee, S., Xie, J. Chen, X. Peptide-based probes for targeted molecular imaging. *Biochemistry*, **2010**, 49, (7), 1364-1376.

156. Du, W., Wang, Y., Luo, Q., Liu, B. F., Optical molecular imaging for systems biology: from molecule to organism. *Analytical and Bioanalytical Chemistry*, **2006**, 386, (3),444-457.

157. Lavis, L. D., Raines, R. T., Bright ideas for chemical biology. *ACS Chemical Biology* **2008,** 3, (3), 142-155.

158. Schantz, S. P., Savage, H. E., Sacks, P., Alfano, R. R., Native cellular fluorescence and its application to cancer prevention. *Environ Health Perspect*, **1997,** 105, (Suppl 4), 941-944.

159. a) Katika, K., Pilon, L., Steady-state directional diffuse reflectance and fluorescence of human skin. *Applied Optics*, **2006**, 45, (17), 4174-4183.
b) Masilamani, V., Al-Zhrani, K., Al-Salhi, M., Al-Diab, A., Al-Ageily, M., Cancer diagnosis by autofluorescence of blood components. *Journal of Luminescence*, **2004**, 109, (3-4), 143-154.

160. Frangioni, J. V., *In vivo* near-infrared fluorescence imaging. *Current Opinion in Chemical Biology*, 2003, 7, (5), 626-634.

161. Yang, Y., Lowry, M., Xu, X., Escobedo, J. O., Sibrian-Vazquez, M., Wong, L., Schowalter, C. M., Jensen, T. J., Fronczek, F. R., Warner, I. M., Strongin, R. M., Seminaphthofluorones are a family of water-soluble, low molecular weight, NIR-emitting fluorophores. *Proceedings of the National Academy of Sciences U S A*, **2008**, 105, (26), 8829-8834.

162. Doja, M. Q., The cyanines dyes. *Chemical Reviews*, **1932**, 11, (3), 273-321.

163. Lopalco, M., Koini, E. N., Cho, J. K., Bradley, M. Catch and release microwave mediated synthesis of cyanine dyes. *Organic& Biomolecular Chemistry*, **2009**, *7*, (5), 856-859.

164. Bouteiller, C., Clavé, G., Bernardin, A., Chipon, B., Massonneau, M., Renard, P. Y, Romieu, A., Novel water-soluble near-infrared cyanine dyes: synthesis, spectral properties, and use in the preparation of internally quenched fluorescent probes. *Bioconjugate Chemistry*, **2007**, 18, (4), 1303-1317.

165. Chan, W. S., Marshall, J. F., Svensen, R., Bedwell, J., Hart, I. R., Effect of sulfonation on the cell and tissue distribution of the photosensitizer aluminum phthalocyanine. *Cancer Research*, **1990**, 50, (15), 4533-4538.

166. Yang, X., Shi, C., Tong, R., Qian, W., Zhau, H. E., Wang, R., Zhu, G., Cheng, J., Yang, V. W., Cheng, T., Henary, M., Strekowski, L., Chung, L. W., Near IR heptamethine cyanine dye-mediated cancer imaging. *Clinical Cancer Research*, **2010**, 16, (10), 2833-2844.

167. Alander, J. T., Kaartinen, I., Laakso, A., Pätilä, T., Spillmann, T., Tuchin, V. V., Venermo, M., Välisuo, P., A review of indocyanine green fluorescent imaging in surgery. *International Journal of Biomedical Imaging*. **2012,** 2012, 940585, doi: 10.1155/2012/940585.

168. Alexander, L., Dhaliwal, K., Simpson, J., Bradley, M., Dunking doughnuts into cells-selective cellular translocation and in vivo analysis of polymeric micro-doughnuts. *Chemical Communications (Cambridge)*, **2008**, 14, (30), 3507-3509.

169. Berger, C., Gremlich , H.-U., Schmidt, P., Cannet, C., Kneuer, R., Hiestand , P., Rausch, M., Rudin, M., In vivo monitoring the fate of Cy5.5-Tat labeled T lymphocytes by quantitative near-infrared fluorescence imaging during acute brain

inflammation in a rat model of experimental autoimmune encephalomyelitis. *Journal of Immunological Methods*, **2007,** 323, (1), 65-77.

170. Christian, D. A., Cai, S., Garbuzenko, O. B., Harada, T., Zajac, A. L., Minko, T., Discher, D. E., Flexible Filaments for *in Vivo* Imaging and Delivery: Persistent Circulation of Filomicelles Opens the Dosage Window for Sustained Tumor Shrinkage, *Molecular Pharmaceutics*, **2009**, *6* (5), 1343-1352.

171. De León-Rodríguez, L. M., Lubag, A., Udugamasooriya, D. G., Proneth, B., Brekken, R. A., Sun, X., Kodadek, T., Dean Sherry, A., MRI detection of VEGFR2 in vivo using a low molecular weight peptoid-(Gd)8-dendron for targeting. *Journal of the American Chemical Society*, **2010**, 132, (37), 12829-12831.

172. a) Cai, W., Hong, H., Peptoid and positron emission tomography: an appealing combination. *American Journal of Nuclear Medicine and Molecular Imaging*, **2011**, 1, (1), 76-79.
b) Hao, G., Hajibeigi, A., De León-Rodríguez, L. M., Öz1, O. K., Sun, X., Peptoid-based PET imaging of vascular endothelial growth factor receptor (VEGFR) expression. *American Journal of Nuclear Medicine and Molecular Imaging* , **2011**, 1, (1), 65-75.

173. Dhaliwal, K., Alexander, L., Escher, G., Unciti-Broceta, A., Jansen, M., Mcdonald, N., Cardenas-Maestre, J. M., Sanchez-Martin, R., Simpson, J., Haslett, C., Bradley, M., Multi-modal molecular imaging approaches to detect primary cells in preclinical models. *Faraday Discussions,* **2011**, 149, 107-114.

174. Dhaliwal, K., Escher, G., Unciti-Broceta, A., Mcdonald, N., Simpson, J. A., Haslett, C., Bradley, M., Far red and NIR dye-peptoid conjugates for efficient immune cell labelling and tracking in preclinical models. *MedChemComm*, **2011**, 2, (11), 1050-1053.

175. Galindo, F., Altava, B., Burguete, M. I., Gavara, R., Luis, S. V., A sensitive colorimetric method for the study of polystyrene merrifield resins and chloromethylated macroporous monolithic polymers. *Journal of Combinatorial Chemistry*, **2004**, 6, (6), 859-861.

176. M. Lopalco, Ph.D. Thesis, University of Edinburgh, 2009.

177. L. M. Alexander, Ph.D. Thesis, University of Edinburgh, 2009.

178 . Xu, K., Wang, L., Qiang, M., Wang, L., Li, P., Tang, B., A selective near-infrared fluorescent probe for singlet oxygen in living cells. *Chemical Communication*, **2011**,47, (26), 7386-7388.

179 . Kulbacka, J., Pola, A., Mosiadz, D., Choromanska, A., Nowak, P., Kotulska, M., Majkowski, M., Hryniewicz-Jankowska, A., Purzyc, L., Saczko, J., Cyanines as efficient photosensitizers in photodynamic reaction: photophysical properties and in vitro photodynamic activity. *Biochemistry (Moscow)*, **2011**,76, (4), 473-479.

180 . Kim, K., Lee, M., Park, H., Kim, J. H., Kim, S., Chung, H., Choi, K., Kim, I. S., Seong, B. L., Kwon, I. C., Cell-permeable and biocompatible polymeric nanoparticles for apoptosis imaging. *Journal of the American Chemical Society*, **2006**, 128, (11), 3490-3491.

181 . Alford, R., Simpson, H. M., Duberman, J., Hill, G. C., Ogawa, M., Regino, C., Kobayashi, H., Choyke, P. L., Toxicity of organic fluorophores used in molecular imaging: literature review. *Mol Imaging*, **2009**, 8, (6), 341-354.

182. Wilkinson, T. S., Dhaliwal, K., Hamilton, T. W., Lipka, A. F., Farrell, L., Davidson, D.J., Duffin, R., Conway Morris, A., Haslett, C., Govan, J.R.W., Gregory, C.D., Sallenave, J.-M., Simpson, A.J., Trappin-2 promotes early clearance of Pseudomonas aeruginosa through CD14-dependent macrophage activation and neutrophil recruitment. *The American Journal of Pathology*, **2009**, 174, (4), 1338-1346.

183. Rossi, A. G., Hallett, J. M., Sawatzky, D. A., Teixeira, M. M., Haslett, C. Modulation of granulocyte apoptosis can influence the resolution of inflammation. *Biochemical Society Transactions*, **2007**, 35, (Pt 2), 288-291.

184. Haslett,C., Granulocyte apoptosis and its role in the resolution and control of lung inflammation. *American Journal of Respiratory and Critical Care Medicine*, **1999**,160, (5 Pt 2), S5-11.

185. Lindsay, M. A., Peptide-mediated cell delivery: application in protein target validation. *Current Opinion in Pharmacology*, **2002**, 2, (5), 587-594.

186. Schimmer, A. D., Hedley, D. W., Chow, S., Pham, N. A., Chakrabartty, A., Bouchard, D., Mak, T. W., Trus, M. R., Minden, M. D., The BH3 domain of BAD fused to the Antennapedia peptide induces apoptosis via its alpha helical structure and independent of Bcl-2. *Cell Death and Differentiation*, **2001**, 8, (7), 725-733.

187. Schmidt, W., Steinlein, P., Buschle, M., Schweighoffer, T., Herbst, E., Mechtler, K., Kirlappos, H., Birnstiel, M. L., Transloading of tumor cells with foreign major histocompatibility complex class I peptide ligand: a novel general strategy for the generation of potent cancer vaccines. *Proceedings of the National Academy of Sciences of the United States of America*, **1996**, 93, (18), 9759-9763.

188. Myou, S., Zhu, X., Myo, S., Boetticher, E., Meliton, A. Y., Liu, J., Munoz, N. M., Leff, A. R., Blockade of airway inflammation and hyperresponsiveness by HIV-TAT-dominant negative Ras. *Journal of Immunology*, **2003**, 171, (8), 4379-4384.

189. Bruyninckx, W. J., Comerford, K. M., Lawrence, D. W., Colgan, S. P., Phosphoinositide 3-kinase modulation of beta(3)-integrin represents an endogenous "braking" mechanism during neutrophil transmatrix migration. *Blood*, **2001**, 97, (10), 3251-3258.

190. Jones, S. W., Christison, R., Bundell, K., Voyce, C. J., Brockbank, S. M., Newham, P., Lindsay, M. A., Characterisation of cell-penetrating peptide-mediated peptide delivery. *British Journal of Pharmacology*, **2005**, 145, (8), 1093-1102.

191. Riedel, H., Yousaf, N., Zhao, Y., Dai, H., Deng, Y., Wang, J., PSM, a mediator of PDGF-BB-, IGF-I-, and insulin-stimulated mitogenesis. *Oncogene*, **2000**, 19, (1), 39-50.

192. a) Jimi, E., Aoki, K., Saito, H., D'Acquisto, F., May, M. J., Nakamura, I., Sudo, T., Kojima, T., Okamoto, F., Fukushima, H., Okabe, K., Ohya, K., Ghosh, S., Selective inhibition of NF-kappa B blocks osteoclastogenesis and prevents inflammatory bone destruction in vivo. *Nature Medicine*, **2004**, 10, (6), 617-624.
b) May, M. J., D'Acquisto, F., Madge, L. A., Glöckner, J., Pober, J. S., Ghosh, S., Selective inhibition of NF-kappaB activation by a peptide that blocks the interaction of NEMO with the IkappaB kinase complex. *Science*, **2000**, 289, (5484), 1550-1554.

193. Snyder, E. L., Meade, B. R., Saenz, C. C., Dowdy, S. F., Treatment of terminal peritoneal carcinomatosis by a transducible p53-activating peptide. *PLoS Biology*, **2004**, 2, (2), E36.

194. Jans, D. A., Xiao, C. Y., Lam, M. H., Nuclear targeting signal recognition: a key control point in nuclear transport? *Bioessays*, **2000**, 22, (6), 532-544.

195. a) Abdel-Malek, Z. A., Melanocortin receptors: their functions and regulation by physiological agonists and antagonists. *Celullar and Molecular Life Sciences*, **2001**, 58, (3), 434-441.

b) Mountjoy, K. G., Robbins, L. S., Mortrud, M. T., Cone, R. D., The cloning of a family of genes that encode the melanocortin receptors. *Science*, **1992**, 257, (5074), 1248-1251.

196. Robinson, S. J., Healy, E., Human melanocortin 1 receptor (MC1R) gene variants alter melanoma cell growth and adhesion to extracellular matrix. *Oncogene*, **2002**, 21, (52), 8037-8046.

197. Meek, D. W., Tumour suppression by p53: a role for the DNA damage response? *Nature Reviews Cancer*, **2009**, 9, (10), 714-723.

198 . Poyurovsky, M. V., Priest, C., Kentsis, A., Borden, K. L., Pan, Z. Q., Pavletich, N., Prives, C., The MDM2 RING domain C-terminus is required for supramolecular assembly and ubiquitin ligase activity. *The EMBO Journal*, **2007**, 26, (1), 90-101.
199 . Manfredi, J. J., The MDM2-p53 relationship evolves: MDM2 swings both ways as an oncogene and a tumor suppressor. *Genes & Development*, **2010**, 24, (15), 1580-1589.

200 . K. L. Ball, Institute of Genetics and Molecular Medicine, University of Edinburgh, Edinburgh, Scotland, UK, EH4 2XR

201 . Worrall, E. G., Wawrzynow, B., Worrall, L., Walkinshaw, M., Ball, K. L., Hupp, T. R., Regulation of the E3 ubiquitin ligase activity of MDM2 by an N-terminal pseudo-substrate motif. *Journal of Chemical Biology*, **2009**, 2, (3), 113-129.

202. Chan, W. C., White, P. D., Fmoc solid phase peptide synthesis, A pratical approach, **2000**, Oxford University Press.

203 . Harre, M., Nickisch, K., Tilstam, U., An efficient method for activation and recycling of trityl resins. *Reactive and Functional Polymers*, **1999**, 41, (1), 111-114.

204. Díaz-Mochón, J. J., Bialy, L., Bradley, M., Full orthogonality between Dde and Fmoc: the direct synthesis of PNA-peptide conjugates. *Organic Letters*, **2004**, 6, (7), 1127-1129.

205. Fischer, R., Mader, O., Jung, G., Brock, R., Extending the applicability of carboxyfluorescein in solid-phase synthesis. *Bioconjugate Chemistry*, **2003**, 14, (3), 653-660.

206. Ma, Y., Sun, Q., Zhang, H., Peng, L., Yu, J. G., Smith, S. C., The mechanism of cyclization in chromophore maturation of green fluorescent protein: a theoretical study. *The Journal of Physical Chemistry B*, **2010**, 114, (29), 9698-9705.

207. Tsien, R. Y., The green fluorescent protein. *Annual Review of Biochemistry*, **1998,** 67, 509-544.

208. a) Zimmer, M., Green fluorescent protein (GFP): applications, structure, and related photophysical behavior. *Chemical Reviews*, **2002,** 102, (3), 759-781.
b) Tavaré, J. M., Fletcher, L. M., Welsh, G. I., Using green fluorescent protein to study intracellular signalling. *Journal of Endocrinology*, **2001**,170, (2), 297-306.
c) Yang, M., Baranov, E., Jiang, P., Sun, F. X., Li, X. M., Li, L., Hasegawa, S., Bouvet, M., Al-Tuwaijri, M., Chishima, T., Shimada, H., Moossa, A. R., Penman, S., Hoffman, R. M., Whole-body optical imaging of green fluorescent protein-expressing tumors and metastases. *Proceedings of the National Academy of Sciences of the U S A*, **2000**, 97, (3), 1206-1211.

209. The Nobel Foundation, The Nobel Prize in Chemistry 2008, <http://www.nobelprize.org/nobel_prizes/chemistry/laureates/2008/>, accessed 15th April 2011.

210. Kogure, K., Moriguchi, R., Sasaki, K., Ueno, M., Futaki, S., Harashima, H., Development of a non-viral multifunctional envelope-type nano device by a novel lipid film hydration method. *Journal of Controlled Release*, **2004**, 98, (2), 317-323.

211. Suzuki, R., Yamada, Y., Harashima, H., Efficient cytoplasmic protein delivery by means of a multifunctional envelope-type nano device. *Biological & Pharmaceutical Bulletin*, **2007**, 30, (4), 758-762.

212. Ford, K. G., Souberbielle, B. E., Darling, D., Farzaneh, F., Protein transduction: an alternative to genetic intervention? *Gene Therapy*, **2001**, 8, (1), 1-4.

213. a) Green, M., Loewenstein, P. M., Autonomous functional domains of chemically synthesized human immunodeficiency virus tat trans-activator protein. *Cell*, **1988**, 55, (6), 1179-1188.
b) Frankel, A. D., Pabo, C. O., Cellular uptake of the tat protein from human immunodeficiency virus. *Cell*, **1988**, 55, (6), 1189-1193.

214. Simon, M. J., Gao, S., Kang, W. H., Banta, S., Morrison, B. 3rd. TAT-mediated intracellular protein delivery to primary brain cells is dependent on glycosaminoglycan expression. *Biotechnology and Bioengineering*, **2009**, 104, (1), 10-19.

215. Shokolenko, I. N., Alexeyev, M. F., LeDoux, S. P., Wilson, G. L., TAT-mediated protein transduction and targeted delivery of fusion proteins into mitochondria of breast cancer cells. *DNA Repair*, **2005**, 4, (4), 511-518.

216. Chin Lee, S. H., Jefferies, R., Watt, P., Hopkins, R., Sotzik, F., Reid, S., Armson, A., Boxell, A., Ryan, U., In vitro analysis of the TAT protein transduction domain as a drug delivery vehicle in protozoan parasites. *Experimental Parasitology*, **2008**, 118, (3), 303-307.

217. Pooga, M., Kut, C., Kihlmark, M., Hällbrink, M., Fernaeus, S., Raid, R., Land, T., Hallberg, E., Bartfai, T., Langel, U., Cellular translocation of proteins by transportan. *FASEB Journal*, **2001**, 15, (8), 1451-1453.

218. Han, K., Jeon, M. J., Kim, K. A., Park, J., Choi, S. Y., Efficient intracellular delivery of GFP by homeodomains of Drosophila Fushi-tarazu and Engrailed proteins. *Molecules and Cells*, **2000**, 10, (6), 728-732.

219. a) Cho, J. H., Hwang, I. K., Yoo, K. Y., Kim, S. Y., Kim, D. W., Kwon, Y. G., Choi, S. Y., Won, M. H., Effective delivery of Pep-1-cargo protein into ischemic neurons and long-term neuroprotection of Pep-1-SOD1 against ischemic injury in the gerbil hippocampus. Neurochemistry International, 2008, 52, (4-5), 659-668.
b) Lundberg M, Wikström S, Johansson M. Cell surface adherence and endocytosis of protein transduction domains. Molecular Therapy, 2003 Jul;8(1):143-150.

220. Harmanson, G. T., Bioconjugate techniques, Second edition, 2008, Elsevier Inc.

221. a) Smyth, D. G., Blumenfeld, O. O., Konigsberg, W., Reactions of N-ethylmaleimide with peptides and amino acids. *The Biochemical Journal*, **1964**, 91, (3), 589-595.
b) Kida, S., Maeda, M., Hojo, K., Eto, Y., Nakagawa, S., Kawasaki, K., Studies on heterobifunctional cross-linking reagents, 6-maleimidohexanoic acid active esters. *Chemical & Pharmaceutical Bulletin (Tokyo)*, **2007**, 55, (4), 685-687.

222. Collins-Racie, L. A., McColgan, J. M., Grant, K. L., DiBlasio-Smith, E. A., McCoy, J. M., LaVallie, E. R., Production of recombinant bovine enterokinase catalytic subunit in Escherichia coli using the novel secretory fusion partner DsbA. *Biotechnology*, **1995**, 13, (9), 982-987.

223. Rich, D. H., Gesellchen, P. D., Tong, D., Cheung, A., Buckner, C. K., Alkylating derivatives of amino acids and peptides. Synthesis of N-maleoylamino acids, [1-(N-maleoylglycyl)cysteinyl]oxytocin. Effects on vasopressin-stimulated water loss from isolated toad bladder. *Journal of Medicinal Chemistry*, **1975**, 18, (10), 1004-1010.

224. Kalgutkar, A. S., Crews, B. C., Marnett L. J., Design, synthesis, and biochemical evaluation of N-substituted maleimides as inhibitors of prostaglandin endoperoxide synthases. *Journal of Medicinal Chemistry*, **1996**, 39, (8), 1692-1703.

225. de Figueiredo, R. M., Oczipka, P., Fröhlich, R., Christmann, M., Synthesis of 4-Maleimidobutyric Acid and Related Maleimides. *Synthesis*, **2008**, 39, (34), 1316-1318.

226. Scigelova, M., Green, P. S., Giannakopulos, A. E., Rodger, A., Crout, D. H. G., Derrick, P. J., A practical protocol for the reduction of disulfide bonds in proteins prior to analysis by mass spectrometry. *European Journal of Mass Spectrometry*, **2001**, 7, (1), 29-34.

227 . Cleland, W. W., Dithiothreitol, a new protective reagent for SH groups. *Biochemistry*, **1964**, 3, 480-482.

228. Gee, N. S., Knowles, M., Production of conjugates. *Innova Biosciences LTD*, **2007**, Patent number WO2007/068906 A2.

229 . Frederick, H., White, Jr., Armando, S., The Thiolation of Ribonuclease, *Biochemistry*, **1962**, 1 (6), 938-946.

230. Singh, R., Kats, L., Blättler, W. A., Lambert, J. M., Formation of N-substituted 2-iminothiolanes when amino groups in proteins and peptides are modified by 2-iminothiolane. *Analytical Biochemistry*, ***1996***, 236, (1),114-125.

231. Kamruzzahan, A. S., Ebner, A., Wildling, L., Kienberger, F., Riener, C. K., Hahn, C. D., Pollheimer, P. D., Winklehner, P., Hölzl, M., Lackner, B., Schörkl, D. M., Hinterdorfer, P., Gruber, H. J., Antibody linking to atomic force microscope tips via disulfide bond formation. *Bioconjugate Chemistry*, **2006**, 17, (6), 1473-1481.

232. Page, P., Bradley, M., Walters, I., Teague, S., Solid-Phase Synthesis of Tyrosine Peptide Aldehydes. Analogues of (S)-MAPI. *Journal of Organic Chemistry*, **1999**, 64, (3), 794-799.

233. Kovacs, J., Kisfaludy, L., Ceprini, M. Q., On the optical purity of peptide active esters prepared by N,N'-dicyclohexylcarbodiimide and "complexes" of N,N'-dicyclohexyl carbodiimide-pentachlorophenol and N,N'-dicyclohexylcarbodiimide-pentafluorophenol. *Journal of the American Chemical Society*, **1967**, 89, (1), 183-184.

234. Xu, Z. P., Walker, T. L., Liu, K. L., Cooper, H. M., Lu, G. Q. M., Bartlett, P. F., Layered double hydroxide nanoparticles as cellular delivery vectors of supercoiled plasmid DNA. *International Journal of Nanomedicine*, **2007**, 2, (2), 163-174.

235. Zhang, P., Liu, W., ZnO QD@PMAA-co-PDMAEMA nonviral vector for plasmid DNA delivery and bioimaging. *Biomaterials*, **2010**, 31, (11), 3087-3094.

236. Liberska, A., Lilienkampf, A., Unciti-Broceta, A., Bradley, M., Solid-phase synthesis of arginine-based double-tailed cationic lipopeptides: potent nucleic acid carriers. *Chemical Communications*, **2011**, 47, (48), 12774-12776.

237. Borger, J.G., Cardenas-Maestre, J.M., Zamoyska, R., Sanchez-Martin, R.M., Novel strategy for microsphere-mediated DNA transfection. *Bioconjugate Chemistry*, **2011**, 22, (10), 1904-1908.

238. Trabulo, S., Mano, M., Faneca, H., Cardoso, A. L., Duarte, S., Gomes, P., Simoes, S., Pedroso de Lima, M. D., Association of S4(13)-PV cell penetrating peptide with cationic liposomes: A synergistic effect on the intracellular delivery of plasmid DNA. *Journal of Peptide Science*, **2008**, 14, (8), 135-135.

239. Morris, M. C., Deshayes, S., Heitz, F., Divita, G., Cell-penetrating peptides: from molecular mechanisms to therapeutics. *Biology of the Cell*, **2008**, 100, (4), 201-217.

240. Chen, X., Kube, D. M., Cooper, M. J., Davis, P. B., Cell surface nucleolin serves as receptor for DNA nanoparticles composed of pegylated polylysine and DNA. *Molecular Therapy*, **2008**, 16, (2), 333-342.

241. Klapper, A., MacKay, B., Resh, M. D., Rapid high resolution western blotting: from gel to image in a single day. *Biotechniques*, **1992**, 12, (5), 650-654.

242. Veronese, F. M., Pasut, G., PEGylation successful approach to drug delivery. *Drug Discovery Today*, **2005**, 10, (21), 1451-1458.

243. Mishra, S., Webster, P., Davis, M. E., PEGylation significantly affects cellular uptake and intracellular trafficking of non-viral gene delivery particles. *European Journal of Cell Biology*, **2004**, 83, (3), 97-111.

244. Schumann, W., Chapter 1: Structure of Bacterial Cell. *Dynamics of the Bacterial Chromosome: Structure and Function*, **2006**, 1-27, Wiley-VCH Verlag GmbH & Co.

245. Claus, D., A standardized Gram staining procedure. *World Journal of Microbiology and Biotechnology*, **1992**, 8, (4), 451-452.

246. Gram, H. C., Über die isolierte Färbung der Schizomyceten in Schnitt- und Trockenpräparaten. *Fortschritte der Medizin*, **1884,** 2, 185–189. Translation in English: Brock, T. D., The differential staining of Schizomycetes in tissue sections and in dried preparations. Milestones in microbiology: 1546 to 1940, *Second Edition*, **1999,** 215-217, AMS press publishing.

247. Allen, M. J., Edberg, S. C., Reasoner, D. J., Heterotrophic plate count bacteria—what is their significance in drinking water? *International Journal of Food Microbiology*, **2004**, 92, (3), 265-274.

248. Sears, C. L., A dynamic partnership: Celebrating our gut flora. *Anaerobe*, **2005**, 11, (5), 247-251.

249. Nelson, E. J., Harris, J. B., Morris, J. G. Jr, Calderwood, S. B., Camilli, A., Cholera transmission: the host, pathogen and bacteriophage dynamic. *Nature Review Microbiology*, **2009**, 7, (10), 693-702.

250. Singh, A. E., Romanowski, B., Syphilis: review with emphasis on clinical, epidemiologic, and some biologic features. *Clinical Microbiology Review*, **1999**, 12, (2), 187-209.

251. Nathwani, D., Hamlet, N., Walker, E., Lyme disease: a review. *The British Journal of General Practice,* **1990**, 40, (331), 72-74.

252. Singanayagam, A., Chalmers, J.D., Hills, A.T., Severity assessment in community-acquired pneumonia: a review. *Quarterly Journal of Medicine,* **2009,** 102, (6), 379-388.

253. Hanekom, W. A., Lawn, S. D., Dheda, K., Whitelaw, A., Tuberculiosis research update. *Tropical Medicine and International Health,* **2010,** 15, (8), 981-989.

254. Chain, E. H., Florey, H. W., Gardner, A. N. D., Healthy, N. G., Jennings, M. A., Orr-Ewing, J., Sanders, A.G., Penicillin as chemotherapeutic agent. *Lancet*, **1940**, 2, 226-228.

255. Fleming, A. Classics in infectious diseases: on the antibacterial action of cultures of a penicillium, with special reference to their use in the isolation of B. influenza. *Reviews of Infectious Diseases*, **1980,** 2, (1), 129-139. Reprinted from *British Journal of Experimental Pathology*, **1929,** 10, 226-236.

256. Drlica, K., Zhao, X., DNA gyrase, Topoisomerase IV, and the 4-Quinolones. *Microbiology and Molecular Biology Reviews*, **1997**, 61, (3), 377-392.

257. a) Moellering, R. C., Jr., In vitro antibacterial activity of the aminoglycoside antibiotics. *Reviews of Infectious Diseases*, **1983,** 5, S212-S232.
b) Forge, A., Schacht, J., Aminoglycoside Antibiotics, *Audiology & Neurotology*, **2000,** 5, (1), 3-22.

258. Tomasz, A., The mechanism of the irreversible antimicrobial effects of penicillins: how the beta-lactam antibiotics kill and lyse bacteria. *Annual Review of Microbiology,* **1979**, 33,113-137.

259. Buynak, J. D.,Cutting and stitching: the cross-linking of peptidoglycan in the assembly of the bacterial cell wall. *Chemical Biology*, **2007**, 2, (9), 602-605.

260. Andersson, D. I., Hughes, D., Antibiotic resistance and its cost:
is it possible to reverse resistance? *Nature Reviews Microbiology*, **2010**, 8, (4), 260-271.

261. Levy, S. B., Marshall, B., Antibacterial resistance worldwide: causes, challenges and responses. *Nature Medicine*, **2004**, 10, (12), S122-S129.

262. Kaye, K. S., Fraimow, H. S., Abrutyn, E., Pathogens resistant to antimicrobial agents: epidemiology, molecular mechanisms, and clinical management. *Infectious Disease Clinics North America*, **2000**, 14, (2), 293-319.

263. Madigan, M. T., Martinko, J. M., Parker, J., Brock biology of microorganisms, *Tenth edition*, **2003,** Pearson International Edtition.

264. De Sarro, A., De Sarro, G., Adverse reactions to fluoroquinolones. An overview on mechanistic aspects. *Current Medicinal Chemistry*, **2001**, 8, (4), 371-384.

265. Anwar, S., Prince, L. R., Foster, S. J., Whyte, M. K.,Sabroe, I., The rise and rise of Staphylococcus aureus: laughing in the face of granulocytes. *Clinical and Experimental Immunology*, **2009**, 157, (2), 216-224.

266. Rosen, D. A., Hooton, T. M., Stamm, W. E., Humphrey, P. A., Hultgren, S.J., Detection of intracellular bacterial communities in human urinary tract infection. *PLoS Medicine*, **2007,** 4, (12), e329, 1949-1958.

267. Hu, Y., Shamaei-Tousi, A., Liu, Y., Coates, A., A new approach for the discovery of antibiotics by targeting non-multiplying bacteria: a novel topical antibiotic for staphylococcal infections. *PLoS One*, **2010,** 5, (7), e11818, 1-10.

268. Gratia, A., Sur un remarquable example d´antagonisme entre souches de colibacille. *Comptes Rendus des Séances et Mémoires de la Société de Biologie*, **1925**, 93, 1040-1041.

269. Whitehead, H. R., A substance inhibiting bacterial growth, produced by certain strains of lactic streptococci. *Biochemistry Journal*, **1933**, 27, 1793-1800.

270. Mattick, A. T. R., Hirsch, A., Further observations on an inhibitory substance (nisin) from lactic treptococci. *Lancet*, **1947**, 250, 5-8.

271. Chan, W.C., Dodd, H.M., Horn, N., Maclean, K., Lian, L.Y., Bycroft, B.W., Gasson, M.J., Roberts, G.C., Structure-activity relationships in the peptide antibiotic nisin: role of dehydroalanine 5. *Applied and Environmental Microbiology*, **1996**, 62, (8), 2966-2969.

272. a) Leach, F. R., Snell, E. E., The absorption of glycine and alanine and their peptides by Lactobacillus casei. *The Journal of Biological Chemistry*, **1960,** 235, (12), 3523-3531.
b) Gilvarg, C., Katchalski, E.,Peptide utilization in Escherichia coli. *The Journal of Biological Chemistry*, **1965,** 240, (7), 3093-3098.

273. Steiner, H., Hultmark, D., Engstrom, A., Bennich, H., Boman, H. G., Sequence and specificity of two antibacterial proteins involved in insect immunity. *Nature*, **1981**, 292, (5820), 246-248.

274. Zasloff, M., Magainins, a class of antimicrobial peptides from Xenopus skin: isolation, characterization of two active forms, and partial cDNA sequence of a precursor. *Proceedings of the National Academy of Sciences of the United States of America*, **1987**, 84, (15), 5449-5453.

275. Boman, H., Peptide antibiotics and their role in innate immunity. *Annual Review of Immunology*, **1995,** 13, 61-92.

276. Ganz, T., Defensins: antimicrobial peptides of innate immunity. *Nature Review. Immunology*, **2003**, 3, (9), 710-720.

277. a) Wang, G., Li, X., Wang, Z., APD2: the updated antimicrobial peptide database and its application in peptide design. *Nucleic Acids Research*, **2009**, 37, D933-D937.
b) Antimicrobial Sequences Database: www.bbcm.univ.trieste.it/~tossi/pag5.htm, accessed 30th November 2012.
c) The Antimicrobial Peptide Database: *http://aps.unmc.edu/AP/main.php*, accessed 30th November 2012.

278. Fukase, K., Kitazawa, M., Sano, A., Shimbo, K., Fujita, H., Horimoto, S., Wakamiya, T., Shiba, T., Total synthesis of peptide antibiotic nisin. *Tetrahedron Letters*, **1988**, 29, (7), 795-798.

279. Hinton, J. F., Jordan, B., Horne, E., Molecular structure heterogeneity of gramicidin analogs incorporated into SDS micelles: a NMR study. *Journal of Molecular Structure*, **2002**, 602-603, 245-256.

280. Yeaman, M. R., Yount, N. Y., Mechanisms of antimicrobial peptide action and resistance. *Pharmacological Reviews*, **2003**, 55, (1), 27-55.

281. Fehri, L.F., Sirand-Pugnet, P., Gourgues, G., Jan, G., Wróblewski, H., Blanchard, A., Resistance to antimicrobial peptides and stress response in *Mycoplasma pulmonis*. *Antimicrobial Agents and Chemotherapy*, **2005**, 49, (10), 4154-4165.

282. Pasupuleti, M., Schmidtchen, A., Malmsten, M., Antimicrobial peptides: key components of the innate immune system. *Critical Reviews in Biotechnology*, **2012**, 32, (2), 143-171.

283. Ge, Y., MacDonald, D. L., Holroyd, K. J., Thornsberry, C., Wexler, H., Zasloff, M., In vitro antibacterial properties of pexiganan, an analog of magainin. *Antimicrobial Agents and Chemotherapy*, **1999**, 43, (4), 782-788.

284. Xiao, Q., Pei, D., High-throughput synthesis and screening of cyclic peptide antibiotics. *Journal of Medicinal Chemistry*, **2007**, 50, (13), 3132-3137.

285. Noto, P. B., Abbadessa, G., Cassone, M., Mateo, G. D., Agelan, A., Wade, J.D., Szabo, D., Kocsis, B., Nagy, K., Rozgonyi, F., Otvos, L. Jr., Alternative stabilities of a proline-rich antibacterial peptide in vitro and in vivo. *Protein Science*, **2008**, 17, (7), 1249-1255.

286. Yeaman M. R., Yount, N. Y., Code among chaos: Immunorelativity and the AEGIS model of antimicrobial peptides, *American Society for Microbiology News*, **2005**, 71, (1), 21-27.

287. Gordon, Y. J., Romanowski, E. G., McDermott, A. M., A review of antimicrobial peptides and their therapeutic potential as anti-infective drugs. *Current Eye Research*, **2005**, 30, (7), 505-515.

288. Fowler, S. A., Blackwell, H. E., Structure-function relationships in peptoids: recent advances toward deciphering the structural requirements for biological function.
Organic & Biomolecular Chemistry, **2009**, 7, (8), 1508-1524.

289. Miller, S. M., Simon, R. J., Ng, S., Zuckermann, R. N., Kerr, J. M., Moos, W. H., Proteolytic studies of homologous peptide and N-substituted glycine peptoid oligomers. *Bioorganic & Medicinal Chemistry Letters*, **1994,** 4, (22), 2657-2662.

290. Ng, S., Goodson, B., Ehrhardt, A., Moos, W. H., Siani, M., Winter, J., Combinatorial discovery process yields antimicrobial peptoids. *Bioorganic & Medicinal Chemistry*, **1999,** 7, (9), 1781-1785.

291. Goodson, B., Ehrhardt, A., Ng, S., Nuss, J., Johnson, K., Giedlin, M., Yamamoto, R., Moos, W. H., Krebber, A., Ladner, M., Giacona, M. B., Vitt, C., Winter, J., Characterization of novel antimicrobial peptoids. *Antimicrobial Agents and Chemotherapy*, **1999**, 43, (6),1429-1434.

292. Humet, M., Carbonell, T., Masip, I., Sánchez-Baeza, F., Mora, P., Cantón, E., Gobernado, M., Abad, C., Pérez-Payá, E., Messeguer, A., A positional scanning combinatorial library of peptoids as a source of biological active molecules: identification of antimicrobials. *Journal of Combinatorial Chemistry*, **2003**, 5, (5), 597-605.

293. Patch, J. A., Barron, A.E., Helical peptoid mimics of magainin-2 amide.
Journal of the American Chemical Society, **2003**, 125, (40), 12092-12093.

294. Wu, C. W., Sanborn, T. J., Huang, K., Zuckermann, R. N., Barron, A. E., Peptoid oligomers with alpha-chiral, aromatic side chains: sequence requirements for the formation of stable peptoid helices. *Journal of the American Chemical Society*, **2001,** 123, (28), 6778-6784.

295. Sanborn, T. J., Wu, C. W., Zuckermann, R. N., Barron, A. E., Extreme stability of helices formed by water-soluble poly-N-substituted glycines (polypeptoids) with alpha-chiral side chains. *Biopolymers*, **2002**, 63, (1),12-20.

296. Shankaramma, S. C., Moehle, K., James, S., Vrijbloed, J. W., Obrecht, D., Robinson, J. A., A family of macrocyclic antibiotics with a mixed peptide-peptoid beta-hairpin backbone conformation. *Chemical Communications*, **2003**, 7, (15), 1842-1843.

297. Shankaramma, S. C., Athanassiou, Z., Zerbe, O., Moehle, K., Mouton, C., Bernardini, F., Vrijbloed, J. W., Obrecht, D., Robinson, J. A., Macrocyclic hairpin mimetics of the cationic antimicrobial peptide protegrin I: a new family of broad-spectrum antibiotics. *Chembiochem*, **2002**, 3, (11), 1126-1133.

298. a) Shuey, S. W., Delaney, W. J., Shah, M. C., Scialdone, M. A., Antimicrobial β-peptoids by a block synthesis approach. *Bioorganic & Medicinal Chemistry Letters*, **2006**, 16, (5), 1245-1248.
b) Olsen, C. A., Ziegler, H. L., Nielsen, H. M., Frimodt-Møller, N., Jaroszewski, J. W., Franzyk, H., Antimicrobial, hemolytic, and cytotoxic activities of beta-peptoid-peptide hybrid oligomers: improved properties compared to natural AMPs. *Chembiochem*, **2010**, 11, (10), 1356-1360.

299. Zhu, W. L., Song, Y. M., Park, Y., Park, K. H., Yang, S. T., Kim, J. I., Park, I. S., Hahm, K. S., Shin, S.Y., Substitution of the leucine zipper sequence in melittin with peptoid residues affects self-association, cell selectivity, and mode of action. *Biochimica et Biophysica Acta*, **2007,** 1768, (6), 1506-1517.

300. a) Song, Y. M., Park, Y., Lim, S. S., Yang, S. T., Woo, E. R., Park, I. S., Lee, J. S., Kim, J. I., Hahm, K. S., Kim, Y., Shin, S. Y., Cell selectivity and mechanism of action of antimicrobial model peptides containing peptoid residues. *Biochemistry*, **2005**, 44, (36), 12094-12106.
b) Zhu, W. L., Lan, H., Park, Y., Yang, S. T., Kim, J. I., Park, I. S., You, H. J., Lee, J. S., Park, Y. S., Kim, Y., Hahm, K. S., Shin, S. Y., Effects of Pro --› peptoid residue substitution on cell selectivity and mechanism of antibacterial action of tritrpticin-amide antimicrobial peptide. *Biochemistry*, **2006**, 45, (43), 13007-13017.
c) Lim, S. S., Yoon, S. P., Park, Y., Zhu, W. L., Park, I. S., Hahm, K. S., Shin, S. Y., Mechanism of antibacterial action of a synthetic peptide with an Ala-peptoid residue based on the scorpion-derived antimicrobial peptide IsCT. *Biotechnology Letters*, **2006**, 28, (18), 1431-1437.

301. Ryge, T. S., Hansen, P. R., Novel lysine-peptoid hybrids with antibacterial properties. *Journal of Peptide Science*, **2005**, 11, (11), 727-734.

302. Chongsiriwatana, N. P., Patch, J. A., Czyzewski, A. M., Dohm, M. T., Ivankin, A., Gidalevitz, D., Zuckermann R. N., Barron, A. E., Peptoids that mimic the

structure, function, and mechanism of helical antimicrobial peptides. *Proceedings of the National Academy of Sciences*, **2008**, 105, (8), 2794–2799.

303. Statz, A. R., Park, J. P., Chongsiriwatana, N. P., Barron, A. E., Messersmith, P. B., Surface-immobilised antimicrobial peptoids. Biofouling, 2008, 24, (6), 439-448.

304. 33rd Session of the Sub-Committee of Experts on the Transport of Dangerous Goods (UNSCOE TDG) June 30-July 9, **2008**

305. Malowa, M., Wehrstedt, K. D., Neuenfeld, S., On the explosive properties of 1H-benzotriazole and 1H-1,2,3-triazole. *Tetrahedron Letters*, **2007**, 48, (7), 1233-1235.

306. Subirós-Funosas, R., Prohens, R., Barbas, R., El-Faham, A., Albericio, F., Oxyma: an efficient additive for peptide synthesis to replace the benzotriazole-based HOBt and HOAt with a lower risk of explosion. *Chemistry*, **2009**, 15, (37), 9394-9403.

307. High-Throughput Synthesis, Principles and Practices, Edited by Irving Sucholeiki, CRC Press 2001, Pages 27

308. Zhang, A. J., Russell, D. H., Zhu, J., Burgess, K., A method for removal of N-BOC protecting groups from substrates on TFA-sensitive resins. *Tetrahedron Letters*, **1998,** 39, (41), 7439-7442.

309. Brown, E. G., Nuss, J. M., Alkylation of Rink's amide linker on polystyrene resin: A reductive amination approach to modified amine-linkers for the solid phase synthesis of N-substituted amide derivatives. *Tetrahedron Letters*, **1997,** 38, (49), 8457-8460.

310. Jas, G., Kirschning, A., Continuous flow techniques in organic synthesis. *Chemistry: A European Journal*, **2003**, 9, (23), 5708-5723.

311. Chankeshwara, S. V., Chakraborti, A. K., Catalyst-free chemoselective N-*tert*-butyloxycarbonylation of amines in water. *Organic Letters*, **2006**, 8, (15), 3259-3262.

312 . a) Turczan, J. W., Kram, T. C., Determination of meprobamate in tablets by NMR. *Journal of Pharmaceutical Sciences*, **1967**, 56, (12), 1643-1645.
b) Turczan, J. W., Goldwitz, B. A., Determination of chloral hydrate in soft gelatin capsules by NMR. *Journal of Pharmaceutical Sciences*, **1972**, 61, (4), 613-615.
c) Turczan, J. W., Goldwitz, B. A., Determination of pentylenetetrazol in tablets and injectables by NMR. *Journal of Pharmaceutical Sciences*, **1972**, 61, (8), 1309-1310.
d) Turczan, J. W., Lau-cam, C. A., 1H-Nuclear Magnetic Resonance Spectrosoopic Determination of Haloperidol in Tablets. *Drug Development and Industrial Pharmacy*, **1989**, 15, (1), 107-115.

313 . Pauli, G. F., Jaki, B. U., Lankin, D. C., Quantitative 1H NMR: development and potential of a method for natural products analysis. *Journal of Natural Products,* **2005**, 68, (1), 133-149.

314. Gerritz, S. W., Sefler, A. M., 2,5-Dimethylfuran (DMFu): An internal standard for the "traceless" quantitation of unknown samples via 1H NMR. *Journal of Combinatoral Chemistry,* **2000**, 2, (1), 39-41.

315. Hamper, B. C., Kolodziej, S. A., Scates, A. M., Smith, R. G., Cortez, E., Solid phase synthesis of β-peptoids: N-substituted β-aminopropionic acid oligomers. *The Journal of Organic Chemistry,* **1998**, 63, (3), 708-718.

316. Lammers, H., Peters, J. A., Van Bekkum, H., Reductive amination of aldohexoses with mono- and bifunctional alkyl amines: Conversion of carbohydrates into EDTA type complexing agents. *Tetrahedron*, **1994**, 30, (27), 8103-8116.

317. Han, G., Tamaki, M. Hruby, V. J., Fast, efficient and selective deprotection of the *tert*-butoxycarbonyl (Boc) group using HCl/dioxane (4 M). *The Journal of Peptide Research,* **2001,** 58, (4), 338-341.

318. Gilbert, P., Collier, P.J. & Brown, M.R. Influence of growth rate on susceptibility to antimicrobial agents: biofilms, cell cycle, dormancy, and stringent response. *Antimicrobial Agents & Chemotherapy,* **1990,** 34, (10), 1865-1868.

319. a)Garcia-Medina, R., Dunne, W. M., Singh, P. K., Brody, S. L., Pseudomonas aeruginosa acquires biofilm-like properties within airway epithelial cells. *Infection and Immunity,* **2005**, 73, (12), 8298-8305.
b) Martin, D. W., Mohr, C. D., Invasion and intracellular survival of Burkholderia cepacia. *Infection and Immunity*, **2000**, 68, (1), 24-29.

320. Govan, J. R., Brown, A. R., Jones, A.M. Evolving epidemiology of Pseudomonas aeruginosa and the Burkholderia cepacia complex in cystic fibrosis lung infection. *Future Microbiology*, **2007**, 2, (2), 153-164.

321. Jorgensen, J. H., Ferraro, M. J., Antimicrobial susceptibility testing: a review of general principles and contemporary practices. *Clinical Infection Diseases,* **2009**, 49, (11), 1749-1755.

322. Kadurugamuwa, J. L., Francis, K. P., Bioluminescent imaging of bacterial biofilm infections *in vivo*. *Methods in Moecular Biology* , **2008**, 431, 225-239.

323. Coates, A.R., Halls, G., Antibiotics in phase II and III clinical trials. *Handbook of Experimental Pharmacology,* **2012**, (211), 167-183.

324. Sarin, V. K.; Kent, S. B. H.; Tam, J. P.; Merrifield, R. B., Quantitative Monitoring of Solid-Phase Peptide-Synthesis by the Ninhydrin Reaction. *Analytical Biochemistry,* **1981,** 117, (1), 147-157.

325. Galindo, F., Altava, B., Burguete, M. I., Gavara, R., Luis, S.V., A sensitive colorimetric method for the study of polystyrene Merrifield resins and chloromethylated macroporous monolithic polymers. *Journal of Combinatorial Chemistry*, **2004**, 6, (6), 859-861.

326. Bialy, L., Díaz-Mochón, J. J., Specker, E., Keinicke, L., Bradley, M., Dde-protected PNA monomers, orthogonal to Fmoc, for the synthesis of PNA–peptide conjugates. *Tetrahedron*, **2005**, 61, (34), 8295-8305.

327 . Chhabra, S. R., Hothi, B., Evans, D. J., White, P. D., Bycroft, B. W., Chan, W. C., *Tetrahedron Letters*, **1998**, 39, (12), 1603-1606.

328. Fischer, R., Mader, O., Jung, G., Brock, R., Extending the applicability of carboxyfluorescein in solid-phase synthesis. *Bioconjugate Chemistry*, **2003**, 14, (3), 653-660.

329. Gee, N. S., Knowles, M., Production of conjugates. Innova Biosciences LTD, 2007, Patent number WO2007/068906 A2.

330. Page, P., Bradley, M., Walters, I., Teague, S., Solid-phase synthesis of tyrosine peptide aldehydes: Analogues of (S)-MAPI. *Journal of Organic Chemistry*, **1999**, 64, (3), 794-799.